AIR2022

Proceedings- International Conference on Advancements in Interdisciplinary Research

Motilal Nehru National Institute of Technology (MNNIT) Allahabad, Prayagraj, India

May, 6-7 2022

Organizing Committee

PATRON
Prof. Rama Shanker Verma, Director, MNNIT Allahabad

CHAIRMAN
Dr. Abhishek Kumar, Head, AMD, MNNIT Allahabad

ORGANIZING SECRETARIES
Dr. Ashutosh Mishra, MNNIT Allahabad
Dr. Abhishek Kumar Tiwari, MNNIT Allahabad

PROGRAM CHAIRS
Dr. Ramesh Pandey, MNNIT Allahabad
Dr. Akshoy Ranjan Paul, MNNIT Allahabad
Dr. Ajaya Bharti, MNNIT Allahabad
Dr. Ashutosh Kr. Upadhyay, MNNIT Allahabad
Dr. Anindya Bhar, MNNIT Allahabad
Dr. V. Murari, MNNIT Allahabad

PUBLICATION CHAIRS
Dr. Vijayan Sugumaran, Oakland University USA
Dr. Ashutosh Mishra, MNNIT Allahabad
Dr. Abhishek Kumar Tiwari, MNNIT Allahabad
Dr. Dharmendra Tripathi, NIT Uttarakhand
Dr. Ravindra Kannojiya, Amity University Noida
Dr. Divya Mishra, ABES Engineering College, Ghaziabad
Ms. Shanu Sharma, ABES Engineering College, Ghaziabad

PUBLICITY CHAIRS
Dr. Vivek Kr. Patel, MNNIT Allahabad
Dr. Anubhav Rawat, MNNIT Allahabad
Dr. Satish Kumar, MNNIT Allahabad
Dr. Abhishek Kundu, MNNIT Allahabad
Dr. Tanmoy Mondal, MNNIT Allahabad
Dr. Udhayaraman R., MNNIT Allahabad

Technical Programme Committee

Prof. (Dr.) Sunil Vadera, School of Science, Engineering and Environment, Salford University, Manchester, UK
Prof. (Dr.) Matthias Volk, Otto-von-Guericke-University Magdeburg, Magdeburg, Germany
Prof. (Dr.) Epaminondas Kapetanios, School of Physics, Engineering, and Computer Science, University of Hertfordshire, UK
Dr. Ayush Goyal, Texas A&T University, USA
Prof. (Dr.) Neil Y. Yen, University of Aizu, Japan
Prof. (Dr.) Jordi Conesa Caralt, Multimedia and Telecommunications Open, University of Catalonia, Barcelona, Spain
Prof. (Dr.) Farid Meziane, College of Science and Engineering, University of Derby, UK
Prof. (Dr.) Ram Mohan, Texas A&M University, USA
Prof. (Dr.) Russell P. Main, Purdue University, USA
Prof. (Dr.) Arvind Agarwal, FIU, USA
Dr. M V Reddy, Senior Professional Researcher at New graphite world Montreal, Canada
Dr. Alok Verma, Energy Research Institute, NTU, Singapore
Dr. Shalini Sharma, Institute of Information System and Applications, National Tsing Hua University, Hsinchu, Taiwan
Mr. Soumak Roy, VP & Global Practice Leader - Cyber security VP & Global Practice, SDG Corporation

Dr. D. Loganathan, Department of Computer Science and Engineering, Puducherry Technological University, India
Dr. Ritu Gupta, Department of IT, Bhagwan Parshuram Institute of technology, GGSIPU, Delhi

International Advisory Committee

Prof. (Dr.) Vijayan Sugumaran, Oakland University, USA
Prof. (Dr.) Farid Meziane, Head-Data Science Research Centre, School of Computing and Engineering, University of Derby, UK
Prof. (Dr.) Sunil Vadera, School of Science, Engineering and Environment, Salford University, Manchester, UK
Prof. (Dr.) Matthias Volk, Otto-von-Guericke-University Magdeburg, Magdeburg, Germany
Prof. (Dr.) Epaminondas Kapetanios, School of Physics, Engineering, and Computer Science, University of Hertfordshire, UK
Prof. (Dr.) M Douglas Dagan, Vice President of Strategic Initiatives & Renewable Energy New York City, USA
Dr. Ayush Goyal, Texas A&T University, USA
Prof. (Dr.) Neil Y. Yen, University of Aizu, Japan
Prof. (Dr.) Jordi Conesa Caralt, Multimedia and Telecommunications Open, University of Catalonia, Barcelona, Spain
Prof. (Dr.) Farid Meziane, College of Science and Engineering, University of Derby, UK
Prof. (Dr.) Wynne Chin, Bauer College of Business, University of Houston, USA
Prof. (Dr.) Victoria Yoon, VCU School of Business, Virginia Commonwealth University, Virginia
Prof. (Dr.) Aurona Gerber, Department of Informatics, University of Pretoria, South Africa
Prof. (Dr.) Ram Mohan, Texas A&M University, USA
Prof. (Dr.) Russell P. Main, Purdue University, USA
Prof. (Dr.) Arvind Agarwal, FIU, USA
Prof. (Dr.) Joerg Leukel, University of Hohenheim, Institute of Health Care & Public Management Information Systems II, Germany
Prof. (Dr.) Stefan Kirn, University of Hohenheim, Institute of Health Care & Public Management Information Systems II, Germany
Prof. (Dr.) Elisabeth Metais, CEDRIC Laboratory, Conservatoire National des Arts et Métiers (CNAM), Paris, France
Prof. (Dr.) Ghassan Beydoun, School of Information, Systems and Modelling, University of Technology, Sydney, Australia
Prof. (Dr.) Veda C. Storey, Department of Computer Information Systems, Georgia State University, USA
Prof. (Dr.) Daniel Staegemann, Department of Technical and Business Information Systems (ITI), Otto-von-Guericke-University Magdeburg, Magdeburg, Germany
Prof. (Dr.) Aaron French, Kennesaw State University, Kennesaw, Georgia, United States
Dr. M V Reddy, Senior Professional Researcher at New graphite world Montreal, Canada
Dr. Alok Verma, Energy Research Institute, NTU, Singapore
Dr. Shalini Sharma, Institute of Information System and Applications, National Tsing Hua University, Hsinchu, Taiwan
Mr. Soumak Roy, VP & Global Practice Leader - Cyber security VP & Global Practice, SDG Corporation
Dr. Xiao-Zhi Gao, School of Computing, University of Eastern Finland, Finland
Dr. Geetika Jain, Assistant Professor & Program Director - MSc Business Analytics, Keele University, UK
Dr. Meenal Chaudhari, EnBiSyS Lab, North Carolina State University, North Carolina USA
Dr. Kirti Seth, INHA University, Uzbekistan
Dr. Nallapaneni Manoj Kumar, School of Energy and Environment, City University of Hong Kong, Kowloon, Hong Kong
Dr. Sanjeev Pannala, Washington State University, United States
Dr. Gaurav Sharma, Researcher, Université libre de Bruxelles, Brussels Region, Belgium
Dr. Adarsh Kumar Pandey, Associate Professor Sunway University Kuala Lumpur, Federal Territory of Kuala Lumpur, Malaysia
Mr. Davinder Singh, Snap Finance, Arizona, USA
Mr. Sajal Jain, Wireless Professional Solutions, New South Wales, Australia

Editors

Chief Editor
Prof. (Dr.) Vijayan Sugumaran
Distinguished Professor, School of Business Administration, Oakland University, USA

Associate Editors:
Prof. (Dr.) Divya Mishra
Professor and Head, Department of Computer Science & Engineering, ABES Engineering College, Ghaziabad, India
Ms. Shanu Sharma
Department of Computer Science & Engineering, ABES Engineering College, Ghaziabad, India

Section Editors:
Dr. Abhishek Kumar
Head, Department of Applied Mechanics, Motilal Nehru National Institute of Technology (MNNIT), Allahabad, Prayagraj, India

Dr. Ashutosh Mishra
Department of Applied Mechanics, Motilal Nehru National Institute of Technology (MNNIT), Allahabad, Prayagraj, India

Dr. Abhishek Kumar Tiwari
Department of Applied Mechanics, Motilal Nehru National Institute of Technology (MNNIT), Allahabad, Prayagraj, India

Dr. Ravindra Kannojiya
Department of Mechanical Engineering, Amity University, Uttar Pradesh, India

About the Editors

Prof. Vijayan Sugumaran is Distinguished Professor of Management Information Systems and Chair of the Decision and Information Sciences department at Oakland University. He is also Co-Director of the Center for Data Science and Big Data Analytics at Oakland University. He received his Ph.D. in Information Technology from George Mason University, Fairfax, Virginia, USA. Over the years he has taught courses at the Graduate and Undergraduate level in Object-Oriented Systems Development, C++, Java, Javascript, Database Management Systems and Data Warehouses, Advanced Databases and Big Data Management, Deep Learning and Text Analytics, Systems Analysis and Design, Electronic Commerce, and Introduction to MIS. His research interests are in the areas of Big Data Analytics, Business Intelligence, Ontologies and Semantic Web, Intelligent Agent and Multi-Agent Systems, Component Based Software Development, Knowledge-Based Systems, and Data & Information Modeling. He has published over 275 peer-reviewed articles in Journals, Conferences, and Books. He has edited twenty books. His recent publications have appeared in *Information Systems Research, ACM Transactions on Database Systems, IEEE Transactions on Engineering Management, IEEE Transactions on Big Data, IEEE Transactions on Education, IEEE software, Communications of the ACM, Healthcare Management*

Science, Data and Knowledge Engineering, The DATABASE for Advances in Information Systems, Information Systems Journal, and Journal of Information Systems and E-Business Management.

He is also the editor-in-chief of the *International Journal of Intelligent Information Technologies* and also serves on the editorial board of eight other journals. He was the Program Co-Chair for the International Conference on Applications of Natural Language to Information Systems (NLDB 2008, NLDB 2013, NLDB 2016, NLDB 2019, and NLDB 2023). He was also the Chair of Intelligent Information Systems track for the Information Resources Management Association International Conference (IRMA 2001, 2002, 2005 - 2007) and the Intelligent Agent and Multi-Agent Systems in Business mini-track for Americas Conference on Information Systems (AMCIS 1999 - 2023). He served as Program Co-Chair for the 14th Workshop on E-Business (WeB2015), 29th Australasian Conference on Information Systems (ACIS 2018), 14th Annual Conference of Midwest Association for Information Systems (MWAIS 2019), 5th IEEE International Conference on Big Data Service and Applications (BDS 2019), and 2022 Midwest Decision Sciences Institute Annual Conference (MWDSI 2022). He also served as Chair of the E-Commerce track for Decision Science Institute's Annual Conference, 2004. He was the Information Technology Coordinator for the Decision Sciences Institute from 2007 to 2010. He also regularly serves as a program committee member for numerous national and international conferences.

Dr. Divya Mishra is working as a full-time academician from last 14+ years. She has a PhD (Engineering) from Amity University Uttar Pradesh, MTech (Information Security) from Guru Gobind Singh Indraprastha University, New Delhi. She also holds B. Tech (Computer Science & Engineering) from Sant Longowal Institute of Engineering & Technology, IKJPTU, Punjab. She has published many research papers in reputed international journals and conferences with Scopus & SCI indexing. She was also appreciated by IEEE Sensors Council for the paper "Application of Non-Linear Gaussian Regression-Based Adaptive Clock Synchronization Technique for Wireless Sensor Network in Agriculture", IEEE Sensors Journal, Vol. 18, No. 10, May 2018, for paper being one of the 25 most downloaded Sensors Journal papers in the month of February 2019. She is an active member of International societies like IEEE, IAENG and an organizing committee for many international conferences, workshops, and seminars to enhance the teaching-learning process. She is also associated with a project on Cloud Computing Security funded by the International Bilateral Cooperation Division, Department of Science and Technology, MS&T, Govt. of India. She has guided more than 15 students of M.Tech. Her research area includes Networking, cloud computing, Information Security, IoT.

Ms. Shanu Sharma is an Assistant Professor in the Department of Computer Science & Engineering, ABES Engineering College, Ghaziabad (Affiliated to A.K.T University, Lucknow) as an Assistant Professor. She has12 years of teaching and research experience. Her research areas include Cognitive Computing, Computer Vision, Pattern Recognition, and Machine Learning. She has published and presented her work in various National and International Conferences and Journals and is currently associated with various reputed International Conferences and journals as a Reviewer. She is serving as a Guest Editor of a Special Issue on Intelligent Systems and Applications for the International Journal of Intelligent Information Technologies (IJIIT), IGI Global (Scopus Indexed). She is also editing a special issue on Intelligent Methods for Industrial Transformation towards Smart and Sustainable Society for the International Journal of Operations Research and Information Systems (IJORIS), IGI Global (Scopus Indexed). She is currently editing the book "Revolutionizing Industrial Automation Through the

Convergence of Artificial Intelligence and the Internet of Things", published by IGI Global. She is a senior member of IEEE and also an active member of other professional societies like ACM, Soft Computing Research Society (SCRS), EUSFLAT, and IAENG.

Dr. Abhishek Kumar is Head of the Department of Applied Mechanics at Motilal Nehru National Institute of Technology Allahabad, Prayagraj, Uttar Pradesh. He received his Ph.D. from the Indian Institute of Technology Roorkee, Roorkee, Uttarakhand. He has 18 years of teaching and research experience. Dr. Kumar has published more than 100 research articles in journals and conferences of repute; and supervised 5 Ph.D. and approximately 50 M.Tech. Theses. His current research interests include the Development of Coatings for Microwave Absorption, Severe Plastic Deformation, and Dispersed Polymers.

Dr. Ashutosh Mishra is a Life member of Indian Nuclear Society, Bhabha Atomic Research Centre, Mumbai. He won a prestigious DGFS Fellowship to pursue his PhD from units of Department of Atomic energy (DAE). He completed his M.Tech from IIT BHU (Varanasi) in 2009. He obtained his Doctorate Degree from Indira Gandhi Centre for Atomic Research, Kalpakkam. During his doctoral work, he was working with Reactor Design Group of IGCAR under the leadership of Dr. P. Chellapandi (former CMD BHAVINI and former member of the Technical Working Group on Fast Reactor in International Atomic Energy Agency, Vienna). His area of research is thermo-mechanical studies, structural mechanics, biomechanics and effect of radiation of metals and human tissues. He also worked in Clyde Pumps India Pvt Ltd as APPLICATION ENGINEER and handled several government projects to provide techno-commercial pumping solutions in power plants, refineries, etc. He has filed two Indian patents and authored 2 book chapters, 19 journal papers & conference papers. He has more than five years' experience in computational and experimental mechanics. Dr. Ashutosh Mishra is currently working as Assistant Professor in Motilal Nehru National Institute of Technology Allahabad since 2016. He has been a reviewer of several reputed journals such as: Latin American Journal of Solids and Structures, Journal of Materials Engineering and Performance. He is also serving as guest editor in Composites: Mechanics, Computations, Applications, Begell House, (Scopus, ESCI), Critical Reviews in Biomedical Engineering, Begell House, (Scopus).

Dr. Abhishek Kumar Tiwari received Ph.D. degree from the Department of Mechanical Engineering, IIT Ropar, in 2017 on Computer Modeling of Bone's Adaptation: The Role of Normal and Shear Strains, Fluid Shear, and Strain Gradients. Later on, his doctoral work also appeared in one of the leading newspaper The Telegraph with the title Bone Again. He also worked as an Assistant Professor with the Department of Mechanical Engineering, Manipal University, Jaipur, till 2018, and then joined Department of Applied Mechanics, Motilal Nehru National Institute of Technology (MNNIT) Allahabad, Prayagraj, Uttar Pradesh. His research group at MNNIT Allahabad is currently exploring mechanobiology involved in bone's adaptation, canalicular fluid dynamics within the bone, and design of orthopedic implants and instruments. His research interests include bone fracture healing, poromechanics, finite element simulations, and computational fluid dynamics. He has publications in peer-reviewed journals and conferences along with two patents in his name.

Dr. Ravindra Kannojiya is working as a full-time academician since last 8 years. He has a PhD in Mechanical Engineering from Delhi Technological University, Delhi, and M.Tech (Thermal Engineering) from National Institute of Technology, Silchar, Assam. He also holds B.Tech (Mechanical & Automation Engineering) from Govind Ballabh Pant Govt. Engineering College, GGSIPU, Delhi. He has published research papers in reputed international journals and conferences. He has also Published a patent for his research work. He has presented papers at various international conferences such as Confluence IEEE Conference, India in January 2018 and International Symposium on Fluids and Thermal Engineering India in July 2021. He is working in the area of Thermal engineering, Optimization algorithms, Energy management, and Intelligent systems.

Preface

AIR 2022 Conference Proceedings contain the peer-reviewed articles from the contributions presented during the International Conference on ***"Advancements in Interdisciplinary Research: AIR-2022"*** held online on ***May 6 - 7, 2022***. The AIR-2022 conference was organized by the ***Department of Applied Mechanics, Motilal Nehru National Institute of Technology Allahabad, Prayagraj, India***, in association with Nexance- The Next Generation Alliance for Scientific and Professional Advancements. It focused on fundamental and applied research to design, understand, and promote an environmentally sustainable and socially resilient society.

In today's era, automation and the development of intelligent systems have unlocked the potential for environmental safety and sustainable development. The development of these intelligent systems provides opportunities to resolve the challenges affecting our lives in adverse ways. This rapid progress of global urbanization, urban expansion, and increasing urban population density, also poses unprecedented challenges to the environment, energy/natural resources, and society. This book aims to discuss some of the important issues and their solutions for developing and managing a smart and sustainable society for everyone.

AIR-2022 was aimed to bring together researchers, academicians, scientists and experts from industry in a single platform to exchange their ideas for a sustainable future with sustainable development through interdisciplinary research approach. While sustainable development is needed for a significant impact on worldwide society, this interdisciplinary conference covered various engineering problems of different thrust areas. The areas covered in AIR-2022 were: *Innovative Engineering Solutions*, *Engineering Applications in Health care* and *Transformative Technologies*.

This book presents technological advancements in terms of machines and materials used, advancements in biomedical, energy, and fluid engineering for sustainable growth, and various transformative technologies. Some of these transformative technologies discussed in this book are security and privacy models for a secure society and industries, Intelligent methods, machine learning, deep learning-enabled applications, development of optimized networking infrastructure, optimized solutions, robotics, and computer vision. It also focuses on the latest trends, technological frameworks, and applications of computers in interdisciplinary engineering for solving real-life problems.

The topics covered and presented during AIR2022 represented a vast pool of research knowledge, resources, and expertise of the various research and technological communities from India and other countries like USA, UK, Canada, and South Korea. Such participation in AIR-2022 made a substantial contribution to the overall national development in the emerging field of energy, artificial intelligence, IoT applications in agriculture, and health care systems.

The topics covered and presented during Air2022 must have inspired the participants to take up the challenges in hot areas of engineering applications.

Prof. (Dr.) Vijayan Sugumaran

Chief Editor, AIR 2022 Proceedings

Message from the Organizing Secretaries

It is our great pleasure to present the proceedings of AIR-2022 to the participants of the conference. We hope that the contents of the proceedings will be able to open a challenging avenue of research towards the development of a "Smart and Sustainable Society".

The Department of Applied Mechanics organized conference AIR-2022, Motilal Nehru National Institute of Technology Allahabad, Prayagraj, with the theme of the conference as "**Smart and Sustainable Society**". The theme is anticipated to raise the awareness among the stakeholders regarding the sustainability issues with the technological development that is affecting the personal lives and society as a whole. Considering everything, through this conference, true and detailed insights of the sustainable technological developments in various disciplines were presented.

AIR-2022 is aimed to provide a platform for discussing the challenges, issues, and research findings in the interdisciplinary field of engineering. The main objective of holding this conference is to provide a single platform for researchers to discuss challenges, trends, technologies, and opportunities for the development of a smart and sustainable society from various domains such as bio-medical, computer science, mechanical, electronics, manufacturing, industrial, and management. The conference was a two-day virtual event dedicated to keynote addresses from experts, panel discussions, oral and poster presentations of innovations and research work. The themes of the research findings discussed at the conference are: Innovative Engineering Solutions, Emerging Technologies and Challenges towards Sustainable Healthcare Industry. The various Developments towards Robotics and Automation Engineering, Economic and Sustainable Smart Cities, Advancements in Agri-Food Industry, sustainability in Supply Chain Management covering broad topics from Solid Mechanics, Biomedical Engineering, Fluid Mechanics, Materials Science, and Engineering, Computer Science and Engineering, and other closely related fields with its focus towards developing a sustainable society.

The wide and active participation and the response for the call-for-papers were overwhelming. We received more than 250 submissions reflecting the growing interest in the interdisciplinary field of engineering. The conference concluded with the successful presentation of 126 research papers during AIR2022.

We would like to take this opportunity to express our sincere thanks to the keynote speakers, presenters, authors and River Publishers as our publication partner.

Dr. Ashutosh Mishra, MNNIT Allahabad, Prayagraj, India
Dr. Abhishek Kumar Tiwari, MNNIT Allahabad, Prayagraj, India

Organizing Secretaries
AIR 2022

Message from the Chairman

Dr. Abhishek Kumar, Head, Department of Applied Mechanics, MNNIT Allahabad, Prayagraj

I am honoured and sensing an immense pleasure to welcome all distinguished guests, keynote speakers, contributory authors, reviewers, session chairs, participants and all stakeholders to the International Conference on *Advancement in Interdisciplinary Research* (AIR-22) organized by the prestigious Motilal Nehru National Institute of Technology, Allahabad, at the holy city Prayagraj. This international conference focuses on the automation and development of smart systems for environmental safety and sustainability. Sustainable development requires the exploration of interdisciplinary research to their maximum potential. With the aim to develop a range of intelligent applications in various domains that can positively impact our surroundings, this international conference focuses on the current trends in interdisciplinary research, emphasizing a sustainable future in various domains. The thematic areas of the conference include *Innovative Engineering Solutions*, *Engineering Applications in Health care* and *Transformative Technologies*.

Successful organization of any event depends on the contribution of many people involved directly and indirectly in the organization of that event. It is my pleasure to acknowledge the efforts of the organizing committee, technical committee and all others who have worked tirelessly in this fruitful event organization. All members of the institute extended their full support in the successful organization of the conference.

The keynote speakers of the conference need special mention as they spared their valuable time to enlighten the young participants. The conference marked the presence of keynote speakers from countries such as South Korea, Canada and USA apart from reputed Indian scientists and academicians from IGCAR, IITs, ISRO etc. Their vast knowledge and experience will be highly motivating for our young participants. I express my thanks to *Nexance* for their support in the organization of the conference.

Dr. Abhishek Kumar
Conference Chairman, AIR 2022

Table of Contents

Section A
Mechanics and Materials

Section B
Energy and Fluid Engineering

Section C
Advancements in Biomedical Engineering for Sustainable Growth

SECTION D
Transformative Technologies enabled Development

Analysis of Variation in Mechanical Properties of Glass Fiber Reinforced Polymer Concrete

[1]Mukund Kaushik, [2]Prakhar Duggal, [3]Ravinder Kumar Tomar

Amity University Uttar Pradesh, India

[1]mukund.kaushik1@s.amity.edu, [2]pduggal@amity.edu, [3]rktomar@amity.edu

Abstract

Mixture of cement with a low strength to weight ratio tension and is prone to breaking and scaling, all of which are related to plastic, solidified states, and drying shrinkage. Worldwide a lot of exploration is presently being directed concerning the utilization of fiber overlays and sheets in the maintenance and fortifying of supported substantial individuals. Fiber-supported polymer (FRP) application is extremely compelling method for fixing and reinforce structures that have become fundamentally feeble over their life expectancy. FRP fix frameworks give a monetarily feasible option in contrast to conventional fix framework and materials. In this paper Experimental examinations done on the conduct of the substantial reinforced utilizing irregular hacked glass fiber are done with substantial blend of two unique length of glass fiber (6mm and 12mm) at different rate (0%,0.75%, 1.25% and 1.75%) amount of expansion by the complete load of cement. Trial information on load for pressure, pliable also bending examination has been completed; strength varieties and disappointment methods of every example were gotten.

Keywords. Synthetic Fiber, Waste material, Glass Fiber 6 mm, 12 mm

1. INTRODUCTION

Concrete made with cement is a type of construction element used for underlying components of the building such as pillars, parts, and chunks, among other things. A large number of structures built in the past that use extra highly experienced schedule guidelines through different parts of the world are primarily hazardous as per the new plan guidelines.

Composites of Fiber supported polymers have wind up being amazingly useful for reinforcing of RCC designs to withstand ordinary has well as seismic burdens. One of the challenges in reinforcing substantial designs is deciding on a protective approach for better the design's hardiness & performance while keeping in mind constraints like as buildability, construction works, and budget, adding glass fibre to a concrete mix increases the compressive as well as stiffness of the concrete.

Extra strength might be expected to consider higher burdens to be set on the design. This is frequently required when the fulfillment of the construction changes and a higher burden conveying limit is required. In today's environment, incredibly challenging and hard structural design structures are being developed establish as more amount of Glass Fiber is used in Concrete Mixture is drop the strength of compression and flexural behavior, GFRC

is having the high performance and it is environment friendly, GFRC having more service life in comparison to normal concrete but GFRC is costly.

The most important and widely used material is often concrete, and it is required to have very high strength and acceptable functioning features. Significant innovation is being made in this field to foster such cements with unique properties. Establishing as Flexural Strength, Strength properties and Tensile Splitting Strength are increasing in the different time duration. Specialists all around the world are endeavoring to foster elite execution cements by utilizing filaments and different admixtures in concrete up to specific extents. The different variation comes in Flexural Strength, Compressive Strength and in Split Tensile Strength when they use different size of Glass Fiber at different ratio and all have different Stress- Strain Curves.

Many practical have indicate as the cement mechanical properties can increment significantly (by in excess of a significant degree) with the expansion of strands exclusively. This section manages the insights about the survey of writing on examinations relating to glass fiber mechanical properties built up concrete presently numerous trial examinations are having been completed with the expansion of glass filaments of different kind, arrangement, and thickness.

2. GLASS FIBER

Glass fibre of varying lengths (6mm and 12mm) is used to obtain varying composite mix (Figure 1). The three different volumetric percentages of 0.75%, 1.25% and 1.75% glass fiber are used in concrete mixture. In this review, an experience made between plain concrete and high strength accomplished by substantial utilizing glass fiber of two lengths (6 &1 2mm) for M25 grade of cement. The test (pressure test, split elastic test and flexural strength test) is to be done on the substantial with the expansion of glass strands of different rates (0.25%, 0.50%, and 0.75%) to add up to weight of the substantial. Blend plan of M25 concrete is to be planned according to IS 10262:2009 and to discover the amounts of fixings.

Figure1. Glass Fiber (6mm and 12mm) [15]

3. CONCRETE MIXING, CASTING AND CURING

Concrete 28-day target strength was set to 31.2 MPa, with a large decline of 75–100 mm planned, according to the blend plan of Indian standard code (IS 10262, 2019). The totals for fine and coarse were in SSD condition. In significant composites, two different lengths

of glass fibre (6 mm, 12 mm) & three different volume fractions (0 percent, 0.75 percent, 1.25 percent, 1.75 percent) were used. The plain and composite cements used in this study's blend extents are described in detail. To perform compressive and elasticity tests, a 150 mm concrete cubic shape was produced. Steel molds with a smooth base plate were used to help set up these examples. To test for water penetration during loading, a thin film of form oil was applied to the combination surfaces between the areas of the shape & the base plate of the form. After the shape had been filled with concrete, standard bar was used to finish the temping. A smooth steel scoop was used to create a new significant surface. For 24 hours, the samples were held at a constant temperature. In the aftermath of being free of mold, the samples were smothered in fresh water for 14 and 28 days (Figure 2).

Figure 2. Curing Tank

4. EXPERIMENTAL TEST FOR COMPRESSION

Strength tests were led utilizing pressure testing machine a while later restoring. Pressure test is the appraisal of substantial limit against static burden. The trial of compressive strength was performed utilizing 6-inch (150-mm) 3D shapes by adhering to the rule of IS: 516. During the pressure test, the heap was applied progressively and extreme heap of each substantial example was noted (Figure 3).

Figure 3. Experimental test for compression

5. FIBRE-FORMING PROCESS

A Glass is a formless solid created by cooling rapidly of a liquefy (i.e., fluid stage) to prevent crystallisation (devitrification). Crystallization occur at liquid temperature, TL, where valuable stones & liquefy are in concord, or below, when the soften is gradually cooled. As a result, glass strands are obtained at high cooling speeds. Glass is formed from combining (co-liquefying) silica alongside minerals that contain the oxides needed to make a particular creation. By a process known as fiberization, the liquid mass is rapidly chilled to prevent crystallisation & moulded into glass strands. Almost all consistent glass filaments are manufactured using an immediate draw method & moulded by expelling liquid glass through a platinum composite bushing with thousands of individual apertures ranging in width from 0.793 to 3.175 mm (0.0312 to 0.125 in.).

6. BATCH MIXING AND MELTING

Gauging and mixing of unprocessed components are the first steps in the glass dissolving process. This connection is highly mechanised in today's fiberglass facilities, with automated gauging units and encased material vehicle frameworks. The individual pieces are weighed & transported to a mixing station, where the clump fixings are thoroughly mixed before being transferred to the heater. Fiber-glass heaters are often divided into three distinct components. The cluster is transported into the heater segment for softening, vaporisation, and homogenization. The liquid glass then flows into the purifier portion, where the temperature of the glass is lowered from 1370 degrees Celsius (2500 degrees Fahrenheit) to roughly 1260 degrees Celsius (2300 F). The liquid glass then travels straight over the fiber-shaping stations to the fore hearth segment. The consistency features of the individual glass support the temperatures throughout this contact. Furthermore, the heater's actual design is subject to modification (Figure 4).

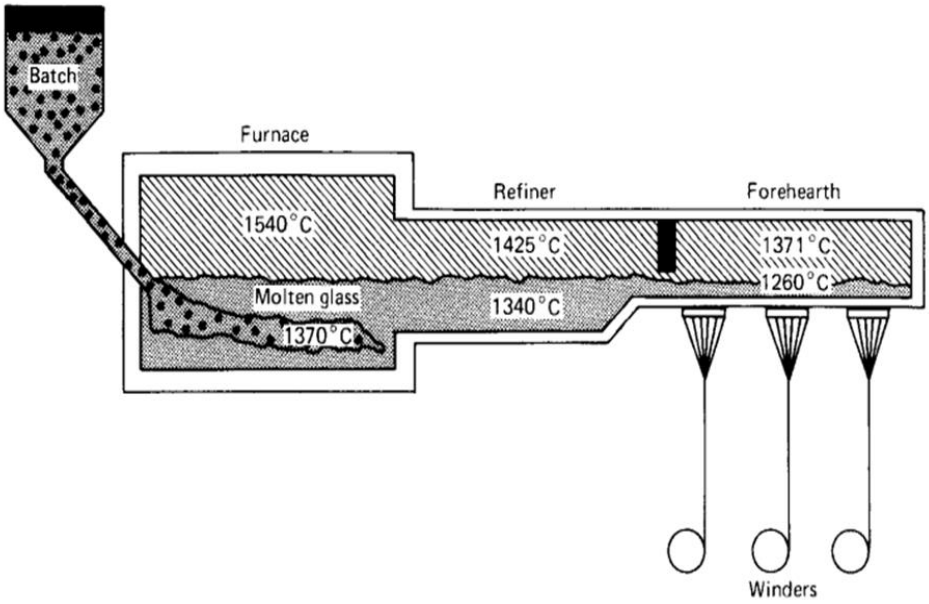

Figure 4. The making of glass fiber [8]

7. SPECIAL PURPOSE PRODUCTS

Glass fibre is used in the construction of basic composites, printed circuit sheets, & a variety of other special-purpose materials. When the nonstop glass strands are finished, they should be transformed into an item structure that is suitable for their intended composite application. The major completed specific reason items are as per the following Fiberglass meandering, Woven wandering, Fiberglass mats, Combinations of a mat and woven meandering, chopped strand items, Milled filaments, Fiberglass paper, Textile yarns, Fiberglass Fabric, Texturized Yarn, Carded Glass Fibers.

8. MIXED DESIGN

Various parameters of the design are listed in Table 1, Table 2 and Table 3. Furthermore various results obtained during compressive strength test are presented in Figure 5, Figure 6 and Figure 7 for different designs.

Table 1: Mix Design of 6mm Glass Fiber

Specimen	Glass Fiber 6 mm(%)	Quantity(kg/m^3)				
		Cement	Glass fiber(6mm)	Water	Coarse Aggregate	Fine Aggregate
M25	0%	448.6	0	197.4	1145.76	677.16
M25+0.75%GF(6mm)	0.75%	448.6	3.285	197.4	1145.76	677.16
M30+1.25%GF(6mm)	1.25%	448.6	5.475	197.4	1145.76	677.16
M30+1.75%GF(6mm)	1.75%	448.6	7.665	197.4	1145.76	677.16

Table 2: Mix Design of 12mm Glass Fiber

Specimen	Glass fiber 12mm(%)	Quantity (kg/m^3)				
		Cement	Glass fiber (12mm)	Water	Coarse Aggregate	Fine Aggregate
M25	0%	448.6	0	197.4	1145.76	677.16
M25+0.75%GF(12mm)	0.75%	448.6	3.285	197.4	1145.76	677.16
M25+12.5%GF(12mm)	1.25%	448.6	5.475	197.4	1145.76	677.16
M25+1.75%GF(12mm)	1.75%	448.6	7.665	197.4	1145.76	677.16

Table 3: Compressive-Strength Test

Specimen	**"Compressive- strength in 7 Days (N/mm^2)"**	**"Compressive-strength in 14 Days (N/mm^2)"**	**"Compressive-strength in 28 Days (N/mm^2)"**
M25	17.12	25.82	29.07
M25+0.75%GF(6mm)	21.02	27.64	31.23
M25+1.25%GF(6mm)	22.18	32.16	34.72
M25+1.75%GF(6mm)	24.37	33.48	36.53
M25+0.75%GF(12mm)	20.58	28.15	30.42
M25+1.25%GF(12mm)	21.18	29.26	31.95
M25+1.75%GF(12mm)	22.13	30.05	32.85

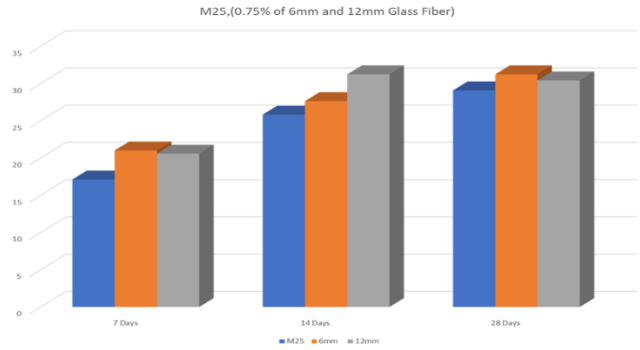

Figure 5: Compressive strength test for dosage 0.75% Glass Fiber

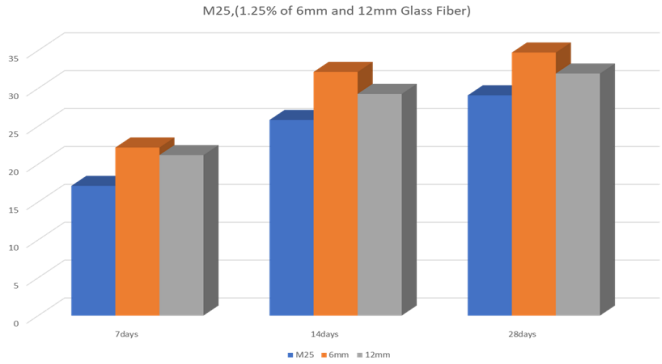

Figure 6: Compressive strength test for dosage1.25% Glass Fiber

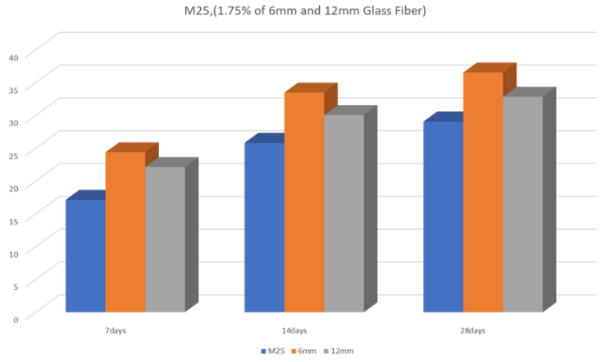

Figure 7: Compressive strength test for dosage 1.75% Glass Fiber

9. DISCUSSIONS

From these results it's clear that high early strength of glass fiber reinforced composite is significantly higher than that of conventional concrete mix regardless of its rate of dosage and its change in size. Other important parameters of significance like higher strength of 6mm based fiber reinforced composite can be explained by understanding basic behavior of matrix (Table 1), that it provides a more homogenous distribution in comparison to that of 12 mm-based composites (Table 2).

12 mm-based composites also acted as a crack bridging secondary reinforcement but its comparatively larger size influenced its homogeneity in comparison to 6 mm alternative, its slump was also significantly smaller, other minor changes also influence its performance. Other possible explanation could be agglomeration of fibers at a single point in composite which can stop proper distribution (Table 3).

A suggestion to properly distribute these fibers would be addition of something like a moderate water reducing admixture because according to technical data sheets and research it's shown that for fiber content beyond 3 kg/m^3 requires moderate water reducing admixtures, this trend follows till the dosage rate of 40 kg/m^3. For dosage rate beyond this value dedicated water reducing admixture should be added.

10. RESULTS

- The Tests on the substantial with and glass strands showed extensive upgrades in properties over the series of expansion of filaments.
- Compressive strength results from change in fiber concentration for a period of 7,14 and 28 days is calculated, and their overall mix consistency, workability and fiber pullout response are observed, which in general shows that the workability decreases with dosage rate and crack bridging effect allows for better mechanical properties than traditional concrete.
- From these results sssss clear that high early strength of glass fiber reinforced composite is significantly higher than that of conventional concrete mix regardless of its rate of dosage and its change in size. Other important parameters of significance like higher strength of 6mm based fiber reinforced composite can be explained by understanding basic behavior of matrix, that it provides a more homogenous distribution in comparison to that of 12 mm-based composites.
- 12 mm-based composites also acted as a crack bridging secondary reinforcement but its comparatively larger size influenced its homogeneity in comparison to 6 mm alternative, its slump was also significantly smaller, other minor changes also influence its performance. Other possible explanation could be agglomeration of fibers at a single point in composite which can stop proper distribution.
- A suggestion to properly distribute these fibers would be addition of something like a moderate water reducing admixture because according to technical data sheets and research its shown that for fiber content beyond 3 kg/m3 requires moderate water reducing admixtures, this trend follows till the dosage rate of 40 kg/m3. For

dosage rate beyond this value a dedicated water reducing admixture should be added.

- From the observed data it can be seen, that for a dosage rate of 0.75%, compressive strength of 6mm glass fiber and 12 mm glass fiber increases by 7.43% and 4.64%. Similarly for the dosage rate of 1.25%, compressive strength of 6mm and 12mm glass fibers increases by 19.43% and 9.91% respectively in comparison to traditional concrete for a time interval of 28 days.

- Lastly for a dosage rate of 1.75%, compressive strength of 6mm and 12mm glass fiber increases by 25.66% and 13.01% respectively in comparison to traditional concrete for a time interval of 28 days.

11. CONCLUSION

The results of using glass fiber with varied cut lengths (6 mm, 12 mm) and varying mix proportions (0.75 percent, 1.25 percent, & 1.75 percent) on concrete compression are presented in this study. The following is a recapitulation of the outcome:

- The most efficient proportion of concrete with glass fiber incorporation was noticed at 1.75% of 6mm size-based glass fiber in which the maximum compressive strength obtained at 28 days was 36.53 N/mm2 for M25 design mix.
- A suggestion to properly distribute these fibers would be addition of something like a moderate water reducing admixture because according to technical data sheets and research its shown that for fiber content beyond 3 kg/m3 requires moderate water reducing admixtures, this trend follows till the dosage rate of 40 kg/m3. For dosage rate beyond this value a dedicated water reducing admixture should be added.
- For dosage rate of 0.75%, compressive strength of 6mm glass fiber and 12 mm glass fiber increases by 22.78% and 20.21%. Similarly for 1.25%, compressive strength of 6mm and 12mm glass fibers increases by 29.55% and 23.7% respectively in comparison to traditional concrete for a time interval of 7 days.
- For a dosage rate of 1.75%, compressive strength of 6mm and 12mm glass fiber increases by 43.18% and 29.26% respectively in comparison to traditional concrete for a time interval of 7 days.
- The Tests on the substantial with and glass strands showed extensive upgrades in properties over the series of expansion of filaments.
- For dosage rate of 0.75%, compressive strength of 6mm glass fiber and 12 mm glass fiber increases by 7.04% and 9.02%. Similarly for 1.25%, compressive strength of 6mm and 12mm glass fibers increases by 24.55% and 13.32% respectively in comparison to traditional concrete for a time interval of 14 days.
- For a dosage rate of 1.75%, compressive strength of 6mm and 12mm glass fiber increases by 29.66% and 16.38% respectively in comparison to traditional concrete for a time interval of 14 days.
- Moreover, optimum incorporation of glass fiber can effectively improve the concrete mechanical properties which may prolong the life of concrete structure.

REFERENCES

[1] S. Das Gupta, M. S. Aftab, H. Mohammod Zakaria, and C. Karmakar, "Scope of Improving Mechanical Characteristics of Concrete using natural Fiber as a Reinforcing Material", Malaysian Journal of Civil Engineering, vol. 32, no. 2, Jul. 2020, doi: 10.11113/mjce.v32.16204.

[2] H. Gholizadeh and S. Dilmaghani, "The Study of Mechanical Properties of High Strength Concrete Containing Steel and Polypropylene Fibers," Civil Engineering Journal, vol. 4, no. 1, p. 221, Feb. 2018, doi: 10.28991/cej-030981.

[3] S. Kamkar and Ö. Eren, "Evaluation of maturity method for steel fiber reinforced concrete," KSCE Journal of Civil Engineering, vol. 22, no. 1, pp. 213–221, Apr. 2017, doi: 10.1007/s12205-017-1761-9.

[4] X. Zhou, H. Saini, and G. Kastiukas, "Engineering Properties of Treated Natural Hemp Fiber-Reinforced Concrete," Frontiers in Built Environment, vol. 3, Jun. 2017, doi: 10.3389/fbuil.2017.00033.

[5] A. Sedaghatdoost and M. Amini, "Mechanical Properties of Polyolefin Fiber-Reinforced Light Weight Concrete," Civil Engineering Journal, vol. 3, no. 9, pp. 759–765, Oct. 2017, doi: 10.21859/cej-030912.

[6] M. Madhuri, J. K. Chandra, B.B. Balakrishna, Comparison of Performance of Non Metallic Fibre Reinforced Concrete and Plain Cement Concrete, IJRET, Vol 4(7), 2017

[7] J.-S. Kim, C.-G. Cho, H.-J. Moon, H. Kim, S.-J. Lee, and W.-J. Kim, "Experiments on Tensile and Shear Characteristics of Amorphous Micro Steel (AMS) Fibre-Reinforced Cementitious Composites," International Journal of Concrete Structures and Materials, vol. 11, no. 4, pp. 647–655, Dec. 2017, doi: 10.1007/s40069-017-0214-7.

[8] J. Dayalan, Study on Strength Characteristics of Glass Fiber Reinforced High Performance-Concrete, IJRET, Vol 4 (2), 2017.

[9] G. M. Sadiqul Islam and S. D. Gupta, "Evaluating plastic shrinkage and permeability of polypropylene fiber reinforced concrete," International Journal of Sustainable Built Environment, vol. 5, no. 2, pp. 345–354, Dec. 2016, doi: 10.1016/j.ijsbe.2016.05.007.

[10] Y.K. Sabapathy, Y.K. Anandan, P. Vaidyanath, P. Baskar, "Strength properties of coated E-glass fibres in concrete," Journal of the Croatian Association of Civil Engineers, vol. 68, no. 09, pp. 697–703, Oct. 2016, doi: 10.14256/jce.1335.2015.

[11] W. Li, Z. Huang, X. C. Wang, and J. P. Zhang, "Study on Tension and Compression Ratio and Discount Ratio of Rubber Modified Silica Fume Concrete," Applied Mechanics and Materials, vol. 670–671, pp. 396–400, Oct. 2014, doi: 10.4028/www.scientific.net/amm.670-671.396.

[12] V. S. Vairagade and K. S. Kene, "Strength of Normal Concrete Using Metallic and Synthetic Fibers," Procedia Engineering, vol. 51, pp. 132–140, 2013, doi: 10.1016/j.proeng.2013.01.020.

[13] K. Chawla, B. Tekwari, Glass fibre Reinforced concrete, IJSCER, Vol 2(3), 2013.

[14] S. Kakooei, H. M. Akil, M. Jamshidi, and J. Rouhi, "The effects of polypropylene fibers on the properties of reinforced concrete structures," Construction and Building Materials, vol. 27, no. 1, pp. 73–77, Feb. 2012, doi: 10.1016/j.conbuildmat.2011.08.015.

[15] S. Guzlena and G. Sakale, “Alkali Resistant (AR) Glass Fibre Influence on Glass Fibre Reinforced Concrete (GRC) Flexural Properties,” RILEM Bookseries, pp. 262–269, Nov. 2020, doi: 10.1007/978-3-030-58482-5_24.

[16] J. Zhao, J. Liang, L. Chu, and F. Shen, “Experimental Study on Shear Behavior of Steel Fiber Reinforced Concrete Beams with High-Strength Reinforcement,” Materials, vol. 11, no. 9, p. 1682, Sep. 2018, doi: 10.3390/ma11091682.

Biographies

Mukund Kaushik received the bachelor's degree in civil engineering from Hindustan College of science and Technology in 2020, the master's degree in Structural engineering from Amity University in 2022. His research areas include green building, supplementary cementitious materials, GFRP Design and Sisal Fiber.

Mr. Prakhar Duggal is a Civil Engineer with vast industry and academic experience. He graduatedin Civil Engineering from Pune University in 2011 and obtained his master’s in Structural Engineering from RTU, Kota in 2013. Subsequently, he is pursuing his doctorate from Amity School of Engineering and Technology, Noida. He has 4 years of industry experience during as a structural engineering consultant for different projectsrelated to building construction. He has worked for more than 08 years in academia in various capacities as Academic Chair, Center Superintendent and Program Leader of the Department.His holds expertise in the area of solar energy and built environment, Building Materials. His research work focuses on application of artificial intelligence for estimation of solar radiation in buildings.

Dr. R.K. Tomar is a Civil Engineer with vast industry and academic experience. He graduatedin Civil Engineering from Pune University in 1990 and obtained his master’s in environmental engineering from Delhi College of Engineering, Delhi in 2006.Subsequently, he completed his doctorate from Indian Institute of Technology, Delhi (IITD) in 2015. He has 8 years of industry experience during which he has extensively worked in the field for different projectsrelated to canal, railways and building construction. He has worked for more than 23 years in academia in various capacities as Academic Chair, Center Superintendent and Head of the Department. He holds expertise in the area of solar energy and built environment. His research work focuses on application of artificial intelligence for estimation of solar radiation in buildings.

An Experimental Study on the Mechanical Properties of Partial Nonreactive Silicate based Sugarcane Bagasse ash and Rice husk ash, along with their Polyolefin and Polyester Fiber based Secondary Reinforcement

[1]Abhishek Nautiyal, [2]Prakhar Duggal, [3]Ravinder Kumar Tomar

Amity University Uttar Pradesh, India

[1]abhishek.nautiyal@s.amity.edu, [2]pduggal@amity.edu, [3]rktomar@amity.edu

Abstract

Supplementary Cementitious Materials, or otherwise known as SCMs are among one of the brightest prospects for substitution of cement in concrete. Addition of these substances enhances efficiency for the mechanical properties in concrete as well as a number of other advantages like reduction in cost and an all-inclusive reduction of carbon emission content. This study provides a detailed overview on some of most abundant SCMs with focus being on use of their less reactive versions that are obtained at higher temperatures, their optimum quantity and proper production process; other than these factors, focus is also shown on providing adequate data on different types of synthetic fibers like polyolefin and polyester fiber for proper understanding, and using their combination as an additive. Consequently, one of the main goals of this study is to create a fiber reinforced composite from discarded less reactive version of sugarcane bagasse ash (SCBA) & rice husk ash (RHA), which are obtained from local jaggery plant and biomass gasifier respectively. Data from technical data sheet is also discussed in the methodology for understanding market and alternatives. A thorough review of literature has also been compiled.

Keywords. supplementary cementitious materials, polyolefin fiber, polyester fiber, rice husk ash, sugarcane bagasse-ash

1. INTRODUCTION

Effects of increasing global warmth have been seen for several decades, the global ocean and land temperature during January 2021 was 0.80 °C above 20th century average, making it the 7th warmest January in 142 years, according to overall global statistics. If that's not enough, considering: 2021 has a 99 percent chance of being among the 10 warmest years on record, with prediction of increased temperature expected in coming years, is a cause for worry.

The worldwide push regarding economic based expansion & infrastructure development puts a considerable strain on the planet's resources, resulting in worrying global warming & carbon emissions. According to Statista data, global cement production needed to fuel the desire for infrastructure development in 2019 was around 4 billion ton, resulting in a terrible 3.5 billion ton of CO^2. Environmental contamination & deterioration, as well as the resource exhaustion of earth during raw material mining, are further concerns related with cement

manufacture. Substituting supplemental cementitious materials (SCMs), also known as pozzolanas, for cement clinker is one of the viable ways for reducing these disadvantages. RHA & SCBA are among most promising SCMs.

Properties of these materials can further be enhanced through treatment, the fineness/specific surface-based area and specific gravity of the treated bagasse ash is more than the untreated-bagasse ash. Strength activity index of the treated SCBA is much higher and loss on ignition is also less [3]. Some of the other factors for their proper use include proper silica concentration and dry density, When SCBA was burned at temperatures ranging from 400 C to 800 C, the chemical compositions and colour changed, and the silica concentration rose from 25.32 to 86.98 percent [15]. When moisture content percentage for bagasse ash is zero, a dry density of 1.06g/cm3 was obtained, and an increase in water content up to 24%, resulted in a maximum dry density of 1.15g/cm3, followed by a reduction in dry density [1].

The fineness/specific surface area & specific gravity of BA is more than the RHA. The higher content of silica in RHA helps in formation of more hydration products. Strength activity index of the RHA is much superior than the BA. Hence RHA is a better pozzolan than BA [4]. However, failure to use them as a constituent material can also be due to lack of proper bonding, absence of adequate bonding between SCBA and RHA particles and the cement-based paste, as well as the non-uniform distribution of SCBA and RHA particles in concrete, might result in non-homogeneous samples, leading in a loss in concrete strength. [8].

Synthetic fibers performances are heavily dependent on temperature and rate of dosage, Up to 150 °C, the structural behaviour and fracture energy of PFRC specimens remained unchanged, according to this study. Some qualities degraded between 150 and 200 degrees Celsius, and at 200 degrees Celsius, a large fraction of the fibres was molten. Damage occurred mostly in the concrete matrix of fibre reinforced concrete specimens exposed to 150 °C, Compressive strength, static modulus of elasticity, and ultrasonic pulse velocity all suffer as a result. The absence of any structural capacity was observed in specimens exposed to 200 °C, yet the specimens did not break or show signs of brittle failure [9].

After the beginning of cracking, the energy absorbed by the fibre deformation generated a significant rise in fracture energy in each examined material. This characteristic revealed the ductile behavior of polyolefin fiber-reinforced concrete. At the limit of proportionality, specimens with a smaller fracture surface exhibited higher strength values. Because the concrete matrix governs the limit of proportionality, this value is consistent with the standard size effect idea for plain concrete [10]. According to Pawaskar et al (2020), Compressive strength, flexural strength, & split tensile strength are shown to be highest at 0.50 percent fibre addition and decrease when the proportion of fibre added exceeds 0.50 percent [12].

Agricultural or industrial wastes with latent hydraulic reactivity that can be activated are commonly used as SCM. Among these, SCBA (sugarcane bagasse ash) has been studied extensively as potential SCM. Along with SCBA several additional types of (SCMs) include options like natural pozzolans, silica fume, fly ash, GGBS, MSW ash, rice husk ash, calcined natural SCMs, calcareous fly ash, activated cooper tailings, wood ash, calcined clays, Biomass ash, Bauxite residue, waste glass etc.

2. RICE HUSK ASH (RHA)

Rice (Oryza glaberrima) is among world's most important staple-based food crop consumed by more over half of the world's population; annual based production of this grain is about [742,541,804 tonnes]. Rice mills, converts the paddy plant into 78 percent rice, 20percent rice husk, and 2% is wasted during the process. During this process, 20 to 25% of the rice husk will hence be converted to Rice husk ash. RHA are generally less than 45µm & average size of particle is in range 6-10µm. Whereas Rice husks main constituents are 50% cellulose, 25-30% lignin, 15-20% silica and a total moisture of about 10-15percent.Bulk density of rice husk is fairly low & lies in reach of 90-150 kg/m3. Rice husk has a calorific value of roughly 15 MJ/kg, and under regulated burning circumstances, the volatile organic content in the rice husk, such as cellulose and lignin, is eliminated, leaving amorphous silica with a microporous cellular structure as the residual ash. However, several factors must be controlled in order to obtain proper ash, one of which is the temperature and conditions under which rice husk-based ash is scorched, for example, ash obtained from uncontrolled combustion, such as open field burning or industrial furnaces at temperatures greater than 700-800°C, will contain significant amounts of non-reactive silica minerals cristobalite and tridymite.

Reactive/amorphous silica (Si02) content, as well as, other pozzolanic oxides (alumina (A1203) & (Fe203) ferrite, are the primary qualifications of any SCM.As a result, many SCM standards concentrate upon establishing a minimum oxide requirement. ASTM C618, for example, needs pozzolanic oxides (Si02 + A1203 + Fe203) to be larger than 70percent, BS EN 197-1 must have a minimum of 25% S102, and IS 3812-1 must have a minimum 35percent Si02 and 70% pozzolanic oxides. As furnace temperature for obtaining RHA from rice husk is increased, the structure goes towards becoming more crystalline in nature, and naturally the surface keeps on decreasing with increase in temperature or hold time of rise husk within favoured equipment. At a temperature of 500-600 structure nature is non-crystalline, 700-800 gives partially crystalline and above 800 results in crystalline structure. Mean diameters for pores in the microscopic structure of RHA is loftiest when they are scorched at temperatures between 600-700°C, therefore e pozzolanic activities of formed ash is highest at this temperature. When we take variations of particle size with grinding time into account, then with increased grinding time particle size reduces and more importantly BET nitrogen adsorption increases with grinding time (Table 1).

Table 1. Average chemical composition data of RHA & Portland limestone cement [19]

S/N	Chemical Components	Portland Limestone Cement %	RHA (%)
1	Silica Oxide (SiO_2)	19.16	88.29
2	Sodium Oxide (NaO_2)	0.40	0.10
3	Potassium Oxide (K_2O)	0.35	2.90
4	Calcium Oxide (CaO)	64.25	0.63
5	Magnesium Oxide (MgO)	2.17	0.46
6	Aluminium Oxide (Al_2O_3)	4.92	0.44
7	Iron Oxide (Fe_2O_3)	0.75	0.65
8	Sulphur Oxide (SO_2)	1.02	0.00
9	Loss on Ignition (LOI)	0.05	5.35

3. SUGARCANE BAGASSE ASH

Sugarcane (SC) is a term used to describe tall perennial grasses from the Saccharum officinarum and its hybrids that have a fibrous stalk rich in sucrose that accumulates in the stems and are used as a staple material in the ethanol and sugar industries. The sugarcane bagasse is a by-product of the extraction of juices from the sugarcane stalk (SCB). Bagasse is a fibrous lignocellulose waste with a high bioconversion efficiency, making it a cost-effective fuel for cogeneration facilities in industry.

After the energy is generated, the SCBA is the last waste. If all sugarcane in the world is processed to extract juice for the ethanol and sugar sectors, 420 to 630 million metric tonnes bagasse are produced each year. This is caused due to the fact that bagasse has been estimated to make up 20 to 30percent of the sugarcane stalk. Similarly, based on a 5% weight of bagasse, yearly global SCBA production is estimated to be between 21 and 31.5 million metric tonnes.

To create additional hydration products, pozzolanic oxides must interact with portlandite from cement hydration. Natural SCBA from the sugarcane sector, on the other hand, frequently requires processing or activation to become sufficiently reactive.

Delignification or in other words chemical treatment, exposes inner cellulose microfibrils for easy oxidation. Commonly chemical based activator includes alkali & acid with dilute acid, which are an economic efficient option. On other hand chemical addition involves addition of minerals like nano silica & limestone which can increase cement hydration rates, creating more portlandite for pozzolanic based consumption.

Treated SCBA is finer in nature than untreated type with an approximate 40 % reduction in size. Treatment do not increase the SAI (strength activity index) performance of SCBA. However chemical addition can improve SAI for example, nano silica improves SAI performance, microstructure based chemical adsorption, chloride ion migration, mercury intrusion, electrical resistivity of a mix containing SCBA especially at higher rate of substitution like 25 % substitution of SCBA.

600°C is the optimum calcination temperature as strength activity index is maximum at that temperature. Recalcination process will further increase SAI by at least additional 10% and can restrict loss on ignition to an average of 2.1 % loss, this is possible because of reduction in detrimental carbon content.

4. POLYOELIFIN FIBER (ECMAS EXF 54- HYBRID SYNTHETIC STRUCTURAL FIBER)

The synthetic-structural fibre was created to increase the durability & mechanical properties of concrete. EXF 54 is a hybrid fibre, meaning it is composed of a non-fibrillated monofilament having a specific mix of Polyolephinic polymers and a fibrillated Polypropylene fibre capable of reducing, if not fully eliminating, plastic shrinkage. It increases concrete flex fatigue, ductility, fatigue resistance, and durability. Unlike metal fibres, these fibres are non-corrosive, non-magnetic, and acid and alkali proof (Table 2).

Table 2. Technical properties of polyolefin fiber [18]

Material	Mix of fibers of a Polyolephin (Polyethylene Co-Polymer) and a fibrillated Polypropylene fiber)
Length	54 mm
Specific Weight	0.91 kg/dm3
Length/Diameter ratio	113
Equivalent diameter	0.48 mm
Chemical Resistance	Total Resistance to acids, bases and salts
Tensile Strength	620 – 758 MPa
Conformity	ASTM C-1116

It reduces floor thickness & eliminates the requirement for electro-welded mesh and metal fibres. It increases concrete's residual tensile strength, and therefore its ultimate strength and resistance to stress induced by dynamic and static overloads, by efficiently controlling temperature/plastic shrinkage fractures.

Fibers should be hurl directly to the mixer at the prefabrication or concrete mixing plant, or to the mixer truck. Fill the conveyor belt with fibres, inert materials, cement, sand, and the first piece of gravel. Fibers should not be introduced at first. Dry mix for at least 5 minutes on high speed before adding water.

In event of fire, polyolefin fibre deteriorates, as do all synthetic fibres once they reach their melting point. When compared to metal fibres, when they reach melting point during a fire, the fibres disintegrate without emitting toxic fumes, transforming the space they previously filled in cement mixes into a system of linked "channels." When water in gaps suddenly boils, these channels act as "escape routes" for the heat and steam produced. This characteristic prevents fibre reinforced concrete from bursting violently, as steel fibre reinforced concrete or unreinforced concrete would. Concrete density of at least 1.5 kg/m3 is required (to be assessed on basis of the application parameters) (Table 3).

Table 3. Properties for different types of polypropylene fibers [14]

Fiber Type	Density (kg/cm3)	Diameter (mm)	Tensile Strength (Mpa)	Modulus of elasticity (GPa)`	Specific Surface (m2/Kg)	Length (mm)
Fibrillated	0.95	0.20-0.30	500-750	5.00-10.00	58	19-40
Microfilament	0.91	0.05-0.20	330-414	3.70-5.50	225	12-20
Monofilament	0.9	0.30-0.35	547-658	3.50-7.50	91	30-50

Polyolefin fibres, often known as PP fibres, offer good mechanical characteristics in general, with their modulus of elasticity being particularly noteworthy. The naturally occurring modulus value is 9 GPa, with some rising as high as 15–20 GPa, which is way greater than 2–3 GPa provided by certain other plastics. Polyolefin fibres have a tensile strength of around 400 MPa. These remarkable properties were attained by the bicomponent manufacturing of two polymers: a high modulus core and a low modulus sheath.

In terms of a fibre form, the optimum macro synthetic fibre-based geometry involves fully using matrix anchoring without breaking the fibres and attaining maximum pullout resistance. The crimped synthetic structural fibres exhibited the best bonding out of all the deformed synthetic structural fibres tested.

5. POYSTER FIBER (RECRON 3S)

They are microfibers with a peculiar "triangular" cross section that are utilized in secondary concrete reinforcement. It works in tandem with structural steel to improve concrete's resistance to shrinkage cracking and improve mechanical qualities such as flexural/split tensile and transverse strengths, as well as abrasion and impact resistance. They operate as a pumping assist in making concrete more homogeneous by inhibiting the growth of cracks, bridging tiny fissures, and providing stability to the concrete. Reduces the absorption of surface water and the permeability of concrete (Table 4).

Table 4. Properties of Recron fiber [16]

S/N	Units	POLYESTER	POLYPROPYLENE	Properties	Remarks
1		Triangular	Triangular	Shape	
2	mm	3/ 4.8/6/12/18/24	3/ 4.8/6/12/18/24	Cut Length	+/- 1mm, Project specific customized lengths can be produced on request
3	Deg C	250-265	160-165	Melting Point	
4		1.34-1.39	0.90-0.91	Specific Gravity	
5	25-40	microns	20-40	Effective Diameter	
6	Gpd	4-6*	4-6*	Tensile Strength	*Estimated tensile strength in Mpa 4-6 *Polyester 480-730, *Polypropylene 320-490
7	%	20-60	60-90	Elongation	Initial Modulus
8	Mpa	>5000	>4000	Young's Modulus	Tests done as per AC
9		Very Good	Very Good	Alkaline Stability	32 standards

Recron 3S Fibers are manufactured from a ISO 9001:2000 facility and are intended for use as secondary reinforcement in concrete at dosage rates ranging from 0.1 to 0.4 percent by volume (0.9 kgs/Cu. M to 3.60 kgs/Cu. M). ASTM (C 1116), Type (111) Fiber Reinforced Concrete requirements are met by the fibres.

These fibres are produced by polymerizing raw ingredients such as Pure-Terephthalic Acid (PTA) & Mono-Ethylene Glycol (MEG) with catalysts, which results in finished polyester yarn via a continuous extrusion process. After that, the finished yarn is automatically cut to

the necessary length and wrapped in pouches. Quality assurance on raw materials & production processes done by ISO 9001:2000 standards.

6. FIBER PULL-OUT RESPONSE

Irrespective of type of fiber used, reinforcement is only successful in concrete when tensile strength of fiber is two to three times higher than that of concrete, when modulus of elasticity of fiber is way higher than conventional concrete & fiber-matrix based strength of bonding is of same order magnitude for tensile strength of the matrix. Crack opening is controlled in an ideal circumstance by fibre bridging, which contains a segment of fibre on either side of the crack with sufficient embedded length to prevent slippage (Figure 1).

Conversely, if fibers slip during the opening process, de-bonding may occur, and the fiber may be pulled out. It's possible that friction shear forces will produce matrix fracture if one fiber is mobilized. In order to identify which of the two situations might emerge, the critical length (lc, the length at which the fiber's tensile strength can be utilized without drawing it out of the matrix) of fibres is the deciding factor. Chemical adhesion & frictional bond one on internal part and other at end of crack is the ideal situation.

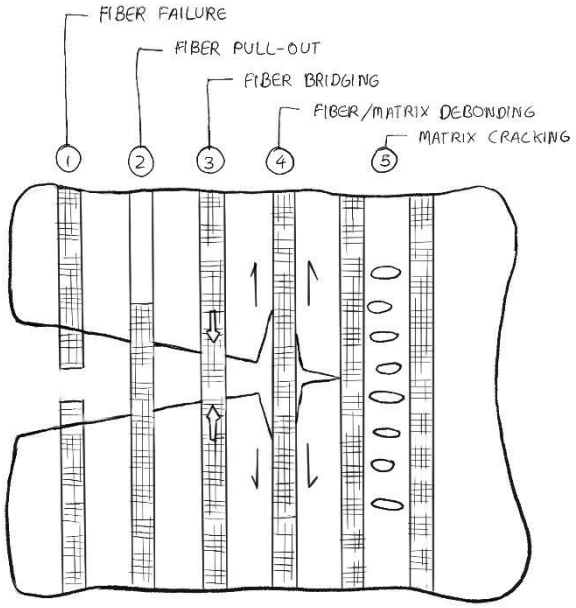

Figure 1. Fiber matrix mechanisms

7. MIX DESIGN

Various parameters of the design are listed in Table 5 and Table 6.

Table 5. Mix Design of Sugarcane Bagasse Ash [20]

Specimen	SCBA (%)	Quantity (kg/m^3)					
		Cement	SCBA	Polyolefin fiber +Polyester fiber (additive)	Water	Coarse Aggregate	Fine Aggregate
M30	0%	426	0	1.5+0.9	192	1186	701
M30+10%SCBA	10%	385.185	42.60	1.5+0.9	192	1186	701
M30+12.5%SCBA	12.5%	373.333	53.25	1.5+0.9	192	1186	701
M30+15%SCBA	15%	361.481	63.90	1.5+0.9	192	1186	701

Table 6. Mix Design of Rice Husk Ash [20]

Specimen	RHA (%)	Quantity (kg/m^3)					
		Cement	RHA	Polyolefin fiber +Polyester fiber (additive)	Water	Coarse Aggregate	Fine Aggregate
M30	0%	426	0	1.5+0.9	192	1186	701
M30+5%RHA	5%	404.691	21.30	1.5+0.9	192	1186	701
M30+7.5%RHA	7.5%	394.074	31.95	1.5+0.9	192	1186	701
M30+10%RHA	10%	385.185	42.60	1.5+0.9	192	1186	701

8. MIXING GUIDELINES

In the case of triangular polyester fibre (Recron 3S), in the event of machine mixing, the fibres are placed in the mixer along with some water (5-10 liters) and then other components are added, followed by a continuing mixing process until all fibres are disseminated, which takes a few minutes. In case of manual mixing, half of the fibers are mixed and stirred in a bucket full of water, which is then mixed with other ingredients. Similarly, balance type fibers are also added to mix, according to MSDS of the product use of more than 0.25% of weight of cement is not recommended. specific gravity of this material is 1.36& placing, curing along with finishing is similar to conventional methods (Table 7).

Table 7. General specification according to application requirement [16]

Type	Application	General specification
CT 2012	Plaster, Concrete	6mm length, 125 gm packing
CT 2024	Concrete	12mm length, 125 gm packing
CT 2424	Ready mix concrete	12mm length, 450 gm dissolvable packing

Fibers for POLYOLEFIN (ECMAS EXF 54) should be put directly to the mixer at the prefabrication or concrete mixing plant, or to the mixer truck. Fill the conveyor belt with fibres, inert materials, cement, sand, and the first piece of gravel. Fibers should not be introduced at first. Dry mix for at least 5 minutes on high speed before adding water [18].

9. RESULTS & DISCUSSIONS

From obtained compressive strength based-results its evident that the sugarcane bagasse ash-based composite obtains high early strength in comparison to rice husk ash-based composite but the ultimate strength provided by rice husk ash is comparatively higher in value. Initial strength of rice husk ash-based composite is less than exemplary and can cause issues while using it as a constituent material, but these issues are as of now has been identified in less reactive version of rice husk ash which has non-reactive silicates in it, due to higher temperature at which it was obtained (Table 8, Figure 2).

Table 8. Compressive strength test

Specimen + (Polyolefin & Polyester fiber)	Compressive strength in 7 Days (N/mm^2)	Compressive strength in 14 Days (N/mm^2)	Compressive strength in 28 Days (N/mm^2)
M30	21.20	28.42	31.55
M30+5%RHA	12.61	18.45	24.35
M30+7.5%RHA	15.56	22.19	27.54
M30+10%RHA	18.89	26.75	33.00
M30+10%SCBA	16.78	22.20	26.78
M30+12.5%SCBA	18.75	25.34	27.55
M30+15%SCBA	19.86	27.36	29.20

The strength obtained from sugarcane bagasse ash composite is almost identical to that of polyolefin and polyester fiber-based composite. But as the no of days increase, the increment in its value becomes significantly less. Through these observations it can be suggested that a composite with a combination of both less reactive versions of SCBA & RHA could provide higher early strength, as well as a comparatively higher compressive strength if superplasticizer is added.

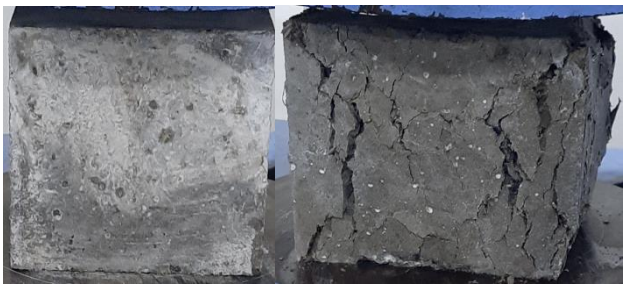

Figure 2. General crack bridging and failure mechanism

10. CONCLUSION

In this experimental study, a comprehensive review on different supplementary cementitious materials (SCMs), polyolefin fibers & polyester fiber have been discussed. Furthermore, technical data on commercially available polyolefin fiber and polyester fiber is discussed with their potential impact on concrete properties. A separate chapter for mixing guidelines & fiber pull-out response is also added for better understanding on handling of these fibres to gain maximum benefit. Some of the noteworthy results obtained from this study are as follows

- The experimental study shows that adequate strength can be achieved through the use of SCBA & RHA even in presence of non-reactive silicates formation like meta stable cristobalite, which is caused by burning at higher temperature than recommended ideal temperature range of 600-700°C.
- The study shows that SCBA reaches high early strength, but it also states that the RHA shows very low strength in its earlier phases like at 7 days or 14 days.
- According to obtained data possibility of obtaining a better specimen by combination of SCBA and RHA is very high, however according to technical data its better if the total replacement level to cement is restricted to 20% replacement by weight and amount of RHA should be properly regulated as it can reduce workability of mix exponentially, at higher concentrations.
- The main goal of this project was to obtain similar or higher value then traditional concrete, and that was achieved according to design mix and lab environment parameters.
- Concrete failure at peak loads is adequate and crack bridging effects show proper fiber pullout response, suggesting tensile strength test of specimen would give exceptional results.
- This fiber reinforced composite is very cost effective as it goes as far as to replace 15% of cement content with a waste material, which is discarded and can be obtained at very cheap rates making it a good alternative.
- Other than the cost factor, this material can be considered as more eco-friendly than conventional concrete. This statement can be justified by simply stating the fact that the majority of carbon emissions in construction are related to cement, its production, etc.
- These results show that with higher quality variants of SCBA and RHA, better results can be obtained. This conclusion is rooted in the fact that silica content can reach up to 90% if these materials are burned at their ideal temperature. An ideal temperature also helps in obtaining the highest values of the strength activity index (SAI).
- From the compressive strength results, it is evident that the sugarcane bagasse ash-based composite obtains high early strength in comparison to the rice husk ash-based composite, but the ultimate strength provided by rice husk ash is

comparatively higher in value. The initial strength of the rice husk ash-based composite is less than ideal and can cause issues while using it as a constituent material, but these issues are, as of now, only identified in the less reactive version of rice husk ash, which has non-reactive silicates in it due to the higher temperature at which it was obtained.

- The strength obtained from sugarcane bagasse ash composite is almost identical to that of polyolefin and polyester fiber-based composites. But as the number of days increases, the increment in its value becomes significantly less. Through these observations, it can be suggested that a composite with a combination of both less reactive versions of SCBA and RHA could provide a higher early strength as well as a comparatively higher compressive strength.

Other potential research on use of SCMs can include options like natural pozzolans, silica fume, fly ash, GGBS, MSW ash, rice husk ash, calcined natural SCMs, calcareous fly ash, activated cooper tailings, wood ash, calcined clays, Biomass ash, Bauxite residue, waste glass etc. Meanwhile fibres can be polypropylene, polyolefin, steel fiber, polyethylene, nylon fiber etc.

REFERENCES

[1] A. Aizaz Dayo, A. Kumar, A. Raja, N. Bheel, Z.H. Shaikh. Use of sugarcane bagasse ash as a fine aggregate in cement concrete. Eng Sci Technol Int Res J 3(3), pp. 8–11, 2019.

[2] V Kavinkumar *et al.* A Study of Partial Replacement for Cement by Bagasse ASH and Coarse Aggregate, *IOP Conf. Ser.: Mater. Sci. Eng.* 1145 012008, 2021.

[2] S. Sindhu, S. Praveenkumar, G. Sankarasubramanian, Evaluation of Pozzolanic Performance of Treated and Untreated Bagasse Ash. In: Shukla, S.K., Chandrasekaran, S., Das, B.B., Kolathayar, S. (eds) Smart Technologies for Sustainable Development. Lecture Notes in Civil Engineering, vol 78. Springer, Singapore, 2021. Doi: 10.1007/978-981-15-5001-0_30

[4] A. Gautam, R.J. Batra, N.K. Singh. A STUDY ON USE OF RICE HUSK ASH IN CONCRETE. *Engineering Heritage Journal*, 3(1): pp. 01-04, *2019*.

[6] M. B. Ahsan and Z. Hossain, "Supplemental use of rice husk ash (RHA) as a cementitious material in concrete industry," Construction and Building Materials, vol. 178, pp. 1–9, Jul. 2018, doi: 10.1016/j.conbuildmat.2018.05.101.

[7] R. Fediuk, V. Lesovik, A. Svintsov, A. Mochalov, S. Kulichkov, N.Y. Stoyushko, N.Y. N.A. Gladkova, R.A. Timokhin, Self-compacting concrete using pretreatmented rice husk ash. Magazine of Civil Engineering. 79. 66-76. 2018. Doi: 10.18720/MCE.79.7.

[8] R. Kumar, M.K Kaushik, Effect of bagasse ash and rice husk ash addition as supplementary cementitious materials on chloride penetration and diffusion in concrete mix(s). International Journal of Technical Research and Applications Volume 6, Issue 1, pp. 44-50, 2018.

[9] M.G. Alberti, J.C. Gálvez, A. Enfedaque, R. Castellanos, Influence of High Temperature on the Fracture Properties of Polyolefin Fibre Reinforced Concrete. Materials (Basel);14(3):601, 2021. doi: 10.3390/ma14030601

[10] A. Picazo, M.G. Alberti, J.C. Gálvez, A. Enfedaque, A.C. Vega. The Size Effect on Flexural Fracture of Polyolefin Fibre-Reinforced Concrete. *Appl. Sci.* 2019, *9*, 1762, doi: 10.3390/app9091762

[11] F. Suárez, J.C. Gálvez, A. Enfedaque, M.G. Alberti, Modelling fracture on polyolefin fibre reinforced concrete specimens subjected to mixed-mode loading, Engineering Fracture Mechanics, Volume 211, pp. 244-253, 2019. Doi: 10.1016/j.engfracmech.2019.02.018

[12] P.D. Pawaskar, V. Shirodkar, Experimental study on behavior of Recron "3s" fibre, IOSR Journal of Mechanical and Civil Engineering (IOSR-JMCE), 2320–334X, pp. 32-38, 2020

[13] C., Neeladharan & Anbarasan, Muralidharan. (2020). Behaviour of Fiber Reinforced Concrete using Recron 3S. 6. 1-3. 10.20256/IJARMATE.2020.0606001.

[14] M. G. Alberti, A. Enfedaque, and J. C. Gálvez, "Polyolefin Fibres for the Reinforcement of Concrete," Alkenes, Feb. 2018, doi: 10.5772/intechopen.69318.

[15] J.T. Kolawole, A.J. Babafemi, E. Fanijo, S.C. Paul, R. Combrinck. State-of-the-art review on the use of sugarcane bagasse ash in cementitious materials, Cement and Concrete Composites, Volume 118, 2021, doi: 10.1016/j.cemconcomp.2021.103975

[16] TDS and MSDS OF TRIANGULAR POLYSTER FIBER (RECRON 3S), [Online] Available: https://www.recron.com/pdf/polyester-3s-short-cut-fibre.pdf

[17] B. Singh, "Rice husk ash," Waste and Supplementary Cementitious Materials in Concrete, pp. 417–460, 2018, doi: 10.1016/b978-0-08-102156-9.00013-4.

[18] TDS and MSDS of polyolefin fiber (ECMAS EXF 54), [Online], Available: https://ecmas.in/our-products/fibers/ecmas-exf-54/

[19] T. Igba, A. Adekunle, O. Abiola, S. Oyebisi, M.O. Osaghale, The Use of Rice Husk Ash in Production of Green Concrete. Proceedings of the 18th International Conference & Annual General Meeting of the Nigerian Institution of Civil Engineers, 2020.

[20] IS 10262; concrete mix proportioning guidelines, [Online] Available: https://civiconcepts.com/wp-content/uploads/2020/11/4.IS-10262-2019-New-Mix-design.pdf

Biographies

Abhishek Nautiyal received the bachelor's degree in civil engineering from SRM University in 2020, the master's degree in Structural engineering from Amity University in 2022. He is currently working as an Graduate Engineer at WS Atkins India which is a part of Global SNC Lavalin Group. His research areas include transparent insulation materials, supplementary cementitious materials, Bridge Assessment Design and Footbridge Dynamics.

.

Mr. Prakhar Duggal is a Civil Engineer with vast industry and academic experience. He graduatedin Civil Engineering from Pune University in 2011 and obtained his master's in Structural Engineering from RTU, Kota in 2013. Subsequently, he is pursuing his doctorate from Amity School of Engineering and Technology, Noida. He has 4 years of industry experience during as a structural engineering consultant for different projectsrelated to building construction. He has worked for more than 08 years in academia in various capacities as Academic Chair, Center Superintendent and Program Leader of the Department. His holds expertise in the area of solar energy and built environment, Building Materials. His research work focuses on application of artificial intelligence for

Dr. R.K. Tomar is a Civil Engineer with vast industry and academic experience. He graduatedin Civil Engineering from Pune University in 1990 and obtained his master's in environmental engineering from Delhi College of Engineering, Delhi in 2006.Subsequently, he completed his doctorate from Indian Institute of Technology, Delhi (IITD) in 2015. He has 8 years of industry experience during which he has extensively worked in the field for different projects related to canal, railways and building construction. He has worked for more than 23 years in academia in various capacities as Academic Chair, Center Superintendent and Head of the Department.He holds expertise in the area of solar energy and built environment. His research work focuses on application of artificial intelligence for estimation of solar radiation in buildings.

Role of Nano Particle Coating in the Progress of Industry 4.O: A Review

[1]Gaurav Verma, [2]Sanjay Kumar Awasthi, [3]Kamal Sharma, [4]Ayush Gupta

[1,2,3,4] GLA University, Mathura, India

[1]gauravverma99@gmail.com, [2]sanjay.mech.jmi@gmail.com

Abstract

A Nanotechnology-The beginning to the Fifth Industrial Revolution and cutting-edge future. Nanotechnology can be described as a new and arising innovation with broad applications in the space of industry 4.0, energy, gadgets, beauty care products, materials, medication, horticulture, climate, etc. In India, both science and financial matters have progressed somewhat recently since post-autonomy. Nanotechnology has filled different mechanical holes and will foster all monetary angles including compensation, work, market monetary standards, the organic market for trade rates, etc. Diminished size nanotechnology makes the computerization of errands that were already distant because of actual work. The current audit focussed on examining the job of nanotechnology that is highly improved in various ventures as well as making the fifth upheaval that will prompt a superior future for the future.

Keywords. Emerging, the industrial revolution, industries 4. o, nanotechnology.

1. INTRODUCTION

The coming of microengineering had contributed a lot to different areas of science. The openness of new nanomaterial advances have added to an upset in all fields including Industry 4. o, biomedicine, Automobile industry, and biotechnology [1]. Nanomaterials (materials with a breadth < 100 nm) showed preferable properties over mass materials of the equivalent nature [2,3]. Different manufactured courses were made for the readiness of nanoparticles (NPs) of various sizes and aspects, remembering compound responses for arrangement (sol-gel techniques), amalgamation in vaporous stages, and mechanical processing. The little size of nanomaterials is like organic atoms like proteins and is profoundly suitable for very long-time natural operations [4]. Another area of science known as "nanomedicine" has as of late been created to foster advances in natural frameworks and nonmaterial's [5]. Nanomedicines offer numerous instances of how nano-mechanical procedures are utilized effectively in the industry. There is a reasonable need in this way to lay out inventive ways to deal with observing new materials that can adapt to these difficult issues. Forerunners of what are now referred to as nanomaterials like silvery (Ag), zinc (Zn), copper (Cu), titanium (Ti), iron (Fe), and silica (SiO2) had been practiced for some time to make use of in injury therapy and related ailments as anti-infection reagents [6].

2. NANOPARTICLES

2.1 About Nanoparticles

(a) A Review on the Study of the Generation of (Nano) particles Aerosols during the Mechanical Solicitation of Materials

Growths in nanoscience are driven by the quick industrialization of items containing nanomaterials with striking properties. These nanomaterials may tend to get deposited in the air as molecule spray [7]. Molecule spray is a technique of accumulation of strong or fluid particles in the vaporous system. It is for the most part settled by the crumbling of fluids or solids into better constituents. Writers have made sense of thoroughly how the particles, after being produced, get accumulated in the air to frame a spray alongside the way of behaving related to their various designs. Different actual peculiarities (e.g., scattering, coagulation, sedimentation, and so forth) are additionally made sense of which guide their size advancement

(b) Advances in green synthesis of nanoparticles

The branch of science known as nanotechnology oversees the evaluation of materials that are typically between 1 and 100 nm in size. Science operates at the nanoscale and lends several central focuses to its many subfields, including bioengineering, pharmaceuticals, and dentistry. The future potential of nanomaterials is greatly impacted by the Green Science approach [8]. With the development of safe, environmentally friendly NPs, this field of nanoscience should come full circle and receive widespread recognition in the field of nanotechnology. The morphology of integrated particles, such as their size, physicochemical characteristics, and form, is affected by the solvents and lowering administrations employed to decrease the NPS, and this morphology affects the usage of NPs. The two innovative NPS combining procedures are "top-down" and "base up." From beginning to end, appropriate bulk material is divided into smaller, finer particles by size using various techniques as crushing, processing, and faltering [9].

(c) The presence of nanosized particles

As soon as in 1997, the Deutsche Commission for the examination of Health Hazards of substance compounds in the workspace characterized the expression "ultrafine particles" [10]. The meaning of "ultrafine particles" as it connects with the working environment compares principally to the term nanoparticles as it is presently being utilized in examination and innovation Nanoparticles are not another disclosure of science, nor are they a development, as respects their definition in light of their molecule size or as a specialized accomplishment.

(d) Nano-based drug delivery systems: Recent developments and prospects

Materials in the nanoscale range are used to operate as a method for symptomatic gadgets or to convey helpful professionals to specifically targeted destinations in a controlled way in nano medication and nano conveyance frameworks, two generally new yet rapidly developing fields of study. By targeting and delivering precise medications at the right places, nanotechnology provides a number of benefits in treating chronic human ailments. Recent advances in nanomedicine (chemotherapeutic specialists, natural specialists,

immunotherapeutic specialists, etc.) have made it useful for treating a variety of infections [11].

(e) Industrial Applications of Nanoparticles

Effective items in the compound business give a particular advantage: Pharmaceuticals communicate with life forms, development polymers support mechanical pressure and paints give surface security. Basic things we know from our daily existence, at the same time, for what reason is the substance business so serious about moving into new business sectors? The accompanying article investigates the job of nanoparticles in modern applications [12]. From the beginning, the utilization of heterogeneous materials (for example mixes of a molecule and a persistent stage like a polymer) seems ugly. Assuming one could stay with a synthetically notable "straightforward" however homogeneous item, later technique shows up additional exquisite and alluring regarding costs, natural effect, and simplicity of the plan.

(f) Synthesis, characterization, applications, and challenges of iron oxide nanoparticles

Nanoparticles (NPs) are at the bleeding edge of quick advancement in nanotechnology. Their select size-subordinate properties make these materials irreplaceable and predominant in numerous areas of human exercise.

(i) Being the latest progress metal on the Earth's outside, iron stands as the foundation of the current framework.
(ii) However, in correlation with a bunch of components like cobalt, nickel, gold, and platinum, iron oxides are fairly neglected. Iron and oxygen synthetically consolidate to frame iron oxides (mixtures), and there are ~16 distinguished iron oxides. In nature, iron (III) oxide is found as rust.
(iii) Generally, iron oxides are common, broadly utilized as they are cheap, and assume a basic part in numerous natural and topographical cycles. They are likewise widely utilized by people, e.g., as iron metals in thermite, impetuses, sturdy shades (coatings, paints, and hued concretes), and hemoglobin [13].
(iv) NPs made out of ferromagnetic materials and with size <10-20 nm exhibit an incomparable type of attraction, i.e., superparamagnetic. The ferromagnetic materials incorporate essential metals, composites, oxides, and other synthetic mixtures that are polarized by an outer attractive field.

(*g) Application of Nanotechnology in Food Science: Perception and Overview*

Nanotechnology has become more widely recognised in recent years as an appealing breakthrough that has altered the food industry. It is a nanoscale innovation that manipulates iotas, atoms, or macromolecules that are around 1-100 nm in size to create and use materials with novel features. The created nanomaterials include at least one external or internal feature on a scale from 1 to 100 nm that enables the perception and management of problems at the nanoscale [14]. Because of the high surface-to-volume ratio and other novel physiochemical properties like tone, solvency, strength, diffusivity, harmfulness, attractiveness, optical, thermodynamic, and so on, it is evident that these materials possess interesting properties that are different from those of their macroscale partners. Both developed and developing countries want to invest more in nanotechnology because it has brought forth fresh modern transformations.

2.2 Properties of Nano particles-Characterization SCM, TEM

(a) Nanoparticles: Properties, applications, and toxicities

This survey gives an outline of the blend, properties, and utilizations of nanoparticles (NPs) that exist in various structures [15]. NPS are small materials having sizes going from 1 to 100 nm. They can be grouped into various classes in light of their properties, shapes, or sizes. The various gatherings incorporate fullerenes, metal NPs, ceramic NPs, and polymeric NPs. NPs has exceptional physical and synthetic properties because of their high surface region and nanoscale size. Their optical properties are accounted for to be reliant upon the size, which grants various tones because of retention in the noticeable locale. Their reactivity, sturdiness, and different properties are additionally reliant upon their remarkable size, shape, and construction.

(b) Synthesis and Characterization Techniques of Nanomaterials

Nanomaterials can be metals, pottery, polymeric materials, or composite materials. Their central quality is a tiny element size in the scope of 1-100 nanometers. The unit of nanometer gets its prefix noon from a Greek word signifying "overshadow" or "tiny." One nnanometertraverses 3-5 molecules arranged in succession. By correlation, the distance across of a human hair is around 5 significant degrees bigger than a nanoscale molecule [16].

Combination Methods: Synthesis techniques assume a vital part to control the size and surface area of nanomaterials. There are a few amalgamation strategies, some of which are depicted in the accompanying segments.

Precipitation Methods: Modified Emulsion Precipitation Method Hydro warm Synthesis/Solvo thermal Synthesis Sol-Gel Method Aerogel Methods Immobilization Methods Citrate Gel Methods Penchini Method Low-Temperature Combustion Synthesis Methods [17].

Precipitation Method Modified Emulsion Precipitation Method - This strategy gives the specific benefit of staying away from the agglomeration of the particles framed in the singular air pockets. This, thus, makes it conceivable resulting in handling courses at abnormally low temperatures.

(*c) Characterization techniques for nanoparticles*

Correlation and complementarily after examining nanoparticles properties - Nanostructures have drawn immense interest as a quickly developing class of materials for some applications. A few strategies have been utilized to describe the size, precious stone construction, basic organization, and an assortment of other actual properties of nanoparticles [18]. In a few cases, there are actual properties that can be assessed by more than one strategy. Various qualities and impediments of every procedure confuse the decision of the most reasonable strategy, while frequently a combinatorial portrayal approach is required.

(d) Techniques for physicochemical characterization of nanomaterials

Propels in nanotechnology have opened up another time of determination, anticipation, and treatment of illnesses and horrible wounds. Nanomaterials, incorporating those with potential for clinical applications, have novel physicochemical properties that affect their

physiological collaborations, from the atomic level to the fundamental level. There is an absence of normalized procedures or administrative conventions for the recognition or portrayal of nanomaterials [19].

(e) Surface characterization of nanomaterials and nanoparticles: Important needs and challenging opportunities

This audit inspects the portrayal challenges innately connected with understanding nanomaterials and the surface and point of the job of interaction portrayal strategies can play in gathering a portion of the difficulties. In pieces of the examination local area, there is developing acknowledgment that reviews and distribution give an account of the properties and ways of behaving of nanomaterials frequently have announced deficient or inadequate portrayal [20].

(f) Nanoparticles: Properties, applications, and toxicities

This paper is given a nitty gritty outline of the blend, properties, and utilization of nanoparticles (NPs) that exist in various structures. NPS are little materials having sizes going from 1 to 100 nm. They can be characterized into various classes given their properties, shapes, or sizes. The various gatherings incorporate fullerenes, metal NPs, ceramic NPs, and polymeric NPs. NPs' have one-of-a-kind physical and synthetic properties because of their high surface region and nanoscale size [21]. Their optical properties are accounted for to be reliant upon the size, which confers various varieties because of ingestion in the apparent locale.

(g) Green Nanobiotechnology: Factors Affecting Synthesis and Characterization Techniques

Nan biotechnology is acquiring a huge driving force in this period inferable from its capacity to tweak metals into their nano size, which proficiently changes their compound, physical, and optical properties. As needs are, extensive consideration is being given to the improvement of novel methodologies for the amalgamation of various types of nanoparticles of explicit structure and size utilizing natural sources. Be that as it may, the majority of the now accessible methods are costly, earth destructive, and wasteful concerning materials and energy use. A few factors, for example, the strategy utilized for amalgamation, pH, temperature, pressure, time, molecule size, pore size, climate, and vicinity significantly impact the quality and amount of the integrated nanoparticles and their portrayal and applications [22].

(h) Metallic Nanoparticles

Metallic nano molecule is nano-measured metals with aspects (length, width, thickness) inside the size scope of 1-100nm. In 1857, Faraday previously examined the presence of metallic nanoparticles in an arrangement. In 1908, Mie gave a quantitative clarification of their variety. Today these nanomaterials can be ready and changed with different synthetic utilitarian gatherings which permit them to tie with antibodies, ligands, and medications [23]. Metallic nanoparticles give a wide scope of use in helpful regions, biotechnology, vehicles for quality, and medication conveyance. This audit sums up the properties, benefits, hindrances, and qualities of metal nanomaterials.

2.3 Coating of Nanoparticles on the base material

(a) Nanocomposite Coatings: Preparation, Characterization, Properties, and Applications

A nanocomposite covering is a material made out of somewhere around two immiscible stages, isolated from each other by an interface area. The material should contain the nanometre scale in no less than one aspect in which the significant part is called the framework in which fillers are scattered.

i. Characterization. The characterization of nanocomposite coatings is given different techniques for managing the kind of nanostructure fillers or sort of network where filler nanostructures are scattered.
ii. Type of Nanostructured Fillers. There are 3 fundamental gatherings of nanocomposite covering as follows [24].
iii. 0D nanocomposite coatings: the filler is nanoparticles (3 aspects on a nanometer scale).
iv. 1D nanocomposite coatings: the fillers are nanotubes or stubbles (2 aspects on a nanometer scale).
v. 2D nanocomposite coatings: the filler is nanolayers (1 aspect in nanometer scale).

(b) Type of Matrix: which are natural and inorganic networks can be found. Subsequently, there are 4 principle gatherings of nanocomposite covering as follows (grid/nanofiller)

i. Organic/inorganic nanocomposite coatings (O/I nanocomposite coatings)
ii. Organic/natural nanocomposite coatings (O/O nanocomposite coatings)
iii. Inorganic/natural nanocomposite coatings (I/O nanocomposite coatings)
iv. Inorganic/inorganic nanocomposite coatings (I/I nanocomposite coatings).

(*c) Materials for Matrix*

For a natural grid, called polymer-based nanocomposite, the most involved polymers for the arrangement of nanocomposite covering can be recorded as follows:

epoxy, polyurethane, Chitosan, polyethylene glycol (PEG), polyvinylidene fluoride (PVDF), Pains, PPy, polystyrene, polyamide corrosive and polyimide, elastic altered polybenzoxazine (PBZ), polymers containing receptive trimethylsilyl (TMOS), pullulan, fluoro acrylic polymer ethylene tetrafluoroethylene (ETFE), polyacrylate, poly(N-vinyl carbazole), polycarbonate, fluorinated polysiloxane, polyester, polyacrylic, polyvinyl liquor (PVA), polydimethylsiloxane polyamide, and UV-treatable polymers[25]. For inorganic framework, like metal network or amalgam grid, these nanocomposite coatings could be ready by different strategies, including substance fume affidavit (CVD), powder metallurgy, actual fume testimony (PVD), warm plasma shower, sol-gel, epitaxial development, cold spray, and electrode position. Metal network composite coatings that scattered a second phase have pulled in broad consideration inferable from special properties, for example, oxidation and consumption opposition wear obstruction and attractive properties [26].

2.4 Nanomaterials Thickness

Nanomaterials allude to materials estimated between 0.2-100 nm. Those materials' properties contrast as their size comes to the nanoscale. The general wealth of surface

molecules influence the properties of such materials. Also, nanomaterials have a high surface region which brings about huge surface-to-volume proportions. Therefore, the condition of electrical energy is particular, which results in uncommon physical, attractive, optical, and mechanical properties [27].

The exceptional physical and synthetic properties of nanomaterials have permitted them to get a ton of Education in the clinical area. Since they are comparative in size to most organic particles, there has been broad utilization of NPs in the biomedical examination. Moreover, most nanomaterials were found to have antimicrobial action against different pathogenic bacterial and viral creatures. Nanomaterials have likewise shown fair biocompatibility when utilized in the assembling of framework materials. Accordingly, nanomaterials in designated drug conveyance, fake inserts, biocompatible platform materials, and detecting, imaging, and antimicrobial materials have been carried out in clinical fields [28]. The nanomaterials enjoy two benefits and inconveniences, and evaluating their general pertinence in both clinical fields is significant.

Since their fantastic antimicrobial exercises, nanomaterials have been utilized in numerous wellbeing-related modern products, for instance, Ag NPs are utilized in clinical items, for example, gauzes and catheters to forestall contamination during twisted healing. Since of their solid photograph catalytical and antimicrobial exercises, zinc oxide NPs have been utilized in sunscreens, coatings, paints, backdrops, beauty care products, salves, and balms [29].

3. USE OF NANO PARTICLES IN INDUSTRY 4. O

Nanotechnology has many uses in similar sectors. It system has a wide variety of everyday life.

3.1 Textile Industry

The utilization of nanotechnology in materials has quickly risen in light of its commitment to service administration. It has colossal rewarding potential for applications in silk and cotton ventures. Financially, it Extends the significance of material and material properties [30]. Nanotechnology is used in an article about the clothing industry expanding the life span of textures dramatically. Nanoparticles of silver and copper are remembered for textures and the future apparel movement. In the expansion, the specialists utilized nano titanium dioxide For self-cleaning materials and UV-hindering properties (Duran and others, 2007). They can utilize zinc nanoparticles in materials for UV assurance. The nano-silica is utilized for further developing cotton wrinkle obstruction and silk [31].

3.2 Paper and Pulp Industry

This examines a considerable lot of the ongoing cycles and innovations to affect the meanings of miniature and nano peculiarities that integrate the ideas genuinely in the initial time. Woodland trees containing agro-deposits and reused fiber miniature designs have driven significant work nano cellulose along. That discusses a considerable lot of the arising cycles and innovations to affect ideas of miniature and nano-phénomènes the first time that coordinates the ideas [32]. Woods Arbore with agro-build-ups and reused fiber miniature designs have fuelled huge examination nano cellulose.

3.3 Nano Technology in Defence

Security is a significant field where nanotechnology can be utilized be summoned. Explicit executions of protection Nanotechnology. The blinds are intended to have persevered through cruel conditions. The nano-arms are utilized for security Detection and Growth. Surprisingly enough nanotechnology will assist us with saving money on fuel, and trooper development for protection and secrecy [33]. One of the essential regions of the prosperity of the litigants is guard. In pathology, nanotechnology, treatment of patients, and the conveyance of the drugs.

3.4 Nano Technology in Automobile Industry

In transport, nanotechnology has been applied for quite a long time, for example, working on the strength and perseverance of autos over a more extended time of time. Nanotechnology might be applied to various pieces of the body like the casing, tires, windows, motors, and so forth. There are, in any case, other well-being and ecological perils related to the use of nanotechnology in transport vehicles that need significant consideration [34]. Consequently, this investigation of assessment is separated into two segments. First and foremost, it presents the nanotechnology applications in vehicles and also, it distinguishes the nanotechnology-related EHS concerns, so this study will be introduced in ongoing advancements Nanotechnology is utilized as a valuable instrument to give insurance against consumption and scraped spot protection from car bodies [35]. It incorporates the "should do" segment, which includes upgrading the nanotechnology for lighter weight, enhancing nanomaterials for self-cleaning and self-recuperating, and hardware with high detecting and high goal.

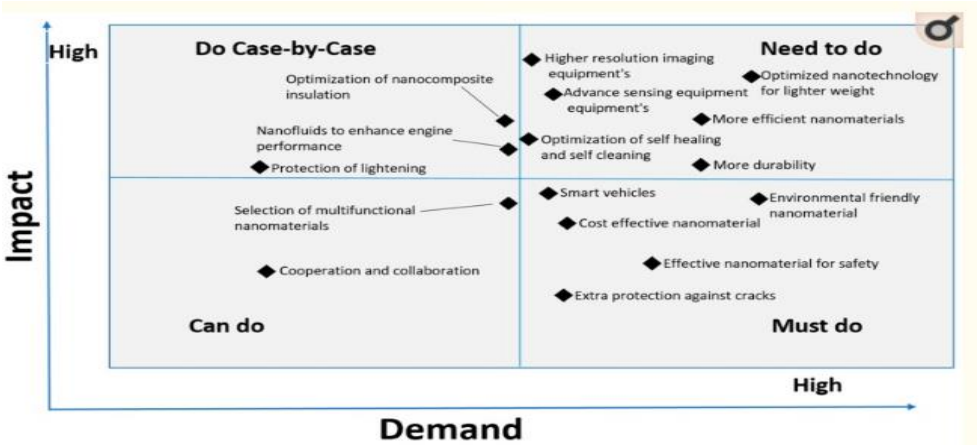

Figure 1. Use of nanocomposite in various fields Reproduced with permission

3.5 Coating, Packing, Papers, and Printing

Nanotechnology is utilized in the fields of printing, bundling, paper and brilliant wood and bundling fabricating security, fake, and microbial materials utilization of various assortments of antibacterial material, paper towel and as of late, newsprint was created in nanotechnology [36]. Extensive further improvement has been made to the surface change

nano strands and movies of cellulose, and screen the Industrial and PFI adventures accomplices showed they can produce nano cellulose economically, in huge scope (1.5 tonnes/day) and with low energy utilization (1600 kWh/ton). That implies the Nan cellulose content, created broadly from wood amount is monstrous. Creation and use sufficient more compressive view of the medication science for nano cellulose, (for example, utilization of paper and mash industries) [37]. The worldwide aggregate is worth all nanotechnologies in 2010. The paper business use was projected to be more including $3.2 billion. By 2015, the venture is supposed to be in this market is supposed to ascend to more than $3.7 billion, Reflecting the expected yearly development pace of the compound (CAGR) for the general interest of 2.8 percent [38].

3.6 Nano Technology in Pharmaceutical Industries

The study is focused on drug organizations on malignant growth, new and arising cardiovascular illnesses, and causes like ebola, HIV, Tuberculosis, and so on. Nanotechnology is utilized to control and orchestrate medications, and as a symptomatic development instrument [39]. One is scaling down and the Most Important Tools are natural union mechanization and bio-screening on a nanometer (Kumar 2011). Most nanomedicines are perhaps more grounded than current prescriptions, and a lot more drug firms have begun to utilize this to support the conveyance and focus of medications (Jain et al, 2015) [40]. Drugs taking a look at the capacity to hit cell limits had more conventional medications, for example, magnet escaped which find itself in some piece of the layer where it ruins the amount of design or position [41].

4. CONCLUSION

Nanotechnology exhibited exceptional potential will the lovely world shift decisively by age of a fresh out-of-the-box new transformation. Nanotechnology application has a huge impact on the world we live in. It's numerous interdisciplinary or alliance applications, like biotechnology, purchaser items, media communications, computers, textiles, food, aviation, guard, and so forth. This impact sets up issues for the scholarly local area and teaches understudies in design and science with the essential mindfulness, and ability to convey and give driving the arising nanotechnology local area.

Nanomaterials, particularly inorganic metals and metal oxides, at present assume an essential part in the re-foundation of different fields of exploration including biomedical. From a natural perspective, its antimicrobial and biocompatible properties are two fundamental parts of most nanomaterials. Nanomaterials are mostly found to have antibacterial, antifungal and viral properties, and nanomaterials target organisms either straight by connection to their cell layer followed by protein and DNA annihilation or by calculation advancing toward smaller nanomaterial aspects has shown a few exceptionally interesting properties of a far greater than mass materials The survey featured the effect of different sorts. This is accordingly inferred that nanomaterials have a wide degree of natural properties profoundly reliant upon their size, design, amount, and sort of cell receptor.

REFERENCES

[1] M.M. Andersen. *Eco-innovation indicators*. European Environment Agency, 2006.

[2] ANF Annual Reports, ANFoS. Asia Nano Forum Summit. Hong Kong Convention and Exhibition Centre & The Hong Kong University of Science and Technology, Hong Kong, 2006. [Online], Available: https://www.asia-anf.org/publications/

[3] P.J.M. Bartos, J.J. Hughes, P. Trtik, W. Zhu. (ed.). Nanotechnology in Construction XVI, Springer, Berlin 2004.

[4] S. H. Boura, M. . Samadzadeh, M. . Peikari, and A. . Ashrafi, "Smart and Multi-Functional Coatings Based on Micro/Nano Sized Additives and Their Implementation," All Days, May 2010, doi: 10.2118/130972-ms.

[5] P. van Broekhuizen, F. van Broekhuizen, R. Cornelissen, and L. Reijnders, "Use of nanomaterials in the European construction industry and some occupational health aspects thereof," Journal of Nanoparticle Research, vol. 13, no. 2, pp. 447–462, Jan. 2011, doi: 10.1007/s11051-010-0195-9.

[6] V. Chauhan & S. Chakrabarti. Use of nanotechnology for high performance cellulosic and papermaking products. Cellulose Chemistry and Technology. 46. 389.

[7] C. Matteo, P. Candido, R. Vera & V. Francesca, "Current and Future Nanotech Applications in the Oil Industry," American Journal of Applied Sciences, vol. 9, no. 6, pp. 784–793, Jun. 2012, doi: 10.3844/ajassp.2012.784.793.

[8] N. Durán, P. D. Marcato, G. I. H. De Souza, O. L. Alves, and E. Esposito, "Antibacterial Effect of Silver Nanoparticles Produced by Fungal Process on Textile Fabrics and Their Effluent Treatment," Journal of Biomedical Nanotechnology, vol. 3, no. 2, pp. 203–208, Jun. 2007, doi: 10.1166/jbn.2007.022.

[9] V. Favier, G. R. Canova, J. Y. Cavaillé, H. Chanzy, A. Dufresne, and C. Gauthier, "Nanocomposite materials from latex and cellulose whiskers," Polymers for Advanced Technologies, vol. 6, no. 5, pp. 351–355, May 1995, doi: 10.1002/pat.1995.220060514.

[10] R.A. Freitas. Progress in Nanomedicine and Medical Nanorobotics, In: Rieth M, Schommers W (eds). Handbook of Theoretical and Computational Nanotechnology. American Scientific Publishers, Stevenson Ranch UK. 2005.

[11] N. Ledbetter, and T. Goswami, "A Review of Nanotechnology Applications," Journal of the Mechanical Behavior of Materials, vol. 13, no. 5–6, pp. 353–362, Dec. 2002, doi: 10.1515/jmbm.2002.13.5-6.353.

[12] A. Gelfert*, "Nanotechnology as Ideology: Towards a Critical Theory of 'Converging Technologies,'" Science, Technology and Society, vol. 17, no. 1, pp. 143–164, Mar. 2012, doi: 10.1177/097172181101700108.

[13] L.E. Grinin, A.L. Grinin. Global technological transformations. Globalistics and Globalization Studies, Uchitel Publishing House (2013): 98-128, 2013.

[14] V. Jain, S. Jain, and S. C. Mahajan, "Nanomedicines Based Drug Delivery Systems for Anti-Cancer Targeting and Treatment," Current Drug Delivery, vol. 12, no. 2, pp. 177–191, Apr. 2015, doi: 10.2174/1567201811666140822112516.

[15] R. Krishnamoorti, "Technology Tomorrow: Extracting the Benefits of Nanotechnology for the Oil Industry," Journal of Petroleum Technology, vol. 58, no. 11, pp. 24–26, Nov. 2006, doi: 10.2118/1106-0024-jpt.

[16] M. Kumar Teli, S. Mutalik, and G. K. Rajanikant, "Nanotechnology and Nanomedicine: Going Small Means Aiming Big," Current Pharmaceutical Design, vol. 16, no. 16, pp. 1882–1892, Jun. 2010, doi: 10.2174/138161210791208992.

[17] L. Barrientos et al., "An Improved Strategy to Recover Large Fragments of Functional Human Neutrophil Extracellular Traps," Frontiers in Immunology, vol. 4, 2013, doi: 10.3389/fimmu.2013.00166.

[18] S. Mann. Nanotechnology and Construction. European Nanotechnology Gateway-Nano forum Report. Institute of Nanotechnology, November 2006: 2-10, 2006.

[19] A.G. Mansoori, P. Mohazzabi, P. McCormack, S. Jabbari. Nanotechnology in cancer prevention, detection and treatment: bright future lies ahead. World Review of Science, Technology and Sustainable Development, 2007 Vol.4 No.2/3, pp.226 – 257. Doi: 10.1504/WRSTSD.2007.013584

[20] W. P. McCray, "Will small be beautiful? Making policies for our nanotech future," History and Technology, vol. 21, no. 2, pp. 177–203, Jun. 2005, doi: 10.1080/07341510500103735.

[21] C. C. M. Mody and H. Choi, "From Materials Science to Nanotechnology: Interdisciplinary Center Programs at Cornell University, 1960–2000," Historical Studies in the Natural Sciences, vol. 43, no. 2, pp. 121–161, Nov. 2012, doi: 10.1525/hsns.2013.43.2.121.

[22] A. Nazari, S. Riahi, S.F. Shamekhi, and A. Khademno. Influence of Al2O3 Nanoparticles on the Compressive Strength and Workability of Blended Concrete. Journal of American Science, 6, 6-9, 2010.

[23] M. Rai, A. Ingle, I. Gupta, S. Birla, A. Yadav, and K. Abd-Elsalam, "Potential Role of Biological Systems in Formation of Nanoparticles: Mechanism of Synthesis and Biomedical Applications," Current Nanoscience, vol. 9, no. 5, pp. 576–587, Aug. 2013, doi: 10.2174/15734137113099990092.

[24] S. Rassenfoss, "Nanotechnology for Sale: The Once-Theoretical Becomes Practical," Journal of Petroleum Technology, vol. 63, no. 10, pp. 32–38, Oct. 2011, doi: 10.2118/1011-0032-jpt.

[25] S. Ryoo et al., "Theoretical and experimental investigation of the motion of multiphase fluids containing paramagnetic nanoparticles in porous media," Journal of Petroleum Science and Engineering, vol. 81, pp. 129–144, Jan. 2012, doi: 10.1016/j.petrol.2011.11.008.

[26] M. Hajjari, M. Ardjmand, and M. Tabatabaei, "Experimental investigation of the effect of cerium oxide nanoparticles as a combustion-improving additive on biodiesel oxidative stability: mechanism," RSC Advances, vol. 4, no. 28, pp. 14352–14356, Mar. 2014, doi: 10.1039/C3RA47033D.

[27] S.M. Hartley, H. Axtell, The Next Generation of Chemical and Biological Protective Material Utilizing Reactive Nanoparticles. Gentex Corporation, Carbondale, PA 18407, 2007.

[28] A. B. Seabra and N. Durán, "Biological applications of peptides nanotubes: An overview," Peptides, vol. 39, pp. 47–54, Jan. 2013, doi: 10.1016/j.peptides.2012.10.007.

[29] S. B, "Nanotechnology in Agriculture," Journal of Nanomedicine & Nanotechnology, vol. 02, no. 07, 2011, doi: 10.4172/2157-7439.1000123.

[30] J. Wu, Y.-L. Shen, K. Reinhardt, H. Szu, and B. Dong, "A Nanotechnology Enhancement to Moore's Law," Applied Computational Intelligence and Soft Computing, vol. 2013, pp. 1–13, 2013, doi: 10.1155/2013/426962.

[31] J. Yu, M.J. Berlin, W. Lu, L. Zhang, A.B. Kan. "Transport Study of Nanoparticles for Oilfield Application," All Days, May 2010, doi: 10.2118/131158-ms

[32] S. Tomar, "Innovative Nanotechnology Applications in Automobiles", International Journal of Engg. Research & Technology, Vol. 1, Dec. 2012.

[33] H. Kang, "A Review of the Emerging Nanotechnology Industry: Materials, Fabrications, and Applications", Sept.2010.

[34] H. Presting and U. König, “Future nanotechnology developments for automotive applications,” Materials Science and Engineering: C, vol. 23, no. 6–8, pp. 737–741, Dec. 2003, doi: 10.1016/j.msec.2003.09.120.

[35] M. C. Coelho, G. Torrão, N. Emami, and J. Gr´cio, “Nanotechnology in Automotive Industry: Research Strategy and Trends for the Future—Small Objects, Big Impacts,” Journal of Nanoscience and Nanotechnology, vol. 12, no. 8, pp. 6621–6630, Aug. 2012, doi: 10.1166/jnn.2012.4573.

[36] A. Baig, I. Mahmood, and S. Das, “Modeling MEMS Devices for Automotive Applications,” SAE Technical Paper Series, Apr. 2005, doi: 10.4271/2005-01-1447.

[37] H. Kantamneni, A. Gollakota, and S. Nimmagadda, “Avant-garde Nanotechnology applications in Automotive Industry,” International Journal of Advanced Materials Manufacturing and Characterization, vol. 3, no. 1, pp. 195–197, Mar. 2013, doi: 10.11127/ijammc.2013.02.034.

[38] R. Kidd, “Leading the charge for panel-powered car”, Queensland University of Technology, Nov, 2014, [Online], Available: https://phys.org/news/2014-11-panel-powered-car.html

[39] D. Kotnarowska, M. Wojtyniak, “Nanotechnology application to automotive coating manufacturing”, Journal of KONES Power train and Transport, 14(2), pp. 253-258, 2007.

[40] F. Monfort-Windels, J. Lecomte, “Nanotechnologies and their applications,” Jan, 2008, [Online], Available: https://www.termpaperwarehouse.com/essay-on/Nanotechnology/326550

[41] P. Louda, “Applications of thin coatings in automotive industry”, Journal of Achievements in Materials and Manufacturing Engineering, Vol. 24, pp. 51-55, 2007.

[42] J. Njuguna, F. Silva, and S. Sachse, “Nanocomposites for Vehicle Structural Applications,” Nanofibers - Production, Properties and Functional Applications, Nov. 2011, doi: 10.5772/23261.

Biographies

Gaurav Verma received a bachelor's degree in Mechanical Engineering from MDU, ROHTAK University in 2008, a master's degree in Applied Mechanics from MNNIT, ALLAHABAD in 2012, and pursuing a doctorate degree in Mechanical Engineering from GLA UNIVERSITY, MATHURA since 2020, respectively. He is currently working as an Assistant Professor at the Department of Mechanical Engineering, at United College oF Engineering and Management, Prayagraj. His research areas composite materials, graphene, reduced graphene, etc.

Sanjay Kumar Awasthi received the bachelor's degree in Mechanical Engineering from Jamia Millia Islamia New Delhi, in 2008, a master's degree in Thermal Engineering from Jamia Millia Islamia New Delhi, in 2011, and pursuing a doctorate in Mechanical Engineering from GLA UNIVERSITY, MATHURA since 2020, respectively. He is currently working as an Assistant Professor at the Department of Mechanical Engineering, at United College OF Engineering and Management, Prayagraj. His research areas are composite material nanomaterial, the hydrophobic effect of materials and carbon nanotubes, etc.

Crystallographic Study of Solid Solutions in the Mg-Ca-Nd Ternary System at 400°C

[1]Yogesh Iyer Murthy*, [2]Sumit Gandhi, [3]Abhishek Kumar

[1,2]Department of Civil Engineering, Jaypee University of Engineering and Technology, Guna, India.

[3]Deprtment of Applied Mechanics, Motilal Nehru National Institute of Technology, Allahabad, India

[1]yogesh.murthy@juet.ac.in, [2]sumit.gandhi@juet.ac.in, [3]abhishek@mnnit.ac.in

Abstract

The homogeneity ranges and crystal structures for the binary substitutional solid solutions, Mg_2Ca, $Mg_{41}Nd_5$, and MgNd extending to the ternary system were discovered using X-ray diffraction and scanning electron microscopy. Mg_2Ca and $Mg_{41}Nd_5$ undergo linear substitution where Ca and Nd replace each other, whereas, MgNd generates a complicated substitutional solid solution where Ca replaces both Mg and Nd. Rietveld analysis in conjunction with Pearson's crystal database and XRD were used to determine the solid solubility ranges of the phases present in the main alloys The lattice parameters and site occupancies were studied for these solid solutions. The experimental investigations were carried out using key alloys annealed at 400°C for four weeks. The solubility limit of Nd in Mg_2Ca is 9.0 at.%. The extended solid solubility of Ca in $Mg_{41}Nd_5$ was determined as 3.9 at.% while that of Ca in MgNd was obtained as 8.9 at.%. The phase Mg_3Nd was found to have negligible solubility and further confirmed by Fourier mapping.

Keywords. Mg-Ca-Nd system, SEM, XRD, Rietveld analysis, solid solutions.

1. INTRODUCTION

The two main processes that help magnesium alloys acquire better mechanical characteristics are solid solution hardening and age hardening. Age hardening becomes possible through precipitation from the supersaturated solution if the solubility of the alloying element decreases with a decrease in temperature. Mg content in precipitates should be high. This enables the increase in volume fraction of precipitate thereby reducing the amount of alloying elements [1]. The alloying element should be selected such that it shows sufficient solubility in Mg at high temperatures and shows considerable improvements in mechanical properties as well. Ca is a low-cost, low-density (1.55 g/cm^3) element with the potential for precipitation hardening [2]. Ca has been reported to be effective in promoting the creep resistance of Mg alloys. Through the refining of grain size, the addition of Ca increases ductility [3], and it also increases strength, castability, creep resistance, and corrosion resistance [4]. The addition of Ca has been discovered to make magnesium more resistant to oxidation at temperatures exceeding 480 °C [5] and to raise the ignition temperature of magnesium [6], making magnesium safer for use in aerospace and

automotive applications [7]. The Mg-Ca-based alloys have also lately discovered a wide range of intriguing uses in the realm of biodegradable implant materials [8–11].

One drawback of alloying Mg with Ca alone is that Mg ignition cannot be avoided during melting. Additionally, the Mg-Ca alloy becomes more brittle as the Ca percentage rises [12]. Therefore, the third element, Nd was considered to be added to the Mg-Ca binary system. The addition of Nd is beneficial in the strengthening of Mg alloys. It purifies the alloy melt thus improving castability. According to Xin et al. [13], adding Nd to magnesium results in a more refined solidified microstructure, which enhances the material's mechanical properties by increasing yield strength, tensile strength at high temperatures [13], and oxidation resistance. The addition of rare earth elements such as Nd also improves ductility and corrosion resistance [14] and creep resistance [15]. Furthermore, Mg-Nd based alloys have many applications as biocompatible materials, such as, bioabsorbable implant devices [16,17], cardiovascular implants [17], and orthopedic applications. [18] .

There hasn't been enough research on the Mg-Ca-Nd ternary phase diagrams in the literature as of yet. Recently, Fei *et al*. [19] studied this system at 400°C in the Mg-rich corner using equilibrated alloys. The partial isothermal is re-drawn as shown in Figure 1. Six samples were used to map this section and the locations for these samples are shown in Figure 1. They identified two three-phase triangulations in this region, Mg + Mg_2Ca + $Mg_{41}Nd_5$ and $Mg_{41}Nd_5$ + Mg_2Ca+ Mg_3Nd. They also reported the solubility limit of Ca in $Mg_{41}Nd_5$ to be 3.57 at.%. and that of Nd in Mg_2Ca to be 1.24 at.%.

The present investigation describes the extended homogeneity ranges of the binary compounds in the ternary Mg-Ca-Nd system. Knowledge of phase relationships and solubility limits is important to understand the microstructure and mechanical properties such as tensile strength and ductility of the resulting alloys. The increased homogeneity enables the easier synthesis of the compound. Moreover, properties such as lower density and higher specific strength could be obtained by tailoring the composition.

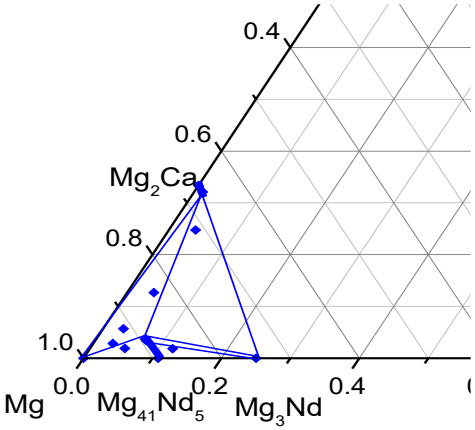

Figure. 1 Partial isothermal section of Mg-Ca-Nd system at 400°C as per Fei *et al* [19]

2. EXPERIMENTAL PROCEDURE

Key alloys were prepared using high purity Mg ingot of 99.8%, Ca with 99%, and Nd with 99.6% all supplied by Alfa Aesar® Company. These samples were initially made using a non-consumable tungsten electrode in an arc-melting furnace that was water cooled in a copper crucible. To ensure uniformity, the samples were crushed and remelted three to four times. Later, the samples were melted at least three times in an induction furnace using Tantalum crucible. To make up for the evaporation losses, extra magnesium (approximately 10 percent) was added. Utilizing an Ultima2 inductively coupled plasma optical emission spectrometer, the exact global composition was discovered (ICP-OES). By averaging the composition of three separate parts from each sample, the true composition was calculated. The deviation the from original composition was found to be negligible in most cases. The actual compositions of the key alloys are shown in Figure 2. The alloys were wrapped in tantalum foils, encapsulated in an argon-purged quartz tube and annealed for four weeks at 400°C. Using a Hitachi S-3400N SEM with EDS, the phase compositions, phase relations, and homogeneity ranges were investigated. With a 2 m probe size, 15 kV accelerating voltage, and 50 nA probe current, samples were analysed.

The XRD patterns were obtained using a PAN analytical X'pert Pro powder X-ray diffractometer with CuKα radiation. The XRD spectrum was acquired from 20 to 90° 2θ with a 0.02° step size. X-ray diffraction study of the samples was carried out using X'Pert High Score Plus Rietveld analysis software. Si was used as an internal calibration standard for correcting the zero shift and specimen surface displacement which are the most serious systematic errors in x-ray powder diffraction patterns. The crystal structure data of the binary compounds were taken from Pearson's crystal structure database [22].

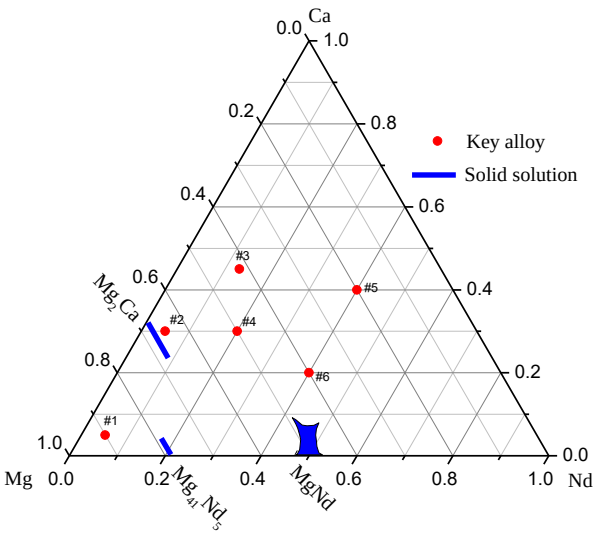

Figure 2. critical alloys' actual compositions and the locations of solid solutions in Gibb's triangle for Mg-Ca-Nd system at 400°C.

3. RESULTS AND DISCUSSION

To study the solubility ranges of the binary compounds, several alloys were prepared and annealed at 400°C for four weeks. The annealed alloys were then quenched in cold water to maintain the microstructure present at the annealing temperature. In the current research, six selected alloys prepared in the ternary system are discussed. The locations of these alloys are shown in Figure 2. The actual composition obtained from ICP and phase identification of the key alloys determined by SEM/EDS and XRD are summarized in Table 1. Figure 3 (a-c) shows the backscatter electron (BSE) images of the sample #1, #2 and #4. To determine the composition of the equilibrated phases and to identify them, the alloys underwent SEM/EDS spot analysis. XRD analysis was performed to identify and to verify the crystal structures of the phases contained in the alloys. The unit cell parameters, lattice volume and phase, composition determined by XRD results are presented in Table 2. The phase relations obtained by SEM/EDS shows great consistency with those obtained by XRD.

Table 1. Actual sample compositions with phase composition determined by XRD results

Sample No.	Actual composition identified by ICP (at %)			Phase identification		Composition of phase by SEM/EDS (at.%)			Composition of phase by Rietveld analysis (at.%)		
	Mg	Ca	Nd	By SEM	By XRD	Mg	Ca	Nd	Mg	Ca	Nd
1	90	5	5	Mg	Mg	100	0	0	100	0	0
				$Mg_2(Ca,Nd)$	$Mg_2(Ca,Nd)$	66.67	31.73	1.6	66.6	31.64	1.7
				$Mg_{41}(Nd,Ca)_5$	$Mg_{41}(Nd,Ca)_5$	88.85	3.83	7.32	88.6	3.85	7.47
2	65	30	5	$Mg_{41}(Nd,Ca)_5$	$Mg_{41}(Nd,Ca)_5$	89.14	2.01	8.85	88.5	1.8	9.7
				$Mg_2(Ca,Nd)$	$Mg_2(Ca,Nd)$	65.57	31.63	2.8	66.6	30.67	2.66
				$Mg_3(Nd,Ca)$	$Mg_3(Nd,Ca)$	75.0	1.0	24.0	75.0	1.0	24.0
3	42	45	13	Mg(Nd,Ca)	Mg(Nd,Ca)	47.62	8.69	43.70	48	8.5	43.5
				$Mg_2(Ca,Nd)$	$Mg_2(Ca,Nd)$	65.46	25.58	8.96	66.6	24.33	9.0
				Ca	Ca	0	100	0	0	100	0
				Mg(Nd,Ca)	Mg(Nd,Ca)	49.13	8.60	42.27	48	8.5	43.5
4	50	30	20	Ca	Ca	0	100	0	0	100	0
				$Mg_2(Ca,Nd)$	$Mg_2(Ca,Nd)$	66.67	24.63	8.7	66.6	24.33	9.0
				Mg(Nd,Ca)	Mg(Nd,Ca)	47.76	7.48	44.76	48	7.5	44.5
5	20	40	40	Ca	Ca	0	100	0	0	100	0
				(Nd)	(Nd)	0	0	100	0	0	100
6	40	20	40	Mg(Nd,Ca)	Mg(Nd,Ca)	47.66	7.50	44.85	48	7	45
				Ca	Ca	0	100	0	0	100	0

3.1 Solubility *study of Mg_2Ca phase*

The binary Mg_2Ca has the C14 type hexagonal structure [22] with *$P6_3/mmc$* (194) space group and the Pearson symbol is hP12. It has a $MgZn_2$ prototype with 12 atoms in the primitive unit cell where Ca atoms in the 4f Wyckoff position and Mg atoms on 2a and 6h

Wyckoff sites. The atomic coordinates are 4f (0.333,0.667,0.562), 2a (0,0,0) and 6h (0.169,0.338,0.250). The EDS spot analysis revealed the substitution of Ca by Nd at constant Mg concentration of 66.67 at. %. Rietveld analysis of the samples annealed at 400°C for four weeks also shows that, Mg_2Ca forms a linear substitutional solid solution where Nd replaces Ca in 4f position and the Mg concentration remains constant. In order to understand this mechanism of substitution and the maximum and minimum solubilities of Nd in Ca, key alloys #1, #2 and #3 were prepared. The XRD patterns of these alloys are presented in Figure 4. The key alloy #1 is in a three-phase region consisting of $Mg+Mg_2Ca+Mg_{41}Nd_5$. Figure 3(a) shows the SEM micrograph of this sample. The solubility of Nd in Mg_2Ca for sample #1 was obtained as 1.6 at.%. This value is consistent with those reported by Fei *et al.* [19], who reported the solubility value as 1.24 at.%. SEM micrograph of the key alloy #2 is presented in Figure 3 (b). This alloy is also located in a three-phase region: $Mg_{41}Nd_5$ + Mg_2Ca+ Mg_3Nd. The solubility of Nd in Mg_2Ca was determined to be 2.8 at.%. Figure 3 (c) shows the BSE image of sample #3. The key alloys #3 and #4 are present in the same triangulation Mg_2Ca+Ca+MgNd and show consistent solubility values. The solubility limit of Nd in Mg_2Ca is found to be 8.56 at. % by SEM and 9.0 at.% by Rietveld analysis and is given by key alloys #3 and #4. The values of unit cell parameters and lattice volume are presented in Table 2.

The characteristics of the unit cell are reduced by replacing Ca with Nd, which has a slightly smaller atomic radius. This is clearly indicated by the shifting of peaks towards higher 2θ values from sample 1 to 3 following the Bragg's Law (Figure 4). In addition, the values of lattice parameters are compared with the standard values of the lattice parameters of Mg_2Ca binary compound taken from Pearson's crystal database [22]. The linear variation of lattice parameters of Mg_2Ca and occupancy of Ca with decreasing concentrations of Ca is presented in Figure 5. Least square approximation was used to establish the relations between unit cell parameters and Ca concentration. The substitution of Ca by Nd is found to be linear obeying the Vegard's Law, thereby clearly indicating the formation of substitutional solid solution. Table 3 describes the refined crystal structure parameters, the occupancies and the reliability factors of all the solid solutions present in the system. The decrease in the value of the reliability factors is also in favour of the well refined unit cell parameters. The coordination spheres and dynamic atomic substitution of Ca by Nd in the 4f Wyckoff position is shown schematically in Figure 6.

Table 2. Actual sample compositions with unit cell parameters, lattice volume and phase composition determined by XRD results.

Sample No.	Actual composition identified by ICP (at.%)			Phase identification	Unit cell parameters and lattice volume		
	Mg	Ca	Nd		*a*(Å)	*c*(Å)	Vol.(Å^3)
1	90	5	5	Mg	3.223	5.219	46.950
				Mg_2(Ca,Nd)	6.24	10.123	341.357
				Mg_{41}(Nd,Ca)$_5$	14.803	10.422	2283.96
2	65	30	5	Mg_{41}(Nd,Ca)$_5$	14.789	10.411	2276.72
				Mg_2(Ca,Nd)	6.228	10.037	333.485
				Mg_3(Nd,Ca)	7.399	7.399	405.060
3	42	45	13	Mg(Nd,Ca)	3.884	3.884	58.592

				$Mg_2(Ca,Nd)$	6.194	10.037	333.485
				Ca	5.479	5.479	164.476
4	50	30	20	Mg(Nd,Ca)	3.884	3.884	58.592
				Ca	5.479	5.479	164.476
				$Mg_2(Ca,Nd)$	6.194	10.037	333.485
5	20	40	40	Mg(Nd,Ca)	3.880	3.880	58.411
				Ca	5.479	5.479	164.476
				(Nd)	3.659	11.796	136.770
6	40	20	40	Mg(Nd,Ca)	3.879	3.879	58.366
				Ca	5.479	5.479	164.476

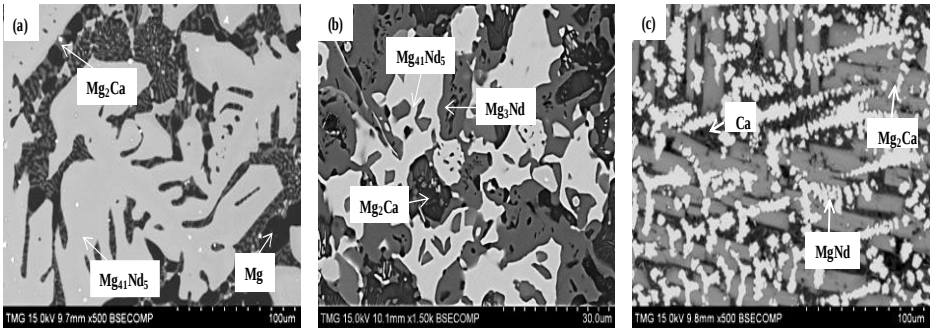

Figure 3. (a-c). BSE images of alloy #1, #2 and #3 all annealed at 400°C for four weeks.

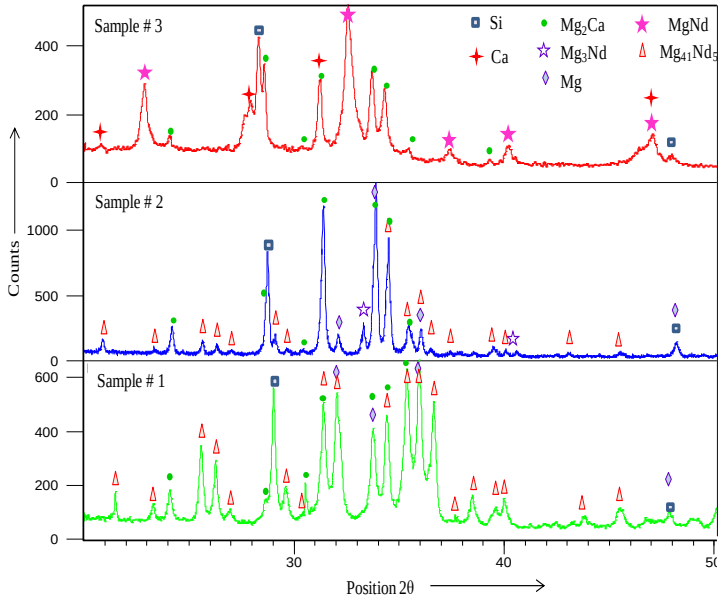

Figure 4. XRD pattern of key alloy #1, #2 and #3 all annealed at 400°C for four weeks.

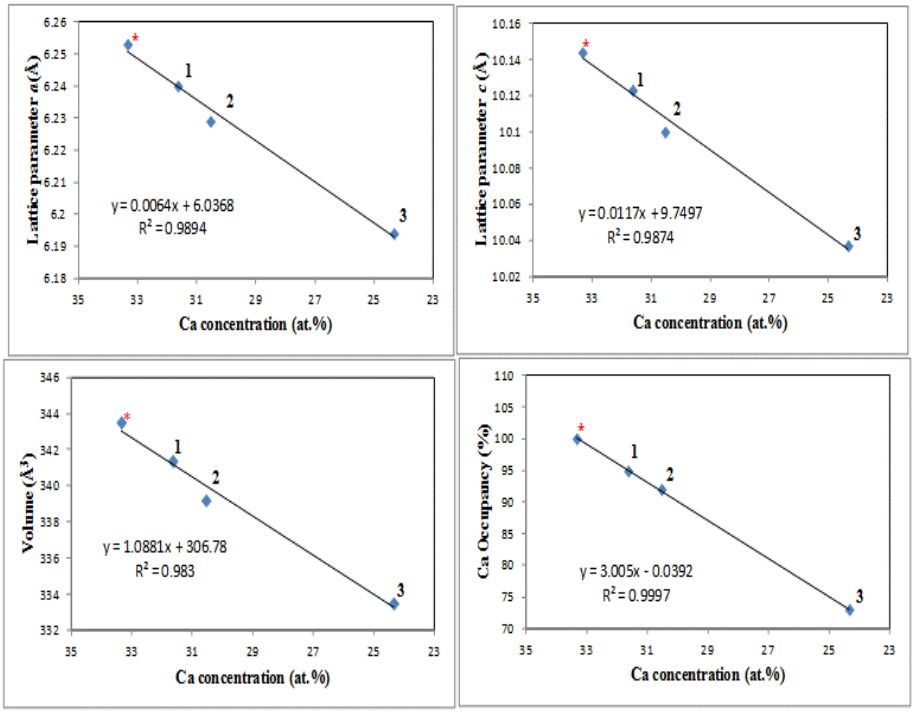

Figure 5. Variation of lattice parameters and occupancy for Mg_2Ca with Ca concentration where progressive substitution of Ca by Nd decreases the cell parameters *a*, *c* and volume and Occupancy of Ca.

* Values obtain by Mg_2Ca binary compound from Pearson's Crystal structure database [21]

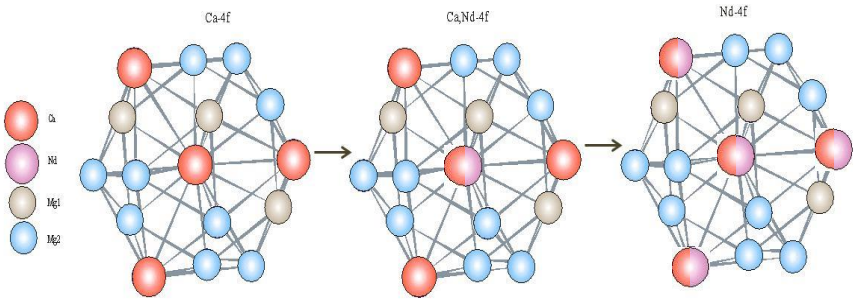

Figure 6. The coordination spheres of dynamic atomic substitution of Ca by Nd in the 4f atomic coordinates

Table 3. Refined crystal structure parameters of the solid solutions.

Sample No.	Phase	Wyckoff position		Occupancy (%)	Reliability Factors*		
					R_e	R_{wp}	*s*
1	$Mg_2(Ca,Nd)$	Mg1	2a	100	11.84	16.68	1.98
		Mg2	6h	100			
		Ca	4f	94.9			
	$Mg_{41}(Nd,Ca)_5$	Mg1	16i	100			
		Mg2	16i	100			
		Mg3	16i	100			
		Mg4	8h	100			
		Mg5	8h	100			
		Mg6	8h	100			
		Nd1	8h	100			
		Mg7	8f	100			
		Mg8	2a	100			
		Nd2	2a	34.4			
2	$Mg_2(Ca,Nd)$	Mg1	2a	100	12.38	13.47	1.18
		Mg2	6h	100			
		Ca	4f	92			
	$Mg_{41}(Nd,Ca)_5$	Mg1	16i	100			
		Mg2	16i	100			
		Mg3	16i	100			
		Mg4	8h	100			
		Mg5	8h	100			
		Mg6	8h	100			
		Nd1	8h	100			
		Mg7	8f	100			
		Mg8	2a	100			
		Nd2	2a	50			
3	$Mg_2(Ca,Nd)$	Mg1	2a	100	11.69	13.25	1.28
		Mg2	6h	100			
		Ca	4f	73			
	Mg(Nd,Ca)	Nd	1b	84			
		Mg	1a	96			
4	$Mg_2(Ca,Nd)$	Mg1	2a	100	15.31	16.46	1.16
		Mg2	6h	100			
		Ca	4f	81			
	Mg(Nd,Ca)	Nd	1b	90			
		Mg	1a	96			
5	Mg(Nd,Ca)	Nd	1b	90	15.25	16.52	1.17
		Mg	1a	96			
6	Mg(Nd,Ca)	Nd	1b	94.7	13.01	21.84	2.82
		Mg	1a	95.5			

*Reliability factors: *s* is the goodness of fit, *Rwp* is the weighted summation of the residuals of the least-squares fit and *Re* is the statistically expected value.

3.2 Solubility study of $Mg_{41}Nd_5$ phase

In the Mg-Nd binary system, $Mg_{41}Nd_5$ is the richest binary compound in Mg content. Like other $Mg_{41}RE_5$ phases, it has a tetragonal structure (tI92-Ce_5Mg_{41} type) [1]. $Mg_{41}Nd_5$ has 92 atoms in the unit cell as presented in Table 2. Key alloy #1 and #2, which were used for the solubility study of Mg_2Ca could also be used for the study of solubility limits of $Mg_{41}Nd_5$.

Similar to Mg_2Ca, $Mg_{41}Nd_5$ also undergoes linear solid substitution, where Ca substitutes Nd in the 2a (0,0,0) position.

The key alloy #1 was determined to be in a three-phase region Mg + Mg_2Ca + $Mg_{41}Nd_5$. The maximum solubility of Ca in $Mg_{41}Nd_5$ is found to be 3.83 at. % by SEM and 3.85 at.% by Rietveld analysis. This value of solubility was found consistent with that of Fei *et al*. [19], who reported the value to be 3.57 at.%. The key alloy #2 also belongs to a three-phase region $Mg_{41}Nd_5$ + Mg_2Ca + Mg_3Nd as discussed previously, yielding a solubility value of Ca of 2.8 at.%. The XRD pattern for the two key samples is shown in Figure 4. In this case, there is a slight shifting of peaks towards lower values of 2θ with the increase in Ca content. This could be explained from the fact that, since Ca atoms are slightly larger than Nd, their substitution results in increasing the interplanar distance, hence resulting in peak shifts towards lower values of 2θ in accordance with Bragg's Law. The values of lattice parameters are presented in Table 2 and their variation with Nd concentration is shown in Figure 7. The dynamic substitution of Nd by Ca in the 2a Wyckoff position is presented in Figure. 8.

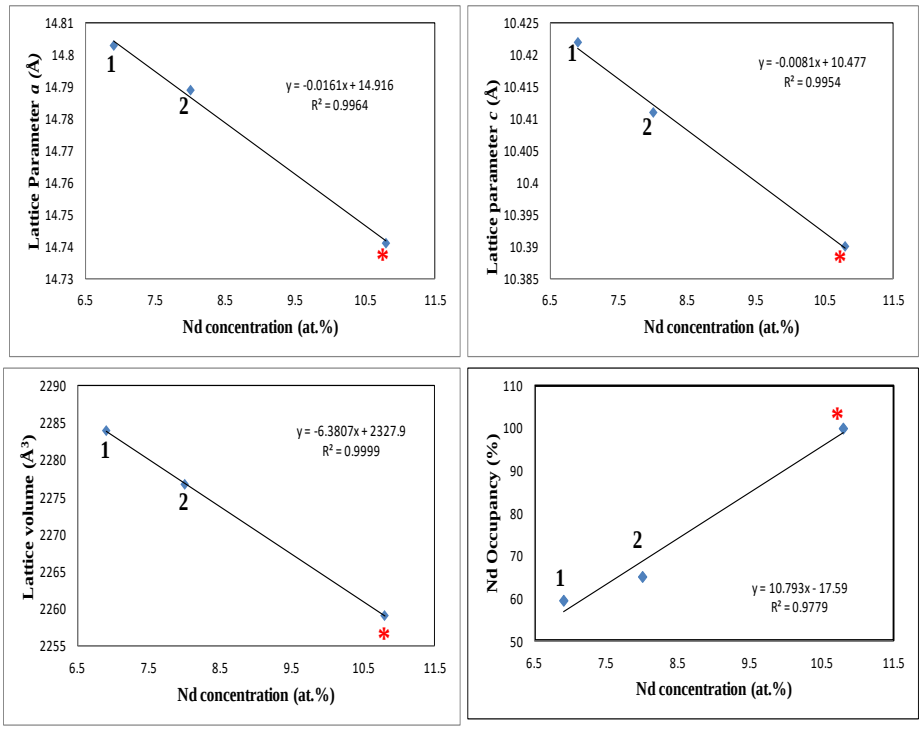

Figure 7. Variation of lattice parameters and occupancy with Nd concentration where progressive substitution of Nd by Ca decreases the cell parameters *a*, *c* and volume and increase the occupancy of Nd.

* Values obtain by $Mg_{41}Nd_5$ binary compound from Pearson's Crystal structure database [21]

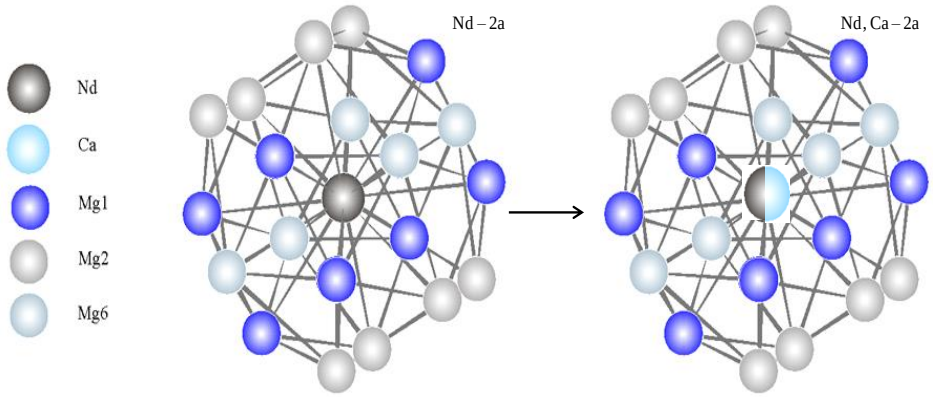

Figure 8. The coordination spheres of dynamic atomic substitution of Nd by Ca in the 2a atomic coordinates

3.3 Solubility study of MgNd phase

The MgNd phase has a ClCs prototype with cubic crystal structure and Pm-3m (221) space group [1]. It has Mg in 1a position with coordinates (0,0,0) and Nd in 1b position with coordinates (0.50,0.50,0.50). This is the only binary phase in this ternary system which undergoes complex substitution, where Ca replaces both Mg of 1a position and Nd of 1b position. Key alloys #4, #5 and #6 were used to study this complex solid solution. Figure 9 shows Rietveld analysis of key alloy #4, #5 and #6 all annealed at 400°C for four weeks.

The key alloy #4 is located in a three-phase region of Mg_2Ca + MgNd + Ca. From this key alloy, the maximum solubility limit of both Nd in Mg_2Ca and Ca in MgNd were established. The maximum solubility limit of Ca in MgNd in this region was found to be 8.6 at. % (Table 1). The key alloy #5 also represents a three-phase region MgNd + Ca + (Nd). This alloy gives the solubility limit of Ca in MgNd to be 6.8 at.% in the Nd rich side of the ternary phase diagram. In addition, the key alloy #6 is in a two-phase region of Ca and MgNd. The solubility of Ca in this region is obtained as 7.5 at. % showing tie-line relationship of the two phases: Ca and MgNd. From the SEM/EDS results and Rietveld analysis of key alloys #4, #5 and #6 (Table 1), it could be verified that with the addition of Ca atoms, the concentrations of both Mg and Nd decrease. Since the atomic size of Ca is larger than both Mg and Nd, there is an increase in volume and lattice parameter *a* with an increase in Ca concentration. The dynamic substitution of Mg and Nd are represented in Figure 10.

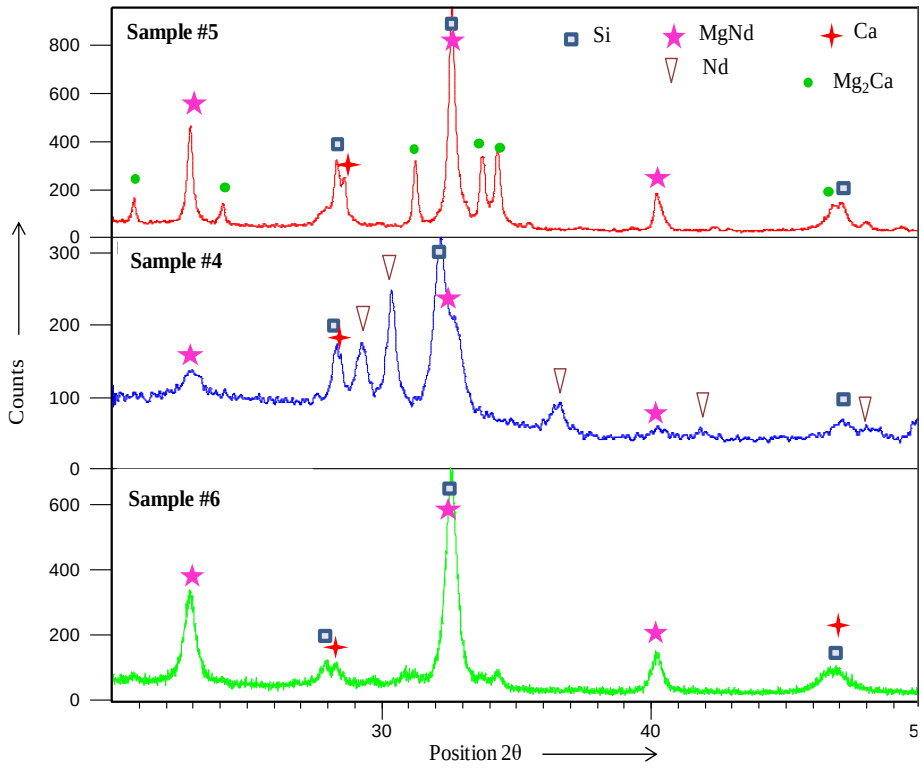

Figure 9. XRD pattern of key alloy #5, #4 and #6 all annealed at 400°C for four weeks

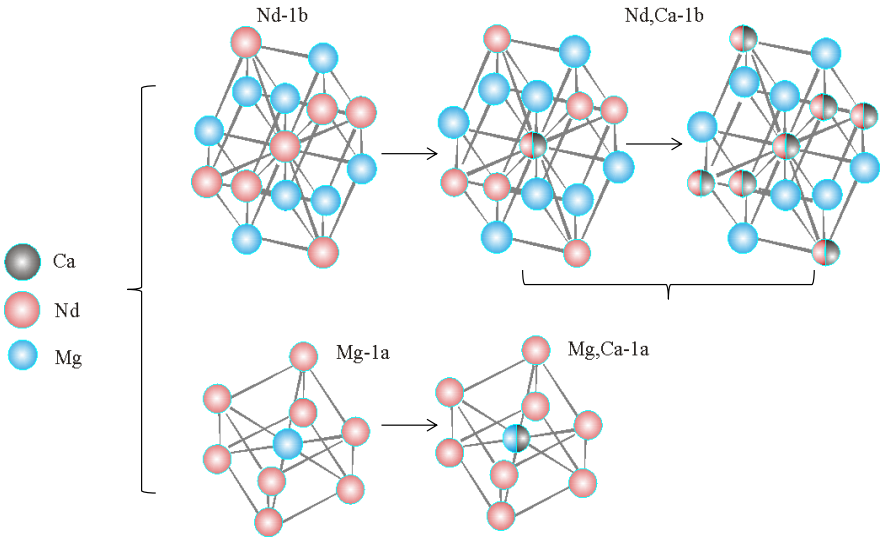

Figure 10. The coordination spheres of dynamic atomic substitution of Ca by Nd with different atomic coordinates

3.4 The Mg_3Nd phase

The Mg_3Nd phase has a BiF_3 prototype with cubic crystal structure and Fd-3m (225) space group [1]. It has Mg1 in 4b position with coordinates (0.50,0.50,0.50), Mg2 in 8c position with coordinates (0.25,0.25,0.25) and Nd in 4a position with coordinates (0,0,0). The phase Mg_3Nd was found to have negligible solubility of Ca in it. For example, in key alloy #2, the solubility of Ca was found to be 1.0 at.% in Mg_3Nd (Table 2), which is within the instrumental error of SEM/EDS. These results are in confirmation with those of Fei *et al*. [19], who found the solubility of Ca in this phase at 0.24 at.%. XRD patterns of key alloy #2 also confirms that there is no shifting of peaks or changes in lattice parameters for this phase. The sliced section of Fourier difference map of Mg_3Nd at all possible atomic coordinates at [0 1 0] plane for key alloy #2 is presented in Figure 11. The Wyckoff position, section and coordinate details are presented in table 4. The Figure 11a shows the Mg1-4b atomic site which was sliced at y = 0.50 level, where the electron density for this position was expected to be maximum. Similarly, the Mg2 and Nd sites were sliced at y = 0.25 (Figure 11b) and y = 0.0 (Figure 11c) levels, respectively. The uniform distribution of electron densities at these positions clearly indicated the absence of any substitution.

Table 4. Wyckoff position, coordinates and slicing levels for Fourier maps of Mg_3Nd

Wyckoff position	**coordinates**			**slicing level**
	x	*y*	*z*	
Mg1-4b	0.50	0.50	0.50	y = 0.50
Mg2-8c	0.25	0.25	0.25	y = 0.25
Nd-4a	0	0	0	y = 0.0

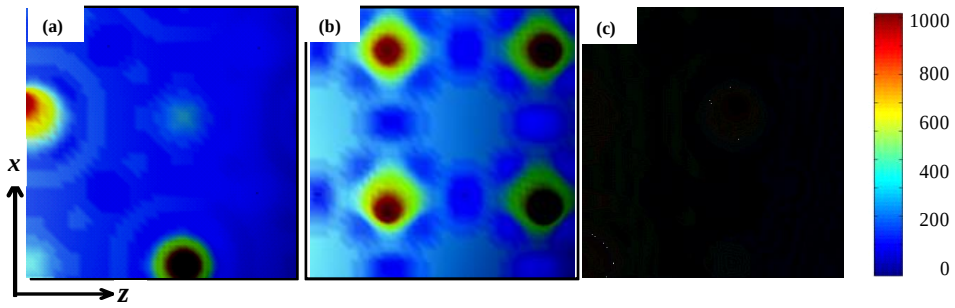

Figure 11. (*a-c*). Fourier maps of Mg_3Nd at (a) Mg1 (b) Mg2 and (c) Nd atomic coordinates.

4. SUMMARY

SEM/EDS and XRD were used to investigate the homogeneity ranges of three binary compounds in the Mg-Ca-Nd system, extending to ternary. The XRD pattern of the six annealed alloys was carried out by Rietveld analysis. In case of Mg_2Ca and $Mg_{41}Nd_5$, linear

substitutions were formed and their lattice parameters were found to obey the Vegard's law. MgNd was found to form complex substitutional solid solution, while Mg_3Nd had negligible solubility. The extended solubilities of the binary compounds as obtained from the SEM/EDS spot analysis were found consistent with those obtained from the Rietveld analysis. The dynamic substitution at different atomic coordinates by the substituting atoms in the coordination spheres is also presented. Based on these results, the solubility limits of these compounds extending to the ternary are established.

ACKNOWLEDGEMENT

The authors would like to acknowledge the financial support provided by NSERC.

REFERENCES

[1] S. Delfino, A. Saccone and R. Ferro, "Phase relationships in the neodymium-magnesium alloy system," *Journal of Metallurgical Transactions A,* vol. 21, p. 2109–2114, 1990.

[2] B.L. Mordike and T. Ebert, "Mg Properties — applications — potential," *Materials Science and Engineering A,* vol. 302, pp. 37–45, 2001.

[3] O. Beffort and Ch. Hausmann, "The Influence of Ca-additions on the Mechanical Properties of T300-C-Fibre/Mg (Al) Metal Matrix Composites," *Mg Alloys and their Applications,* pp. 215–220, 2000.

[4] Y.N. Zhang, X. D. Liu, Z. Altounian and M. Medraj, "Coherent nano-scale ternary precipitates in crystallized $Ca_4Mg_{72}Zn_{24}$ metallic glass," *Scripta Materialia,* vol. 68, p. 647-650, 2013.

[5] Y.N. Zhang, D. Kevorkov, F. Bridier and M. Medraj, "Experimental investigation of the Ca-Mg-Zn system using diffusion couples and key alloys," *Journal of Science and Technology of Advanced Materials,* vol. 12, p.1-13, 2011.

[6] A. A. Luo, "Recent Mg Alloys Development for Elevated Temperature Application," *International Materials Review,* vol. 49, pp. 13-30, 2004.

[7] B.S. You, W.W. Park and I. S. Chung, "The effect of Ca additions on the oxidation behavior in Mg alloys," *Scripta Materialia,* vol. 42, pp. 1089–1094, 2000.

[8] I. Polmear, Ed., *Light Alloys from Traditional Alloys to Nano-crystals*. Butterworth-Heinemann, Oxford, UK 2006.

[9] H. Watari, "Japanese Science and Technology Quarterly Report," 2006.

[10] Y.F. Zheng, X.N. Gu, Y. L. Xi and D.L. Chai, "In vitro degradation and cytotoxicity of Mg/Ca composites produced by powder metallurgy," *Acta Biomateriala,* vol. 6, pp. 1783- 91, 2010.

[11] W. Yizao, X Guangyao, L. Honglin, H. Fang, H. Yuan and Z. Xiaoshong, "Preparation and characterization of a new biomedical Mg–Ca alloy," *Materials and Design,* vol. 29, pp. 2034–37, 2008.

[12] L. Zijian, G Xunan, L. Siquan and Z. Yufeng, "The development of binary Mg–Ca alloys for use as biodegradable materials within bone," *Biomaterials,* vol. 29, pp. 1329- 1344, 2008.

[13] I. Antoniac and M. Dinu, "Microstructural and Mechanical Features of Mg-Ca Alloys," in *3rd International Conference on E-Health and Bioengineering,* 2011.

[14] P.J. Li, B. Tang and E.G.Kandalova, "Microstructure and properties of AZ91D alloy with Ca additions," *Journal of materials,* vol. 59, p. 671−675, 2005.

[15] Z. Jinwang, W. Shebin, Z. Junyuan, Z. Jinling and X. Bingshe, "Effects of Nd on Microstructures and Mechanical Properties of AM60 Magnesium Alloy in Vacuum Melting," *Rare Metal Materials and Engineering,* vol. 38, p. 1141−45, 2009.

[16] S. Gorsse, C.R. Hutchinson, B. Chevalier and J.F. Nie, "A thermodynamic assessment of the Mg–Nd binary system using random solution and associate models for the liquid phase," *Journal of Alloys and Compounds,* vol. 392, pp. 253–262, 2005.

[17] F.V. Fanjul, S. Srimanosaowapak, K.R. McNee, G.W. Greenwood and H. Jones, "The effect of Nd substitution for mischmetal on creep performance of Mg-2.5 RE-0.35 Zn-0.3 Mn-0.03 Zr alloy," *Zeitschrift fuer Metallkunde,* vol. 94, pp. 25-29, 2003.

[18] J.M. Seitz, R. Eifler, J. Stahl, M. Kietzmann and W. Bach, "Characterization of MgNd2 alloy for potential applications in bio-resorb able implantable devices," *Acta Biomaterialia,* pp. 1-13, 2012.

[19] H.Fei, L.Liu, H. Bo, L. Zeng and C. Chen, "Phase equilibria in Mg-rich corner of Mg−Ca−RE (RE=Gd, Nd) systems at 400 °C," *Transactions of Nonferrous Metals Society of China,* vol. 23, p. 881−888, 2013.

[20] A. Ulrich, N. Ott, A. Tournier-Fillon, N. Homazava and P. Schmutz, "Investigation of corrosion behavior of biodegradable magnesium alloys using an online-micro-flow capillary flow injection inductively coupled plasma mass spectrometry setup with electrochemical control," *Spectrochimica Acta Part B,* vol. 66, pp. 536–45, 2011.

[21] F. Witte, V. Kaese, H. Haferkamp, E. Switzer, A. MeyerLindenberg, C. J. Wirth and H. Windhagen, "In vivo corrosion of four magnesium alloys and the associated bone response " *Biomaterials,* vol. 26, pp. 3557–63, 2005.

[22] H. Putz, K. Brandenburg, Pearson's Crystal Data, Crystal Structure Database for Inorganic Compounds, CD-ROM software version 1.3.

Biographies

Dr. Yogesh Iyer Murthy pursued his B.E. (Civil Engineering) from DSCE, Bangaluru and M.E. (Structural Engineering) from SGSITS, Indore. He has worked with L&T ECC as Sr. Bridge Engineer (Chennai Division) and has five years of industrial experience before coming into the academics. He has served various engineering colleges for nearly 12 years teaching UG and PG courses in Civil/Structural engineering and has 2.5 years of international R&D experience as research assistant at the thermodynamics of materials group (TMG), Department of Mechanical and Industrial Engineering, Concordia University, Montreal, Canada. Mr. Murthy has filed for three patents on newer materials in construction industry.

Dr. Abhishek Kumar pursued his B.Tech. (Industrial and Production Engineering) from MIET, Meerut and M.Tech. (Material Science) from MNNIT, Allahabad. He then obtained his PhD degree from IIT Roorkee in the field of Microwave Absorbing Materials in the year 2014. The major areas of his research interest include mechanical behavior of materials, microwave absorbing coatings, dispersed polymers, nano materials and high entropy alloys. He is serving as a reviewer in many reputed journals. Dr. Abhishek has nearly 15 years of teaching experience.

Dr. Sumit Gandhi presently works as an Associate Professor and Head in the Department of Civil Engineering at JUET Guna MP, India. Prior to this he has completed his Ph.D from MNNIT, Allahabad in 2009 in the field of Hydraulic Engineering. He has completed M.Tech from MNNIT Allahabad in 2004 and B.Tech (Civil Engineering) from NMU Jalgaon in 2001. The major areas of his research includes corrugated bed flow, flow over spillways and concrete technology. He is associated with many renowned International Journals as reviewer/editorial board member; and reviewed many research articles and book chapters. He has nearly 15 years of teaching and research experience and also published book & research papers in various journals of repute. Dr. Gandhi has filed two patents.

Woven Fabric for Protection against Stabbing

[1] Sahil Kashyap, [2]Vivek Kumar, [3]A.K. Upadhyay, [4]K.K. Shukla

[1,2,3,4]Department of Applied Mechanics, Motilal Nehru National Institute of Technology, Allahabad, India

[1]sahilkashyap.nr@gmail.com,[2]vivekmnnit01@gmail.com,[3]ashutosh@mnnit.ac.in

[4]kkshukla@mnnit.ac.in

Abstract

Today's law enforcement personnel are regularly spotted with body protection vests. These vests assist them in coping with a variety of threats like from small firearms and others originating from the edge of a sharp metal piece. Light weight and ability to offer better mobility to the wearer, have made soft body armour a preferred choice. The work here presents a numerical study of low velocity impact response on one such soft body armour, prepared as a woven fabric. A multi-layered dimension-wise graded woven fabric is developed using CAD software SolidWorks 2020 and its performance against stab threats is investigated using impact simulations on commercially available FE tool ABAQUS CAE 2019. The investigation involved subjecting the fabric to the standardized energy level E1 (24J) - defined as per the National institute of justice (NIJ) standard 0115 - for a range of attack angles and observing dissipation of energy brought in by the impactor into different forms. The material for yarns is Kevlar 29 while the impactor is considered as a perfect rigid body. There are *three* key observations: *first*, in case of oblique angle impacts, stress and strain distributions are observed to be asymmetric as compared to normal impacts and with increase in obliquity, tendency of yarn slippage increased. *Second*, for energy dissipation, at higher oblique angles, lower plastic dissipation of energy is observed whereas for frictional energy dissipation, higher oblique angles resulted in higher frictional energy dissipation. *Third*, the frictional dissipation energy has a non-linear relationship with inter-yarn coefficient of friction. The simulation depicted that the frictional dissipation energy rose with smaller μ, reached a peak value, in this case, at $\mu = 0.45$, and then decreased with further increase in μ. This is attributed to the fact that high inter-yarn friction could lead to premature yarn breakage, reducing the energy absorption capacity of the fabric. This highlights the importance of administering the inter-yarn coefficient of friction, especially for refining the energy dissipation.

Keywords. Graded woven fabric, Body protection vest, Low-velocity impact, NIJ standard 0115.00, ABAQUS/Explicit

1. INTRODUCTION

Wars have been around since the beginning of the humankind, trying to protect oneself and to keep others at bay, humans looked towards weapons. Initially the weapons were made from wood clay and stones, but as the time progressed and other materials started to surface,

humans started using them in upgrading their weapons like after discovery of metals, the spearheads and arrowheads which were made from stones were upgraded to one's made from metals, similar upgradation happened throughout. With wars and weapons evolving, the need for a body protection shield was felt.

Initial body protection clothing was made from basic materials like wood, clay etc., it all changed once the metals were discovered. With properties like malleability, the metals could be rolled and hammered into body armour suits which provided decent protection to the wearer. It all again changed when gunpowder was discovered, all the earlier developments made for protection against threats like swords, spear and arrows were left useless against these new high-speed firearms. Now the body protection industry again pivoted, the armour developed were in shape of a vest which supplemented the protection by guarding the ribcage and back, by a solid metal plate. This continued till the 1970's until p-aramid materials like Kevlar were developed. These newly developed synthetic fibres showed strength to weight ratio 4-5 times higher than that of steel. So, because of all these properties, also coupled with light weight, these became an epicentre of body protection research industry(Nayak *et al.*, 2017).

Protection clothing can be classified in 2 categories, hard body armour and soft body armour. Hard body armours are supplemented using metal or other ceramic material plates, which comprise different piles in protective clothing. They are used by personnel in operations for protection where high-speed high-calibre bullets are involved. These are bulky and hinder the wearer's mobility. On the other hand, soft body armour is developed by bringing together different plies formed of p-aramid fabric, making it light and comfortable for the wearer, these soft body protection vests compliment mobility of the person wearing it. Police personnel, prison guards etc., prefer these soft armours against threats from small firearms like handguns or from any edged object. Soft body armour can be developed using various techniques like knitted, woven, non-woven etc, and each technique can be implemented with help of different patterns. The study here focuses on stab resistant behaviour of one such soft body armour prepared as woven fabric. Woven fabrics are widely accepted for body protection clothing. Woven fabric provides, when compared to non-woven and knitted structure, better packing of yarns. With their advantages, they also possess certain shortcomings, as they are formed due to interlacing arrangement of warp and weft yarns because of this arrangement crimp is formed. This crimp is the wavy nature of yarns, because of this crimp, yarns develop buckling tendencies when put under compressive loads such as during the action of stabbing, it may happen that the yarns might slip during such an event and can result in injury to wearer. This problem of slipping can be overcome by tightly stacking the yarns into the weave, when the weave is finer it improves the stab resistance behaviour but also can't be too tight as flexibility will be compromised. Soft body armour prepared as woven fabric have shown to be implemented with many techniques like with modification of yarn surface and using different weave patterns (Usman Javaid *et al.*, 2019; Hameed *et al.*, 2021), but Abhijit majumdar *et al*., (2014) research work focused on the impact performance of soft composite with Kevlar-STF. It was noted that the STF coating improved the energy absorption of the soft composite. Similar findings were made by M. J Decker et al. (2007), this research work focused on Kevlar fabric and nylon cloth, impregnated with shear thickening fluid of equal area density for stab resistance. The standard drop tower test was performed and it was noted that the STF addition significantly boosted the stab resistant performance of fabric. Rajesh Mishra *et al*. (2014), prepared a

model of woven Fabric in SolidWorks and then simulated the impact on Ansys workbench, the parameters of deformation, strain and stress were noted on the fabric it was observed that the deformation in the 3D Kevlar epoxy composite was maximum when compared to others. The literature available on protection against threats be it low or high velocity, clearly indicates the body protection clothing available for protection against ballistic impacts may not necessarily perform when subjected to stab threats or vice versa (Nayak *et al*., 2017).

After going through the literature, factor influencing stab resistant behaviour can be listed under following categories as below.

a. Impactor related characteristics like geometry, size, point of impact, angle of impact etc.,
b. Fabric related characteristics like material property, friction, weave pattern, fabric density etc.

Upon going through the literature, it was observed that most of the research carried out related to this low velocity impact study, has been done with impactor positioned to attack at perfectly normal to the target area, but in actual scenario the probability of perfect normal impact is very slim. Also, it was noted that even though a lot of research is available on 2D fabric weaves but the performance a multi-layered fabric is yet to be explored in details. In the study here, an attempt has been made to address these, the study focuses on development of a multi-layered plain-woven fabric and a P1 knife impactor according to the National institute of Justice (NIJ) standard 0115.00, and investigation of the stab resistant behaviour of the prepared woven fabric when subjected to oblique angles of attack by the knife at E1 energy level according to the NIJ standard 0115.00. It was also noted that friction between yarn-yarn and knife-yarn plays an important role in dissipation of kinetic energy brought in by the impactor, an attempt has been made here to study the change in frictional energy dissipation by varying coefficient of friction in model.

2. PREPARATION OF MODEL

2.1 Preparation of geometry of woven fabric and knife

The geometry of both the woven fabric and knife were prepared on commercially available CAD tool SolidWorks 2020. Impactor was developed in accordance with the specifications provided in NIJ standard 0115.00 for single cutting-edge impactor (i.e., P1 type).

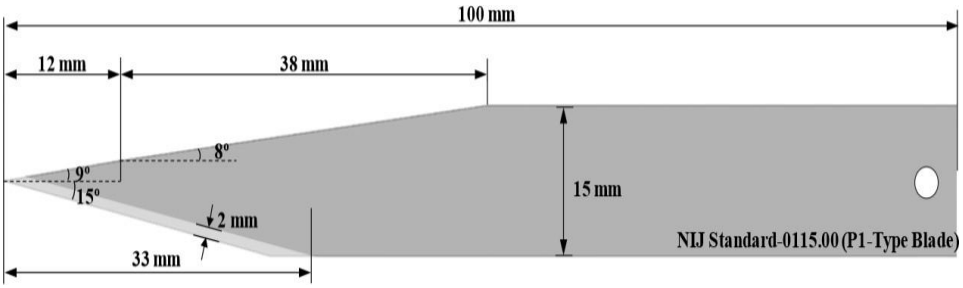

Figure 1. P1 type impactor

Preparation of woven fabric was done with fabric thread density of 7.5 per centimetres for both weft and wrap and linear density is taken as 158 tex. For calculation of strength

parameters, a single yarn is taken and tested experimentally. It is important to note that when the yarn is tested it has a circular shaped cross section but when this same yarn is weaved into a fabric the compression forces make the cross section into lenticular shaped. For this study same arcs of curvature are assumed for lenticular cross section. All geometrical parameters are calculated using equations.

$$L = \frac{2}{thread\ density} \tag{1}$$

$$b = \frac{Fabric\ thickness}{4} \tag{2}$$

$$x = \frac{L}{4} \tag{3}$$

$$R_m = \frac{x^2 + y^2}{2b} \tag{4}$$

$$R_i = R_m - b \tag{5}$$

$$a = (2bR_i - b^2)^{1/2} \tag{6}$$

Where L is yarn path wavelength, Rm is radius of the arc of yarn path, Ri is radius of the arc of yarn cross section, a is half of the width and b is half of the height of cross section of yarn. Based on equation 1- 6 following geometrical parameters are calculated for development of woven fabric geometry.

Table 1. Geometrical parameters for woven fabric development

Layer no.	L	b	x	R_m	R_i	a
1	6	0.255	1.50	4.4400	4.1850	1.40
2	6	0.235	1.50	4.8129	4.5779	1.40
3	6	0.215	1.50	5.2383	5.0233	1.40
4	6	0.195	1.50	5.7707	5.5757	1.40
5	6	0.175	1.50	6.4468	6.2718	1.40

Kevlar 29 is considered for the material assignment of the yarns with properties listed in Table 3. The yarns are modelled with the assumption that they are comprised of homogenous material and rather than being orthotropic, they are considered to be isotropic in nature, the reason behind this is that when energy absorption was considered, there was only a slight difference due to orthotropic nature and this difference was incomparable with other energies being absorbed upon impact.

2.2 Description of Finite element model

The geometric model created as described above, was imported into ABAQUS CAE 2019 for further analysis. The problem was solved using the explicit dynamic solver of the ABAQUS 2019. The fabric (yarns) was meshed with the help of a user defined mesh (Fig 4) with 8 node brick C3D8R type elements whereas the knife was considered as a discrete solid and was meshed using R3D4.

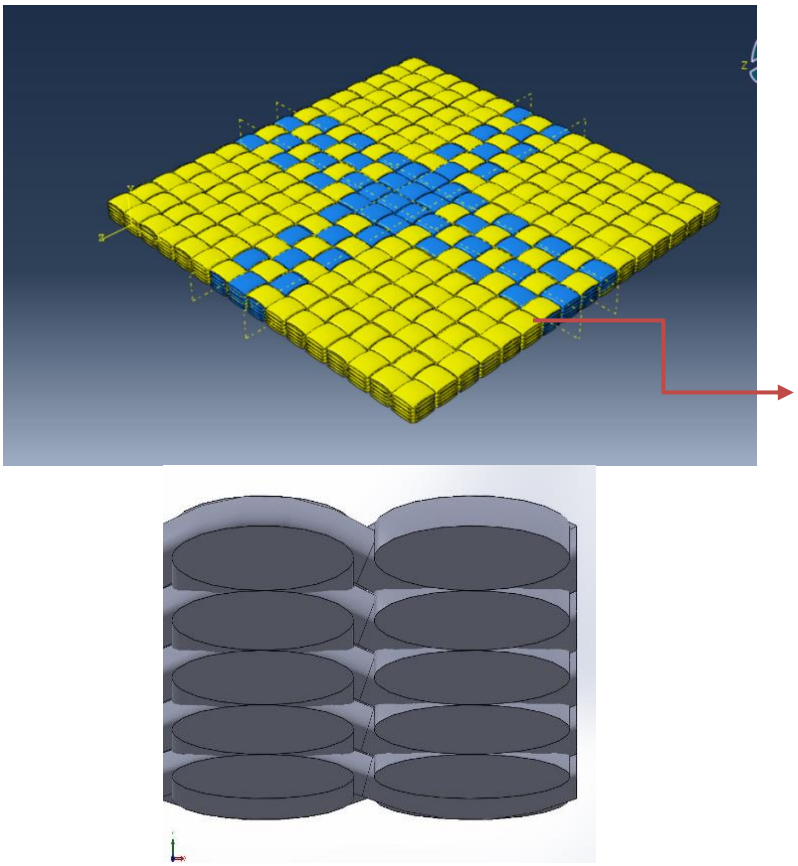

Figure 2. Iso-metric view and cross section of prepared Woven fabric

A) Impactor

It's important to note that this study is carried out at E1 energy level according to the NIJ standard 0115.00, which is 24 ± 0.5 Joules. Now the kinetic energy can be considered as

$$K.E = 0.5\, m\, V^2 \qquad (7)$$

Where m is the mass of the P1 type knife used here, which is considered to be 1.8 kgs and V is magnitude of velocity, which upon simple calculation comes up to be nearly 5.164 m/s.The knife is assumed to be rigid solid and since this analysis involves oblique impacts, the velocity is defined as a vector as shown below

$$\vec{V} = V_x\hat{\imath} + V_y\hat{\jmath} + V_z\hat{k} \qquad (8)$$

Where V_x, V_y and V_z are components in x, y and z axis respectively.

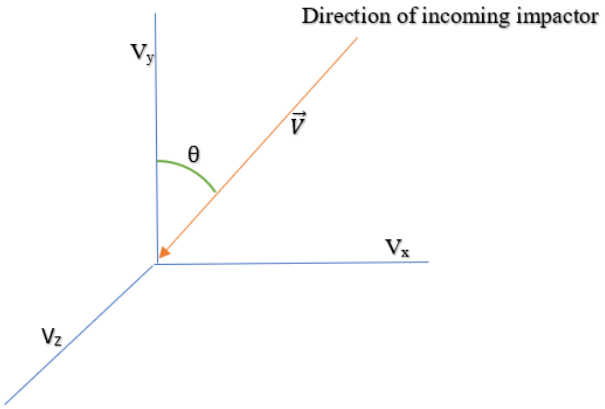

Figure 3. Orientation of components of velocity vector

Where θ is angle of obliquity, based on above orientation, values of components of velocity for different oblique angles of impact is listed below

Table 2. Components of velocity of impactor

θ	**V_x**	**V_y**	**V_z**	**$\|V\|$**
0°	0	-5163.98	0	5163.98
15°	0	-4988.02	1336.54	5163.98
30°	0	-4472.11	2581.99	5163.98
45°	0	-3651.49	3651.49	5163.98

*All values are in mm/s

(B) Fabric

Friction plays an important role in energy dissipation in these kinds of woven fabrics, two kinds of friction are considered in the above model, 1 between yarn and yarn the other being between yarn and knife surface, this study also carries out an investigation with variation of coefficient of friction to see how the energy absorption is affected by this variation. This study proceeds further by ignoring inter fibre friction because, as generally yarns are made of multiple fibres but in this study the yarn is considered to be made up of a continuous and isotropic material, also the inter fiber friction contributes to very negligible amount of energy being absorbed, so it is not considered here. For plastic behaviour of yarns and failure modelling, Johnson-cook model is considered after ignoring the effects of temperature softening on material with total elongation being 4%, along with tensile strength of 3.5 GPa taken as a failure criteria for a yarn. All parameters of J-c model are listed in table 3.

Table 3. Material properties

volumetric density	1440 kg/m^3
Young's modulus	93.5 GPa

Poisson ratio	0.35
A	3500 MPa
B	3560 MPa
n	1
m	0
Melting temperature	0 K
Transition temperature	0 K
Fracture strain	0.04
Stress triaxiality	-0.333
Strain rate	2000 s^{-1}
Fracture energy	74.674 N/mm

To facilitate the friction between yarn-yarn and knife-yarn, a penalty-based contact algorithm is provided by ABAQUS/Explicit finite element package and effect of friction on stabbing performance of woven fabric using analysed by different coefficient of friction. Referring to boundary condition of the problem, all degrees of freedom are constrained at all the four edges of the fabric and a fixed edge boundary condition is modelled, in ABAQUS this is done using encastre condition.

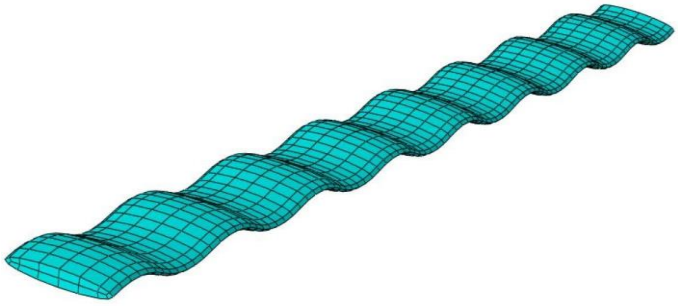

.

Figure 4. Represents the meshed view of yarn with C3D8R element

3. RESULTS AND DISCUSSIONS

3.1 Effects of obliquity of stabbing impact on woven fabric

When knife is attacked normal to fabric, the deformation shape XYZ, surrounding the impact area stay symmetrically. This deformation leads to strains which in turn leads to stresses, it's easy to conclude both stresses and strains in case of a normal impact would be same on both the sides i.e., XY and YZ sides. But in case of angle of attack being at any oblique angle the deformation shape becomes X'Y'Z'. It can be noted that X has moved to X', Y to Y' and Z to Z', it can be easily understood that with high oblique angle the asymmetry will also be higher.

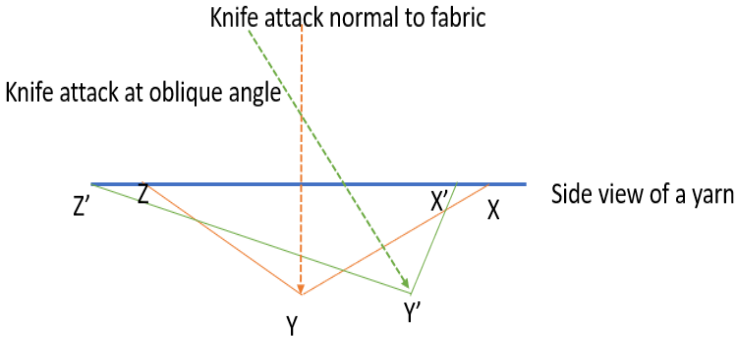

Figure 5. Comparison of knife attack on a yarn at normal and oblique angles of impact

In case of a normal impact, strains on both sides will be symmetric hence would cause a normal reaction to pass through knifes reference axis. This will not be the case when angle of attack is anything expect normal, because with obliquity some asymmetry in deformation will be observed. It can be understood that $\varepsilon_{X'Y'} < \varepsilon_{Y'Z'}$, where ε represents strain. This translates to a stress asymmetry with side Y'Z' experiencing higher stress when compared to X'Y', finally this induces a non-uniform force which is experienced by the knife.

(A) Effect on displacement (slippage) of warp and weft yarns with changing θ

The investigation performed here focuses on considering different angles of attack i.e., θ, to study the slipping of warp and weft fibres. This was done by selecting surrounding nodes of both warp and weft yarns in close proximity of impact zone and tracing their path throughout the simulation. The results obtained (Figure 6) show that with higher obliquity angle θ the slipping increases, as discussed earlier when the impactor impacts the yarn vertically, the strains generated in the surrounding of the impact point are symmetric and the reaction force experienced by the knife is along its axis of travel, but when the impact angle changes the strains are no longer symmetric, which create different stresses in nearby by region.

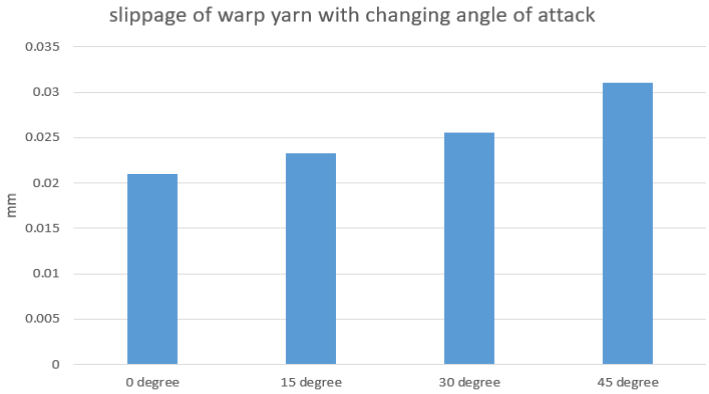

Figure 6(a). Slippage of warp and weft yarns

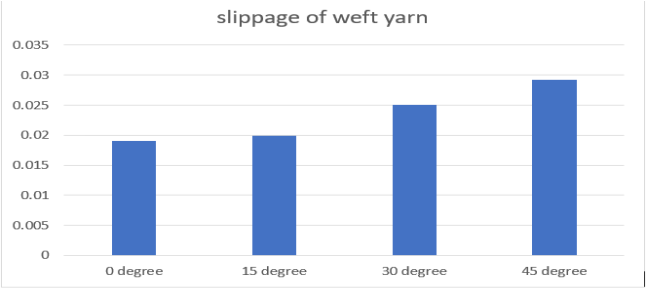

. Figure 6 (b). Slippage of warp and weft yarns

Moreover, initially the primary yarns do not perforate immediately they try to move in the direction of the projectile. This creates a tendency in the secondary yarns present underneath the primary ones to slip, which is countered by the presence of friction between the yarns. As the angle of attack that is the angle of obliquity is increased, the strain and stress distribution's asymmetric character increases, so at high oblique angles knife drives yarns without perforating, causing them to slip by overcoming inter-yarn friction, and hence it can be concluded that, if obliquity is increased the tendency to slip will also increase.

(B) Effects on energy dissipation

The kinetic energy brought in by the impactor has to be dissipated as soon as possible to improve performance of the fabric, dissipation of energy is a phenomenon which involves a lot of variables. Here energy dissipation in fabric is mainly categorised as Elastic Strain energy absorbed by the fabric, the plastic strain dissipated and energy dissipated because of friction.

- ***Effect of elastic strain energy absorbed and plastic energy dissipated***

During impact the primary yarns experience a stretching because of this stretching elastic strain energy starts getting absorbed by the fabric, when this phenomenon continues there comes a point when the yarns enter plastic deformation and depending upon the material property, the fracture happens. The amount of strain energy stored within the fabric is majorly decided by the number of yarns participating in the impact.

It can be noted that plastic energy dissipation in the beginning would be zero (Fig 7) it would continue to be zero for some time, until the yarn enters plastic deformation zone once the yarn enters plastic deformation zone the plastic energy dissipation starts rising it will continue to rise until the yarns fail. Upon failure the plastic energy becomes constant. It can be noted that the plastic energy dissipation is lowest for high oblique angles like 30° and 45° this is because plastic energy dissipation will be higher if the impact involves more number of yarn in impact, as more yarn to store energy, as discussed in the previous section where the displacement of warp and weft yarn is shown, it was evident that at impact angle of 45°, the maximum displacement (slippage) of warp and weft occurred, so those yarns got away from the zone and were not strained till later and hence the plastic dissipation is lower. Similar reasoning can be applied for others to understand the trend of graph (Fig 7).

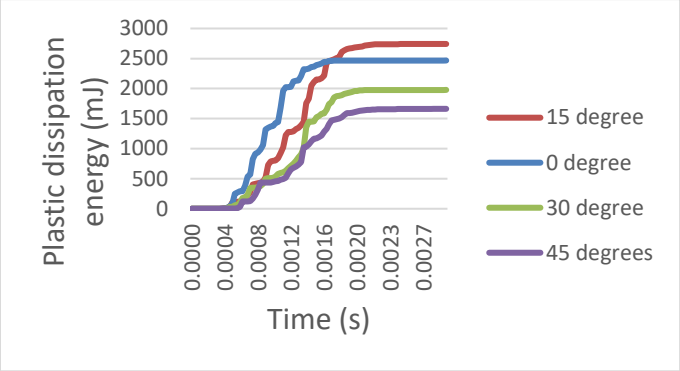

Figure 7. comparison of plastic dissipation at various θ

- ***Effect of frictional dissipation energy***

When the impact occurs in the primary yarns longitudinal wave fronts and transverse wave fronts are generated longitudinal wave travel within that same plane and transverse wave travel out of the plane i.e., in the direction of impactor. Because woven fabric is formed due to interlacing arrangements of yarns at crossovers, frictional contact is higher and in ABAQUS, tangential contact and hard normal contact properties are given in interaction section to accommodate this. Majorly in this model two types of friction are responsible for frictional energy dissipation

a) yarn and yarn and b) between yarn and impactor.

When angle of attack θ is 0° the chances of impactor sliding over yarn are very slim, but when the obliquity is introduced this changes. In the plot (Fig 8) it can be seen that for 45° the frictional energy dissipation is maximum this can be attributed to the fact that was explained earlier frictional energy depends upon yarn-to-yarn friction and also on yarn to and knife fiction so as 45° impact involves slipping of yarn at maximum, this shows the friction induced will be higher that is why frictional energy dissipation can be seen as maximum.

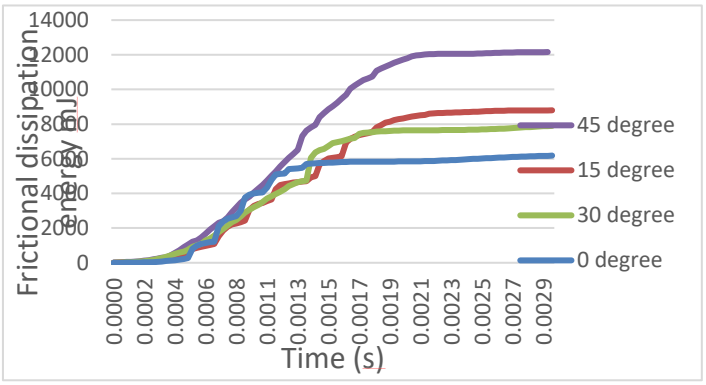

Figure 8. Comparison of frictional energy dissipation at various θ

(C) Knife travel and penetration into the fabric

The knife travel and penetration into the fabric is the most important parameter in determining the stab resistant property of the fabric. The knife travel here was calculated by selecting a node at the tip of the knife and plotting its journey through the entire simulation process. Knife penetration is a complex phenomenon and is dependent on a lot of factors like the energy dissipation, yarn slippage discussed in previous sections.

Because of the minimum dissipation of energy in the case of 45°, it is quite evident that fabrics performance at an obliquity of 45° impact of the knife is the poorest. The results obtained (fig 9) after plotting of the curve are in accordance with our hypothesis.

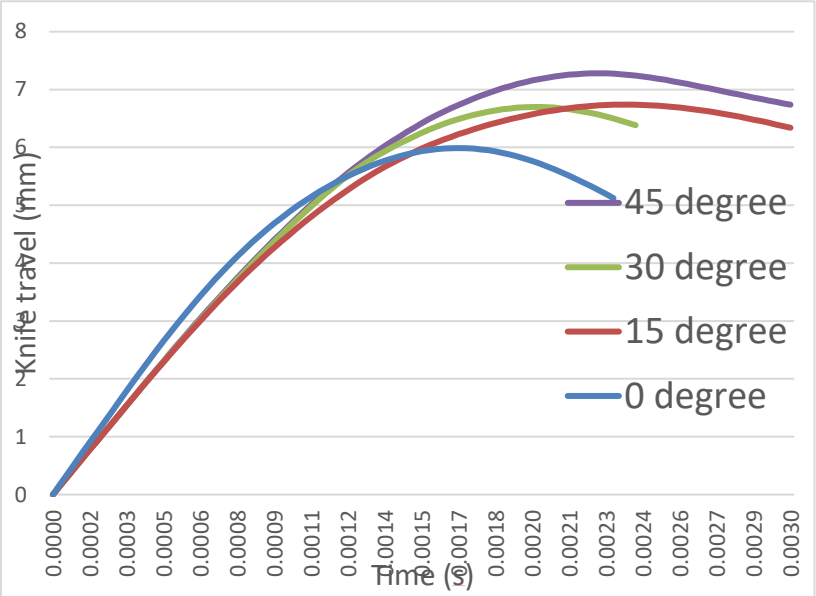

Figure 9. Comparison of Knife travel

3.2 Effect of coefficient of friction on energy dissipated by fabric

The performance of a protective clothing is substantially affected by its frictional behaviour. Factors influencing textile friction behaviour can be divided into fiber friction, yarn friction and fabric friction. As discussed earlier the fibre friction is not considered here, the other two factors are explored here.

Upon impact in woven fabric two kinds of wavefronts are generated longitudinal and transverse, the longitudinal wavefront is the fast-travelling wavefront, travelling in primary yarns, is responsible for stretching of yarns and it travels away from the impact zone i.e. within the plane, at a wave speed $\sqrt{(E/\mathrm{p})}$, where E is young's modulus and p is the density of material, it can be noted it is independent of speed of the impactor whereas the transverse wavefront travels along the projectile, it is the slower wavefront and takes impact out of the plane. Now as woven fabric is formed because of interlacing arrangement of the yarns, there are crossover regions present, where warp and weft yarns overlap, this is where inter yarn

friction comes into play majorly. When the impact occurs, primary yarns are stretched and tensile stresses are induced in them, at crossover region these interact with secondary yarns, present orthogonal to these, secondary yarns are deformed and are subjected to stresses and strains, which results in stress distribution to a large extent and more energy is dissipated. In ABAQUS tangential contact and hard normal contact properties are given in interaction section to accommodate this frictional contact. This study used the developed woven fabric with impactor positioned at θ=0° for observing the changes in frictional dissipation energy when coefficient of friction is varied between yarn-yarn. The simulation results (Fig 10) shows that initially frictional dissipation energy rose with smaller μ, reached a peak value and then came down with further increase in μ. This can be attributed to the fact that, high inter-yarn friction can lead to premature yarn breakdown, reducing the energy absorption capacity of the fabric. So as a result, good control of inter-yarn frictional coefficient is crucial to improve the energy dissipation capability of the fabric. When the μ between yarns surpasses a certain level, the energy dissipated by the fabric will come down, in this case the peak value for max dissipation is $\mu = 0.45$

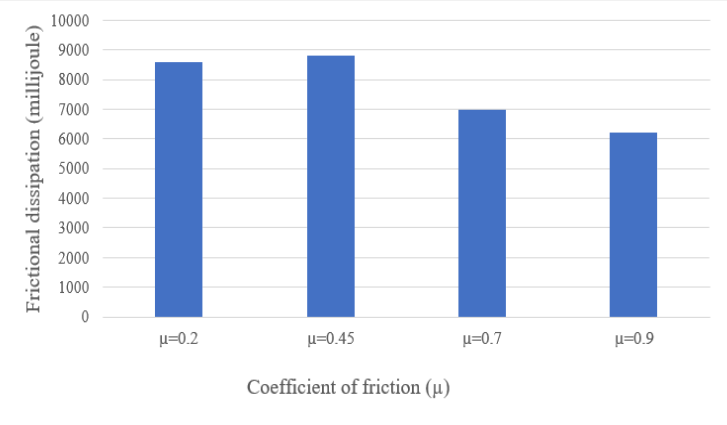

Figure 10. Frictional dissipation for different value of coefficient of friction

4. CONCLUSION

The stab resistant behaviour of the fabric was simulated and studied for effects of impact at oblique angles, the material assigned during simulation was Kevlar 29 for yarns, while impactor was considered as rigid. Along with effects at oblique angle impacts, the stab resistant behaviour of the fabric was also closely observed with variation of inter yarn coefficient of friction. It was noted that in case of oblique angle impact, stresses and strains were not symmetrically distributed as they were in case of normal impact. For different angles of impact, the phenomena of warp and weft yarn slippage was examined, it was noted that higher oblique angles caused higher slippage. The energy coming in through the impactor was considered as kinetic and its dissipation was mainly observed as elastic strain energy absorbed, plastic energy dissipation along with frictional energy dissipation. It was noted that for higher obliques angles plastic dissipation of energy was lower whereas for frictional energy dissipation, it was seen that for high oblique angles frictional energy

dissipation was higher. It was also concluded that among all the cases of oblique angle impacts simulated here, highest knife travel within the fabric i.e., penetration, was observed at θ=45°, yarn slippage was considered a major factor for it. Similarly, when the frictional dissipation energy was observed, with different inter yarn coefficient of friction, simulation results showed that initially frictional dissipation energy rose with smaller μ, reached a peak value and then came down with further increase in μ. This was attributed to the fact that, high inter-yarn friction can lead to premature yarn breakdown, reducing the energy absorption capacity of the fabric, in this case the peak value for maximum dissipation was $\mu = 0.45$. This stressed the importance for good control of inter-yarn frictional coefficient to improve the energy dissipation capability of the fabric. It is important to note that this work was carried out during covid 19 lockdown on a relatively limited capable workstation, improved results maybe obtained on a highly capable workstation.

REFERENCES

[1] K. K. Shukla, K. Yadav, and A. K. Upadhyay, "Effect of obliquity on ballistic impact response of plain-woven fabric," International Journal of Materials and Structural Integrity, vol. 13, no. 1/2/3, p. 93, 2019, doi: 10.1504/ijmsi.2019.10022234.

[2] M. N. Hameed, Y. Nawab, M. Zubair, M. Umair, Z. Ahmad, and K. Shaker, "Double face fabrics: a tailorable solution for puncture resistant applications," The Journal of The Textile Institute, vol. 113, no. 6, pp. 1197–1205, Apr. 2021, doi: 10.1080/00405000.2021.1918882.

[3] D. T. Tien, J. S. Kim, and Y. Huh, "Stab-resistant property of the fabrics woven with the aramid/cotton core-spun yarns," Fibers and Polymers, vol. 11, no. 3, pp. 500–506, Jun. 2010, doi: 10.1007/s12221-010-0500-3.

[4] R. Nayak, I. Crouch, S. Kanesalingam, J. Ding, P. Tan, B. Lee, M. Miao, D. Ganga and L. Wang. "Body armor for stab and spike protection, Part 1: Scientific literature review," Textile Research Journal, vol. 88, no. 7, pp. 812–832, Feb. 2017, doi: 10.1177/0040517517690623.

[5] L. Tian, J. Shi, H. Chen, X. Huang, and H. Cao, "Cut-resistant performance of Kevlar and UHMWPE covered yarn fabrics with different structures," The Journal of The Textile Institute, vol. 113, no. 7, pp. 1457–1463, Jun. 2021, doi: 10.1080/00405000.2021.1933327.

[6] M. Usman Javaid, J. Militký, J. Wiener, A. Jabbar, J. Salačová, and M. Umair, "Effect of surface modification and knife penetration angle on the Quasi-Static Knife Penetration Resistance of para-aramid fabrics," The Journal of The Textile Institute, vol. 110, no. 4, pp. 590–599, Oct. 2018, doi: 10.1080/00405000.2018.1496988.

[7] W., Xungai, L. Xin, H. Christopher and L. Tong, Recent research on natural fibres and textiles, in Natural fibres in Australasia : proceedings of the combined (NZ and AUS) Conference of The Textile Institute, Dunedin 15-17 April 2009, Textile Institute (NZ), [Dunedin, New Zealand], pp. 1-9.

[8] A. Majumdar, B. S. Butola, and A. Srivastava, "Development of soft composite materials with improved impact resistance using Kevlar fabric and nano-silica based

shear thickening fluid," Materials & Design (1980-2015), vol. 54, pp. 295–300, Feb. 2014, doi: 10.1016/j.matdes.2013.07.086.

[9] R. Mishra, B. Kumar Behera and J. Militky, "Impact simulation of three-dimensional woven kevlar-epoxy composite" Journal of Industrial Textiles. Vol 45 (2014) 978-994, doi: 10.1177/1528083714550056

[10] J. B. Mayo, E. D. Wetzel, M. V. Hosur, and S. Jeelani, "Stab and puncture characterization of thermoplastic-impregnated aramid fabrics," International Journal of Impact Engineering, vol. 36, no. 9, pp. 1095–1105, Sep. 2009, doi: 10.1016/j.ijimpeng.2009.03.006.

[11] M. Zako, Y. Uetsuji, and T. Kurashiki, "Finite element analysis of damaged woven fabric composite materials," Composites Science and Technology, vol. 63, no. 3–4, pp. 507–516, Feb. 2003, doi: 10.1016/s0266-3538(02)00211-7.

[12] M. El Messiry, "Investigation of Puncture Behaviour of Flexible Silk Fabric Composites for Soft Body Armour" Fibers & Textiles in Eastern Europe. Vol 5(107), 2014, pp. 71-76

Biographies

Sahil Kashyap completed his master's with faculty of applied mechanics at Motilal Nehru National institute of technology, Allahabad and is presently a research scholar at Applied mechanics department, Indian institute of technology, Delhi, India.

Vivek Kumar completed his master's with faculty of applied mechanics at Motilal Nehru National institute of technology, Allahabad and is presently a research scholar at mechanical engineering department, Indian institute of technology, Patna, India.

Dr. A.K. Upadhyay is an Associate Professor with Applied mechanics Dept. of Motilal Nehru National Institute of Technology, Allahabad with research interests in impact mechanics (low velocity and ballistic), composite structures (Plates and shell), vehicle crashworthiness and energy absorbers like thin-walled tubes, sandwich constructions with honeycomb and metallic foams.

Dr. K.K. Shukla is a Professor with Applied Mechanics Dept. of Motilal Nehru National Institute of Technology Allahabad and currently the director of National institute of technology Jamshedpur. Prof. Shukla's expertise lies in Solid mechanics, composite structures (Plates and shell), retrofitting & strengthening of RCC structure, computational mechanics, stability & dynamics of structure.

Pushover Analysis of a RC Building Resting on Sloping Ground

[1]Nitin Jain and [2]Goutam Ghosh

[1,2]Motilal Nehru National Institute of Technology Allahabad, Prayagraj-211004, UP, India

[1] nitin.jain041995@gmail.com, [2] goutam@mnnit.ac.in

Abstract

Several past earthquakes study suggest that earthquake have had a significant impact on the network system as well as considerable catastrophic effects on human life, buildings, bridges and economy. Hilly buildings are more susceptible to severe damage under lateral forces (earthquake ground motion) as compared to buildings in plains, as they are irregular and unsymmetrical in horizontal and vertical planes and torsionally coupled. Past earthquakes like Kangra (1950), Tokachi-Oki-Japan(1968) and Uttarkashi-India(1991) have proved that the buildings located near the edge of stretch of hills or sloping ground suffered severe damages. In this paper, the seismic behaviour of a G+4 Reinforced Concrete (RC) building is being compared considering two conditions viz. (i) resting on plain terrain and (ii) resting on sloping ground. The seismic design of the building has been performed as per IS 1893 (Part I): 2016 and the ductile detailing provisions have been considered as per IS 13920: 2016. The modelling and analysis of the buildings have been done in ETABS. Plastic hinges have been assigned to the frame elements to incorporate the nonlinear behaviour. A nonlinear static pushover analysis has been performed for the buildings and the capacity curve and ductility demand have been determined. It has been observed that there is a change in the dynamic characteristics and increase in the vulnerability along with variation in ductility demand of the buildings resting on slope. The results obtained from the present study will help in evaluating the seismic performance and risk of failure of the hilly buildings.

Keywords. RC building; pushover; ductility; seismic; performance.

1. INTRODUCTION

The rapid urbanization and economic growth in hilly region has accelerated the real estate development, as an impact of this population density increased enormously in hilly region, which leads to the construction of multi-storeyed buildings on sloping ground [1]. The scarcity of plain terrain compels the construction activities to be done on sloping ground [2]. Varied configurations of buildings in hilly areas results the buildings to be highly irregular and asymmetric, due to the variation in mass and stiffness distributions on different vertical axis at each floor [3,4]. In this study the main focus is the comparison of the seismic behaviour of a G+4 RC building having two different conditions viz. (i) resting on plain terrain and (ii) resting on sloping ground [6]. All the seismic design considerations are being considered as per the IS 1893 (Part I) [5]: 2016 and the ductile detailing provisions have been considered as per IS 13920: 2016 [7]. The modelling and analysis of the buildings have

been done in ETABS [10]. Models are being compared on the basis of their time periods, mass participation ratios, base shear, column forces, storey drifts, capacity curve and ductility demand [8,9,11]. The results obtained from the present study will help in evaluating the seismic performance of the hilly buildings.

2. OBJECTIVES OF WORK

- To study the comparison of the seismic behaviour of a G+4 RC building having two different conditions viz. (i) resting on plain terrain and (ii) resting on sloping ground on the basis of their time periods, mass participation ratios, base shear, column forces, storey drifts.
- A nonlinear static pushover analysis has been performed for the different models and the capacity curves and ductility demands have been determined.

3. DESCRIPTION OF BUILDING

Plan area- 16m X 16m	Number of storey-5
Height of bottom story- 4m and all other stories- 3m	Total height of building- 16m
Cross-section of the column- 300mm X 300mm	Cross-section of the beam- 230mm X 300mm
Thickness of the slab- 150mm	Grade of Concrete- M25
Grade of Steel- HYSD500	Weight density of brick - 20kN/m^3
Roof Live load- 1.5kN/m^2	Live load- 3kN/m^2
Sloping ground angle-15^o	

SEISMIC DATA

Seismic zone-V	Zone factor-0.36
Importance factor-1	Response reduction factor-5
Function damping ratio- 0.05	Soil type- II (Medium Soil)

4. MODELLING

MODEL 1: G+4 Reinforced Concrete (RC) building resting on plain terrain. (Figure 1)

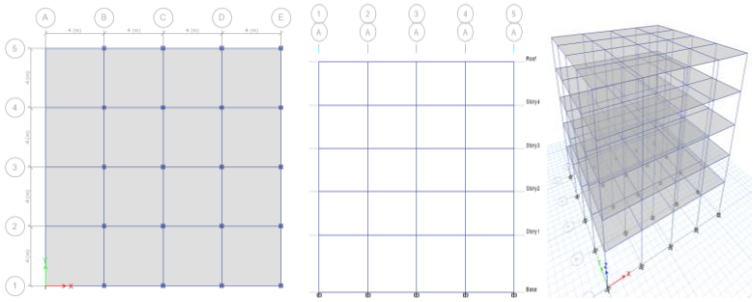

Figure 1. Plan, Elevation and 3D (Model 1)

MODEL 2: G+4 Reinforced Concrete (RC) building resting on sloping ground with one extra slab at the plinth level so that the space can be utilized (Figure 2).

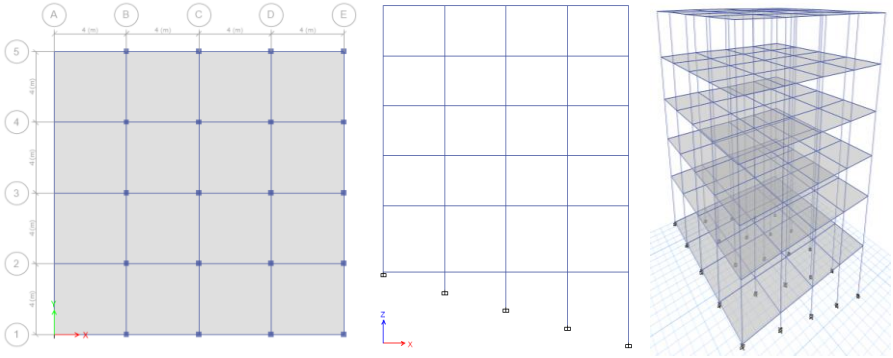

Figure 2. Plan, Elevation and 3D (Model 2)

5. ANALYSIS AND RESULTS

5.1. Time Period

Building acts as an inverted pendulum and has been considered as lumped mass system. One lumped mass get increased with increase in the storey. When earthquake occur building start vibrating under forced vibration and when earthquake completes then building vibrates as free vibration and vibrates at natural frequency. The time required to complete one complete cycle of oscillation when it was disturbed and left free is called natural time period. Natural time period is inverse of natural frequency. It depends on mass and stiffness of the building. Time period for Model 1 and Model 2 is presented in Table 1.

$$\mathbf{Tn = 2\pi\sqrt{m/k}}$$

Table 1. Time period for model 1 and model 2

Mode	Time Period(sec)	
	Model 1	Model 2
1	1.124	1.58
2	1.124	1.578
3	0.984	1.397
4	0.354	0.492
5	0.354	0.491
6	0.311	0.437

5.2. Mass Participation Ratio

The percent of structural mass that is participating in a given direction and mode is known as the mass participation ratio. The ration for Model 1 and Model 2 is given in Table 2 and 3 respectively.

Table 2. Mass participation ratios for model 1

Mode	UX	UY	RZ
1	0.894	0.00001354	0
2	0.00001354	0.894	0
3	0	0	0.8958
4	0.0805	0.00001162	0
5	0.00001162	0.0805	0
6	0	0	0.0794

Table 3. Mass participation ratios for model

Mode	UX	UY	RZ
1	0.0075	0.893	0.0088
2	0.9017	0.0075	0.00000429
3	0.00004003	0.0086	0.9011
4	0.0021	0.0688	0.0002
5	0.0692	0.0021	0
6	0.000004542	0.0005	0.0705

5.3. Base Shear

The total amount of shear acting in a lateral direction on all the storeys of a building is known as the Base Shear of the building. Base shear plays a crucial role while selecting the type of foundation. Stronger foundations are required when the base shear of a building is as high as compared to low base shear. The following expression is used for the calculation of base shear:

$$\mathbf{Vb = Ah} \times \mathbf{W}$$

Where Ah= Design horizontal seismic coefficient for structure.

W= Seismic weight of the building.

Table 4. Base shear for model 1 and model 2

Model	Base Shear	
	X-direction (kN)	Y-direction (kN)
Model 1	468.65	468.65
Model 2	240.64	238.13

5.4. Column Forces

Comparison of forces on 5 exterior columns of both the models is presented in Table 5.

Table 5. Column forces in exterior columns of model 1 and model 2

Column	Model 1			Model 2		
	P (kN)	M_2 (kN-m)	M_3 (kN-m)	P (kN)	M_2 (kN-m)	M_3 (kN-m)
1	334.7348	46.137	46.7623	342.7071	51.1434	58.0688
2	611.6728	44.2977	57.172	810.923	38.466	23.2983
3	609.6403	44.3312	56.4659	818.2662	41.7977	20.6865
4	607.8509	44.4752	56.8283	820.5263	38.5937	17.6855
5	334.7239	46.4941	53.8438	443.8706	31.4064	15.9027

5.5. Storey Drift

As we have discussed in this paper, the building acts as a spring mass system. In which the floor level acts as a mass and the columns impart stiffness to the structure. When a seismic load acts on the structure, each mass vibrates differently depending on the location and amount of its mass value. The relative displacement between two adjacent storeys is known as storey drift. Storey drift for Model 1 when response spectrum in X and Y-direction is presented in Figure 3 and Table 6 and in Figure 4 and Table 7 respectively. Storey drift for Model 2 when response spectrum in X and Y-direction is presented in Figure 5 and Table 8 and in Figure 6 and Table 9 respectively.

For Model 1

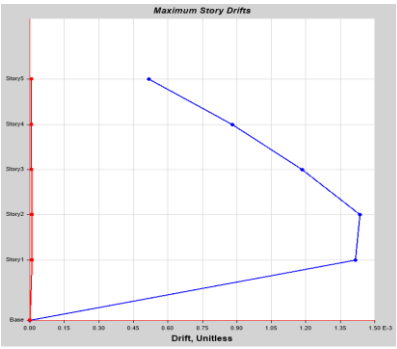

Figure 3. Storey drift for model 1 when response spectrum in X-direction

Storey	Elevation M	Location	X-Dir	Y-Dir
Roof	16	Top	0.000518	0.000008
Storey4	13	Top	0.000882	0.000008
Storey3	10	Top	0.001185	0.000007
Storey2	7	Top	0.001434	0.00001
Story1	4	Top	0.001415	0.000009
Base	0	Top	0	0

Table 6. Storey drift values for model 1 when response spectrum in X-direction

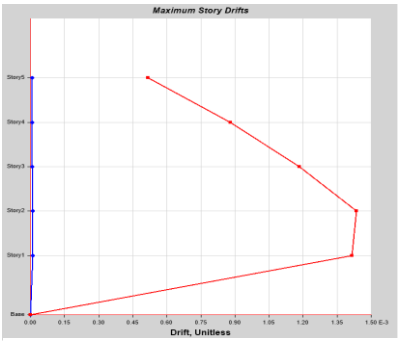

Figure 4. Storey drift for model 1 when response spectrum in Y-direction

Story	Elevation	Location	X-Dir	Y-Dir
	M			
Roof	16	Top	0.000008	0.000518
Story4	13	Top	0.000008	0.000882
Story3	10	Top	0.000007	0.001185
Story2	7	Top	0.00001	0.001434
Story1	4	Top	0.000009	0.001415
Base	0	Top	0	0

Table 7. Storey drift values for model 1 when response spectrum in Y-direction

For Model 2

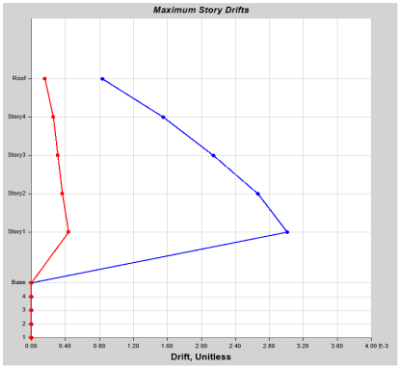

Figure 5. Storey drift for model 2 when response spectrum in X-direction

Storey	Elevation	Location	X-Dir	Y-Dir
	M			
Roof	20.288	Top	0.000833	0.00016
Storey4	17.288	Top	0.001553	0.000259
Storey3	14.288	Top	0.002142	0.000312
Storey2	11.288	Top	0.002668	0.000364
Storey1	8.288	Top	0.003011	0.000441
Base	4.288	Top	0	0
4	3.216	Top	0	0
3	2.144	Top	0	0
2	1.072	Top	0	0
1	0	Top	0	0

Table 8. Storey drift values for model 2 when response spectrum in X-direction

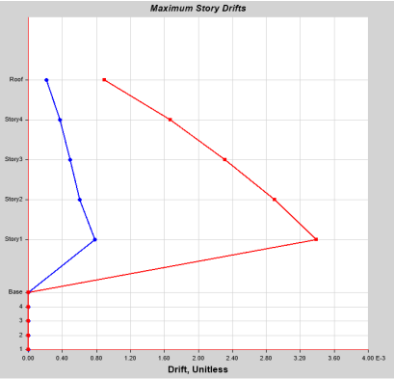

Figure 6. Storey drift for model 2 when response spectrum in Y-direction

Storey	Elevation	Location	X-Dir	Y-Dir
	M			
Roof	20.288	Top	0.000214	0.000895
Storey4	17.288	Top	0.000374	0.001674
Storey3	14.288	Top	0.000489	0.002316
Storey2	11.288	Top	0.000602	0.002897
Storey1	8.288	Top	0.000785	0.003388
Base	4.288	Top	0	0
4	3.216	Top	0	0
3	2.144	Top	0	0
2	1.072	Top	0	0
1	0	Top	0	0

Table 9. Storey drift values for model 2 when response spectrum in Y-direction

5.6. Capacity Curve

The non-linear behaviour of the structure can be shown by the Capacity Curve or Pushover Curve. It is the load deformation curve of the base shear and the horizontal roof displacement of the building. Capacity curve for model 1 when response spectrum in X and Y-direction is presented in Figure 7 and 8 respectively. Capacity curve for model 2 when response spectrum in X and Y-direction is presented in Figure 9 and 10 respectively.

For Model 1

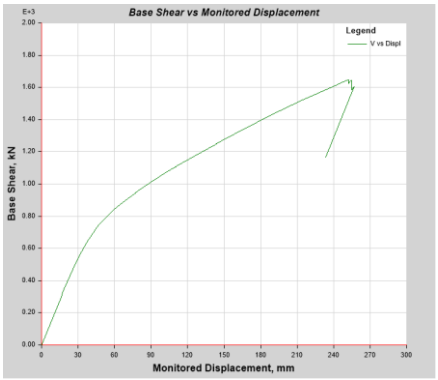

Figure 7. Capacity Curve for model 1 when response spectrum in X-direction

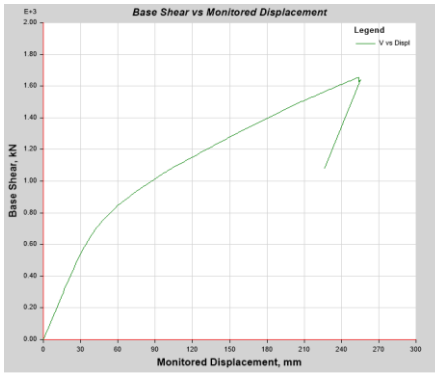

Figure 8. Capacity Curve for model 1 when response spectrum in Y-direction

For Model 2

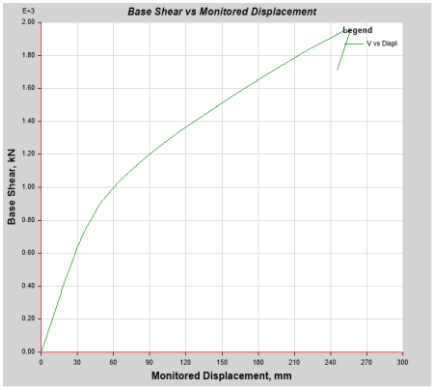

Figure 9. Capacity Curve for model 2 when response spectrum in X-direction

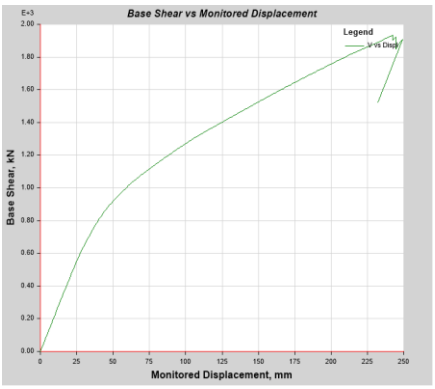

Figure 10. Capacity Curve for model 2 when response spectrum in Y-direction

5.7. Performance Point

The intersection point between the capacity spectrum and the demand spectrum at a given damping ratio is termed the Performance Point. It is the maximum inelastic capacity of the structure. Performance point for model 1 when pushover analysis in X and Y direction is presented in Figure 11 and 12 respectively and for module 2 is presented in Figure 13 and 14 respectively.

For Model 1

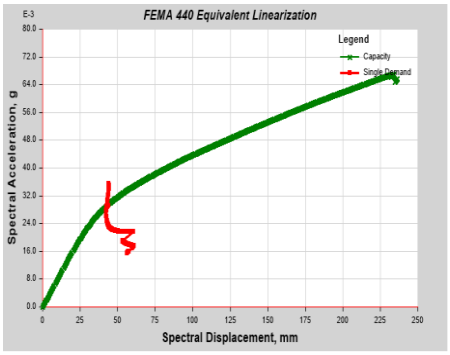

Point Found	Yes	T secant	2.43 sec
Shear	740.7828 kN	T effective	2.407 sec
Displacement	46.634 mm	Ductility Ratio	1.668543
Sa	0.029309	Effective Damping	0.0686
Sd	42.991 mm	Modification Factor	0.980907

Figure 11. Performance point for model 1 when pushover analysis in X-direction

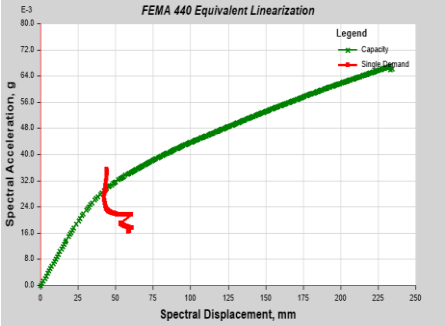

Point Found	Yes	T secant	2.43 sec
Shear	743.2573 kN	T effective	2.409 sec
Displacement	46.688 mm	Ductility Ratio	1.672114
Sa	0.029313	Effective Damping	0.0688
Sd	43.015 mm	Modification Factor	0.982096

Figure 12. Performance point for model 1 when pushover analysis in Y-direction

For Model 2

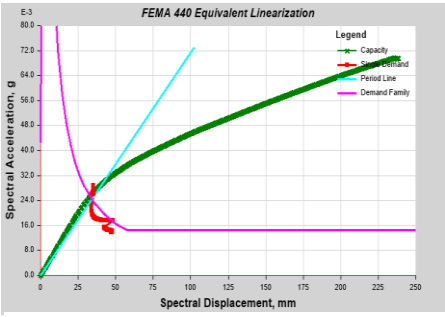

Point Found	Yes	T secant	2.305 sec
Shear	756.6875 kN	T effective	2.316 sec
Displacement	37.443 mm	Ductility Ratio	1.519953
Sa	0.026431	Effective Damping	0.0617
Sd	34.873 mm	Modification Factor	1.00973

Figure 13. Performance point for model 2 when pushover analysis in X-direction

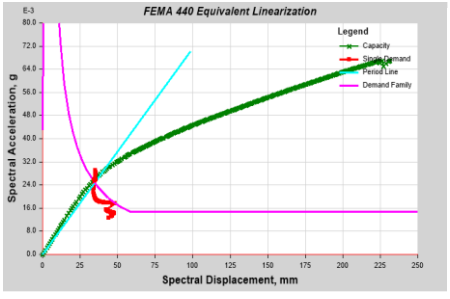

Point Found	Yes	T secant	2.323 sec
Shear	770.4671	T effective	2.335 sec
Displacement	37.701	Ductility Ratio	1.567648
Sa	0.025992	Effective	0.0638
Sd	34.843	Modification	1.010133

Figure 14. Performance point for model 2 when pushover analysis in Y-direction

6. CONCLUSION

In the present paper, the seismic analysis of a G+4 Reinforced Concrete (RC) building has been done considering the building is resting on plain and hilly terrains. The seismic design of the building has been performed as per IS 1893 (Part I): 2016 and the ductile detailing provisions have been considered as per IS 13920: 2016. The following conclusions can be drawn. A. The time period of the building resting on hilly slope is found to be higher than the same resting on plain ground which might be due to additional flexibility because of unsymmetrical configuration in the former case. B. The base shear for the hilly building is found to be lesser than the same resting on plain ground which might be due to increased flexibility in the former case. C. The storey drift is found to be higher in case of hilly terrain building than the building resting on plain ground. However, for both the buildings, the drifts are within the desired limit as per IS:1893-2016 code. D. The ductility demand of the building resting on hilly terrain is higher than the same resting on plain ground which might be due to unsymmetrical configuration in the former case.

REFERENCES

[1] R. B. Khadiranaikar and A. Masali, "Seismic Performance of Buildings Resting on Sloping Ground," Advances in Structural Engineering, pp. 803–813, Dec. 2014, doi: 10.1007/978-81-322-2193-7_63.

[2] S. Goyal. Dynamic Analysis of Sloped Buildings: Experimental and Numerical Studies (Doctoral dissertation), 2015. [Online], Available: http://ethesis.nitrkl.ac.in/6801/1/DYNAMIC_Goyal_2015.pdf

[3] Z. Mohammad, A. Baqi, and M. Arif, "Seismic Response of RC Framed Buildings Resting on Hill Slopes," Procedia Engineering, vol. 173, pp. 1792–1799, 2017, doi: 10.1016/j.proeng.2016.12.221.

[4] IS: 456:2000 Plain and Reinforced Concrete-Code of Practice by Bureau of Indian Standards, 2000. [Online], Available: https://archive.org/details/gov.in.is.456.2000

[5] IS: 1893(Part-1):2016 Criteria for Earthquake Resistant Design of Structures by Bureau of Indian Standards, 2016. [Online], Available: https://www.studocu.com/in/document/birla-institute-of-technology-and-science-pilani/foundation-engineering/1893-part-1-2016-criteria-for-earthquake-resistant-design-of-structures-is-code-1893/9255021

[6] IS: 875 (Part 2) - 1987, Code of Practice Design Loads (Other Than for Earthquake) For Buildings and Structures by Bureau of Indian Standards, [Online], Available. https://law.resource.org/pub/in/bis/S03/is.875.2.1987.pdf

[7] IS: 13920:2016 Ductile Design and Detailing of Reinforced Concrete Structures Subjected to Seismic Forces- Code of Practice by Bureau of Indian Standards, 2016. [Online], Available. https://idoc.pub/documents/13920-2016-vlr0k1ryxjlz

[8] FEMA-440: Improvement of Nonlinear Static Seismic Analysis Procedures June, 2005. [Online], Available. https://mitigation.eeri.org/resource-library/building-professionals/improvement-of-nonlinear-static-seismic-analysis-procedures-fema-440

[9] ASCE/SEI 41-17(2017): Seismic Rehabilitation of Existing Buildings (ASCE/SEI 41-17). [Online], Available. https://ascelibrary.org/doi/pdf/10.1061/9780784414859.fm

[10] ETABS 2017- Building Analysis and Design- Computers & Structures, Inc., Berkley, CA, USA. [Online], Available. https://www.csiamerica.com/products/etabs

[11] D. E. Hudson, “Dynamics of structures: Theory and applications to earthquake engineering, by Anil K. Chopra, Prentice-Hall, Englewood Cliffs, NJ, 1995. No. of pages: xxviii + 761, ISBN 0-13-855214-2,” Earthquake Engineering & Structural Dynamics, vol. 24, no. 8, pp. 1173–1173, Aug. 1995, doi: 10.1002/eqe.4290240809.

Biographies

Mr Nitin Jain is a Ph.D student in the Civil Engineering Department, MNNIT Allahabad, Prayagraj, India. He did his M.Tech. in Structural Engineering from IET Lucknow. His present area of research is Seismic performance evaluation of building structures.

Dr Goutam Ghosh, is currently an Associate Professor in the Civil Engineering Department, MNNIT Allahabad, Prayagraj, India. He did his Ph.D. from IIT Roorkee in the area of seismic performance of bridge structures. He has more than 15 years of teaching experience and has published several research papers in reputed Journals/Conferences. His area of interest is earthquake engineering, performance-based design of structures, base isolation of structures and bridge engineering.

An Identification of Unbalance in Rotor Bearing System and Fault Classification using Adaptive Neuro Fuzzy Interface System (ANFIS)

Prasad V. Shinde, R.G. Desavale

Mechanical Engineering Department, RIT, Sakhrale-415414, Shivaji University, Kolhapur, Maharashtra, India

prasadshinde7174@gmail.com, ramchandra.desavale@ritindia.edu

Abstract

In rotating machinery, unbalance creates excessive vibration and causes a catastrophic or sudden system failure. Unbalance is produced inside the system due to shaft deformation, inhomogeneity in material, and manufacturing tolerance. This current study proposed an experimental approach to identifying unbalance in the rotor-bearing system. The dominant peak is obtained at the first and multiple harmonics of the shaft frequency. It is seen from the pilot experiments the vibration amplitude increases as speed increases. Also, defect frequency corresponds to the first harmonics of the shaft's rotating speed, which conforms to the theoretical results. The Adaptive Neuro-Fuzzy Interface System (ANFIS) is implemented to classify multiple fault presents in the rolling element bearing. ANFIS reveals good fault classification over multiple fault classes of vibration data with an accuracy of 91.66 %.

Keywords: Rotor Bearing System, Unbalance, ANFIS, Defect

1. INTRODUCTION

Rotating machines are found in a wide variety of applications, including power plants, marine propulsion systems, aviation engines, machine tools, vehicles, home products, and futuristic micro- and nano machines. In modern engineering, the design trend for such systems is toward lighter weight and supersonic speeds. A precise estimate of the rotor system's dynamic properties is critical when developing any form of machinery. In real machines, rotors may display many defects at the same time, such as unbalance, rotor bow, crack, and misalignment, either during continuous operation or at the start of manufacturing of the various components due to design issues or during assembly of the rotor system setup.

Any disobedience on the part of machinery causes huge damage to the entire system as well as significant financial loss. As a result, researchers have focused their efforts on detecting defects with maximal accuracy.

At present, different fault finding techniques have been introduced for rolling bearing, such Zhang et al. [1] investigated the compound faults of vibration signatures of gearbox using

genetic algorithm. Also, vibration characteristics were analyzed by energy operator demodulating, and vibration signals of bearing and gears were effectively studied. Jing [2] studied vibration signals of several defects using the blind source separation approach. This method effectively identified the compound defects. Li et al. [3] studied a vibration response of compound faults in the gears and bearing uses nonlinear feature extraction with blind source separation. The results obtained are more effective for the multi-fault diagnosis for bearings and gears. Tang et al. [4] considered the compound fault of roller bearing using the variational mode decomposition. The compound defects are separated effectively for the analysis of the individual components. Also, experimental results were carried out to validate the results, and this shows that the technique is more reliable to study compound defects. Jiang et al. [5] applied empirical wavelet transform to rolling element bearing vibration signals to identify compound faults. Experimentation was performed on rolling bearing for combine faults to validate the empirical wavelet transform-duffing oscillator results, and this shows that the method proposed was more reliable.

At present, number of methods and techniques are available for fault identification in rolling element bearing, such as Wavelet Transform-based [6-8], mode decomposition-based [9, 10] methods, and intelligent composite fault diagnosis methods [11, 12]. Many authors use the dimensional analysis approach, neural network approach, ANFIS, etc., to study the fault characteristics of rotor-bearing systems. [13-26]. Intelligent algorithms, such as neuro-fuzzy classifiers and support vector machines, are frequently used as popular methods for compound fault diagnosis since they can effectively classify different types of fault data.

From the literature findings, most of the research is going on in vibration analysis with localized defects. But there is a comprehensive scope to study multiple faults in the rotor-bearing system that needs to be investigated.

The current paper proposes a duo study of unbalance response of the vibratory system and fault classification using the Adaptive Neuro-Fuzzy Interface System (ANFIS) for the rotating system.

2. ADAPTIVE NEURO-FUZZY INFERENCE SYSTEM (ANFIS)

For improvement in the accuracy of complex system analysis, Jang created an ANFIS approach. ANFIS is a data-learning technique that transforms a given input into a desired output. It is based on a fuzzy inference model. This method encompasses various membership functions, fuzzy logic operators, and conditional rules.

The statistical features retrieved from a vibration characteristics were used as input ANFIS classification models in this investigation.

The output of the fuzzy inference system is subjected to the first-order polynomial. Using IF-THEN rules in human cognitive systems, the ANFIS technique creates a neural-fuzzy system. Membership functions can be better represented and identified using the system's entry point. As a result, ANFIS has been developed to incorporate both the advantages of an artificial neural network and a fuzzy reasoning system.

ANFIS architecture shows two inputs and a single output with five layers of neurons in Figure1.

The first layer denotes the fuzzyfying layer, in which each neuron is an adaptable node made up of premise parameters. The second layer denotes the product layer, or the implication layer indicates a product of inputs. The normalizing layer function is to normalize the weight functions indicated by layer 3. Layer 4 is defined as a defuzzyfing layer whose nodes or neurons are adaptive. All the input is into a single neuron representing an output or results represented by layer 5.

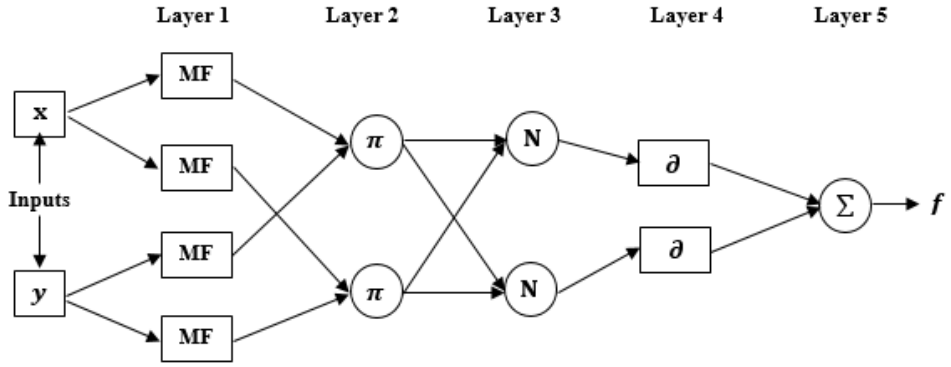

Figure 1. ANFIS Architecture

2.1 Feature Extraction

The obtained data is extracted in five features: peak value, crest factor, RMS, Range, and standard deviation.

The details of these features are given below,

- **Root mean square (RMS) -**This function measures the total level of a discrete signal.

$$\mathrm{RMS} = \sqrt{\frac{1}{\mathrm{M}}\sum_{\mathrm{m=1}}^{\mathrm{M}} f_n^2}$$

- **Peak value ($\boldsymbol{\rho}$)**
  The peak value is the highest acceleration measured in its amplitude.

$$\mathrm{P} = \frac{1}{2}[f_{nmax} - f_{nmin}]$$

- **Crest factor($\boldsymbol{\varsigma}$)**
  The crest factor is the contrast between peak and RMS acceleration. This measurement can identify accelerant bursts even though the signal RMS remains unchanged.

$$\text{Crest Factor} = \frac{\mathrm{P}}{\mathrm{RMS}}$$

- **Standard deviation ($\boldsymbol{\sigma}$)**
  The standard deviation is a quantity that expresses the distribution's variability or the divergence of signals from the mean.

$$\sigma = \left(\frac{1}{\mathrm{N}-1}\sum_{\mathrm{m=1}}^{\mathrm{M}}(f_n - f)^2\right)^2$$

- **Range ($\boldsymbol{\gamma}$) -** The difference is between the high and low extremes.

3. EXPERIMENTATION

For the rotor-bearing setup, the dynamic response of the test setup is investigated by taking unbalanced mass and shaft speed into account. Figure 2 shows a schematic view of experimental. The setup consists of an unbalance disc supported by a shaft between two ball bearings driven at operating speed by a DC motor via a dimmer stat.

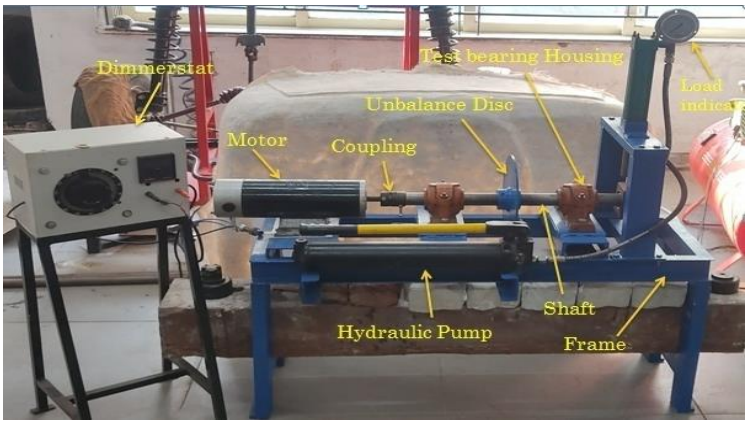

Figure 2. Experimental Setup

To measure vibration signals, Adash VAPro 4400 Fast Fourier transforms (FFT) with an accelerometer of the piezoelectric type was placed on the test bearing housing. The ball bearing specifications mentioned in Table 1 are used for experimentation. The deep groove ball bearing is mounted on the pedestal carrying a shaft. The mild steel shaft of 600 mm in length and 40 mm in diameter is used for experimentation. The unbalance disk is attached to the shaft, and variable unbalances are created throughout the experiment. The 1 HP DC motor is used to rotate the shaft with the help of a dimmer stat. Stat jaw coupling is used to attach the motor shaft and bearing shaft. The proximity sensor is used for the speed measurement of the shaft.

The different combination of bearing speed and unbalanced mass was simulated between 500 rpm to 1300 rpm. A total of 25 trials were conducted to acquire vibration signals and defect frequencies.

Table 1. Bearing Specifications
Bearing - SKF 6209-K
d- Bearing Inner Dia. - 45 mm
D- Bearing Outer Dia. - 85 mm
No. of Balls (N)- 9
Diameter of balls- 9 mm

4. RESULTS AND DISCUSSION

4.1 Influence of Unbalance on Vibration Characteristics

The figure 3 to 6 shows frequency response spectra of vibratory setup under the influence of unbalance present in system. The unbalance of 25 gm to 125 gm is considered for experimentation.

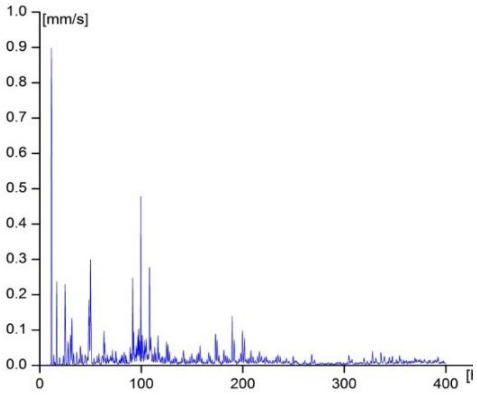

Figure 3. Vibration response at 700 rpm and 25 gm of unbalance mass

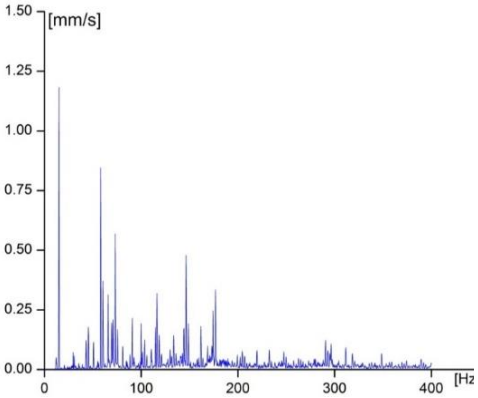

Figure 4. Vibration response at 900 rpm and 75 gm of unbalance mass

Figure 3 shows a vibratory response at 25 gm unbalance and 700 rpm speed of shaft. The vibration amplitude recorded at the first harmonics of the shaft frequency is 0.898 mm/s, which corresponds to the first harmonic of the shaft frequency. The defect frequency is closely matches with the experimentally obtained frequency. Figure 4 shows a vibration response for trial 75 gm of unbalanced mass and shaft rotational speed of 900 rpm. The peak amplitude of vibration is obtained at 1×fs is 1.18 mm/s. The significant peak is obtained at 15 Hz, matching the theoretical study.

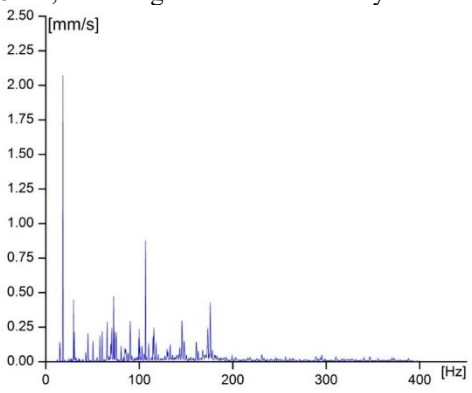

Figure 5. Vibration response at 1100 rpm and 100 gm of unbalance mass

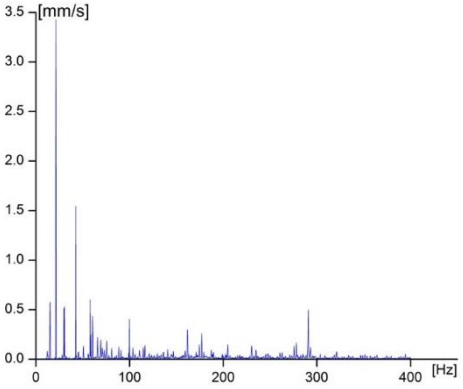

Figure 6. Vibration response at 1300 rpm and 125 gm of unbalance mass

This trial was conducted with a shaft unbalance of 100 gm and a 1100 rotor speed. The vibration plot for the above test is given in Figure 5. The dominant peak occurs around 18.3 Hz, close to the first harmonic of the shaft frequency. Other distinct low amplitude spikes are also observed at different frequencies.

The frequency response plot for unbalance mass of 125 gm and shaft speed of 1300 rpm is observed in Figure 6. The significant peak is observed at 21.5 Hz which is of amplitude of 3.4 mm/s.

Table 2. Vibration Response of all trials

Speed	**25 gm**	**50 gm**	**75 gm**	**100 gm**	**125 gm**
RPM	**Vibration Amplitude (mm/s)**				
500	0.566	0.598	0.784	0.854	0.902
700	0.898	0.927	0.997	1.09	1.29
900	0.945	1.02	1.18	1.49	1.58
1100	1.415	1.59	1.65	2.07	2.35
1300	1.894	2.354	2.89	3.17	3.4

Similarly all other trials are conducted for various speeds and unbalance mass and vibration amplitude is reported in Table 2.

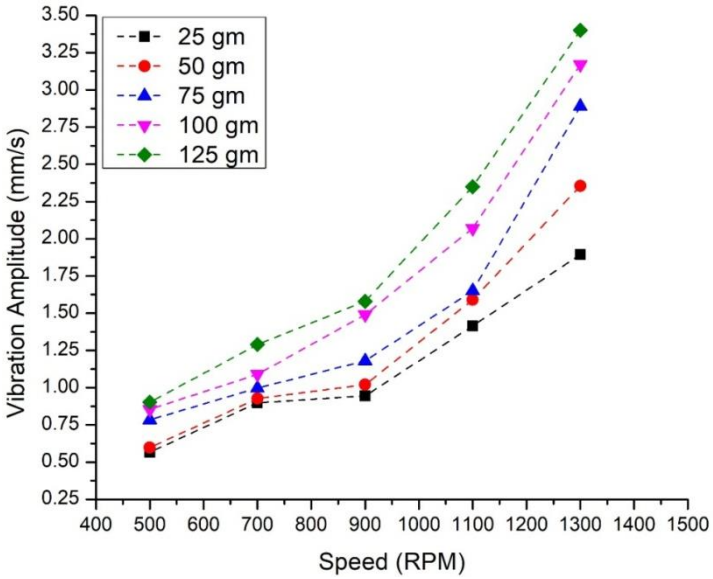

Figure 7 Influence of unbalance mass on vibration amplitude

Preliminary experimentation was performed successfully in the range of 25gm-125gm and the speed range of 500 rpm to 1300 rpm, as shown in Table 3. It is observed from the pilot experiments that amplitude of vibration increases as speed increases. Also, defect frequency corresponds to the shaft's rotating speed fs, which conforms to the theoretical results.

4.2 Fault Classification

A five bearing faults classes are considered for ANFIS, viz. unbalance, outer race fault, misalignment, inner race fault, and clearance. Overall, 60 fault cases are trained and tested in ANFIS. 80% of data is used for training, and 20% is utilized for testing. The details of ANFIS parameters are provided in table 3.

Table 3. ANFIS Parameter	
No of Membership functions	5
Optimization method	Linear
Type of membership functions	Trimf

Table 4 compares the performance of the ANFIS using statistical measures such as root mean square error (RMSE) and correlation coefficient (R). These characteristics are typically expressed in terms of predicting error, which is defined as the difference between the observed and predicted values.

Table 4. ANFIS Results	
Accuracy	91.67
R	0.9775
RMSE	0.4978

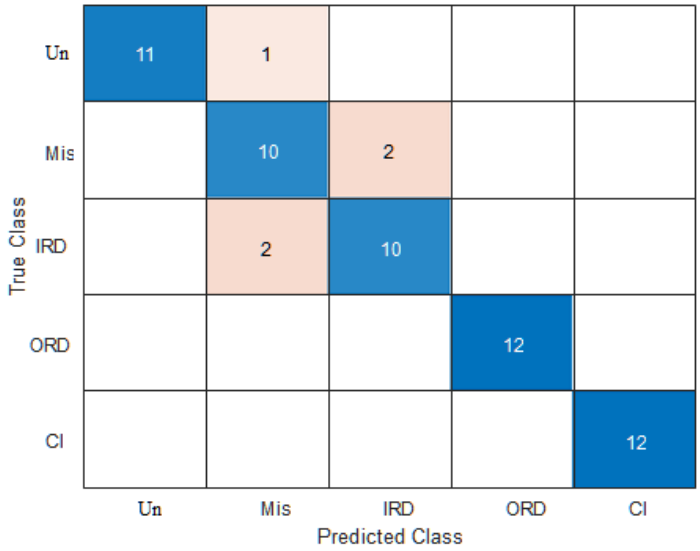

Figure 8. Confusion Matrix

The correlation coefficient (R) of 0.9775 and root mean square error (RMSE) of 0.4978 is acquired using data classification. Figure 7 shows a confusion matrix that offers an actual class vs. a predicted class. The 60 fault cases are considered, 55 fault cases are predicted correctly, and five are wrongly classified. ANFIS gives a 91.66 % of fault classification accuracy.

5. CONCLUSION

The current study proposes a duo study of unbalance response of the vibratory system and fault classification using the Adaptive Neuro-Fuzzy Interface System (ANFIS) for the rotating system.

The results obtained are summarized as follows,

1. It is observed that as unbalanced mass with shaft speed increases, the amplitude of vibration increases.
2. Experimental defect frequencies closely match the theoretical defect frequencies that validate the experimental investigation.
3. The linear nature of vibration is observed as an increase in unbalanced mass, which changes the system's dynamics.
4. Adaptive Neuro-Fuzzy Interface System (ANFIS) classified 55 fault cases out of 60 fault cases with a 91.66 % of classification accuracy over multiple fault cases.

The current work can be extended with the application of convolutional neural network (CNN), support vector machine (SVM), K- nearest neibour network (KNN).

ACKNOWLEDGEMENTS

This work is financially supported Chhatrapati Shahu Maharaja National Research fellowship 2020, SARTHI, Pune.

REFERENCES

[1] D. Zhang, D. Yu, and W. Zhang, “Energy operator demodulating of optimal resonance components for the compound faults diagnosis of gearboxes,” Measurement Science and Technology, vol. 26, no. 11, p. 115003, Sep. 2015, doi: 10.1088/0957-0233/26/11/115003.

[2] J. Jing and G. Meng, “A novel method for multi-fault diagnosis of rotor system,” Mechanism and Machine Theory, vol. 44, no. 4, pp. 697–709, Apr. 2009, doi: 10.1016/j.mechmachtheory.2008.05.002.

[3] Z. Li, X. Yan, Z. Tian, C. Yuan, Z. Peng, and L. Li, “Blind vibration component separation and nonlinear feature extraction applied to the nonstationary vibration signals for the gearbox multi-fault diagnosis,” Measurement, vol. 46, no. 1, pp. 259–271, Jan. 2013, doi: 10.1016/j.measurement.2012.06.013.

[4] G. Tang, G. Luo, W. Zhang, C. Yang, and H. Wang, “Underdetermined Blind Source Separation with Variational Mode Decomposition for Compound Roller Bearing Fault Signals,” Sensors, vol. 16, no. 6, p. 897, Jun. 2016, doi: 10.3390/s16060897.

[5] Y. Jiang, H. Zhu, and Z. Li, “A new compound faults detection method for rolling bearings based on empirical wavelet transform and chaotic oscillator,” Chaos, Solitons & Fractals, vol. 89, no. 1, pp. 8–19, Aug. 2016, doi: 10.1016/j.chaos.2015.09.007.

[6] R. Shao, W. Hu, and J. Li, “Multi-Fault Feature Extraction and Diagnosis of Gear Transmission System Using Time-Frequency Analysis and Wavelet Threshold De-Noising Based on EMD,” Shock and Vibration, vol. 20, no. 4, pp. 763–780, 2013, doi: 10.1155/2013/286461.

[7] M.-C. Pan and W.-C. Tsao, “Using appropriate IMFs for envelope analysis in multiple fault diagnosis of ball bearings,” International Journal of Mechanical Sciences, vol. 69, pp. 114–124, Apr. 2013, doi: 10.1016/j.ijmecsci.2013.01.035.

[8] S. Abbasion, A. Rafsanjani, A. Farshidianfar, and N. Irani, “Rolling element bearings multi-fault classification based on the wavelet denoising and support vector machine,” Mechanical Systems and Signal Processing, vol. 21, no. 7, pp. 2933–2945, Oct. 2007, doi: 10.1016/j.ymssp.2007.02.003.

[9] X. Yan, M. Jia, and L. Xiang, “Compound fault diagnosis of rotating machinery based on OVMD and a 1.5-dimension envelope spectrum,” Measurement Science and Technology, vol. 27, no. 7, p. 075002, May 2016, doi: 10.1088/0957-0233/27/7/075002.

[10] Z. Wang, Z. Han, F. Gu, J. X. Gu, and S. Ning, “A novel procedure for diagnosing multiple faults in rotating machinery,” ISA Transactions, vol. 55, no. 1, pp. 208–218, Mar. 2015, doi: 10.1016/j.isatra.2014.09.006.

[11] R. Zhao, R. Yan, Z. Chen, K. Mao, P. Wang, and R. X. Gao, “Deep learning and its applications to machine health monitoring,” Mechanical Systems and Signal Processing, vol. 115, no. 1, pp. 213–237, Jan. 2019, doi: 10.1016/j.ymssp.2018.05.050.

[12] P. Comon, “Independent component analysis, A new concept?,” Signal Processing, vol. 36, no. 3, pp. 287–314, Apr. 1994, doi: 10.1016/0165-1684(94)90029-9.

[13] R. G. Desavale, R. Venkatachalam, and S. P. Chavan, “Antifriction Bearings Damage Analysis Using Experimental Data Based Models,” Journal of Tribology, vol. 135, no. 4, Aug. 2013, doi: 10.1115/1.4024638.

[14] R. G. Desavale, “Dynamics Characteristics and Diagnosis of a Rotor-Bearing’s System Through a Dimensional Analysis Approach: An Experimental Study,” Journal of Computational and Nonlinear Dynamics, vol. 14, no. 1, Nov. 2018, doi: 10.1115/1.4041828.

[15] P. V. Shinde, R. G. Desavale, V. R. Patil, P. M. Gawali, and S. M. Patil, “Modeling, attenuation and flow field analysis of diesel engine muffler using fluid structure interaction approach and experimental analysis,” SN Applied Sciences, vol. 2, no. 5, Apr. 2020, doi: 10.1007/s42452-020-2683-6.

[16] M. A. Vishwendra et al., “A Novel Method to Classify Rolling Element Bearing Faults Using K-Nearest Neighbor Machine Learning Algorithm,” ASCE-ASME J Risk and Uncert in Engrg Sys Part B Mech Engrg, vol. 8, no. 3, Mar. 2022, doi: 10.1115/1.4053760.

[17] S. M. Patil, R. G. Desavale, and S. G. Kumbhar, “Roller Element Bearing Fault Size Estimation Using Adaptive Neurofuzzy Inference System,” ASCE-ASME J Risk and Uncert in Engrg Sys Part B Mech Engrg, vol. 7, no. 1, Jan. 2021, doi: 10.1115/1.4048656.

[18] P. M. Jadhav, S. G. Kumbhar, R. G. Desavale, and S. B. Patil, “Distributed fault diagnosis of rotor-bearing system using dimensional analysis and experimental methods,” Measurement, vol. 166, no. 1, p. 108239, Dec. 2020, doi: 10.1016/j.measurement.2020.108239.

[19] S. G. Kumbhar, E. Sudhagar P, and R. G. Desavale, “Theoretical and experimental studies to predict vibration responses of defects in spherical roller bearings using dimension theory,” Measurement, vol. 161, no. 1, p. 107846, Sep. 2020, doi: 10.1016/j.measurement.2020.107846.

[20] P. V. Shinde and R. G. Desavale, “Application of dimension analysis and soft competitive tool to predict compound faults present in rotor-bearing systems,”

Measurement, vol. 193, no. 1, p. 110984, Apr. 2022, doi: 10.1016/j.measurement.2022.110984.

[21] R. A. Kanai, R. G. Desavale, and S. P. Chavan, “Experimental-Based Fault Diagnosis of Rolling Bearings Using Artificial Neural Network,” Journal of Tribology, vol. 138, no. 3, p. 031103, Apr. 2016, doi: 10.1115/1.4032525.

[22] R. G. Desavale, R. A. Kanai, S. P. Chavan, R. Venkatachalam, and P. M. Jadhav, “Vibration Characteristics Diagnosis of Roller Bearing Using the New Empirical Model,” Journal of Tribology, vol. 138, no. 1, Aug. 2015, doi: 10.1115/1.4031065.

[23] R. G. Desavale and A. R. Mali, “Detection of Damage of Rotor-bearing Systems Using Experimental Data Analysis,” Procedia Engineering, vol. 144, no. 1, pp. 195–201, 2016, doi: 10.1016/j.proeng.2016.05.024.

[24] Patil, S. M., Desavale, R. G., Shinde, P. V., Patil, V. R., Comparative Study of Response of Vibrations for Circular and Square Defects on Components of Cylindrical Roller Bearing Under Different Conditions, In : Lecture Notes in Mechanical Engineering Innovative Design, Analysis and Development Practices in Aerospace and Automotive Engineering, Springer, pp. 189-198, 2020.

[25] V. R. Patil and P. V. Jadhav, “Dynamic response analysis of unbalanced rotor-bearing system with internal radial clearance,” SN Applied Sciences, vol. 2, no. 11, Oct. 2020, doi: 10.1007/s42452-020-03608-y.

[26] M. A. Vishwendra, P. S. Salunkhe, S. V. Patil, S. A. Shinde, P. V. Shinde, R. G. Desavale, P. M. Jadhav and N. V. Dharwadkar. “A Novel Method to Classify Rolling Element Bearing Faults Using K-Nearest Neighbor Machine Learning Algorithm.” ASME. ASME J. Risk Uncertainty Part B. Vol. 8, No. 3,p. 031202, September 2022, doi: https://doi.org/10.1115/1.4053760

Biographies

Mr. Prasad Vishwasrao Shinde received the bachelor's degree in mechanical engineering from D. Y. Patil College of Engineering, Kolhapur in 2013, the master's degree in mechanical engineering from Shivaji University, Kolhapur in 2016, and pursuing the philosophy of doctorate degree in mechanical engineering from Shivaji University, Kolhapur, respectively. He is currently working as a Research Scholar at the Department of Mechanical Engineering, Rajarambapu Institute of Technology, Islampur. His research areas include bearing vibration, machine learning, and acoustic analysis.

.

Dr. R. G. Desavale received the bachelor's degree in Automobile engineering from Rajarambapu Institute of Technology, Islampur in 2005, the master's degree in mechanical engineering from Shivaji University, Kolhapur in 2008, and the philosophy of doctorate degree in mechanical engineering from National Institute of Technology, Warangal respectively. He is currently working as an associate professor at the Department of Mechanical Engineering, Rajarambapu Institute of Technology, Islampur. His research areas include bearing vibration, FEA, and signal analysis.

Optimization of Turning Parameters of AISI 4340 Steel Using Parallel Textured Tool

Manjari Malviya, Sunil Kumar, Apurva Anand

Department of Mechanical Engineering, Babu Banarasi Das University, Lucknow

manjarimalviya1997@gmail.com, sonkar.sunil@gmail.com, apurva2050@yahoo.co.in

Abstract

The current work examines how input factors affect the surface quality of AISI 4340 steel while cutting the material with a parallel textured cutting tool. A copper electrode with a diameter of 500 m is used to create textures on the rake face of the tool that are parallel to the cutting edge. The distance between two consecutive lines is maintained at 100 m, while the line depth is maintained at 50 m. Cutting speed, feed rate, and depth of cut are taken into consideration as input parameters. The response parameter is chosen to be surface quality. The Taguchi L9 approach is used to optimize the parameters to enhance the quality of the surface. The contribution of each parameter to surface quality is determined using ANOVA. Results discovered that feed rate has maximum contribution on surface quality with 61.71% followed by depth of cut with 24.31% contribution, and cutting speed with 14.06% contribution. Confirmation experiment shows an improvement in surface roughness by 19.21% when it is compared with experiment number one of Taguchi L_9 OA.

Keywords. ANOVA; Parallel Texture; Surface Roughness; Taguchi

1. INTRODUCTION

Nowadays, demand for materials possessing rich surfaces is rapidly increasing in market because of their excellent performance characteristics. Turning is a metal cutting process in which material is removed from a rotating surface using single-point tool to get desired surface quality. Turning process is shown in Figure 1.

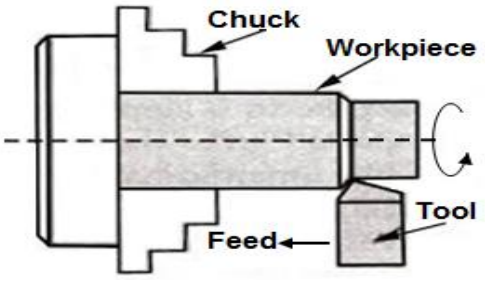

Figure 1. Turning process [1]

Cutting tools used for this purpose are generally made up of High-speed steel, ceramics, carbide, diamonds, cubic boron nitride, etc. Turning of alloy steel such as AISI 4340 steel is

a challenging task since excess friction and adhesion at tool-chip interface increases the temperature of cutting area leading to high tool wear, reduction in tool life, and also reduces surface quality. Thus, cutting tool should be modified in such a way that it produces a better-turned surface. Surface texturing is relatively a new application that overcomes above-stated drawbacks by introducing different textures such as vertical, parallel, and dot at flank or rake face of tool inserts. Surface texturing reduces cutting forces, increases load-carrying capacity, and improves wear resistance and surface quality. Textured tools reduced tool chip contact thereby reducing cutting forces, cutting temperature, and coefficient of friction [2].

Gap provided between grooves in textured tools helped in reducing heat at surface of tool of titanium alloy, thus reducing cutting temperature [3]. Textures produced on rake face helped reduce friction on tool surface and also reduced cutting forces [4]. Turning was performed on annealed 1045 steel and 6061 aluminum workpieces using an isotropic parallel textured tool with a width and depth of 100µm produced on rake face and a significant decrease in feed rate and improvement in surface quality were found [5]. Effect of different textured tools on built-up edge formation and tool wear while machining carbon steel concluded that textured tools helped in destabilizing BUE resulting in a better surface quality [6]. Impact of built-up edge formation on surface quality with orthogonal cutting tests on titanium alloy was investigated. It was found that effect of BUE on surface roughness changes according to cutting speed and uncut chip thickness. Better surface values were also found at cutting speed = 62m/min [7]. Influence of rake angle of milling cutter on quality of TB17 was investigated. Researchers concluded that surface quality increases with rake angle [8]. Textures produced on rake face of tool reduced friction coefficient and improved lubrication of tool [9]. There are no certain guidelines made for producing surface textures and thus, input parameters can be optimized only by trial-and-error method [10].

Type of surface texturing greatly influences turning parameters and surface roughness of hard materials and alloys. Texturing of tools helped in improving wear resistance by reducing cutting zone temperature and also caused a reduction in machining forces [11]. Less BUE was found on tool edge having texture grooves 45º inclined to cutting edge [12]. Textured tools improved surface quality, tool wear, and cutting zone temperature as compared to conventional tools [13]. Therefore, demand for textured tools is rapidly increasing in market as it helps in reducing manufacturing costs, yields higher productivity, and also safeguard health of operators and environment. In present study, surface quality of AISI 4340 steel is evaluated with a parallel textured cutting tool. Taguchi L_9 OA is used with input parameters considered as cutting speed, feed rate, and depth of cut while surface roughness is considered as response parameter. Optimum results are verified by performing validation experiments.

2. LITERATURE REVIEW

Many researchers have found that textured tools significantly help in reducing surface roughness. A comparative analysis between spot and dimple textured tools at different cutting speeds showed that spot-textured cutting tools produced better surface quality than dimple and conventional tools [14]. Authors found that parallel textured tools produced lesser wear than non-textured tools. It was also found that textured tools produced better surface quality and lower cutting temperature [15]. In another study, surface roughness of steel was compared and analyzed by three different types of textures that were vertical,

parallel, and dot with a non-textured tool. It was concluded that surface quality improved at high values of cutting speed for all types of texturing [16].

When cutting AISI 420 steel, the effects of changing turning parameters such cutting speed, feed rate, and depth of cut were examined. Results showed that feed rate, which contributed 80.71% to surface quality, was the most important element [17]. Studying the impact of turning parameters on the surface roughness of AISI 4140 steel revealed that feed rate had the greatest influence on the quality, whilst cutting speed and depth of cut had the least. Additionally, it was found that increasing feed rate causes surface roughness to rise [18]. It was found that with cutting speed = 350m/min and feed rate = 0.15mm/rev, surface quality improved. It was also revealed that surface quality deteriorates at a higher feed rate [19]. Optimum condition for reducing surface quality of AISI 1045 steel was found as cutting speed = 116m/min, feed rate = 0.06mm/rev, and depth of cut = 0.25mm. Authors also inferred that surface roughness improves at a lower feed rate [20].

For obtaining high productivity and low manufacturing costs, industries need to operate in perfect conditions. Taguchi methodology is very useful for optimizing machining parameters and producing good quality and cheaper products. It is the most effective approach for solving complex problems as it makes use of an orthogonal array that studies parametric space with less experiments. Therefore, researchers utilized this approach in many research papers and optimal results provided by this approach showed a significant improvement in all types of responses. When Taguchi L_9 OA was utilized during turning of AISI D3 steel, it was found that feed rate had maximum contribution on surface roughness [21]. Taguchi L_9 OA was used on turning parameters like cutting speed, feed rate, and depth of cut during machining of SS-304 steel with carbide tools. After result analysis, best combination was found at cutting speed = 350m/min, feed rate = .12mm/rev, and depth of cut = .40mm [22]. Based on Taguchi optimization technique, at cutting speed = 90m/min, feed rate = .15mm/rev, and depth of cut = .5mm, improvement in surface roughness was seen to be 244% when compared with initial setting [23]. Minimum value of surface roughness of 52100 hardened alloy steel was achieved at optimum condition of cutting speed = 140m/min, feed rate = .08mm/rev, and depth of cut = .19mm [24].

3. EXPERIMENT DETAILS

3.1. Materials

AISI 4340 steel is selected as a workpiece for experiment. AISI 4340 steel is widely used in manufacturing industries as it possesses high hardness and can be machined by all conventional techniques. Dimensions of workpiece are taken as diameter = 25mm and length = 78mm. Composition of workpiece in terms of weight% is shown in Table 1.

Table 1. AISI 4340 steel composition

Component	C	Mn	P	S	Si	Ni	Cr	Mo	Fe
Weight (%)	.38-.43	.6-.8	.035	.035	.15-.35	1.65-2.00	.7-.9	.2-.3	Bal.

3.2. Machine tool and cutting tool

All experiments are performed on a lathe machine. Its specification is listed below:

Range of spindle speed: 45-800 rpm

Height of centers: 200mm

Diameter of a hole through spindle: 41mm

Required H.P.: 2 HP (1.5 KW)

Cutting tool inserts used for experimentation are carbide with ISO designation of E10-TH20. A ZNC 25 EDM machine with a capacity of 250L is used for making parallel textures on rake face of tool as shown in Figure 2. Copper electrode with a diameter of 500µm is used for making lines parallel to cutting edge. Distance between two successive lines is kept at 100µm and depth of lines is kept at 50µm. Parallel textures produced by EDM are depicted in Figure 3(a) and dimensions of parallel textures are depicted in Figure 3(b). These textured inserts are then brazed on a left-hand cutting tool holder. A TR200 surface roughness is used to measure the surface roughness of workpiece. To minimize variation in surface roughness, each experiment is performed three times and average surface roughness is considered.

Experimental setup in actual condition is shown in Figure 3(c). A minimum of three experiments at each level are performed to minimize variability. Pilot experiments are performed and a range of machining parameters is identified. Factors and their levels (Table 2) are selected and Taguchi L_9 OA is used (Table 3). Degree of freedom (DF) is calculated by equation (3.2) [25]

$$\mathrm{DF} = [(\text{level} - 1) + (\text{level} - 1) \times (\text{level} - 1) + 1] \quad (3.2)$$

Surface roughness values obtained for all nine experiments are then converted into S/N ratio which is further utilized for obtaining optimum level as well as to perform ANOVA analysis. Taguchi L_9 OA and surface roughness values are provided in Table 3. S/N ratio (Table 3) is solved by equation (4.1).

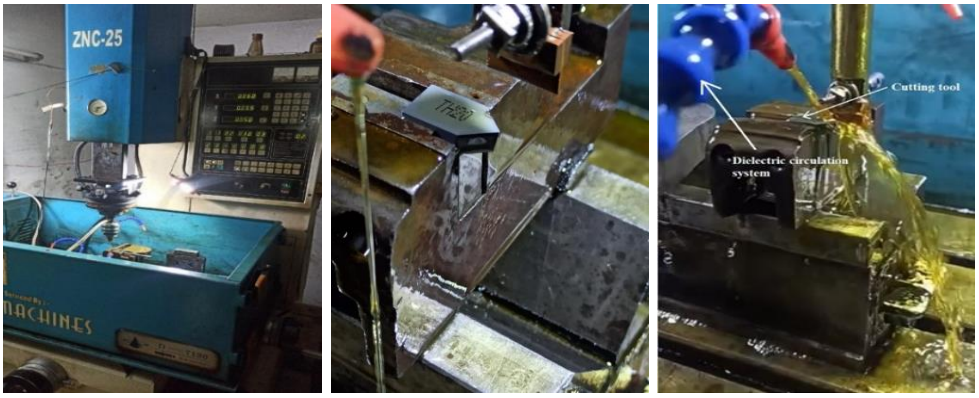

Figure 2. Texturing performed on EDM

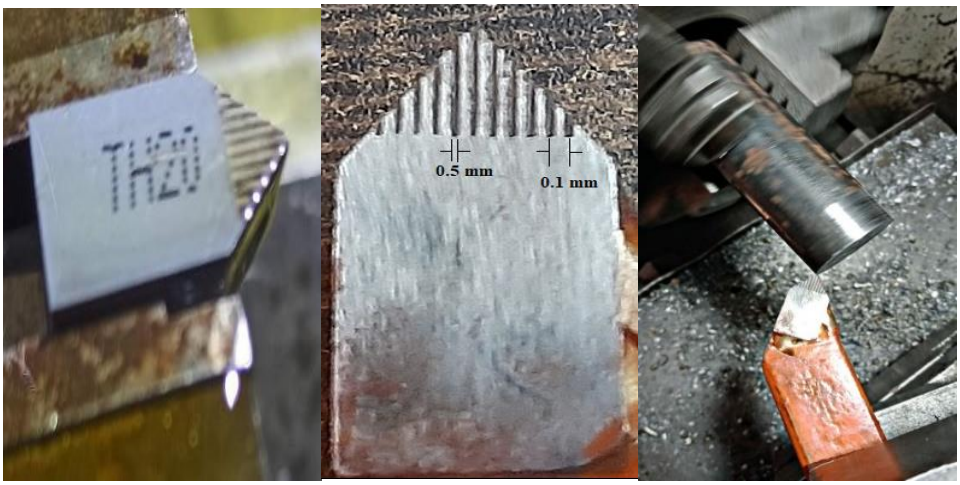

(a) (b) (c)

Figure 3: (a) Parallel textures produced by EDM; (b) Dimensions of parallel texture (c) Turning performed on AISI 4340 by parallel textured cutting tool

Table 2. Factors and levels

Factors	Symbols	1	2	3
Cutting speed (m/min)	V	80	100	120
Feed rate (mm/rev)	f	.16	.20	.24
Depth of cut (mm)	t	.25	.50	.75

Table 3. Experimental results for L_9 OA on parallel-texture

Trial No.	Input Conditions			Parallel-textured	S/N ratio
	V (m/min)	f (mm/rev)	t (mm)	Ra(μm)	
1	1	1	1	2.732	-8.7296
2	1	2	2	1.784	-5.0278
3	1	3	3	3.997	-12.0346
4	2	1	2	1.213	-1.6772
5	2	2	3	2.468	-7.8469
6	2	3	1	3.784	-11.5590
7	3	1	3	1.171	-1.3711
8	3	2	1	2.214	-6.9035
9	3	3	2	2.512	-8.0003

4. RESULT AND DISCUSSION

In this section, results obtained from Taguchi L_9 OA are analyzed in form of ANOVA and average value of S/N ratio. Confirmation experiments are performed to verify feasibility of the experiments.

4.1. Taguchi Method

Taguchi is a method of optimization in which parameters are optimized by using S/N ratio. It is calculated by using equation (4.1) [13] and values obtained are presented in Table 3.

$$\mathbf{S/N} = -\mathbf{10}\log\left[\frac{\mathbf{1}}{\mathbf{n}}\sum_{\mathbf{i=1}}^{\mathbf{n}}\mathbf{y_i^2}\right] \quad (4.1)$$

Here, yi = observed response, n = number of trials.

4.2. ANOVA analysis

S/N ratio (Table 3) is used for calculating ANOVA in sum of squares (SS), their adjusted values, F-ratio, and percentage contribution. ANOVA results are shown in Table 4. Graphical representation of percentage contribution is shown in Figure 4. Variation of S/N ratio for each level is shown graphically in Figure 5.

Table 4. ANOVA analysis

Parameters	DF	Adj SS	Adj MS	F-ratio	PC (%)
V	2	15.10	7.548	1	14.06
f	2	66.25	33.127	4.387	61.71
t	2	26.01	13.00	1.722	24.31
Pooled error[#]	--	15.10[#]	7.548	--	--
Total	6	107.36	--	--	--

Table 5. Average S/N ratio at each level

Mean	V	f	t
Level 1	-8.5973	-3.9259*	-9.0640
Level 2	-7.0277	-6.5927	-4.9017*
Level 3	-5.4249*	-10.5313	-7.0842

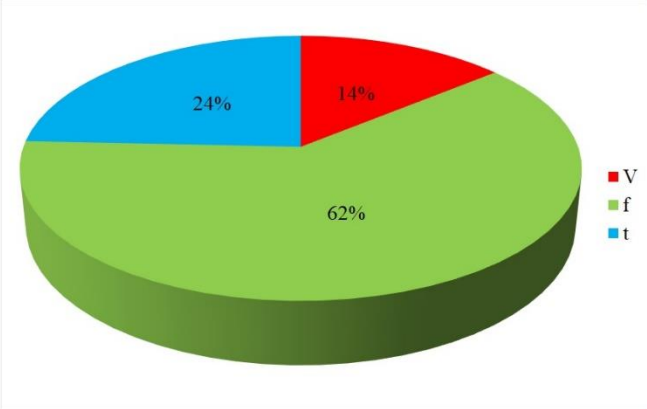

Figure 4. Percentage contribution of each factor

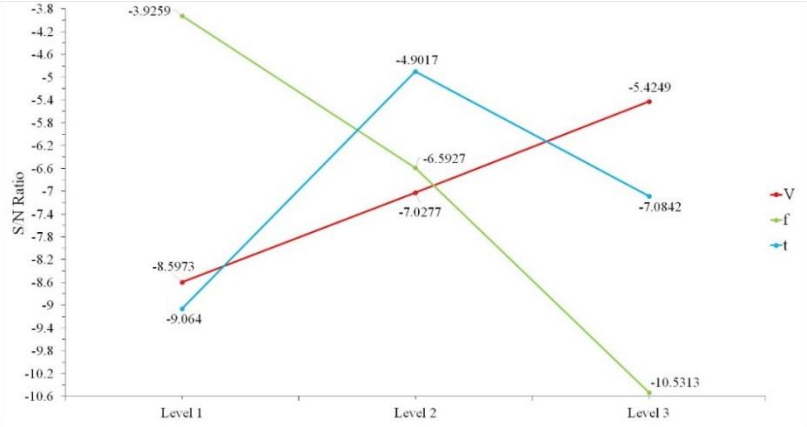

Figure 5. Variation of S/N ratio for each level

4.3. Validation of optimal level

Optimal level obtained after the analysis is V_3-f_1-t_2 (V = 120m/min, f = .16mm/rev, and t = .50mm). Experiments are conducted at optimal condition and then compared with initial setting. From analysis of Table 6, it is observed that surface roughness, Ra improves by 19.21% from initial setting parameters.

Table 6. Confirmation experiment

Response	Initial Setting	Optimum results		
		Predication	Experiment	%Improvement
	V_1-f_1-t_1	V_3-f_1-t_2	V_3-f_1-t_2	
Ra	2.732	–	2.207	19.21%

5. CONCLUSION

In present work, optimum level of textured tool is experimentally tested and verified. It is concluded that:

1. Percentage contribution of each factor on response is, cutting speed = 14.06%, feed rate = 61.71%, and depth of cut = 24.31%.
2. Optimal level of input parameter using Taguchi L_9 technique is, cutting speed = 120m/min, feed rate = .16mm/rev, and depth of cut = .50mm.
3. ANOVA analysis indicates that feed rate has maximum contribution on surface quality.
4. Improvement in response obtained during confirmation experiment is, Ra = 19.21%.

ACKNOWLEDGMENTS

The authors express their sincere gratitude to BBD University, Lucknow for providing support in this experimental study.

REFERENCES

[1] S. Kumar, R.N. Yadav, and R. Kumar, 'Modelling and optimization of duplex turning of titanium alloy (grade 5) using Taguchi methodology-response surface methodology', Int. J. Ind. Syst. Eng., 35(4), pp. 463-481, 2020.

[2] D. Jianxin, W. Ze, L. Yunsong, Q. Ting and C. Jie, 'Performance of carbide tools with textured rake-face filled with solid lubricants in dry cutting processes', Int. J. Refract. Met. Hard Mater.,30(1), pp. 164-172, 2012.

[3] J. Xie, M.J. Luo, K.K. Wu, L.F. Yang, and D.H. Li, 'Experimental study on cutting temperature and cutting force in dry turning of titanium alloy using a non-coated micro-grooved tool', Int. J. Mach. Tools Manuf, 73, pp. 25-36, 2013.

[4] N. Kawasegi, H. Sugimori, H. Morimoto, N. Morita, and I. Hori, 'Development of cutting tools with microscale and nanoscale textures to improve frictional behavior', Precis. Eng., 33(3), pp. 248-254, 2009.

[5] P. Koshy, and J. Tovey, 'Performance of electrical discharge textured cutting tools', CIRP Ann., 60(1), pp. 153-156, 2011.

[6] J. Kummel, D. Braun, J. Gibmeier, J. Schneider, C. Greiner, V. Schulze, and A. Wanner, 'Study on micro texturing of uncoated cemented carbide cutting tools for wear improvement and built-up edge stabilization', J. Mater. Process. Technol., 215, pp. 62-70, 2015.

[7] S.N.B. Oliaei, and Y. Karpat, 'Investigating the influence of built-up edge on forces and surface roughness in micro-scale orthogonal machining of titanium alloy Ti6Al4V', J. Mater. Process. Technol., 235, pp. 28-40, 2016.

[8] S.Y. Du, M.H. Chen, Z.S. Zhu, and X.N. Wang, 'Experimental research on Surface Integrity of Milling New Ultra-High Strength Titanium Alloy TB17', Modul. Mach. Tool Autom. Manuf. Tech, 4, pp. 125-129, 2017.

[9] T. Sugihara, and T. Enomoto, 'Performance of cutting tools with dimple textured surfaces: a comparative study of different texture patterns', Precis. Eng., 49, pp. 52-60, 2017.

[10] V. Sharma, P.M. Pandey, 'Recent advances in turning with textured cutting tools: a review', J. Clean. Prod., 137, pp. 701–715, 2016.

[11] Y. Wei, M.R. Kim, D.W. Lee, C. Park, and S.S. Park, 'Effects of micro-textured sapphire tool regarding cutting forces in turning operations', Int. J. Precis. Eng. Manuf. - Green Technol., 4(2), pp. 141-147, 2017.

[12] P. Sivaiah and U. Bodicherla, 'Effect of Surface Texture Tools and Minimum Quantity Lubrication (MQL) on tool Wear and Surface Roughness in CNC Turning of AISI 52100 Steel', J. Inst. Eng. (India): Series C, 101(1), pp. 85-95, 2019.

[13] P. Sivaiah, M. Revantha Kumar, S. Bala Subramanyam, and K.L.V. Prasad, K.L.V., 'A comparative study on different textured and untextured tools performance in turning process', Mater. Manuf. Process., 36(8), pp. 926-935, 2021.

[14] M.S. Sawant, N.K. Jain, I.A. Palani, 'Influence of dimple and spot-texturing of HSS cutting tool on machining of Ti-6Al-4V', J. Mater. Process. Technol., 261, pp. 1-11, 2018.

[15] S.K. Rajbongshi and D.K. Sarma, 'Performance parameters studies in the machining of AISI D2 steel with parallel-textured, groove-textured & non-textured cutting tool at the flank face', Int. J. Refract. Met. Hard Mater., 83, p. 104970, 2019.

[16] C. Pan, Q. Li, K. Hu, Y. Jiao, Y. Song, 'Study on surface roughness of Ger15 machined by micro-texture PCBN tools', Mach. 6(3), p. 42, 2018.

[17] A. Zerti, M.A. Yallese, I. Meddour, S. Belhadi, A. Haddad, and T. Mabrouk, 'Modeling and multi-objective optimization for minimizing surface roughness, cutting force, power, and maximizing productivity for tempered stainless steel AISI 420 in turning operations', Int. J. Adv. Manuf. Technol., Vol. 102, Issue 1 (4), pp. 135-157, 2019.

[18] A. Sahinoglu, and M. Rafighi, 'Investigation of vibration, sound intensity, machine current, and surface roughness values of AISI 4140 during machining on the lathe', Arab J Sci Eng., 45(2), pp. 765-778, 2020.

[19] P. Chandra, C.R.P. Rao, and R. Kiran, 'Influence of machining parameter on cutting force and surface roughness while turning alloy steel', Mater. Today: Proc. 5(5), pp. 11794-11801, 2018.

[20] A.T. Abbas, M.K. Gupta, M.S. Soliman, M. Mia, H. Hegab, M. Luqman and D.Y. Pimenov, 'Sustainability assessment associated with surface roughness and power consumption characteristics in nanofluid MQL-assisted turning of AISI 1045 steel', Int. J. Adv. Manuf. Technol., 105(1), pp. 1311-1327, 2019.

[21] J.S. Dureja, R. Singh, and M.S. Bhatti, 'Optimizing flank wear and surface roughness during hard turning of AISI D3 steel by Taguchi and RSM methods', Prod. Manuf. Res., 2(1), pp. 767-783, 2014.

[22] N.J. Rathod, M.K. Chopra, P.K. Chaurasiya, U.S. Vidhate, and A. Dasore, 'Optimization on the Turning Process Parameters of SS 304 Using Taguchi and TOPSIS'. Ann. Data Sci., pp.1-15, 2022.

[23] A. Hascalik, and U. Caydas, 'Optimization of turning parameters for surface roughness and tool life based on the Taguchi method', Int. J. Adv. Manuf. Technol., 38(9), pp. 896-903, 2008.

[24] S. Mane, and S. Kumar, 'Analysis of surface roughness during turning of AISI 52100 hardened alloy steel using minimal cutting fluid application', Adv. Mater. Process. Technol., pp. 1-12, 2020.

[25] P.J. Rose, 'Taguchi Technique for Quality Engineering', Tata McGraw-Hill, New York, 1996.

Finite Element Analysis of Laser Cladding Process

[1]Devendra Kumar Gautam, [2]Audhesh Narayan, [3]Satish Kumar, [4]Ajaya Bharti

Department of Applied Mechanics, Motilal Nehru National Institute of Technology Allahabad, Prayagaraj Uttar Pradesh 211004

[1]gautamdevendra070@gmail.com, [2]anarayan@mnnit.ac.in, [3]satistme@mnnit.ac.in, [4]abharti@mnnit.ac.in

Abstract

Laser cladding (LC) is a novel manufacturing process that can be used for coating and prototyping, among other things. In most situations, complex processing processes and the development and growth of thin clads in the micrometer to millimeter range remain unsolved. A thermo-mechanical finite element model with a Gaussian moving heat source and an element birth and death technique has been developed to describe powder injection laser cladding of CPM9V over H13 tool steel. The temperature distribution over the clad material is determined using Ansys software and a finite element analysis. During the FEA change of laser power and scanning speed, I discovered a temperature gradient. I also discovered a correlation between temperature gradient and laser power, as well as a correlation between temperature gradient and scanning speed. This understanding should come in useful when it comes to repairing structures that are subjected to cyclic thermo-mechanical loads.

Keywords. — Heat transfer, FEA, Laser Cladding Process, Simulation.

1. INTRODUCTION

The laser cladding is a weld forming process and is costing technology that complements thermal spray. It is gradually used as an alternative to the Plasma Transferred Arc (PTA) welding and simply outperforms conventional welding methods as the Tungsten Inert Gas (TIG) designed for advanced weld repairing applications[1]. The heat source's laser beam is dimmed on the workpiece with a predetermined spot size during the LC process. A powder nozzle deli vers the powder coated material into the melting area with inert gas. Single grooves, entire layers, or even huge agglomerates are deposited by moving laser beam and powder nozzles over the workpiece surface. LC process is a material deposition method in which a wire or powder material is melted and consolidated using a laser to clad part of the substrate or to fabricate a shape close to the array. It has ability to mix two or more powders and control the feed rate of each powder stream makes laser coating a versatile process for manufacturing heterogeneous components or functional grade material[2].

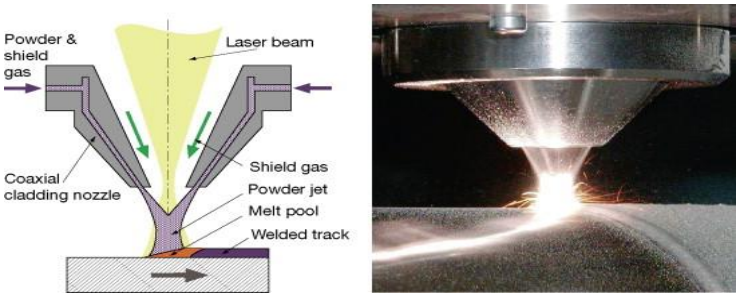

Figure 1. Laser Cladding Process[3]

2. FINITE ELEMENT MODELLING OF LC PROCESS

To determine simulation results of temperature dispersion, a FEM-based transient thermal model was constructed. Different materials Such as the clad material CPM9V vanadium carbide steel and substrate material H13 tool steel are used such as the work material with a size of the clad material 6 × 3 × 0.6 mm and substrate material 6 × 6 × 6 mm for performing the FEM analysis[4]. The model is further discredited into smaller size elements for more obtain more precise results. Standard ANSYS software was used to estimate the temperature distribution inside the work material during the laser cladding process.

2.1 Three-dimensional (3-D) Model

A semi-symmetric model measuring 6 mm 6 mm 6 mm was designed for simulation. It is intended to conduct a combined investigation of these thermal and mechanical processes. Eight nodded coupled temperature distributions were used to calculate the influence of the thermal stress generated throughout this operation.

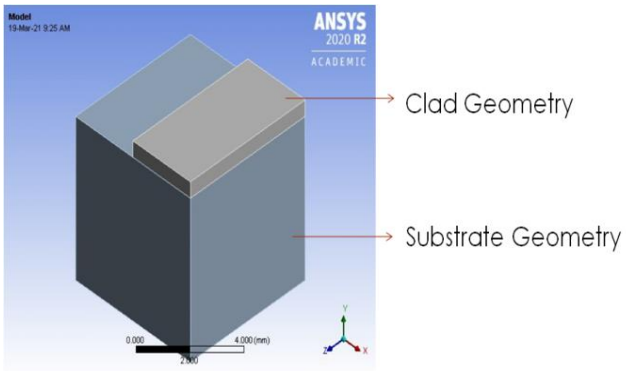

Figure 2. Geometry of the 3-D model

In 3-D model 8- Nodded Fine Meshing of the both clad and substrate body. The node has 9790 elements, and the total number of elements is 1968.

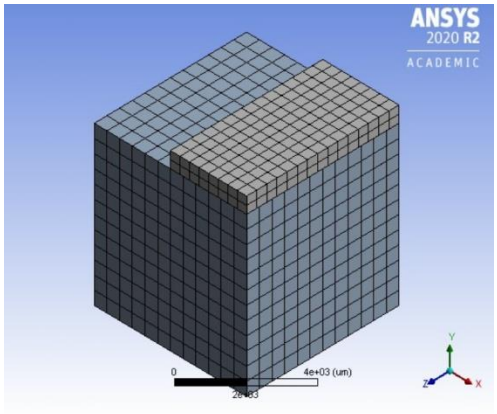

Figure 3. Meshing of 3-D Model

2.2 Loading and boundary condition

With a linear decrease in heat input with depth of penetration, the source is predicted to emit a Gaussian moving heat source distribution of laser power. Heat transfer via convection with a heat transfer coefficient of 15 W/m^{2}K is one of the thermal boundary conditions and heat transfer by radiation with emissivity of 0.3 lead to thermal damage of the surfaces[5].

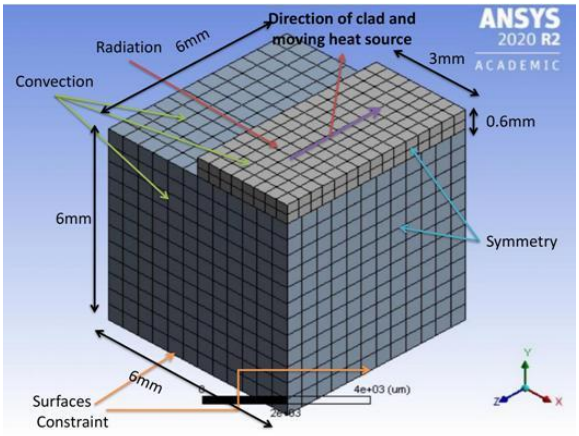

Figure 4. Geometry of 3-D model showing with thermal loading and boundary conditions

In the laser cladding process, the powder injection procedure is adopted to clad over the surface of the substrate material. It's used to model the effect of powder deposition, along with the element birth-death methodology.

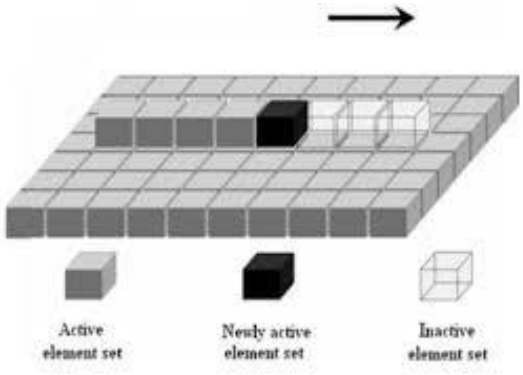

Figure 5. The element birth methodology is used to model powder deposition on the surface of the substrate material during the LC process[5].

3. MODEL VALIDATION

The present model was compared with the previously developed model. The Nodal temperature plots over the work material surface in depth were compared for clad material CPM9V vanadium carbide steel and substrate material H13 tool steel. Even though there were some different temperature values but the trend was quite similar to the previous model. It was observed that the previous model was based on constant the laser power: 1700 Watt, feed rate: 5 gram/min, beam diameter of laser: 3 mm and scanning speed: 200 mm/min[5]. This model was based on the empirical relationship of nodal temperature over depth. Also the previous model took into consideration a varying he figures below predict the difference of nodal temperature with depth distance for materials and a comparison is made between the present data.

3.1 Nodal temperature changes with depth

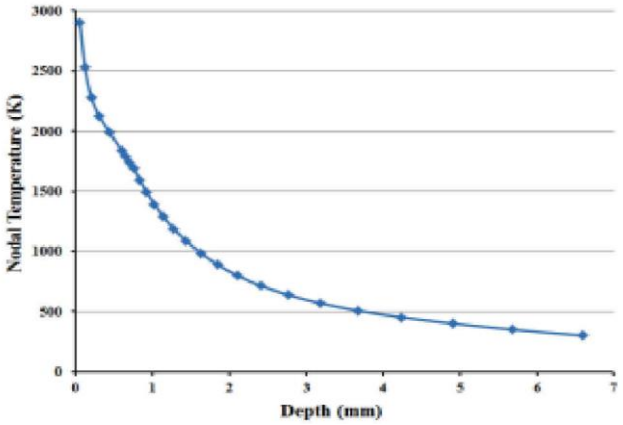

Figure 6. Variation of nodal temperature vs. Depth[5]

1) Nodal temperature changes with depth (input parameter in Ansys)

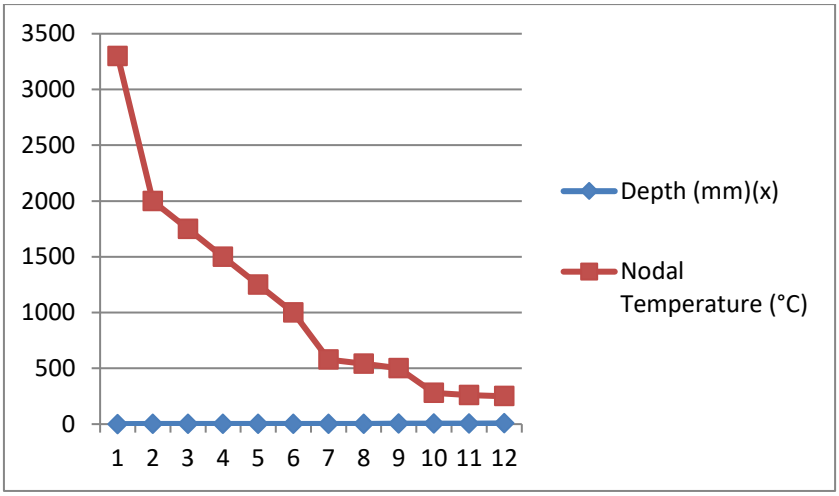

Figure 7. Nodal temperature vs. Depth with input parameter in Ansys.

2) Comparison of nodal temperature with depth

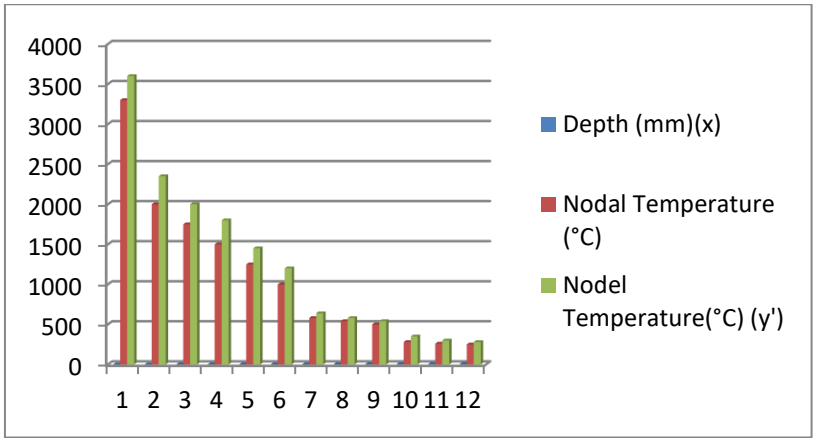

Figure 8. Comparison of nodal temperature vs. depth

Where: Nodal Temperature (^{0}C) taken from literature and Nodal Temperature (^{0}C) (y') input parameter is Ansys.

When comparing the clad height predicted by the 3-D model during the LC process via Ansys simulation to the experimental data, there was a 14 percent variation in the clad height forecast.

4. STUDY OF PARAMETER VARIATION OF TEMPERATURE WITH INPUT PARAMETER

With the laser power (1500–2000) watt input parameter, Ansys software was utilized to model the LC process. The laser beam has a diameter of 3 mm and a scanning speed of 2–4 mm/sec. During the LC process, determine the correlation between thermal and material properties, as well as the thermal gradient.

1) The coupled thermo-mechanical 3-D model predict the coating value for the Beam diameter of laser 3 mm, scanning speed of 240 mm/min, feed rate of 5 gram/min and the laser power of 1200 Watt.

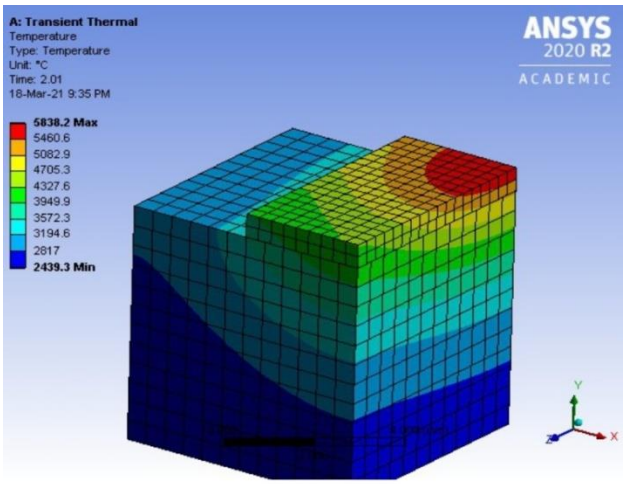

Figure 9. Contour plot of nodal temperature

2) The coupled thermo-mechanical model input parameter for simulation the beam diameter of laser 3 mm, scanning speed of 240 mm/min, feed rate of 5 gram/min and the laser power of 1500 Watt.

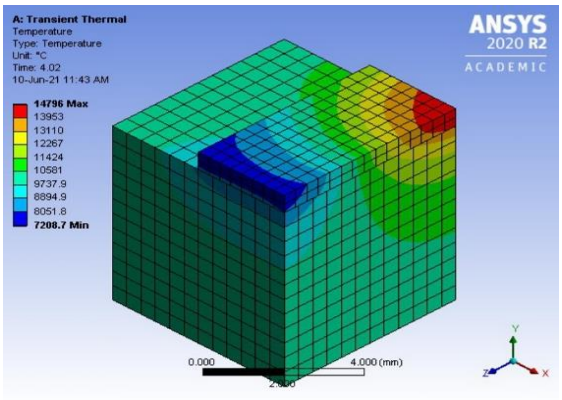

Figure 10. Contour plot of nodal temperature

5. RESULTS

In this chapter I have to show the improvement in the performance and parameters obtain by Finite element analysis of LC process.

5.1 Convection

Table1: Transient thermal analysis (Convection)

Temperature [°C]	Convection Coefficient [W/mm²·°C]
1.	1.24e-006
10.	2.67e-006
100.	5.76e-006
200.	7.25e-006
300.	8.3e-006
500.	9.84e-006
700.	1.101e-005
1000.	1.24e-005

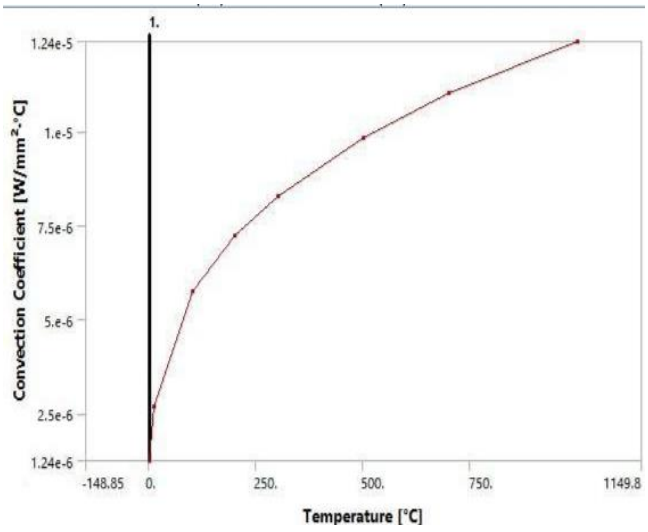

Figure 11. Convection during laser cladding

1) Temperature Distribution

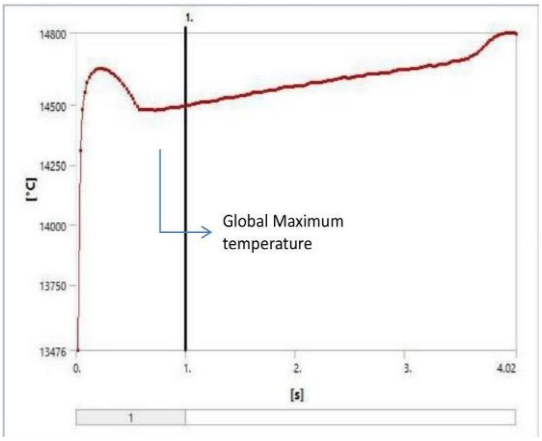

Figure 12. Global maximum temperature by FEM

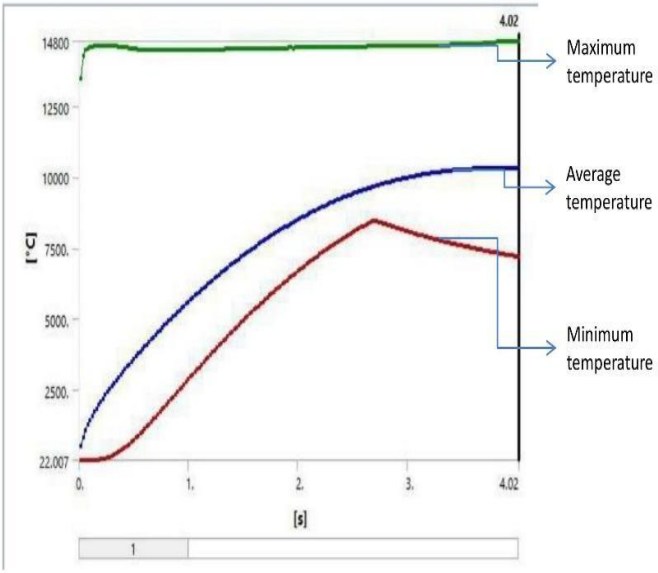

Figure 13. Variation of temperature by FEM

2) Transient Heat Transfer Analysis

1) With increasing laser intensity, the temperature gradient increases, with the largest gradient in the vertical Z direction, followed by the X and Y directions. The thermal gradient in the X and Y directions is smaller in the present FEA results as compared to the Z direction.

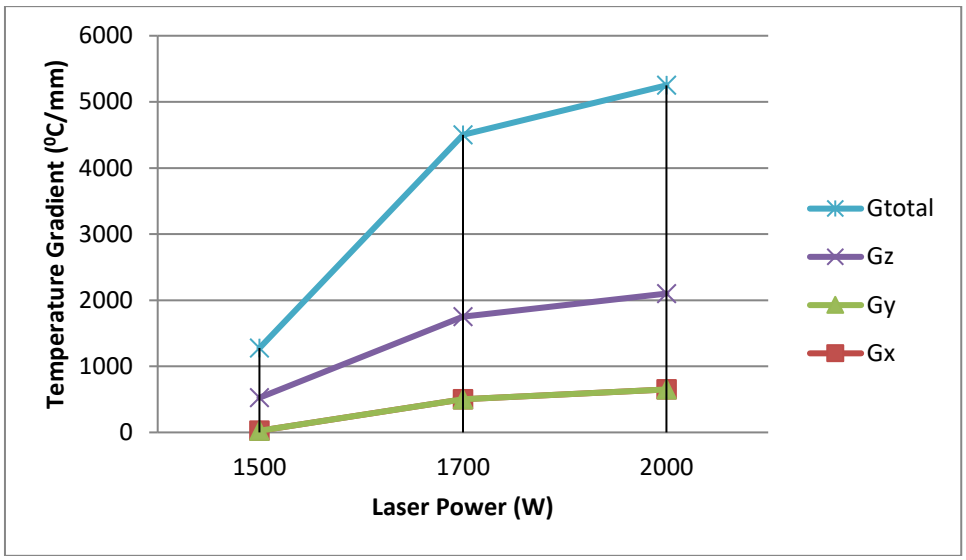

Figure 14. Changes in the simulated thermal gradient as a function of laser power

2) It is computed how scanning speed affects the thermal gradient. The temperature gradient is clearly minimized as the scanning speed increases.

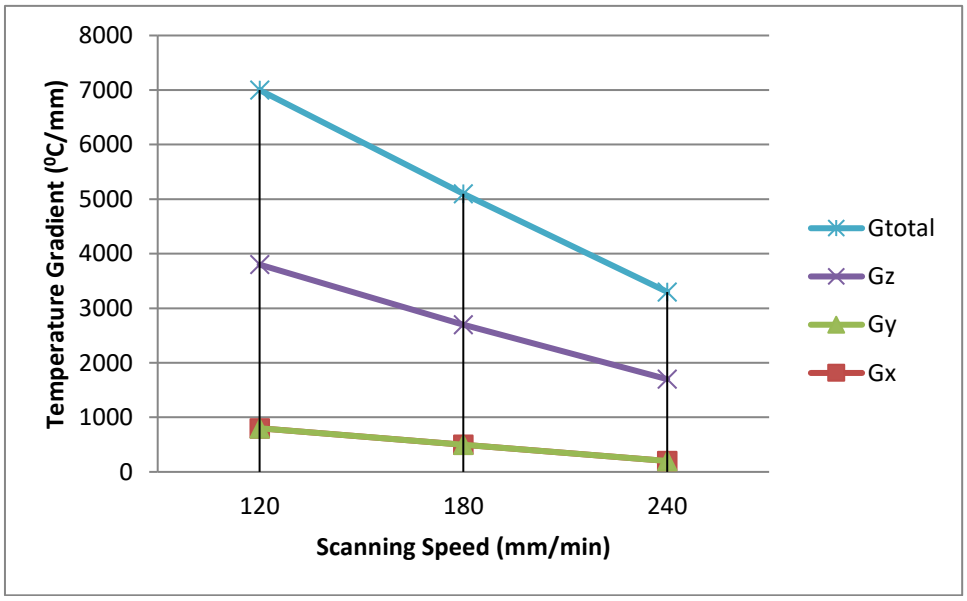

Figure 15. Scanning speed affects the calculated thermal gradient.

Thermal gradients in the x, y, and z directions are represented by G_x, G_y, and G_z, respectively due to LC process clad over the surface of the substrate materials.

6. DISCUSSION

It is observed that temperature gradient of work material increases with increases when the laser power increases. The thermal gradient decreases as the scan speed increases.

- In the present FEA results when the laser power increases 1500Watt - 2000Watt the total temperature gradient increases between 1200 ^{0}C/mm – 5200 ^{0}C/mm. the temperature gradient in X direction and Y direction are obtained on the lower side as compared with Z direction (depth).
- When the scanning speed increases 120 mm/min – 240 mm/mm the total temperature gradient reducing between 7000 ^{0}C/mm – 3200 ^{0}C/mm.

In the LC process, clad material (CPM9V) provides decreased heat distortion, reduced dilation, low porosity levels, and greater surface uniformity over the substrate material (H13). It can be used to create a protective layer as well as restore broken or damaged surfaces.

7. CONCLUSIONS

The cladding process' combined thermo-mechanical analysis is built on the concept that the temperature profile produced from thermal analysis may be utilized to predict the temperature distribution across the LC process' duration. A thermal analysis of a process can yield temperature profiles, which can be used to calculate dilution and heat affected zones. In the current FEA results, the temperature gradient in the Z direction is larger than in the X and Y directions. The influence of scanning speed on temperature gradient is greatly reduced as scanning speed increases.

REFERENCES

[1] Gu ST, Chai GZ, Wu HP, Bao YM. Characterization of local mechanical properties of laser-cladding H13-TiC composite coatings using nanoindentation and finite element analysis. Mater Des. 2012;39:72-80. doi:10.1016/j.matdes.2012.02.028

[2] Parekh R, Buddu RK, Patel RI. Multiphysics Simulation of Laser Cladding Process to Study the Effect of Process Parameters on Clad Geometry. Procedia Technol. 2016;23:529-536. doi:10.1016/j.protcy.2016.03.059

[3] Nazemi N, Urbanic J. A FINITE ELEMENT ANALYSIS FOR THERMAL ANALYSIS OF LASER CLADDING OF MILD STEEL WITH P420 STEEL POWDER.; 2016. http://proceedings.asmedigitalcollection.asme.org/pdfaccess.ashx?url=/data/conferences/asmep/90978/

[4] Vundru C, Paul S, Singh R, Yan W. Numerical analysis of multi-layered laser cladding for die repair applications to determine residual stresses and hardness. In: Vol 26. Elsevier B.V.; 2018:952-961. doi:10.1016/j.promfg.2018.07.122

[5] Paul S, Singh R, Yan W. Thermo-mechanical modelling of laser cladding of CPM9V on H13 tool steel. Proc 5th Int 26th All India Manuf Technol Des Res Conf (AIMTDR 2014). 2014;(Aimtdr):10-16.

Biographies

Devendra Kumar Gautam is from Prayagraj, Uttar Pradesh, India**.** He has completed his Bachelor's degree in Mechanical Engineering from Rajkiya Engineering College Azamgarh in 2018, Master's degree in Computer Aidded Design and Manufacturing from MNNITA, Prayagraj in 2021, and Pursuing philosophy of doctorate degree from MNNITA, Prayagraj. His research interests lie in Fatigue damage analysis of alloys and composites.

Dr. Audhesh Narayan is an associate professor in the Department of Mechanical Engineering at Motilal Nehru National Institute of Technology Allahabad, Prayagraj, India. He received his Ph.D. degree in Mechanical Engineering in 2012 from Motilal Nehru National Institute of Technology Allahabad, Prayagraj, India. His current research interests include Conventional and Advanced Machining Processes, Deep Grinding Processes, Hybrid Machining Processes, Micromachining Processes and FEM Applications in Manufacturing.

Dr. Satish Kumar is currently working as an Assistant Professor at Applied Mechanics Department, Motilal Nehru National Institute of Technology Allahabad, Prayagraj, India. He has completed his B. Tech from NIT Jalandhar, M. Tech, and Ph.D. from IIT Roorkee. His research interests lie in the design, fabrication, and mechanical characterization of adaptive membrane-based lightweight structures for space applications, which he plans to study using a combined experimental and numerical approach. He has published seven peer-reviewed journal articles, seventeen international conference papers, and filled two Indian patents. He has successfully completed one research project and three consultancy projects.

Dr. Ajaya Bharti is an associate professor in the Department of Applied Mechanics at Motilal Nehru National Institute of Technology Allahabad, Prayagraj, India. He received his Ph.D. degree in Applied Mechanics in 2014 from Motilal Nehru National Institute of Technology Allahabad, Prayagraj, India. His current research interests include Fatigue and Fracture Mechanics, Wear, Corrosion, Powder Metallurgy, Physical Metallurgy, Synthesis and Characterization of Advanced Materials, Biomaterials, Severe Plastic Deformation (SPD), Structural Health Monitoring.

Dynamic Analysis and Shape Control of Membrane Structures

[1]Amiy Chandraul, [2]V. Murari, [3]Satish Kumar

Motilal Nehru National Institute of Technology Allahabad, Prayagraj, India

[1]chandraul.amiy@gmail.com,[2]vmurari@mnnit.ac.in, [3]satistme@mnnit.ac.in

Abstract

This research examines the dynamic analysis and shape control of membrane structures designed to function as space structures under a variety of loading conditions. The finite element method was used in commercially available software to perform the analysis. Square membrane structures have been analyzed under on-orbit loading conditions. The present analysis gives the results of various dynamic properties of membranes such as natural frequencies, mode shapes, etc. PVDF and PZT smart materials were used at optimized locations of membranes to minimize shape error. It has been observed that the shape error of the membrane is minimized significantly after using smart materials.

Keywords: Membrane Structures, Pre-Stressed, FEM, Natural Frequency, Mode Shape, Shape Error, Finite Element Method, Smart Materials.

1. INTRODUCTION

Membrane structures play a vital role in the fields of architecture, civil engineering, and space technology. In space, these structures are widely used as communication satellite antennas, space telescopes, solar arrays, etc. [1]. Membrane structures have the capability to play an advanced role in space-borne structures due to their inherent characteristics like ultra light weight, ability to stow in small volume, demanding small space requirements, high flexibility to change their shape etc. These structures show very similar properties to conventional materials like Aluminium, Carbon Fiber, etc. These membrane structures are very thin and possess negligible bending and compressive stiffness. So these thin structures need to be pre-tensioned to function as an engineering structural element [2, 3]. For the current study, an ultra-lightweight inflatable space-based membrane structure made of Kapton, Mylar, and Kevlar was used. Inflatable structures, often known as gossamer structures and are inflated with gas, usually air [4]. In space, ambient conditions are perilous and unpredictable. As a result, the challenges for the long-term survival of space-borne structures are complex. Space-borne structures like inflatable antennas and solar arrays are subjected to thermal distortion, bombarding particles (meteoroids) and huge vibrations while being launched. These unwanted elements reduce the performance of these structures. That's why dynamic properties calculation is paramount for safety and accuracy of the system. Huge vibrations create large amount of out-of-plane displacement which affects the shape

accuracy and the main concern with these structures is how they keep their shape intact. Shape accuracy creates the new opportunities in the field of space exploration and structures with high performance. One such technique is using smart materials, for instance, Lead Zirconate Titanate (PZTs), Polyvinylidene Fluoride (PVDFs), etc [5]. These materials will behave as sensors and actuators. These smart materials will help to reduce large deformations by controlling them and maintaining the shape as smoothly as possible. So PVDF and PZT are going to be used at optimal locations. This paper deals with FEM based numerical analysis of square membrane structures at various on-orbit loading conditions. Natural frequencies, mode shapes, and out of plane displacement have been calculated using the finite element method in ABAQUS. Out-of-plane displacement with and without using smart materials (PVDF and PZT) was also compared.

2. MEMBRANE MATERIALS PROPERTIES

For exploring space at a level of admiration with minimal cost and the utmost possible performance, researchers must use materials that possess high mechanical and thermal stability over a long period of time in their proposed orbital environment. All space-borne structures are comprised of a light and very thin film-based material that would be amenable to compact stowage volume and deployment in space. The achievement of light-weight, large-deployable, and compact launch volume structures poses a great challenge to the scientific community. Numerous thin polymeric films have been used in space applications. Table 1 lists the properties of the membrane.

Table 1. Membrane material properties [6]

Materials	Kapton	Mylar	Kevlar
Density[ρ](Kg/m3)	1430	1390	1400
Young's Modulus[E](MPa)	2000	5000	100000
Poisson's ratio[μ]	0.34	0.35	0.30
Thermal conductivity(w/mk)	0.12	0.14	0.04

3. MATHEMATICAL MODELLING OF MEMBRANE STRUCTURE

A membrane assumed as a thin plate loaded with tension. It cannot sustain bending resistance and restoring forces arises only when subjected to tensile loading [7]. Membrane behaves similarly to a plate, while string behaves similarly to a beam. The perfect example of membrane is a drumhead.

The membrane structures are analyzed by considering the following assumptions;

1. The effect of gravity is insignificant.
2. Displacement is small and takes place only in z-direction.
3. Membrane is very thin.
4. Pre-stress and mass density is considered to be uniform throughout the membrane structure.

5. The transverse shear stresses are insignificant.

A flat curve S bounds a region in *xy* plane to formulate the equation of motion for membrane structures, as shown in Fig. 1. Pressure loading acts normal to the plane surface of membrane (z-direction) denoted by *f*(*x*, *y*, *t*) and *p* is the tension at a point.

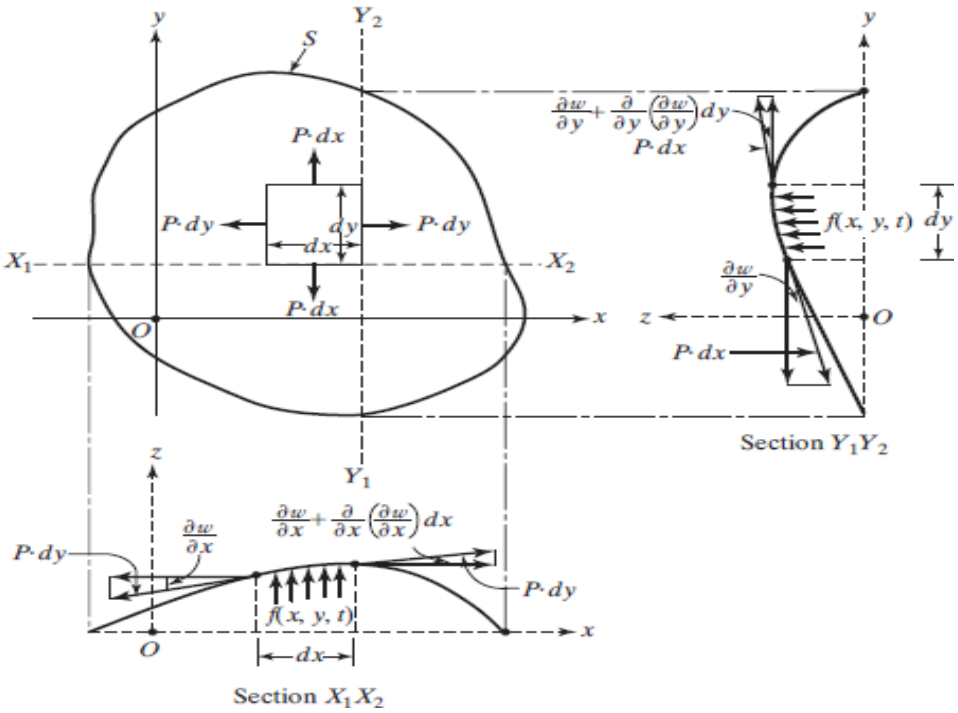

Figure 1. A membrane under uniform tension [7]

The magnitude of tension *p* typically remains invariable at every point of the membrane, making it completely visible in the drumhead. A very small elemental area *dxdy is considered in the x-y* plane, forces of magnitude *pdx* and *pdy* will act on the sides that are parallel to the *x* and *y*-axes, respectively, as shown in Fig. 1. A resultant force in the z direction emerges as a result of these two forces.

$$\left(p\frac{\partial^2 w}{\partial y^2}dxdy\right) \quad \text{and} \quad \left(p\frac{\partial^2 w}{\partial x^2}dxdy\right)$$

The pressure force acting normal to the plane surface of membrane is f (x, y, t) dx dy, and the inertia force is

$$\rho \text{ (x, y) } p\frac{\partial^2 w}{\partial t^2}dxdy$$

where ρ (x, y) is the mass of membrane per unit area. The following is the equation of motion for the membrane's forced vibration

$$p\left(\frac{\partial^2 w}{\partial x^2}+\frac{\partial^2 w}{\partial y^2}\right)+ f = \rho\frac{\partial^2 w}{\partial t^2} \quad (1)$$

Eq. (1) gives the equation of free vibration if force f (x, y, t) = 0

$$c^2\left(\frac{\partial^2 w}{\partial x^2}+\frac{\partial^2 w}{\partial y^2}\right)=\frac{\partial^2 w}{\partial t^2} \quad (2)$$

Where, $c=\left(\frac{p}{\rho}\right)^{1/2}$ and $\nabla^2=\frac{\partial^2}{\partial x^2}+\frac{\partial^2}{\partial y^2}$ (3)

Equations (1) and (2) can be written in the following way

$$p\nabla^2 w+ f = \frac{\partial^2 w}{\partial t^2} \quad (4)$$

And

$$c^2\nabla^2 w=\frac{\partial^2 w}{\partial t^2} \quad (5)$$

Equation (5), with c representing wave velocity, is sometimes known as the 2-D wave equation. Variable separable method is going to be used for free vibration condition. A square membrane with side a along x and y direction is considered. *w*(x, y, t) is assumed to be

$$w(x, y, t) = W(x, y)\, T(t) = X(x)\, Y(y)\, T(t) \quad (E.1)$$

By using Eq. (E.1), we obtain

$$\frac{\partial^2 w}{\partial t^2}=w(x,y)T''(t)$$

$$\frac{\partial^2 w}{\partial x^2}=\frac{\partial^2 w(x,y)}{\partial x^2}T(t)$$

$$\frac{\partial^2 w}{\partial x^2}=\frac{\partial^2 w(x,y)}{\partial y^2}T(t)$$

Using variable separable method, we obtain

$$\frac{T''(t)}{T(t)} = c^2 k^2 \quad \text{(i)}$$

$$\frac{X''(x)}{X(x)} = j^2 \quad \text{(ii)}$$

$$\frac{Y''(y)}{Y(y)} = k^2 - j^2 \quad \text{(iii)}$$

We get the solutions of Equations by solving Equations (i), (ii) and (iii)

$$T(t) = c_1 \cos ckt + c_2 \sin ckt \quad \text{(A)}$$

$$X(x) = c_3 \cos jx + c_4 \sin jx \quad \text{(B)}$$

$$Y(y) = c_5 \cos \sqrt{k^2 - j^2}\, y + c_6 \sin \sqrt{k^2 - j^2}\, y \quad \text{(C)}$$

The boundary and initial conditions can be used to determine the constants $c_1 to c_6$.

3.1 Initial and Boundary Conditions-

Initial and boundary conditions are required to determine a unique solution. Typically, the displacement and velocity of the membrane at time t = 0 are $w_0(x, y)$, $w_0'(x, y)$. Hence the initial conditions are specified by

$$w(x, y, 0) = w_0(x, y)$$

$$\frac{\partial w}{\partial t}(x, y, 0) = w_0'(x, y)$$

The boundary conditions are as follows:

1. If the square membrane is hinged at the all four corners, the boundary conditions will be-

$$w(0,0,t) = 0; w(a,0,t) = 0; w(0,a,t) = 0 \text{ and } w(a,a,t) = 0 \qquad t \geq 0$$

4. RESULTS AND DISCUSSIONS

The finite element method (FEM) in ABAQUS is used to analyze free and forced vibrations of single-layer flat square-shaped membranes. The square membrane has a thickness (t) of 0.05 mm and side length of 200 mm. It is supported on knife edges, which essentially implies that all four corners are hinge supported. As shown in Fig. 2, all membrane models are pre-stressed by 10 N/m in the *x-y* plane. For meshing of the configuration, Quadrilateral membrane elements have been used (the M3D4 membrane element, which is a 4 node quadrilateral element). A membrane element is a surface or 2D element that transmits only in-plane forces. So it is necessary to pre-stress these elements to carry out the vibration analysis. According to the assumption, the modulus of elasticity of the membrane will be

equal to E when the membrane is in tension and will be very small when subjected to compression. This explains why the membrane elements cannot endure any in-plane compressive loads. Static and linear perturbation analyses with pre-stress effects have been performed in ABAQUS. The effects of various parameters, such as pre-stress, boundary conditions, thickness, and materials behavior, are analyzed using FEM. The analysis has been performed on several models whose results are exposed below;

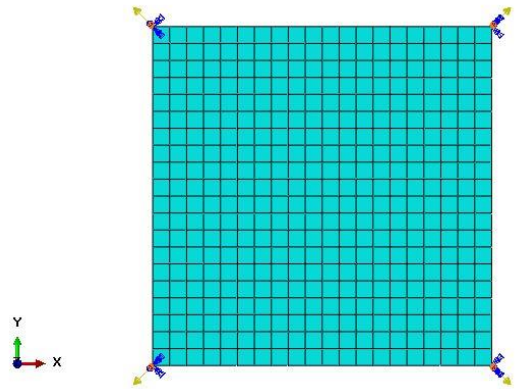

Figure 2. Meshed square membrane showing BCs

4.1 Square membrane with free vibration

Table 2 presented the computational results of natural frequencies obtained by the finite element analysis. The analysis is performed for various space materials. The graph between mode number and natural frequency is plotted for all three materials and shown in Fig. 3. Fig. 4 shows the various mode shapes of kapton membrane.

Table 2. Comparison of Natural frequencies of various square membranes

Mode No.	**Kapton (Hz)**	**Myla r(Hz)**	**Kevlar (Hz)**
1	1.573	2.523	11.246
2	1.573	2.523	11.246
3	2.477	3.973	17.704z
4	2.477	3.973	17.704
5	2.477	3.973	17.704

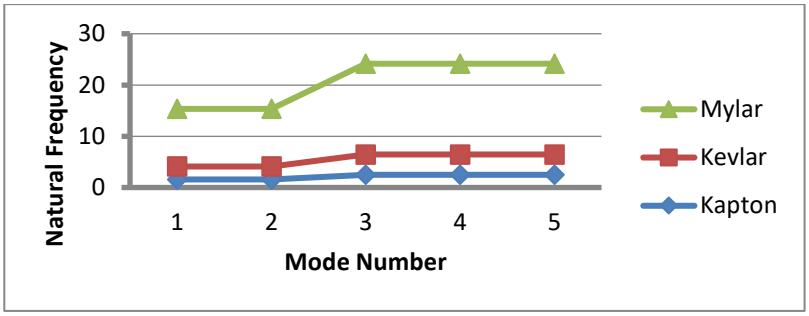

Figure 3. Graphical representation of natural frequencies for different membrane materials

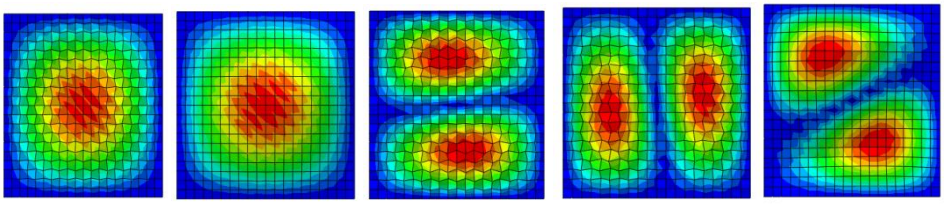

i) Mode 1 ii) Mode 2 iii) Mode 3 iv) Mode 4 v) Mode 5

Figure 4. Different mode shapes of the Kapton square membrane

4.2 Square membrane with forced vibration

The forced vibration analysis will focus on the steady-state behavior of the kapton membrane due to transversely applied periodic loading at the centre of the surface. The applied load is in the form of;

$$F = Fo*\sin(\omega t)$$

The magnitude of loading is 10 N and 500 Hz is the frequency applied. Fig. 5 shows the various mode shapes of kapton membrane. Fig. 6 shows the plot between transverse displacement (units in cm) and mode number.

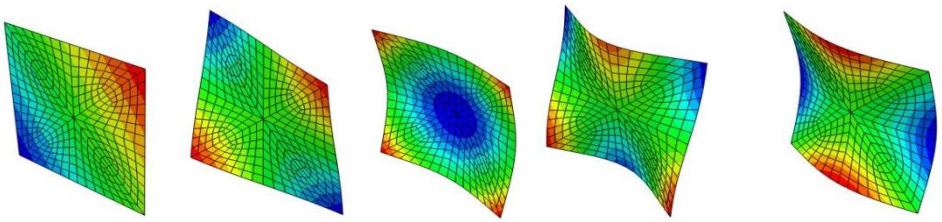

i) Mode 1 ii) Mode 2 iii) Mode 3 iv) Mode 4 v) Mode 5

Figure 5. Different mode shapes of the Kapton square membrane during periodic loading

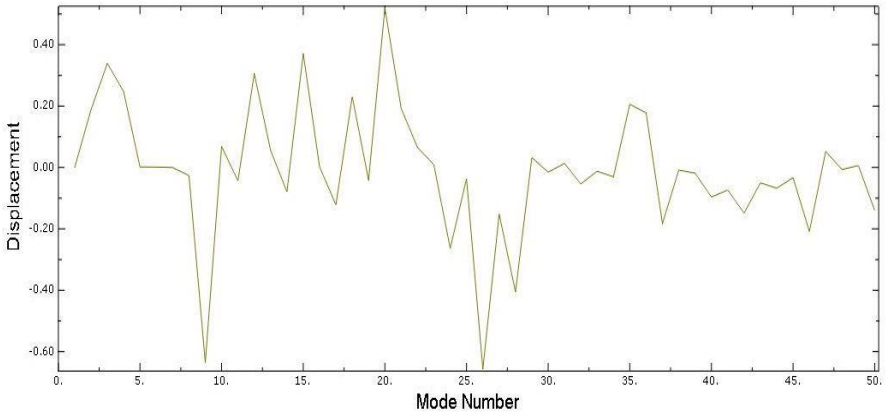

Figure 6. Displacement response with mode number

4.3. Square membrane with forced vibration attached with one smart material

PVDFs and PZTs are smart materials that are linked to the membrane near the centre (Node No.85), as shown in Fig. 7. Loading conditions will be similar to those in the prior scenario. The smart material's shape deforms as a result of the voltage applied to it. PVDF and PZT undergo induced deformation, which aids membrane recovery from a damaged state. Fig. 8 shows a plot of transverse displacement (units in mm) vs. mode number for kapton coupled to PVDF and PZT. As seen in Fig. 8, PVDFs are substantially more efficient than PZTs since PVDFs have less transverse displacement.

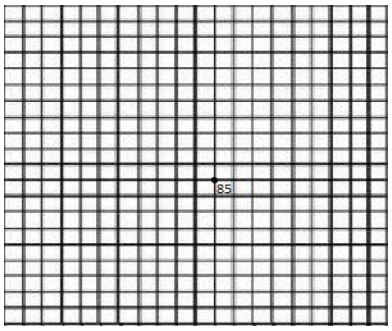

Figure 7**.** Meshed square membrane showing node 85

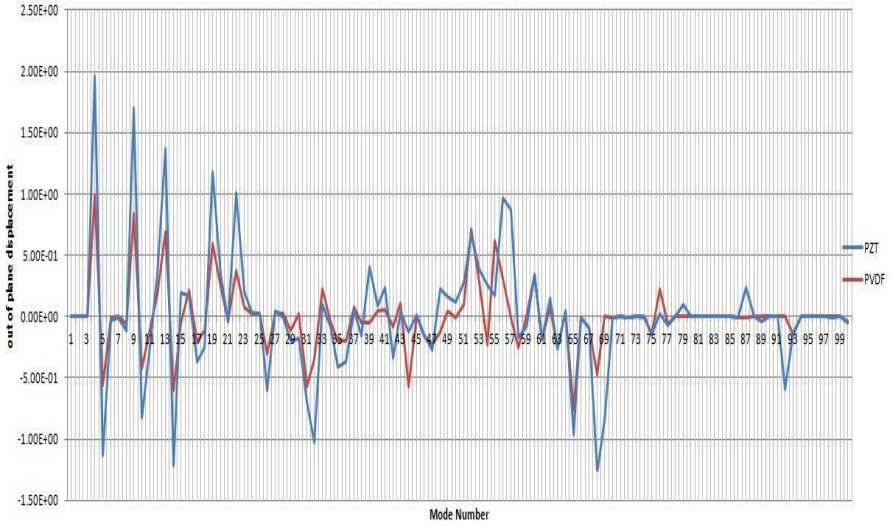

Figure 8. Out-of-plane displacement corresponding to mode numbers

4.4 Square membrane attached with eight smart materials

This model is the same as the previous one. The only change is the placement of PVDF materials into the membrane structure. PVDFs are tied at eight locations, as shown in Fig. 9.

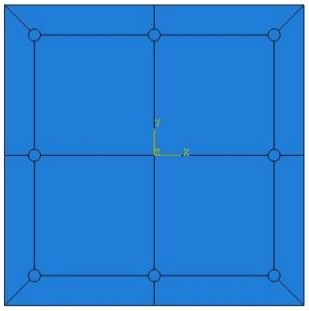

Figure 9. Square membrane coupled with eight PVDFs

Fig. 10 evidently shows that the use of smart materials at optimum locations minimizes the out-of-plane displacement substantially.

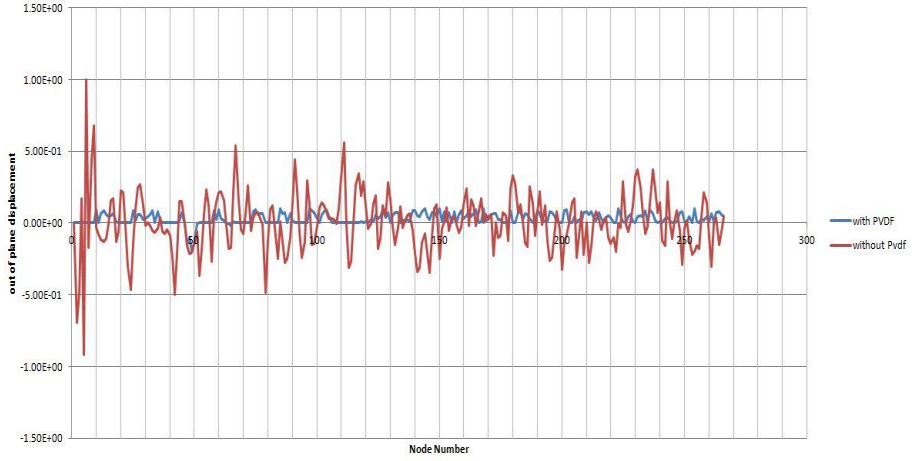

Figure 10. Out-of-plane displacement using PVDF and without PVDF

5. CONCLUSION

Kapton, Kevlar, and Mylar have emerged as the most viable prospects as space materials, replacing traditional materials such as aluminum, carbon fiber reinforced plastic (CFRP), and so on, due to their ultra-lightweight and flexibility. FEM analysis has been carried out on square membrane with the help of ABAQUS. Free and forced vibration condition applied on membrane. At these loading conditions, various natural frequencies, mode shapes and out-of-plane displacement was collected.Membrane structures are flexible and this inherent property of membrane structure makes it incompetent to abide bending or compressive stresses and this leads to shape deformation (wrinkle formation). At this stage, membrane structure needs to recover its original smooth shape for proper signal transmission. Thanks to PVDF and PZT for controlling the shape exceptionally well. Smart material PVDF and PZT have enough capability to improve the surface accuracy.

REFERENCES

[1] J. Santiago-Prowald, H. Baier, 'Advances in deployable structures and surfaces for large apertures in space', CEAS Space Journal, 5(3-4), 89-115, 2013.

[2] S. Kukathasan, S. Pellegrino, 'Vibration of pre stressed membrane structures in Air', AIAA, pp. 13-68, 2002.

[3] S. C. Gajbhiye, S.H. Upadhyay, S.P. Harsha, 'Free vibration analysis of flat thin membrane', International Journal of Engineering Science and Technology 4, no. 8, pp. 3942-3948, 2012.

[4] C.H. Jenkins, (Ed.), 'Gossamer spacecraft: membrane and inflatable structures technology for space applications. In: Progress in Astronautics and Aeronautics', vol. 191. Published by the American Institute of Aeronautics and Astronautics, Inc., 1801 Alexander Bell Drive, Reston, VA 20191-4344. December 2000, pp. 103–105, 2001.

[5] I. Bruant, L. Gallimard, S. Nikoukar, 'Optimal piezoelectric actuator and sensor location for active vibration control', using genetic algorithm. Journal of Sound and Vibration, 329(10), pp. 1615-1635, 2010.

[6] Y. Lecieux, and R. Bouzidi, 'Experimental analysis on membrane wrinkling under biaxial load–Comparison with bifurcation analysis', International Journal of Solids and Structures 47, no. 18, pp. 2459-2475, 2010.

[7] S.S. Rao, 'Mechanical vibrations', Prentice Hall; 5th Revised edition, pp. 739-742, 2011.

[8] C.H. Jenkins, (Ed.), 'Recent advances in Gossamer Spacecraft. Progress in Astronautics and Aeronautics', vol. 212. Published by the American Institute of Aeronautics and Astronautics, Inc., 1801 Alexander Bell Drive, Reston, VA 20191-4344, September 2005, pp. 109–164, 2006.

[9] W. Wong, S. Pellegrino, 'Wrinkled membranes I: experiments', Journal of Mechanics of Materials and Structures 1, no. 1, pp. 3-25, 2006.

[10] C. G. Wang, H. F. Tan, X. W. Du, Z. M. Wan, 'Wrinkling prediction of rectangular shell-membrane under transverse in-plane displacement', International Journal of Solids and Structures 44, no. 20, pp. 6507-6516, 2007.

[11] S. Timoshenko, 'Theory of Plates and Shells', McGraw–Hill, New York, pp. 457–465, 1940.

[12] R. E. Newnham, 'Piezoelectric sensors and actuators: smart materials', In Frequency Control Symposium, 46th. Proceedings of the 1992 IEEE, pp. 513-524, 1992.

[13] C. Y. Chee, L. Tong, G.P. Steven 'A review on the modeling of piezoelectric sensors and actuators incorporated in intelligent structures', Journal of Intelligent Material Systems and Structures, 9(1), pp. 3-19, 1998.

[14] J. L. Gasper, R.S. Pappa, 'Membrane Vibration Tests Using Surface-Bonded Piezoelectric Patch Actuation', NASA TM, 2003.

[15] H. Fang, M.C. Lou, 'Analytical characterization of space inflatable structures-an overview', *AIAA paper*, 99-1272, 1999.

[16] B.S. Munjal, 'Challenges in Spacecraft Reflector Technologies–A Few Potential Applications of Smart Materials', 2007.

[17] A. A. Liepins, 'Free vibrations of prestressed toroidal membrane', *AIAA journal*, *3*(10), pp. 1924-1933, 1965.

[18] C. H. Jenkins, U. A. Korde, 'Membrane vibration experiments: an historical review and recent results', *Journal of Sound and Vibration*, *295*(3), pp. 602-613, 2006.

Biographies

Amiy Chandraul is from Fatehpur, Uttar Pradesh, India**.** He has completed his Bachelor's degree in Mechanical Engineering from Babu Banarasi Das National Institute of Technology and Management, Lucknow in 2014, Master's degree in Machine Design Engineering from IIT Roorkee in 2016, and currently pursuing philosophy of doctorate degree from MNNITA, Prayagraj. His research interests lie in Modal analysis of membrane structures for space applications.

Dr. V. Murari is an Associate Professor in the Department of Applied Mechanics at Motilal Nehru National Institute of Technology Allahabad, Prayagraj, India. He received his Ph.D. degree in Aerospace Engineering in 2011 from IIT Kanpur, India. His current research interests include continuum damage modeling of composite materials and structures, damage mechanics of repaired and recycled composites, damage response of composite structures under dynamic loads, and correlation of energy absorption with damage propagation.

Dr. Satish Kumar is currently working as an Assistant Professor at Applied Mechanics Department, Motilal Nehru National Institute of Technology Allahabad, Prayagraj, India. He has completed his B. Tech from NIT Jalandhar, M. Tech, and Ph.D. from IIT Roorkee. His research interests lie in the design, fabrication, and mechanical characterization of adaptive membrane-based lightweight structures for space applications, which he plans to study using a combined experimental and numerical approach. He has published seven peer-reviewed journal articles, seventeen international conference papers, and filled two Indian patents. He has successfully completed one research project and three consultancy projects.

Modelling of RCC Framed Structure on Sloping Ground using ANN and Random Tree techniques

[1]Sukh Sagar Shukla and [2]Yogesh Aggarwal

Department of Civil Engineering, NIT Kurukshetra, Kurukshetra, Haryana, India
[1] hariom.edu7607@gmail.com, [2] yogeshkumar@nitkkr.ac.in

Abstract

Framed buildings built on hill slopes exhibit structural behaviour that differs from those built on flat ground. Because these structures are unsymmetrical in nature, they draw a high quantity of shear pressures and torsional moments, and their distribution is uneven owing to different column lengths. Because analysing complex structures takes a significant amount of time and effort. The aim of this paper is to create a model to predict seismic analysis parameters using machine learning methods and evaluate the outcomes of various techniques utilised.

Keywords. Seismic Analysis, Sloping Ground, Machine learning, Artificial Intelligence.

1. INTRODUCTION

Structures are typically built on level land however, due to a paucity of level ground, construction activities have begun on sloping terrain. The mountainous region's economic prosperity and fast urbanisation have hastened real estate development. As a result, population density in the hilly terrain has skyrocketed. As a result, there is a need for multi-story structures on hill slopes in and surrounding cities **[1]**. It is extremely difficult and expensive to dig or level in such conditions. Structural Engineers face the difficulty of achieving the most efficient and inexpensive design with precision in solution while guaranteeing that the final design of a building is serviceable for its intended purpose during its design lifetime. Previous studies attempted to analyse the behaviour of these frames located on sloping ground with various software available and given the value of critical seismic parameters like base shear, storey drift, and fundamental time period **[2-4]**. Also, on hills various configuration of buildings are possible for instance step back and step back-setback so researchers have also tried to predict most suitable configuration **[5- 9]**. But these processes are time-consuming and require a lot of effort. Researchers have used modelling techniques in various processes to make them easy to use **[10-12]**. Therefore, present paper aims at use of machine learning tools and their comparison to predict the seismic behaviour of building, constructed on hilly regions. The model developed using these techniques, will be capable of prediction of base shear in step back configuration. Thereby, resulting in saving of multiple use of various software and manual calculations for the design of these buildings.

2. METHODOLOGY

2.1 Artificial Neural Network

An ANN is a mathematical model that is driven by the organisation and functioning characteristics of biological brain networks in humans. Many applications have been done in this sector from the discovery of ANN in 1943 and till today. The main idea is to use computers to simulate complex problems in order to produce accurate estimates or facts using arithmetic operations, reasoning, and past knowledge, especially when the relationships between variables are not known or non-linear, and to recognise correlations between certain relevant features. ANN may be used to solve a variety of issues, including multivariate regression, categorization, control systems, associative memory, simulation forecasting etc.

Learning in ANN may be done in a variety of methods. For example, supervised learning makes use of a dataset made up of numerous characteristics and their related output values. The neural network learns over numerous iterations, adjusting its weights repeatedly while taking prior deviations into account in order to estimate the outputs. The most popular supervised learning model is the multilayer perceptron (MLP), which is made up of multiple layers of neurons with information moving feed-forward from inputs to outputs through various layers of neurons and a back-propagation (BP) method connecting back to the network.

MLP is made up of three layers, each of which is made up of clusters of neurons that execute similar jobs. The Input Layer, which accepts input from the user application, is the initial layer. The second sort of layer is Hidden Layer(s), in which neurons are only linked to other neurons and never interact directly with the end user. Finally, the neurons in the Output Layer provide data to the user application. Processing may happen at any layer in the neural network (i.e., the input and output layers aren't merely interface points), therefore every neuron in a neural network can do it. Weights play a part in the establishing relation between neurons in determining the relative intensity of the signal; when the weight varies, the network produces varied results. As a result, choosing the right weight values is crucial to constructing a good neural network. This is accomplished through the training phase in the learning process.

Figure 1 shows the artificial neural network model developed in this research. This is the multilayer perceptron of a single-layer feed-forward Neural Network, in which there are twelve main parameters that are mentioned in the previous section. Total 6 neurons were employed for the hidden layer and 1 neuron for the output layer, and the output layer neuron's final value represents the Base Shear value.

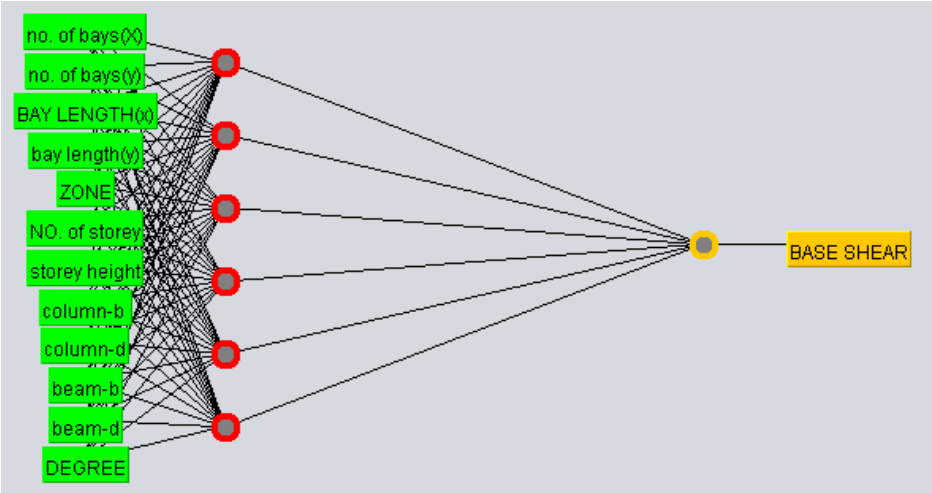

Figure 1. ANN model for base shear evaluation

2.2 Decision Tree

Decision Tree is extremely popular and widely used classification prediction tool. It is a tree structure that look like a flow chart, in which each internal node represents a test on an attribute, each branch represents the test's conclusion and each leaf node (terminal node) holding class label

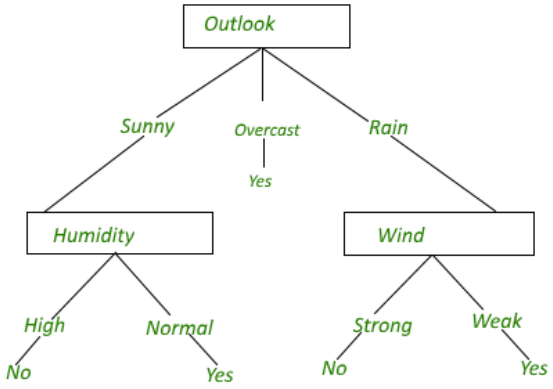

Figure 2. Decision Tree for tennis play

Decision Tree in Figure 2 categorises a particular morning based on whether it is suitable for playing tennis and returned the classification linked with specific leaf

2.3 Data set used

The experimental dataset of 101 sample set has been collected from various literature available, this dataset includes twelve input variables i.e. (no of bay (X), no of bay (Y), bay length (X), bay length (Y), zone, no. of storey, storey height, column depth, column width, beam width, degree beam depth,). Bay length are in meter (m) but cross section dimensions are in millimetre (mm). The minimum, maximum and average value are shown in Table 1

Table 1. Range of various input parameters used.

Name of input	Maximum value	Minimum value	Average value
no of bay (X)	11	3	4.19
no of bay (Y)	7	1	2.71
bay length (X)	7	3	5.39
bay length (Y)	5	3	4.44
zone	5	2	3.92
no. of storey	19	4	7.84
storey height	3.66	3	3.27
column width	600	230	395.54
column depth	1000	300	534.65
beam width	550	230	308.71
beam depth	750	350	516.83
degree	45	0	22.49

To compare the outcomes of the random tree and ANN models, statistical measures such as root relative square error (RRSE), coefficient of correlation (CC), mean absolute error (MAE), relative absolute error and root mean square error were determined. The performance of the models is affected by user-defined parameters in both models. As a result, choosing the best settings for these parameters is critical. The optimised values of user defined parameter in both the modelling approaches are given in Table 2.

Table 2. Statistical parameters used in the predictive models.

Modeling Technique	**Parameters**
Multilayer perceptron (ANN)	L-0.1, M-0.21, N-1000
Random Tree	M-1

3. RESULT AND DISCUSSION

Base shear with varied parameters was predicted and compared to the actual results using MLP and RT models. The fitness level of anticipated Base Shear values was calculated using

statistical metrics such as CC, MAE, RMSE, RAE, and RRSE. Figure 3 depicts the statistical characteristics of Base shear predicted by both modelling Techniques.

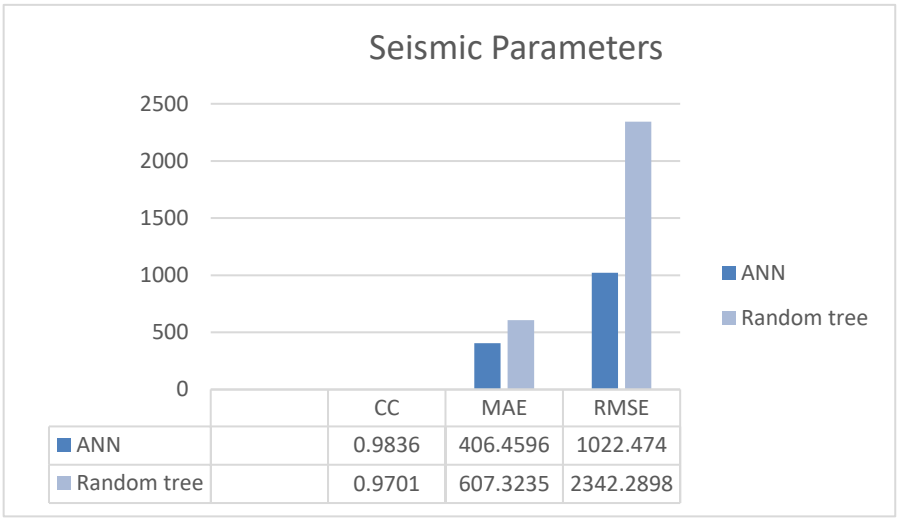

Figure 3. Statistical parameters of MLP and Random Tree

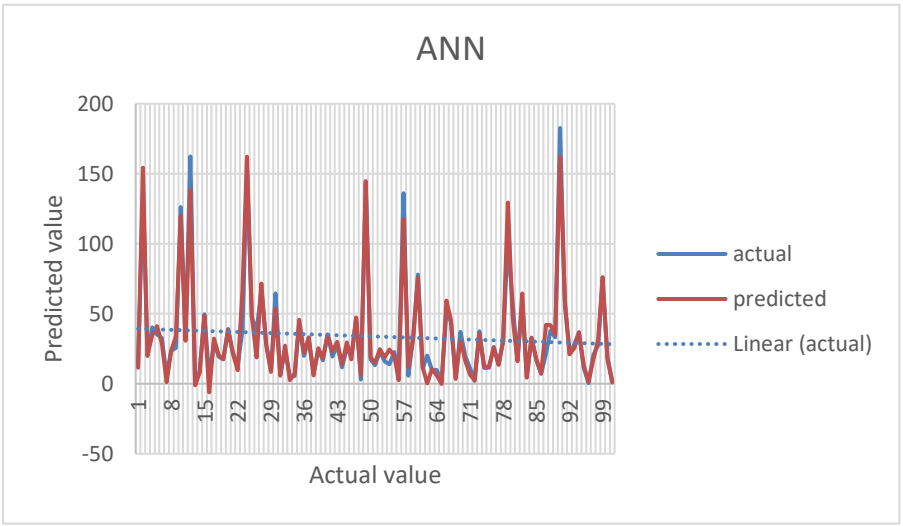

Figure 4. Actual Vs Predicted value from ANN model

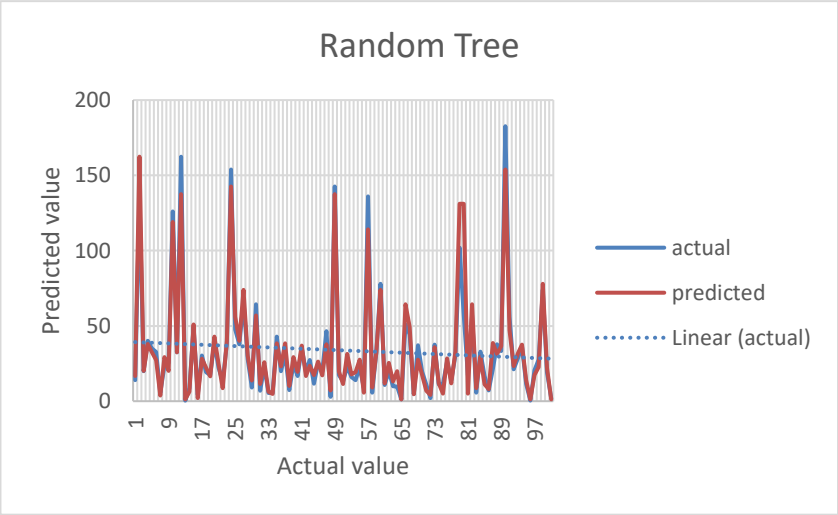

Figure 5. Actual Vs Predicted Value for Random Tree

Scattered graph between the observed and predicted values of Base shear obtained from MLP and RT model with dataset is presented by Figure 4 and Figure 5. According to the graphical results, the projected Base shear values by both models are in excellent agreement with the Base shear values gathered in the data set, while the ANN model predicts negative Base shear values against low Base shear values. Based on statistical metrics (Figure 1), the ANN model performs somewhat better than the Random Tree model in forecasting Base shear values due to higher CC and lower errors (CC- 0.9836, MAE- 405.4596, RMSE- 1022.474).

For validation part dataset was randomly divided into 70/30 ratio and 70 percent was used to train the model and remaining 30 percent was used to test it. Statistical parameters thus obtained were recorded but it was observed that these parameters were better in case of cross validation.

4. CONCLUSION

In this paper, ML approaches like ANN and RT is used to predict the model for Base shear value. We can conclude following points from the result

- The ANN model developed in this paper showed its capability to predict the base shear value based on various input parameters mentioned earlier. This will help in predicting the value of base shear in similar type of building hence will save lot of effort and time.
- Among both ANN and RT models ANN performed better on the taken dataset due to higher correlation coefficient and lesser error values obtained.

REFERENCES

[1] Z. Mohammad, A. Baqi, and M. Arif, "Seismic Response of RC Framed Buildings Resting on Hill Slopes," Procedia Engineering, vol. 173, pp. 1792–1799, 2017, doi: 10.1016/j.proeng.2016.12.221.

[2] S. K. Dangi and S. Akhtar, "Seismic analysis of a RC building on sloping ground with shear wall at different positions," PROCEEDINGS OF THE INTERNATIONAL CONFERENCE ON SUSTAINABLE MATERIALS AND STRUCTURES FOR CIVIL INFRASTRUCTURES (SMSCI2019), 2019, doi: 10.1063/1.5127154.

[3] P. Manjunath and Y. R. Holebsgilu, "Seismic Analysis of Multi Storey Building with Flat Slab Resting on Plain and Sloping Ground," Bonfring International Journal of Man Machine Interface, vol. 4, no. Special Issue, pp. 20–25, Jul. 2016, doi: 10.9756/bijmmi.8150.

[4] S. Kulkarni, "Seismic Analysis of Building Resting on Sloping Ground," International Journal for Research in Applied Science and Engineering Technology, vol. 9, no. VII, pp. 1340–1352, Jul. 2021, doi: 10.22214/ijraset.2021.36647.

[5] Birajdar BG, Nalawade SS. Seismic analysis of buildings resting on sloping ground. In13th World conference on Earthquake engineering 2004 Aug 1 (No. 1472).

[6] V. Kumar, "ANALYSIS OF 3D RC FRAME ON SLOPING GROUND," International Research Journal of Engineering and Technology, 2017.

[7] Y. S. Sontakke, "Seismic Analysis of Multi-Storey Building on Sloping Ground," International Journal of Recent Technology and Engineering, 2016.

[8] M. Islam, "Analysis of building on Sloping Ground subjected to Seismic Forces," International Journal of Advanced Engineering Research and Science, 2020.

[9] Kiran.T, "Seismic Performance of RC Frame Buildings Resting on Sloping Ground," IOSR Journal of Mechanical and Civil Engineering, 2017.

[10] Y. S. Alsalman, "Using Decision Tree and Artificial Neural Network to Predict Students Academic Performance," International Conference on Information and Communication Systems (ICICS), 2019.

[11] S. Sebastian, "Performance Evaluation By Artificial Neural Network Using WEKA," International Research Journal of Engineering and Technology, 2016.

[12] S. saad, "selection of most relevant input parameters using weka for artificial neural network based concrete compressive strength prediction model," IEEE, 2016.

[13] A. PRAJAPATI, "PARAMETRIC STUDY ON STEP BACK & STEP BACK-SET BACK BUILDING ON SLOPING GROUND," INTERNATIONAL JOURNAL OF ENGINEERING , 2021.

[14] M. HASAN, "Seismic Analysis of RC Buildings Resting on Sloping Ground with Varying Hill Slopes," Proceedings of International Conference on Planning, Architecture and Civil Engineering, 2019.

[15] S. Arjun, "A Study on Dynamic Characteristics of RC Buildings on Hill slopes," International Journal of Science and Research, 2013.

Modelling of RC Frames with Shear walls and Openings using ANN and M5P Techniques

[1]Priya Agrawal, [2]Paratibha Aggarwal

Department of Civil Engineering, NIT Kurukshetra, Kurukshetra,Haryana, India
[1]agrawalpriya2140@gmail.com, [2]paratibha@nitkkr.ac.in

Abstract

Shear wall is a RC structural element that resists lateral loads, majorly due to wind and seismic loads. The aim of the given study is to know the responses of shear walls for 5 to 40 story RC frame structures provided with different percentages of openings. Equivalent static method of seismic analysis in staad pro is performed to collect the data set for 240 models in terms of Maximum Story Displacement (MSD). Also, Machine learning (ML) techniques is being applied to predict the similar model within the given range. The analysis data can be further used directly as modelling of shear walls in staad pro requiresa lot of effort, time, and practice, so this predicted model will simply help us to predict the seismic response of any similar RC Frame structures provided with shear walls and various percentages of openings.

Keywords. Shear walls, Equivalent static method, Machine learning, Seismic analysis, Maximum storey displacement

1. INTRODUCTION

In a building structure, along with slabs, beams, and columns, reinforced concrete buildings frequently contain vertical plate like structure made of RCC called shear walls. These RC walls usually began at the foundation and continue to the building's top storey. In high-rise buildings, the thickness can be as low as 150mm or as thick as 400mm. Shear walls are typically installed along the breadth and length of structures. Shear walls resemble vertically oriented wide beams that transport earthquake loads to the base.

To resist the stresses due to seismic hazards, shear walls must have sufficient lateral strength. Also, Shear walls provide lateral rigidity to avoid excessive sway movement of the roof or the floor above. Shear walls that are sufficiently rigid will keep floor and roof framing members from shifting off their supports. In addition, buildings that are sufficiently rigid are less likely to sustain non-structural damage.

Buildings having RC shear walls and those were properly designed and constructed have performed well in past earthquakes. "We cannot afford to build concrete buildings built to withstand severe earthquakes without shear walls," a quote by Mark fintel, sums up the effectiveness of RC structures with shear walls in resisting the strong earthquakes. Mark Fintel is a well-known consulting engineer in the United States. In earthquake prone areas, shear walls demand special attention. Buildings that were not designed for seismic

activities but as they consist of enough number of walls with well-distributed reinforcement were also protected from damages in previously occurred earthquakes. Shear wall structures are common in seismic prone countries such as New Zealand, Chile, and the United States. Shear walls are easier to construct since detailing of reinforcementis straightforward and hence simple to execute on site. Shear walls are also useful for reducing earthquake damage caused to both structural and non-structural materials in termsof cost of construction as well as effectiveness for the building [1].

Shear wall provided in apartment complexes will be perforated by rows of openings that are necessary for exterior windows or interior entrances or corridors. The position and size of openings may have a negative impact on the seismic reactions of frame-shear wall constructions. Because lateral forces are transferred to individual shear walls considering their relative stiffness and it plays a significant role in shear walls. Several design guides offer simplified approaches for shear walls with openings for analyzing stiffness. As a designer, you must understand the impacts of opening in shear walls on stiffness, as well as seismic reactions and behavior of the structure, to select an appropriate configuration of openings in the shear wall [2].

In this study shear walls are considered as major earthquake resisting member, and location of shear walls majorly affects the behavior of the buildings. Researchers Studied for different opening conditions for story drift and diaphragm displacement and theyconcluded that provision of opening in shear wall ultimately helps to achieve the economy [3].So, it is important to provide the shear walls in proper position as it will minimize the effect and damages due to earthquakes, and thus Researchers has concluded that shear walls should be placed symmetrically on the periphery of the buildings [4, 5, 6]. The openings in shear walls also affects the maximum story displacement, on providing shear walls displacement is reduced [7], but on increasing the area of openings Displacement increases [8, 9]. Also, comparison of shear walls with openings with shear wall and without shear walls is done for seismic parameters for twelve storied structures. [10]

Artificial intelligence can be used as a tool in civil engineering for analysis and design of structures, it may be for pavement design, structural damages, Risk analysis etc. [11]. Various ML models for ANN and Decision trees is being analyzed for prediction of strength parameters [12, 13]. Also, A model of prestress concrete is predicted for time in seismic analysis using Machine learning models [14].

2. DATA SET

The data used for this study were recorded using staad pro software by modelling of building models for 5, 10, 15, 20, 25, 30, 35 and 40 stories. The data were analyzed for earthquake zones i.e., III, IV and V. The RC structured shear walls and various sizes of square openings in meters (0, 1, 1.5, 1.75, 2, 2.25, 2.5, 2.7, 2.85, 3) were considered. The dataset collected comprises a total dataset of 240 models out of which 168 randomly selected were used for training of models and the rest 72 models used for Testing. Based on the obtained data, six input variables were considered to predict the dependent variable i.e., Maximum story displacement. The analytical parameters of the variables are providedin Table 1 and 2 for training and testing dataset respectively.

Table 1: Details of statistical parameters of training data set

		Minimum	Maximum	Mean	Standard Deviation
INPUT DATA PARAMETERS	**Stories**	5	40	22.55	11.68
	Elevation (m)	20	160	90.2	0.924
	Size of openings (m)	0	3	1.9	0.92
	Openings %	0	45	22.8	14.87
	Zone	3	5	4	0.87
	Zone factor	0.16	0.36	0.25	0.08
OUTPUT DATA	**Max Displacement (m)**	3.453	351.233	99.042	92.528

Table 2: Details of statistical parameters of testing data set

		Minimum	Maximum	Mean	Standard Deviation
INPUT DATA PARAMETERS	**Stories**	5	40	22.36	11.511
	Elevation (m)	20	160	89.44	46.04
	Size of openings (m)	0	3	2.01	0.845
	Openings %	0	45	23.544	14.15
	Zone	3	5	4.01	0.93
	Zone factor	0.16	0.36	0.25	0.086
OUTPUT DATA	**Max Displacement (m)**	3.524	349.962	96.633	77.33

3. METHODOLOGY

The maximum story displacement of RC Frame shear wall systems is a critical parameter to consider while analyzing and designing the structure. As we know the value of MSD varies with variation of different structural parameters. Hence in this study, the effect of parameters like earthquake zone, height of buildings, size of openings in shear walls for 5 to 40 stories has been observed assuming the other parameters to be constant.

The unique properties of ML modelling as artificial neural network (ANN) and M5P Tree model have been used to develop and correlate the models and identify the factors influencing the parameter to predict the model for the same. These machine learning techniques can learn from any complex problem's input output relationship, avoiding the need for any predefined equation form. The ability of model to predict the MSD based on the trained data that determines whether it has been accepted or rejected. To evaluate the performance of the computational approach in predicting displacement, the mean absolute error (MAE), root mean square error (RMSE) and correlation coefficient (CC) are used. The statistical method for non-linear relationships is complicated. In contrast, the modelling approach is more straightforward because mathematical relationship cannot be established between theoutput and input variables.

3.1 Artificial neural network (ANN)

The artificial neural networks using Multilayer perceptron technique is a computational system that models it in the way the brain of a healthy human analyses and operated the information. The model is also a machine learning process that is being utilized in construction engineering for different types of numerical predictions and issues. The input layer, hidden layers, and the output layer constitute an ANN model. Transfer function, weight, and bias helps to connect the hidden layer to the other layers. The inputs for the multi-layer feed forward network were stories, stories heights, seismic zones, and the size and percentages of openings, and the output was maximum story displacement. A standard approach for developing or selecting a network architecture does not exist. As a result, the trial-and-error test was used to determine the optimum number of hidden layers and neurons considering the criteria for lowest average squared error. The second phase in the network design procedure was to determine the optimum number of epochs to use during training to achieve the best mean absolute error (MAE), Root mean square error (RMSE), and Correlation coefficient (CC). The obtained data set (total of 240 data) was divided into two parts after the ideal architecture was designed: the first portion that is
(168) used for training the model was 70% of the overall data set, and the rest part was 30% of the total data set (72) for testing the model. To generate the best structure to predict the maximum storey displacement, various transfer functions and ANN models with varying numbers of neurons and hidden layers were tested. One hidden layer modelled on three neurons was employed in each network, as illustrated in Figure 1. The ANN model was utilised in this phase of the study to calculate the maximum storey displacement in various seismic zones for various shear wall models and different percentages of openings.

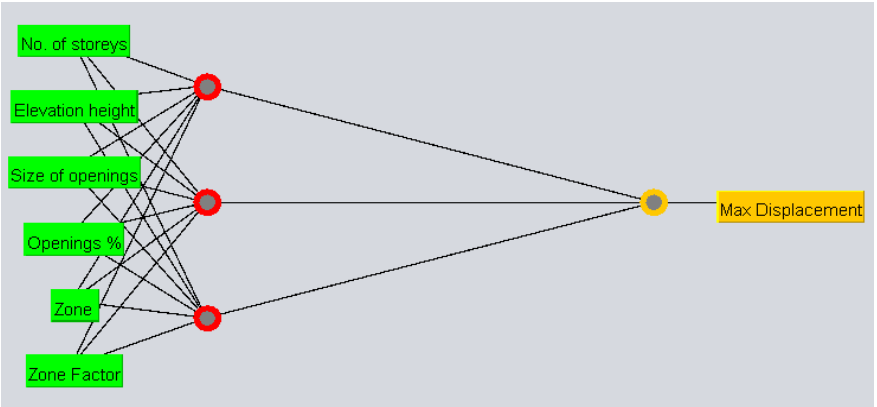

Figure 1. ANN Model

3.2 M5P-tree model (M5P)

The M5P tree model focuses on regression issues using genetic algorithms. The strategy of tree models in M5P adds linear regression characteristics to the nodes at the end and fits into a multivariable model like linear regression at every sublocation by separating various sets of data into numerous sublocations. Instead of discrete segments, the M5P-treemethod is used to solve continuous issues of class, and it can handle functions with many dimensions. It shows the result component of every linear model that was developed to represent the non-linear relationship between the datasets. The M5P-tree model tree division criteria, as well as the error estimation, are displayed on each node. To determine the mistakes, the variance of the default value of the class entering the node is used. The parameter at which the expected error reduction is maximised is being considered for evaluation of any function of that node. The M5P-tree model tree division criteria are determined using error computations per node [15] .

The optimized parameters concluded for the ANN and M5P models are-

Modeling Technique	Parameters
Multilayer Perceptron	L-0.3 M-0.2 N-500
M5P model tree	M-4

4. RESULTS

Maximum displacement with varied parameters was predicted and evaluated using the ANN and M5P models. Statistical measures such as correlation coefficient (CC), Mean absolute error (MAE), and Root mean square error (RMSE) were used to determine the fitness level of predicted Maximum storey displacement (MSD) values. Figure 2 depict the statistical parameters for training and testing dataset of both the models. Figure 3 shows the scatter line graph between the actual and predicted values of MSD derived from the ANN model and Figure 4 for M5P models with training and testing datasets. According to the representation of data in graphical format, Testing models predicted MSD values correspond linearly with the Trained data, although the M5P model predicts lower values for CC, MAE and RMSE compared to ANN model. Thus ANN (Multilayer perceptron) model shows slightly better performance with CC=0.998, MAE= 11.5, RMSE= 14.79.

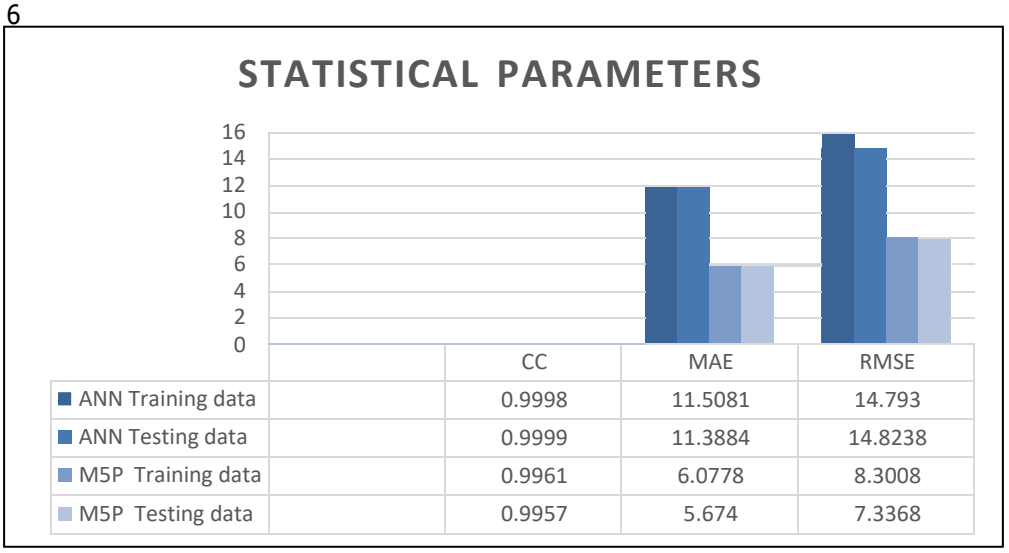

	CC	MAE	RMSE
ANN Training data	0.9998	11.5081	14.793
ANN Testing data	0.9999	11.3884	14.8238
M5P Training data	0.9961	6.0778	8.3008
M5P Testing data	0.9957	5.674	7.3368

Figure 2. Comparison of statistical parameters of ANN and M5P models

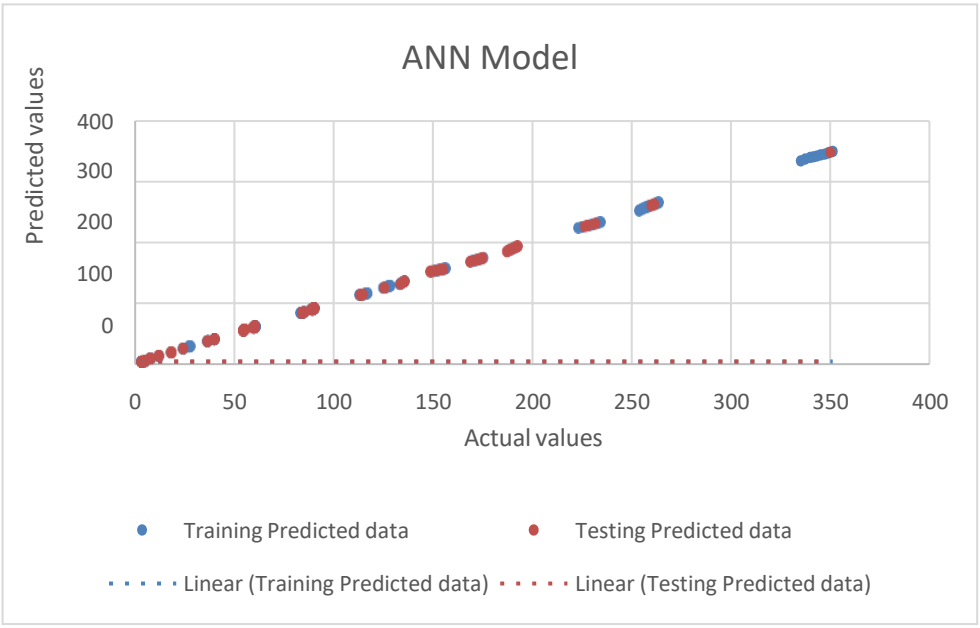

Figure 3. Actual v/s Predicted values of MSD for ANN Model

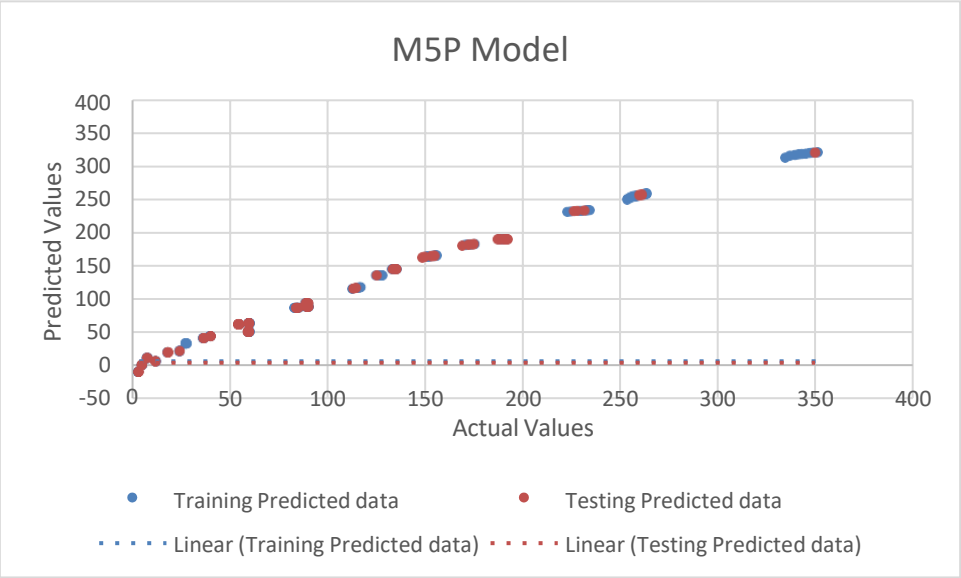

Figure 4. Actual v/s Predicted values of MSD for M5P Model

5. CONCLUSION

In this research, Machine learning approach like ANN and M5P is used to predict the model of Maximum storey displacement. The results obtained from this paper lead us tothe following conclusions:

1. The ANNs model proposed in this current study showed its ability to predict the MSD based on storey heights in different seismic zones of earthquake. This study will help in predicting the similar model type and thus it will reduce time, cost and labour.
2. The statistical parameters obtained shows good results, but ANN model shows more Correlation coefficient (CC), MAE and RMSE for both training and testing models, Thus ANN gives better performance as compared to M5P for MSD results.
3. The actual and predicted results are satisfactory and are varying linearly for ANN as well as M5P Models in training and testing datasets, but ANN is again showing more precise graphs as compared to M5P. Thus, the ANNs model is a powerful tool for predicting the Maximum storey displacement of shear walls.
4. RC Shear wall have been proved to perform good in earthquakes, the effect of opening provided for architectural aspects considering MSD is being observed in various seismic zones.
5. It is concluded that on increasing zones of earthquakes, MSD increases. Also, on increasing opening percentages and number of storeys the MSD values again increases.

REFERENCES

[1] D. H. Hosseini, “Numerical Analysis of High Rise Building with Openings on Shear walls,”American Journal of Engineering Research (AJER), vol. 6, no. 2, p. 30, 2017.

[2] M. J. A. M. FAROOQ, International journal of Earth sciences and Engineering, vol. 7, no. 4, p. 8, August, 2014.

[3] B. H. S. Harshal M. Banubakode, “Influence of openings in shear wall in high rise structures,” IJASRE, 2017.

[4] P. N. R. Mahdi Hosseini, “Seismic Analysis of Multi-Storey Building Structure with Shear Walls at the center core and center side of each parameter.,” International Journal of Engineering and Management Research, vol. 6, no. 6, p. 10, December 2016.

[5] D. I. E. Ravi Sonani, “Behaviour of R.C. Structure with and Without Provision of Shear Wall Including Openings against lateral loads,” GRD Journals, p. 5, March 2016.

[6] N. K. G. Mallika.K, “Analysis of Shear Wall in High Rise Unsymmetrical Building Using Etabs,” IJIRSET, vol. 5, no. 11, November 2016.

[7] M. M. et.al., “Seismic Analysis of Multistorey Building with shear wall using Staad pro,” IJERT, June 2021.

[8] D. P. P. et.al., “Seismic analysis of an R.C. multistorey building frame with varying sizes of openings in shear wall”, IRJET, July 2016.

[9] S. R. Chowdhury, “Effects of Openings in Shear Wall on Seismic Response of structures”, International journal of computer applications, December 2012.

[10] D. G. D. A. Susmeet D. Bagde, “Comparing the Effect of Earthquake on High Rise Building with & without Shear Wall and Shear Wall with Opening”, IRJET, 2021.

[11] A. P. et.al., “Artificial intelligence as a tool in civil engineering,” IOSR-JCE, 2017.

[12] M. A. Yaman, “Predicting the ingredients of SCC using ANN,” Alexandria Engineering Journal, 2017.

[13] W. b. c. et.al., “Machine learning prediction of mechanical properties of concrete,” Construction and building materials, 2020.

[14] H. Babita Saini, “ML based modelling of estimation of fundamental time period of precast concrete structures,” Civil engineering journal, 2021.

[15] A. M. et.al., “ANN, M5P-tree and nonlinear regression approach with statistical evaluations to predict the compressive strength of cement-based mortar modified with fly ash,” Journal of materials research and technology, 2020.

Biographies

Priya Agrawal received the bachelor's degree in Civil engineering from Amity University Chhattisgarh. She is currently pursuing a Master’s degree in structural engineering from National Institute of Technology, Kurukshetra. She is currently working on Modelling and analysis of RC frame structures with shear walls and openings using Machine learning techniques.

Modelling of RCC Framed Structure with Bracing Using Random Forest and M5P Technique

[1]Shubham Kumar Goyal, [2]Paratibha Aggarwal

Department of Civil Engineering, NIT Kurukshetra, Kurukshetra, Haryana, India
[1]shubhamku530@gmail.com, [2]paratibha@nitkkr.ac.in

Abstract

When an earthquake strikes a region, most of the RC buildings collapse. As a result, selecting a lateral load resisting system that is effective is critical. The safety of the structure against lateral loads is prioritised in RCC frames. Steel bracings of various types are used to withstand lateral loads operating on the structure. The structural performance is greatly influenced by the bracing scheme. Steel bracing offers a potential benefit over alternative bracing because it allows for a substantial increase in stiffness with a little increase in weight, making it ideal for existing structures with weak lateral stiffness. Thus, the natural frequency is increased while the lateral displacement and drift are generally reduced. Steel bracing is inexpensive, easy to install, takes up less space, and may be customised to meet particular strength, stiffness, and stability requirements. With the aid of the Etabs software, the impact of steel bracing on the seismic behaviour of RC frames was investigated. In a G+7-story reinforced concrete skyscraper, many models were built with various types of bracing systems. Using E-TAB software, the models were examined for different seismic zones, characteristic strength, location of bracing, and type of bracings in accordance with IS 1893:2016. The results (maximum story displacement) of several CBF bracing system such as X bracing, V bracing, Inverted-V, Diagonal bracing were gathered through seismic analysis by response spectrum method. In this comparison between two AI techniques were discussed using Weka software on maximum story displacement data obtained through Etabs models. The results showed that Random Forest is more reliable than M5P technique.

Keywords. Seismic analysis, steel Bracings, Maximum story displacement, Random forest (RF), M5P, Etabs.

1. INTRODUCTION

In order to strengthen and stiffen multi-story structures, which are more sensitive to earthquake and wind stresses, the cross sections of the members rise from top to bottom, making the construction uneconomical due to structural safety. As a result, unique procedures and/or techniques to strengthen the lateral stability of the structure are required. Braced frames create their lateral force confrontation through the bracing action of diagonal elements. Frames that are fully braced are more rigid. Arbitrarily braced ones have the least forces produced in the structure while producing maximal displacement within set limitations.

In past many studies were carried out to find which type of bracing is suitable for RC building having different story height and symmetric or non-symmetric plan subjected to seismic analysis through various softwares [1-3]. But this process is time consuming and uneconomical. Therefore, the main aim of this study is to develop a trained model (AI) which can predict the output with the help of various input parameters available.

Steel bracing for reinforced concrete buildings has several advantages, including the fact that it is relatively inexpensive, does not considerably increase structural weight, is simple to install, and can be designed with the required strength and stiffness. The fundamental advantage of this technology is that no foundation system rehabilitation is required.

Considering the usage of tree - based regression in many civil engineering applications [4], two such techniques (I) RF regression and (II) M5P model tree-based modelling approaches [5-6] are employed in this research work to estimate the maximum story displacement of a building structure. Data set obtained through seismic analysis (Response spectrum analysis) of models in Etabs- structural analysis and design software for modelling purpose.

2. METHODOLOGY

Seismic analysis of models were done using Response spectrum method in Etabs.

Using this method of analysis, multiple modes of response may be considered Except for exceptionally complicated or basic structures, many building codes require such technique. The structure reacts in a way that may be described as a hybrid of several special modes. Dynamic analysis is used to figure out these modes. A response from the design spectrum is examined for each mode, taking into account the modal mass and modal frequency, and then combined to offer an assessment of the structure's overall reaction. In order to do so, we must first determine the magnitudes of the forces in all directions (X, Y, and Z) and then look at the repercussions for the structure. The following are a few different ways to combine things: 1) CQC, 2) SRSS, 3) Absolute-peak values are summed together.

2.1 AI Techniques

Random Forest Technique

The supervised learning approach is used by Random Forest, a well-known machine learning algorithm. In machine learning, It may be used for both classification and regression problems. It's based on ensemble learning, which is a method for merging several classifiers to solve a complex problem and improve the model's performance. Based on the decision trees' projections, the RF algorithm decides the outcome. It anticipates the production of numerous trees based on an average of their output. M and k [9] are the only user-defined variables. According to Breiman [7], the number of trees used enhances the accuracy of the result. The limitations of a decision tree algorithm are eliminated by using a random forest technique. It enhances accuracy while reducing dataset over fitting. It can provide forecasts without a significant number of package configurations (like scikit-learn). Random forests can generate non-linear relationships between input and output variables. Class labels are translated into numerical values throughout the regression procedure [7].

M5P Technique:

M5P is an enhanced version of Quinlan's M5, in which a conventional decision tree is merged with linear regression functions at the nodes. The M5 model's construction is divided into three major phases. To begin, a tree model is constructed using a splitting criterion to divide the data into subgroups. Then, in order to overcome data over fitting that occurred during tree creation, tree pruning is undertaken to delete or combine unnecessary sub trees. Finally, a smoothing procedure is carried out to compensate for the severe discontinuities that occur between consecutive linear models at the clipped tree leaves. The decision tree is created using a divergence metric known as Standard Deviation Reduction (SDR). Pruning, evacuation, and tree substitution are all part of the process. As a result, a final tree model is created.

The M5P algorithm produces accurate classifiers, especially when the majority of the characteristics are numerical. To evaluate the proposed model, the M5P method measures both MAE and MASE. The M5P has been utilised in a variety of disciplines, like predicting soaked CBR value of stabilized pond ash.

3. DATASET

For the modelling, Input parameters were type of bracing [x- bracing (1), v-bracing (2), inverted v-bracing (3) and diagonal bracing (4)], Fck (30, 40, 50), zone (III, IV, V) and location of bracing (model type) as shown in Figure 1. Data was obtained by keeping one parameter varying and other parameter constant in a model. A total of 369 data sets were gathered and seismic analysis of models were done in Etabs software. Using the WEKA 3.9 software [8], the maximum story displacement was estimated using random forest regression and the M5P model. In both models, 70 percent of the data was randomly picked for training, while 30 percent was utilized to test the models. Type of bracing, seismic zone, characteristic strength (Fck), and placement of bracing are all input parameters/dependent variables in models. The maximum story displacement, on the other hand, was used as an output parameter.

To compare the outcomes of the RF and M5P models, statistical measures such as coefficient of correlation (CC), mean absolute error (MAE), root relative square error (RRSE), root mean square error (RMSE), and relative absolute error (RAE) were discovered. The performance of both models is influenced by user-defined parameters. As a result, picking the correct choices for these parameters is crucial. Table 1 shows the statistical properties of various analytically obtained data. Table 2 shows the ideal values of the needed user-defined parameter in both modelling techniques.

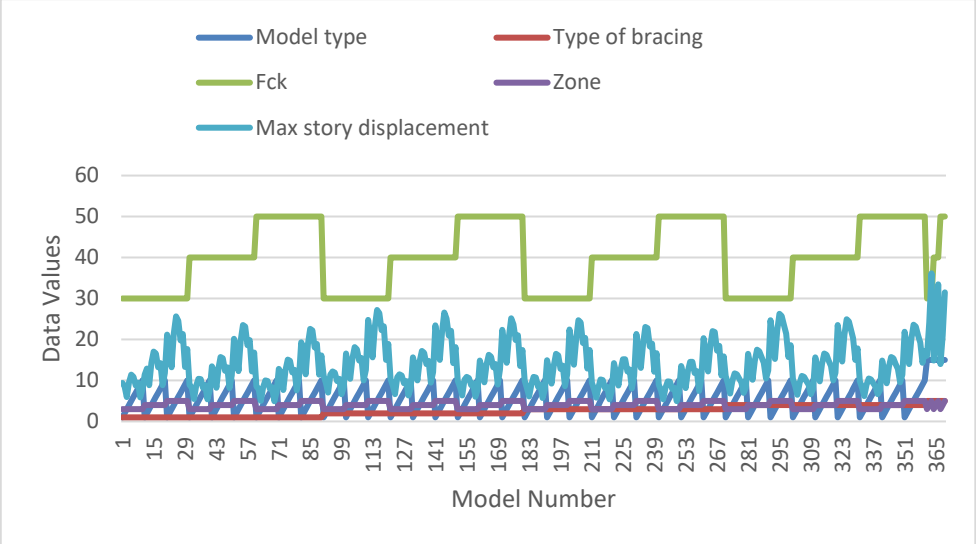

Figure 1. Data values of parameters with model number of full data set (Training-Testing)

Table 1. Predictive models' details of statistical parameters over training data

Used Parameters		Training dataset			
		Min.	Max.	Avg.	Standard deviation
Input data	zone	3	5	-	-
	F_{ck}	30	50	-	-
Output data	MSD	4.9629	36.127	14.083	5.799

Table 2. Predictive models' details of statistical parameters over testing data

Utilized parameters		Testing Dataset			
		Min.	Max.	Avg.	Standard deviation
Input data	zone	3	5	-	-
	F_{ck}	30	50	-	-
Output data	MSD	4.9704	33.4819	13.781	5.3064

Table 3. Details of numerical parameters in predictive models of RF over training and testing data

Methodology (RF) Training			Methodology (RF) Testing		
Parameters		CC	Parameters		CC
I-1, M-1, K-3		0.9769	I-1, M-1, K-3		0.8972
I-10, M-1, K-2		0.9917	I-10, M-1, K-2		0.9516
I-50, M-1, K-1		0.9903	I-50, M-1, K-1		0.9001
I-100, M-1, K-2		0.9944	I-100, M-1, K-2		0.9429
I-100, M-1, K-3		0.9967	I-100, M-1, K-3		0.9642
Optimized	I-100, M-1, K-3	0.9967	Optimized	I-100, M-1, K-3	0.9642

Table 4. Details of numerical parameters in predictive models of M5P over training and testing data

Methodology (M5P) Training				Methodology (M5P) Training			
Parameters	M-4	M-3	M-2	Parameters	M-4	M-3	M-2
CC	0.9443	0.9433	0.9433	CC	0.8352	0.8352	0.8352
Optimized	0.9443			Optimized	0.8352		

Table 3 and 4, depicted the implementation of AI technique i.e. RF and M5P. The variation in the performance criteria of correlation coefficient (CC) is given in Table 3, 4 and finally

summarized in Table 5, 6 based on the optimization of various factors like I, M and M in RF and M in M5P models.

4. RESULTS AND DISCUSSIONS

The maximum story displacement with varied parameters was predicted using the RF and M5P models and compared to the analytically determined results. The adequacy level of anticipated MSD reading was determined using statistical metrics such as CC, MAE, RMSE, RAE, and RRSE. Tables 5 and 6 demonstrate the statistical parameters of MSD predicted by both modelling techniques. Figures 2, 3 show a scatter graph of the actual and predicted MSD values derived from the RF and M5P models using training and testing datasets, respectively.

The graphical results indicate that the projected MSD value by both models is in good accordance with the actual MSD value, although the M5P model predicts more error in both training and testing values. In comparison to the M5P model in predicting MSD values, the random forest model performs somewhat better than the M5P model due to greater CC and lower errors values (CC- 0.9642, RMSE-1.4467, MAE-1.1823, RAE-27.6024, and RRSE-27.3412).

Table 5. Details of numerical parameters over training data using prediction models

Methodology used	**Data set for training**				
	Coefficient correlation	**MAE**	**RAE (%)**	**RMSE**	**RRSE (%)**
RF	0.9967	0.3276	6.8518	0.5081	8.7772
M5P model	0.9443	1.4467	30.2583	1.9547	33.774

Table 6. Output data of testing data using prediction models

Methodology used	**Data set for testing**				
	Coefficient correlation	**MAE**	**RAE (%)**	**RMSE**	**RRSE (%)**
RF	0.9642	1.1823	27.6024	1.4467	27.3412
M5P model	0.8352	2.4086	56.234	3.0583	57.8013

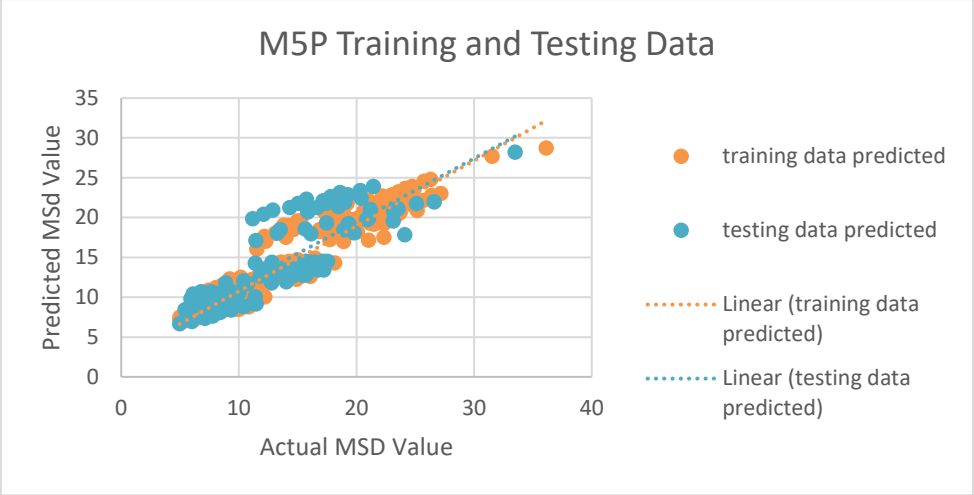

Figure 2. Predicted VS Actual MSD value using M5P with training and testing data set

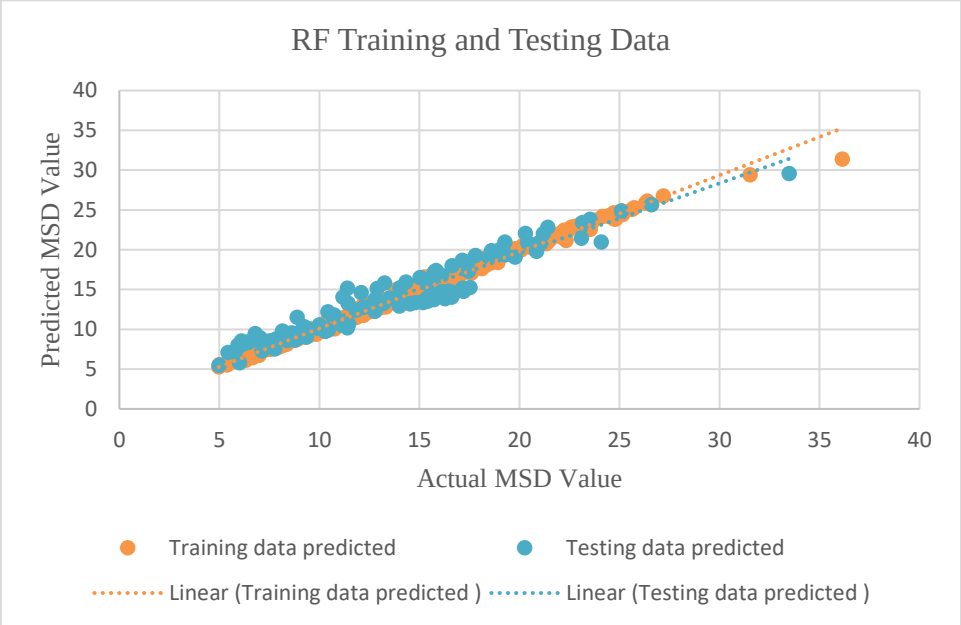

Figure 3. Predicted versus Actual MSD value calculated with RF utilising training and testing data sets

5. CONCLUSION

The present work models the analytically obtained MSD value of frames utilising two modelling methodologies (i) Random Forest and (ii) M5P. Figures 2 and 3 clearly show that the dispersion of data from the trend line is greater in M5P than in RF. Statistical parameters

are used to assess the fitness of models. Random Forest performs better than M5P because to larger CC and smaller errors in Tables 5 and 6. RF has the following advantages over other machine learning tools: (a) It takes less time to train than other methods, (b) It estimates output with great precision, even for big datasets, and (c) It can retain accuracy even when a significant amount of data is absent.

REFERENCES

[1] Kulkarni JG, Kore PN, Tanawade SB. Seismic response of reinforced concrete braced frames. International Journal of Engineering Research and Applications (IJERA) ISSN. 2013 Jul:2248-9622.

[2] Sagar, T., Tupe, D.H. and Gandhe, G.R., 2019. Seismic Analysis of Steel Frame Building using Bracing in ETAB Software.

[3] Viswanath, K.G., Prakash, K.B. and Desai, A., 2010. Seismic analysis of steel braced reinforced concrete frames. International journal of civil and structural engineering, 1(1), p.114.

[4] B. A. Omran, Q. Chen, and R. Jin, "Comparison of Data Mining Techniques for Predicting Compressive Strength of Environmentally Friendly Concrete," Journal of Computing in Civil Engineering, vol. 30, no. 6, p. 04016029, Nov. 2016, doi: 10.1061/(asce)cp.1943-5487.0000596.

[5] M. Suthar and P. Aggarwal, "Modeling CBR Value using RF and M5P Techniques," MENDEL, vol. 25, no. 1, pp. 73–78, Jun. 2019, doi: 10.13164/mendel.2019.1.073.

[6] Singh, B., Sihag, P., Tomar, A. and SEHGAL, A., 2019. Estimation of compressive strength of high-strength concrete by random forest and M5P model tree approaches. Journal of Materials and Engineering Structures «JMES», 6(4), pp.583-592.

[7] Breiman, L., 1999. 1 RANDOM FORESTS--RANDOM FEATURES.

[8] Lang, S., Bravo-Marquez, F., Beckham, C., Hall, M. and Frank, E., 2019. Wekadeeplearning4j: A deep learning package for weka based on deeplearning4j. Knowledge-Based Systems, 178, pp.48-50.

[9] I.S. 456-2000, Indian standard code of practice for plain and reinforced concrete (fourth revision), Bureau of Indian Standards, New Delhi.

[10] I.S. 1893 (Part 1)-2002, Criteria for earthquake resistant design of the structure, general provision, and building, Bureau of Indian Standards, New Delhi.

Compressive Strength Prediction of SCC using ANN

[1]Gulshan Kumar Gurjar, [2]Paratibha Aggarwal

Department of Civil Engineering, NIT Kurukshetra, Kurukshetra, Haryana, India
[1]*gulshance2@gmail.com*, [2]*paratibha@nitkkr.ac.in*

Abstract

The optimal use of supplementary cementing materials (SCMs) in Portland cement blends, such as limestone filler (LF), fly ash (FA), and silica flume (SF), has produced numerous environmental and technical benefits, including enhanced physical properties, increased concrete industry sustainability, and decreased CO2 emissions. Artificial neural networks (ANNs) have been utilized in civil engineering to handle a number of issues, including forecasting the compressive strength of self-compacting concrete. A good correlation was found between the results of earlier studies and the impacts and advantages of limestone filler (LF), fly ash (FA), and silica flume (SF) on the hardened qualities of self-compacting concrete, such as compressive strength. The outcomes showed that the created ANNs model was indeed a workable and effective tool for simulating the compressive strength prediction of self-compacting concrete for LF, FA, and SF.

Keywords: Self compacting concrete (SCC), limestone filler, fly ash (FA), silica flume, compressive strength (CS), prediction, artificial neural networks (ANN)

1. INTRODUCTION

Prof. Hajjim Okamura developed self-compacting concrete three decades earlier in Japan [1] . SCC is a highly flowable concrete that can fill forms without the usage of mechanical vibration. It's a self-consolidating, non-segregating concrete that's deposited down by gravity. Self-compacting concrete (SCC) is important since it maintains all the concrete's durability and properties while achieving performance standards. As a result, SCC is capable of self-consolidation without the use of external or internal vibrators. Therefore, bleeding and segregation are avoided while maintaining stability. According to, changing the production process and aggregate type due to variations in mineral additives or cement can have a significant impact on the characteristics of fresh SCC, therefore having a robust combination with minimal influence from external sources is crucial. Scholars are taking priority the use of powder industries by products and waste as mineral additives in this direction because of the environmental benefits. Fly Ash (FA), Silica fume(SF), limestone filler(LF) and a new generation of super plasticizers (SP) have all been proposed to be incorporated into the mix . The type of admixture used is determined by the properties of the concrete. In past few years, silica, fly ash, lime powder, and have been the most commonly used admixtures in civil engineering research.

SCM's can be used in Portland cement replacement for these reasons: (1) their cost is significantly lower than that of Portland cement; (2) some of SCM's increases the early-age

mechanical properties and reduces the aggressive environmental impacts of concrete; (3) improve the long-term performances of concrete.
Artificial neural networks (ANNs), a type of soft computing, are intended to mimic how the human brain system learns from training patterns or data. They are capable to solve extremely complex problems, such as highly non-linear problems, using interconnected computing elements to approximate the non-linear input-output relationship for a variety of applications. In the field of civil engineering, neural network technology is being used more and more to predict or improve more or less complex phenomena, such as the effectiveness of slag and fly ash concrete, the design of concrete mixes incorporating natural pozzolans, the characteristics of self-compacting concrete (SCC) containing fly ash, and the carbonation depth of fly ash concrete. Some have used self-compacting, high-performance concrete with large volume fly ash to improve the compressive strength (CS) of concrete including cement additives of silica fume. This study's objective is to develop an accessible ANNs model for foretelling the mechanical characteristics (compressive strength) of concrete incorporating fly ash, silica flume, and limestone filler. The ANN model was trained using a set of experimental data that included input parameters such as binder content (B), limestone filler (LF), fine aggregate (FA), coarse aggregate (CA), fly ash (FA), silica flume (SF), water/binder ratio (W/B), superplasticizer (SP), and compressive strength (CS) that were determined through experimentation.In addition, for evaluating the performance of the developed ANNs model, the analysis is done based on parameters and a comparison were conducted between the experimental and predicted results.

2. METHODOLOGY

A soft computing technology called "ANNs" operates on the idea of neural networks that are modeled after the biological nervous systems of living things. It is capable of learning from data instances, including each of the intelligence models. The architecture of ANNs is typically made up of a collection of interconnected, numerous simple computational nodes that operate in parallel and are referred to as neurons. These neurons are typically arranged into groups systematically to form layers in the network and provide a response, or output, in response to a series of inputs. Thus, neural networks can be single or multilayered, with an input layer that does not do any computations while it distributes data from the outside world to one or more hidden layers of the network that then process it to produce the desired output. With the exception of input layers, the hidden and output layers make up the activation function, and the number of neurons in each is equivalent to a model variable. The hidden and output layers of the neural network are where all information processing for this purpose takes place. Links channels carrying so-called weights, which are initially set to a random value and modifiable throughout the training process, are used to reflect the strength of connections between the layers. As seen in Figure 1, the incorporation of nonlinear activation functions in hidden layers enhances ANNs' capacity to learn nonlinear correlations between collections of input and output data. The modelling with ANNs required five main stages:

(a) Acquisition and analysis the data, (b) determining the architecture of model, (c) learning process determination, (d) training of the networks and (e) testing and validation of the model proposed for generalization evaluation.

Therefore, Inputs, weights, sum function, activation function, and outputs are the five fundamental components of an artificial neuron. The weighted sums of the input component $(net)_j$ are found by using Eq. (1) as follow:

$$(net)_j = \sum w_{ij} x_i + b \quad (1)$$

Where x_i is the input data; w_{ij} is the weight of the neural model; b is the bias.

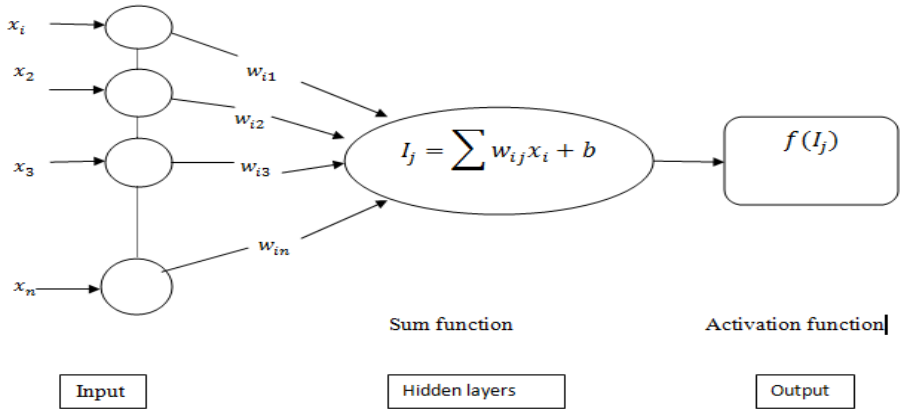

Figure 1. Typical neural network architecture

Experimental database collections and normalization

The major goal of this work is to build an ANNs model to forecast the mechanical properties (compressive strength) of self-compacting concrete using a large database. The first stage in achieving this goal is to gather and select a wide range of pre-existing experimental data and build a trustworthy database for training and testing samples as well as ANN modeling. Numerous datasets with 179 cases were gathered and chosen from sixteen different independent literary sources {20 data [2], 6 data [3], 28 data [4], 8 data [5], 12 data [6],42 data [7], 8 data [8],4 data [9], 3 data [10], 4 data [11], 4 data [12],11 data [13], 5 data [14], 11 data [15], 12 data [16] ,6 data [17]}, were used to construct the ANNs model. The testing data must be used to evaluate the performance of the best model produced by ANNs. After the training and testing phases are complete, the network must use the validation data to improve network generalization and to determine the generalization capability of the selected model on data that was not used during training and just in the input data range. The data sets are randomly separated into three subsets in order to achieve a consistent division: A total of 149 data sets, or about 83% of the database, were allotted for the training stages, and the remaining 30 data sets, or about 17% of the database, were allotted for the testing phases. Table 1 provides a summary of the various input and output variables from the complete data sets utilized to create the ANNs model.

Table 1. Model input and output parameter range

		Cement*	Water*	Silica*	SP %	FA*	CA*	Filler*	Compressive strength (MPa)
Mean	Training data	386.78	0.36	26.52	1.13	915.74	763.83	103.69	59.62
	Testing data	384.77	0.37	25.58	1.06	935.44	701.35	99.95	58.41
Maximum	Training data	600.00	0.50	150.00	6.00	1180.00	986.00	420.00	101.00
	Testing data	513.00	0.50	100.00	4.00	1160.00	917.00	390.00	85.30
Minimum	Training data	146.88	0.28	0.00	0.00	407.55	578.00	0.00	40.30
	Testing data	180.00	0.30	0.00	0.15	407.55	578.00	0.00	43.10

* Kg/m^3

Test for Mechanical properties - Compressive strength test

Figures 2 (before failure) and 3 show the results of compression strength tests on 150mmX150mmX150mm cubes using a compression testing apparatus (Sample after failure). The specimens were thoroughly cleaned and dried with care after being taken out of the curing tank. Afterward, the cube was put into the testing device with the cast faces contacting the platens. The cube received tension at a consistent pace. The compressive strength was assessed after 28 days to compare the strength of various SCC blends.

Figure 2. Sample before failure

Figure 3. Sample after failure

Figure 4. SCC mix specimen

Table 2. Experimental data sheet

Sr. No.	Cement*	w/b	Silica*	SP (%)	FA*	CA*	Filler*	Compressive strength (MPa)
1	350	0.4	20	1	960	600	220	60.15
2	250	0.35	18	1	1000	650	250	55.21
3	225	0.4	20	1	1050	650	200	47.73
4	300	0.35	60	1	950	600	240	78.76
5	400	0.3	10	1	950	670	150	63.52
* Kg/m^3								

3. RESULTS

ANNs model Development

Table 3. ANN model Learning Parameters

Parameters	
Number of hidden layers	2
No. of hidden neurons in left and right	8(left),7(right)
Learning rate	0.03
Momentum	0.5
Iterations	10000

Table 1 provides the statistics of data which was used for modelling. To examine the accuracy of result a line and bar chart graph is plotted between actual and predicted value in Figure 6-8. The results of performance evaluation parameters shows that ANN based model is R^2=0.9642, MAE=2.9501, RMSE=3.7021, RAE(%)=25.1982, RRSE(%)=26.5630 for training and R^2=0.9049, MAE=3.8729, RMSE=4.6531, RAE(%)=54.6531,

RRSE(%)=51.8477 for testing and R^2=0.9891, MAE=3.8195, RMSE=6.6269, RAE(%)=47.8989, RRSE(%)=63.6111 for validating given the result best in using two hidden layer [left neuron(8),Right neuron(7)]. So the actual and predicated strength are obtained with minimum error.

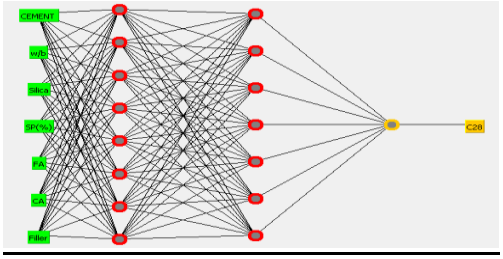

Figure 5. ANN with two hidden layers

The interpretable ANN model for 28 days compressive strength prediction as obtained for two [left neuron (8), Right neuron (7)] of the nodes in the hidden layer is-

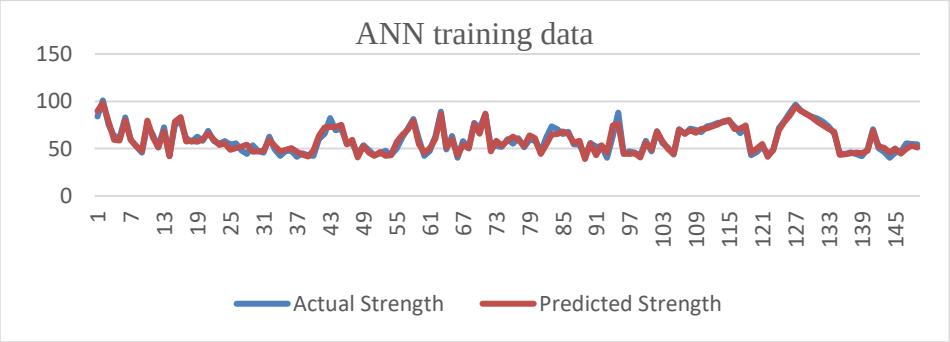

Figure 6. Training set

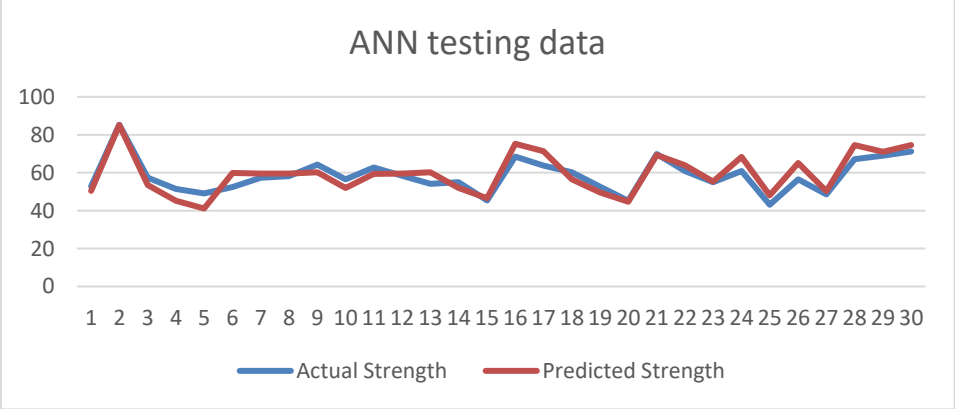

Figure 7. Testing set

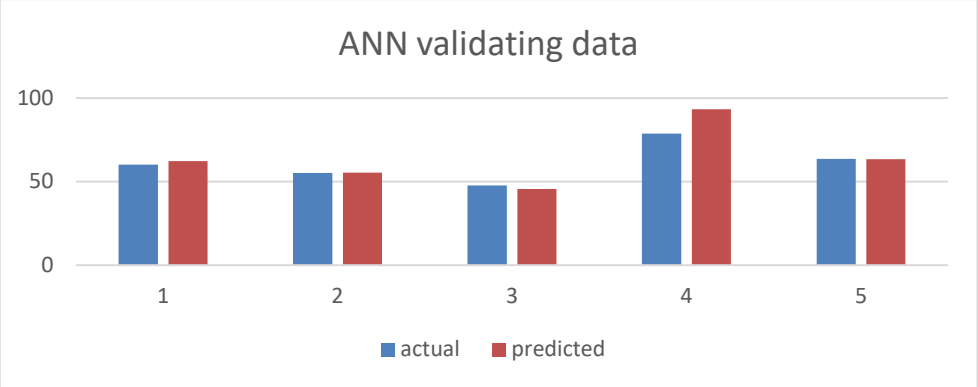

Figure 8. Validating set

Study of literature/research already published shows that generally the modal development using ANN involves the data obtained from another research [18] [19] . The novelty of the present study involves the actual data obtained from experimental work. The validation of the experimental data was also carried out keeping the various input parameters within the range for the model development.

4. CONCLUSIONS

In this Paper, Compressive Strength model using ANN is predicted for SCC including limestone powder, silica flume, and fly ash filler. Thus, following conclusions can be observed:

- The ANNs model proposed in this current study showed its ability to predict the CS of limestone powder, silica flume and fly ash filler self-compacting concrete and the best ANN's architecture of the proposed model is 7-8-7-1.
- To forecast the CS of self-compacting concrete while related the concrete mixes, a back-propagation ANN model can be trained.
- The modeling results are excellent and closely match the experimental values in all phases of training, testing, and experimental validation, proving the proposed ANNs model's accuracy. As a result, the ANNs model is a useful tool for estimating the compressive strength of self-compacting concrete.
- A parametric study was carried out to see the effect of each parameter considered in the proposed model on compressive strength. The results agreed with the literature.
- There are a lot of potential avenues for further works. In the future, the work can be extended by applying the ANN's for predicting several proprieties of SCC with limestone powder, silica flume and fly ash filler such as the workability, elasticity module, durability etc.

REFERENCES

[1] H. Okamura and M. Ouchi, "Self-Compacting Concrete," Journal of Advanced Concrete Technology, vol. 1, no. 1, pp. 5–15, 2003, doi: 10.3151/jact.1.5.

[2] W. Wongkeo, P. Thongsanitgarn, and A. Chaipanich, "Compressive strength and drying shrinkage of fly ash-bottom ash-silica fume multi-blended cement mortars," Materials & Design (1980-2015), vol. 36, pp. 655–662, Apr. 2012, doi: 10.1016/j.matdes.2011.11.043.

[3] A. Mohan and K. M. Mini, "Strength and durability studies of SCC incorporating silica fume and ultra fine GGBS," Construction and Building Materials, vol. 171, pp. 919–928, May 2018, doi: 10.1016/j.conbuildmat.2018.03.186.

[4] M. Y. Durgun and H. N. Atahan, "Strength, elastic and microstructural properties of SCCs' with colloidal nano silica addition," Construction and Building Materials, vol. 158, pp. 295–307, Jan. 2018, doi: 10.1016/j.conbuildmat.2017.10.041.

[5] J. Bernal, E. Reyes, J. Massana, N. León, and E. Sánchez, "Fresh and mechanical behavior of a self-compacting concrete with additions of nano-silica, silica fume and ternary mixtures," Construction and Building Materials, vol. 160, pp. 196–210, Jan. 2018, doi: 10.1016/j.conbuildmat.2017.11.048.

[6] R. Choudhary, R. Gupta, and R. Nagar, "Impact on fresh, mechanical, and microstructural properties of high strength self-compacting concrete by marble cutting slurry waste, fly ash, and silica fume," Construction and Building Materials, vol. 239, p. 117888, Apr. 2020, doi: 10.1016/j.conbuildmat.2019.117888.

[7] M. Abu Yaman, M. Abd Elaty, and M. Taman, "Predicting the ingredients of self compacting concrete using artificial neural network," Alexandria Engineering Journal, vol. 56, no. 4, pp. 523–532, Dec. 2017, doi: 10.1016/j.aej.2017.04.007.

[8] M. Jalal, A. Pouladkhan, O. F. Harandi, and D. Jafari, "Comparative study on effects of Class F fly ash, nano silica and silica fume on properties of high performance self compacting concrete," Construction and Building Materials, vol. 94, pp. 90–104, Sep. 2015, doi: 10.1016/j.conbuildmat.2015.07.001.

[9] S. H. V. Mahalakshmi and V. C. Khed, "Experimental study on M-sand in self-compacting concrete with and without silica fume," Materials Today: Proceedings, vol. 27, pp. 1061–1065, 2020, doi: 10.1016/j.matpr.2020.01.432.

[10] Behforooz B, Eftekhar MR, Amin E, Ghias A. Effects of using silica fume (SF) in improving cermeability properties of Self-compacting concrete (SCC). InProceedings of the 9th International Congress on Civil Engineering, Isfahan, Iran 2012 May (Vol. 8).

[11] O. M. Ofuyatan, A. M. Olowofoyeku, S. O. Edeki, J. Oluwafemi, A. Ajao, and O. David, "Incorporation of Silica Fume and Metakaolin on Self Compacting Concrete,"

Journal of Physics: Conference Series, vol. 1378, no. 4, p. 042089, Dec. 2019, doi: 10.1088/1742-6596/1378/4/042089.

[12] F. A. Mustapha, A. Sulaiman, R. N. Mohamed, and S. A. Umara, "The effect of fly ash and silica fume on self-compacting high-performance concrete," Materials Today: Proceedings, vol. 39, pp. 965–969, 2021, doi: 10.1016/j.matpr.2020.04.493.

[13] Y. Esen and E. Orhan, "Investigation of the effect on the physical and mechanical properties of the dosage of additive in self-consolidating concrete," KSCE Journal of Civil Engineering, vol. 20, no. 7, pp. 2849–2858, Feb. 2016, doi: 10.1007/s12205-016-0258-2.

[14] D. A. J. K.S. Johnsirani, "Study on Effect of Self-Compacting Concrete with Partial Replacement of Mineral Admixtures Using Quarry Dust," 2015.

[15] M. Rita M. Rathod, "To study the effect of varying proportion of Fly Ash and Silica Fume on Fresh and Mechanical Properties of High Strength Self Compacting Concrete," 2015.

[16] Hakim Abdelgader, Abdullah Saud and Ali El-Baden, "EFFECT OF SILICA FUME ON SELF-COMPACTING CONCRETE," Tripoli University, Tripoli, Libya.

[17] Henriette Szilagyi, Ofelia Cornelia Corbu, "SCC with silica fume for precast concrete industry".

[18] Ayat H, Kellouche Y, Ghrici M, Boukhatem B. Compressive strength prediction of limestone filler concrete using artificial neural networks. Adv. Comput. Des. 2018 Jul 1;3(3):289-302.

[19] O. Belalia Douma, B. Boukhatem, M. Ghrici, and A. Tagnit-Hamou, "Prediction of properties of self-compacting concrete containing fly ash using artificial neural network," Neural Computing and Applications, vol. 28, no. S1, pp. 707–718, Jun. 2016, doi: 10.1007/s00521-016-2368-7.

Thermal Analysis of Laser Welding of 304L Austenitic Stainless Steel

[1]M. Zubairuddin*, [2]R. Ravi Kumar, [3]M. S. Reddy, [4]Z. Ahmed, [5]A. Mishra

[6]A. K. Singh, [7]P. Kumar, [8]P. S. Ranjit, [9]A. Saravanan, [10]P. V. Elumalai

[1,3,4,8,9,10] *Aditya Engineering College, Surampalem, Andhra Pradesh, India*

[2]*Indira Gandhi Centre for Atomic Research, Kalpakkam, Tamil Nadu, India*

[5]*Motilal Nehru National Institute of Technology Allahabad, Uttar Pradesh, India*

[6,7]*Aditya College of Engineering and Technology, Surampalem Andhra Pradesh, India*

**zubersiddiqi09@gmail.com*

Abstract

Austenitic stainless steel 304L high temperature applications steel used for different power plants, boilers, oil and gas industries etc. This paper investigates the FEM based thermal analysis of Nd-YAG Laser welding for 1 mm thick 304L stainless steel. FEM based thermo-elastic-plastic model is developed for thermal analysis of Laser welding using SYSWELD. Two different Gaussian distribution heat source models are used for heat source distribution. Initially heat source fitting of bead-on-plates was carried using two different models conical and combined Goldak double ellipsoidal plus conical heat source models then transient analysis of square butt joint was carried out using same models.

Keywords. 304L, SYSWELD, Laser welding, Thermal analysis.

1. INTRODUCTION

Laser beam welding using laser as the energy source is used to weld a variety of materials and composites available today. Laser beam welding can be precisely controlled in intensity and position for joining of metals. The laser beam focus to a small spot size to perform welding. Based on the power intensity and the resulting weld bead profile the laser welding can be classified as conduction mode and deep welding. The advantage of laser compared to Electron Beam (EB) welding process is that the laser can be welded in atmospheric condition whereas the latter needs a complicated vacuum environment.

M. Zubairuddin studied the FEM based analysis of Grade 91 steel using SYSWELD. Author studied the Heat Source Fitting (HSF) analysis on different bead-on-plate, further thermo-mechanical analysis of predicted results validated with measured values of residual stresses and distortion [1-5]. J. Chakkan studied the thermal plus mechanical analysis of 304L and 316L laser welding. Author compared the FEM based calculated residual stresses and distortion with experimental measured values [5-6]. Goldak et al discussed double

ellipsoidal model for GTA welding [7]. Various authors discussed thermo-mechanical analysis of Mod 9Cr-1Mo steel, Al and austenitic stainless steel for different welding processes like GTA, EB and Laser welding analysis [8-15].

In this paper, stainless steel AISI 304 is selected for laser welding as this material has wide application. FEM analysis was carried out using SYSWELD. In this analysis two different heat source models were selected later predicted models were compare with experimental measured width. In second stage, FEM based transient analysis of square butt joint 304L steel plate was carried out.

2. EXPERIMENTAL WORK

The material selected for this experiment is AISI 304L thickness 1 mm. Initially bead on plate experiment was carried out using given below parameters later dimension of each 304L Stainless steel is 150 x 100 x 1 mm is welded using butt joint. The power parameters of Laser Welding, TruPulse 556 is as been given in Table. 1. Experimental setup of Laser welding is shown in Figure 1.

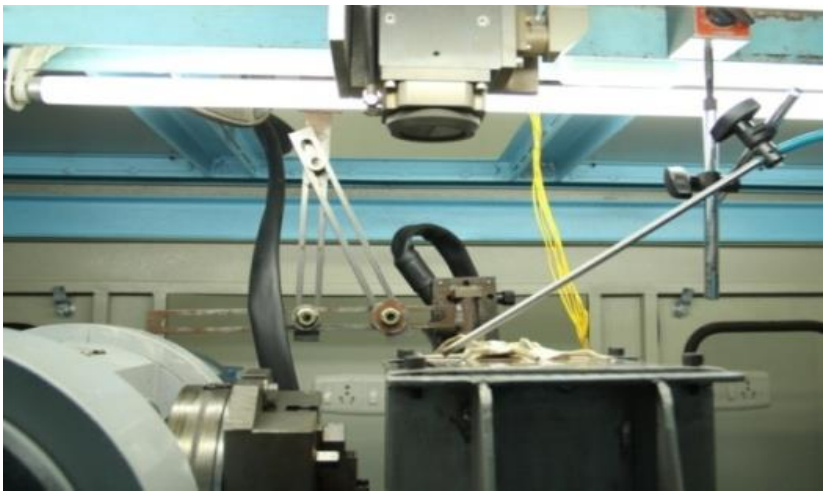

Figure 1. CNC based Laser welding machine

3. WELDING HEAT SOURCE MODEL

Selection of heat source model is a first criterion for finite element analysis and must be calculated to explain the practical physical phenomena in laser welding. Based on literature, it can be seen that defining a reliable and simple model for welding processes is very important step. Heat transfer is the main phenomena happening while welding. Modelling of heat source model for laser welding is a very challenging in finite element method. In this work, two different models have been selected as beam source model by investigating the bead cross section of bead on plate welding.

Table 1. Laser Welding Parameters

Parameters	Value
Peak Power	1.3k W
Average Power	240 W
Velocity	3 mm/s
Pulse Energy	15.1 J
Pulse Width	11 ms
Shielding Gas (Ar)	10l pm
Frequency	14 Hz

3.1. 3D Conical model

3D Conical model as shown in Figure 2 is reliable heat source model used for high depth of penetration of laser welding modelling. Heat power density is higher at the top surface of plate and lower at the bottom surface. The power density at any plane is expressed in Eq. 1.

$$Q_r = Q_0 \exp\left(\frac{-3r^2}{r_0^2}\right) \tag{1}$$

Where r and r_0 is given by

$$r = \sqrt{x^2 + y^2}$$

$$r_0 = r_e - \frac{(r_e - r_i)(z_e - z)}{(z_e - z_i)}$$

Where Q_r is heat source intensity, Q_0 is the maximum intensity, r_e and r_i are surface radius in planes $z=z_e$ and $z=z_i$ respectively.

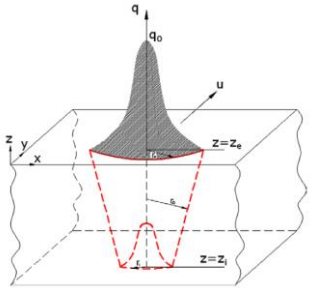

Figure 2. Conical heat source model

3.2. Combined Goldak's double ellipsoidal plus conical heat source model

Laser welded bead cross section shows an elliptical upper portion like a nail head. In order to account for that nail head shape a Goldak double ellipsoidal heat source is attached on top

of 3D conical heat source. The power for each heat source is then distributed according to HSF. Figure 3 shows the combined double ellipsoidal plus conical model.

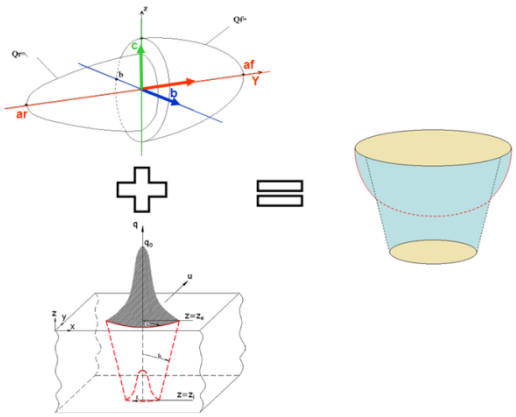

Figure. 3 Combined Goldak's double ellipsoidal plus conical model

4. GEOMETRICAL MODEL

For butt weld experiment, two plates dimensions 150 mm x 100 mm x 1 mm are used. Throughout meshing 8-node hexahedron elements of varying size has been used. Total number of nodes and element are 92123 and 113512. FZ and HAZ will be having a very high thermal gradient; hence, mesh in this zone is very fine. Element size in HAZ and FZ are 0.5 mm x 0.5 mm x 0.5 mm. Since temperature gradient is low in next to HAZ hence mesh is coarser. Visual Mesh, a sub package in SYSWELD has been used for creating the plate model and meshing. The meshed model used for simulation is shown in Figure 4.

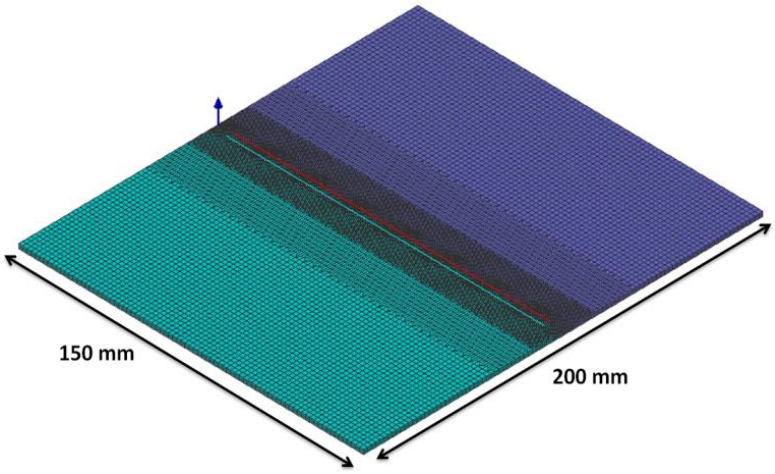

Figure 4. Meshing of butt joint plate

5. THERMAL ANALYSIS OF LASER WELDING

Heat flux distribution decides the accuracy of FEM analysis, based on right choice of model. HSF tool is used for predicting fusion zone. In SYSWELD software, HSF tool is used to

calculate the parameters, based on number of trial close to predicted FZ nearby arc energy input to give the values of heat power density. Experimental based weld profile of bead on plate at 15.1 Joule heat input power is shown in Figure 5. FZ and HAZ of weld profile is measured using microscope.

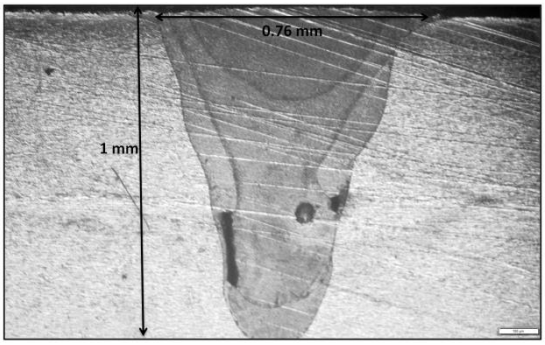

Figure 5. Weld profile of 1 mm thick 304L plate

The HSF analysis of considering conical and combined double ellipsoidal plus conical model heat source model keeping same heat input as bead on plate is shown in Figure 6 (a-b). Predicted FZ width size using conical model shown in Figure 6 (a) is 0.8 mm and depth of penetration is 1 mm, where experimentally measured value is 0.75 mm with 1 mm depth. In case of combined double ellipsoidal plus conical model predicted FZ width is 1.2 mm, where as experimental FZ width is 0.75. HAZ width in case of conical model is 1.3 mm while in case of combined double ellipsoidal plus conical model is 1.9 mm, where as experimental measured using optical microscope is 1.25 mm.

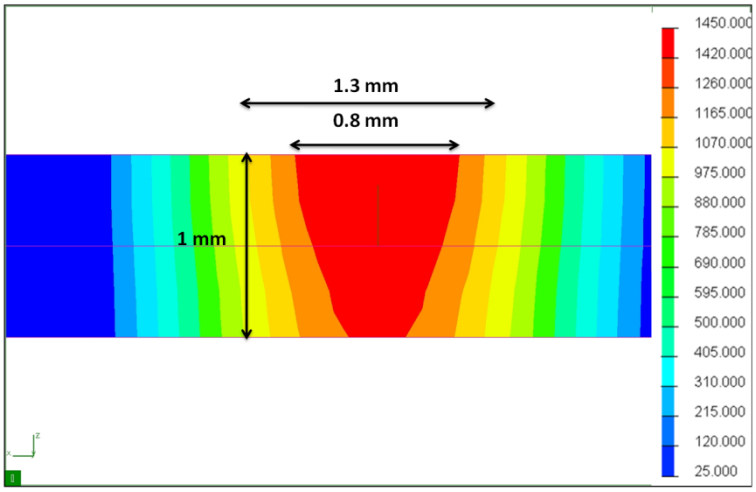

(a) Conical Model

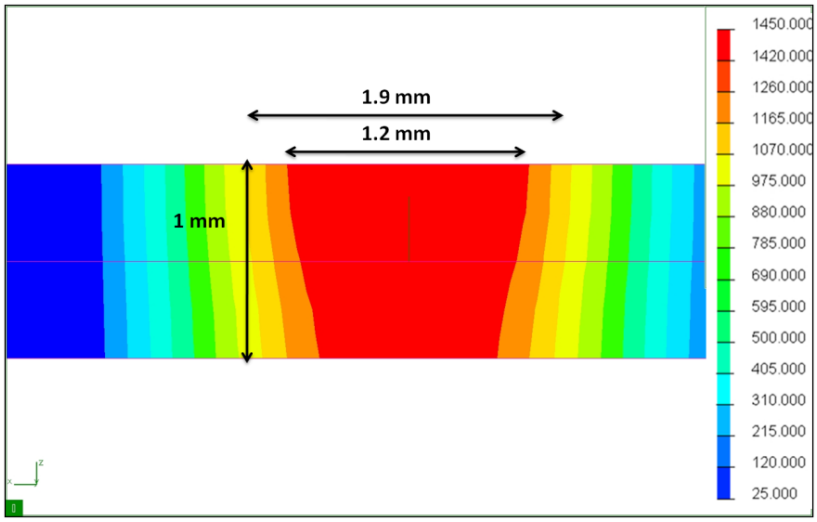

(b) Conical and Goldak's combined Model

Figure 6. Heat Source fitting Analysis

Based on above results, it is observed that conical model is more accurate as compare to combined double ellipsoidal plus conical model, conical model shows 0.04 mm only, where as combined model shows 0.44 mm error. Transient analysis of butt joint plate considering same heat input parameters is carried put in welding advisor. Figure 7 (a-b) shows the thermal analysis of butt joint at the mid of weld plate. Peak temperature reached during welding analysis shows1450ºC in case of conical model as shown in Figure 7 (a), whereas in case of combined double ellipsoidal plus conical model as shown in Figure 7 (b) temperature is reached 1740ºC, above melting point of 304L (1410ºC value).

This high temperature is the main attribute in the formation of the FZ and converting solid to liquid and immediate vicinity of FZ (i.e. weld zone) is defined as HAZ.

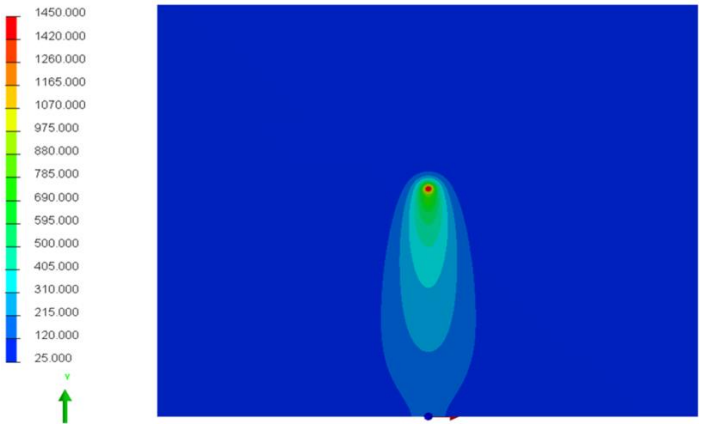

(a) Conical Model

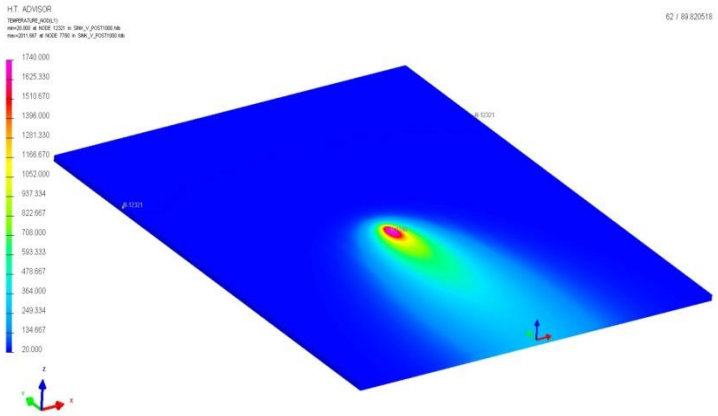

(b) Double ellipsoidal plus conical model

Figure 7. Thermal Analysis of laser welding of 304L butt Joint

6. CONCLUSION

In this study, initially work bead on plate welding is carried out in the next stage same heat input parameters was used for transient analysis.

- Comparison of predicted FZ and HAZ showed that conical model predicts more accurate as compare to combined double ellipsoidal plus conical models.
- FEM based steady state analysis of HAZ and FZ of bead on plate of 304L carried out using two different heat source models, results shows 0.8 and 1.3 mm, which is nearer to measured value 0.76 mm.
- Second stage of FEM analysis shows maximum temperature reached in case of conical model is 1450ºC as compare to combined model double ellipsoidal plus conical model is 1740ºC.

REFERENCES

[1] M. Zubairuddin, R. Ravi Kumar, B. Ali, Thermo-mechanical analysis of Laser welding of Grade 91 steel, Optik, 245 (2021) 167510.

[2] M. Zubairuddin, S. K. Albert, S. Mahadevan, M. Vasudevan, V. Chaudhari, V. K. Suri. Experimental and Finite element analysis of residual stress and distortion in GTA welding of modified 9Cr-1Mo steel. J. Mech. Sci. Techn. 28 (12) (2014) 5095-5105.

[3] M. Zubairuddin, S. K. Albert, S. Mahadevan, M. Vasudevan, V. Chaudhari, V. K. Suri. Thermo-mechanical analysis of preheat effect on Grade P91 steel during GTA welding. Mat. Manuf. Proc. 31 (3) (2014) 366-371.

[4] M. Zubairuddin, S. K. Albert, S. Mahadevan, M. Vasudevan, V. Chaudhari, V. K. Suri. Numerical simulation of multi-pass GTA welding of grade 91 steel J. Manuf. Proc. 27 (2017) 87-97.

[5] J. R. Chukkan, M. Vasudevan, S. Muthukumaran, K. C. Ganesh. R. Ravi Kumar, S. Murugan. V. Madhuaimuthu, Numerical simulation of pulsed Nd-YAG Laser butt

welding of AISI 304L stainless steel sheet and experimental validation, App. Mech. Mater. 2014, 592-594, 565-570.

[6] J. R. Chukkan, M. Vasudevan, S. Muthukumaran, R. Ravi Kumar, N. Chandrasekhar, Simulation of laser butt welding of AISI 316L stainless steel sheet using various heat sources and experimental validation, J. Mater. Process. Technol, 2015, 219, 48-59.

[7] Goldak, A. Chakravati, M. Bibly, A new finite element model for welding heat sources, Metall. Trans. B. 15 (2) (1984) 299-305.

[8] S. Saravanan, K. Raghukandan, G. Shanthos Kumar, Comparison of numerical and experimental macrostructure in Nd-YAG laser welding Hastelloy C-276, Optik, 2019, 180, 562-568.

[9] S. Kumar, R. Awasthi, C. S. Vishwanadham, K. Bhuanumurthy, G. K. Dey, "Thermo-metallurgical and thermo-mechanical computations for laser welded joint in 9Cr–1Mo (V, Nb) ferritic/martensitic steel" Material and Design, 2014, Vol. 59, 211-220.

[10] C. Heinze, A. Pitter, M. Rethmeier, S. Babu, "Dependency of martensite start temperature on prior austenite grain size and its influence on welding induced residual stresses", Computational Material Science, 2013, Vol. 69, Issue 1, 251-260

[11] H. Serizawa, S. Nakamura, M. Tanaka, Y. Kawahito, H. Tanigawa, S. Katayama, "Effect of mechanical restraint on weldability of reduced activation ferritic/martensitic steel thick plates", Journal of Nuclear Material, 2011, Vol. 417, 55-58.

[12] Z. HU, J. Zhao, "Effects of martensitic transformation on residual stress of P91welded joint", Material research express, 2018, Vol. 5, No. 9, 96528-96529..

[13] Z. Muhammad, N. Daniel, J. Jullien, D. Dominique, Experimental investigation and finite element simulation of laser beam welding induced residual stresses and distortion in thin sheets of AA 6056-T4, Journal of Material Processing Technology, 2012, 1705-1715.

[14] J. Sun, X. Liu, Y. Tong, D. Deng, A comparative study on welding temperature fields, residual stress distribution and deformations induced by laser beam welding and CO2 gas arc welding, Mater. Des, 2014, 63, 519-530.

[15] B. Shanmugarajan, G. Padmanabham, H. Kumar, S. K. Albert, A. K. Bhaduri, "Autogenous laser welding investigations on modified 9Cr-1Mo (P91) steel", Science and Technology of Welding and Joining, 2011, Vol. 16, 6, 528-534.

Biographies

Dr. M. Zubairuddin received the bachelor's degree in Mechanical engineering from Dr. BAMU University in 2006, the master's degree in Machine Design and Analysis from National Institute of Technology Rourkela in 2009, and the philosophy of doctorate degree in Engineering Science Homi Bhabha National Institute in 2020, respectively. He is currently working as an Assistant Professor at the Department of Mechanical Engineering, Faculty of Engineering, Aditya Engineering College Surampalem. His research areas include Welding analysis, residual stress, and artificial intelligence. He has been serving as a reviewer for many highly-respected journals.

A Review on Design Consideration for Reconfigurable Manufacturing System

Anurag Anand, Prakash Kumar

Production & Industrial Engineering Department, BIT Sindri, Dhanbad

anurag2k87@gmail.com, hod.pe@bitsindri.ac.in

Abstract

In the present paper, a review of design methodologies for reconfigurable manufacturing systems is discussed, with a focus on different combinations of interchangeable designs in alignment with symmetric and asymmetric combinations of the system are analyzed. With the different combinations of the crossover and without crossover it was concluded that machine reliability and gantry reliability of RMS with crossovers have higher degree of productivity. It can be said, that better the machine average reliability, larger is the solution of parallel line configuration or the vice versa. It can be concluded that in a larger system, the RMS has an extended degree of capability in comparison to parallel line combinations.

Keywords: Reconfigurable Manufacturing System, Reliability, Productivity, Maintainability

1. INTRODUCTION

The beginning of the mass production era marked in 1913 with the introduction of the moving assembly line. It has significant contribution towards the possibility of the emergence of the dedicated machining line (DML), which further led to the development of advanced production for engines, transmissions, and major components contributing towards the automotive sector. The introduction of DML provided the capability of high production rates for the specific part types, which drastically enhanced production time as well as the entire cycle time of the product. Furthermore, NC and CNC systems were introduced which again acted as a revolutionary trend change in the entire manufacturing scenario of the world, facilitating the entry of the flexible manufacturing system in the early 1980s [7]. Stecke and Solberg [16] who previously introduced the operation policies of FMS, again developed the concept for the mathematical modelling of flexible systems, easing the ideal objective of a manufacturer, that is flexibility, productivity and quality, to enhance the capability of the entire system in 1980s and 1990s. In the forthcoming era, the changing pace of the globalization and the increasing competitiveness in the manufacturing scenario FMS also found to be a partial solution for the economic prospects. Therefore, rising need for the rapid change in the production capabilities in responsive acts towards the sudden market demands the concept for reconfigurable manufacturing systems are introduced [5]. In reconfigurable manufacturing system, the capability of scaling up and scaling down the system structure both at the software and hardware levels in response to

sudden market changes makes it a very effective solution for the manufacturers leading to proper cost effectiveness as well as the inventory control solution [6].

2. CHARACTERISTICS OF RMS

A typical Reconfigurable Manufacturing System has six characteristics as shown in fig 1 that includes Modularity, Integrative design features, Customized flexibility, Scalability, Convertibility, and Diagnosability [10]. Y.Koren applied these characteristics in the event of transformation of the entire manufacturing system for different attributive components of the system.

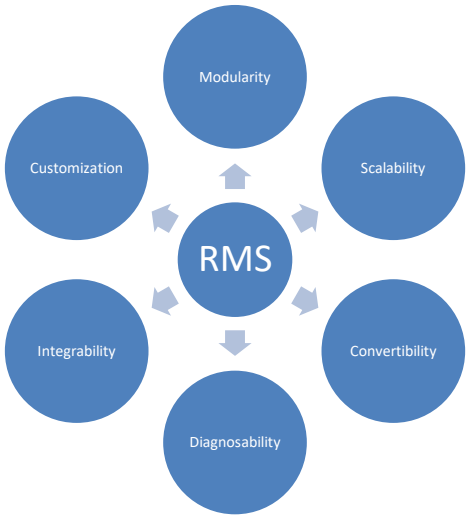

Figure 1. Characteristics of RMS

Modularity*:* It is the most important indicative component of the reconfigurable manufacturing system responsible for the reduction of complexity both at design and evaluation level of the system. The system includes different type of components that are typically commutable in nature which can be machines, axes of motion, controls, and tooling that can be replaced or upgraded to a better version when found to be necessary suiting new applications.

Scalability*:* It expresses the performance ability with adjustment of production capability of the system as per the needs with optimum cost consideration alongwith minimised time, over a large range of capacity within its capacitive increments. It can also be said as the ability to maintain cost effectiveness when there is a change in market demands or workloads as shown in the fig 2 and fig 3.

Convertibility*:* Convertibility explains the capability to adjust operational functionality that can be changed from one form to another. It includes the capability to switch over the spindles of a machine as per the requirements of the system. Also, it can be adjusted

manually with a passive degree of freedom for the production of different parts within a part family.

***Diagnosability**:* It is the capability to find and optimise the basic cause of problems for output defects of the products which further can be corrected or adjusted quickly. However, diagnosability can be further categorized into delectability, predictability and distinguish-ability.

***Customization**:* It explains the capability of modifying or designing machine capability to achieve a higher degree of flexibility. It significantly classifies the RMS and its enhanced superiority over the classical FMS /CNC system. The typical feature of the customization provides feasible designing of the system for the operational output of the similar type of part, irrespective of a particular part type integration.

Integrability: It is the integrative capability of different modules in a very quick and accurate manner with different sets of interface controls as well as different mechanical and software information. It allows a typical system designer to relate various types of part type and their capability for respective machines for corresponding operations to be performed which further leads to the product-process integration.

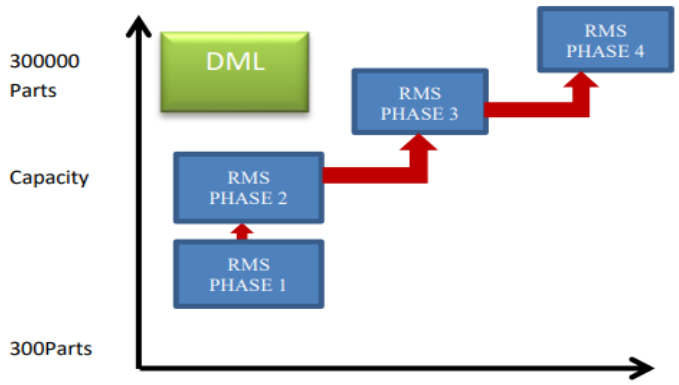

Figure 2. Static Nature of DML and FMS Vs Dynamic Nature of RMS

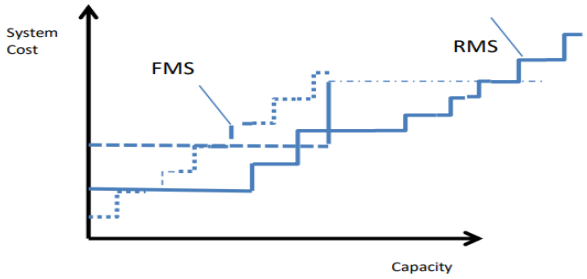

Figure 3. Comparison of Manufacturing System Cost and Capacity

3. CLASSIFICATION OF THE CONFIGURATIONS

In order to classify the configurations, there should be known daily demands of part types per day (Q), total time required by part type (t) in minutes, are given. In real kind scenario, the equipment used attribute towards the machining time but in general here it is represented as:

$$N = \frac{Q*T}{\frac{Min}{Day}*Machine\ Reliablity}$$

Here, the system is to be assumed to be 100% reliable for all pieces of equipment, which therefore, represent the reliability = 1. To calculate the number of machines it can be rounded off the data towards the nearest higher side of the integer

On considering that, if 300 parts per day are needed and thereby the time required by each part type for processing is 9.5 min then minimum requirement of the machine time that are assumed to be in the work becomes 1000 min/day [12]. In general, the total number of combinations for the machines are higher, therefore a logarithmic scale was considered which led to the increase in the configuration on a linear scale. Here, with the linear arrangement it was found that with the aforementioned number of machines, the possible configuration for the RMS is pretty much lower to meet the possible demands of products.

No. of Machines	No. of Possible Configurations	No. of RMS Configurations
3	3	3
5	18	9
7	198	36

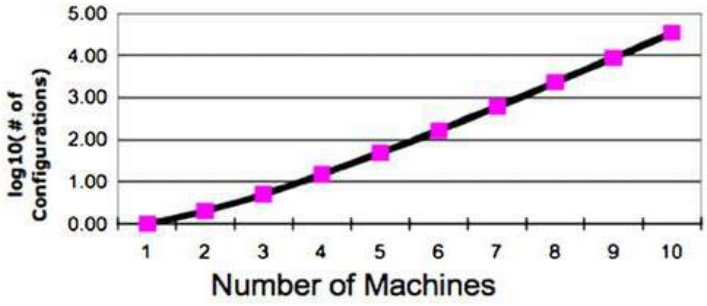

Figure 4. Representation of Total System Combination or Configuration on the Basis of Different Numbers of Machines

Here, different combinations are classified as symmetrical or asymmetrical, which is further evaluated by its typical arrangement of connections with respect to machines. For instance, if configurations have almost similar kind of arrangements, i.e they are identical, but they are considered differently because of cross coupling between different stages of machines,

In the present system, the symmetrical system has only 18 configurations for the 5 machines (Fig. 4) and will be considered as the symmetric configuration by the designer as shown in fig 5. However, asymmetric combinations of configurations add very higher degree of complexity and are practically feasible in real-world kind operational lines. The different combinations led to a very higher possible configuration of the asymmetric configurations as compared to symmetric configurations. It is only due to the different position as per the reconfiguration science as per their requirements.

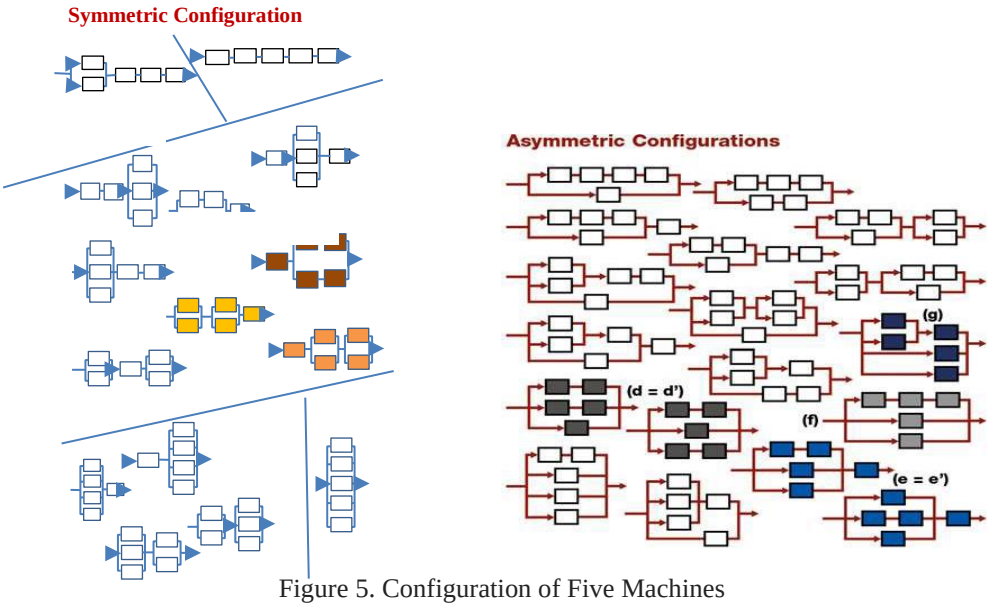

Figure 5. Configuration of Five Machines

In general, it was found that asymmetric configurations are typically not suitable for real time machining scenarios, which can be categorised into variable-process configurations and single-process configurations, which are represented by Fig. 6. below. With the non-identical flow paths, variable configurations are characterised for the different parts [19]. For instance, the aforesaid system shown in fig 6 can have different sequences of flow paths such as g–c–f-e, g–c–d–e, a–b–c–d–e, etc. It was not possible for a designer to design multiple prospective designs for the same part type with different corresponding flow paths. It is due the very higher possibility of the error in the part quality which are very tough in nature to be detected, which might led in the failure of the system.

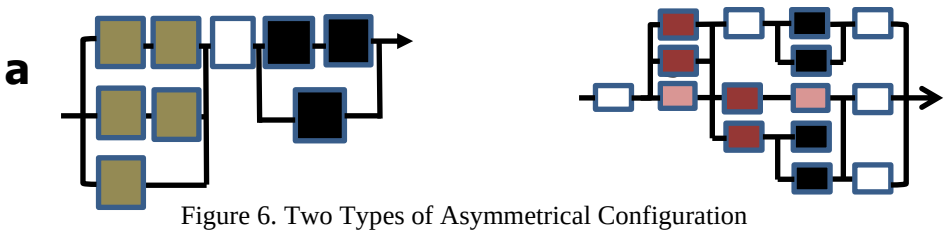

Figure 6. Two Types of Asymmetrical Configuration

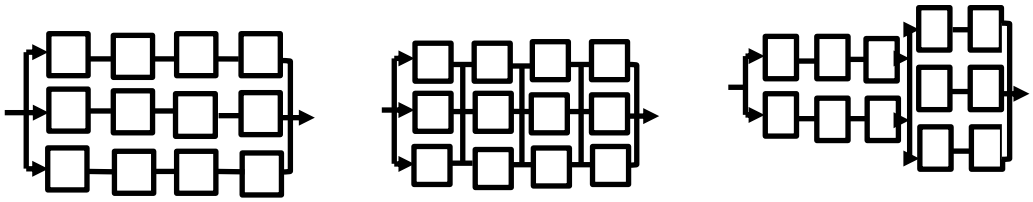

Class I
Series in Parallel = Cells

Class II RMS
Configuration with Crossovers

Class III
No Crossovers

Figure 7. Three Types of Symmetrical Combination

The processing time for the symmetric configuration in a particular stage is almost equal due to the similarity in the sequence of operation that can be attributed to the different combinations of machine types. Here, system designers also not consider them because of excessive competitiveness and impractical considerations [4]. It can be said that practically only symmetric configurations are the only possible design consideration for the real time performance which is further classified into three stages [12] as shown in the above figure7.

4. CONCLUSION

The aforesaid configuration discussed represents that RMS has a spine gantry having identical reliability to that of the conveyors as shown in the fig 10. which further attributed towards the complex calculation of trade-offs between creditability of responsiveness(reliability) of cell gantry and hence the overall machine that is Gr = 0.96 and Mr = 0.96 respectively [12]. As per various research and analysis on the basis of machine and gantry reliability, respectively proven that RMS with crossovers have a higher degree of productivity and hence, they are preferred. It can be said that the better the machine's average reliability, there is higher extended solution of parallel line configuration or vice versa. It can be concluded that in a larger system, the RMS has the higher capability than parallel line configurations. Secondly, with respect to higher machine reliability, the productivity of cell configuration becomes on the higher side. Although, the installation cost of the RMS is higher but with the changing market demand scenario, and the need of scaling up or down of the system RMS can easily cope up with the highly un-predictive boundaries.

REFERENCES

[1] Cochran DS, Arinez JF, Duda JW, Linck J. A decomposition approach for manufacturing system design. Journal of Manufacturing Systems 2001–2002; 20(6):371–89.

[2] Dupont-Gatelmand C. A survey of flexible manufacturing systems. Journal of Manufacturing Systems 1981;1(1):1–16

[3] Freiheit T, Koren Y, Hu SJ. Productivity of parallel production lines with unreliable machines and material handling. IEEE Transactions on Automation Science and Engineering 2004;1(1):98–103.

[4] Freiheit T, Shpitalni M, Hu SJ. Productivity of paced parallel-serial manufacturing lines with and without crossover. Journal of Manufacturing Science and Engineering 2004;126(2):361–8.

[5] Koren Y, Ulsoy AG. Reconfigurable manufacturing systems. Engineering Research Center for Reconfigurable Machining Systems. ERC/RMS report #1. Ann Arbor; 1997.

[6] Koren Y. The global manufacturing revolution—product-process-business integration and reconfigurable systems. John Wiley & Sons; 2010.

[7] Koren Y. Computer control of manufacturing systems. McGraw-Hill; 1983.

[8] Lee HF, Stecke KE. An integrated design support method for flexible assembly systems. Journal of Manufacturing Systems 1996;15(1):13–32

[9] Koren Y, Kota S. Reconfigurable machine tools. US patent no. 5,943,750. August 1999

[10] Koren Y, Heisel U, Jovane F, Moriwaki T, Pritschow G, Ulsoy AG, et al. Reconfigurable manufacturing systems. CIRP Annals 1999;48(2):6–12.

[11] Koren Y, Ulsoy AG. Vision, principles and impact of reconfigurable manufacturing systems. Powertrain International 2002;14–21.

[12] Koren, Y., Shpitalni, M.: Design of reconfigurable manufacturing systems. Journal of Manufacturing system. 2011

[13] Koren Y, Ulsoy AG. Reconfigurable manufacturing system having a production capacity, method for designing same, and method for changing its production capacity. US patent no. 6,349,237. February 2002.

[14] Landers R, Min BK, Koren Y. Reconfigurable machine tools. CIRP Annals 2001; 49:269–74

[15] Pritschow G, Altintas Y, Jovane F, Koren Y, VanBrussel H, Weck M. Opencontroller architecture—past, present, and future. CIRP Annals 2001;50(2):463–70.

[16] Stecke KE, Solberg J. Loading and control policies for a flexible manufacturing system. International Journal of Production Research 1981;19(5):481–90.

[17] Son YK, Park CS. Economic measure of productivity, quality and flexibility in advanced manufacturing systems. Journal of Manufacturing Systems 1987; 6(3):193–207.

[18] Spicer P, Yip-Hoi D, Koren Y. Scalable reconfigurable equipment design principles. International Journal of Production Research 2005;43(22):4839–52.

[19] Spicer P, Koren Y, Shpitalni M. Design principles for machining system configurations. CIRP Annals 2002;51(1):276–80.

Biographies

Anurag Anand received the bachelor's degree in Mechanical Engineering from Ranchi University in 2010, the master's degree in Automated Manufacturing System from Birla Institute of Technology, Mesra, Ranchi in 2013, and currently pursuing philosophy of doctorate degree in Production and Industrial Engineering from BIT Sindri, respectively. He has interdisciplinary work experience both in the teaching as well as in the corporate sector handling the major projects. His research areas include reconfigurable manufacturing system, maintenance strategy, forecasting, fuzzy applications and soft computing analysis

Dr. Prakash Kumar received the bachelor's degree in Production Engineering from Birla Institute of Technology, Mesra, Ranchi in 1996, the master's degree in Production Technology from BIT Sindri in 2009, and the philosophy of doctorate degree in Production Engineering (Maintenance Management) from Vinoba Bhave University in 2017, respectively**.** He has over two decades of experience in technical education and is currently serving as a Professor and Head, Department of Production and Industrial Engineering, BIT Sindri, Dhanbad. He began his career in Tata Motors Ancillary industry and later moved on to Jojobera Power Plant and BIT Mesra. He is President of IIC (4.0). Also contributing significantly as an Expert Representative for Centre of Innovation, Incubation & Entrepreneurship (CIIE) of IIT(ISM) Dhanbad. His fields of interest are Maintenance Technology, Productivity Improvement through Lean Manufacturing, Expert System, Change Management and Industrial Management.

Improvements of Quality in SMT line through Overall Equipment Effectiveness

[1]Manish Kumar Ojha, [2]Bharath Kumar S., [3]Ravindra Kannojiya, [4]Poonam Ojha

[1,2,3] Amity University Uttar Pradesh, Noida, India

[4] School of Management, Graphic Era Hill University, Bhimtal Campus, Bhimtal, Uttarakhand, India

mkojha@amity.edu, bharathsiva01@gmail.com, rkannojiya@amity.edu, poonamojha@gehu.ac.in

Abstract

In the 21st century, everything is improving faster, and manufacturing sectors are not excluded. Technological advancements have exponentially improved the manufacturing sector in the past three decades and have also advanced in increasing the quality of products produced in a manufacturing industry. TPM, one of the most famous and used methodologies founded by Seiichi Nakajima has a quantitative tool called Overall Equipment Effectiveness (OEE), which gives the quantification of an industry's Total Productive efficiency. The electronics sector is a growing sector in India and this paper is an attempt to deliver a case study on the Improvement of OEE in an SMT line. In this case study, several quality tools from Lean Manufacturing have been integrated and incorporated for the OEE improvement. OEE data has been assumed from various articles on the Semi-conductor industry. The tools like VSM, Fishbone Analysis, FMEA are used to identify the main slow-down process and then the paper discusses the various methodologies that can be adopted for this specific SMT line so that the result would be an improvement in OEE.

Keywords. Total Productive Maintenance, Overall Equipment Effectiveness, Surface Mount Technology, Value-Stream Mapping, Fishbone analysis, Process-failure mode analysis.

1. INTRODUCTION

The rise of the industrial revolution in the 19th century and early 20th century led to technological advancements in the electronics sector and the growth of the global economy. European countries, Japanese, and many other countries were improving to be the industrialized nation and as a result, the technology saw a rapid advancement. The First World War adversely affected many countries, and they were forced to adopt different methodologies to be more efficient. The lean Manufacturing model from the Toyota Production System in 1930 gave a new insight into discrete manufacturing. This Lean Manufacturing focussed on eliminating wastages, speeder

production, and cost-effectiveness. Later in the 1950s the Father of the Total Production System Seiichi Nakajima devised a quantitative measure to standardize the production efficiency called OEE i.e., Overall Equipment Effectiveness. OEE is a small part and a lean tool of this Lean manufacturing which deals with the equipment effectiveness, it takes the most common sources of manufacturing which gives us a measure to calculate the efficiency the manufacturing process. The three categories are Availability, Performance and Quality. Since the 1950s OEE has evolved in many ways for various kinds of manufacturing sectors. OEE consists of three attributes Availability, Performance, and quality. OEE is the product of all these three values. Nakajima also states that the losses while calculation of OEE can be grouped into six big losses which further helps us to classify the losses.

In the past two decades, Electronics Manufacturing Sector has been growing exponentially all over the world and countries like India which has a growing number of skilled workforces is a perfect place for this industry. Printed Circuit Boards are the building blocks of an electronic component, and these PCBs are manufactured using Surface Mount Technology. Developing VSM from the data gathered and identifying the bottleneck manufactured using Surface Mount Technology. Improvement of OEE[8] of SMT line is a continuous improvement strategy and This paper is a case study on the Linear Surface Mount Technology line. Single-sided PCBs are taken into consideration, so that model can follow a linear path and single workflow.

2. METHODOLOGY

Basic area to focus in improving OEE is to look after the major losses i.e., breakdown**,** setups and adjustment, small stops**,** reduced speed**,** startup rejects, production rejects and try to reduce it**.** This case study focusses on how to improve the OEE by focussing on the quality attribute and availability of the equipment unlike only on availability as discussed in [9], The prime objective of this study is to analyse the process flow of the SMT line, and to apply the quality tools over the gathered data about SMT line and finding out the bottleneck. Integration of quality tools like FMEA as mentioned in [7] and identification of appropriate methodologies for OEE improvement is the secondary goal is to be achieved. The proposed framework of the adopted methodology for the same is shown in Figure 1.

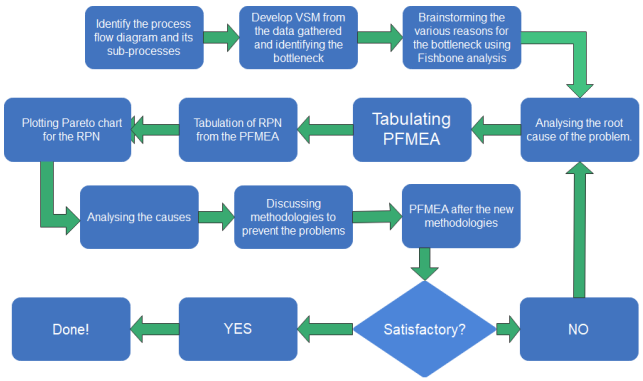

Figure 1. Methodology for this case study

The process workflow Figure 2 formulated in this paper is primarily focused on the linear model. The SMT line usually starts from the arrival of components, solder paste and other products to the warehouse, then it follows the major value-added processes and then unloading occurs which then proceeds for logistics or other processes depending upon the, if it is an automotive electronics manufacturer, it proceeds for ICEF testing processes. This paper has considered standard sized PCBs and the simple major value-added processes to the PCB boards. The machinery is arranged in a linear manner and connected to each other via conveyor belt.

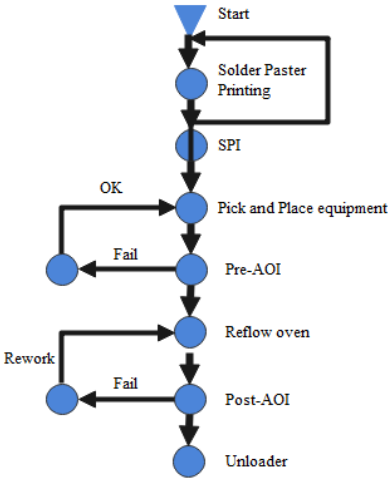

Figure 2. Process flow in considered SMT line

The Process workflow considered in this paper:

1. The Surface Mount Technology process starts from the loading of PCBs onto the loader, the worker loads the plain PCBs on to the UD/LD loader, which proceeds to push the PCBs onto conveyor belt.
2. This takes the boards to their first value-added process where the automated solder paste printer prints the solder paste. The PCB is placed under a Stencil and a squeegee moves left to right printing the Solder paste onto the board. This printing involves loading the raw solder paste in liquid or solid state into the machinery prior to the start of the processes, this involves different methods depending upon the industries.
3. After this printing process the conveyor belt takes this board to Solder Paste Inspection, this inspection is usually automatic because it saves a lot of time, and this machine can detect whether the print is applied or not but cannot detect the quality of the solder printing. If any fault is detected in the SPI the defective parts is excluded and sent to the buffer, it may be a vertical or horizontal buffer depending on the industry. The defective boards are then corrected and then set back in the conveyor belt.
4. The Board then passes to the major value adding process i.e., Chip mounting machinery or pick and place equipment. The considered environment is high-mix low volume, so this process is very crucial in the Surface Mount Technology line. Components like chips, resistors are loaded to the machine and this loading process is considered in downtime. The automated pick and place fit the components onto the board where the solder paste is printed.
5. After the chip mounting process, the board passes through the Automated Optical Inspection before entering the reflow oven, x-ray inspectors are used for this inspection. The Pre-AOI is placed right before the reflow oven to detect any missing part. This equipment is very essential in the entire process because once the fault is not detected before a board enters a reflow oven, rework cannot be done over the board and eventually the defective board will be discarded. I have considered an automated OI.
6. After this inspection the board enters the reflow oven, I have considered 8-layer reflow oven and a linear flow. The incomplete board then passes over the solder paste enters the reflow oven and gets heated up and the soldering is done.
7. When the board exits the oven, it is subjected to cooling or other trivial processes depending upon the manufacturers, but I have made a simple SMT line so, the board goes through the post-AOI which is the final process of my considered SMT line, Here the board is checked for every aspect. Same as the pre-AOI equipment, if any detect is found, it is sent to the buffer and the rework is done. Then the board are unloaded from the conveyor belt.

2.1 Developing VSM

Value stream mapping is a lean management tools which provides the big picture of the entire process. The conventional usage of this tool is by creating a current VSM, analysing the causes, implement new methodologies and implement future VSM. In this paper, two to three quality tools have been integrated for improvement of OEE. VSM helps visualise the entire process and quickly discover in which way it may go wrong and gives an idea for improvement. Data has been gathered for SMT line from [5] by Amir Azizia and Thulasi a/p Manoharan which was based on a PCB manufacturer in Malaysia and from other sources to implement the VSM. This

Data has been checked properly and considered after some recommended changes. The data has been displayed in the Table 1.

Table 1. VSM data for the considered line.

Process name	Solder Print	SPI	Chip mounter	Pre-AOI	Reflow oven	Post-AOI
Manual Cycle time	55.8	6	0	34	0	62.5
Machine cycle time	5	14	48	6	20	7.5
Changeover time	65	0	0	0	105	0
Batch size	300	300	300	300	300	300
Effective cycle time	61	20	48	40	20	70
Available time	50400	50400	50400	50400	50400	50400

2.2 Analysis of VSM

It indicates a main point that Manual Cycle time for post-Automated Optical Inspection is more than a minute for single board. The VSM has been attached as *Figure 3.* This is due to the importance of quality of the soldering. If the AOI detects any quality degradation it sends it to the buffer and a worker checks any rework is possible or else the board is discarded. So, the important reason for this rejection and increasing manual cycle time is Improper soldering in Reflow oven.

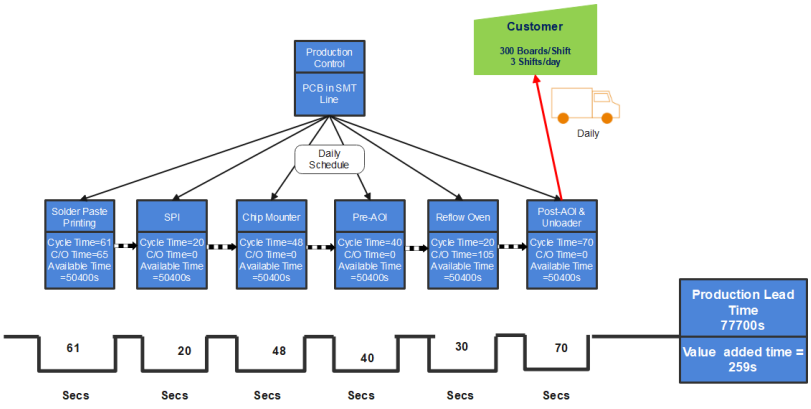

Figure 3. Current VSM for the considered line

2.3 Fishbone diagram and its analysis

Figure 4. Fishbone analysis over the bottleneck

Fishbone analysis is a lean management tool and used to take all the causes for the main problem. The main purpose of this tool is to quickly factor out the major causes for the problem. The main effect should be discussed and clearly stated out.[8] The main effect is written at the right edge of the paper or sheet; a line is drawn from the effect in the middle and branches are drawn out of the line to factor out the causes. This resembles a fishbone with the main effect as the head. Hence it is also called as Fishbone analysis. The Fishbone analysis has been attached as *Figure 4*. Improper soldering from VSM has given us the main area to focus and it is a solid effect to be focussed on.

2.4 PFMEA

Failure mode effective analysis is a lean tool which quantifies the risk involved in a process or components [15] . Process-FMEA is formulated here because this tool helps identify the errors precisely and provides with a solution for that. This tool also helps to eliminate the unwanted processes in a manufacturing line. From the fishbone analysis the causes for the effects are known now PFMEA can be performed on the main value-added processes in SMT line to sort them out based on their stages. PFMEA is quantified by three attributes *Severity, Occurrence and Detection*. Product of these attributes gives us the Risk Priority Number. The limit set to RPN varies across manufacturing sectors. The Scale for the quantification of Severity, Occurrence and the detection varies across industries. The considered Scale here is designed by considering data from various sources.

Table 2. PFMEA over Solder paste printing

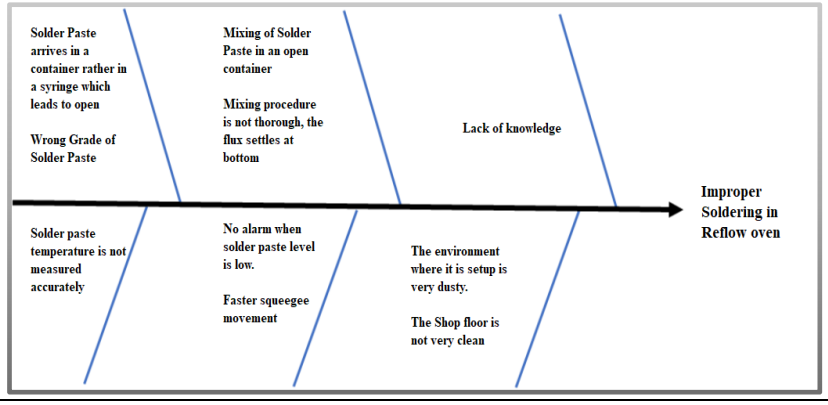

Process/Product Potential Failure Modes and Effects Analysis (FMEA)

Process or Product Name:	PCB							**Prepared by:**	Bharath										
Responsible:	Process Engineer							**FMEA Date:**	**(Orig.)**1/06/21		**(Rev.)** 10/08/21					**Page**		**of**	
Process Step/Input	**Potential Failure Mode**		**Potential Failure Effects**		**Potential Causes**		**Current Controls**				**Actions Recommended**	**Responsible**	**Actions Taken**						
		Effect					**Prevent**	**Detect**											
What is the process step/input under investigation?	**In what ways does the input go wrong?**	**NP-NEXT PROCESS SP-SUBSEQUENT PROCESS OP-OTHER PROCESS**	**What is the impact on the Output Variables (Customer Requirements) or internal requirements?**		**What causes the input to go wrong?**		**What are the existing controls and procedures (inspection and test) that prevent/detect either the Cause or Failure Mode?**				**What are the actions for reducing the occurrence of the Cause, or improving detection? Should have actions only on high RPN's or easy fixes.**	**Who is responsible for the recommended action?**	**What are the completed actions taken with the recalculated RPN? Be sure to include completion month/year.**						

Solder Paste Printing	Improper attachment of components	NP		8	Low Temperature of the Solder	8	Using Solder Paste after 6 hours taken from refrigerator.	SPI	2	128	Poka yoke for Solder paste temperature and not based on hours	Engineer 03/06/2021	Poka yoke for Solder paste temperature and not based on hours.23/06/21	2	6	6	72
		SP								0							0
		OP	Rejection of Products							0							0
										0							0
										0							0
	Improper attachment of components	NP		5	Improper mixing of Solder paste	6	Stirring the paste before application	SPI	3	90	Employment of Solder Paste centrifuge machine	Engineer 16/06/2021	Employment of Solder Paste centrifuge machine. 30/06/2021	3	3	4	36
		SP								0							0
		OP	Rejection of Products							0							0
										0							0
										0							0
	Improper attachment of	NP		3	Paste stuck in Stencil	5	Replacement of Stencils	SPI	4	60	Usage of frameless stencils	Engineer 05/07/2021[1	Usage of frameless stencils 20/07/2021	3	2	2	12
		SP								0							0

	components	OP	Rejection of Products							0							0
										0							
	Improper attachment of components	NP		3	Faster Printing	2	nil	SPI	7	42	Slower Squeege action	Engineer 27/07/2021	Slower Squeegee action 10/08/21	1	2	4	8
		SP								0							
		OP	Rejection of Products							0							0

PFMEA is a very tedious process and can be exceptionally long, PFMEA is updated whenever a new methodology is applied and for this case study, this paper has considered what can go wrong in SMT line and a PFMEA is made, a sample of PFMEA done over Solder printing has been attached as table 2. The main deduction from the PFMEA is the RPN. RPN has been segregated for three main Value-added processes in table 3 and pareto chart has been plotted for that in Figure 5.

Table 3. Compilation of RPN from PFMEA

Effect	RPN	Cumulative Percentage	Percentage
Sol.Print	320	38	38
Chip.Mt	288	72	34
Reflow Soldering	232	100	28

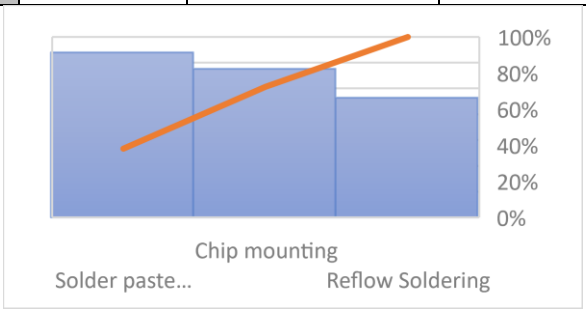

Figure 5 Pareto chart of RPN.

2.5 Pareto Chart

This Pareto is also a lean tool, and it is because 80 percent of disruption in a manufacturing line is caused by 20 percent of the process and the remaining 20 percent disruption is caused by 80 percent of the line. This helps to identify the main area to focus on terms of quantified risks. Pareto chart is combination of bar graph and a line graph. In this case the RPN for each process is plotted in bar graph and their cumulative percentages are plotted as the line graph.

3. RESULTS AND DISCUSSION

3.1 Quality

From the above performed quality tools it can be deduced, which area should be focused. PFMEA performed after this analysis quantified and allowed to visualize the various effects and their causes. The Pareto analysis clearly indicates where to focus the most and it is the pre soldering process followed by chip mounting process Following are the main factors:

Table 4: Methodologies for quality aspects

Problems	Methodologies	Implementation goals
Using Solder Paste after 6 hours.	Implementing poka-yoke [18] for the solder printing process.	Poka-yoke for Solder paste temperature.
Stirring the paste before application	Employment of Solder Paste Centrifuge machine.	This ensures the proper mixing of solder paste without any synthetic errors.
Paste stuck in Stencil, thickness of the stencil	Usage of frameless stencils	This is cheap and allows the operator to replace it without any hinderance.
Faster printing and Squeegee angle	Slowing done the action.	This ensures the proper solder printing.
Excess or Low solder paste volume	Employment of ML algorithms [16] to study the effect of temperature and volume of solder paste on the soldering process.	This has been proved to be a good methodology to identify the good solder paster type and their temperature operating window.

- Low temperature of the solder[4], improper mixing of solder paste, paste stuck in Stencil, thickness of the stencil, damaged stencil faster printing, squeegee angle, Wrong cleaning fluid in the printer,
- Oxidation of the solder paste and faulty heater.

The components are heat sensitive and undergo thermal stress, which causes the damage, should use appropriate mounter tools.

3.2 Availability

The VSM has given the data, and it indicates the availability of the machine. It clearly indicates the set-up time, break down considering change over time during solder paste printing and Reflow oven is more and it can be optimized. It can be also observed that all these processes can be made continuous by segregating and performing it as internal and external activities over time. SMED is a lean manufacturing tool, developed by Toyota in 1950s. Which eliminates the unwanted time. Motive of SMED is to reduce the change over time under 10 minutes. This directly reduces the lead time and reduces the idle time. SMED methodology can be applied to the entire process.

In a high-mix low-volume production changeover time is generally higher and it specifically caused during the components loading into the chip mounter. Above mentioned data considers only a single type of PCB board. Change-over time is considered under Down Time loss. We can reduce the change over time by implementing SMED. Two cases with use of DES software and WITNESS simulation over SMT line have been shown in [10]. For Case 1, the only maintenance strategy used is Corrective Maintenance. Hence, the maintenance is performed only when the machine breakdown. The breakdown of machine will cause stoppage to whole production line. As for case 2, PM is introduced to all machines. The maintenance task that should be done during PM and its frequency were decided qualitatively after discussion with the stakeholders. The PM was scheduled to be done daily. The time for adjustment and setup task during PM is 15 minutes.

The result proved that Preventive maintenance was much effective than the corrective maintenance. Though not all machines showed improvement under preventive maintenance the overall availability of the manufacturing line saw a decent increase. This concludes that SMT manufacturing line should adopt Preventive Maintenance strategy.

Preventive maintenance can also be improved by various methods. By installing sensors and a storage we can start gathering data as mentioned in [1] and [2], SMT line can produce rich data within a week giving us the needed information. We can employ machine learning algorithms to analyze the data and predict the model. This can be incorporated with Preventive maintenance strategies.

Table 5 Methodologies for availability aspects

Methodologies	Implementation goals
Labelling components (RFID)	We can reduce the time utilized for component search
Changing Warehouse layout to accommodate the above said changes	Improvising the shop floor towards [17] Industry 4.0
Preventive maintenance using gathered data	Installing sensors and tagging the boards to gather data and predict the equipment wear.

4. CONCLUSION

This report has accomplished the above-mentioned objectives with clear explanation. This Report has integrated the tools and have performed a valid case-study providing the insights of SMT line. The PFMEA can be performed after the chosen methodologies, and it can clearly give us the efficiency of our implemented methods. It can be quantified into numbers by RPN and paretto chart and since it is a continuous improvement strategy, we can periodically assess this and improve the manufacturing line. Growing trend of Industry 4.0 in India [11] is a point to be noted as all quality tools are data driven and integration of the lean tools with them will result in

a more efficient production line. The methodologies provided in this paper may further studied in detail for future studies.

REFERENCES

[1] Parviziomran, I., Cao, S., Yang, H., Park, S., & Won, D. (2019). Data-driven prediction model of components shift during reflow process in surface mount technology. *Procedia Manufacturing*, *38*, 100-107.

[2] Kim, D., Koo, J., Kim, H., Kang, S., Lee, S. H., & Kang, J. T. (2019). Rapid fault cause identification in surface mount technology processes based on factory-wide data analysis. *International Journal of Distributed Sensor Networks*, *15*(2), 1550147719832802.

[3] Zhang, Q., Zhang, M., Gamanayake, C., Yuen, C., Geng, Z., Jayasekaraand, H., ... & Liu, X. (2020, July). Deep Learning Based Defect Detection for Solder Joints on Industrial X-Ray Circuit Board Images. In *2020 IEEE 18th International Conference on Industrial Informatics (INDIN)* (Vol. 1, pp. 74-79). IEEE.

[4] Okafor, P. U., & Eneh, I. I. (2013). Investigation of printing performance of solder paste at different temperatures. *International Journal of Engineering Research and Applications*, *3*(5), 818-829.

[5] Azizi, A. (2015). Designing a future value stream mapping to reduce lead time using SMED-A case study. *Procedia Manufacturing*, *2*, 153-158.

[6] Eswaramurthi, K. G., & Mohanram, P. V. (2013). Improvement of manufacturing performance measurement system and evaluation of overall resource effectiveness. *American Journal of Applied Sciences*, *10*(2), 131-138.

[7] Chong, K. E., Ng, K. C., & Goh, G. G. G. (2015, December). Improving Overall Equipment Effectiveness (OEE) through integration of Maintenance Failure Mode and Effect Analysis (maintenance-FMEA) in a semiconductor manufacturer: A case study. In *2015 IEEE International Conference on Industrial Engineering and Engineering Management (IEEM)* (pp. 1427-1431). IEEE.

[8] Singh, S., Khamba, J. S., & Singh, D. (2021). Analyzing the Role of Six Big Losses in OEE to Enhance the Performance: Literature Review and Directions. *Advances in Industrial and Production Engineering: Select Proceedings of FLAME 2020*, 411.

[9] Puvanasvaran, P., Kim, C. Y., & Siang, T. Y. (2012, October). Overall equipment efficiency (OEE) improvement through integrating quality tool: case study. In *International Conference on Design and Concurrent Engineering* (Vol. 402864, No. 182700, p. 585564).

[10] Swaim, W. (2011). *SMT line improvements for high mix, low volume electronics manufacturing* (Doctoral dissertation).

[11] Tan, S. M., Hwang, J. Q., & Ab-Samat, H. (2019, May). WITNESS simulation of preventive and corrective maintenance for Surface Mounted Technology (SMT) line.

In *IOP Conference Series: Materials Science and Engineering* (Vol. 505, No. 1, p. 012047). IOP Publishing.

[12] Vyshnevskyi, O., Liashenko, V., & Amosha, O. (2019). The impact of Industry 4.0 and AI on economic growth. *Zeszyty Naukowe. Organizacja i Zarządzanie/Politechnika Śląska*.

[13] Dos Santos Caetano, F. A. (2017). SMED streamlining applied to SMT production.

[14] Waghmare, S. N., Raut, D. N., Mahajan, S. K., & Bhamare, S. S. (2017). Enhancing reliability and quality for SMEs in India by using failure mode effect analysis and total productive maintenance. *International Journal of Indian Culture and Business Management*, *14*(1), 44-64.

[15] Braglia, M., Castellano, D., Gabbrielli, R., & Marrazzini, L. (2021). A Revised PFMEA Approach for Reliable Design of Assembly Activities. *Designs*, *5*(1), 12.

[16] Halldórsson, Á. (2016). *IIoT data collection for OEE measurements* (Doctoral dissertation).

[17] Singh, R., Shah, D. B., Gohil, A. M., & Shah, M. H. (2013). Overall equipment effectiveness (OEE) calculation-Automation through hardware & software development. *Procedia Engineering*, *51*, 579-584.

[18] MAHTO, D., & MASTORAKIS, N. Identifying and measuring operational performance through Overall Equipment Effectiveness: An empirical study.

[19] MOHAMAD, E., TUKIRAN, M. A., ITO, T., JAMLI, M. R., MOHAMAD, N. A., SALLEH, M. R., ... & SULAIMAN, M. A. (2020). Improving Overall Equipment Effectiveness Using Lean Six Sigma in Lube Blending Plant: A Case Study.

[20] Bhat, V. S., Bhat, S., & Gijo, E. V. (2020). Simulation-based lean six sigma for Industry 4.0: an action research in the process industry. *International Journal of Quality & Reliability Management*.

Experimental and Simulated Analysis of Tractor Seat during Tillage

Harbhinder Singh, Munish Mehta

School of Mechanical Engineering, Lovely Professional University, Phagwara, India

harry2211@rediffmail.com, munishmehta1@rediffmail.com

Abstract

The tractor operators are subjected to negative vibrations because most of the tractors are without any type of suspensions. Because drivers have to work for long hours, these vibrations are hazardous to their health. The present study is focused to analyse the seat of tractor experimentally by collecting the real time data from tractor seat while working in fields with implements during tillage process. Tri-axial accelerometer was used to collect the actual data from seat base and was stored in data collection unit. Based on the real-time data a dynamic model of tractor along with seat was developed in MATLAB-Simulink for further analysis of vibrations. Measurement of vibrations is the basis for developing a good tractor seat with reduced vibrations. Although, there still remained many problems to be solved but this study will provide a good base to work in this direction.

Keywords -Tractor, Implements, Vibration, Modelling and Simulation.

1. INTRODUCTION

Vibrations in the range of 12 Hz affect all organs of operator, whereas vibrations above 12 Hz have a local effect on organs. Low frequency (less than 6 Hz) movement, such as movements of tires over an irregular road, can cause body resonance [1]. Biodynamic research has shown that prolonged exposure to vibrations increases the risk on health [2].

Many characteristics of mechanical vibrations strongly influence the operators. These characteristics include the direction of vibrations, point of contact with the body, frequency, and duration [3, 4, and 5]. If external force frequency matches with natural frequency, resonance occurs [6] due to which undesirable oscillations of large amplitude are produced. When a system is disturbed and can vibrate on its own, the natural frequency is the frequency of the vibrations without damping or external force [7, 8]. If damping is present, it is referred to as the system's damped natural frequency. Most seats exhibit low-frequency resonance, resulting in greater magnitude of vertical vibrations on the seat [10, 11].

MATERIALS AND METHODS

The tractor seat was used to collect real-time data. The experiment was conducted for two different implements. First time data was taken from tractor seat when the tractor was moving with plough and second time disc harrow (Figure 1) was used as implement for tillage process.

Figure 1. Tractor with Chisel Plough and Disc Harrow

During both cases vibrations were measured with tri-axial piezoelectric accelerometer (Figure 2). Vibrations measuring accelerometer was fitted on the seat base of test tractor to measure vibrations on seat of tractor. The frequency sensitivity range of an accelerometer was 2-8000 Hz. Every time, acceleration levels were recorded simultaneously in three perpendicular directions, X longitudinal (pitching), Y lateral (rolling), and Z vertical (bouncing/heave) on the base of the tractor seat.

Figure 2. Location of accelerometer on the base of tractor seat.

A vibration measurement setup in the X, Y, and Z directions was created (Figure 3). At a frequency of 10 Hz, the vibration measuring accelerometer could quantify the vibration of the X, Y, and Z axes

Figure 3. Tri-axial Sensor and Data Acquisition unit setup used for the measurement of vibrations

The tractor was made two runs at two constant speed during both cases and the real time data was recorded separately for each case along horizontal, transverse and vertical directions.

2. DATA ANALYSIS

Accelerations measured are shown in Figure 4 in horizontal (x), transverse (y) and vertical (z) direction. The speed of tractor was kept constant at 2.30 Km/hr. As the Figure shows when tractor was made to work with tillage implements (chisel plough) the measured RMS values of acceleration was highest in transverse (y) direction and lowest in horizontal (x) direction and the vertical (z) direction values lies in between that of lateral (y) direction and longitudinal (x) direction.

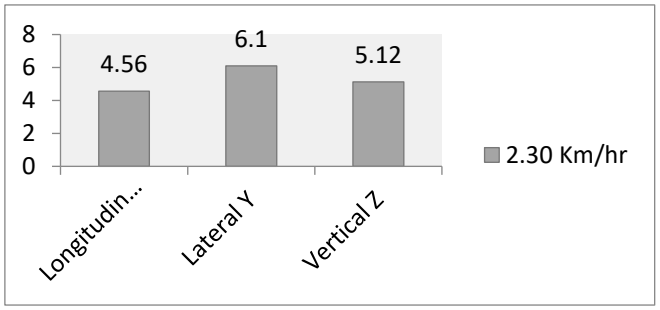

Figure 4. RMS acceleration in all three directions at tractor's seat with implements

3. IMPLEMENTATION- SIMULATED MODEL OF TRACTOR

A full tractor vibration model along with implements was simulated. The tractor-implement structure was represented by the characteristics like MOI and mass of tractor with implements. Figure 5 depicts the dynamic model of the tractor and implement. Due to surface roughness, the tractor's front and rear tyres experience displacement excitations qfz(t) and qrz(t), respectively. A displacement with respect to the centre of mass is introduced by the change in amplitudes of qfz(t) and qrz(t). Roll, yaw, and pitch movements of the tractor were introduced as a result of this displacement with respect to the mass centre. Rough road force between front axle and rear axle with a time lag of $q_{fz}(t)$and $q_{rz}(t)$of the tractor-implement system at an instant i can be expressed as

$$q_{fzi}(t) = q_{rzi}(t + \tau) \qquad (1)$$

Where $q_{fzi}(t)$ and $q_{rzi}(t)$ are displacement excitations, Ƭ is time lag and can be calculated as

$$\tau = \frac{l_{bf} + l_{br}}{v} \qquad (2)$$

Where lbf is the distance between the chassis and the front axle, and lbr is the distance between the chassis and the rear axle. v represents the velocity of the tractor-implement system.

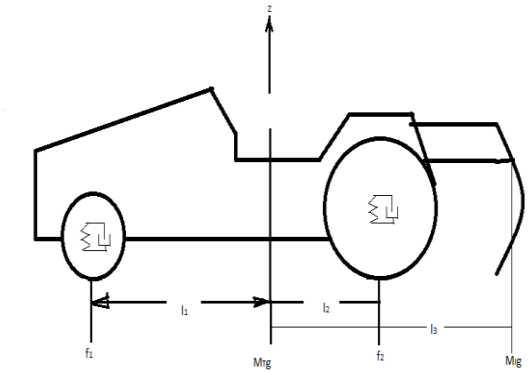

Figure 5. Schematic diagram of Tractor Implement System

The motion equations can be written as follows:

$$(M_T + M_I)\ddot{z} = f_1 + f_2 - (M_T + M_I)g \tag{3}$$

Wheel displacement can be calculated as

$$z_1 = z + \left(l_1 + l_3 \frac{M_I}{M_T + M_I}\right) \tag{4}$$

$$z_2 = z + \left(l_2 - l_3 \frac{M_I}{M_T + M_I}\right) \tag{5}$$

Equations (3) and (4) can be used to calculate the effect of implement on wheel displacement. So M_T will be used to express the effective mass of the tractor and implement. Equations (1) to (4) represents roll, yaw, and pitch effect on wheel displacements. Tractors and other off-road vehicles do not have primary suspension. This complete model is made up of three parts: four wheels, a body, and a vibration model. Figure 6 depicts the physical model of the entire tractor, including the driver's seat.

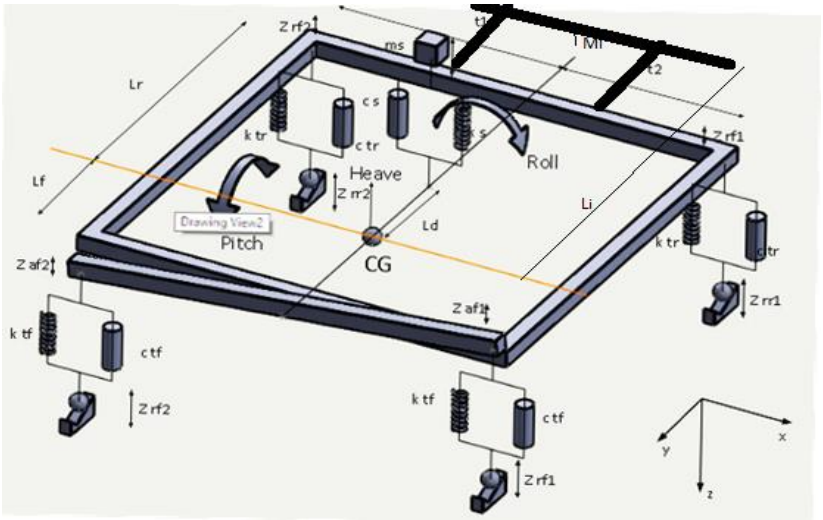

Figure 6. Complete tractor implement vibration model

4.1 Mathematical Full Tractor with Suspended Seat Model

In mathematical modelling, the motion of equations were derived for each of the five degrees of freedom. It is well known fact that the force of spring is proportional to the variation of the length of the spring and that the strength of the shock absorber that is damper force is proportional to variation of the length of damper over time. The vibratory forces transmitted by each wheel at the point of contact between the axle and the wheel can be formulated as follows:

$$k_t(z_a - z_R) + c_t(\dot{z}_a - \dot{z}_R) \quad (6)$$

The mathematical equations for the forces transmitted to chassis are given as:

$$F_{f1} = k_{tf}\left(z_{af1} - z_{Rf1}\right) + c_{tf}\left(\dot{z}_{af1} - \dot{z}_{Rf1}\right) \quad (6a)$$

$$F_{f2} = k_{tf}\left(z_{af2} - z_{Rf2}\right) + c_{tf}\left(\dot{z}_{af2} - \dot{z}_{Rf2}\right) \quad (6b)$$

$$F_{r1} = k_{tr}(z_{ar1} - z_{Rr1}) + c_{tr}(\dot{z}_{ar1} - \dot{z}_{Rr1}) \quad (6c)$$

$$F_{r2} = k_{tr}(z_{ar2} - z_{Rr2}) + c_{tr}(\dot{z}_{ar2} - \dot{z}_{Rr2}) \quad (6d)$$

The mathematical equations of the body of tractor are the following:

(i) for the linear acceleration of the centre of gravity of the tractor in Z direction

$$\ddot{z}_{cg} = -\frac{1}{m_t}\left(F_f + F_{r1} + F_{r2}\right) \quad (7)$$

(ii) for angular accelerations of the tractor body about X-axis which crosses the center of gravity of the tractor

$$\ddot{\theta} = \frac{1}{I_{xxt}}\left(F_f l_f - (F_{r1} + F_{r2}) l_r\right) \quad (8)$$

(iii) for angular accelerations of the tractor body about Y axis

$$\ddot{\phi} = \frac{1}{I_{yyt}}(F_{r2}t_2 - F_{r1}t_1) \quad (9)$$

The calculation of the tractor body's bouncing, rolling, and pitching motion results in an acceleration of the tractor's driver's seat base. If the distance between the tractor's centre of gravity and the seat base is known, the elements of the seat base can be calculated. The equation of motion of seat base of tractor is given as (Ahmadi, 2014):

$$\ddot{Z}_{seat\ base} = \ddot{Z}_{cg} \quad (9a)$$

$$\ddot{Y}_{seat\ base} = R\ddot{\phi} \quad (9b)$$

$$\ddot{X}_{seat\ base} = R\ddot{\theta} \quad (9c)$$

$\ddot{Z}_{seat\ base}, \ddot{Y}_{seat\ base}, \ddot{X}_{seat\ base}$ – acceleration of tractor seat base in z direction, y direction and z direction (m/s^2) respectively.

The accelerations of the points of force application to the tractor body (comprising the acceleration of the pivot point of front axle and acceleration of the joints of the tractor rear wheels of the tractor body) may be computed as following (Sarami 2009):

$$\ddot{z}_{afc} = \ddot{z}_{cg} - l_f\ddot{\theta} \quad (10)$$

$$\ddot{z}_{ar_1} = \ddot{z}_{cg} - l_r\ddot{\theta} + t_1\ddot{\phi} \quad (11)$$

$$\ddot{z}_{ar2} = \ddot{z}_{cg} - l_r\ddot{\theta} - t_1\ddot{\phi} \quad (12)$$

The accelerations in linear direction of the joints between front axle and front wheels are indicated as follows:

$$\ddot{\alpha} = \frac{1}{I_{xxa}}\left(F_{f1}t_1 + F_{f2}t_2\right) \quad (13)$$

Finally, the mathematical equations for the accelerations in linear of the axles of front wheel joints can be computed as follows:

$$\ddot{z}_{af_1} = \ddot{z}_{afc} + t_1\ddot{\alpha} \quad (14)$$

$$\ddot{z}_{af2} = \ddot{z}_{afc} + t_2\ddot{\alpha} \quad (15)$$

4. FULL TRACTOR MODELLING USING SIMULINK

Table 1 Full tractor vibration model parameters.

Notations	Description	Values	Units
k_{tf}	stiffness of tractor front tire	90,000	N/m
c_{tf}	damping of tractor front tire	1,000	N-s/m
k_{tr}	stiffness of tractor rear tire	90,000	N/m
c_{tr}	damping of tractor rear tire	2,000	N-s/m
m_t	Tractor weight	2,800	Kg

t_1	Tractor center of gravity from left portion of chassis	0.87	M
t_2	Tractor centre of gravity from right portion of chassis	0.87	M
l_r	Distance of center c.g. of tractor from rear portion of chassis	0.91	M
l_f	Distance of c.g of tractor from front portion of chassis	1.35	M
I_{xxt}	Tractor MOI about the x axis	600	kg-m^2
I_{yyt}	MOI of tractor about y axis	2,000	kg-m^2
I_{xxa}	Tractor front axle MOI about pivot point	5	kg-m^2
m_s	Mass of seat	35	Kg
l_d	Seat's longitudinal distance from the centre of gravity	0.69	M
k_s	stiffness of seat	8000	N/m
c_s	Damping of seat	130	N-s/m

Figure 7 illustrates a MATLAB-Simulink computer model of the entire tractor.

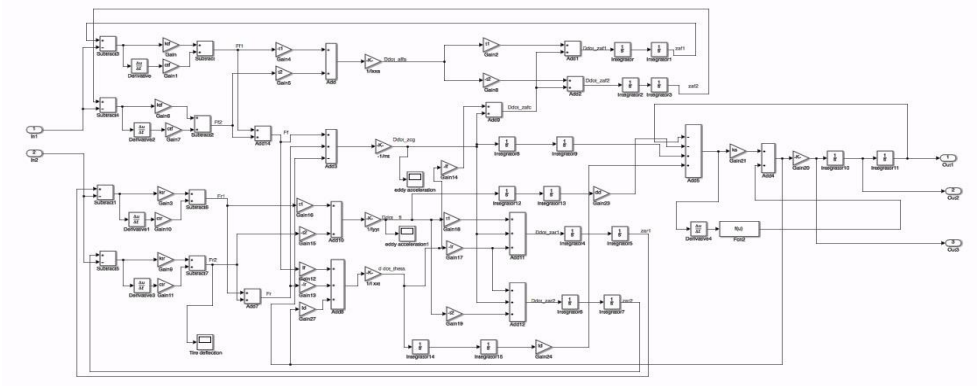

Figure 7. Full Tractor-Implement Simulink Model

The source block or input is the signal generator representing the sine input with 0.01m amplitude and 35 Hz frequency and step function with the height of 1 unit up at 5 sec and 1 unit down at 7 sec for front wheel were selected. The steps up and down for the rear wheel took 8 and 10 seconds, respectively. The road inputs were applied to the front and rear wheels of the modelled tractor at times t0 and t1, respectively. The time intervals t0 and t1

are considered in relation to the distance between the front and back axles. (Wheel Base), WB, and the speed (v) of the tractor as:

$$t_1 - t_2 = \frac{Wheel\ Base\ (WB)}{Velocity\ of\ tractor\ (v)} \tag{16}$$

Figure 8 (a) and (b) show the developed Simulink model of disturbance input for the front and rear wheels, respectively.

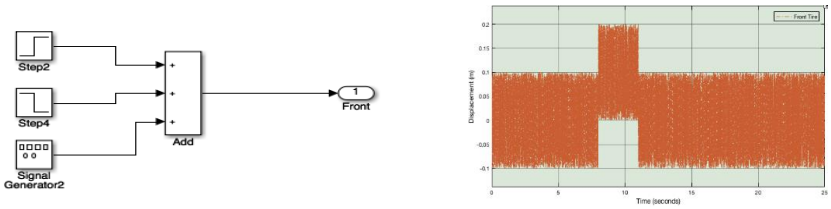

(a)

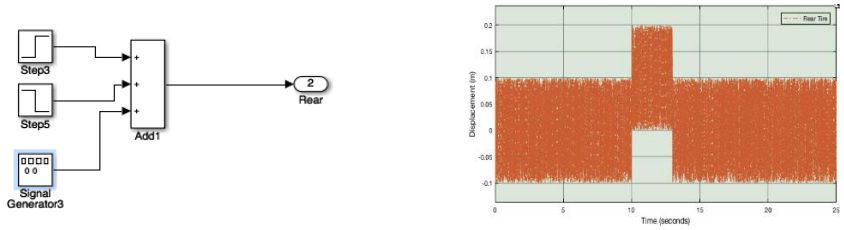

(b)

Figure 8. Road Input (a) Front wheels (b) Rear wheels

5.1 Simulated Dynamic Tractor-Implement Model Validation

In the quantitative comparison, as the input displacement functions, a step function was chosen. To simulate a moving tractor at 3.5 km/h and a wheel base of 1970 mm (as for the test tractor) over a step-like hurdle, the rear wheels were delayed for two seconds as follows:

$$t = \frac{1970(mm)}{3.5(\frac{km}{hr})} = \frac{1.97}{0.972(m/s)} = 2.026s \tag{17}$$

Based on the time domain results, a comparison of the simulation acceleration and the real test acceleration was performed using Root Mean Square (RMS) values.

5.2 Comparison of Simulated and Experimental Results

The modified inputs resulted in RMS errors of 1%, 2.2%, and 5.2% in the X, Y, and Z directions, respectively. As a result, the modified model demonstrated the model's dependability in simulating the seat base acceleration caused by a tractor moving over a step-like random irregularity. The results of the modified model obtained in this investigation were compared with the calculation of the RMS value of acceleration and the

estimation of the simulation error used by other researchers to validate the developed vibration model. The modified model produced excellent results, with simulation errors of 1%, 2.2%, and 5.2%, which were found to be lower than 10% of other studies' developed models. The results indicate that the computer model developed could accurately model the induced vibrations caused by the field irregularity transmitted to the tractor seat. As a result, this model can be used to simulate the test required for the design of the tractor seat suspension controller.

5. RESULTS AND DISCUSSION

The tractor parameter values were entered into a MATLAB Simulink model of the tractor with implements, and the RMS values of the simulated model were compared to the experimental RMS values. To reduce the percentage error in measured and simulated values, some parameters were redefined. The modified inputs resulted in RMS errors of 5.2%, 1%, and 2.2% in the X, Y, and Z directions, respectively. As a result, the modified model demonstrated that the model is reliable in simulating seat acceleration caused by a tractor moving over random irregularity. The results of the modified model obtained in this investigation were compared with the calculation of the RMS value of acceleration and the simulation error used by other researchers to validate the developed vibration model. The modified model produced excellent results, with simulation errors of 5.2%, 1%, and 2.2%, which were found to be less than 10% of other studies' developed models.

6. CONCLUSION

Because the differences between simulated and measured values are less than 10%, this model can accurately predict tractor seat vibrations during tillage. Because the model is comparable to the actual tractor-implement system, a variety of other studies can be conducted by changing the input parameters such as speed and type of tillage implement in the simulated model without actually performing on the tractor. Further research into designing a controller to reduce tractor seat vibrations can be conducted using this model.

REFERENCES

[1] Gu, Z.Q.,Oyadiji, S. O., "Application of MR damper in structural control using ANFIS method", *Computers and Structures*, 86, pp. 427–436, 2008.

[2] Han,Y. M., Jung, J. Y., Choi, S. B., Choi, Y. T., Wereley, N. M., "Ride Quality Investigation of an Electrorheological Seat Suspension to Minimize Human Body Vibrations," *Proceedings of the Institution of Mechanical Engineers, Part D: Journal of Automobile Engineering*, Volume: 220, pp. 139–150, 2006.

[3] Han, Y. M., Nam, M. H., Han, S. S., Lee, H. G., Choi, S. B., "Vibration control evaluation of a commercial vehicle featuring MR seat damper , *Journal of Intelligent Material Systems and Structures*,13(9), pp. 575-579, 2002.

[4] Hansen, M. R., & Andersen, T. O., "Active Damping of Oscillations in Off Road Vehicles," *8th Scandinavian Intl Conference on Fluid Power*, 2, pp. 1073-1085, 2003.

[5] Hansson, P. A., "Optimization of Agricultural Tractor Cab Suspension Using the Evolution Method, "*Computers and Electronics in Agriculture*, 12, pp. 35-49, 1995.

[6] Hansson, “Rear axle suspensions with controlled damping on agricultural tractor,” *Computers and Electronics in Agriculture*, 15, pp. 123-147, 1996.

[7] Hansen, M. R., Andersen, T. O., “Active damping of oscillations in off road vehicles,” *8th Scandinavian International Conference on Fluid Power*, 2, pp. 1073-1085, 2003.

[8] Heo, S., Park, K., Hwang, S., “Performance and design consideration for continuously controlled semi-active suspension systems,” International Journal of Vehicle Design, 23 (3), pp.376-389, 2003.

[9] He, Y., McPhee, J., “Multidisciplinary design optimization of mechatronic vehicles with active suspensions,” *Journal of Sound and Vibration*, 283, pp. 217–241, 2005.

[10] Hiemenz, G. J., Hu, W., Wereley, N. M., “Semi-active magnetorheological helicopter crew seat suspension for vibration isolation,” *Journal of Aircraft*, 45, pp. 945–953, 2008.

[11] Hilton, D. J., Moran, P., “Experiments in improving tractor operator ride by means of a cab suspension,” *Journal for Engineering Research*, 20 (4), pp. 433-448, 1975.

[12] Ho, D. W., Niu,Y.,“Robust fuzzy design for nonlinear uncertain stochastic systems via sliding-mode control,” *IEEE Trans Fuzzy System*, 15, pp. 350–358, 2007.

Biographies

Harbhinder Singh is presently working as an Assistant Professor in Mechanical Engineering Department, University Institute of Engineering and Technology, Panjab University Chandigarh. He completed his M.Tech from I.K. Gujral Punjab Technical University in 2005 and B.Tech. from Punjab Technical University in 1998. He is research scholar at School of Mechanical Engineering, Lovely Professional University, Phagwara, Punjab His research interests include design engineering, controls modeling and simulation. He has published various research papers and book chapters in different national/international journals and conferences of repute. He has supervised and guided various dissertations and projects at PG and UG level. He has 20 years of teaching experience to his credit.

Dr. Munish Mehta is presently working as Professor in the School of Mechanical Engineering, Lovely Professional University, Phagwara, Punjab. He completed his Ph. D. from I.K. Gujral Punjab Technical University in 2018 and M. Tech. from National Institute of Technical Teachers Training and Research (NITTTR) Chandigarh in 2010. He obtained his B.E. from Nagpur University in 1997. His research interests include reliability engineering, optimization, stochastic modeling, mechatronics and genetic algorithm etc. A lifetime member of ISTE, he has published various research papers and book chapters in different national/international journals and conferences of repute. His academic achievements include serving as reviewer of many reputed journals. He has supervised and guided various dissertations and projects at PG and UG level. He has organized an international and a national conference as organizing secretary. He has 7 years of industrial and 18 years of teaching experience to his credit.

Effect of Notch on Arrival Time of Lamb Wave in Plates of Different Thicknesses: A Simulation Study

Md Sajjad Alam, Anindya Bhar

[1,2]*Department of Applied Mechanics, Motilal Nehru National Institute of Technology, Allahabad, Prayagraj, UP (India);*

sajjadalam927@gmail.com, *anindyab@mnnit.ac.in*

Abstract

Lamb wave is the kind of ultrasonic wave guided between two parallel surfaces. It is a special wave which acts like a standing wave in X direction and travelling wave in Y direction and is highly dispersive in nature. Due to these reasons, it has good capacity to scan a whole structure. This is why Lamb wave is used widely in structural health monitoring. In this work, we have studied on lamb wave propagation in isotropic aluminium plate using finite element simulation. It first consists of the convergence and validation of results on propagation of lamb wave in normal isotropic homogenous plate with varying plate thickness. Then we study the effect of presence of notch on time of arrival of lamb wave, that is, how much time it would take from start where it is excited to reach the end of the plate having the notch.

Keywords: Lamb wave, Isotropic plates, Notch.

1. INTRODUCTION

Guided waves are the type of waves which remain confined in structure and propagate through long distance with minimum energy/amplitude loss. These waves are extremely important for structural health monitoring systems due to their properties like they travel through long distance, remain confined in structure and they can also travel through curved walls. Lamb waves are the waves which is guided between two surfaces, upper and lower surface and during the propagation, show two types of mode shapes symmetric mode shapes designated as S_0, S_1, S_2…… S_n and antisymmetric mode shapes designated as A_0, A_1, A_2…… A_n. All of these mode shapes are present at different frequency-thickness product, but due to highly dispersive nature of lamb wave we are able to see zero order mode shape (S_0, A_0) mainly.

The zero-order mode shapes deserve special attention among all mode shapes because it is only mode shape which present at all frequency spectrum range from zero to high frequencies. At low frequency it is known as extensional mode which outline elastic stiffness and nature of motion that govern the propagation velocity. The zero-order symmetric mode shape at lowest frequency is called as extensional mode. As the frequency increases, the phase velocity drops and group velocity approaches towards a minimum and at this frequency each velocity converges towards the Rayleigh wave velocity.

The existence of lamb wave was first examined by Lamb [1], by using some Rayleigh wave equations developed by Rayleigh [2]. The lamb wave was mostly used in detection or quantification of damage. Toyamaa *et al* [3] saw that there was decrease in velocity of S_0 mode shape as transverse crack density increases. Then Yang *et al* [4] observed that the propagation of lamb wave was not much affected when stringer material and height kept same, but there were series of effects created on lamb wave when material and height were varied. Janarthan *et al* [5] used A_0 lamb wave mode shape for detecting the damage in stiffened composite panels and antisymmetric mode shape successfully detected the damage present in carbon-epoxy composites. Damages are present in different forms like cracks of different shape and size which is buried in the plate. Wan *et al* [6] used nonlinear lamb wave to detect the presence of micro crack in the plate. Elgamal *et al* [7] studied the arrival time of lamb wave with a different plate thickness like if we increased the plate thickness with increase in frequency of excitation then how much time the wave takes to reach from one point to another. Senyurk [8] extended this work and used lamb wave for detecting cuts and impact damages which generally occurred at the aircraft wing slat and also found out S_0 mode shape was more suitable for detecting impact damage than the A_0 mode shape. When the lamb wave comes in contact with a notch or crack, we can see the conversion of mode. Alkasam *et al* [9] studied the conversion of mode of lamb wave after interacting with a damage in thin plate. Zheng *et al* [10] extended the work on lamb wave by combining the lamb wave technique with electro – mechanical impedance for detecting the damage so that we can also get the characteristics property of damage. For finding the displacement of lamb wave there are number of theories which have been used. Orta *et al* [11] seen that higher order theory gave accurate results.

In the paper, Elgamal *et al* [7] studied the arrival time of waves in a standard isotropic plate with varying thicknesses of that plate. We extended the work by creating a notch, and its size is comparable to the thickness of the plate, see how much effect is created by a notch on the arrival time of wave. We have used a Finite Element Software Abaqus CAE to run the simulation. First, we validated the Elgamal *et al* [7] and then created a notch to study the wave arrival time further; the detailed procedure is given in the next section.

2. PROBLEM DEFINITION

In this work, a two-dimensional finite element simulation of Lamb wave propagation through isotropic Aluminium plates is carried out in Abaqus CAE. The dimension of the plate is considered to be 300 mm × (1.98, 2.64, 3.3) mm, as shown in Figure 1, with the latter dimension representing the thickness of the plate.

Figure 1. Geometry of Aluminium Plate

The material properties of the aluminium plate considered are as given in Table-1.

Table 1. Material Properties of Aluminium Plate (Elgamal et al [7])

Material	**Elastic Modulus, E (GPa)**	**Shear Modulus, G (GPa)**	**Poisson's Ration, υ**	**Density, ρ kg/m^3**
Al 2024-T3	73.1	27	0.33	2780

The excitation is carried out by lamb wave at 150 kHz excitation frequency using 5.5 bursts of sinusoidal wave in the time domain in which time is in second, as shown in Figure 2. The excitation pulse is given at the x=0 mm (where x is the distance measured length-wise) on the middle node in *the y direction*. At least one node has fixed boundary conditions to create

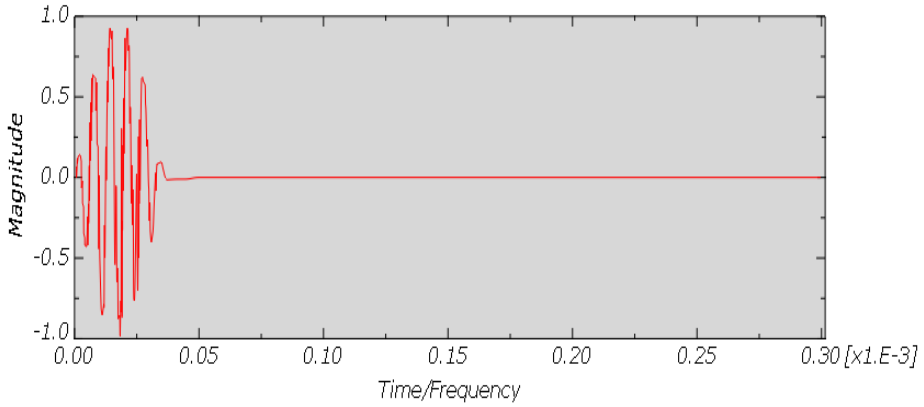

Figure 2. 150 kHz Actuator Signal in time domain

3. RESULTS AND DISCUSSIONS

The results obtained from the stated finite element simulations are presented and discussed in the following sub-sections. It includes the convergence study regarding the effect of mesh density and validation of the time of arrival of wave in the isotropic plate. After that, the impact on the wave's arrival time with varying notch sizes in the isotropic plate is analysed.

3.1 Convergence and Validation Study

The simulation starts in a standard isotropic plate with a CPS4R element, a 4-node bilinear plane stress element, and a Quad-dominated (1×1) mm element shape size with a free type technique. As we decreased the element size, our result converged towards the solution. The

time step is selected as 0.001 sec for completing the simulation in Finite Element Software because at this time step, we got a good agreement with Elgamal *et al* [7].

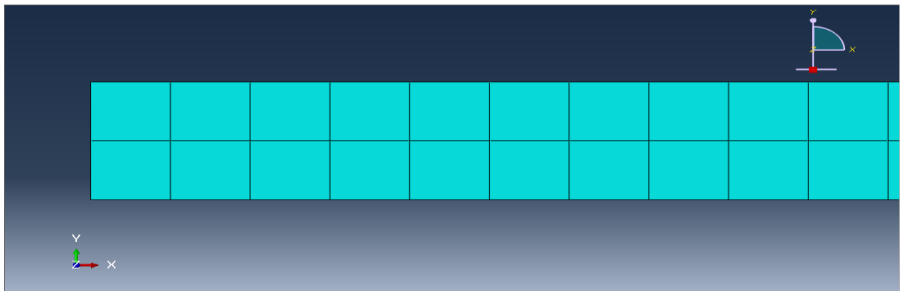

Figure 3. 600 Elements Quad- Dominated Mesh Element

Next the convergence study of the arrival time of lamb wave at receiver end follows, as in Figure 4.

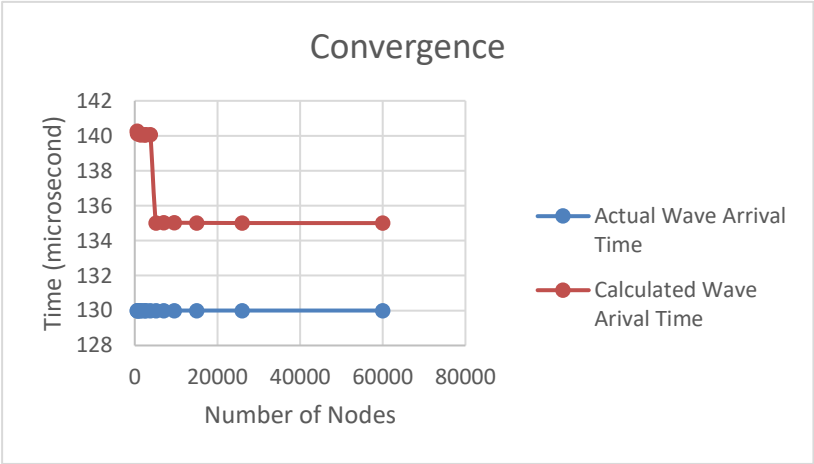

Figure 4. Graphical Representation of Convergence

The Table-2 shows the convergence study of the isotropic normal plate

Table 2. Convergence Study

Quad Element Size (mm)	**Number of Elements**	**Actual Result (micro second) (Elgamal *et al* [7])**	**Simulated Result (micro second)**	**Error in Percentage**
1×1	600	130	140.27	7.9
0.9×0.9	666	130	140.13	7.79230
0.8×0.8	750	130	140.18	7.83076
0.7×0.7	1287	130	140.06	7.73846
0.6×0.6	1500	130	140.07	7.74615
0.5×0.5	2400	130	140.04	7.7230
0.45×0.45	2668	130	140.06	7.7384

0.4×0.4	3750	130	140.07	7.746
0.35×0.35	5142	130	135.016	3.85846
0.3×0.3	7000	130	135.033	3.8715
0.25×0.25	9600	130	135.024	3.8646
0.2×0.2	15000	130	135.018	3.86
0.15×0.15	26000	130	135.006	3.85076
0.1×0.1	60000	130	135.004	3.8492

Now, based on this convergence study, the element size of 0.1 × 0.1 mm, is the best suited for meshing and is used for further simulations. Figure 5 shows the arrival of the wave at the end of the plate without notch.

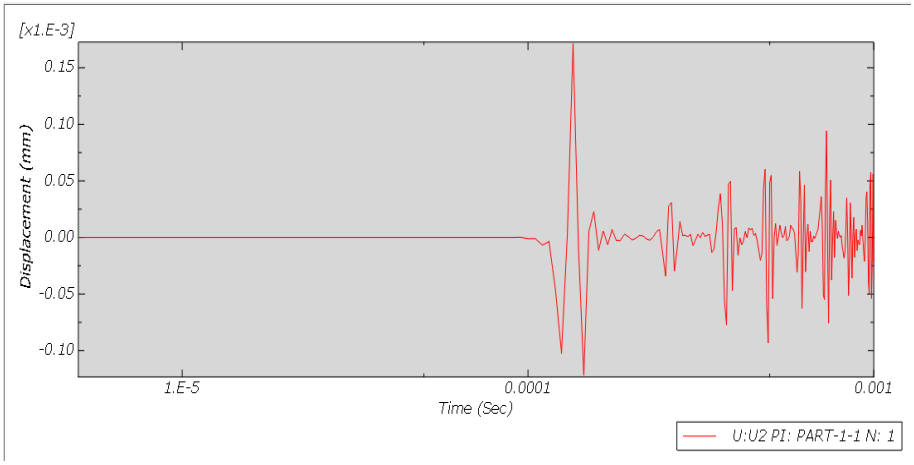

Figure 5. Wave Captured for 1.98 mm plate at Receiver end

After selecting the mesh size and done with all the algorithms, now we are moving towards the validation part here; the time of arrival of lamb wave for different plate thicknesses has been validated, as presented in Table 3.

Table 3. Validation of Base Paper (Elgamal *et al* [7])

Thickness of plate (mm)	**Actual Result (micro second) (Elgamal *et al* [7])**	**Simulated Result (micro second)**	**Error in percentage**
1.98	130	135.004	3.8492
2.64	125	125.013	0.0104
3.3	120	120.009	0.0075

3.2 Effect of Notch

Now we have created a notch having varying dimensions and are trying to see how much time it will take to reach from start point to endpoint. A circular notch is created at the centre of the plate with a starting radius of the notch is 0.3 mm, and its size increases with an

increment of 0.1 mm till it is comparable to the thickness of the plate. Such a typical plate with a notch is shown in Figure 6.

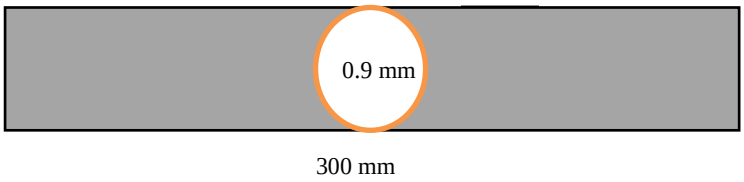

Figure 6. Isotropic Aluminium plate with notch

The wave arrival time for Plate thickness of 1.98 mm, with varying notch dimensions, are presented in Table 4.

Table 4. Simulated Result for Plate thickness 1.98 mm, with varying notch dimensions

Radius of Circular Notch (mm)	**Actual Result (microsecond)**	**Simulated Result (microsecond)**	**Error in percentage**
0.3	135.004	135.003	0.001
0.4	135.004	135.001	0.002
0.5	135.004	135.007	0.002
0.6	135.004	140.002	0.002
0.7	135.004	140.002	3.702
0.8	135.004	140.002	3.702
0.89	135.004	140	3.700
0.9	135.004	140	3.700

As we see from Table 4, if the size of the notch is comparable to the plate thickness, then it affects the wave arrival time of the lamb wave. Figure 7 shows the wave received at the plate end; wave arrival time is the first maximum displacement obtained at the plate end. Here as we see, if the circular notch dimension is about 0.9 mm, then the wave takes 140 micro-second, just a little more than a normal plate, which shows a circular notch creates a significant increment in wave arrival time.

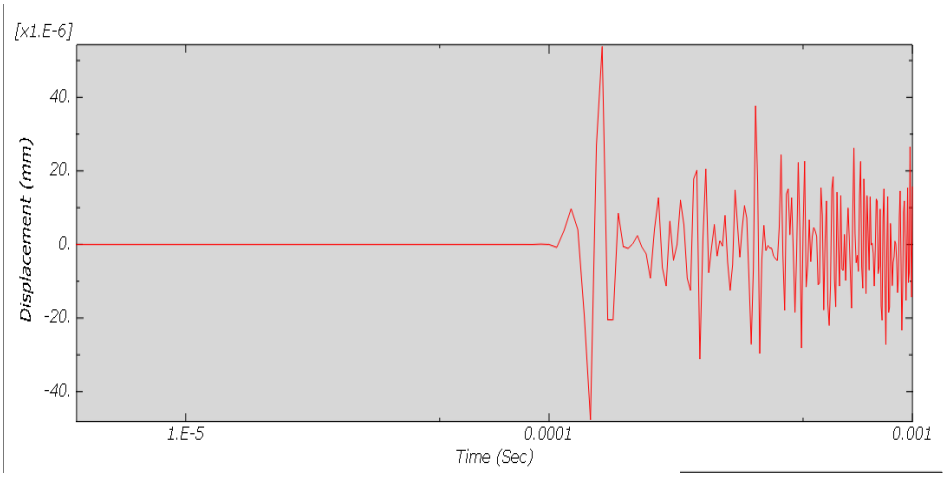

Figure 7. Wave Captured for 1.98 mm plate with notch at Receiver end

Figure 8 shows the wave arrival time for a 2.64 mm plate with a circular notch of the radius of 1.30 mm, so as discussed, for a 1.98 mm plate, it will produce little effect on the wave arrival time. This means if the notch dimension is approximately equal to the plate thickness, then it creates a significant effect on arrival time.

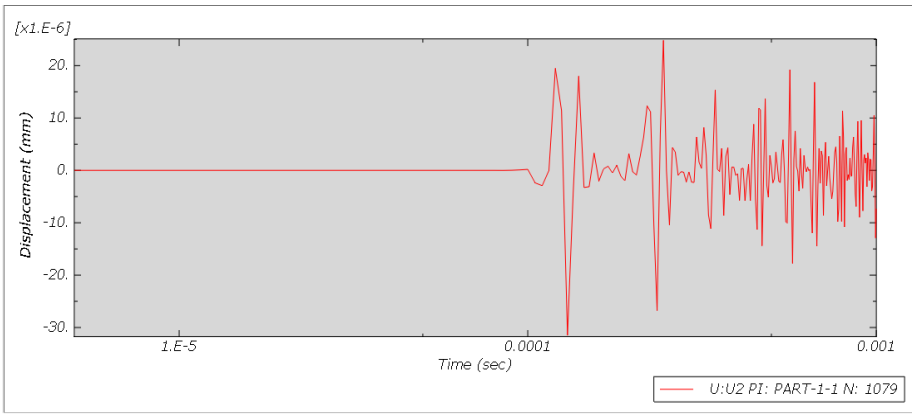

Figure 8. Wave Captured for 2.64 mm plate with notch at Receiver end

Figure 9 shows the arrival time for a 3.3 mm plate with a circular notch of radius 1.30 mm. The result shows more or less the same expected scenario as discussed in Figures 7 and 8. The wave takes more time to reach the receiver end, thereby indicating a significant effect on arrival time for thicker plates.

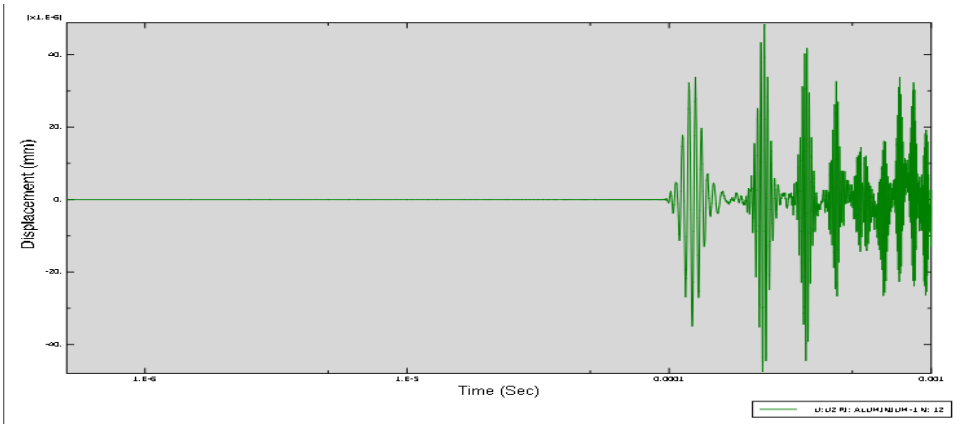

Figure 9. Wave Captured for 3.3 mm plate with notch at Receiver end

Table 5. Comparing the arrival time of wave propagating through normal plate and plate with notch

Thickness of plate (mm)	Radius of notch (mm)	Result of normal plate (micro second)	Result of Plate with Notch (micro second)
1.98	0.9	135.004	140
2.64	1.30	125.013	130.002
3.3	1.60	120.009	126.004

4. CONCLUSION

The results of wave propagation in a simple homogenous isotropic plate show the wave arrival time decreases as the thickness of the plate increases. For the notch section, if the notch size is not comparable with plate thickness, it will not affect wave arrival time. However, if the notch size is comparable with the plate thickness, it shows some effect on the wave arrival time of the lamb wave. So, we can conclude that whether it is a standard plate or a Plate with a notch, the wave arrival time decreases as plate thickness increases. One can also extend the work by increasing the number of notches, and varying the material property of the plate.

REFERENCES

[1] Lamb H, "On waves in elastic plate", Proc.R. Soc.Lond A 93 (1917), 114-128.

[2] Lord Rayleigh, "On waves propagation along the plane surfaces of an elastic solid", Proceedings of the London mathematical society IV (1885), 45.

[3] N. Toyamma, J. Nodaa, T. okabeb, "Quantitative damage detection in cross ply laminates using lamb wave", Composite Science and Technology 63 (2003), 1473-1479.

[4] Chunhui Yang, Zhongqing Su, Lin Ye, Ye Lu, Michael Bannister, “Propagation Characteristics of lamb wave in stringer-stiffened panels”, Key Engineering Materials 334-335 (2007), 637-640.

[5] B. Janarthan, M. Mitra, P.M. Mujumdar, “Damage Detection in stiffened composite panels using lamb wave”, Structural Health Monitoring (2013).

[6] Xiang Wan, Qing Zhang, Guanghua Xu, Peter W. Tse, “Numerical Simulation of Nonlinear lamb waves used in a thin plate for detecting buried micro-cracks”, Sensors 14 (2014), 8528-8546.

[7] Hamada M. Elgamal, Yang Zailin, Zhang Jian, Wei, “Numerical Simulation of lamb wave propagation in isotropic materials with different plate thickness”, Advance Materials 1094 (2015), 500-504.

[8] V.Y. Senyurek, “Detection of cuts and impact damage at the aircraft wing slat by using lamb wave method”, Measurement 67 (2015), 10-23.

[9] Yassin Alkasarm, V.K. Agarwal, Eman Alshrihi, “Simulation of lamb wave mode conversions in a thin plate for damage detection”, Procedia Engineering 173 (2017), 945-955.

[10] Yuebin Zheng, Kehai Liu, Zhanjun Wu, Dongyue Gao, Rahim Gorgin, Shuyi Ma, Zhenkun Le, “Lamb Waves and Electro- Mechanical impedance-based damage detection”, Ultrasonics 92 (2019), 13-20.

[11] Adil Han Orta, Jeroen Vandendriessche, Wim Van Paepegem, Nicolaas Bernardus Roozen, Koen Van Den Abeele, “Modelling lamb wave propagation in visco- elastic composite plates using fifth-order plate theory”, Ultrasonics 116 (2021), 106482.

Biographies

Md Sajjad Alam received the Bachelor's degree in Mechanical Engineering from Mahavir Swami Institute of Technology which is affiliated to Guru Gobind Singh Indraprastha University. He is Currently Pursuing Master’s in Engineering Mechanics and Design from Motilal Nehru National Institute of Technology Allahabad.

Dr. A. Bhar received his Bachelor's degree in Civil Engineering from Bengal Engineering College (Presently IIEST Shibpur, Howrah) in the year 2000. After a short duration of Industrial experience that he left for higher studies, he earned the Master's degree in Structural Engineering (Civil) from the same institute in 2003. Thereafter, he went on to join his doctoral research to obtain his Doctorate degree in Solid Mechanics from Indian Institute of Technology Kharagpur in 2011. He is presently working as an Associate Professor at the Department of Applied Mechanics in Motilal Nehru National Institute of Technology Allahabad. His research areas include Solid Mechanics, Structural Analysis, Stiffened Plates, Wave Propagation, Isogeometric Finite Element Methods etc.

Application of Matrix Method of Dimensional Analysis (MMDA) and Experimental Approach for investigation of Unbalance in Rotor Bearing

Prasad V. Shinde, R.G. Desavale

Mechanical Engineering Department, RIT, Sakhrale-415414, Shivaji University, Kolhapur, Maharashtra, India

prasadshinde7174@gmail.com, ramchandra.desavale@ritindia.edu

Abstract

Rotor deformation, material in homogeneity, and manufacturing tolerance lead to unbalance inside the rotor-bearing system. Industrial maintenance follows condition monitoring to diagnose the faults present. This work employs the matrix method of dimensional analysis to identify the unbalance in the rotor-bearing system. Experimentation performed under the various operating conditions on the test rig reveals that the vibration amplitude increases as unbalanced mass increases; defect frequency corresponds to the shaft frequency of the rotating shaft, which conforms to the theoretical results. The method reduced the excessive number of variables considered due to simplicity, ultimately reducing the time and effort required. Also, the detection potential of the method for unbalance endorses application to industrial machines.

Keywords: rotor-bearing system; dimensional analysis; unbalance fault

1. INTRODUCTION

The rotor-bearing system is vital in modern industry and is predominantly used in machines like gensets, aero engines, fabrizer, and gas turbines. A series of failures will happen in bearing with localized or distributed faults such as unbalance, misalignment, crack, inner race, outer race fault, and ball pits. This ultimately results in increasing the ideal time of machinery and loss of production. In rotating machinery, unbalance creates excessive vibration and causes a catastrophic or sudden system failure. Unbalance will produce inside the system due to deformation of the shaft, in homogeneity in material, and manufacturing tolerance. Various techniques have been implemented for the diagnosis of the fault, such as condition monitoring using vibration analysis, acoustic analysis, and lubrication analysis.

Many products and processes rely on rotating systems, from machine tools to autos to rockets to ships to submarines to power plants to gadgets in the home to medical equipment. The dynamic systems need accurate and reliable predictions of the dynamic properties of their important parts as well as the detection of the corresponding fault parameters for proper

working. Identifying these systems' multiple fault parameters (MFPs) is a crucial goal for researchers in this field.

Liu et al.[1] studied the rotating system with an outer ring defect is modeled using the energy technique. A unique strategy for rotor mass distribution was used to increase the model's accuracy with the experimental data. The dynamic equations could be solved using the Runge-Kutta method and the simulated vibration signal generated. Mufazzal et al.[2] examined vibration response of ball bearings using a modified two-DOF lumped parameter model. An extra deflection and multi-impact theory are used to simulate how healthy and faulty bearings behave under varying loads and speeds. The bearing response characteristics were studied using numerical simulations run at various speeds, loads, defect sizes, and locations. Suryawanshi et al. [3] analyzed rolling contact bearing under the influence of inclined surface fault. The Buckingham Pi theorem of DA is used to cultivate a mathematical model by considering the rotor speed, angle of the incline, surface fault, load, and other bearing parameters. Experiments are conducted to determine the impact of the slope and size inclined surface fault on the vibration characteristics of spherical roller bearings. Han et al. [4] use the rotor-bearing system unbalance parameters identified using an evolutionary algorithm and a kriging surrogate model. Yaxi Shen [5] implemented a linear elastic plate, actuators, and piezoelectric sensors to model a dynamic structural system. Simulation confirms that steady-state resonance vibrations are suppressed. Genetic Algorithm-designed PID and Hybrid Fuzzy-PID control aim to minimize performance output error. Wan [6] introduced Soft Competitive Learning as a novel approach to classification. The proposed diagnosis is implemented for faulty bearings using SFART, or Fuzzy Adaptive Resonance Theory. The closeness of neurons was measured using Yu's lateral inhibition theory. Sanches et al. [7] uses a finite element approach for modeling the dynamic system, and the faults were found utilizing time-domain rotor responses and correlation analysis. A simplified system model's Lyapunov matrix equation uses least-squares fitting to identify fault parameters. The damping of rotor and coupling is determined using a differential evaluation optimization. Sugumaran et al. [8], Using the retrieved features, created a rule set for a fuzzy classifier. To identify bearing fault scenarios in train data, a decision tree is used to select the best few histogram characteristics. A fuzzy classifier is created and evaluated on real-world data. The findings are positive.Tiwari and Chakravarthy [9] provided an approach based on force response measurements for identifying unbalance parameters. De Queiroz [10] presented an unbalance force identification approach based on harmonic response to determining unbalanced parameters. Li et al. [11] developed an expert system for identifying unbalance utilizing a acoustic signal and Artificial Neural Network (ANN). Harsha [12] studied the unbalanced rotor on roller bearings using nonlinear dynamic analysis. They demonstrated the dynamic response's appearance of chaos and instability as the speed of the system was altered. Shinde et al. [13] studied a matrix method of dimensional analysis to find the effect of unbalance and misalignment. The author uses a support vector machine for multi-fault classification in a rotor-bearing system. A support vector shows a promising performance for a given input parameter.

The dimensional analysis is a powerful method to predict the vibration characteristics of a rolling element bearing (REB) under variety of conditions. The latest machine learning tools also increase fault diagnosis performance at different fault conditions [14-22].

2. DIMENSIONAL ANALYSIS (MATRIX METHOD)

The matrix method of dimensional analysis has been used to determine the unbalance rotor-bearing system characteristics. Fourteen dependent and independent variables have been used to generate a mathematical model under the influence of rotor unbalance. All variables affecting the dynamic behaviour of a taper roller contact bearing can be defined in terms of three fundamental dimensions: length (L), time (T), and either force (F) or mass (M). Variables used for the FLT (Force, Length, and Time) model are shown in table no.1 with their dimensionless unit. The functional relation between vibration amplitude in terms of velocity and 13 dependent variables is shown by the equation,

$$\dot{x} = f(d_m, D_b, B, K_d, \rho, E, \delta, c, N, W, F_u, K, m_r) \quad (1)$$

Details of each parameter are given in table no.1 Table 1 represents 14 dimensionless parameters

Table 1. Dimensions to study the system [14]

Symbol	Parameter (Unit)	Dimension
d_m	Diametric Pitch (mm)	L
D_b	Diameter of Ball (mm)	L
E	Modulus of Elasticity ($\frac{N}{mm^2}$)	FL^{-2}
K_d	Contact force for deformation ($\frac{N}{mm^{-1.5}}$)	$FL^{-1.5}$
ρ	Material Density ($\frac{kg}{m^3}$)	$FL^{-4}T^2$
δ	Bearing deflection (mm)	L
c	Coefficient of Damping ($\frac{Ns}{m}$)	$FL^{-1}T^1$
N	Speed of Shaft(rpm)	T^{-1}
W	Load (N)	F
U	Unbalance mass (kg)	$FL^{-1}T^2$
B	Bearing Width (mm)	L
Ks	Stiffness (N/m)	FT^{-2}
m_r	Rotor mass (Kg)	$FL^{-1}T^2$
$\dot{x}$	Velocity(Amplitude of Vibration- m/s)	LT^{-1}

Table 1 depicts a matrix with fourteen variables. The dependent variables are represented on the left side of the matrix, while the independent variables are represented on the right side of the matrix.

Figure 1 represents the following manner

A matrix- Repeating variables

B Matrix- Dimensionless parameter

C Matrix- Derived from equation

$$C = -(A^{-1} B)^T \text{ [15]}$$

D Matrix- No. of 'π' terms

	B Matrix										A Matrix		
	d_m	D_b	E	K_d	ρ	δ	c	B	Ks	Mr	$\dot{x}$	F_u	N	W
F	0	0	1	1	1	0	1	0	1	1	0	1	0	1
L	1	1	-2	-1.50	-4	1	-1	1	0	-1	1	-1	0	0
T	0	0	0	0	2	0	1	0	-2	-2	-1	2	-1	0
					D Matrix							C Matrix		
π_a	1	0	0	0	0	0	0	0	0	0	0	1	2	-1
π_b	0	1	0	0	0	0	0	0	0	0	0	1	2	-1
π_c	0	0	1	0	0	0	0	0	0	0	0	-2	-4	1
π_d	0	0	0	1	0	0	0	0	0	0	0	-1.5	-3	0.5
π_e	0	0	0	0	1	0	0	0	0	0	0	-4	-6	3
π_f	0	0	0	0	0	1	0	0	0	0	0	1	2	-1
π_g	0	0	0	0	0	0	1	0	0	0	0	-1	-1	0
π_h	0	0	0	0	0	0	0	1	0	0	0	1	2	-1
π_i	0	0	0	0	0	0	0	0	1	0	0	0	-2	-1
π_j	0	0	0	0	0	0	0	0	0	1	0	-1	-4	0
π_k	0	0	0	0	0	0	0	0	0	0	1	1	1	-1

Figure 1. Dimensionless Set [14]

From the above dimensionless matrix 11 π terms are obtained and listed in the Table No. 2.

Table 2. Dimensionless Variables

Variable	π-terms	Variable	π-terms
U, N, W and d_m	$\pi_a = \frac{d_m U\, N^2}{W}$	U, N, W and C	$\pi_g = \frac{C}{U\, N}$
U, N, W and D_b	$\pi_b = \frac{D_b\, U\, N^2}{W}$	U, N, W and B	$\pi_h = \frac{B\, U\, N^2}{W}$
U, N, W and E	$\pi_c = \frac{E\, W}{U^2 N^4}$	U, N, W and K_s	$\pi_i = \frac{K_s}{N^2\, W}$
U, N, W and K_d	$\pi_d = \frac{K_d\, W^{0.5}}{U^{1.5} N^3}$	U, N, W and Mr	$\pi_j = \frac{M_r}{U\, N^4}$
U, N, W and ρ	$\pi_e = \frac{\rho\, W^3}{U^4 N^6}$	U, N, W and $\dot{x}$	$\pi_k = \frac{\dot{x}\, U\, N}{W}$
U, N, W and δ	$\pi_f = \frac{\delta\, U\, N^2}{W}$		

Vibration amplitude is function of all the π terms and represented by equation no. 2,

$$\frac{\dot{x}\, U\, N}{W} = f\left(\frac{d_m U\, N^2}{W}, \frac{D_b\, U\, N^2}{W}, \frac{E\, W}{U^2 N^4}, \frac{K_d\, W^{0.5}}{U^{1.5} N^3}, \frac{\rho\, W^3}{U^4 N^6}, \frac{\delta\, U\, N^2}{W}, \frac{C}{U\, N}, \frac{B\, U\, N^2}{W}, \frac{K_s}{N^2\, W}, \frac{M_r}{U\, N^4}\right) \quad (2)$$

It is reasonably challenging to manage a number of π terms in such a way that dimensional reduction occurs in following way,

$$\pi_I = \frac{\pi_a}{\pi_b} = \frac{d_m}{D_b} \quad (3)$$

$$\pi_{II} = \frac{\pi_f}{\pi_h} = \frac{\delta}{B} \tag{4}$$

$$\pi_{III} = \frac{\pi_i \times \pi_j}{\pi_g} = \frac{W\ M_r}{K_s C\ N} \tag{5}$$

Eq. 3 indicates vibration amplitude after a sequence of reductions in the dimensionless parameter.

$$\pi_k = (\varphi\ \times \pi_I \times \pi_{II} \times \pi_{III}) \tag{6}$$

Where,φ is the dimensional groups which not assorted during experimental analysis. After putting the π terms we get

$$\frac{\dot{x}W^2}{U\ N} = \left(\varphi \times \frac{d_m}{D_b} \times \frac{\delta}{B} \times \frac{W\ M_r}{K_s C\ N}\right) \tag{7}$$

The above equation represents a mathematical equation for the rotor-bearing system under unbalance conditions.

3. EXPERIMENTATION

For the rotor-bearing setup, the dynamic response of the test setup is investigated by taking unbalanced mass and shaft speed into account. The schematic view of the test setup, as shown in figure 2, consists of a shaft with a disc supported between two bearings that are driven at operating speed by a DC motor via a dimmer stat. The shaft is coupled with a DC motor with a flexible coupling.

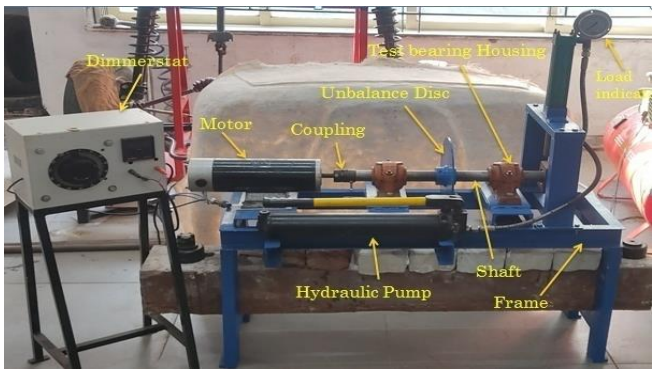

Figure 2. Experimental Setup

Table 3. Specifications of Bearing	
Bearing Type	SKF 6209-K
(d)- Bearing Inner Dia.	45 mm
(D)- Bearing Outer Dia.	85 mm
No. of Balls (N)	9
Diameter of balls	9 mm

Two deep groove ball bearings, specifications mentioned in table 3, are used for experimentation. To measure vibration signals, Adash VAPro 4400 Fast Fourier transforms (FFT) with an accelerometer of the piezoelectric type with a sensitivity of 100 mV/g was placed on the test bearing housing. The different combination of bearing speed and unbalanced mass was simulated between 500 rpm to 1300 rpm. Table 2 shows the bearing specifications that were used in the experiment.

4. RESULTS AND DISCUSSION

Different combinations of unbalance mass of 50 gm to 125 gm and shaft speed of 700 rpm to 1300 rpm are considered for experimentation. Sixteen experiments were performed on the test setup, and frequency responses were obtained below.

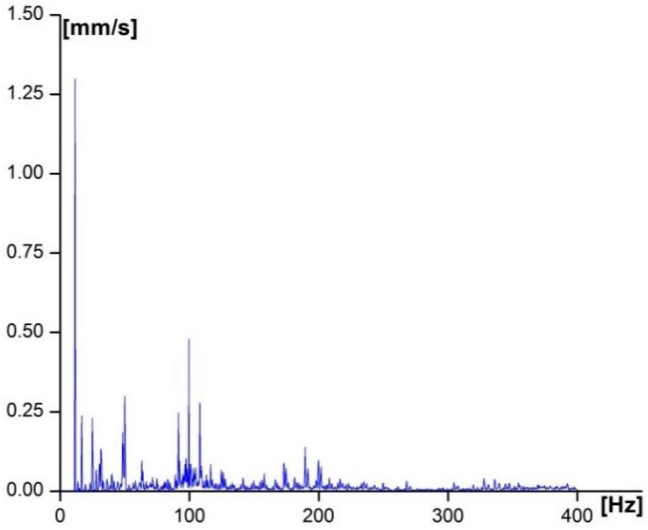

Figure 3. Vibration characteristics for trial-2

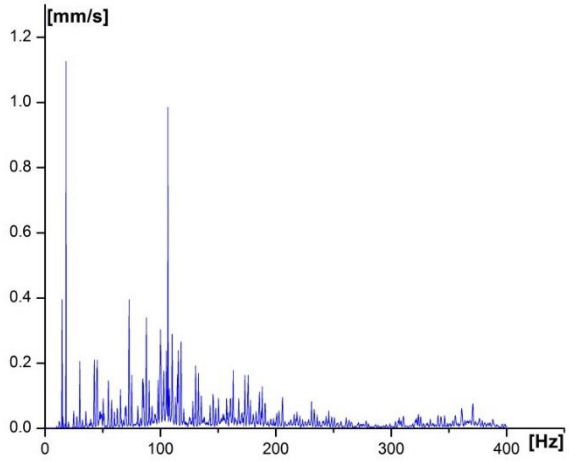

Figure 4. Vibration characteristics for trial-8

An unbalance mass of 125 gm and speed of 700 rpm is a combination for trial 2 is considered. The vibration response obtained using the test is shown in figure 3. The figure depicts that vibration spectrum is obtained at first harmonics of shaft frequency ($1 \times f_s$). The vibration amplitude for a given unbalance mass is 1.29 mm/s.

A combination of unbalance mass and speed for trial 2 is 75 gm and 900 rpm, respectively, shown in figure 4. The vibration response obtained using the test is shown in figure 4. The vibration amplitude for conducted trial is 1.18 mm/s. As the unbalance mass increase with speed, vibration amplitude also increases.

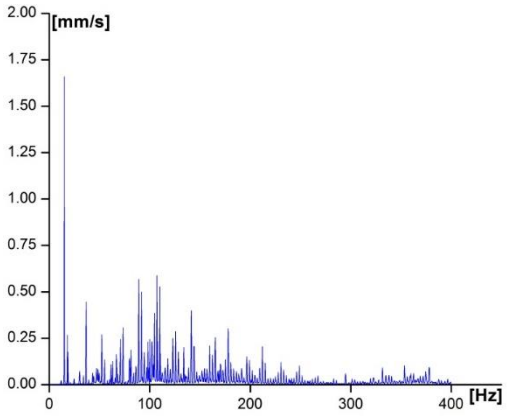

Figure 5. Vibration characteristics for trial-13

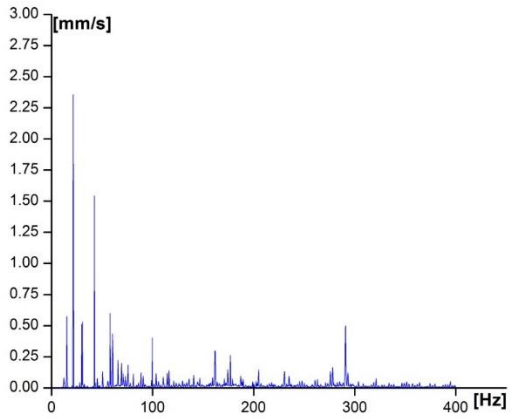

Figure 6. Vibration characteristics for trial-15

The above trial is conducted for rotor speed of 1100 rpm and 75 gm of unbalance mass. The peak amplitude is obtained for a given speed, and the mass is 1.65 mm/s. The peak amplitude is obtained at first harmonics of shaft frequency. The vibration response for the above trial is shown in figure 5.

Similarly, a combination of unbalance mass and speed of 1300 rpm and 50 gm unbalance, the vibration responses are shown in figure 6. The vibration amplitude for conducted trial is 2.354 mm/s.

Table 4. Summary of the vibration responses					
Trial No.	**Speed**	**Unbalance Mass**	**Experimental vibration amplitude (mm/s)**	**Model vibration amplitude (mm/s)**	**% Error in amplitude**
1	700	50	0.927	0.91	1.83
2	900	75	1.18	1.12	5.08
3	1100	100	2.07	2.03	1.93
4	1300	125	3.4	3.31	2.65
5	700	75	0.997	1.04	4.31
6	900	100	1.49	1.43	4.03
7	1100	125	2.35	2.3	2.13
8	1300	50	2.354	2.28	3.14
9	700	100	1.09	1.05	3.67
10	900	125	1.58	1.5	5.06
11	1100	50	1.59	1.52	4.40
12	1300	75	2.89	2.84	1.73
13	700	125	1.29	1.26	2.33
14	900	50	1.02	0.97	4.90
15	1100	75	1.65	2.06	0.48
16	1300	100	3.17	3.15	0.63

Similarly, all trials are conducted for different speeds and unbalanced mass. The combination of unbalanced mass and speed and respective vibration response is reported in table 4. It is observed from trials that as unbalanced mass is introduced with combinations of speed increases the vibration levels of the system and shows a vibration peak at first harmonics of shaft frequency, i.e. (1 × fs). Speed, geometric proportions, and mass distribution of the rotor and the shaft, bearings, and foundation's dynamic rigidity primarily determine the unbalance response. The disc unbalance is created by attaching the unbalance mass to the disc.

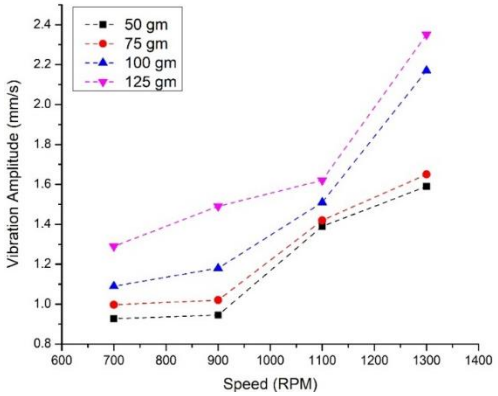

Figure 7. Influence of unbalance mass to speed of the shaft

Figure 7 shows the vibration amplitude vs. speed of the rotor in rpm. The maximum vibration amplitude is obtained at 125 gm of unbalance and at 1300 rpm of speed, while at 700 rpm

of speed and at 50 gm of unbalance amplitude of vibration is minimum. It is observed from the pilot experiments that the amplitude of vibration increases as speed increases. Also, defect frequency corresponds to the shaft's rotating speed fs, which conforms to the theoretical results.

5. CONCLUSION

A model-based matrix method (MMDA) is proposed for the rotor-bearing system under the influence of unbalance. An unbalance mass can cause complete failure of the rotating machine. The proposed method is found to be accurate and effective in obtaining the vibration amplitude under unbalance conditions.

The following findings are noted.

- The difference between the vibration amplitude measured experimentally and the amplitude calculated using a mathematical model demonstrates a close match with a marginal error.
- Experimentation shows that the dominating peak is obtained at first and several harmonics of the shaft frequency.
- The mathematical model proposed is consistent with the results found experimentally.
- The findings indicate that the vibration amplitude is enhanced as the unbalance mass increases.

ACKNOWLEDGEMENT

This work is financially supported by the Chhatrapati Shahu Maharaja National Research fellowship 2020, SARTHI, Pune.

REFERENCES

[1] Y. Liu, C. Yan, K. Wang, X. Gao, X. Zhang, and L. Wu, "Dynamic modeling of rotor-bearing-housing system with local defect on ball bearing using mass distribution and energy methods," Proceedings of the Institution of Mechanical Engineers, Part K: Journal of Multi-body Dynamics, vol. 235, no. 3, pp. 412–426, 2021.

[2] S. Mufazzal, S. Muzakkir, and S. Khanam, "Theoretical and experimental analyses of vibration impulses and their influence on accurate diagnosis of ball bearing with localized outer race defect," Journal of Sound and Vibration, vol. 513, p. 116407, Nov. 2021, DOI: 10.1016/j.jsv.2021.116407.

[3] G. L. Suryawanshi, S. K. Patil, and R. G. Desavale, "Dynamic model to predict vibration characteristics of rolling element bearings with inclined surface fault," Measurement, vol. 184, p. 109879, Nov. 2021, doi: 10.1016/j.measurement.2021.109879.

[4] F. Han, X. Guo, and H. Gao, "Bearing parameter identification of rotor-bearing system based on Kriging surrogate model and evolutionary algorithm," Journal of Sound and Vibration, vol. 332, no. 11, pp. 2659–2671, May 2013, doi: 10.1016/j.jsv.2012.12.025.

[5] Y. Shen and A. Homaifar,D. Chen"Vibration Control Of Flexible Structures Using Fuzzy Logic and Genetic Algorithms,"Proceedings of the American Control Conference Chicago, Illinois, no. 1: 448–52, 2000

[6] X.-J. Wan, L. Liu, Z. Xu, Z. Xu, Q. Li, and F. Xu, "Fault diagnosis of rolling bearing based on optimized soft competitive learning Fuzzy ART and similarity evaluation technique," Advanced Engineering Informatics, vol. 38, pp. 91–100, Oct. 2018, doi: 10.1016/j.aei.2018.06.006.

[7] F. D. Sanches and R. Pederiva, "Theoretical and experimental identification of the simultaneous occurrence of unbalance and shaft bow in a Laval rotor," Mechanism and Machine Theory, vol. 101, pp. 209–221, Jul. 2016, doi: 10.1016/j.mechmachtheory.2016.03.019.

[8] V. Sugumaran and K. I. Ramachandran, "Fault diagnosis of roller bearing using fuzzy classifier and histogram features with focus on automatic rule learning," Expert Systems with Applications, vol. 38, no. 5, pp. 4901–4907, May 2011, doi: 10.1016/j.eswa.2010.09.089.

[9] R. Tiwari and V. Chakravarthy, "Simultaneous identification of residual unbalances and bearing dynamic parameters from impulse responses of rotor–bearing systems," Mechanical Systems and Signal Processing, vol. 20, no. 7, pp. 1590–1614, Oct. 2006, doi: 10.1016/j.ymssp.2006.01.005.

[10] M. S. De Queiroz, "An Active Identification Method of Rotor Unbalance Parameters," Journal of Vibration and Control, vol. 15, no. 9, pp. 1365–1374, Mar. 2009, doi: 10.1177/1077546308096103.

[11] S. Lotfan, N. Salehpour, H. Adiban, and A. Mashroutechi, "Bearing fault detection using fuzzy C-means and hybrid C-means-subtractive algorithms," 2015 IEEE International Conference on Fuzzy Systems (FUZZ-IEEE), Aug. 2015, doi: 10.1109/fuzz-ieee.2015.7338049.

[12] W. Li, Y. P. Tsai, and C. L. Chiu, "The experimental study of the expert system for diagnosing unbalances by ANN and acoustic signals," Journal of Sound and Vibration, vol. 272, no. 1–2, pp. 69–83, Apr. 2004, doi: 10.1016/s0022-460x(03)00317-1.

[13] S. P. Harsha, "Nonlinear dynamic analysis of an unbalanced rotor supported by roller bearing," Chaos, Solitons & Fractals, vol. 26, no. 1, pp. 47–66, Oct. 2005, doi: 10.1016/j.chaos.2004.12.014.

[14] P. V. Shinde and R. G. Desavale, "Application of dimension analysis and soft competitive tool to predict compound faults present in rotor-bearing systems," Measurement, vol. 193, no. 1, p. 110984, Apr. 2022, doi: 10.1016/j.measurement.2022.110984.

[15] T. A. Jadhav and P. J. Awasare, "Enhancement of particle damping effectiveness using multiple cell enclosure," Journal of Vibration and Control, vol. 22, no. 6, pp. 1516–1525, Jul. 2014, doi: 10.1177/1077546314543725.

[16] Patil, S. M., Desavale, R. G., Shinde, P. V., Patil, V. R., Comparative Study of Response of Vibrations for Circular and Square Defects on Components of Cylindrical Roller Bearing Under Different Conditions, In : Lecture Notes in Mechanical Engineering Innovative Design, Analysis and Development Practices in Aerospace and Automotive Engineering, Springer, pp. 189-198, 2020

[17] V. R. Patil and P. V. Jadhav, "Dynamic response analysis of unbalanced rotor-bearing system with internal radial clearance," SN Applied Sciences, vol. 2, no. 11, Oct. 2020, doi: 10.1007/s42452-020-03608-y.

[18] R. G. Desavale, "Dynamics Characteristics and Diagnosis of a Rotor-Bearing's System Through a Dimensional Analysis Approach: An Experimental Study," Journal of Computational and Nonlinear Dynamics, vol. 14, no. 1, Nov. 2018, doi: 10.1115/1.4041828.

[19] R. G. Desavale, R. Venkatachalam, and S. P. Chavan, "Antifriction Bearings Damage Analysis Using Experimental Data Based Models," Journal of Tribology, vol. 135, no. 4, Aug. 2013, doi: 10.1115/1.4024638.

[20] P. M. Jadhav, S. G. Kumbhar, R. G. Desavale, and S. B. Patil, "Distributed fault diagnosis of rotor-bearing system using dimensional analysis and experimental methods," Measurement, vol. 166, no. 1, p. 108239, Dec. 2020, doi: 10.1016/j.measurement.2020.108239.

[21] S. G. Kumbhar, E. Sudhagar P, and R. G. Desavale, "Theoretical and experimental studies to predict vibration responses of defects in spherical roller bearings using dimension theory," Measurement, vol. 161, no. 1, p. 107846, Sep. 2020, doi: 10.1016/j.measurement.2020.107846.

[22] R. A. Kanai, R. G. Desavale, and S. P. Chavan, "Experimental-Based Fault Diagnosis of Rolling Bearings Using Artificial Neural Network," Journal of Tribology, vol. 138, no. 3, p. 031103, Apr. 2016, doi: 10.1115/1.4032525.

[23] T. Szirtes And P. Rozsa,Applied Dimensional Analysis and Modeling,New York: McGraw Hill, December. 2007.

[24] M. A. Vishwendra, P. S. Salunkhe, S. V. Patil, S. A. Shinde, P. V. Shinde, R. G. Desavale, P. M. Jadhav and N. V. Dharwadkar. “A Novel Method to Classify Rolling Element Bearing Faults Using K-Nearest Neighbor Machine Learning Algorithm.” ASME. ASME J. Risk Uncertainty Part B. Vol. 8, No. 3,p. 031202, September 2022, doi: https://doi.org/10.1115/1.4053760

Biographies

Mr. Prasad Vishwasrao Shinde received the bachelor's degree in Mechanical engineering from D.Y.Patil College of Engineering, Kolhapur in 2013, the master's degree in mechanical engineering from Shivaji University, Kolhapur in 2016, and pursuing the philosophy of doctorate degree in mechanical engineering from Shivaji University, Kolhapur, respectively. He is currently working as an Research Scholar at the Department of Mechanical Engineering, Rajarambapu Institute of Technology, Islampur. His research areas include bearing vibration, machine learning, and acoustic analysis.

Dr. R. G. Desavale received the bachelor's degree in Automobile engineering from Rajarambapu Institute of Technology, Islampur in 2005, the master's degree in mechanical engineering from Shivaji University, Kolhapur in 2008, and the philosophy of doctorate degree in mechanical engineering from National Institute of Technology, Warangal respectively. He is currently employed as an associate professor at Rajarambapu Institute of Technology, Islampur, in the Department of Mechanical Engineering. His research areas include bearing vibration, FEA, and signal analysis.

Finite Element Analysis of a Shape Memory Polymer for Space Actuator Applications

Sreetam Das, Sourabh Kumar Singh, Avadesh Yadav, Satish Kumar* and Abhishek Kumar

Department of Applied Mechanics, Motilal Nehru National Institute of Technology Allahabad, Prayagraj, India

sreetam28197@gmail.com, sks314285@gmail.com, avadesh.yadav2008@yahoo.com, satistme@mnnit.ac.in, abhishek@mnnit.ac.in

Abstract

Shape memory polymer (SMP) belongs to a unique class of smart materials that has the ability to return to its original shape from a deformed temporary shape when subjected to external stimuli such as electricity, light, magnetism, pH value, moisture, and heat. This external stimulus helps the polymer recover its permanent shape by increasing the temperature above the polymer's glass transition temperature (Tg). The popularity of inflatable space structures has increased due to their low weight, high reliability, low volume, low cost, and easy packing. Antennas are one such space structure used to send and receive information over large distances. Antennas keep on moving in a constant path around the earth in different orbits. During movement in the orbits, the antennas are exposed to a constant variation in the temperature. This variation in temperature affects the dimensions of the antenna, thus having an adverse effect on the transmission of desired information. So, the idea of using shape memory polymer is to restrict the deviation of required dimensions. SMP plays a vital role in compensating for the dimension variation to keep the antenna structure in a definite shape due to its shape memory effect (SME). In the present study, the property of an SMP material is assigned to a beam which is modeled and simulated on a commercial finite element software Abaqus FEA. A hyperelastic model (Neo-Hookean) and generalized Maxwell model with viscoelastic property were used for simulation. It was found that when heat is provided to the SMP, viscoelastic prony's parameters, thermal expansion coefficient with varying heating rates, and temperature range have a significant effect on the total time taken to regain the desired shape.

Keywords: Shape memory polymer, glass transition temperature, finite element, viscoelastic, hyperelastic, antenna.

1. INTRODUCTION

Shape memory materials have the property to remember their original state of shape when deformed. Shape memory alloy (SMA) is a prime shape memory material which has varied applications ranging from space to biomedical. These alloys are able to transform between austenite and martensite phases based on temperature variation. This phase transition is used to deform the permanent shape and also to recover the distorted shape. Some of the common

examples of SMAs are Ni-Ti and Cu-Zn. One such recent advancement is the emergence of shape memory polymer (SMP). Nowadays, polymers and their composites are widely used due to their outstanding properties like high strength to weight ratio, higher corrosion resistance, as well as excellent tailorability with low processing cost. SMPs return to their previous shape after a substantial plastic deformation under externally applied stimuli like direct heating, electrically induced heating, magnetically induced heating, light, and chemicals [1–4]. The most frequent triggering stimuli is heat, which raises the polymer's temperature over its glass transition temperature (Tg), where the permanent shape is distorted and regained.

Moreover, SMPs have extraordinary properties, such as higher recoverable strain (~400%) than conventional SMAs (~8%), which makes them viable for many researchers and industrialists [5–7]. Since weight is an important factor in any space mission, the use of SMP becomes advantageous as they have a weight significantly lower than that of SMA. Antennas are one of the most often used space structures for transmitting and receiving data over long distances. Antennas constantly rotate around the earth, experiencing a continuous temperature variation. These temperature variations alter the antenna component, changing the size and inhibiting data transmission. To limit the deviation of the components, SMPs can be used to constrain the changes allowing the antenna to maintain its shape without any change in the dimensions [8]. When the temperature hits a particular threshold value, the SMP starts to deform. As the temperature on the surface of the antenna is constantly fluctuating owing to the earth's rotation, SMP goes through many stages of expansion and contraction in a single day. Hence, there would be many recovery cycles during the course of its lifespan and experimentally verifying these cycles could be a challenging task. Polymeric bonds, cross-linking (chemically or physically), and functional groups all have a role in determining SMP characteristics [9]. There are primarily five steps to program a shape memory polymer. The polymer is first heated above Tg. The polymers stretch a little when the heat opens up the bonds. The chains are twisted around each other and locked while the polymer is below Tg. However, when the temperature increases above Tg, the polymeric chains gets soften and starts to behave like rubber. In the second stage, an external load is given to the polymer, altering its dimension to achieve a temporary shape occurring at a high temperature. In the third stage, the temperature is allowed to lower below Tg. In the presence of load applied from the outside, cooling the polymer locks it in the transitional form. Unloading is done in the fourth stage, which determines the stress relaxation factor, thereby helping to find the shape fixity of the polymer. In the final stage, the polymer is reheated to regain its original permanent shape. External stimuli such as heat, electricity, and light are delivered to the SMP, activating the polymer's bond and causing it to restore its form. The temperature at which an SMP transitions is determined by a number of parameters [1,10,11]. The Tg varies in direct proportion with the molecular weight of the polymer. A higher molecular weight means the chains are less mobile, which raises the Tg. Due to double bonds and bulky functional groups, the chain's mobility is restricted, resulting in a more significant Tg. The Tg value also increases due to cross-linking in the polymer.

The thermomechanical properties of an SMP are determined by using the constitutive equations. A typical linear viscoelastic model may be used to characterise the polymer's overall properties. Under varied conditions, the constitutive equation may predict the strain for different programming stages [12]. In the present study, programming of an SMP material is done to analyse the compression behaviour for three temperature ranges from 25-

45, 25-55 and 25-65 °C. The strain fixity and shape recovery ratio have been reported for the listed temperature ranges.

2. MODELLING AND PROGRAMMING

In the present work, two constitutive models are used to model SMPs. Primarily, the thermo-viscoelastic is the first model, while the secondary is phase transition model. The material is considered viscoelastic in the thermo-viscoelastic model, which is just an assembly of springs and dashpot, commonly known as the Maxwell model [13]. The thermo-viscoelastic model is quietly able to predict the polymer's behaviour based on time-temperature dependent responses for a full shape memory cycle. The thermo-viscoelastic model requires a high number of material parameters, and fitting the numerous parameters into one equation to obtain a generalized curve is complex and cumbersome.

2.1. Viscoelastic Model

Viscoelasticity is a term that refers to materials that are both viscous and elastic. One of the most prominent viscoelastic models is the generalized Maxwell model, which recognizes that material relaxation is a continuous process rather than an instantaneous event. A dashpot and a spring are linked in series in the Maxwell model. They are placed in parallel in the extended Maxwell model. When the temperature reaches the material's glass transition, the relaxation modulus (E) has a strong reliance on time. However, this dependency is greatly reduced when the temperature range is far away from Tg [14].

$$\mathrm{E}(t, T_{ref}) = \mathrm{E}(a_T t, T) \tag{1}$$

The Time-Temperature Superposition (TTS) principle is very well applicable to explain the influence of viscoelastic materials over a varied time and temperatures [15]. The shift factor (a_T) is used to connect the modulus at a reference temperature (T_{ref}) and time (t) to the modulus of relaxation at any time ($a_T t$) and temperature (T), as shown in equation (1). The T_{ref} and shift factor are usually determined from the Tg of the polymer as stated by WLF or Arrhenius equation [16]. After changing the curves, the master curve is obtained. Finally, the equation is fit onto the master curve where prony's series parameters are produced as shown in the equation (2).

$$\mathrm{E}(t) = E_\infty + \sum_{i=1}^{n} E_i \, e^{\frac{-t}{\tau_i}} \tag{2}$$

2.2. Hyperelastic Model

Rubber-like materials with a high elastic deformation region relative to other materials are modeled using the hyperelastic material model [17]. The stress-strain relationship in a hyperelastic model is derived from the density function of strain energy. This model is utilized near Tg in which the rubbery state of polymer is seen. The material hyperelastic reaction is modeled using the Neo-Hookean material model with a slow uniaxial strain rate.

2.3. Programming

The simulation is performed using the finite element-based software Abaqus FEA. Five phases of programming are performed on the SMP. The first stage is heating the polymer to a specific temperature and maintaining it. The second phase entails introducing uniaxial compression as an external load. The dimension of the beam is 200 mm x 15 mm x 3 mm

where one end is rigidly fixed, and a compressive deformation of 20 mm is given in the form of load on the other end. The material is cooled to room temperature in the third stage. The load is removed and then reheated again in the final stage to witness the SME. For this purpose of model analysis, the Neo-Hookean parameters and viscoelastic parameters are drawn from the paper of Arrieta et al. [18]. Shape memory behaviour was observed for the polymer for different temperature ranges and the recovery and fixity ratios were calculated.

3. RESULTS AND DISCUSSION

The relationship between shape memory effect, and the temperature variation were found to be in good agreement. The simulation of SME in the temperature range of 25-45 °C is shown in Figure 1. After compression, when unloading takes place, the strain developed in the polymer significantly reduces from 20 mm to 11.49 mm, showing the shape fixity to be 58.95%, indicating poor SME. This indicates that the transition temperature is far away as many spring-back effects are seen. But as the temperature increases, it is seen that the shape fixity reaches 90.95% in the temperature range of 25-55 °C (Figure 2), which improves even further in the range of 25-65 °C (Figure 3), showing a fixity value of 93.29%. This indicates that the spring-back effect gets lower as the temperature increases up to a certain value offering a good range of shape fixity.

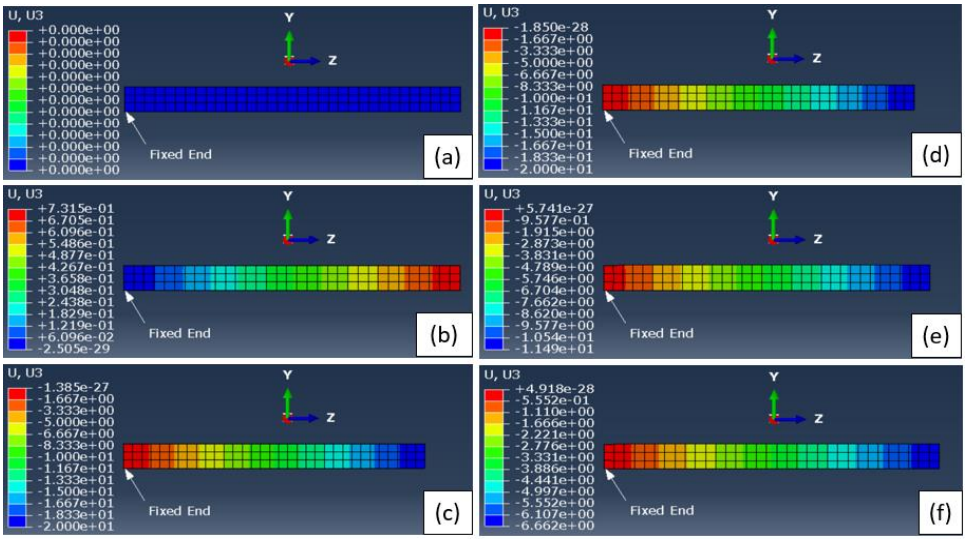

Figure 1. SME simulated in Abaqus FEA subjected to a compressive load during 25-45 °C: (a) Initial temperature of 25 °C, (b) Heat at 45 °C, (c) Load at 45 °C, (d) Cool up to 25 °C, (e) unload, (f) and again, reheat up to 45 °C.

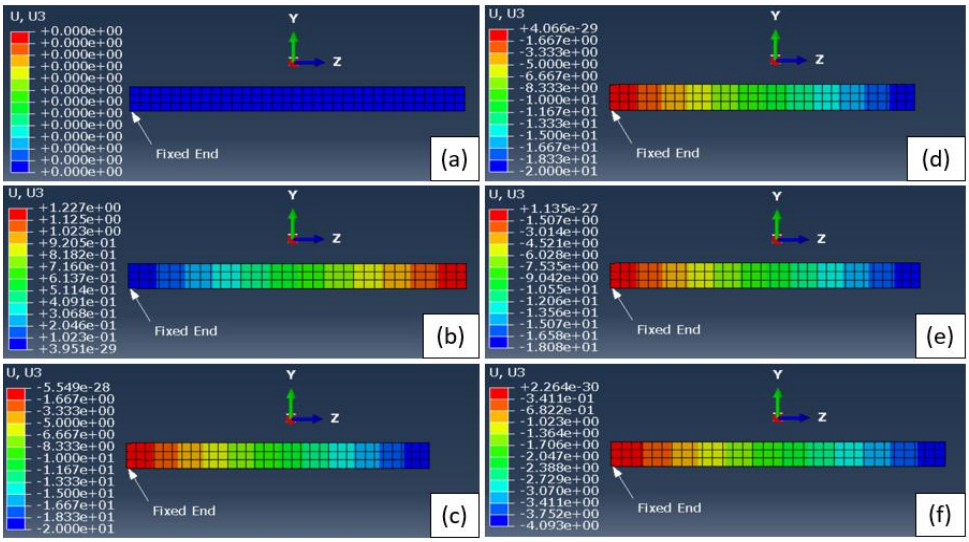

Figure 2. SME simulated in Abaqus FEA subjected to a compressive load during 25-55 °C: (a) Initial temperature of 25 °C, (b) Heat at 55 °C, (c) Load at 55 °C, (d) Cool up to 25 °C, (e) Unload, (f) and again, reheat up to 55 °C.

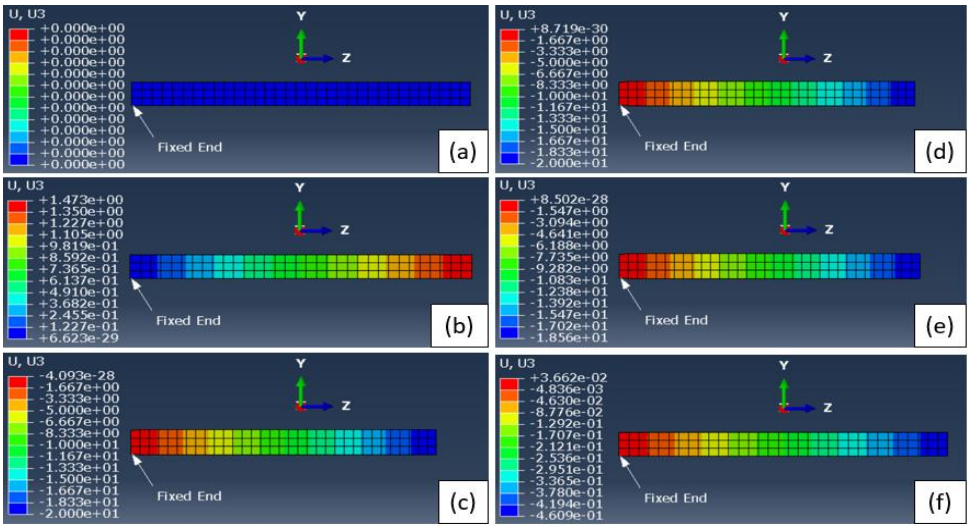

Figure 3. SME simulated in Abaqus FEA subjected to a compressive load during 25-65 °C: (a) Initial temperature of 25 °C, (b) Heat at 65 °C, (c) Load at 65 °C, (d) Cool up to 25 °C, (e) Unload, (f) and again reheat up to 65 °C.

Similarly, the shape recovery ratio also increases as the temperature reaches Tg. The values obtained are 64.33%, 74.93% and 90.99% when temperature rises from 45, 55 and 65 °C, respectively (Figure 1-3). This shows that as we move towards Tg, the spring back effect decreases, thus increasing fixity and recovery, which is depicted in Figure 4. Initially, the stresses are high at lower temperatures, and the polymeric chain is intact. As temperature increases, the chain starts opening and bond breakage takes place, making it more flexible and easy to recover. Hence, it can be inferred that the SMP is not programmable at lower temperatures showing poor fixity and recovery. But as the temperature keeps on rising and reaches in the range of Tg, a good amount of shape fixity and recovery is achieved, which makes it suitable for various space applications.

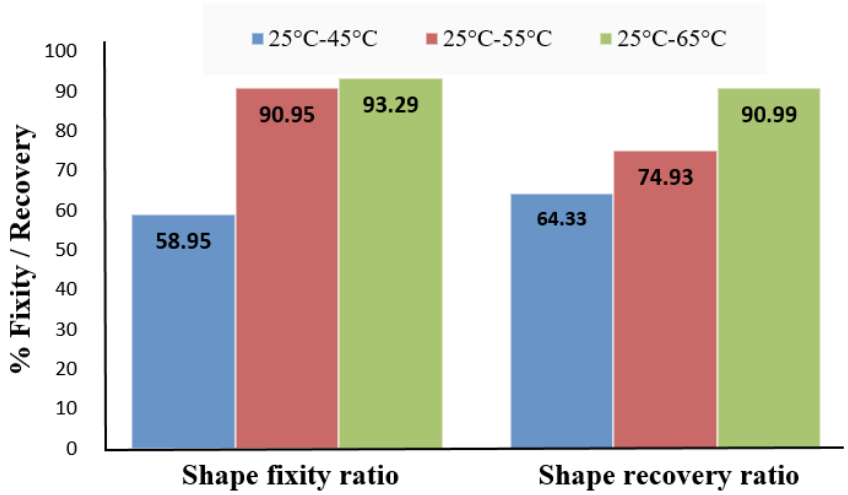

Figure 4. Shape fixity and shape recovery ratio for different temperature ranges.

4. CONCLUSION

In the current work, the shape memory effect of the SMP under uniaxial compressive strain was investigated using temperature variations as the external stimulus. Modeling and simulation is performed using the Abaqus FEA software by adopting the thermo-visco-hyperelastic theory. Many space actuators are subjected to compressive loads, and this model helps to determine the variation of SMEs under this loading condition. It is observed that the temperatures have a tremendous impact on the shape fixity and shape recovery of smart materials. At temperatures lower than that of Tg, the shape fixity is low due to the large spring-back effect as the material is unable to retain its shape. With the increase in temperature, the shape fixity and recovery improve. The fixity ratio increases with temperature because of stable and rigid bonds after the unloading stage, which keeps the deformed shape intact. As the polymer reaches a rubbery state in Tg region, the shape recovery becomes easier. In the temperature range of 65 °C, the fixity along with recovery was found to be above 90%. Thus, for an SMP to show a good SME, it has to be

programmed just above the value of Tg. There are still many parameters that may affect the recovery behaviour of SMP and needs to be explored, which include holding duration, rate of temperature rise, environmental conditions, loading rate and polymer composition.

5. LIMITATIONS AND FUTURE SCOPE

During modeling and simulation, the material's properties are required to input which are obtained from the experimental results and it itself is a challenging task. The SMP made for the antenna has to be tested before being actually deployed in space. To test the SMP for the cycle of contraction and expansion, as well as its fatigue life, rigorous tests and space testing conditions must be further developed.

ACKNOWLEDGMENTS

The authors express their sincere obligation to Motilal Nehru National Institute of Technology Allahabad, Prayagraj for allocating finite element based simulation facility in order to model and simulate the shape memory behaviour.

REFERENCES

[1] Q. Zhao, H.J. Qi, T. Xie, Recent progress in shape memory polymer: New behavior, enabling materials, and mechanistic understanding, Prog. Polym. Sci. 49–50 (2015) 79–120.

[2] J. Hu, Y. Zhu, H. Huang, J. Lu, Recent advances in shape–memory polymers: Structure, mechanism, functionality, modeling and applications, Prog. Polym. Sci. 12 (2012) 1720–1763.

[3] A. Yadav, B.N.V.S.K.G. Gupta, A.O. Fulmali, R.K. Prusty, B.C. Ray, Effect of cure kinetics and nanomaterials on glass fiber/vinyl ester composites: An assessment on mechanical, thermal and fracture morphology, Mater. Today Proc. 33 (2020) 4937–4941.

[4] S.K. Singh, D. Singh, A. Kumar, A. Jain, An Analysis of Mechanical and Viscoelastic Behaviour of Nano-SiO_2 Dispersed Epoxy Composites, Silicon 2019 1210. 12 (2019) 2465–2477.

[5] L. Sun, W.M. Huang, Z. Ding, Y. Zhao, C.C. Wang, H. Purnawali, C. Tang, Stimulus-responsive shape memory materials: A review, Mater. Des. 33 (2012) 577–640.

[6] W.M. Huang, Z. Ding, C.C. Wang, J. Wei, Y. Zhao, H. Purnawali, Shape memory materials, Mater. Today. 13 (2010) 54–61.

[7] H. Li, C. Yu, R. Chen, J. Li, J. Li, Novel ionic liquid-type Gemini surfactants: Synthesis, surface property and antimicrobial activity, Colloids Surfaces A Physicochem. Eng. Asp. Complete (2012) 116–124.

[8] M. Chandra, S. Kumar, S. Chattopadhyaya, S. Chatterjee, P. Kumar, A review on developments of deployable membrane-based reflector antennas, Adv. Sp. Res. 68 (2021) 3749–3764.

[9] S.C. Arzberger et al., Elastic memory composites (EMC) for deployable industrial and commercial applications, SPIE. 5762 (2005) 35–47..

[10] R. Xiao, C. Zhang, W.M. Huang, Programming of Shape-Memory Polymers, Shape-Memory Polym. Device Des. (2017) 113–137.

[11] O.K.C. Tsui, H.F. Zhan, Effects of Chain Ends and Chain Entanglement on the Glass Transition Temperature of Polymer Thin Films, Macromolecules. 34 (2001) 9139–

9142.
[12] H. Tobushi, K. Okumura, S. Hayashi, N. Ito, Thermomechanical constitutive model of shape memory polymer, Mechanics of Materials. 33 (2001) 545–554.
[13] B. Radovskiy, B. Teltayev, Relaxation modulus and complex modulus, Struct. Integr. 2 (2018) 41–72.
[14] K.K. Westbrook, P.H. Kao, F. Castro, Y. Ding, H. Jerry Qi, A 3D finite deformation constitutive model for amorphous shape memory polymers: A multi-branch modeling approach for nonequilibrium relaxation processes, Mech. Mater. 12 (2011) 853–869.
[15] W.B. Luo, C.H. Wang, R.G. Zhao, Application of Time-Temperature-Stress Superposition Principle to Nonlinear Creep of Poly(methyl methacrylate), Key Eng. Mater. 340–341 (2007) 1091–1096.
[16] P. Liu, Viscoelastic bilinear cohesive model and parameter identification for failure analysis of adhesive composite joints using explicit finite element analysis, Damage Model. Compos. Struct. (2021) 175–190.
[17] J. Bergström, Mechanics of Solid Polymers: Theory and Computational Modeling, Mech. Solid Polym. Theory Comput. Model. (2015) 1–509.
[18] S. Arrieta, J. Diani, P. Gilormini, Experimental characterization and thermoviscoelastic modeling of strain and stress recoveries of an amorphous polymer network, Mech. Mater. 68 (2014) 95–103.

Biographies

Sreetam Das received his bachelor's degree in Mechanical Engineering from College of Engineering and Technology, Bhubaneswar in 2018. He is currently pursuing his master's degree in Material Science & Engineering from Motilal Nehru National Institute of Technology Allahabad, Prayagraj.

Sourabh Kumar Singh received his bachelor's degree in Mechanical Engineering from Lovely Professional University, Punjab in 2020. He is currently pursuing his master's degree in Material Science & Engineering from Motilal Nehru National Institute of Technology Allahabad, Prayagraj.

Avadesh Yadav received his bachelor's degree in Mechanical Engineering from Dr. A.P.J. Abdul Kalam Technical University, Lucknow in 2017 and completed his master's in Metallurgical and Materials Engineering from National Institute of Technology Rourkela in 2020. He is currently pursuing his Ph.D. in the Applied Mechanics Department from Motilal Nehru National Institute of Technology Allahabad, Prayagraj. His thesis work is focussed on the shape memory polymer for structural applications

Dr. Satish Kumar is currently working as an Assistant Professor at Applied Mechanics Department from Motilal Nehru National Institute of Technology Allahabad, Prayagraj, India. He has completed his B. Tech from NIT Jalandhar, M. Tech, and Ph.D. from IIT Roorkee. His research interests lie in the design, fabrication, and mechanical characterization of adaptive membrane-based lightweight structures for space applications, which he plans to study using a combined experimental and numerical approach.

Dr. Abhishek Kumar is currently working as an Associate Professor in the Applied Mechanics Department from Motilal Nehru National Institute of Technology Allahabad, Prayagraj. He completed his Ph.D. in the Department of Metallurgical and Materials Engineering from Indian Institute of Technology Roorkee in 2014. His research areas include design and development of microwave absorbers, synthesis and characterisation of nanomaterials, mechanical and corrosion behaviour of metals and alloys.

Finite Element Analysis of Re-Entrant and Modified Curved Re-Entrant Auxetic Structure for Energy-Absorption

Prabhakar Kumar[a*], Prashant Singh[a], Nigatu D. Tilahun[b], R. Sujithra[a], Abhishek Kumar[a]

[a] *Motilal Nehru National Institute of Technology Allahabad, Prayagraj, India*

[b] *Debre Berhan University, Ethiopia*

**prabhakark73@gmail.com,singhprashant2296.ps25@gmail.com, r-sujithra@mnnit.ac.in, abhishek@mnnit.ac.in*

Abstract

Auxetic cellular materials have unique and superior physical properties with negative Poisson's ratio which is caused by the structural deformation of the cells, which increases their lateral dimension when stretched. The re-entrant and the proposed curved re-entrant structure with varying thicknesses (1 mm and 0.5mm) is analyzed in ABAQUS by considering the properties of Acrylonitrile butadiene styrene (ABS). A curved re-entrant structure with a thickness of 1 mm was found to be capable of bearing more load than that of a 0.5 mm thickened structure. Also, the nominal stress was found to increase by 6 times when the thickness was doubled.

Keywords Auxetic cellular material, Poisson's ratio, Re-entrant structure, curved re-entrant.

1. INTRODUCTION

In a confined space and weight, where high damping absorption is required that too with high strength, rigidity, lightweight, and good impact resistance. The auxetic materials stand at the top with the above-mentioned properties [1-2]. It has the properties to shrink when applied with compressive force as it is defined as a negative poison's ratio material. The deformation modes, structure, loading circumstances, material qualities, and hybrid configurations all have an impact on the energy-absorption capacity of materials [3].

Many writers have proposed various structures for auxetic materials, such as hexagonal, re-entrant, kagome, diamond, star-shaped honeycomb, and many more. A hexagonal structure [13] consists of a 2D structure with a hexagon as a unit cell as shown in Fig. 1(a). These hexagonal unit cells get repeated horizontally and vertically as per the required property and energy absorption capacity. When a hexagonal unit cell is put on an orthogonal plane, such that the opposing sides are parallel and horizontal, and both neighboring sides are pushed inside, the hexagonal unit cell is turned into a re-entrant structure. Fig. 1(b) depicts the re-entrant structure's unit cell [9]. To investigate the desired qualities, the angle of inclination of inclined sides can be changed. Kagome structure [7] consists of two triangle-shaped

structures placed inverted such that all the three sides of both the triangles intersect each other twice, forming a shape as shown in Fig. 1(c). As illustrated in Fig. 1(d), a diamond-shaped [7] unit cell is made up of two triangular-shaped structures that are inverted such that the peak points of both structures coincide with the base of each triangle. When an eight-sided polygon is made in such a way that all alternate vertices are pushed towards the center and other remaining alternate vertices are constrained at their original position as shown in Fig. 1(e) to form a star-shaped structure [8].

In terms of differences in deformation and mechanical reactions of different cells many experiments and simulation has been studied and also new designs are proposed. Gao et al. [2020] purposed a double arrowed honeycomb (DAH) and studied its deformation under different impact velocity conditions and found that crushing strength increase with impact velocity and relative density [4]. The re-entrant structure possesses better energy absorption properties as compared to conventional hexagonal structure and also possesses anisotropic dynamic mechanical properties [5]. The honeycomb structure is considered the basic structure for such properties. As the honeycomb structure was made hierarchical with the first and second-order, the specific energy absorption increases many times as compared to the basic structure [6] thus increasing the potential in the energy absorption field. Quadri-arc honeycomb designed by Zhang et al. shows a better energy absorption efficiency than that of circular in quasi-static and low-velocity impact and relative density [7]. In-plane dynamic crushing and energy absorption characterization were also studied by Lu et al. with the different proposed structures. The result showed that the star-circle honeycomb structure's energy absorption efficiency increased as impact velocity increased as compared to star-shaped honeycomb indicating higher impact resistance [8]. When the load is applied at in-plane and out-of-plane for re-entrant samples, the in-plane is applied to provide a better impact strength and absorption of energy than another plane [9]. Till now, several reviews and works have been published. Because of the folding and rotation of cell walls, the auxetic structure's load-bearing abilities are limited [10]. Therefore, the mechanical properties enhancement became the main concern of the researchers through different structure design, material, and parametric variations. To check the mechanical response Wang et al. [11] developed the 3D cross-chiral structures. The author examines the result theoretically and also performed experiments and simulation work. The authors found that the young's modulus of the structure is also dependent on the tilt angle and the proposed design by the author showed a significant increase of approximately 8-fold this structure shows a wide range of mechanical properties stability. To check the effect of cell numbers Carneiro et al. concluded that as the cell numbers increases, the Poisson's ratio value also increases exponentially. It is also stated that to get the internal bulk behavior, the structure must contain a minimum of 13 cells per row [12].

(a) (b) (c) (d) (e)

Figure 1. Various auxetic structure (a) Hexagonal (b) Re-entrant (c) Kagome (d) diamond (e) star shaped

The present study proposes a modification in the pre-existing design for the auxetic behavior. Here, we compare existing re-entrant and modified curved re-entrant structure with varying parameters in ABAQUS to study and shows the comparison of the in-plane dynamic response.

2. NUMERICAL ANALYSIS

2.1 Model Design

In this study, the basic model was simulated and the result was studied. A modified re-entrant curved design is also proposed for the auxetic properties. The re-entrant and proposed models are shown in Fig. 2 (a) and 2 (b)

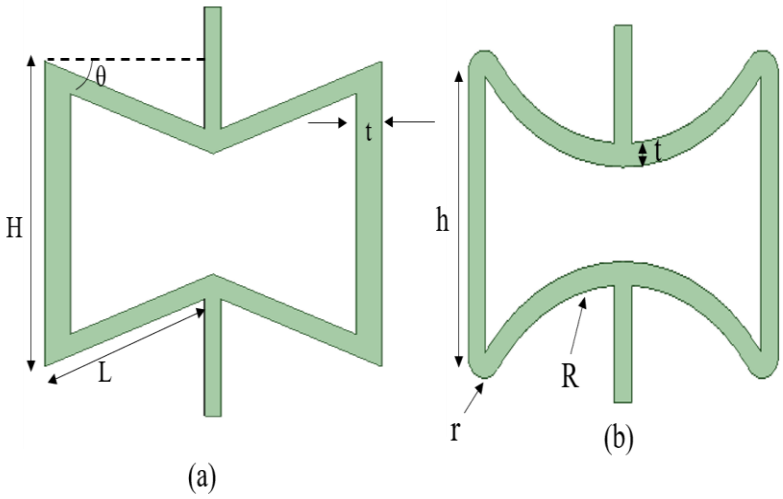

Figure 2. Unit cell of structure design (a) Re-entrant (b) Curved re-entrant

The dimension of two different structures is as follow: H and h is the height of the vertical strut of the re-entrant and curved re-entrant respectively, L is the length of the inclined strut of the re-entrant structure, θ is the angle of incidence of the inclined strut, R is the radius of curvature of the curved strut of curved re-entrant, r is the radius of curvature of corner joining vertical strut and curved re-entrant and t is the thickness of both the structures. The values of all the parameters are given in table 2. The depth of all the structures is kept at 45 mm. The three models whose analysis is studied are re-entrant unit cell structure, curved re-entrant unit cell with thicknesses 1 mm and 0.5 mm. The code given to the models is tabulated in table 1.

Table 1. Model code for different Structure

Sl. No.	Structure	Model code
1.	Re-entrant Unit cell	RS

2.	Curved re-entrant Unit cell with a thickness of 1 mm	CRS1
3.	Curved re-entrant Unit cell with a thickness of 0.5 mm	CRS2

Table 2. Dimension of the structures

Re-entrant Structure (RS)	
Parameter	Value
H	10 mm
	5 mm
θ	- 30˚
t	1 mm

Curved Re-entrant Structure (CRS)	
Parameter	Value
h	9 mm
R	5 mm
r	0.5 mm
t	CRS1 =1 mm CRS2 = 0.5mm

The proposed structure i.e., curved re-entrant was modeled and analyzed with two different thicknesses, t, that is thickness t=1mm and t=0.5 mm. The proposed models were analyzed using ABAQUS and the results are compared with the re-entrant model.

2.2. Simulation

The finite element method was done to analyze the result using ABAQUS. An explicit dynamic model was done for all the structures. The ABS thermoplastic material properties is assigned to the model which has young's modulus E_s of 2.2 GPa with Poisson's ratio of 0.35 and density of 1.05g/cm^3 [2]. The unit cell of both the structure is modeled with five unit cells horizontal such that the right vertical strut of one cell coincides with the left vertical strut of another cell and three in a vertical direction as shown in Fig. 3. In total, 23 unit cells were considered for simulation and analysis.

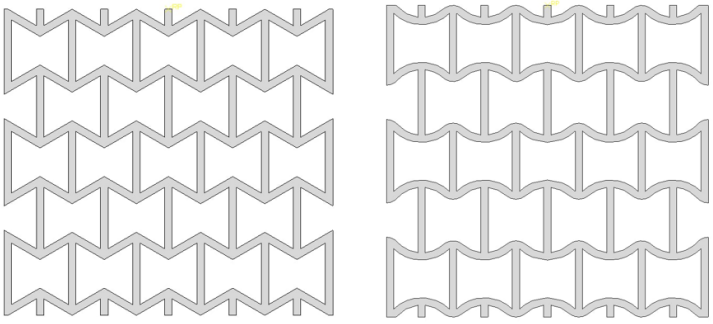

Figure 3. Model of re-entrant and curved re-entrant structure

These models are kept between two rigid plates in a sandwich style. The bottom plate was fixed restricting any movement in all directions and the top plate was given displacement only in the negative y-direction while movement in the other two directions was constrained to perform a uniaxial compression test in the y-direction. The maximum downward movement of the top plate given was 20 mm. Interaction of the upper and lower side of the structure with top and bottom plates respectively penalized with a frictional coefficient of 0.2. The depth of the structure was kept at 45 mm to avoid the buckling of the structure. The aforementioned boundary condition applied is shown in Fig. 4. S4R elements were used to mesh the model, which was swept with a quad-dominated elemental shape utilizing a free technique and linear geometric order. The element size of mesh was half the thickness of the model.

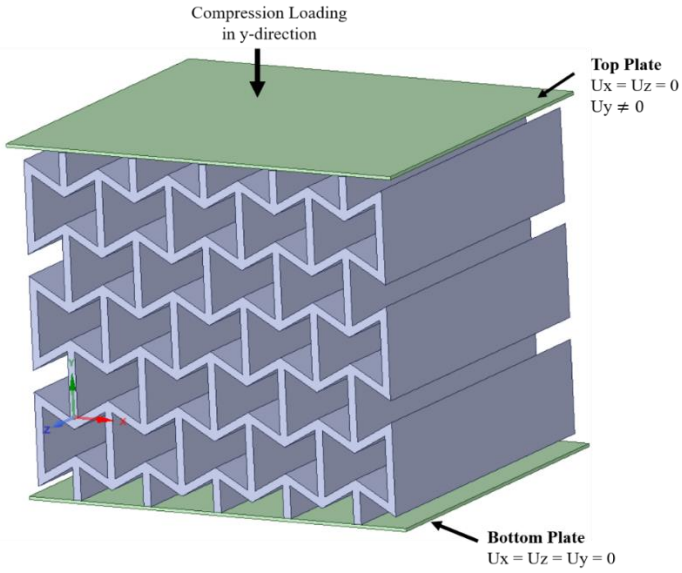

Figure 4. Boundary conditions are used in the model.

3. RESULTS AND DISCUSSIONS

The structures are crushed in the y-direction to study the mechanical properties such as stress, strain, force, and displacements of the structures. The stress-strain curve of the re-entrant structure, the curved re-entrant structure with a thickness of 1 mm, and the curved re-entrant structure with a thickness of 0.5 mm are shown in Fig. 5. The maximum stress induced in the re-entrant structure is 1.10741 MPa at a strain of 0.029056 mm/mm. The maximum stress occurred for curved re-entrant structure CRS1 (thickness 1mm) is 0.93991 MPa at a strain value of 0.03782 mm/mm whereas CRS2 (thickness 0.5mm) has the maximum stress of just 0.15029 MPa at a strain of 0.04741 mm/mm.

From the Stress-strain curve shown in Fig. 5, the stress produced in the Re-entrant structure (RS) is higher than compared to the proposed design. At a particular strain value, the maximum stress reached is more than 1 MPa whereas the curved re-entrant has a stress of less than 1 MPa. The CRS1 has a stress value much higher than that of CRS2. The

deformation of structures under compression load at different strain values is shown in Fig. 7. The deformation pattern in all three structures is same as the strain in the structure increases.

The load variation concerning the deformation displacement of all structures is shown in Fig. 6. The re-entrant-shaped structure has the maximum load applied is 2208.7 N displacing 1.2125 mm of structure in the negative y-direction. When the top plate is displaced downward in negative y-direction compressing the structure the curved re-entrant CRS1 is imposed by a maximum load of 1873.7 N at the displacement of the plate at 1.6178 mm vertically downward whereas the CRS2 suffered a maximum load of 310.6 N at plate displacement of 1.9769 mm vertically downward. The pattern of the curve shows that when the structure is compressed, at the beginning the structure is imposed with linearly increasing loads and this load continues to decrease up to a certain limit after which it again starts increasing exponentially as the structure is further compressed. The stress-strain plot of the structure also depicts that the modified curved re-entrant structure has lower toughness as compared to the base re-entrant structure for ABS material.

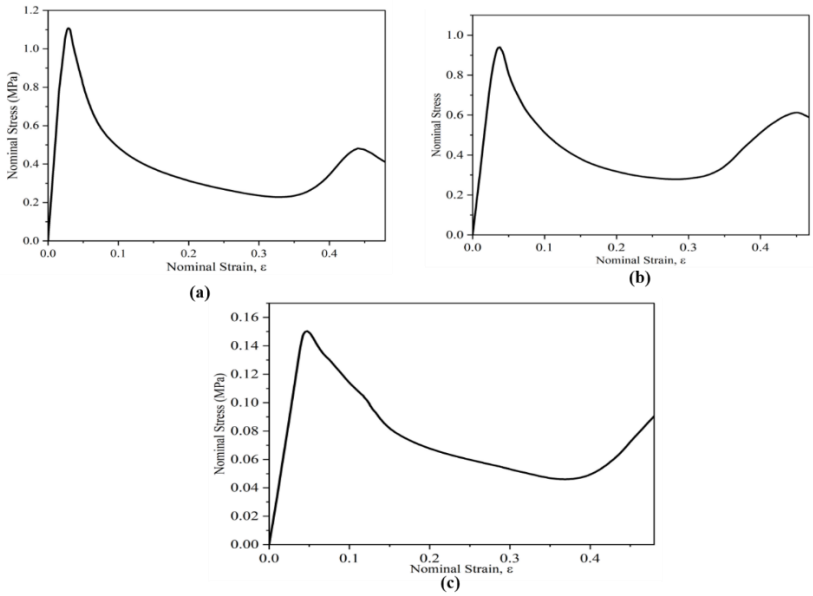

Figure 5. Stress-strain plots for (a) RS (b) CRS1 and (c) CRS2

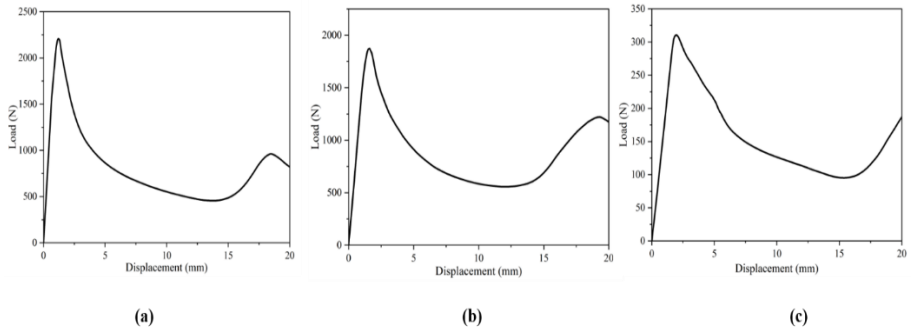

Figure 6. Load-displacement plot of (a) RS (b) CSR 1 (c) CSR 2

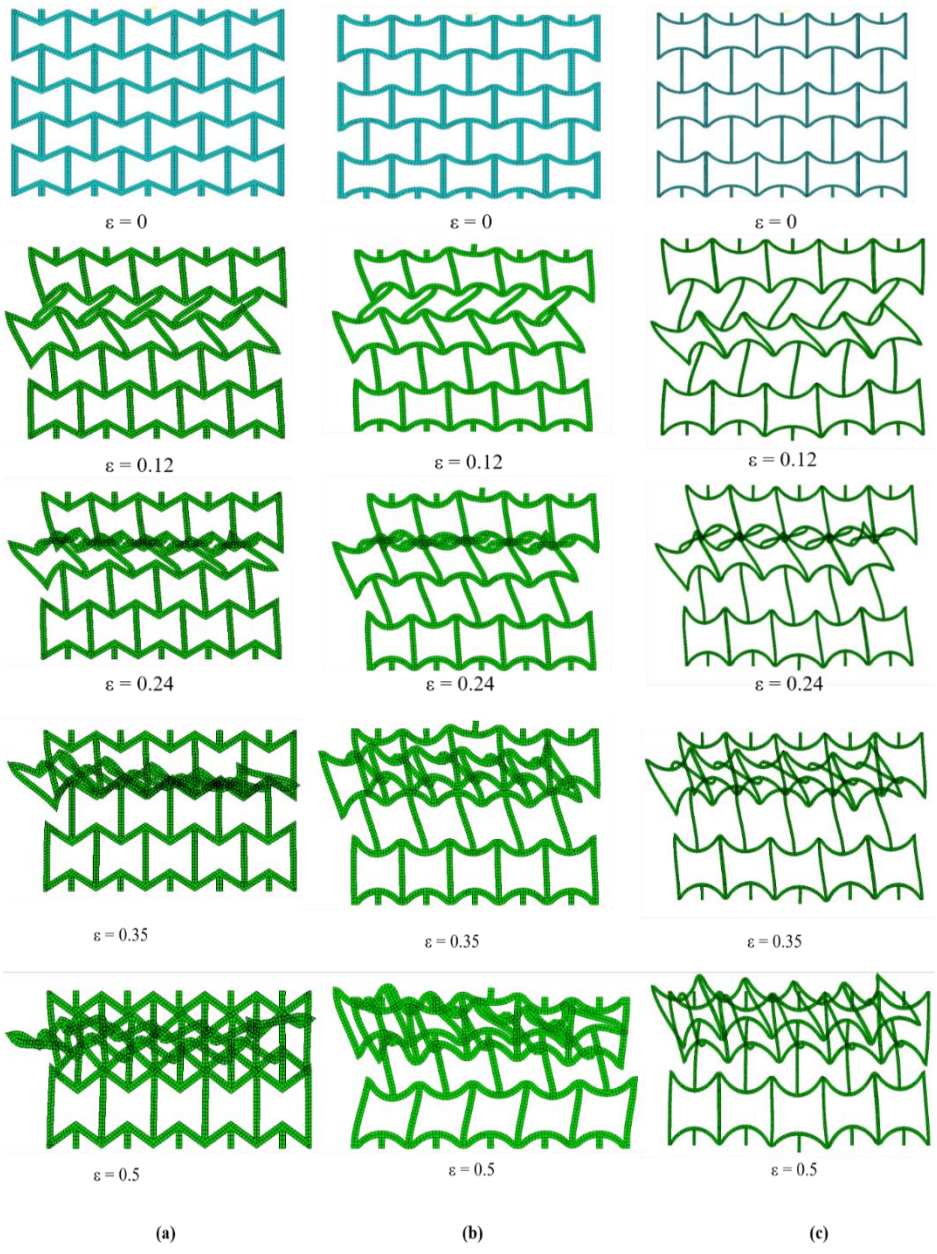

Figure 7. Deformation of shape under compression at different strain values (from ε=0 to ε=0.5) of **(a)** RS (**b)** CRS1 **(c)** CRS2

4. CONCLUSION

In this paper, investigation is done on the ABS-based curved re-entrant structure with a thickness of 1mm which is capable of bearing about 6 times more load than that of 0.5mm thick. When the thickness was doubled, the nominal stress is raised by 6 times, demonstrating that the 1mm thick structure had a larger energy absorption capacity. The modified curved structure has lower energy absorption as compared to the base re-entrant structure. Further studies will focus on improving the energy absorption property of this modified structure by varying the geometric parameters.

REFERENCES

[1] Gill, Harjot Singh. "Mechanical and structural properties of cellular auxetic materials." *Materials Today: Proceedings* 37 (2021): 3320-3323.

[2] Ingrole, Aniket, Ayou Hao, and Richard Liang. "Design and modeling of auxetic and hybrid honeycomb structures for in-plane property enhancement." *Materials & Design* 117 (2017): 72-83.

[3] Zhang, Jianjun, Guoxing Lu, and Zhong You. "Large deformation and energy absorption of additively manufactured auxetic materials and structures: A review." *Composites Part B: Engineering* 201 (2020): 108340.

[4] Gao, Qiang, Wei-Hsin Liao, and Liangmo Wang. "On the low-velocity impact responses of auxetic double arrowed honeycomb." *Aerospace Science and Technology* 98 (2020): 105698.

[5] Hou, Xiuhui, Zichen Deng, and Kai Zhang. "Dynamic crushing strength analysis of auxetic honeycombs." *Acta Mechanica Solida Sinica* 29.5 (2016): 490-501.

[6] Sun, Guangyong, et al. "Crashworthiness of vertex-based hierarchical honeycombs in out-of-plane impact." *Materials & Design* 110 (2016): 705-719.

[7] Zhang, Dahai, Qingguo Fei, and Peiwei Zhang. "In-plane dynamic crushing behavior and energy absorption of honeycombs with a novel type of multi-cells." *Thin-Walled Structures* 117 (2017): 199-210.

[8] Lu, Huan, Xiaopeng Wang, and Tianning Chen. "In-plane dynamics crushing of a combined auxetic honeycomb with negative Poisson's ratio and enhanced energy absorption." *Thin-Walled Structures* 160 (2021): 107366.

[9] Özen, İsmail, et al. "Low-energy impact response of composite sandwich panels with thermoplastic honeycomb and re-entrant cores." *Thin-Walled Structures* 156 (2020): 106989.

[10] Zhang, Jianjun, et al. "Tensile behavior of an auxetic structure: Analytical modeling and finite element analysis." *International Journal of Mechanical Sciences* 136 (2018): 143-154.

[11] Feoktistova, Natalia A., et al. "Bioactivity of catalase loaded into vaterite CaCO3 crystals via adsorption and co-synthesis." *Materials & Design* 185 (2020): 108223.

[12] Carneiro, V. H., Nuno Peixinho, and J. Meireles. "Significance of cell number on the bulk elastic properties of auxetic re-entrant lattices." *Science and Technology of Materials* 30.1 (2018): 8-12.

[13] Xu, Mengchuan, et al. "Mechanical properties and energy absorption capability of AuxHex structure under in-plane compression: Theoretical and experimental studies." *International Journal of Mechanical Sciences* 159 (2019): 43-57.

Biographies

Prabhakar Kumar received his bachelor's degree in Mechanical Engineering from O.P Jindal University, Raigarh in 2019. He is currently pursuing his master's degree in Material Science & Engineering from Motilal Nehru National Institute of Technology Allahabad, Prayagraj.

Prashant Singh received his bachelor's degree in Mechanical Engineering from GLA University, Mathura in 2017. He is currently pursuing his master's degree in Material Science and Engineering from Motilal Nehru National Institute of Technology Allahabad, Prayagraj.

Nigatu Desta Tilahun is a lecturer of Mechanical Design Engineering at Department of Mechanical Engineering, College of Engineering, Debre Berhan University. He earned his MSc degree in Mechanical Engineering from Addis Ababa Science and Technology University in 2019. He is looking research on mechanical engineering disciplines, composite materials, dynamics of machines and vibration analysis of mechanical systems.

R. Sujithra is currently working as an Assistant Professor in the Applied Mechanics Department from Motilal Nehru National Institute of Technology Allahabad, Prayagraj. She completed his Ph.D. in the Department of applied mechanics from Indian Institute of Technology Madras. Her research areas includes Smart materials, Polymers and Composites, Biomaterials, Material Modeling, Additive Manufacturing

Abhishek Kumar is currently working as an Associate Professor in the Applied Mechanics Department from Motilal Nehru National Institute of Technology Allahabad, Prayagraj. He completed his Ph.D. in the Department of Metallurgical and Materials Engineering from Indian Institute of Technology Roorkee in 2014. His research areas include design and development of microwave absorbers, synthesis and characterisation of nanomaterials, mechanical and corrosion behaviour of metals and alloys.

Review of Isogeometric Analysis based Shape Optimization Methods and Applications

Raja Sekhar Konatham and Hari Kumar Voruganti*

Department of Mechanical Engineering, National Institute of Technology Warangal, Telangana, India

rajasekhark@rguktn.ac.in, *harikumar@nitw.ac.in* *

Abstract

Shape optimization is an important technique to improve the efficiency of engineered components by achieving the optimized geometry of the component. In the optimization process, three steps are involved, namely design, analysis, and optimization. Different numerical methods can be used during the analysis stage. One of the popular numerical methods is classical Finite element analysis. This study examines how the traditional Finite element method is used to solve shape optimization problems covering structural problems, thermal problems, fluid-structure interactions, and contact problems. The key issues raised by researchers in the field of FEM based shape optimization are also examined in this study. Recently, Isogeometric analysis has evolved as a powerful tool for solving shape optimization problems. The purpose of this study is to see how successfully IGA can tackle shape optimization problems and how it performs in comparison to standard FEM. An overview of the methods based on finite element analysis and current Isogeometric analysis are discussed with their applications to shape optimization.

Keywords: Isogeometric analysis, Shape optimisation, FEM

1. INTRODUCTION AND BACKGROUND

Shape optimization is the process of designing a structure for better performance. It has been applied in a variety of domains, including structural analysis, fluid analysis, acoustics, nano-photonics, and micro-scale optimisation. The shape optimisation process relies heavily on geometric parameterization and a correct boundary description. In shape optimization, proper boundary representation and selection of design variables are essential to the success of the optimization. The coordinates of the nodes of elements are used as design variables in finite element based approaches [1]. Because of discrete representation and further changes in nodal coordinates, optimized designs are often irregular in shape thereby making the manufacturing of the design difficult [2]. Some engineering structures shapes are very complex. To represent the geometry more precisely, a very finer mesh is required, thus increasing the computational time as the number of design variables will be very high. In Iso-parametric formulation of FEM, for geometry representation and field variable, a Lagrange polynomial with c^0 continuity across the elements is used. Hence, the first order derivatives of field variable are discontinuous across the element [3, 4]. Therefore, it becomes difficult to perform a sensitivity analysis. As a result, the gradient-based optimization methods do not succeed, and the most sensitive studies are being performed

using other techniques. Using higher-order Lagrange polynomials is one of the techniques to deal with this issue [5]. However, the robustness of the method and efficiency are compromised. The drawbacks can be addresses by using a different set of basis functions such as B-spline, NURBS(Non Uniform Rational B spline), and T-spline to precisely describe the geometry and also field variable. A recent analysis approach, Isogeometric analysis (IGA) has brought a new direction to numerical analysis. This study is yielding fresh insights into shape optimization. Several researchers have focused on studies relating to the benefits of Isogeometric analysis and have achieved significant improvements. The fundamental benefit of IGA is that it uses the same NURBS basis function for representing geometry and field variable. The function variable, shape design, and analysis all share the same domain space in the context of shape optimization, making it easier to do sensitivity analysis. This reduces communication with the CAD in every phase of the optimization process, which saves time and enables faster results. Moreover, the IGA based methods results in a smooth structure. The resulting structures are manufacturable. Classical FEM boundaries are not properly captured, which leads to various inaccuracies in the final results. With splines in IGA, boundaries are captured accurately.

In this paper first, an overview of FEM-based shape optimization methods is given, followed by a discussion of the shortcomings. A brief overview of the IGA-based shape optimization is discussed in the later part. The overall paper is divided into the following sections 2) Process of shape optimisation 3) Shape optimisation using Finite element technique 4) Shape optimisation with IGA 5) Comments and future scope 6) Conclusion and discussion

2. PROCESS OF SHAPE OPTIMISATION

In general, shape optimization involves either minimizing or maximizing an objective function that is constrained in some way. Mathematically the shape optimisation equation can be written as below

$$\text{Min } C(u)$$

$$\text{Subjected to } \sigma \leq \sigma_{max}$$

where, C is the compliance, u is the design variable, $and\ \sigma_{max}$ is the max stress induced in the component. The objective could be to reduce the amount of weight or to reduce the amount of stress. Design variables are bounded with some upper and lower limits. Constraints can sometimes be either equality or inequality. In certain instances, objective functions are linear, while in others, they are nonlinear, based on the scale of complexity involved.

There are several optimization algorithms in the literature, which are divided into two types: gradient-based optimization and gradient-free optimization. Sensitivity information is required for gradient-based optimization, while it is not required for gradient-free optimization. The techniques used so far are mentioned in the next section. Figure 1 represents a flow chart to understand this shape optimisation process.

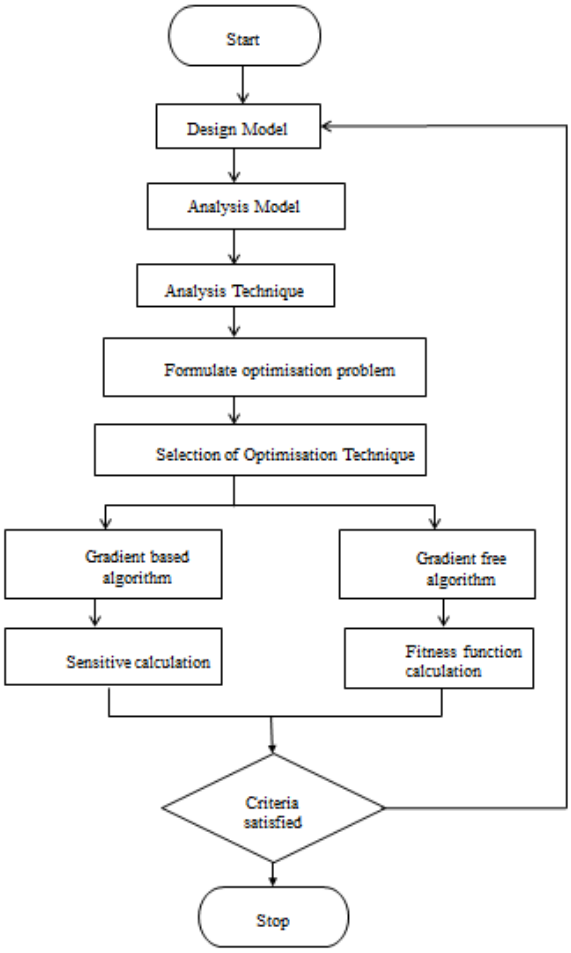

Figure 1. Shape optimisation process

3. SHAPE OPTIMISATION USING FINITE ELEMENT TECHNIQUE

The subject of structural optimization arose at the same time as finite element analysis technology. However, due to the fact that it has to undergo repetitive analysis the development of structural optimization lags behind. Several commercial analysis softwares e.g., Ansys , Abaqus, Nastran offer separate module for structural optimisation. Although the finite element technique is a well-developed numerical technique, the utility of this method in shape optimization has some issues like re-meshing of the model in each optimization phase; Geometry model and analysis model have different parameterization schemes. Following section deals with research papers focussed on fem technique especially in application to structural problems.

3.1. Finite element analysis steps

In finite element method the domain is discretised into a collection of preselected finite elements. It mainly consists of three features those are given below

- The entire domain is divided into small shapes
- Lagrange basis functions are used over each element depending on the dimension and location of nodes (Ex 1D element, Triangular element, rectangular element , Hex element)
- Assembly of elements are done by ensuring continuity of field variables across each element.

They are mainly three types of errors present in the finite element method based on above process

- Domain approximation errors occur in complex geometry where curvature are present
- Approximation error which is due to the approximation of the solution by piecewise polynomials
- Computational error occurred due to inexact evaluation of stiffness and force matrix

3.2. Applications

Several review articles [6, 7, 31] are published on FEM based shape optimisation. Hence, focus of this paper mainly on shape optimisation using IGA. Although shape optimisation is used in variety of fields like structural, fluid, and aerodynamic. This paper is focused mainly on structural optimisation.

In early shape optimisation methods based on FEM, boundary nodes of mesh are used as design variables [9]. This process offers more design options, but increases computational effort and generates an infeasible geometric shape [2]. Due to random deformation of the elements, this leads to inaccurate stresses in the final design (Figures 2 and 3).

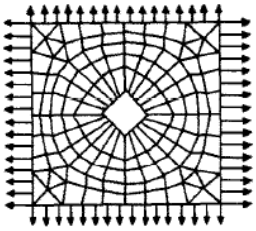

Figure 2. Initial design [2]

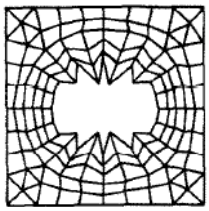

Figure 3. Final design [2]

Separation of finite element mesh and design variable could be one solution. Polynomials are also explored as an alternative to represent the boundaries [11]. The idea was to define the boundary as a linear combination of shape function with coefficients. The coefficients will act as design variable. Thus, Kristensen [5] has used linear combination of orthogonal function to represent the boundary and its coefficient are design variable. Dems [12] has solved by considering simple linear boundaries. Most approaches are restricted to solving

linear boundaries since; with higher order polynomials suffers from oscillatory behaviour. This is a well-recognized issue which necessitates a better approach for representing the boundary. This issue can be tackled by representing boundary with Splines. Splines can have high order smoothness with lower order polynomial. So it becomes another alternative for boundary representation (e.g., [5]). Yang and Choi showed that the spline representation has better sensitivity accuracy than a piecewise linear representation of the boundary. Briabant [2] has used Bezier and B-spline blending functions to describe design element boundaries. With the B-spline formulation, boundary regularity requirements are automatically taken into consideration and also an analytical formulation of the sensitivity derivatives can be established.

Shape optimization has proven to be very effective in the area of computational fluid dynamics. Chan et al [13] have enhanced the power coefficient of the wind turbine blade using shape optimisation. To improve the power coefficient, the geometry of the semi-circular blade is optimized using an evolutionary-based genetic algorithm. It is solved through the ANSYS Fluent software. Additive manufacturing may be used to manufacture the optimised blade shape. Artificial intelligence is progressing, and deep learning-based algorithms are increasingly being applied in a variety of fields. Shape optimisation is one such area. Jichao et al. [14] has verified the abnormality in aerofoil wings using a surrogate-based optimization approach. The standard neural network is first trained using 20,000 existing data and then coupled to a surrogate-based optimization framework. The algorithm produced timely and accurate findings. Ramadan et al.[15] have developed an optimised vertical axis wind turbine blade using a genetic algorithm method. FEA software, Ansys fluent is used for the CFD analysis. The power coefficient is increased about four times for the optimized blade shape and validated experimentally.

Tada et al.[16] used FEM to optimize the contact forces between two elastic bodies. Contact forces between the bodies are optimized. Butt et al.[17] developed the material derivation method for shape optimization of contact problems. Weil et al. (2001) worked on the uniform distribution of contact stresses between two- and three-dimensional elastic bodies. In this work, evolutionary techniques are used in combination with the finite element method.

In the work of Daniel Hilding et al. [18], shape optimization software was developed based on the following four blocks- namely, account analytic sensitivity analysis, adaptive finite element method, contact solver, and sequence convex programming. Ou et al. [10] focused on reducing boundary stress and contact pressure between multi-body contact systems. He has proposed a novel way that does not require sensitive studies.

3.3. Limitations of FE shape optimisation

The limitations of the numerical analysis techniques also prevent a successful structural shape optimization, as the solution accuracy and the computation time for the shape optimization strongly depend on them. Because FEM is widely used for structural analysis, the resulting framework features FEM-related difficulties such as mesh distortion and subsequent re-meshing, discontinuous stresses across element borders due to linear approximation field function, and so on. Despite its success in several domains, the FEM approach still has limitations, some of which are listed below.

1) Different basis functions used to describe geometry in design and analysis models are the crucial bottleneck in classic FEM-based shape optimization [19]
2) To reduce computational cost, it is desirable to use as few design variables as possible. But, it is not possible in FEM for accurate results.
3) Each iteration of the optimization process necessitates back-and-forth communication with CAD. As a result, it takes a long time to compute.
4) Sensitive analysis needs to carry out in gradient-based optimisation methods and it is difficult with classical FEM.
5) Traditional FEM has discontinuous stresses across the elements because it approximates linear interpolation for design variables. The first derivative of stresses concerning the design variable is necessary for sensitive analysis. So higher-order representation of the field variable is required.
6) In FEM-based form optimization, a wavy or uneven shape will emerge, which is unsuitable for manufacturing.

4. SHAPE OPTIMISATION WITH IGA

Many commercial software packages employ an Iso-parametric formulation in their FEM code, which means that the field variable and geometry descriptions share the same basis. Those are Lagrange basis with c^0 continuity. NURBS are used in CAD modelling software to describe geometry. IGA approach uses the same NURBS basis function for the filed variable also. This new concept has opened the opportunity for a better type of analysis known as Isogeometric analysis. They have successfully implemented these new improvements in a variety of fields. Those publications that employed IGA shape optimization are discussed in the following section.

4.1. Isogeoemtric analysis steps

CAD geometry is represented using NURBS from past two decades because of their inherent properties. In Isoparametric FEM the field variable is discretised first and then the same basis discretisation is used for domain. In IGA the domain is discretised by NURBS and same is used for field variable.

In B-spline curve is represented with a set of basis function combines n+1 control points.

$$\text{P(u)}=\sum_{i=0}^{n} P_i \quad N_{i,k}(u)$$

Where k is the order of B-spline and k-1 is the degree of the B-spline. It is independent of number of control points

The NURBS are recursively defined by the following

$$N_{i,1}(u)= 1 \quad \text{if } t_i \leq u \leq t_{i+1}$$

$$=0 \quad \text{otherwise}$$

and

$$N_{i,k}(u) = \frac{(u - t_i)N_{i,k-1}(u)}{t_{i+k-1} - t_i} + \frac{(t_{i+k} - u)N_{i+k,k-1}(u)}{t_{i+k} - t_{i-1}}$$

k value ranges from 2,…,k where k is the order of the B-spline and controls the degree (k-1) of the resulting polynomial in u and also controls the continuity of the curve.. The t_i are called knot values, and set of knot values comprise a knot vector. They relate the parametric variable u to the P_i control points where i=0,…,n. For an open uniform curve the t_i are calculated once using k:

$$t_j = 0 \quad \text{if} \quad j<k$$

$$t_j = j-k+1 \quad \text{if} \quad k \leq j \leq n$$

$$t_j = n+k+2 \quad \text{if} \quad i>n$$

Using above knot values the basis functions can be generated. B spline surface is generates using tensor product of bi-variant and Tri-variant B splines. Third order and fourth order B-spline curves generated using MATLAB code are shown below

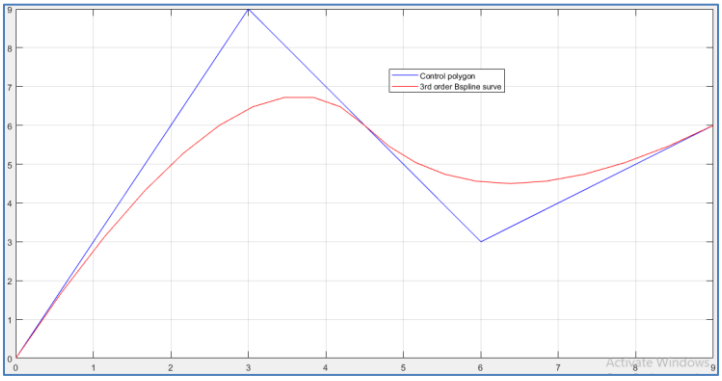

Figure 4. Third order B-spline with four control points

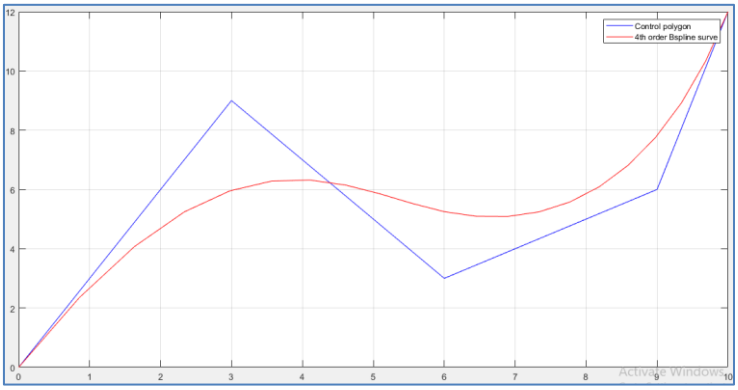

Figure 5. Fourth order B-spline with five control points

4.2. Applications

Due to its precise shape representation, NURBS-based geometry representation analysis has become increasingly popular in shape optimization applications in recent years. Because the approach uses a higher-order foundation, sensitive studies are simple to perform. Wall et

al.[20] worked on shape optimization of structures with IGA. The effectiveness of linking the design and analysis model is intensified. Simple 2D problems like a plate with a hole and wrench are solved using NURBS. The sensitive analysis is performed using a gradient-based optimization method. The majority of studies have used NURBS control points as a decision variable in their sensitivity analysis. For the sensitivity analysis, Qian et al. [27] employed both control points and weights. In his study, he used a gradient-based optimization approach. According to this approach, weights and control points as design variables help achieve optimal shapes.

Another area of application is the optimization of shell structures. Boilers, roof structures, and the automotive and aerospace industries use shells. In all these cases, optimizing the shell structure is very important. Keindl et al. [22] has pointed out that when representing geometry using splines, the rotational degree of freedom need not be a field variable due to their higher-order continuity. In addition, the flow structure of the rotor blade interaction of the wind turbine is optimized. It is mentioned that the flexibility of this IGA-based representation has many advantages and reduces the computational time. The 2D plate and shell problems are optimised using Iso-geometric analysis in the work of Yudeok Seo et al. [23]. The optimization of vibrating membranes with IGA is performed by Nguyen et al [24]. Two methods, namely the quasi-conformal mapping and the spring-based mesh method, are proposed to map the boundary of the domain to its interior. IGA goes well with shape optimization of vibration problems. The IGA has also been used for topology optimisation using the trimming technique. For topology optimization, trimmed surface analysis is used, which was recently proposed to analyse any complex topology problem. Some benchmark problems are solved in shape and topology optimisation. Li et al. [25] have studied shape optimisation using the Iso-geometric boundary integral method. The author has performed an h-p-k refinement and concluded that the NURBS technique offers better performance. The sensitive analysis can be done either with NURBS control points or its weights. In shape optimization, a sensitivity analysis is much more important to see how sensitive the objective functions are to design variables. Hassani et al. [26] have solved two and three-dimensional simple problems using the NURBS basis function and obtained a very smooth optimised surface. The boundary variable and field variable are approximated with NURBS basis in the Iso-geometric boundary integral method.

Xiaoping Qian et al. [21] has used multi patch coons to generate the complex geometry. It allows to user to design boundary shapes without specifying the internal control points. The specification of internal nodes can be avoided in this process. It is applied to maximise the band gap in photo crystal design. The internal nodal data is embedded in the NURBS formulation itself. Analytical and semi-analytical techniques have been used for performing sensitivity analysis.

An optimised location quadrature point has been proposed by Zhen Lei et al. [28], which addresses the locking issue in shell formulation. A mixed grid Reissner-Mindlin shell formulation is used in this work. The classic modal synthesis method and the Craig-Brampton fixed interface method are used for shell-patch coupling. The analysis time decreases more in the modal synthesis method. Ummidivarapu et al. [29] has optimized the acoustic horn with TLBO (Teaching Learning-based algorithm). The acoustic field is modelled and analysed in the IGA framework. The optimal shape of the horn speaker has resulted in reduced back reflection. This IGA analysis has shown significant improvement

and surpassed the FEM results. The shape of the horn is also easy to manufacture. Recently, Qin et al. [31] worked on the shape and material optimization of functionally graded material (FGM). MMA method and SQP are used for shape and material optimization respectively. The optimal shape of the stiffener is obtained to minimize the flexibility of the plate subjected to a volume constraint.

Ummidivarupu et al. [32] has used IGA on cantilever beams and square plates with a circular hole to achieve an optimal area under a given load condition. Genetic algorithm and Nelder and Mead simplex algorithm were used to solve the problems. Lopez et al. [4] performed an automated sensitive analysis using a differential toolbox. Automatic differentiation can be used to perform a forward and reverse mode sensitive analysis. This AD (automatic differentiation) is far superior to analytical and semi-analytical sensitive techniques, as demonstrated by the practical application.

The analysis of shells required a curvilinear representation of the surface. IGA and NURBS are very suitable for shell analysis, as they reproduce the geometry very smoothly. Hirschler et al. [34] optimized the shape of solid shell and Kirchhoff Love Shells. The author observed that both methods gave similar results. The size and shape optimisation are integrated by the author and applied to the cylinder.

The majority of engineering components are subjected to thermal conditions. As a result, one of the most important areas to focus on is heat exchange. Components are optimised either to increase or decrease the heat exchange. The shape and material selection plays a key role in efficient performance. Wang et al. [28] have worked on optimised shapes subjected to steady-state heat conduction. Active control of heat is not feasible in fluctuating thermal conditions. Shape optimization is a more effective method that acts as a passive control for thermal conditions.

Any machine consists of more elements under relative motion. Because of their relative motion, engineering components are prone to wear. Engineers are always concerned with wear and stress distribution between contact surfaces. Shape optimization can be applied to control these parameters. The contact problems are nonlinear since the point before contact is unknown. These boundary conditions are nonlinear. It is difficult to perform a sensitivity analysis using a gradient-based method since most contact equations are non-differentiable. So gradient-free optimisation techniques are adopted by most cases in contact problems.

Li w et al. [35] solved the optimal distance between contact bodies to limit the contact stress between multi-body systems. An evolutionary optimization method is used to solve the problem. In this multiple contact problems are solved by adopting individual criteria and the unified criteria method. Nam Ho Kim et al. [36] used a material-derivative approach for sensitive analysis of the three-dimensional contact problem. Mesh-free methods are used to solve the design sensitivity equation. Not much of the work is reported on shape optimization with IGA for contact problems.

4.3. Comments and future scope

Iso-geometric analysis can be more potential in shape optimisation problems, shell structure analysis. The domain discretisation error present in FEM can be avoided in Iso geometric analysis. Contact problems is another important where it require to represent the geometry exactly. Recently Functionally graded materials (FGM) have been analysing for estimating

the strength and stability. FGM requires higher order basis for better analysis. In these problems IGA make the process more robust and computationally more efficient.

5. CONCLUSION AND DISCUSSION

The structural shape optimisation topic is widespread. It is difficult to describe all of the interesting aspects in one paper. An attempt is made to review of literature related to shape optimisation. The scope of the present article is restricted to only FEM and IGA based shape optimisation. One particular advantage of IGA is using the same basis for analysis and design models. The researchers have focussed on thermal, structural, fluid-structure interaction, and contact problems. Due to its attractive features, IGA is expected accelerate the shape optimization research further. In brief, the advantages of IGA-SO are listed below.

- complex geometry can be represented accurately
- Analysis and geometry model share the same basis.
- Number of design variables are less in IGA based shape optimization
- Stresses are continuous across the elements so sensitive analysis is easy.
- CAD and analysis communication can be avoided
- Re-meshing tasks can be avoided in every iteration process

REFERENCES

[1] Zienkiewicz OC, C. J. (1973). Shape optimisation and sequential linear programming. 109-26.

[2] Braibant V, F. C. (1983). Shape optimal design: An approach matching CAD and optimisation concept. Belgium: Aerospace Laboratory of the university of Liege.

[3] Lacroix D, B. P. (2003). Improved sesitive analysis by a coupled FE-EFG Method. *Computer structure, 81*, 2431-9

[4] Lopez Jorge, A. c. (2021). Isogeometric structural shape optimisatoin using automatic sensitivity analysis. *Applied mathematical modelling,89,1004-1024*.

[5] K S Kristensen, N. F. (1976). On the optimum shape of fillets in plates subjected to multiple in-plane loading case. *International Journal Numerical methods Engineering, 10*, 1007-1009.

[6] Bhavik D Upadhyay, S. S. (2021). Numerical analysis perspective in structural shape optimisation: A review post 2000. *Advances in engineering software*.

[7] Haftka RT, G. R. (1986). Structural shape optimisaiton : a survey. *Computationla methods applied Mechanical engineering, 57(1)*, 91-106.

[8] Vinay K Ummidivarapu, H. K. (2019). Isogeometric Boundary Element Method for analysis and design optimisation- A survey. In K. S. D Srinivasacharya, *Numerical Heat transfer and fluid flow,Lecture Notes in Mechanical Engineering* . Springer.

[9] Yukio Tada, S. N. (1993). Optimum shape design of contact surface with finite element method. *Advances in Engineering software*, 75-85.

[10] H Ou, B. L. (2013). A direct shape optimisation approach for contact problems with boundary stress concentration. *Journal of mechanical science and technology, 27(9)*, 2751-2759.

[11] P Pederson, C. L. (1983). Design for minimum stress concentrtion by finite elements and linera programming. *Jounrla of structural Mechanics, 10(4)*, 375-391.

[12] Dems, K. (1980). Multiparameter shape optimisation of elastic bars in torsion. *International Journal of Numerical Methods*, 1517-1539

[13] C M Chan, H. B. (2018). Blade shape optimization of the Savonius wind turbine using a genetic algorithm. *Applied energy*.

[14] Jichao Li, M. Z. (2020). Effieceint Aerodynamic shape optimisaiton with Deep learning based geometric filtering. *American Institute of Aeronautics and Astrobnautics Inc*.

[15] Ramadan A, Y. k. (2018). Shape Optimization and Experimental Validation of a Drag Vertical Axis Wind Turbine. *Energy* .

[16] Yukio Tada, S. N. (1993). Optimum shape design of contact surface with finite element method. *Advances in engineering software*, 75-85.

[17] R Butt, J. E. (1992). Optimal shape design for a fricitonless contact problem. *Journal of computational and applied mathematics*, 1-17.

[18] Daniel Hilding, B. T. (2001). A computational methodology for shape optimisation of structures in frictionless contact. *Computational method applied mechanical engineering*, 4043-4-60.

[19] Schramm U, P. W. (1993). Coupling of geometric description and finite element using NURBS a study in hsape optimisation. *Finite Elem Anal Des*, 11-34.

[20] Wolfgang A Wall, M. A. (2008). Isogeometric structural shape optimisation. *Computational Methods Applied Mechanical Engineering*, 2976-2988.

[21] Xiaoping Qian, O. s. (2011). Isogeometric shape optimisaiot of photonic crystal via coons patch . *Computational methods applied mechanical Engg*, 2237-2255.

[22] Keindl, J. M. (2010). Isogeometric analysis and shape optimal design of shell structures. *Thesis*.

[23] Yu Deok Seo, H. J. (2010). shape optimisation and its extension to topological design based on isogeomtric anlaysis. *International journal of solids and structures* , 1618-1640.

[24] Nguyen Dang Manh, A. E. (2011). Isogeometric shape optimisaiotn of vibrating membranes. *Computational method applied mechanical engineering* , 1343-1353.

[25] Kang Li, X. Q. (2011). Isogeometric analysis and shape optimisation via boundary integral. *Computer Aided Design*, 1427-1437.

[26] B Hassani, S. M. (2011). Application of isogeometric analysis in structural shape optimisation. *Scientia Iranica A*, 846-852.

[27] Qian, X. (2010). Full analytical sensitivities in NURBS based isogeometric shape optimization. *Computational methos in Applied mechancis and Engineeering* , 2059-2071.

[28] Zhen Poe Wang, S. T. (2017). Shape optimisation and optimal control for transient heat conduction problems using as isogeometric approach. *Computers and strucutres*, 59-74.

[29] Vinay K Ummmidivarapu, H. K. (2020). Isogeometric shape optimisation of an acoustic horn using teaching learning based optimisation(TLBO) algorithm. *Computer aided geometric design*, 101881.

[30] X C Qin, C. Y. (2021). NURBS based isogeometric shape and material optimisation of curvilinearly stiffened plates with FGMs. *Thin walled structures*, 162.

[31] Vinay K Ummidivarapu, H. K. (2019). Isogeometric Boundary Element Method for analysis and design optimisation- A survey. In K. S. D Srinivasacharya, *Numerical Heat transfer and fluid flow,Lecture Notes in Mechanical Engineering* . Springer.

[32] Vinay K Ummidivarupu, H. K. (2017). Shape optimisation of two dimensional structures using IGA. *International Journal Engineering systems modelling and simulations, 9*(3).

[33] Lopez Jorge, A. c. (2019). Isogeometric structural shape optimisatoin using automatic sensitivity analysis. *Applied mathematical modelling*.

[34] T Hirschler, R. B. (2018). Isogeoemetric sizing and shape optimisation of thin structures with solid shell approach. *Hal open science*.

[35] W Li, Q. L. (2003). An evolutionary shape optimisation procedure for contact problems in mechanical design. *Part C: Journal of mechanical engineering sciences*.

[36] Nam Ho Kim, K. Y. (2002). A material derivative approach in design sesnitivity analysis of three dimensional contact problems. *International Journal of solids and structures, 39*, 2087-2108.

[37] Sachi D Daxini, J. M. (2017). Parametric shape optimisaiton techniques based on meshless methods: A review. *Structural multidisp optimisation*.

[38] R J Yang, K. K. (1985). Accuracy of finite element based shape design sensitivity analysis. *ASCE Journal structural Mech, 13(2)*, 223-239.

[39] Nafia A R, S. M. (2017). Shape optimisation using a NURBS based interface enriched generalized FEM. *International Journal Numerical Methods Engineering, 111(10)*, 927-54.

[40] A ramadan, K. Y. (2018). Shape optimisation and experimental validation of a drag vertical axis wind turbine. *Energy*

[41] M Weck, P. S. (1983/84). An efficient technique in shape optimisation. *Journal of structural mech*, 433-449.

Biographies

Hari Kumar Voruganti received the bachelor's degree in mechanical engineering from Kakatiya Institute of Technology & Science, Warangal in 2001, the master's degree in mechanical engineering from Osmania University in 2003, the philosophy of doctorate degree in the centre for robotics, Mechanical Engineering from Indian Institute of Technology, Kanpur in 2009. He is currently working as an Associate Professor at the Department of Mechanical Engineering, National Institute of Technology, Warangal. His research areas include robotic kinematics, motion planning and applied optimization, finite element/isogeometric analysis, geometry modelling for CAD. He has been serving as a reviewer for many highly-respected journals.

Raja Sekhar K is a PhD student at the National Institute of Technology Warangal, India. He completed his M.Tech from IIT Delhi with machine design as specialisation. His areas of interest are shape optimisation, and isogeometric analysis(IGA).

An Investigation into Carbon/Epoxy Composites for Conceptual Design of Automobile Vehicle Under Various Loads

Abdul Rehman*, G. S. Lathkar

MGM College of Engineering Nanded, India

**rehman_ai@mgmcen.ac.in*

Abstract

In this study the finite element analysis of CFRP square beam, which is used for chassis have been studied using bending and torsion loading cases. Total 8 sequences have been studied using ANSYS software. According to the Tsai–Wu failure theory and the results of reserve factor (strength to stress ratios) the fiber direction and stacking sequence design for square section beam have been discussed. Based on the finite element analysis it is observed that the stacking sequences [0/90/45/-45]s , [-45/45/0/90]s and [90/0/0/90]s are the better for the composite structural members of a vehicle.

Keywords. Carbon fiber reinforced polymer, stacking sequence, finite element analysis, automotive, lightweight Design.

1. INTRODUCTION

Composite material consists of fibre and matrix materials which are used in automotive industries because of its high strength to weight ratio, high impact strength, and low density and flexible in the design. Understanding the structural behaviour of composite materials with the complicated geometrical profiles under various loading situations is a challenging task. Different FEA software like ANSYS, ABAQUS, NASTRAN etc predicts the behaviour of the structure efficiently in terms of stresses and deformations. Finite element analysis is very challenging when designing an anisotropic material like carbon-glass fibre reinforced members which is used for a vehicle [1-6.

Many researchers have made attempts to understand the structural behaviour of composites, using FEA software and to replace the existing metallic automotive components with Fiber Reinforced Plastic (FRP) composites [1-10]. Finite element analysis predicted well the stress distribution and failure stress of the critical regions observed during experimental tests. Composite monocoque chassis analysed using finite element analysis on the geometry and laminate lay-ups of a chassis [1]. Optimal stacking sequence determined according to the maximum stress theory and the results of strength to stress ratios [2]. Finite element analysis of simplified part samples have been carried out under various loads. By calibrating the test sample at the coupon and element level, it is possible to predict the structural response at a higher structural level [3]. The damage behaviour of an aluminium–composite hybrid beam under three point bending loading was investigated by a finite element analysis [4]. Different

various designs of glass carbon thermoplastic (GCMT) were discussed using FEA [5]. Stacking sequence of the automotive composite lower arm using carbon-epoxy was optimized using micro-genetic algorithm [8]. Development of CFRP lightweight structure for electric vehicles carried out. The multi-scale analysis approach proposed is generic and can be used for other lightweight vehicle structure made of composites [9]. The effect of stacking sequence and fiber orientation angle on the performance of drive shaft was investigated numerically [10].

Objective of this present study is the FEA of hollow beam with different stacking sequence, under the bending and torsional loads. In this paper ANSYS composite pre-post tool is used for composite analysis. Reserve Factor (RF) has been determined based on Tsai-Wu failure criteria for all eight different stacking sequences.

2. MATERIALS AND DESIGN

In this study unidirectional carbon-epoxy composite material has been used. Material properties of these composite is given in Table 1. Carbon-epoxy composite material consists of two parts: a matrix and reinforcement. In carbon-epoxy composite material the reinforcement is carbon fiber, which provides its strength. The matrix is epoxy a polymer resin, which binds the reinforcements together. Carbon-epoxy composite material consists of two distinct elements, the material properties depend on these two elements. Figure 1 shows the material co-ordinates system.

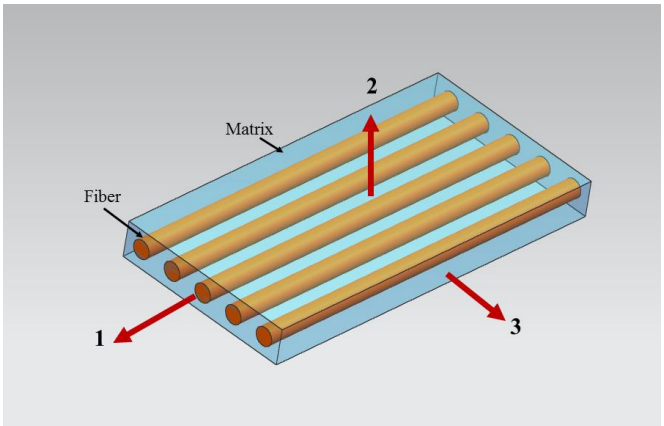

Figure 1. Material coordinate system for hollow square beam (1, 2, 3)

Four different fiber directions have been selected based on reference, which are 0º, +45º, -45º, and 90º [2]. Total 8 layers of each thickness 0.64 mm with total thickness 5.12mm are used for FEA.

Table. 1. Material properties of carbon-epoxy composite [11]

Property	Value	Unit
E1	1.21x105	Mpa
E2	8600	Mpa

E3	8600	Mpa
Density	1.49x10-6	Kg/mm3
G12	4700	Mpa
G23	3100	Mpa
G13	4700	Mpa
µ12	0.27	
µ23	0.4	
µ13	0.27	

Axis of the beam (X axis of structure coordinate system) is taken as a reference direction for stacking up as shown in Figure 2. Total 8 different stacking sequences considered in FEA are given in Table 2.

Table 2. Stacking sequence

Sample	Stacking sequence
1	[00/00/00/00]s
2	[00/90/45/-45]s
3	[-45/45/90/00]s
4	[-45/45/00/90]s
5	[00/90/90/00]s
6	[90/00/00/90]s
7	[90/90/90/90]s
8	[45/45/45/45]s

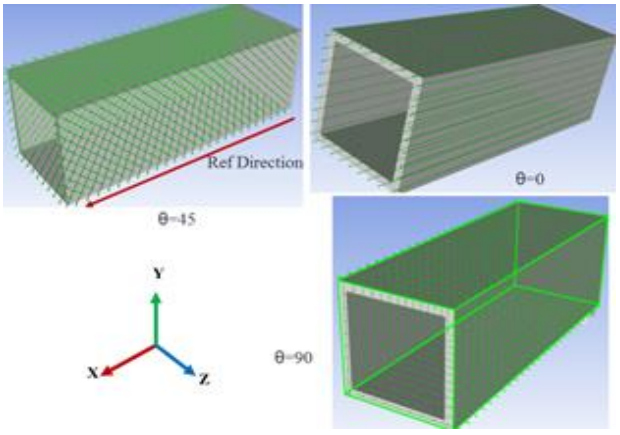

Figure 2. Structure Coordinate system (X, Y, Z)

3. FAILURE CRITERIA

In this study, the Tsai-Wu failure theory is used [9]. This criterion implies the quadratic equation to express a failure envelope surface, which attempts to fit experimental values. It accounts for the stress interaction but does not predict the specific failure mode.

$$f = \frac{\sigma_1^2}{X_t X_c} + \frac{\sigma_2^2}{Y_t Y_c} + \frac{\sigma_3^2}{Z_t Z_c} + \frac{\tau_{12}^2}{S_{xy}^2} + \frac{\tau_{13}^2}{S_{xz}^2} + \frac{\tau_{23}^2}{S_{yz}^2} - 0.5\frac{\sigma_1\sigma_2}{\sqrt{X_t X_c Y_t Y_c}} - 0.5\frac{\sigma_2\sigma_3}{\sqrt{Y_t Y_c Z_t Z_c}} - 0.5\frac{\sigma_1\sigma_3}{\sqrt{X_t X_c Z_t Z_c}} + \sigma_1\left(\frac{1}{X_t} - \frac{1}{X_c}\right) + \sigma_2\left(\frac{1}{Y_t} - \frac{1}{Y_c}\right) + \sigma_3\left(\frac{1}{Z_t} - \frac{1}{Z_c}\right)$$

Reserve Factor = Ultimate Strength/Ultimate Load

Failure RF ≤1

Safe RF ≥1

4. FINITE ELEMENT MODEL

A square hollow beam is selected for the analysis. The meshing of the beam is shown in Figure 3- 4 with total number of 936 SHELL elements and 972 Nodes. For determining the performance of the beam under bending, 3 point bend virtual test is carried out by applying a central static load of 40 KN, which leads to a maximum bending moment of 1700 Nm as shown in Figure 3. For determining the performance of the beam under torsional loading, a twisting moment of 1.7KN-m is applied at the one end, while the other end is fixed as shown in Figure 4.

For bending as well as for torsional loading (other parameters constant) the stacking sequence has been changed. The Reserve Factor (RF) is calculated as per Tsai-Wu failure theory, the maximum deflection is also determined for each sample.

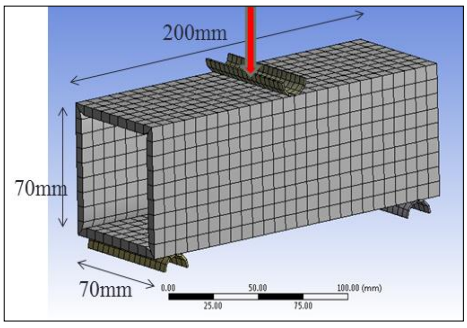

Figure 3. 3 point bend test

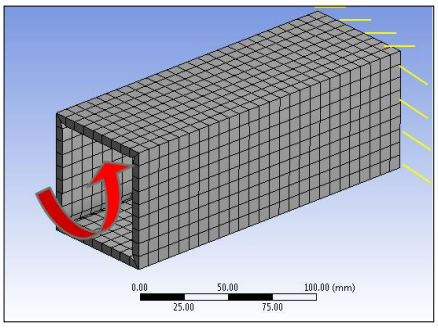

Figure 4. Torsion test

5. RESULT AND DISCUSSION

Results of deflection of the beam with [0/0/0/0] stacking sequence in bending is shown in Figure 5 and deformation with [90/0/0/90] stacking sequence in twisting respectively is shown in Figure 6. Table 3 and 4 list all values of RF, deflection and angle of twist for 8 samples under the bending and torsional loading.

Table 3. Point Bend Test Results

Sample	Stacking sequence	Reserve factor bending	Max Deflection (mm)
6	[90/00/00/90]s	0.693	0.795
2	[00/90/45/-45]s	0.651	0.470
5	[00/90/90/00]s	0.544	0.798
4	[-45/45/00/90]s	0.524	0.486
3	[-45/45/90/00]s	0.467	0.488
7	[90/90/90/90]s	0.417	1.172
8	[45/45/45/45]s	0.346	1.041
1	[00/00/00/00]s	0.230	1.170

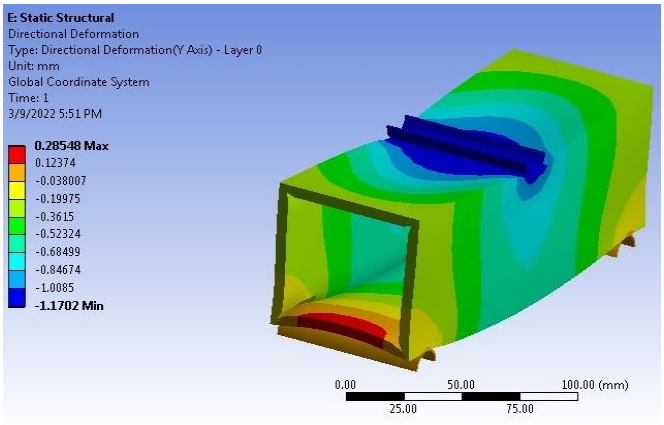

Figure 5. Deflection of the beam for [00/00/00/00] stacking sequence in Bending.

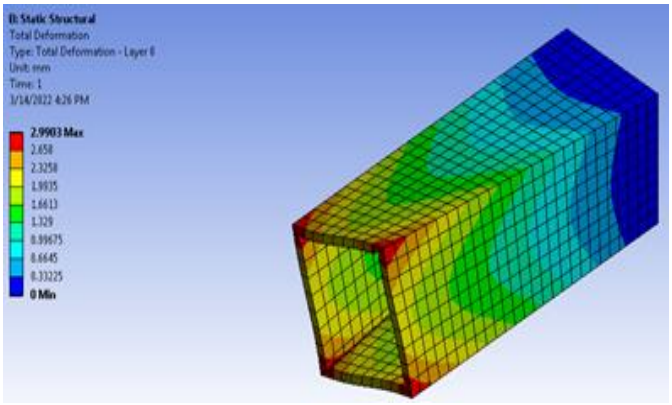

Figure 6. Deformation of the beam for [90/00/00/90] stacking sequence in twisting

Table 4. Torsion test results

Sample	Stacking sequence	Reserve factor torsion	Angle of twist (Deg)
4	[-45/45/00/90]s	0.5988	1.00
8	[45/45/45/45]s	0.5827	1.02
6	[90/00/00/90]s	0.5467	1.72
2	[0/90/45/-45]s	0.5424	1.11
7	[90/90/90/90]s	0.4433	1.75
3	[-45/45/90/00]s	0.4274	0.99
5	[00/90/90/00]s	0.4236	3.41
1	[00/00/00/00]s	0.2827	3.44

The structural members of a vehicle can be subjected to various loads, the best stacking sequence for both the test can be predicted based on above results. In bending [90/00/00/90]s stacking sequence has the highest value of RF which is 0.6934, whereas [00/00/00/00]s stacking sequence has the lowest value of RF 0.2302. In torsion [-45/45/00/90]s stacking sequence has the highest value of RF which is 0.5988 whereas [00/00/00/00]s stacking sequence has the lowest value of RF which is 0.2827. Hence stacking sequences [0/90/45/-45]s, [-45/45/00/90]s and [90/00/00/90]s are the better designs in bending as well as torsion. It is also observed that the unidirectional laminates, i.e. [00/00/00/00]s, [90/90/90/90]s, and [45/45/45/45]s, are the poor designs.

Under three point bending, the deflection of [00/90/45/-45]s stacking sequence is lowest, where as[90/00/00/90]s stacking sequence is at highest. In torsion [-45/45/90/00]s stacking sequence is having minimum angle of twist, while [00/00/00/00]s stacking sequence is having maximum angle twist. Considering all three parameters i.e. RF, deflection and angle of twist in all eight cases the [-45/45/00/90]s is the optimum stacking sequence.

6. CONCLUSION

In this study the finite element analysis of square beam have been carried out with bending and torsional loading. The finite element analysis results comparison showed that the stacking sequences [00/90/45/-45]s, [-45/45/00/90]s and [90/00/0/90]s are the better designs for the composite structural members of a vehicle. Unidirectional laminates, i.e. [00/00/00/00]s, [90/90/90/90]s, and [45/45/45/45]s, are the poor designs which are not recommended for designing. Finally it is concluded that [-45/45/00/90]s is the optimum stacking sequence for bending and torsional loads.

REFERENCES

[1] Denny J, Veale K, Adali S, Leverone F. Conceptual design and numerical validation of a composite monocoque solar passenger vehicle chassis. Engineering science and technology, 2018 Oct 1;21(5):1067-77.

[2] Liu, Thomas Jin-Chee, and Huang-Chieh Wu. Fiber direction and stacking sequence design for bicycle frame made of carbon/epoxy composite laminate. Materials & Design 31, no. 4 (2010): 1971-1980.

[3] Krishnamoorthy, Sivakumara Kannappan and Höptner, Johannes and Kopp, Gundolf and Friedrich, Horst E. (2011) *Prediction of structural response of FRP composites for conceptual design of vehicles under impact loading.* 8th European LS-DYNA Conference, 23-24. 2011, Frankreich.

[4] H.C. Kim, D. K. Shin, J.G. Kim, K.C. Shin, J.J. Lee. Damage analysis of aluminum / cfrp hybrid beam Under three point bending.19th International Conference on Composite Materials July 28 to August 2, 2013 Montréal, Canada.

[5] Kim, Do-Hyoung, Hyun-Gyung Kim, and Hak-Sung Kim. "Design optimization and manufacture of hybrid glass/carbon fiber reinforced composite bumper beam for automobile vehicle." Composite Structures 131 (2015): 742-752.

[6] Koricho, Ermias Gebrekidan, and Giovanni Belingardi. "An experimental and finite element study of the transverse bending behavior of CFRP composite T-joints in vehicle structures." Composites Part B: Engineering 79 (2015): 430-443.

[7] Murray, Robynne & Doman, Darrel &Pegg, Michael. (2015). Finite element modeling and effects of material uncertainties in a composite laminate with bend–twist coupling. Composite Structures. 121. 362-376. 10.1016/j.compstruct.2014.11.035

[8] Do-Hyoung Kim Dong-Hoon Choi Hak-Sung Kim. Design optimization of a carbon fiber reinforced composite automotive lower arm. Composites Part B: EngineeringVolume 58, March 2014, Pages 400-407.

[9] Qiang Liu ,, Yongzhou Lin , ZhijianZong , Guangyong Sun , Qing Li. Lightweight design of carbon twill weave fabric composite body structure for electric vehicle. Composite Structures 97 (2013) 231–238

[10] M.A. Badie, E. Mahdi, A. M. S. Hamouda. An investigation into hybrid carbon/glass fiber reinforced epoxy composite automotive drive shaft. Materials and Design 32 (2011) 1485–1500.

[11] ANSYS Composite Prep-Post User's Guide, [Online] Available: https://dlscrib.com/download/ansys-composite-preppost-users-guide_5a0b7960e2b6f5c2218c3cf6_pdf

Influence of Copper Slag, Rice husk ash mixed with Alkali Activator for Pavement Construction

[1]Kunal Jee Thakur, [2]Arvind Kumar, [3]Kuldeep Sharma[3]

[1,2,3] Department of Civil Engineering, Dr. B. R. Ambedkar NIT Jalandhar, Punjab, India

[1]kunaljee111@gmail.com, [2]agnihotriak@nitj.ac.in, [3]kuldeepsha333@gmail.com

Abstract

The demand for ecologically friendly and long-lasting building materials has required the search for new materials for pavement sub-base design. A sub-base design utilizing an alkaline activator involving the use of wastes and by-products from various industrial processes may be considered a promising alternative to sub-base traditional materials (crushing aggregates and gravel). This research studies emphasize Rice Husk Ash (RHA), Copper Slag (CS), and mixed with Alkaline Activator (Sodium Hydroxide (SH) and Sodium Silicate (SS)) are used as an alternative material for the construction of pavement. This paper is an experimental investigation by performing Compaction Tests, and Unconfined Compressive Strength (UCS) tests as per Indian Standard Code. The compaction tests and UCS tests have been performed for various combinations and various combinations were made using CS (90%, 80%, 70%, 60%, and 50%) and RHA (10%, 20%, 30%, 40%, and 50%). The percentage of alkali activator 3% and 6% was used. Further, the ratio of SH/SS 1:2 was used and the concentration of SH is 10M (molarity) used. Prepared samples have been cured for 7 days in the thermostatic temperature-controlled chamber at 60℃. On behalf of experimental results, the replacement of this waste material with traditional constructional material is beneficial economically as well as for the environment.

Keywords: Copper slag, Rice husk ash, Alkaline Activator, Compaction test, UCS test.

1. INTRODUCTION

Industrial waste disposal has become the most difficult problem to solve in today's world [1]. Globally, enormous amounts of trash are produced. Waste comes in two forms: liquid and solid. Residential buildings, medical facilities, and industries all generate a significant amount of waste. Due to the direct dumping of these wastes over the ground and near water bodies, soil and water pollution may increase, thereby depleting fertile land [2]. This has negative consequences for the ecosystem. Industrial wastes may be recycled and repurposed with the right tools for maximum efficiency. The current research emphasizes the usage of CS and RHA in pavement design.

Compared to the manufacture of copper, two to three times more CS is produced during the smelting process. Because CS and fine sand’s comparable in physicochemical qualities, they may be used in a variety of applications, including soil stabilization, backfilling in retaining walls, embankment construction, pavement construction, rail ballast, concrete manufacture, and cement [3].

At various temperatures, the burning of rice husk, the RHA is also produced in rice mills. Approximately 200 kg of rice husk can be obtained from 1000 kg of paddy, which, when burned, creates around 40 kg of RHA. According to ASTM C-168, it has a large proportion of amorphous silica, making it a pozzolanic material (ASTM 1997) [4].

Cement and lime are widely used as additional materials in pavement building and soil stabilization across the world [5]. A large quantity of CO_2 is emitted during cement manufacture, which is hazardous to the environment. During the manufacture of one tonne of cement, about one tonne of CO_2 gas is emitted, which contributes to global warming. As a result, additional sustainable pozzolanic materials must be used to partially or entirely replace cement. Replacement for cement in soil stabilization and improvement, as well as in the development of novel composite materials AA can be used as a partial or complete [6].

Calcined clay and metakaolin are some of the natural sources of pozzolans. The chemical makeup of aluminosilicate materials influences the alkali-activation reaction products. AA reacts with high calcium binders to produce calcium-silicate-hydrate (C-S-H) gels. Low calcium binder gels (K-A-S-H) or Sodium Aluminosilicate Hydrate Gels (N-A-S-H) are made of potassium aluminum silicate hydrate and sodium aluminum silicate hydrate, respectively, where K stands for K+ cations and N stands for Na+ [7].

The composite includes CS and RHA combined with an AA are investigated for the compaction and UCS. This research might aid in the development of novel composite materials for pavement construction with improved mechanical qualities (sub-grade and sub-base). This study is part of a larger experimental examination that includes a particular compaction characteristic (OMC and MDD), UCS test, and the value of composite materials made up of AA, CS, and RHA. The current research is mostly concerned with:

- To study the different combinations of RHA, CS, and AA percentages that affect the compaction behavior.
- To study In RHA treated with AA composite material with CS, the curing period of 7 days affects the UCS of stress-strain behavior.

2. Experimental Investigation

RHA, CS, and AA (SS and SH) were employed in this experimental investigation. As described by Sharma and Kumar the CS and RHA have the same physical characteristics as reported in [8].

2.1. Copper slag

The experiment employed a blackish-colored CS. From the Hindustan Copper Limited (HCL) in Bharuch, Gujarat, India; CS was obtained and a sample is displayed in Figure 1. 18%, 3.50, 2.5, and 1.715 gm/cc respectively, are the OMC, SG, Fineness Modulus (FM), and MDD of CS. Table 1. summarises the physical characteristics of CS [8].

Figure 1. Raw materials copper slag

Table 1. Copper slag’s physical propert

Copper slag’s physical property		
S. No.	Physical properties	Value
1	Particle shape	Irregular
2	Appearance	Black and glassy
3	Maximum Dry Density	1.715 gm/cc
4	Optimum moisture content	18%
5	Fineness modulus	2.5
6	Specific gravity	3.50
7	Coefficient of Uniformity(Cu)	1.534 (Poorly graded)
8	Coefficient of Curvature (Cc)	0.960
	Particle Size	
9	> 425 micron	-
10	> 300 micron	4.16 %
11	> 150 micron	91.07 %
12	> 75 micron	3.65 %
13	< 75 micron	1.12 %

2.2. Rice husk ash

From Jalandhar, Punjab, India a local rice mill RHA was collected as shown in Figure 2. RHA's SG, OMC, MDD, and FM, respectively, were determined to be 2.06, 64%, 0.52 g/cc, and 1.43. Table 2. summarises the physical characteristics of CS [8].

Figure 2. Raw materials image Rice husk Ash

Table 2. The physical property of rice husk ash

The physical property of rice husk ash		
S.no	Physical properties	value
1	Particle shape	Irregular
2	appearance	Dark grey
3	Optimum moisture content	64%
4	Maximum Dry Density	0.52 gm/cc
5	Specific gravity	2.06
6	Fineness modulus	1.43
7	Coefficient of Uniformity	7.08
8	Coefficient of Curvature	0.44
	Particle Size	
9	> 425 micron	-
10	> 300 micron	0.32 %
11	> 150 micron	47.35 %
12	> 75 micron	5.760 %
13	< 75 micron	46.34

2.3. Alkali activator

In this experiment, SS and SH were employed as AA. As indicated in Figures 3. (a), (b), and (c), with 98 percent purity SH was accessible in flake form and SS was available in solution form as shown in Figure 3. Whereas an Activator Modulus (Ms) of 3.3 was observed. The term "activator modules" refers to the mass ratio of silicon dioxide to sodium oxide in AA. In a 1:2 ratio, sodium hydroxide and sodium silicate are mixed. 24 hours before usage dissolve the sodium hydroxide flakes in distilled water to make a 10M sodium hydroxide solution. A high pH environment is formed when an AA is used, which speeds up the

hydration processes. So while using AA in lab work or other work we should wear proper gas masks and gloves to take care of its side effects.

Figure 3. Raw materials (a) sodium hydroxide solution, (b) sodium hydroxide flakes, (c) sodium silicate solution

3. EXPERIMENTAL PROGRAM

On RHA and CS with combinations of the binder AA treated with various percentages, sequences of laboratory tests are carried out. UCS test and the Standard proctor compaction test are the most common laboratory tests conducted. Both the UCS test and the standard proctor compaction test were conducted in accordance with Table 3, which lists the different ratios of RHA and CS when treated with AA, along with each combination's percentages. Combinations with RHA of Standard proctor compaction are conducted at 10%, 20%, 30%, 40%, and 50%, as well as AA of 3%, and 6%, and the Rest of the percentages CS. The same percentages of RHA of 10 %, 20 %, 30 %, 40 %, and 50 % are used in the UCS test, as well as CS of 90 %, 80 %, 70 %, 60 %, and 50 %, respectively, with AA of 3% and 6%.

Table 3. Combination scheme

Combinations	Mixed proportions	Title	Molarity of NaOH solution (M)	$NaOH/Na_2SiO_3$ ratio
A	90%CS+10%RHA+3%AA	A1	10 M	1:2
	80%CS+20%RHA+3%AA	A2		
	70%CS+30%RHA+3%AA	A3		
	60%CS+40%RHA+3%AA	A4		
	50%CS+50%RHA+3%AA	A5		
B	90%CS+10%RHA+6%AA	B1	10 M	1:2
	80%CS+20%RHA+6%AA	B2		
	70%CS+30%RHA+6%AA	B3		
	60%CS+40%RHA+6%AA	B4		
	50%CS+50%RHA+6%AA	B5		

4. THE TESTING PROCEDURE AND SAMPLE PREPARATION

In the beginning, oven-dried RHA and CS were completely mixed in a big steel tray by hand. To avoid moisture, RHA and CS were placed in sealed containers. At a temperature of 105^{o} C in an ambient temperature-controlled chamber, the airtight container was put. Following that, standard proctor compaction tests were performed. The mold size is 105 mm in diameter and 115.5 mm height was taken for all A and B combinations and also following the IS code-2720, part VII, 1980 [9]. In this experiment, the making of AA was employed by SH and SS. Before the 24-hour test, the SH solution was mixed. All of the combinations A and B are specified in Table 3.1. A 10 M (molarity) SH solution was utilized. The SS on the other hand is in a solution form so the mixing of both (SS and SH) was employed immediately. The SH/SS ratio utilized for all AA combinations is 1:2.

The UCS samples (38 mm in diameter and 76 mm in height) were made with a mixture of CS, RHA, and AA. Standard compaction was used to prepare all of the specimens. The molds were cast after 24-hour samples of UCS were extracted as shown in Figure 4. Furthermore, the UCS samples were ambient cured for 7 days, respectively. UCS testing is carried out following IS code-2720, part X, 1991 [10] at the displacement of 1.25 mm/min.

Figure 4. UCS samples after 24 h casting

5. RESULTS AND DISCUSSION

Standard proctor compaction tests and UCS tests are used to calculate the impact of RHA and CS treated with AA on mechanical characteristics. The following segments provide a comprehensive discussion and analysis of the findings.

5.1. Results from compaction test

Figures 5. and 6. Show how OMC and MDD change with different amounts of AA and RHA. The values of OMC and MDD were found to increase and decrease respectively, while the amount of RHA was increased from 10% to 50% at a constant amount of AA 3%, and 6%. In combination A, where the amount of AA is held constant at 3%, Figure 5 demonstrates that when the amount of RHA added to CS increases There is a decrease in MDD value but an increase in OMC value. For combinations-B with 6% of AA, similar MDD and OMC patterns were observed as shown in Figure 6. The highest MDD values found for combinations A and B are 1.77 g/cc and 1.84 g/cc respectively, with OMC values of 15.25 % and 12.50 %. A1 (90%CS+10%RHA+3%AA) and B1 (90%CS+10%RHA+6%AA) are the best mixes for combinations A and B. Furthermore, the lowest MDD values In combination A and B, results are obtained at 0.76 g/cc and 0.71 g/cc respectively, with OMC values of 38.20 % and 29.20 %. Figures 5 and 6 indicate the

cumulative effects of increasing RHA on OMC and MDD with individual AA content is increases of 3% and 6% denoted by combinations A and B, respectively. Increasing the RHA content decreases the MDD while increasing OMC in all of the combinations. The lower SG relative to that of CS is responsible for the reduction in MDD value that occurs when RHA concentration is increased. The lower SG values of lightweight materials account for the decrease in MDD values [8]. Because the AA utilized in Some of the water content is replaced by this research, which is in liquid form so necessary the MDD decreases with the OMC increase. These findings show an innovative, environmentally friendly composite material produced in this work by combining CS and RHA with AA may be employed in a variety of a wide range of civil engineering applications retaining wall backfill, pavement sub-base, and subgrade.

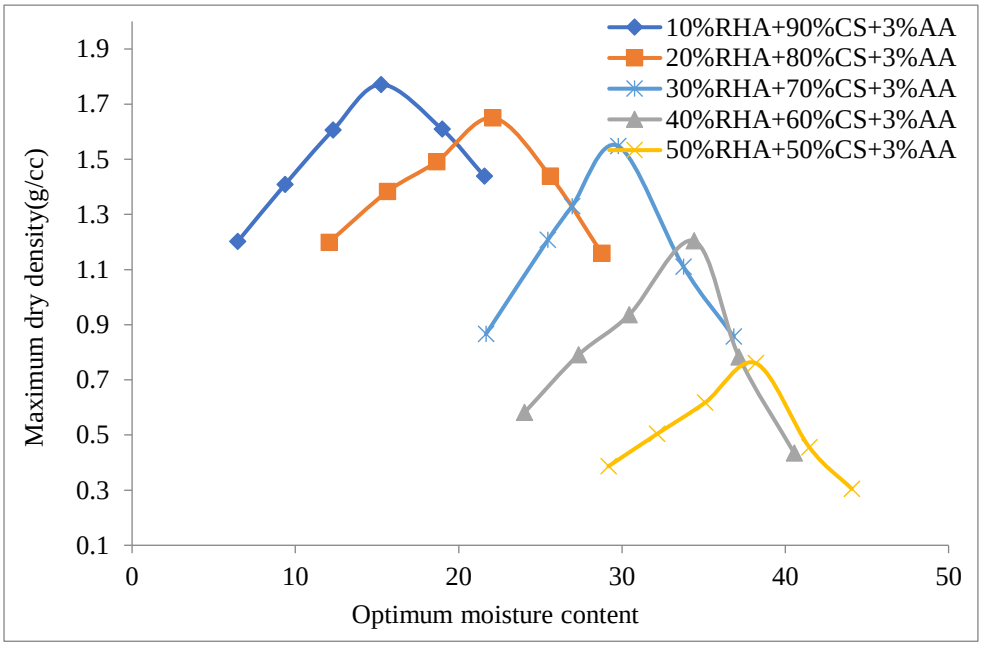

Figure 5. Combination- A Standard Proctor compaction curve with 3% AA

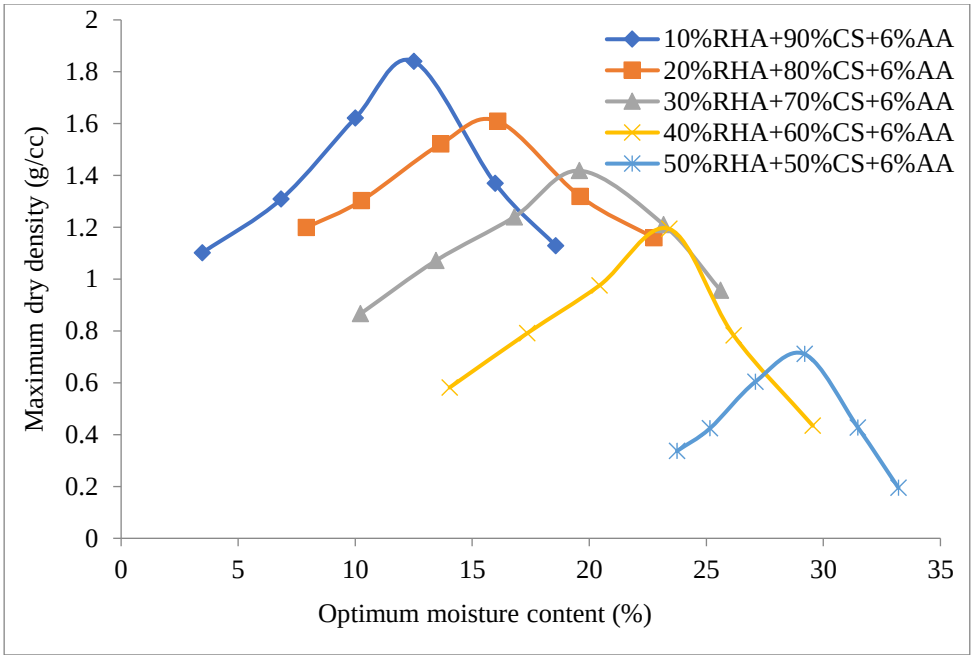

Figure 6. Combination- B Standard Proctor compaction curves with 6% AA

5.2. Unconfined compressive strength test

Behavior responses of strain and stress Figure 7 and 8 demonstrate the stress-strain behavior of various mixtures (combination-A and B) after 7 days of curing. The stress increase as the strain values increase up to a particular maximum level, beyond which the stress values drastically decreased as the strain values increase. For combinations A and B, the composite materials demonstrate brittle failure. The relation between strain and stress behavior of combination-A the RHA with CS at different percentages of 10%, 20%, 30%, 40%, and 50% constant quantity of AA is shown in Figure 7. (3%). The curve shows that increasing the percentage of RHA (up to 20%) while keeping the quantity of AA (3%) constant increases the UCS values. Stresses and strains that lead to maximum failure of around 3815.68 kPa and 1.97 %, respectively, have been observed at 20% RHA and 3% AA. Furthermore, the stated Stresses and strains that lead to minimum failure, are 1130.44 kPa and 1.57 percent, respectively. Figure 8. Depicts the relation behavior of combination-B under stress and strain the CS with RHA at various percentages of AA, such as 10%, 20%, 30%, 40%, and 50% at AA content 6%. The graph shows that as the proportion of RHA is raised to 20% but the percentage of AA is kept constant (6%), the UCS values increase. Stresses and strains that lead to maximum failure for 20% RHA and 6% AA were determined to be 4410.11 kPa and 2.36%. Furthermore, the reported Stresses and strains that lead to minimum failure are 1408.34 kPa and 1.97 percent, respectively.

With the inclusion of alumina, and calcium, After hardening, CS is bound to AA by its cementitious properties and the silica in the CS, RHA, and AA are all factors that contribute to the increase in UCS values.

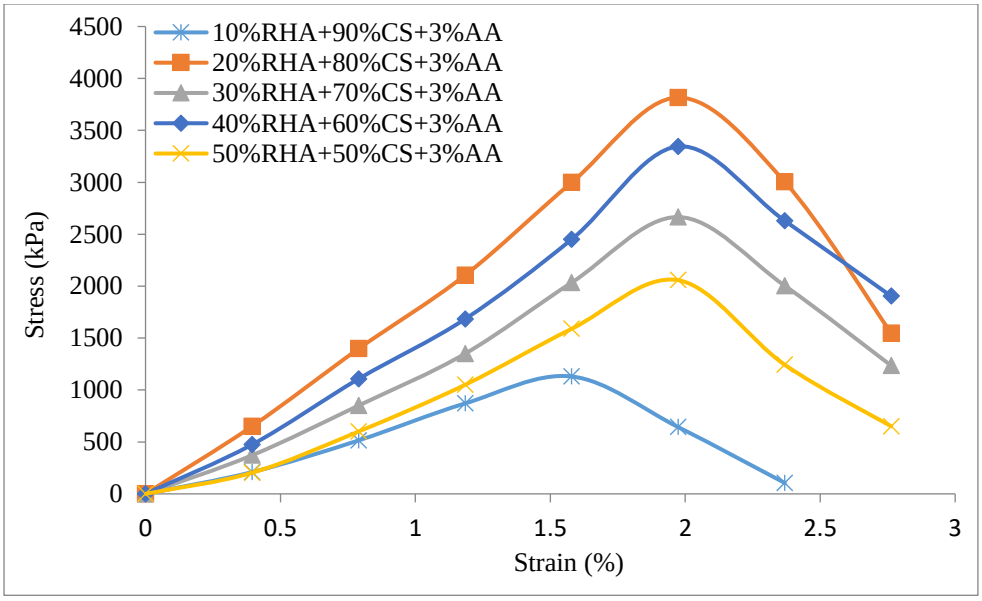

Figure 7. Combination-A's Stress-strain curves after 7 days of curing

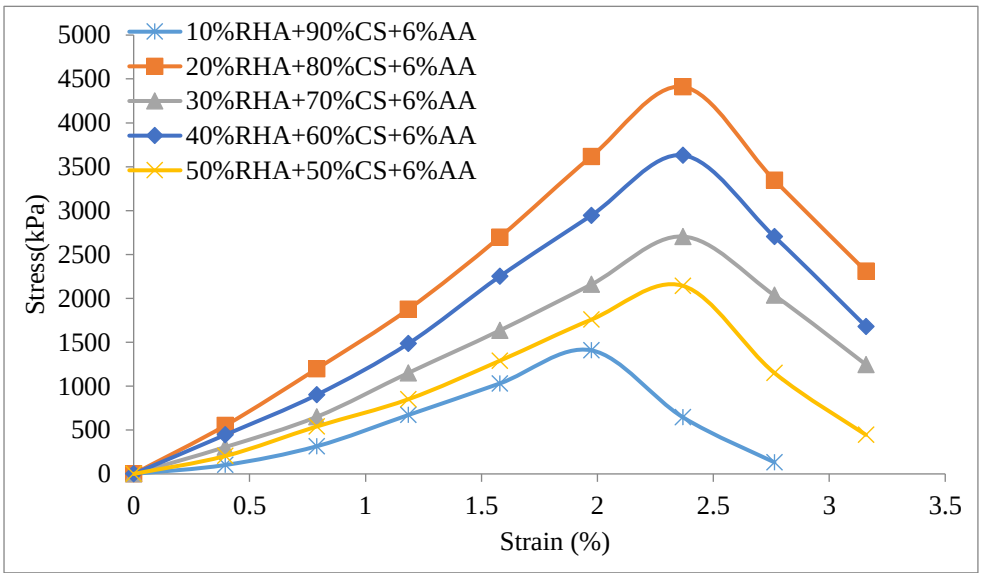

Figure 7. Combination-B's Stress-strain curves after 7 days of curing

6. CONCLUSIONS

An experimental evaluation of compaction and UCS in a composite including RHA and CS mixed with an AA was provided in this paper. These tests' results are given and analyzed in depth. The following are the primary results gained from this research:

- The best combination for the newly created sustainable composite material is 80%CS+20%RHA+6%AA they may be used in a variety of applications, including soil stabilization, backfilling in retaining walls, and embankment construction, pavement construction, rail ballast, concrete manufacture, and cement since it has improved geotechnical qualities.
- Using AA as a binder material instead of traditional binders like cement and lime minimizes the carbon footprint and CO_2 emission, which would otherwise be substantial when traditional binders are manufactured.
- For RHA content of roughly 20% and 20%, respectively, the maximum UCS values for combination-A and B are observed. The combination-B with 20% RHA (80% CS+20% RHA+6% AA) achieved the greatest UCS value (4410.11 kPa).
- The stress-strain curve behavior demonstrated that the UCS tested materials have brittle fractures for varied combinations. The percentages of RHA and CS, as well as the amount of additional material, influence it.
- The creation of composite materials use of industrial wastes, such as the RHA and CS treated with AA used in this study, provides a cost-effective way to dispose of waste, as well as solving the waste disposal problem, environmentally benign, and saves virgin resources.
- The demand for ecologically friendly and long-lasting building materials has required the search for new materials for pavement sub-base design. A sub-base design utilizing an alkaline activator involving the use of wastes and by-products from various industrial processes may be considered a promising alternative.

REFERENCES

[1] J. Singh, R. Laurenti, R. Sinha, and B. Frostell, "Progress and challenges to the global waste management system," Waste Manag. Res. J. a Sustain. Circ. Econ., vol. 32, no. 9, pp. 800–812, Sep. 2014, doi: 10.1177/0734242X14537868.

[2] Jihan Khalid Abdel Karim Ali, "The Impact of Industrial Waste on Human and Natural Resources : A Case Study of Khartoum North Industrial Area, B . Sc Environmental Science Omdurman Ahlia University A thesis submitted to the University of Khartoum partia," 2004.

[3] B. Gorai, R. K. Jana, and Premchand, "Characteristics and utilization of copper slag—a review," Resour. Conserv. Recycle., vol. 39, no. 4, pp. 299–313, Nov. 2003, doi: 10.1016/S0921-3449(02)00171-4.

[4] F. Celik and H. Canakci, "An investigation of rheological properties of cement-based grout mixed with rice husk ash (RHA)," Constr. Build. Mater., vol. 91, pp. 187–194, Aug. 2015, doi: 10.1016/j.conbuildmat.2015.05.025.

[5] P. Shekhawat, G. Sharma, and R. M. Singh, "Potential Application of Heat Cured Eggshell Powder and Flyash-Based Geopolymer in Pavement Construction," Int. J. Geosynth. Gr. Eng., vol. 6, no. 2, p. 28, Jun. 2020, doi: 10.1007/s40891-020-00213-2.

[6] I. Tekin, "Properties of NaOH activated geopolymer with marble, travertine and volcanic tuff wastes," Constr. Build. Mater., vol. 127, pp. 607–617, Nov. 2016, doi: 10.1016/j.conbuildmat.2016.10.038.

[7] S. Thiha, “Shear strength enhancement of compacted soils using high-calcium fly ash-based geopolymer,” int. j. geomate, vol. 15, no. 48, Aug. 2018, doi: 10.21660/2018.48.35692.

[8] K. Sharma and A. Kumar, “Influence of rice husk ash, lime and cement on compaction and strength properties of copper slag,” Transp. Geotech., vol. 27, p. 100464, Mar. 2021, doi: 10.1016/j.trgeo.2020.100464.

[9] Bureau of Indian Standards, “Methods of test for soils, determination of water content dry density relation using light compaction,” IS 2720 (Part VII-1980), pp. 1–16, 2011.

[10] IS: 2720 (Part 10):1991, “Indian Standard: Methods of test for soils, Part 10: Determination of unconfined compressive strength,” Bur. Indian Stand. New Delhi, no. Reaffirmed 2006, pp. 1–6, 1991.

Contemporary Development on the Mechanical Properties of HDPE/Natural Fiber Composites

Uma Dutt Chaubey, Rajesh Kumar Verma*

Materials and Morphology Laboratory, Department of Mechanical Engineering

Madan Mohan Malaviya University of Technology, Gorakhpur- 273010, India

*umaduttchaubey@gmail.com, rajeshverma.nit@gmail.com**

Abstract

In today's world, with the critical impact caused due to manufacturing and disposal of man-made fiber reinforced polymer composite, there is always a scope for producing eco-friendly composite. It has vast applications opportunities in the manufacturing sector, such as automobiles, marine, piping, and grocery items. Several natural fibers such as banana, rice, sisal, oil palm, coconut, and kenaf are looked up to nowadays because they are readily available, environment friendly, and have better mechanical properties. Natural fiber will always stand out in developing several industrial products with various polymer matrices. High-density polyethylene (HDPE) plays a key role among many polymers as it acquires numerous benefits such as strength and excellent chemical stability. HDPE has several other advantages, such as being durable, lightweight, and easily machinable, making it usable in medical, construction, maritime, and food. This review article proposed with an objective of mechanical properties of natural fiber reinforced in HDPE and various parameters affecting the structural features of polymer composite, like loading, fiber dimensions, and fiber structure. A critical observation is also done to understand the broader effect of the mechanical properties on varying the fiber wt.% and loading. This review article outlined to survey and collect the earlier works demonstrating the mechanical properties of natural fiber and its polymer composite to give a well-made source of information for performing future research to clarify the properties of synthetic fibers.

Keywords. HDPE, Natural fiber, Processing techniques, Mechanical Properties.

1. INTRODUCTION

High-density polyethylene (HDPE) was not discovered till the 1950s. Low-density polyethylene (LDPE) was more utilized [1]. But a requirement of the more strengthened polymer was in demand. Thus, several scientists were much interested in the production of denser polyethylene. The difference between the high density and low-density polyethylene is that HDPE is of higher molecular weight and has less molecular chain branching. The mechanical properties acquired by HDPE are much better than other polyethylene. HDPE has carbon and hydrogen as its main constituent. The higher density of HDPE is due to its long-linear molecular arrangement. HDPE was found to have high temperature-resistant properties[1]. HDPE acquiring certain unique features has vast applications, including grocery items, pipes, fuel tanks, cable insulators. HDPE is mostly used as a base material or

so-called matrix because of its greater strength to density ratio. It is also equipped with a better specific strength. It is also very cheap and readily available in the market.

A fiber-reinforced polymer (FRP) has its constituents as a polymer matrix reinforced with strengthened fiber like glass, and carbon forms a composite material. Polymers are basically divided into two groups, thermosetting plastic and thermoplastics. Thermoplastic materials nowadays play a prominent part in bio-fibers; the most widely used thermoplastics are PE, PVC, and PP, whereas epoxy and polyester resins are the most widely used thermosetting matrices [2]. In the recent past, natural fibers as a substitute for additives in polymer composites have gained the attention of several researchers and scholars because of their uniqueness over conventional glass and carbon fibers [3]. The natural fibers are sisal, hemp, kenaf, jute, coir, banana, and many others [4]. Natural fibers have various benefits over the synthetic glass and carbon fibers: low cost, low density, good tensile properties, not hazardous to the body, renewable, recyclable, and biodegradable nature [2]. The polymer composite thus developed has a vast application which includes aerospace, construction, sport, automotive industry, and packaging industry. However, natural fibers are a few limitations reinforced in a polymer composite, which could be the instability between the hydrophobic thermoplastic matrices and natural hydrophilic fibers. This may be a cause for the unfavorable properties of the composite. Hence, there is a requirement to improve the fiber interface by modifying the chemical composition of the surface between fiber and matrix.Many parameters can impact the performance of natural fiber impregnated composite. Hydrophilic behavior is not the only property that affects, but the proportion of additive added a significant effect. There is always a need for more excellent fiber content for acquiring better mechanical properties of the composite. This illustrates the importance of fiber amount added to the matrix. Several works have improved the mechanical properties by increasing the fiber loading [5]. This comparative study highlights the effect of different natural fibers with HDPE as a polymer matrix. It also makes us understand the physical and mechanical characteristics of different natural fiber reinforced HDPE composites in various aspects such as industrial, biomedical, structural, etc.

Thus, the following study provides a basic understanding of the relationship between natural fiber and polymer matrix. Natural fiber has vast application due to its better properties and superior advantages over synthetic fiber in terms of lower cost, weight, and less fiber content.

2. FEATURES OF NATURAL FIBER POLYMER COMPOSITE

There is much variation in the mechanical properties of the reinforcement of different kinds of fibers reinforcement. Certain factors affect the properties: composition, structure, defects, and behavior with the base material. There are certain limitations as mixing natural fiber and polymer has certain ill behavior. It is due to the chemical structure of the matrix and reinforcement. This can be a significant cause of misleading the stress transfers. Hence, there is always a need for chemical treatment for the natural fiber to get an excellent interfacial property. While developing natural fiber polymer composites, there is a creation of a weak bond between the hydrophobic polymer and hydrophilic fiber. This hydrophilic property in the natural fiber is due to a functional group known as the hydroxyl group. This results in inferior mechanical properties.

2.1. Mechanical Properties of natural fiber polymer Composite

There are many efficient methods for the natural fiber that can be performed to improve the mechanical properties. Once the foundation is made strong, the polymers can easily have high strength and improvement. Many things have impacted the performance level, such as the position of fiber [6]., fiber strength, physical properties of fibers, etc. Natural fiber Polymer composite is a type of composite with a mechanical efficiency that depends on the interface made by fiber and matrix. Due to this, the stress is transferred from fiber to matrix [7]. Different aspects of natural fibers such as position, moisture absorption, impurities, and volume fraction are several properties that play a role in finding mechanical properties. Natural fiber polymer composites show good mechanical properties compared to a pristine matrix where jute fibers are involved in polylactic acid (PLA). Till now, mostly, there has been a growth in composites where jute is reinforced and showed 121% improvement is found in comparison to pristine polyester [8]. Essabir et al. developed a composite with the inclusion of oil palm fiber and clay particles as reinforcement with HDPE. Clay as reinforced material reduces thermal interruption and with better mechanical properties. Oil palm fiber is hard. Several tests were performed to analyze the properties, The result observed was satisfying, with a hike of 11% in tensile strength. Elastic properties were also enhanced.[9]. Mazur et al. carried out the inclusion of NF with HDPE matrix to assess the effect on the composite. Wood flour, flax fiber, and wall nutshell flour was used with 40% wt.%. The performance was assessed with several tests, namely Differential Scanning Calorimetry (DSC), and roughness test. Growth in density and reduction in impact strength was improved. Significant flexural strength was found with 262% growth. Composites with NF showed a par level of tensile strength of 156% with basalt and 16% with flax fiber [10]. Savini and Orifice studied on the composite produced by HDPE mixed with micro talc. Thermogravimetric analysis, DSC was carried out to check the variability of the composite's nature. ANOVA was also performed for statistical analysis. The elastic property got enhanced. There was a little drop in tensile strength. Hence, talc showed a better composite improvement with increased ductility, toughness, and rigidity [11]. Li et al. developed a composite reinforced with sisal fiber with an HDPE matrix. Sisal fiber possesses high strength and durability, and its composite is also environmentally friendly. The interfacial shear strength of sisal fiber, including the HDPE matrix, was improved.[12]. Yao et al. developed a composite by reinforcing four rice straw components and wood fiber with an HDPE matrix.The result showed a larger storage modulus and a decrease in tensile and impact strength. Heat flow rate also showed variation. The recycled HDPE and its derivative had much better moduli with respect to virgin HDPE [13]. Mohanty and Nayak developed a composite of bamboo fiber reinforced HDPE. Tensile, flexural, SEM, and heat deflection temperature tests were carried out. The tensile strength was found to be 25.27MPa and flexural strength 27.86 MPa.[14]. Panthapulakkal and Sain prepared a composite with agro-based residue as reinforcement material in the HDPE matrix. Tensile strength showed an improvement. The percentage improvement in strength and stiffness of wheat straw is 47% and 36%, respectively [15]. Table 1 depicts much improvement in tensile properties and flexural and impact strength of HDPE on being reinforced with different natural fibers.

Table 1. Natural fiber reinforcement-based HDPE composites

Matrix	Reinforcement	Matrix Size	Reinforcement Size	Result	Ref.
HDPE	Char	Density = 0.957 g/cm^3	-	32 % rise in tensile properties.	[16]
HDPE	Oil Palm Fiber	Grade HD-6705	10 cm in length	11% rise in tensile strength	[9]
HDPE	Basalt Fiber	94% Biobased Content	40 wt. %	590% rise in young modulus	[10]
HDPE	Micro Talc	Density of 0.957 g/cm^3	60 wt.%	200 % rise tensile strength	[11]
HDPE	Sisal Fiber	Density of 0.96 g/cm^3	100-300 µm	Significant Increase in IFSS.	[12]

3. PROCESSING TECHNIQUES FOR THERMOPLASTIC MATERIALS

The processing of natural fiber composites is affected by several variables, including the kind of fiber, the volume fraction of the fibers, and the temperature. The moistening effect between the fiber and matrix must be reduced before processing. Other factors affecting composite performance are length, aspect ratio, and chemical proportion. The temperature that must be maintained while processing should also be addressed. Temperatures beyond 200°C should be avoided if the product is not to disintegrate prematurely. The most used methods are compression, injection, and extrusion molding [17-19].

3.1. Compression molding

Since the 1990s, compression molding has been the most common method of processing thermoplastic materials. As time went on, demand for lightweight and high-performance materials grew steadily. In this method, materials are heated to a high temperature before being poured into a mound hole. Afterward, these are squeezed and warped by the mold's middle portion while the cavity is subjected to high pressure [17]. It should be subjected to significant pressure until the mold is released and the composite formed reaches a solid-state. For the mechanism to perform well, the heating time, the pressure exerted, and the cooling period must all be regulated. Sheet molding, which is a kind of compression molding, is among the essential processing procedures for the production of polymer composites [18]. It is necessary to inject a fluid mass of a specific resin into the plastic film before it can be used to cut the fibers. Figure 1 illustrates a clear visualization of each component of the compression molding press. The charge or resin is placed in the mold as shown below, giving the final composite the required shape to be developed.

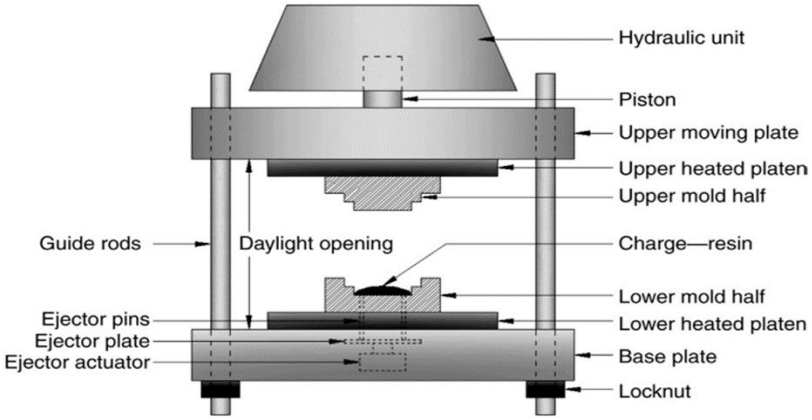

Figure 1. Major parts of a compression molding press [19].

3.2. Injection molding

When mass manufacturing of polymer composites is required, this is one of the processing methods used. The process initiates with feeding the granules of polymers in the hopper. After that, the melting process is completed by a heating procedure done at high temperatures. The liquid components are then pumped into an empty cavity. In the mold, the molten shape solidifies and is extracted using a split die mold [20].

3.3. Extrusion molding

Extrusion molding could be a widely used manufacturing industry procedure to produce or develop natural fiber composites. The reason behind its importance is the high stiffness and strength of the polymer composite. This process gets started by keeping the polymer material in the shape of pellets [21]. After which, they are given heat to get converted into a molten state. Hence it gets heated up, so it is made to cool down.

Figure 2 exemplifies a brief description of the life cycle of natural fiber. Initially, the raw fiber gets processed into intermediate products like fiber mats, fleece, etc., then into the final product. The final product after usage, when it becomes of no use and is referred to as waste, gets decomposed into fiber crops after several chemical processes. Hence, fiber extraction is finally done. This process continues cyclically.

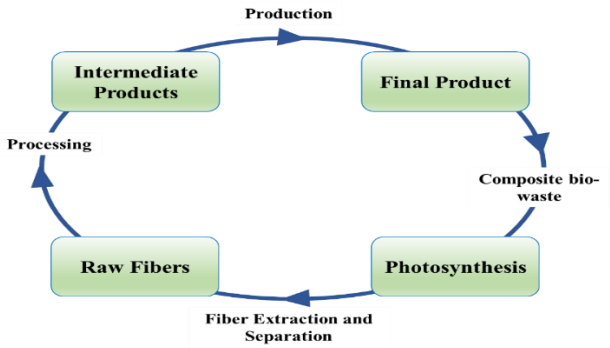

Figure 2. Life cycle of natural fiber.

4. APPLICATIONS OF NATURAL FIBER REINFORCED POLYMER COMPOSITES

Natural fiber composites have been reported to be primarily employed in the automotive, construction, aviation components, packaging, electrical parts, and biomedical sectors due to their eco-friendly nature, superior mechanical qualities, and lightweight nature, among other factors. Due to a few drawbacks, such as a lack of endurance in wet environments, such as piping and boats may eventually be replaced with glass fiber reinforced composite (GFRC) [22]. In 1941, Henry Ford was the first person to use flax and hemp fibers in the automobile industry [23]. In the construction area, natural fibers are employed to produce load-carrying elements such as beams, roofs, walls, and bridges. For safety purposes, jute fiber composites are used in indoor parts housing and outdoor housing [24].

5. CONCLUSION

The most striking features of natural fiber are cost-effective and environment-friendly, making it a better option and replacing conventional fibers like glass and carbon as an additive in the polymer matrix. HDPE stands out to be a better matrix than other polymer matrices such as LDPE, Polypropylene and Polyester because of its high strength and hardness. HDPE could be utilized for pipes, biomedical implantation, packaging and sporting equipment etc. One of the major concerns encountered in today's world is solid waste management. HDPE-based composite reinforced with natural fiber is most effective due to its eco-friendly behavior and is easily decomposable. Various natural fibers can be added for developing new and advanced composites, such as sisal, wheat, rice etc. There are many processing techniques available for the development of the composite, under which some are discussed as per the requirement. The above discussions in this review article had already shown that natural fibers reinforced with HDPE have greater tensile strength, modulus of elasticity, and bending strength. The strength of the HDPE-based composite is also much dependent on the fiber loading, which shows improvement up to a certain level on increasing the wt. %.

REFERENCES

[1] Kumar, S., Panda, A.K. and Singh, R.K., 2011. A review on tertiary recycling of high-density polyethylene to fuel. *Resources, Conservation and Recycling*, *55*(11), pp.893-910.

[2] Malkapuram R, Kumar V, Yuvraj SN. Recent development in natural fibre reinforced polypropylene composites. J Reinf Plast Compos 2008;28:1169–89.

[3] Nabi Saheb D, Jog JP. Natural fiber polymer composites: a review. Adv Polym Technol 1999;18:351–63. [

[4] Li X, Tabil LG, Panigrahi S, Crerar WJ. The influence of fiber content on properties of injection molded flax fiber-HDPE biocomposites. Can Biosyst Eng 2009;08–148:1–10. [

[5] Ahmad I, Baharum A, Abdullah I. Effect of extrusion rate and fiber loading on mechanical properties of Twaron fiber-thermoplastic natural rubber (TPNR) composites. J Reinf Plast Compos 2006;25:957–65.

[6] A. Shalwan and B. F. Yousif, "In state of art: mechanical and tribological behaviour of polymeric composites based on natural fibres," Materials & Design, vol. 48, pp. 14–24, 2013.

[7] V. K. Thakur and M. K. Thakur, “Processing and characterization of natural cellulose fibers/thermoset polymer composites,” Carbohydrate Polymers, vol. 109, pp. 102–117, 2014.

[8] A. Shalwan and B. F. Yousif, “In state of art: mechanical and tribological behaviour of polymeric composites based on natural fibres,” Materials & Design, vol. 48, pp. 14–24, 2013.

[9] H. Essabir, R. Boujmal, M. O. Bensalah, D. Rodrigue, R. Bouhfid, and A. E. K. Qaiss, “Mechanical and thermal properties of hybrid composites: Oil-palm fiber/clay reinforced high density polyethylene,” Mech. Mater., vol. 98, pp. 36–43, 2016, doi: 10.1016/j.mechmat.2016.04.008.

[10] K. Mazur, P. Jakubowska, P. Romańska, and S. Kuciel, “Green high density polyethylene (HDPE) reinforced with basalt fiber and agricultural fillers for technical applications,” Compos. Part B Eng., vol. 202, no. August, 2020, doi: 10.1016/j.compositesb.2020.108399.

[11] G. Savini and R. L. Oréfice, “Comparative study of HDPE composites reinforced with microtalc and nanotalcs: high performance filler for improving ductility at low concentration levels,” J. Mater. Res. Technol., vol. 9, no. 6, pp. 16387–16398, 2020, doi: 10.1016/j.jmrt.2020.11.090.

[12] Y. Li, C. Hu, and Y. Yu, “Interfacial studies of sisal fiber reinforced high density polyethylene (HDPE) composites,” Compos. Part A Appl. Sci. Manuf., vol. 39, no. 4, pp. 570–578, 2008, doi: 10.1016/j.compositesa.2007.07.005.

[13] F. Yao, Q. Wu, Y. Lei, and Y. Xu, “Rice straw fiber-reinforced high-density polyethylene composite: Effect of fiber type and loading,” Ind. Crops Prod., vol. 28, no. 1, pp. 63–72, 2008, doi: 10.1016/j.indcrop.2008.01.007.

[14] S. Mohanty and S. K. Nayak, “Short bamboo fiber-reinforced HDPE composites: Influence of fiber content and modification on strength of the composite,” J. Reinf. Plast. Compos., vol. 29, no. 14, pp. 2199–2210, 2010, doi: 10.1177/0731684409345618.

[15] S. Panthapulakkal and M. Sain, “Agro-residue reinforced high-density polyethylene composites: Fiber characterization and analysis of composite properties,” Compos. Part A Appl. Sci. Manuf., vol. 38, no. 6, pp. 1445–1454, 2007, doi: 10.1016/j.compositesa.2007.01.015.

[16] M. Sogancioglu, E. Yel, and G. Ahmetli, “Pyrolysis of waste high density polyethylene (HDPE) and low density polyethylene (LDPE) plastics and production of epoxy composites with their pyrolysis chars,” J. Clean. Prod., vol. 165, pp. 369–381, 2017, doi: 10.1016/j.jclepro.2017.07.157.

[17] Campilho RDSG (2015) Natural fiber composites. CRC Press, Boca Raton

[18] Dai D, Fan M (2014) Wood fibres as reinforcements in natural fibre composites: structure, properties, processing and applications. In: Hodzic A, Shanks R (Eds) Natural fibre composites. Elsevier, Amsterdam, pp 3–65

[19] Kutz, M. (Ed.). (2011). Applied plastics engineering handbook: processing and materials. William Andrew.

[20] Scheru¨bl B, Hintermann M (2005) Application of natural fibre reinforced plastics for automotive exterior parts, with a focus on underfloor systems. In: Proceedings of the 8th international AVK-TV conference, Baden, Germany, 2005. p D5

[21] Campilho RDSG (2015) Natural fiber composites. CRC Press, Boca Raton

[22] Dicker MPM, Duckworth PF, Baker AB, Francois G, Hazzard MK, Weaver PM (2014) Green composites: a review of material attributes and complementary applications. Compos Part A Appl Sci Manuf 56:280–28

[23] Mohanty AK, Misra M, Drzal LT (2005) Natural fibers, biopolymers, and biocomposites. CRC Press, Boca Raton
[24] Dweib MA, Hu B, Shenton Iii HW, Wool RP (2006) Biobased composite roof structure: manufacturing and processing issues. Compos Struct 74(4):379–388.

Biographies

Uma Dutt Chaubey received the bachelor's degree in mechanical engineering from ABES engineering college in 2018. He is currently pursuing M.Tech, in Computer Integrated Manufacturing from Madan Mohan Malviya University of Technology, Gorakhpur, Uttar Pradesh, India. His research area includes material recycling, composite material, Polymer composite, nanomaterials.

Dr. Rajesh Kumar Verma is an Associate Professor and Doctoral Supervisor at the Department of Mechanical Engineering at the Madan Mohan Malaviya University of Technology, Gorakhpur, India. He received his Ph.D. (Engg.) from Jadavpur University, Kolkata, India. He is actively involved in teaching and research in nanomaterial, polymer composites, modeling, simulation, optimization, advanced machining, Machinability aspects of composites/nanocomposites materials. He has completed/ongoing more than eight nos. of research and development projects sponsored by various govt. agencies

.

Experimental Prediction of Failure Progression of Lithium-ion battery under Lateral and Longitudinal Compression

[1]Vishesh Shukla, [2]Ashutosh Mishra, [3]R.P. Tewari

[1,2,3]Department of Applied Mechanics, Motilal Nehru National Institute of Technology Allahabad, Prayagraj, UP, India

[1]vishesh.2018ram52@mnnit.ac.in, [2]ashutoshjssate@gmail.com, [3]rptewari@mnnit.ac.in

Abstract

The safety issues of lithium ion batteries (LIBs) is a recent topic of research nowadays because of rapidly growing market of LIBs in electric vehicles. Present work consists of experimental findings covering the failure progression of LIB under mechanical abuse conditions of lateral and longitudinal. The compression tests were performed on commercial 18650 battery. The load vs. displacement curve was recorded during deformation under lateral and longitudinal compression. The results are compared and governing failure mode was identified. It was found that battery samples are failed at 53 kN and at 5 kN under lateral and longitudinal compression respectively. This demonstrates the significance of types of loadings considered, to predict the failure behavior of LIB during mechanical abuse conditions.

Keywords. Lithium Ion battery, Electric vehicle, Mechanical abuse, Battery Safety.

1. INTRODUCTION

Batteries are commonly used in devices such as laptops, trimmers, electric cars, drones, power banks etc. and its market is growing with its wider applications. With its increasing use, there is an increasing safety concerns associated to its use in electric transports (public/private). In the crash events of automobiles, the safety concerns of lithium ion batteries have become a frequently discussed topic. There are several aspects of safety of batteries that includes electrical, thermal and mechanical failure. Mechanical integrity of the batteries is the ability to withstand mechanical load. The impact of mechanical integrity on electric vehicle against electric short circuit is that the safety of LIB packs highly depends on their mechanical integrity. In the case of crash of electric vehicles due to lack of mechanical integrity the LIB packs are subjected to internal short circuit and fire. It is very important to understand the mechanical integrity of the batteries and consequently the electric vehicles against electric short circuit as a result of mechanical failure during vehicle crash. The events of catastrophic failure of batteries due to small intrusion in the battery pack during crash necessitate the requirements of increase research activities in the area of battery safety [1]. There are various chemical reactions, involving conversion of energies

apart from the energy involved during lithiation and de-lithiation process, that are responsible for considerable amount of heat released. In the case of high load or short circuits caused by manufacturing defects or abuse load, these reactions are triggered and may cause thermal runaway and even explosion. Xu et. al [2] have performed the study on separators of two types of materials i.e., Celgard 2400 having single layer and Celgard 2340 with three-layered structures. It was found that there was decrease in the failure strain while there is increase in failure stress with the strain rate in the considered separator materials. Studies by Wang et al. [3], covering quasi-static mechanical loading on cylindrical LIB, revealed the essential mechanical behavior and properties of the jellyroll. The study by Wang et al shows the suitability of considering clay-like properties for jellyroll adopting plastic flow rule with homogenized mechanical properties. Studies by Sahraeia et al. [4] shows an accurate model representing a single LIB to simulate the mechanical failure of LIB subjected to mechanical abuse conditions. Extensive experiments have been conducted on 18650 lithium ion battery to explore the failure behavior of LIB due to indentation with a hemispherical punch, indentation (lateral) by a cylindrical rod, three-point bending and compression between flat plates. Wierzbicki et al [5] preformed combined experimental and analytical approach to identify the averaged mechanical properties of LIB. It was revealed in the study that jellyroll is the source of the major mechanical resistance offered from the LIB. Further, the analytical studies showed that the end-caps and shell casing had little contribution to the overall crash resistance of the LIB. Goret al. [6] have tested the mechanical stability of inactive components viz. binder and separator due to their important role in the life cycle of LIBs. They investigated the effects of solvents in the electrolyte. It was observed by them, that there is a significant influence of solvents on the mechanical properties of battery separator made of polypropylene due to its chemical compatibility. The effect was studied by measuring the thickness and elastic modulus of separator samples immersed in different solvent environments. It was noticed that certain electrolyte solvents like ethyl- acetate, dimethyl-carbonate and diethyl -carbonate, cause separators softening. Zhu et al. [7] carried out several indentation tests on LIB with different capacities to identify the effect of internal short circuit (ISC). The failure response batteries were investigated, wherein the batteries of different state of charges (SOC) and capacities showed different behaviors. Wang et al. [8], performed the safety assessment studies using a numerical approach considering second-order oscillation. The simulation results showed an error of approximately 8.8% and 4.0% for the force-displacement and failure displacement respectively using safety performance model and Crushable-Foam model. Ma et al. [9] have used computed tomography, mechanics analysis and simulation techniques to characterize the evolution of the battery's internal components during nail penetration tests using multi-methods concepts. Liao et al. [10] reviewed the various work done int the field of battery abuse. They performed a comparative study to understand the sensitivity of various methods to monitor and detect the battery abuse. Authors [9] have discussed possible future research directions towards enhancing the safe functionality of LIBs. The failure of LIBs, as stated earlier, is governed by thermal, electrical, mechanical or cascading effect due to one of these reasons. In this regard, thermal abuse conditions due to inappropriate thermal behavior of LIB are also a widely researched area. Ahmad et al [11], discussed efficient cooling by comparing the effectiveness of "both-tab" and "radial cooling" cooling approach to prevent the possibility of thermal runaway. These results show, the significance of cooling strategy

that should be adopted for different battery chemistries. Failure of a single LIB may lead to failure of a whole battery pack that may subsequently results into the failure of the electric vehicle using it. Such failures of batteries with different battery chemistries [12, 13] are a cause of concern to occupant safety and environment both.

It is to be noted here, that most of the work discussed the different abuse conditions for different battery chemistries. In the present work, comparison of failure progression of LIB, having lithium-cobalt oxide (ICR 18650) cathode, is done considering, lateral and longitudinal compression. The distinct failure behavior of considered LIB at various failure stages depicts the changing rate of failure progression.

2. MATERIAL AND METHOD

Commercially available 18650 lithium ion battery (3.2 V/2200 mAh, 65 mm* 18 mm* 18 mm) with lithium-cobalt oxide chemistry are used in this study as they are widely used in laptops, drones etc. The considered batteries at 2.5 V with states of charge (SOC) 0%. The SOC of the battery is 0% to avoid severe thermal runaway or fire at the start of internal short circuit during deformation. The present work does not include the temperature and voltage measurements as this work only deal with the mechanical behavior of batteries not the thermal and electrical aspect or short circuit behavior of batteries. A Universal Test Machine (MTS 100 T) is used to perform the compression test as per the loading direction shown in figure 1. The cylindrical battery was compressed between two flat plates in lateral and longitudinal directions at a quasi-static rate of 5 mm/min. The applied load and plate displacement were measured during the experiments. The test was repeated at least three times to ensure the accuracy of the measured data.

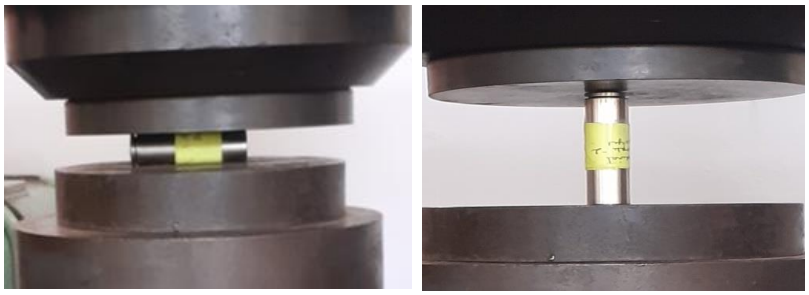

Figure 1. Experimental setup for (a) lateral compression, and (b) longitudinal compression of 18650 lithium-ion batteries.

3. RESULTS AND DISCUSSION

The, loading at specified rate of feed is provided once the initial contact of the crosshead with the considered LIB as shown in figure 1. (a) and (b). The measured load-displacement curve corresponding to the loadings are shown in figure 2.

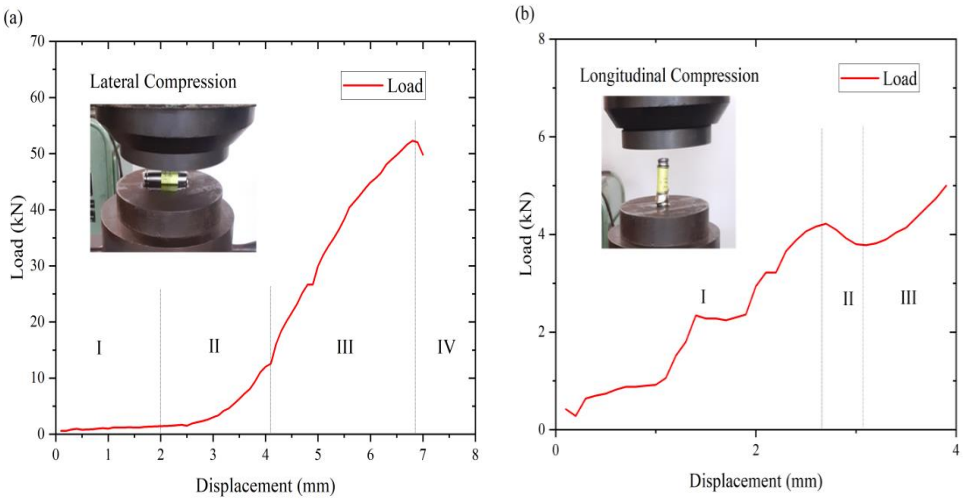

Figure 2. Load vs. displacement behavior and stages of failure progression of LIB (ICR 18650) under (a) lateral compression, and (b) longitudinal compression.

During lateral compression, the load increases at small rate for Stage I showing compression of the casing of cell. The load vs. displacement curve seems to be linear in Stage I but it is not linear. The load then displays a platform stage called as Stage II that signifies the onset of jellyroll compression after casing compression is complete. Stage II is followed by the Stage III depicting compaction stage wherein jellyroll is compressed (space between the layers of jellyroll is reduced during this stage), and finally a load drop is seen in Stage IV illustrating complete rupture (figure 2a). The peak load is approximately 53.04 kN, and the corresponding displacement is 7 mm.

For longitudinal compression, figure 2b highlights the slow rate of increases in load during Stage I until the peak force is reached showing compression of end-cap and space between end-cap and jellyroll. The force then fluctuates around 440 N because of the buckling of cylindrical casing in Stage II and finally increases with the formation of multiple compression rings in the casing during Stage III due to repetitive buckling of casing and compression resistance offered by jellyroll. Buckle rings form mainly in Stage II, and Stage III as shown in the figure 2 b. Buckle rings forms mainly in Stage II and Stage III because in Stage I the end cap and space between end cap and jellyroll is compressed, after that the compression of shell casing starts which results in buckling of shell and formation of

multiple rings. The peak load in this case is approximately 5 kN, and the corresponding displacement of cross head is 3.9 mm.

4. CONCLUSION

Compression tests were performed on 18650 (IFR) LIB. The LIBs were tested with 0% state of charge. Lateral and longitudinal compression tests were carried out to quantitatively analyze the failure of LIB by measuring the maximum load bearing capability of considered LIB.

- It was found that battery samples failed at 53 kN and at 5 kN under lateral and longitudinal compression respectively. The corresponding displacement at the instant of failure is 7 mm in case of lateral compression and 3.9 mm in case of longitudinal compression.
- The results of the tests describe the different stages of the failure depicting the onset of failure and complete failure. The different stages of failure in lateral compression are compression of casing, jellyroll compression, compaction and rupture or load drop. Similarly, the stages of failure in longitudinal compression are compression of casing with caps (considering space between end cap and jellyroll), buckling of casing and ring formation and compression in jellyroll along with casing. The formation of ring in longitudinal compression test revealed the criticality of such loading configuration in comparison to the lateral loading.
- It was concluded that the local failure of cell in the test can be detected by local peak in the force-displacement curve.

REFERENCES

[1] R. A. Austin. Lower Extremity Injuries and Intrusion in Frontal Crashes. (Report No. DOT HS 811 578). Washington, DC: National Highway Traffic Safety Administration, (2012, March).

[2] J. Xu, L. Wang, J. Guan, and S. Yin, “Coupled effect of strain rate and solvent on dynamic mechanical behaviors of separators in lithium ion batteries,” Materials & Design, vol. 95, pp. 319–328, Apr. 2016, doi: 10.1016/j.matdes.2016.01.082.

[3] W. Wang, S. Yang, and C. Lin, “Clay-like mechanical properties for the jellyroll of cylindrical Lithium-ion cells,” Applied Energy, vol. 196, pp. 249–258, Jun. 2017, doi: 10.1016/j.apenergy.2017.01.062.

[4] E. Sahraei, J. Campbell, and T. Wierzbicki, “Modeling and short circuit detection of 18650 Li-ion cells under mechanical abuse conditions,” Journal of Power Sources, vol. 220, pp. 360–372, Dec. 2012, doi: 10.1016/j.jpowsour.2012.07.057.

[5] T. Wierzbicki and E. Sahraei, “Homogenized mechanical properties for the jellyroll of cylindrical Lithium-ion cells,” Journal of Power Sources, vol. 241, pp. 467–476, Nov. 2013, doi: 10.1016/j.jpowsour.2013.04.135.

[6] G. Y. Gor, J. Cannarella, C. Z. Leng, A. Vishnyakov, and C. B. Arnold, “Swelling and softening of lithium-ion battery separators in electrolyte solvents,” Journal of Power Sources, vol. 294, pp. 167–172, Oct. 2015, doi: 10.1016/j.jpowsour.2015.06.028.

[7] X. Zhu et al., “Internal short circuit and failure mechanisms of lithium-ion pouch cells under mechanical indentation abuse conditions : An experimental

study," Journal of Power Sources, vol. 455, p. 227939, Apr. 2020, doi: 10.1016/j.jpowsour.2020.227939.
[8] W. Wang, Y. Li, L. Cheng, F. Zuo, and S. Yang, "Safety performance and failure prediction model of cylindrical lithium-ion battery," Journal of Power Sources, vol. 451, p. 227755, Mar. 2020, doi: 10.1016/j.jpowsour.2020.227755.
[9] T. Ma, L. Chen, S. Liu, Z. Zhang, S. Xiao, B. Fan, L. Liu, C. Lin, S. Ren, F. Wang. "Mechanics-morphologic coupling studies of commercialized lithium-ion batteries under nail penetration test," Journal of Power Sources, vol. 437, p. 226928, Oct. 2019, doi: 10.1016/j.jpowsour.2019.226928.
[10] Z. Liao, S. Zhang, K. Li, G. Zhang, and T. G. Habetler, "A survey of methods for monitoring and detecting thermal runaway of lithium-ion batteries," Journal of Power Sources, vol. 436, p. 226879, Oct. 2019, doi: 10.1016/j.jpowsour.2019.226879.
[11] T. Ahmad, A. Mishra, S. Ghosh, and C. S. Casari, "Identifying Efficient Cooling Approach of Cylindrical Lithium-Ion Batteries," Energy Technology, vol. 10, no. 2, p. 2100888, Nov. 2021, doi: 10.1002/ente.202100888.
[12] S. Kala and A. Mishra, "Battery recycling opportunity and challenges in India," Materials Today: Proceedings, vol. 46, pp. 1543–1556, 2021, doi: 10.1016/j.matpr.2021.01.927.
[13] S. Kala, A. Mishra, V. Shukla, Battery technologies and its future prospects, Journal of the Indian Chemical Society, Vol 97, 10a, pp. 1683-1687, 2020.

Biographies

Vishesh Shukla received the bachelor's degree in Mechanical Engineering from Sam Higginbottom University of Agriculture, Technology and Sciences (SHUATS), Prayagraj, UP, India in 2016, the master's degree in Energy Technology and Management from Madan Mohan Malaviya University of Technology (MMMUT), Gorakhpur, UP, India in 2018, and currently pursuing the philosophy of doctorate degree in Battery Safety and its Assessment from Department of Applied Mechanics, Motilal Nehru National Institute of Technology Allahabad, Prayagraj, UP, India.

.

Dr. Ashutosh Mishra received the bachelor's degree in Manufacturing Technology, the master's degree in Production Engineering from IIT BHU, Varanasi, India, and the philosophy of doctorate degree in Structural Mechanics, Mechanical Engineering from Indira Gandhi Centre for Atomic Research (IGCAR), Kalpakkam, Chennai, India. He is currently working as an Assistant Professor at the Department of Applied Mechanics, Motilal Nehru National Institute of Technology Allahabad, Prayagraj, UP, India. His research areas include Mechanics of composites and 3D printed parts, Battery modeling and battery abuse testing, Mechanical

behavior of metals, Macro mechanics of bones and tissues under time dependent and radioactive load, Application of mechanics in multidisciplinary field.. He has been serving as a reviewer for many highly-respected journals - Latin American Journal of Solids and Structures (SCI-IF=1.289), Journal of Materials Engineering and Performance (SCI-IF=1.652).

Prof. R P Tewari received the bachelor's degree in Mechanical Engineering from MMMUT Gorakhpur, India, the master's degree in Biomedical Engineering form IIT BHU, Varanasi, India, and the philosophy of doctorate degree from IIT BHU, Varanasi, India, respectively. He is currently working as a Professor at the Department of Applied Mechanics, Motilal Nehru National Institute of Technology Allahabad, Prayagraj, UP, India. His research areas include Biomechanics, Robotics, Rehabilitation Engineering, Biomaterials. He has been serving as a reviewer for many highly-respected journals - Computer Methods in Biomechanics and Biomedical Engineering, Journal of Composites & Biodegradable Polymers, Executive Council Guest Editor in Current Chinese Science – Bioinformatics.

Solar Cookers and their Present Global Status: A Review

[1]Bhupendra Koshti[*], [2]Rahul Dev, [3]Ajaya Bharti, [4]Audhesh Narayan, [5]Priyank Srivastava

Motilal Nehru National Institute of Technology, Allahabad, Prayagraj, India

bhupendra@mnnit.ac.in, rahuldsurya@gmail.com, abharti@mnnit.ac.in, anarayan@mnnit.ac.in, priyank.srivastava25@gmail.com

Abstract

Nowadays, peoples in the world concentrate on energy, the environment. Presently developing countries are rising concerned about deforestation and finding alternatives to non-renewable energy sources. In recent times developing countries utilize a large percentage of solar energy as a power requirement. Solar cooking contributes to energy saving in the world, control of indoor pollution in homes, cost-saving, and preserving non-renewable energy sources for the future, and also maintaining the earth's global temperature. Solar Energy is the most promising and suitable option to meet energy demands in the cooking sector. But its widely used is remains limited. Most works in solar cookers are studied for research purposes only. In this paper, an effort has been made on various types of solar cookers Design, materials, and present conditions. Eventually, different appropriate technology is explained for future analysis in solar cooking, and Various performance parameters, like FOM, and the power of the cooker are also considered.

Keywords. Solar cooker, Figure of Merits(FOM), Manual solar cooker, cooking power, etc.

1. INTRODUCTION

Sunlight an immense origin of heat and generates vitality at the rate of 3.8×10^{23} kWh in the form of radiant Energy with the help of a nuclear fusion reaction [1]. Solar energy application is immemorial from the origin of human beings on earth. The life of people relies on energy production and its utilization that affects the supply and demand of society. A large amount of Energy depends upon non-renewable sources like fossil fuels, firewood, animal dung, agriculture waste, etc. while the Energy comes in urban places by petroleum and LPG. In the twenty-first century, 82% of world energy comes from the burning of fossils fuels, which results in increased greenhouse gases, global warming, release pollution, and decreases the ozone layer in the environment and more chances of environmental risk therefore to protect the environment it is essential to a renewable source of Energy [2]. The world health organization (WHO) predicts that 4 million people prematurely die due to minute particle pollution that is effect in cooking along the burning of conventional fuels in homes [3]. Solar Energy is the most suitable option for thermal application and is also present in the most abundant quantities among all renewable energy sources [4]. Cooking is essential for the human being and also the life human will depend upon on cooking. However, with increment in population and depletion of resources, food will be scarce in the future [5]. The solar cooker has significant potential to overcome the exhaustion of

conventional fuels in cooking. However, to increase curiosity in solar cookers, therefore required to develop a different type of solar cooker, specific customer needs, satisfaction, economics, and climate condition [6]. Solar cooking is a trouble-free and peculiar method to cook food and sunlight is drop down on the earth. This technique is very constructive in a developing country where the people will depend upon the availability of solar radiation in these regions, where most common peoples people used resources for cooking [7]. Pasteurization and sterilization processes take place in solar cookers. Therefore, researchers are regularly modified solar cookers to increase their performance [8]. In India, only 36% of energy is utilized in solar cooking. solar cooking is the most convenient option due to its economical and extensible [9]. Almost heavily populated countries are blessed in the world with a sufficient amount of solar radiation with a daily mean value between 5 to 7 kWh/m^2 and 274 bright days in the year [10]. Conventional fuels increase carbon dioxide by 1.07% in the short period and 1.9% in the long period respectively [11]. In the contemporary scenario, the average annual energy used is increased by 1% in advanced countries, 5% increases in developing countries, and becomes an economic development of their nation. [12,13]. The purpose is to provide information and strengthen the current accomplishment of solar cookers and their future potential.

2. WORKING PRINCIPLE

Solar power cooker changes solar radiation towards thermal Energy. This thermal Energy is utilized to prepare food, which is kept inside the cooking utensil. [14]. This trapped heat is present inside the container used to assist in heating and converting it into healthily cooking food. There are three modes of heat transfer in which solar cooker works are concentration, absorption, and retention [15]. The simple flat solar cooker is the cheapest and a temperature 100-150°C (300 F). The sun's radiant energy incident on the glass cover and reached at bottom base. The inside air gets heated due to the contact of the bottom plate, heats, and transfers its thermal energy to the food present inside the pots.

The bottom plate of the solar cooker should be made of black material in order to transfer maximum heat to the utensils (pots). To minimize heat, condition a single transparent window must be replaced with a double transparent window. Reflective glass is used to maximize the incoming solar radiation which can be varied from 0° to 120°. Also, the box must be made like airtight via possible, by decrease the hot airflow from inside to outside. [14].

3. CLASSIFICATION

In the current situation of renewable Energy, scientists and researchers working on the efficient design of solar cookers. The classification of solar cookers is a difficult task. Therefore, solar cookers are reclassified into two main categories one is an automatic type of solar cooker and the other is a manual solar cooker which is evidenced in diagram. Generally, box-type cooker and concentrating cooker is mostly used in cooking applications all around the world. [16].

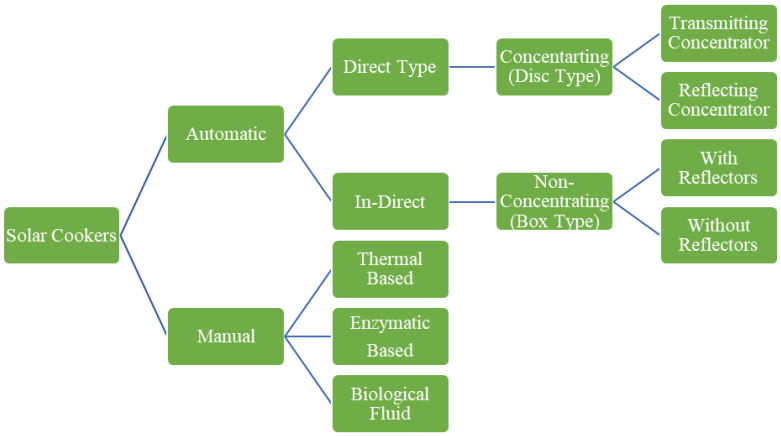

Figure 1. Classification of solar cookers [16]

4. TESTING AND PERFORMANCE

Solar cooking is an inspiring technology showing signs of future success and uninterrupted application of solar Energy. The availability of solar Energy and its sustainability in the environment become the most suitable option for energy supply non-renewable energy sources. Therefore, most people are interested in increasing the performance of the solar cooker [17]. Existing International testing standards are applied to estimate the performance of a solar cooker. There are three types of international standards used for testing solar cookers. These are (i) American Society of Agricultural Engineers Standard (ASAE, 2003), (ii) Bureau of Indian Standards Testing Method (BIS 2000), and (iii) European Committee on Solar Cooking Research Testing Standard and others (ECSCR, 1994) [18]. The Figures of merits, Standardized cooking power, and cooking efficiency terms were used to predict the performance of the solar cooker [19]. The figure of merit F_1 is described as the ratio of optical efficiency to the heat loss factor by absorber plate and the measure of the differential temperature gained by the absorber plate at a particular level of solar insolation. F_2 is more or less independent of climatic conditions and indicates heat transfer from the absorber plate to the water in the containers placed [20]. The first figure of merit, F_1, is calculated with the help of a stagnation test under the no-load condition. The second figure of merit, F_2 is calculated under full load conditions when water is taken in pots, and reflector is not considered in this test [21]. F_1 is based on stagnation-load at without load which is empirically shown as

$$F_1 = \frac{\eta_o}{u_L} = \frac{(T_P - T_\infty)}{I_S} \quad (1)$$

(F_2) is based on complete load and is mathematically expressed as:

$$F_2 = \frac{F_1(mc)_W}{A(t_2 - t_1)} \ln\left[\frac{1-((T_{W1}-T_\infty)/F_1 I_a}{1-((T_{W2}-T_\infty))/F_1 I_a}\right] \quad (2)$$

The higher value of the figure of merits (F_1 and F_2) is used in healthy cooking. The temperature range of T_{W2} between 90 to 95ºC and T_{W1} should be taken between ambient and boiling temperatures. From experimental data, it concluded that the water quantity depends on the F2 test in solar cookers. Hence performance tests depend on the amount of water to be taken. The lower limits of F_1 and F_2 are preferred in order to satisfactory accomplishment

of solar cooker. The eligibility criterion for qualified ISI mark in solar cooker the value of F_1 should not than 0.12 and F_2 should greater than 0.40[22].

Standardized cooking power- Express in terms of following equations.

$$P = \frac{T_{W1} - T_{W2}}{t} mc_w \quad (3)$$

Where, T∞ is ambient temperature (K), T_p is plate temperature (K), Is is solar insolation, (W/m2), T_{w1} is beginning temperature of water (°C), T_{w2} is finishing temperature of water (°C), P is standardized cooking time to 700, (W/m2), mcw is quantity of water multiplied by specific heat (J $°C^{-1}$), U_L is heat loss factor, $\eta_o$is efficiency of solar cooker, Ia is average solar radiation (W/ m^2).

5. STUDIES AND ADVANCEMENT IN SOLAR COOKING SYSTEM DESIGN FEATURES OVER RECENT TIMES

In the modern world, many researchers are focused on creating new designs, geometry, and material to increase the cooking power, and efficiency of solar cookers. Mullick conceived and built a box-style solar oven in 1987, the outer body is made from teakwood, the inner body from aluminum sheet, and the cooking pot is aluminum. Carried the thermal test on solar cooker under different climate conditions and various food and formed the figure of merit (F_1 and F_2) [36].

Hot-box solar cooker developed for late evening purpose. The material used is a galvanized, aluminum sheet for the outer and inner body, having double walled. A 5kg used engine oil is filled between the inner body and sealed for storage purposes. The maximum stagnation temperature is found to be the same as without storage during the day, the temperature in the storage cooker is raised by 23°C from 1700 to 2400 h, and the efficiency is reported to be 27.5 percent. [10]. Mahavar et al created a small-scale solar rice cooker in 2012 from transparent acrylic (PMMA) thickness of 2.75 mm with an air gap of 13 mm. solar cookers made from opaque material have the disadvantage of the maximum area of the container covered with shadow this leads to increases thermal stress and non-uniform heating. In this work, the radiation enters from the top and horizontal sides of the solar cooker. therefore, increasing the thermal performance of the cooker. The maximum temperature reaches 144°C and cooking 103.5 W. Acrylic and polycarbonate materials have been shown to be appropriate for glazing materials. [23]. Kumar used geometry and Design and build a solar oven with a truncated pyramid shape. the main purpose of this solar cooker was it acts as a dryer for domestic uses, the principle behind was to increase the absorber tray temperature due to its geometry Sunlight falls and is reflected with high intensity in order to maintain a higher temperature. Maximum temperatures of 140 °C and 98.6 °C were attained in the no-load and full-load water conditions, respectively. [26]. Namrata et. al fabricated a masonry and cement plaster solar cooker having a cylindrical shape in 2011. Comparative thermal performance results show that a building-material-housing solar cooker (BHMC) is slightly better than a commercially solar cooker (CSC) [29]. Verma manisha et. al developed a solar cooker made of hardboard for the nuclear family in 2011 and tested on a hot climate for various food. Concluded that it was suitable for the nuclear family due to low cost, less weight as also compared to other good cooking capacities [30]. In 2018 The box-type solar oven, developed and produced by Yettou, is made out of a wooden box. for the hot box, as well as a mirror, aluminium is used for making absorber plate painted black with inclined

area has many benefits When compared to traditional box cookers, expanding the horizontal width improves the amount of sunlight falling on the solar cooker and minimises the level of shadow falling on the absorber. Trials were performed with 2 kg of water in the cookers from 08:00 to 15:00 solar time. Temperature gain in the box-type solar cooker was around 69.8° C during the testing. [24]. In 2018, Ademe introduced a box-style solar cooker with a glazed wiper function. The outer wall is made of a single-walled cardboard box of 50mm. A 1.5 mm thickness iron sheet using for making the inner box. The gap between the outer and inner box is filled with compressed sawdust (insulator) 50 mm thick. Three-reflector is used in this mechanism, the inner one is composed of a 1.5 mm thick iron sheet. The tilted intercept is controlled from the horizontal plane. The foam strip is attached with the exterior glazing and thin threads to the back and front side wooden sticks. The ASA International Test Procedure and the Bureau of Indian Standards were used to evaluate thermal performance. Without a wiper mechanism, F_1 = 0.123 Km^2/W, F_2 = 0.540, the standard cooking power 36 W, and the total efficiency is 22%. With wiper mechanism, F_1 = 0.123, F_2 = 0.827, standard cooking power 51 W, and a total efficiency of 31.4%. [28]. Mohamad Zeeshan Siddiqui developed a unique design a solar oven that combines the functions of cooker and dryer in a single unit, and conducted an outdoor experiment for evaluating performance. A separate section was made for the cooker and dryer and connected with a small opening provided for air passage to transfer lower portion higher temperature to upper portion higher temperature, which behaves as with a dryer, the air is moved across the box by buoyancy-driven free convection flow. The temperature values of the solar cooker segment were (80 °C – 135 °C) and the dryer segment was (35 °C – 65 °C) under the same environmental conditions. The F_1 and F_2 were found to be 0.11, 0.303. Utilization factor, COP, and drying performance were calculated to be 34%, 66%, and 14%. [27] Saxena modified the solar cooker and introduced a hybrid design in 2018. To enhance the overall movement of warm air within the cooker, a trapezoidal shape duct is placed Inside the duct is a cooker and a halogen light bulb. Also, spherical balls were kept inside the box. The author found that with these designs the overall efficiency increases from 38.10% to 45.11 [31]. Some researchers also concentrated on improving the Design of solar cooker vessels/pots/utensils and considered very crucial parts of solar cookers and their effects on these parts analyzed [32-35]. Hermelinda presented newly designed pots and applied them to the different numbers of pots to test their thermal performances and found that 35%, 16%, and 12% for first, second, and third cooking pots designs, respectively [36]. In 2019 Samdarshi used a technique to maximize the cooking performance of solar cookers by improving the Design of cooking utensils/pots. In this pot which is made up of stainless steel, the top middle surface of the box is replaced with the glass using an appropriate high-temperature sealant. The heating performance of the box cooker increases due to capture from the top of cooking pots as well as sides of cooking pots [37].

Concentrate type of solar cooker used due to its faster cooking ability and the high-temperature range than simple box cooker. It is based on the three-dimensional parabola principle when directed into the sun and reflected onto the focus.

Badran used reflective aluminum thin foil in a dish satellite for making a portable parabolic solar cooker. Cooking and heating were two fundamental considerations for the analyzed solar cooker. In the cooking method, the pot placed inside the glass box and uncovered pots were analyzed deeply, whereas, in the heating method, the heat transfer of heat energy with the help of a collector [44] Regattieri builds a parabolic-type solar cooker out of a cardboard

box that was previously applied for mankind's relief material and logistic support to the public who need help. The main aim is to utilize the waste cardboard, and performances are measured through the elephant test and disc solar cooker test. The various shapes are tested, and the best result is obtained from parabolic geometry, and efficiency was about 14–18%, like of raw fire [49]. Masum Ahmed used stainless, thin aluminum baffles and mayer tape. For making concentrating solar cooker. Heat conduction takes place in the aluminum vessel cast black is more prominent. This material is easily available and provides good results in cooking food and the efficiency of solar cookers. After conducting the experimental test on parabolic solar cookers with Mylar tape and results showed that reflective materials better as compared to others [56].

Contribution of some legendary researchers in Concentrating-type cookers.

Work	**Highlighted Feature**
El-Kassaby 1991	Developed solar cooker which employs for cooking and distillation of water. the shape of the cooker is a parabolic square dish type. If the bottom portion of the pot of the solar cooker is maintained black then efficiency is increased by 30%.[25]
Patel and Philip (2000)	Consider three types of concentrated solar cookers and conclude that the Fresnel reflector cooker is better than the parabolic type [38]
Oztürk (2004)	Performances of solar cookers were found, 2.8–15.7% and 0.4–1.25% in terms of energy and exergy[39]
Pohekar and Ramachandran 2006	The author described that liquefied petroleum gas (LPG) performance is fast as compared to other cooking devices [40].
Kaushik and Gupta (2008)	Predicted the enhancement of different geometry with Exergy analysis. [41].
Sosa-Montemayor (2009)	A coffee device was developed using a small circular TV dish [42].
Al-Soud et al. (2010)	A biaxial sun tracking system and programmable logic controller were used [43]
Badran et al. (2010)	Designed and developed truncated cone-shaped receiver at the focal point made from copper [44].
Purohit and Purohit 2011	Instruments error around 1-5.5% on solar cookers thermal performance [45].
Prasanna and Umanand 2011	A new technique is used for circulating the fluid in a kitchen in the form of solar Energy [46].
Huang et al., 2013	The various optical error was found under the typical condition to maximize the solar power energy to net head efficiency. The results of the experiments revealed that a concentrate-type solar cooker with a spherical receiver had the highest solar energy efficiency [47].
Suple And Thombre, 2013	A tracking system is used for a concentrated type cooker using the circular disc for indoor cooking [48].
Regattieri 2015	Modified portable solar cooker using waste cardboard packing the function of this cooker is heating, cooking food, and filtration of raw water and rivers [49].
Krishnan 2015	Developed disc type solar cooker and found that faster ability to cook food at a specified time with the help of solar radiation [50].

(Akoy and Ahmed, 2015).	Different solar cookers were fabricated and their performance was examined. The highest temperature was achieved at 86.5 °C for a concentrated solar cooker, 52.36 °C for a simple box cooker, and 43.5 °C for a panel cooker.[51].
Wimmer et al. (2017)	Consider different types of the solar cooker and research on public views on why solar cooker is not used in Austria and Thailand [52].
Indora and Kandpal 2018	Provides institutional parabolic solar cookers for cooking food also concentrated on features of the economy [53].
Sagade et al. 2018	Obtained technique for calculating Rating in various box cooker and concentrating type solar cooker using experimental data [54].
Jayaleka 2020	Working on Spiral Concentrating solar cooker and calculated Optical efficiency and instantaneous efficiency. the overall efficiency found to be 73.5% [55].
Masum Ahmed 2020	The important objective of this type of cooker is to use various reflective materials to concentrate the solar radiation into thermal Energy [56].

These are the calculated results of the researcher on various materials in which tests are conducted in a solar cooker to increase the performance of solar cooker in the world to provide an alternate solution for conventional fuel in the world. These values depend on cooking power, figures of merits, efficiency, temperature, etc.

6. CONCLUSION

Solar cookers' present circumstances are focused on increasing their thermal performance and efficiency. Another parameter is also kept in mind regarding safety issues in solar cooking and awareness among the public on how to use the solar cooker and how it is very beneficial for public health and eco-friendly nature. The conventional fuel costs also increase day by day therefore alternate options for cooking. To develop solar cookers for practical purposes, stimulate studies, an experimental approach is needed to find out the most appropriate with different geometries, different materials to improve performance with aesthetic looking and economic costs, and socially acceptable geometry and Design. Reflector can be increase to maximise solar cooker performances and Double glass also used to reduce convection losses. Further studies are also needed regarding the portable transparent solar cooker with time constraints, and it is excellent for when you are working outside from home, and you do not want to waste time in the kitchen.

REFERENCES

[1] D.Y. Goswami, F. Kreith, JF Kreider, Principles of solar engineering. Taylor and Francis 2000.

[2] A. Lotfalian, M.Ghazavi, B. Hoseinzadeh B, “Reviewing drying of dill and spearmint by a solar dryer and comparing with traditional dryers”. World Appl Sci J, 2010; 8:364–8.

[3] Funk P A, Larson D L. Parametric model of a solar cooker. Solar Energy 1998; 62: 63–68.

[4] H.H Ozturk, “Comparison of energy and exergy efficiency for solar box and parabolic cookers”. J Energy Eng,133:53–62, 2007.

[5] M.Thirugnanasambandam, S. Iniyan, R. Goic, “A review of solar thermal technologies. Renew Sustain Energy Rev”. 14:312–2, 2010

[6] A. Abhat, “Low temperature latent thermal energy storage system: heat storage materials”. Solar Energy, 30: 313–332, 1983.
[7] P.J Lahkar, S.K Samdarshi, “A review of the thermal performance parameters of box type solar cookers and identification of their correlations”. Renew Sustain Energy Rev, 2010; 14:1615–21, 2010.
[8] E Cuce, P.M Cuce, “Theoretical investigation of hot box solar cookers having conventional and finned absorber plates”. International Journal of Low-Carbon Technologies, 10:238–245, 2015.
[9] N.M Nahar, “Performance and testing of a hot box storage solar cooker”. Energy Conversion and Management, 44:1323–31, 2003.
[10] S. Adams, C. Nsiah, “Reducing carbon dioxide emissions: does renewable energy matter”. Sci. Total Environment, 693: 1-9, 2019.
[11] K. Sanglimsuwan, “Carbon dioxide emissions and economic growth: an econometric analysis”. International Research Journal of Finance and Economics, 67: 97-102, 2011.
[12] F. Yettou, B. Azoui, A. Malek, A. Gama, N.L Panwar, “Solar cooker realizations in actual use: an overview”.Renew Sustain Energy Rev, 37:288–306, 2014.
[13] Manual for solar box cookers How to build and use them Published by Technology for Life, Finland, 1995.
[14] J.R Fanchi, “Energy technology and directions for the future. 1st ed. London”.Elsevier Academic Press, 2004.
[15] A. S. Boudghene, H. Koinuma, “A primary study on a long-term vision and strategy for the realization and the development of the Sahara Solar Breeder project in Algeria”. Renew Sustain Energy Rev, 16:591–8, 2012.
[16] A.H Zafar, M.Y Khan, A.W Badar, R.Tariq, F.S Butt, “Introducing a novel design in the realm of box type solar cookers: An experimental study”. Journal of renewable and sustainable Energy, 10: 043707, 2018.
[17] E.C, Ugwuoke, C.M Aburu, I. Ofili, N.P Oputa, Shaibu. N, “Determination of Temperature Variation of a Box-Type Solar Cooker”. The Pacific Journal of Science and Technology, 19: 12-16, 2018.
[18] E. Biermann, M. Grupp, “Palmer R. Solar cooker acceptance in South Africa: results of a comparative field test' Solar Energy”. 66:401–7, 1999.
[19] S. Poonia, A.K. Singh, P. Santra, D. Jain, “Development and performance evaluation of high insulation box type solar cooker”.Journal of agricultural engineering, 43:1-10,2019.
[20] N. Kumar, T. Chavda, H.N. Mistry, “A truncated pyramid non-tracking type multipurpose domestic solar cooker/hot water system”.Applied Energy, 87: 471–477, 2010.
[21] N.L Panwara, S.C Kaushika, S. Kotharib, “State of the art of solar cooking: An overview”. Renewable and Sustainable Energy Reviews, 3776– 3785, 2016.
[22] D. Buddhi, S.D Sharma, R.L Sawhney, “Performance test of a box type solar cooker: effect of load on the second figure of merit”. Int J Ener Res, 23:827–30, 1999.
[23] S. Mahavar, N. Sengar, P. Rajawat, M. Verma. P. Dashora, “Design development and performance studies of a novel single-family solar cooker”. Renew Energy, 47:67–76,2012.
[24] F. Yettou, B. Azoui, A. Malek, A. Gama, N.L Panwar, “Experimental investigation and thermal modelling of box and parabolic type solar cookers for temperature mapping”. Journal of Thermal Analysis and Calorimetry, 136:1347–1364, 2019.

[25] M.M El-Kassaby. “New solar cooker of parabolic square dish: design and simulation”. Renewable Energy, 1:59–65, 1991.
[26] N. Kumar, S. Agravat, T.Chavda, H.N Mistry, “Design and development of efficient multipurpose domestic solar cookers/dryers”. Renew Energy, 33:2207–11, 2018.
[27] M.Z Siddiqui, A.W Badar, S.A Jakhrani, SA, M.Y Khan, F.S Butt, MS. Siddiqui, “Development and experimental investigation of a novel combined solar cooker and dryer unit. Energy Sources”. Part A: Recovery, Utilization, and Environmental Effects, 2020.
[28] A. Zeleke, H.Sameer, “Design, construction and performance evaluation of a Box type solar cooker with a glazing wiper mechanism”. AIMS Energy,6: 146–169, 2018.
[29] N. Senger ,S. Mahavar, M. Gupta, P Dashora. “Experimental Studies, Energy Savings and Payback Periods of a Cylindrical Building-Material-Housing Solar Cooker”. International Journal of Energy Information and Communications, 2:75-84, 2011.
[30] M. Verma, S. Mahavar, P. Dashora, “Extensive Experimental Studies of a Single-Family Solar Cooker. International Journal of Energy”. Information and Communications' 2:169-179, 2011.
[31] A. Saxena, N. Agarwal, “Performance characteristics of a new hybrid solar cooker with air duct”. Solar Energy, 159: 628–637, 2018.
[32] A.R Reddy, A.V. Rao, “Narasimha. Prediction and experimental verification of performance of box type solar cooker e Part I. cooking vessel with central cylindrical cavity” Energy Convers. Manag, 48: 2034-2043, 2007.
[33] A.R Reddy, A.V. Rao, “Prediction and experimental verification of performance of box type solar cooker” Part II: cooking vessel with depressed lid. Energy Convers. Manag, 49: 240-246, 2008.
[34] Rao A.V. Rao, S. Subramanyam, “Solar cookers-part I: cooking vessel on lugs” Sol. Energy, 75:181-185, 2003.
[35] Rao A.V. Rao, S. Subramanyam, “Solar cookers part-II- cooking vessel with central annular cavity” Sol. Energy, 78:19-22, 2005.
[36] SC Hermelinda, GA Mauricio, “Development of the solar cooker Jorhejpatarnskua: thermal standard analysis of solar cooker with several absorber pots” Energy Proced, 57:1573-1582, 2014.
[37] A.A Sagade, S.K Samdarshi, P.J Lahkar, S.N Sagade, “Experimental determination of the thermal performance of a solar box cooker with a modified cooking pot”. Renewable Energy, 150:1001-1009, 2020.
[38] NV Patel, S.K Philip, “Performance evaluation of three solar concentrating cookers”. Renew. Energy, 20: 347-355,2000.
[39] H.H Ozturk, “Experimental determination of energy and exergy efficiency of the solar parabolic-cooker”.Sol. Energy 77:67-71, 2004.
[40] S. D. Pohekar, M. Ramachandran, “Multi-criteria evaluation of cooking energy alternatives for promoting parabolic solar cooker in India”.Renewable Energy, 29:14 49-1460, 2004.
[41] S.C Kaushik, M.K Gupta, “Energy and exergy efficiency comparison of community-size and domestic-size paraboloidal solar cooker performance”.Energy Sustain Dev, 12:60-64, 2008.
[42] F. S Montemayor, O.A Jaramillo, J.A, Río Del, “Thermodynamic analysis of a solar coffee maker”.Energy Conversion and Management, 50: 2407-2412, 2009.
[43] Al-Soud M.S, Abdallah. E, Akayleh. A, Abdallah. S, Hrayshat. E.S, “A parabolic solar cooker with automatic two axes sun tracking system”. Appl. Energy, 87 :463-470,2010.

[44] A.A Badran, I. A Yousef, N. K Joudeh, R. A Hamad, H.K Hassouneh, “Portable solar cooker and water heater”. Energy Convers. Manag, 51:1605-1609, 2010.
[45] I. Purohit, P. Purohit, “Instrumentation error analysis of a box-type solar cooker”. Energy Conversion and Management, 50: 365-375, 2009.
[46] U.R Prasanna, L. Umanand, “Modeling and design of a solar thermal system for hybrid cooking application”. Applied Energy 88:140-1755, 2011.
[47] W. Huang, “ Prediction and optimization of the performance of parabolic solar dish concentrator with sphere receiver using analytical function”. Renewable Energy 53: 18-26, 2013.
[48] Y.R Suple, S.B Thombre, “Performance evaluation of parabolic solar disc for indoor cooking”.OSR Journal of Mechanical and Civil Engineering (IOSR-JMCE), 4: 42-47,2013.
[49] A. Regattieri A, F.Pian, M. Bortolini, M. Gamberi, E. Ferrari, “Innovative portable solar cooker using the packaging waste of humanitarian supplies”. Renewable and Sustainable Energy Reviews, 57: 319-326, 2016.
[50] V.K Krishnan, T. Balusamy, “Simulation studies on concentrating type solar cookers”. World Academy of Science Engineering and Technology, 15:1143-1147, 2015.
[51] O.M Akoy, A. Ahmed, “Design, Construction and Performance Evaluation of Solar Cookers”. Journal of Agricultural Science and Engineering, 1: 75-82, 2015.
[52] R. Wimmer, J.M Kang, C. Pokpong, A. Mahdavi, “Analysis of user needs for solar cooker acceptance. Sustainability Through Innovation in Product Life Cycle Design”. Eco Production. Springer Japan, 151-165, 2017
[53] I, Sunil, C. T Kandpal, “Institutional and community solar cooking in india using sk-23 and scheffler solar cookers”. Renewable Energy,120: 501-511, 2018.
[54] A. Sagade, S.K Samdarshi, P.S Panja, “Enabling rating of intermediate temperature solar cookers using different working fluids as test loads and its validation through a design change”.Solar Energy 171: 354-365, 2018.
[55] T.K Jayaleka, J.P. Julius, D Usha, “Performance analysis of cooking experiments with a spiral concentrating type solar cooker”. Studies in Indian Place Names, 18:1209-1212, 2020
[56] SMM Ahmed, M R Al-Amin, S. Ahammed, F. Ahmed, A.M Salequeb, M.A Rahman, “Design, construction and testing of parabolic solar cooker for rural households and refugee camp”. Solar Energy 205: 230-240, 2020.

Biographies

Bhupendra Koshti received the bachelor's degree in Mechanical engineering from RGPV University in 2009, the master's degree in Heat Power Engineering from RGPV University in 2011, Research scholar in Department of Mechanical Engineering, (M.N.N.I.T.) Allahabad, Prayagraj-211004,U.P, INDIA.

Dr. Rahul Dev received the bachelor's degree in Mechanical engineering in 2004 from IET Lucknow 2009, the master's degree in Energy Studies from IIT Delhi in 2007, and the philosophy of doctorate degree in Solar Distillation from IIT Delhi in 2017, respectively. He is currently working as an Assistant Professor at the Department of Mechanical Engineering, M.N.N.I.T. Allahabad,Prayagraj-211004,U.P, INDIA. His research areas include Renewable Energy, Solar Energy Applications like Solar Thermal (Solar Energy Storage, Passive Buildings, Solar Stills, FPC), Daylighting and Photovoltaics. Consultancy in Solar Energy applications.

Dr. Ajaya Bharti received the bachelor's degree in Mechanical engineering from KNIT Sultanpur, Sultanpur, UP, India in 2001, the master's degree in Materials Science and Engineering) from MNNIT Allahabad, Prayagraj, UP, India in 2005 , and the philosophy of doctorate degree in PhD (Applied Mechanics) from MNNIT Allahabad, Prayagraj, UP, India, respectively. He is currently working as an Associate Professor at the Department of Applied Mechanics M.N.N.I.T. Allahabad,Prayagraj-211004,U.P, INDIA. His research areas include Fatigue and Fracture Mechanics, Wear, Corrosion, Powder Metallurgy, Physical Metallurgy, Synthesis and Characterization of Advanced Materials, Biomaterials, Severe Plastic Deformation (SPD), Structural Health Monitoring.

Dr. Audhesh Narayan received the bachelor's degree in received the bachelor's degree in Mechanical engineering, the master's degree in M. Tech. CAD/CAM, and the philosophy of doctorate degree in Mechanical Engineering, respectively. He is currently working as an Associate Professor at the Department of Mechanical Engineering, Motilal Nehru National Institute of Technology (M.N.N.I.T.) Allahabad,Prayagraj-211004,U.P, INDIA. His research areas include Conventional & Unconventional Manufacturing Processes, FEM in Manufacturing.

Mr. Priyank Srivastava received the bachelor's degree in Mechanical engineering from Dit University Dehradun Uttarakhand in 2017, (MTech) Research scholar in Department of Mechanical Engineering, (M.N.N.I.T.) Allahabad,Prayagraj-211004,U.P, INDIA.

Prediction of Occupational Accidents in Steel Industry using Bayesian Belief Network

[1]Shivam Singh, [2]Arunjeet Chakraborty, [3]Shatrudhan Pandey, [4]Abhishek Kumar Singh

Department of Production & Industrial Engineering, Birla Institute of Technology, Mesra, Ranchi, India
[1]btech10472.18@bitmesra.ac.in, [2]arunjeet22@gmail.com, [3]er.shatrudhanp@gmail.com, [4]abhishekkumar@bitmesra.ac.in

Abstract

Nowadays, emphasizing health and safety in the process industry, building a proper model for predicting occupational safety and health hazards is essential. In general, accidents in the steel industry are often overlooked because of their sheer numbers compared to other more accident-prone sectors such as Oil and Gas. However, recent studies have shown that the number of casualties in steel industries is increasing, and this issue needs to be taken care of urgently. Some of the factors that lead to occupational hazards in the steel industry are unfavorable working setup, machine conditions, lagging Standard Operating procedures (SOP), and physical, chemical and radiation issues leading to poor health and safety conditions for workers and various property damage. Given the data set retrieved from an integrated steel plant via Incident Data Reporting System (IDRS), multiple parameters can be obtained, which can help us identify whether a casualty will occur. Various ML algorithms can be applied to detect the probability of a loss arising from this data. Each of the ML algorithms has its advantages and disadvantages. Given the complexity of the dataset, Bayesian Belief Network proves to be the ideal fit in terms of accuracy.

Keywords - Process Safety, Steel Industry, Bayesian Belief Network

1. INTRODUCTION

India's steel industry, primarily iron and steel, is the country's largest ferrous metal sector and a key economic component. India is ranked second among all countries in terms of crude steel production. Steel consumption per capita has become an indicator of a country's economic growth as a result of the Indian economy's globalization and the expansion of industries that use steel as raw material, such as the automobile industry, railways, and defence. Steel usage is also rising in the country. The availability of domestic raw resources and low labor wages, compared to the rest of the globe, are the key advantages for Indian steel companies. Steelmaking has always been a risky, and accidents are unavoidable. However, due to enhanced safety system implementation, the world has changed once more. Steel manufacturing is complicated, which means workers are exposed to a variety of hazards, including extreme heat, high pressure, radiation, heights, heavy machinery, and

hazardous pollutants, all of which put them at risk of accidents. In the process sector, it is critical to developing a system for recognizing occupational dangers.

It has also been seen that steel industry workers take long-term sick leave more often than in other industries, which more or less can be explained because of constant exposure to hot, humid, noisy, gaseous, and dusty environments, which negatively impacts the production in the steel industry thus affecting various interrelated output in sectors such as railways, housing construction, shipbuilding, etc. [1], [2].

In a recent study, it has been found that the total number of industrial accidents (major /minor) has risen to 30 crores per year, with more than 3 lakh reported deaths [3].

It must also be noted that advancements in technology and automation have resulted in different types of accidents; thus, a proper prediction of hazards taking all critical parameters must be built on an urgent basis.

To identify the parameters necessary for building our model on "Prediction of occupational hazards in steel industry using Bayesian Belief Network," thorough research has been done. The Quality Management System Standard ISO 9001 has been used by the Steel Industry for many years, along with ISO 14001:2015 for Environmental Management and ISO 45001:2018 for Health and Safety Management. The Bureau of Indian Standards (BIS) has helped our cause identify the parameters necessary for safe operation in an everyday process industry [4].

A knowledge graph is then used to identify, separate, and establish a rough relationship between the key factors responsible for occupational accidents in the steel industry [5], [6]. The knowledge model needs to be known first to understand a knowledge graph. A knowledge model is a collection of interdependent descriptions of concepts, relationships, events, etc., that allows both people and machines to process efficiently—the reports contributing to each other form an extensive network, from which meaningful output can be obtained.

Now, to understand the interrelation between different factors and to predict the possible outcomes of the accident, "Bayesian Belief Network" is used, which is a graphical method used to predict uncertain events using the conditional probability theorem (CPT) [7]. Bayesian Belief Networks are used when the real-world applications are probabilistic and there is a probabilistic connection between various events/nodes. It is mainly used for anomaly detection, diagnostics, classification, and prediction under uncertainty. It is also commonly known as the Bayes network, belief network, decision network, and Bayesian model. A Directed Acyclic Graph (DAG) is used, which helps establish relationships between various factors through a network of nodes and ultimately leads to determining the Joint Probability of each node through the conditional probability theorem (CPT). The probabilistic dependence/independence between each variable is observed through a network of arcs. It is also noted that each node is conditionally independent of its non-descendants, given its immediate parents.

The Tree Augmented Naive Bayes algorithm (TAN algo) is used for structure learning of the model leading to the identification of various measures required for process safety in steel plants. In other words, it is used for finding the approximation of the dependencies between multiple factors.

CART (classification and regression trees) and CHAID (chi-square automated interaction detection) are two decision trees used to make predictions in data mining. These predictions may reveal traits of people who are vulnerable to workplace accidents. The CART and CHAID algorithms can forecast the outcome of workplace accidents in a steel plant. Furthermore, safety authorities can reduce the rate of accidents by using predictions for detecting vulnerable workers in steel plants. However, there are some limitations to these techniques for predicting accidents in steel plants as it has often been reported that the system becomes unstable when the structure gets complicated, and therefore it is recommended that the use of Bayesian networks to predict the outcome of injuries is done in steel industries as it is better suited to capture the complexity.[8].

Other methods such as BN Augmented Naïve Bayes (BANs) and General BNs (GB) can also be used. Still, through various researchers it is found that TAN algo is comparably faster than the above-mentioned unrestricted BN methods [9], [10]. Finally, the model has been validated through Sensitivity analysis.

2. METHODOLOGY

First, various parameters responsible for accidents in the steel industry have been identified and segregated through the help of a knowledge graph. Figure 1. shows us all the essential parameters taken for our model. Then based on our critical parameters, all the datasets were retrieved through an integrated steel plant via Incident Data Reporting System (IDRS) [11]. Data wrangling has been done to obtain our desired output from the vast dataset.

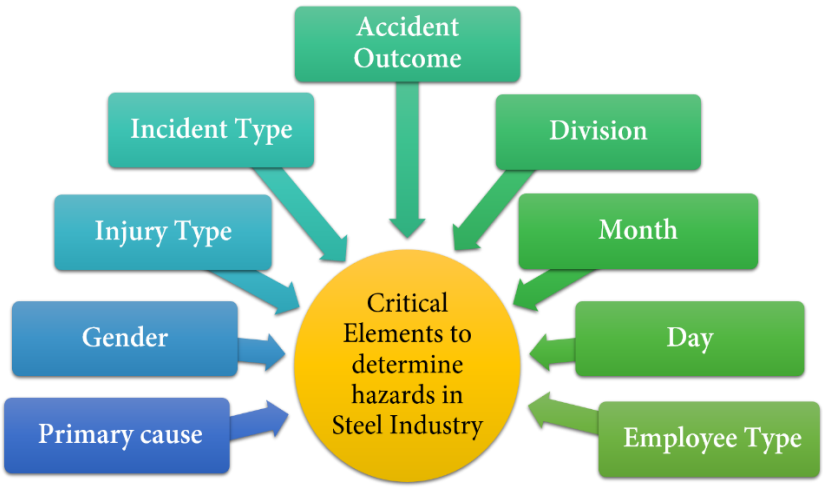

Figure 1. Critical elements to determine hazards in steel industry

Then through the application of TAN algo, an approximation of dependencies between various factors has been determined. This method is used in different fields, like medicine [12], reliability [13], and lifecycle engineering [14].

Finally, Directed Acyclic Graph (DAG) has been obtained as shown in Figure 2. before applying the conditional probability theorem (CPT) responsible for finding the Joint probability of each factor/node.

As shown in Figure 2. various probabilistic inter-dependencies have been generated between the factors through a chain of arcs.

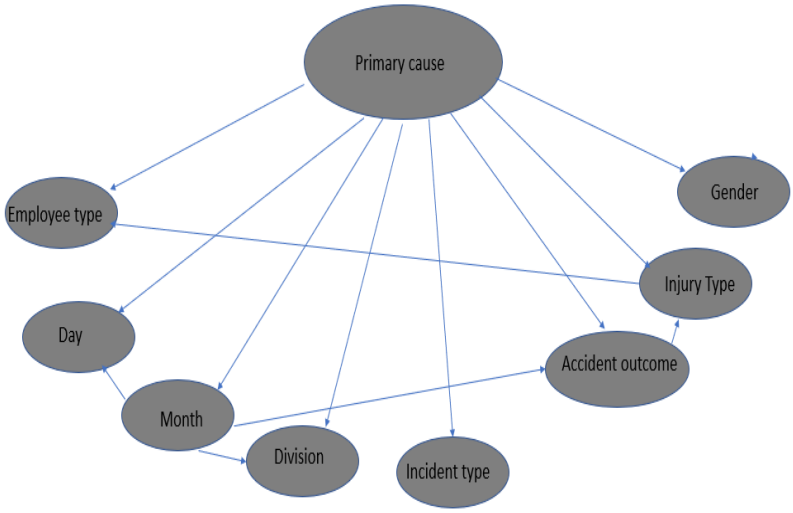

Figure 2. Structure of Bayesian Belief Network

Real possibilities of each node based on the number of parent nodes is to be determined:

- Primary cause has only one possibility because of the absence of any parent node.
- Gender has two possibilities because of 1 parent (Primary cause).
- Injury type has two parent nodes (Primary cause, Accident outcome) and a child node (employee type). So, it has four real possibilities.
- Accident outcome having two parents (Primary cause, Month) and one child (Injury type) has four possibilities.
- Incident type having only one parent (Primary cause) has two possibilities.
- Division having two parents (Primary cause, Month) has four possibilities.
- Month having one parent (Primary cause) and three children (Day, Accident outcome, Division) has two possibilities.
- Day having two parents (Primary cause, Month) has four possibilities.
- Employee type having two parents (Primary cause, Injury type) has four possibilities.

So, there are 27 total conditional possibilities in our model.

Now, using the conditional probability theorem (CPT), the Joint probability of each node is to be found.

To find the joint probability of each node, the formula for conditional probability theorem (CPT). Equation 1 has been used [4].

$$P(Xi|Xi-1, \ldots\ldots\ldots, X1) = P(Xi \mid Parents(Xi)) \quad - \quad \text{Equation 1.}$$

Finally, validate our model through sensitivity analysis.

3. RESULT AND DISCUSSION

To understand the effect of different factors on accident outcomes, Bayesian Belief Network model (BBN) has been used; for modelling of BBN software package, Netica is used, which is based on the Tree Augmented Naïve Bayes Algorithm (TAN algo).

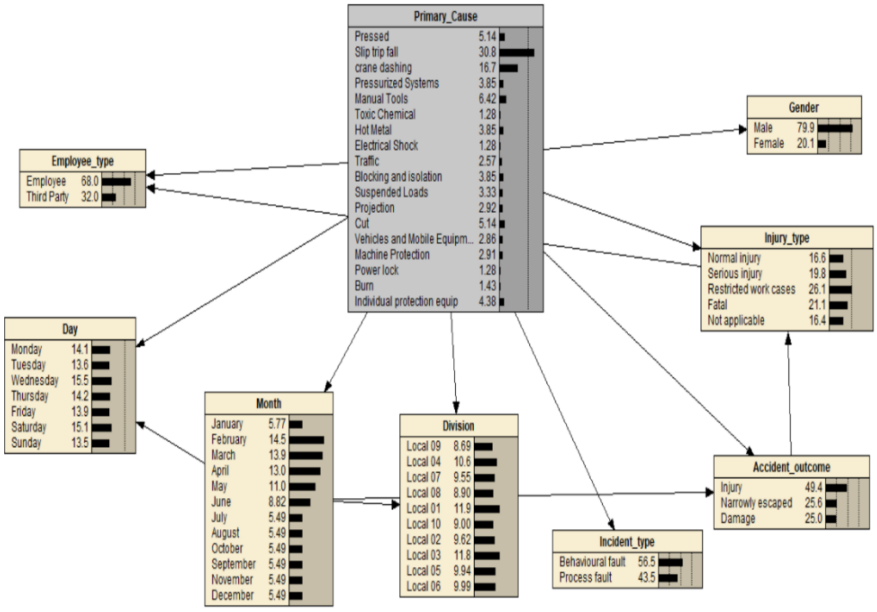

Figure 3. Bayesian Belief Network

Using a tree structure, TAN algo approximates the dependencies between different factors (variables). Based on the experimental analysis of (Jie Cheng Russell Greiner) it has been found that TAN algo is a few times faster than other unrestricted BN-learning methods like BN augmented Naïve Bayes (BANs) and general BNs (GB). Tree Augmented Naive Bayes (TAN) is more suitable for BN than Naive Bayes and selective Naive Bayes [9]. Figure 3. shows the belief network for all the nodes of the Bayesian Network and the probability percentage of each state of each variable. Further, the use of probability percentage of states for sensitivity analysis to analyze how other factors affect accident outcomes has been done.

3.1. Sensitivity analysis

A. Primary Cause

Table 1. Sensitivity analysis of primary cause.

Sensitivity analysis of 'Primary_cause':

Accident_outcome Primary_causes	Injury	Narrowly_escaped	Damage
Initial	24.2	41.8	34
Pressed	28.9	43.1	28
Slip_trip_fall	30.3	41.1	28.6
Crane_dashing	24.5	48.9	26.6
Pressurized_Systems	26.3	55.2	18.6
Manual_Tools	25.5	41.4	33.3
Toxic_Chemical	26.8	43.1	30.1
Hot_Metal	26.6	42.5	30.9
Electrical_Shock	25.8	41.6	32.6
Traffic	21.4	56	22.6
Blocking_and_isolation	23.8	49.3	26.9
Suspended_Loads	27	65.7	7.29
Projection	32.1	35.9	32.1
Cut	28.4	43.1	28.4
Vehicles and Mobile-Equipments	38.9	32	29.1

As shown in Table 1. The initial probability percentage of Injury narrowly escaped and damage (property damage) is 24.2, 41.8, and 34, respectively. As a result, the injury cases are highest for state Vehicles, and Mobile Equipment's probability percentage is 38.9. The instances of narrowly escaped are highest for Suspended state loads, and its probability percentage is 65.7. The property damage cases are significantly low for state Suspended loads and highest for state Manual tools.

B. Employee Type

Table 2. Sensitivity analysis of employee type

Sensitivity analysis of 'Employee_type':

Accident_outcome Employee_type	Injury	Narrowly_escaped	Damage
Initial	49.4	25.6	25
Employee	21.6	29.9	48.5
Thirdparty	31.2	34.6	34.2

Table 2. shows an analysis of employee type and explains how it directly affects accident outcomes. The case of narrowly escaping is the least sensitive, with the highest variation of 9.2% from the initial probability percentage for the state of Third-party employees. Here, injury and property damage cases significantly differ from the initial probability.

C. Month

Table 3. Sensitivity analysis of month

Sensitivity analysis of 'Month':

Accident_outcome Month	Injury	Narrowly_escaped	Damage
Initial	49.4	25.6	25
January	23.2	31.7	45.1
February	24.6	37.2	38.1
March	19.7	43.8	36.5
April	42.2	21.8	36
May	19.7	36.2	44.1
June	16.8	27.3	55.9
July	25.2	36.4	38.4
August	37.4	38.2	24.4
September	51.8	19.2	29
October	21.3	37.6	41.1
November	31.2	43.4	25.4
December	34.8	26.2	39

As depicted in Table 3., the initial probability percentage of injury narrowly escaped and damaged the (property damage) is 24. It's 41.8 and 34, respectively. As a result, the harm cases are highest in September, and its probability percentage is 51.8. The instances of narrowly escaped are highest for March. Its probability percentage is 43.8. Here on, September is significantly sensitive for Property damage; There is a variation of 30.9% from the initial probability rate/percent.

4. CONCLUSION

The above analysis helps us understand the nature of accidental hazards in the steel industry and how accident outcomes depend on different factors (variables). This analysis will help us understand the situation that can lead to accidents and focus on sensitive parameters to prevent accidents. The above result shows that the factors like primary cause, month, and employee type have a powerful influence on accident outcomes; the rest of the elements were less sensitive to accident outcomes, so their analysis is not discussed. This model can be used for safety enhancement in the steel industry by developing a decision support system.

REFERENCES

[1] H. Nordlöf, B. Wiitavaara, U. Winblad, K. Wijk, and R. Westerling, "Safety culture and reasons for risk-taking at a large steel-manufacturing company: Investigating the worker perspective," Saf. Sci., vol. 73, no. March, pp. 126–135, 2015, doi: 10.1016/j.ssci.2014.11.020.

[2] C. Li, J. Qin, J. Li, and Q. Hou, "The accident early warning system for iron and steel enterprises based on combination weighting and Grey Prediction Model GM (1,1)," Saf. Sci., vol. 89, pp. 19–27, 2016, doi: 10.1016/j.ssci.2016.05.015.

[3] ILO, Protecting Workplace Safety and Health in Difficult Economic Times. 2013.

[4] G. Ministry of Steel, "25 Safety Guidelines for Iron & Steel Sector," Gov. India, pp. 1–17, 2019, [Online]. Available: https://steel.gov.in/sites/default/files/Framework Document for Safety Guidelines.pdf.

[5] S. Mao, B. Wang, Y. Tang, and F. Qian, "Opportunities and Challenges of Artificial Intelligence for Green Manufacturing in the Process Industry," Engineering, vol. 5, no. 6, pp. 995–1002, 2019, doi: 10.1016/j.eng.2019.08.013.

[6] S. Sarkar, A. Patel, S. Madaan, and J. Maiti, "Prediction of occupational accidents using decision tree approach," 2016 IEEE Annu. India Conf. INDICON 2016, no. December, pp. 3–9, 2017, doi: 10.1109/INDICON.2016.7838969.

[7] S. Sarkar, A. Kumar, S. K. Mohanpuria, and J. Maiti, "Application of Bayesian network model in explaining occupational accidents in a steel industry," Proc. - 2017 3rd IEEE Int. Conf. Res. Comput. Intell. Commun. Networks, ICRCICN 2017, vol. 2017-Decem, pp. 337–342, 2017, doi: 10.1109/ICRCICN.2017.8234531.

[8] G. A. Shirali, M. V. Noroozi, and A. S. Malehi, "Predicting the outcome of occupational accidents by CART and CHAID methods at a steel factory in Iran," J. Public health Res., vol. 7, no. 2, 2018, doi: 10.4081/jphr.2018.1361.

[9] N. Friedman, D. Geiger, and M. Goldszmidt, "Bayesian Network Classifiers," Mach. Learn., vol. 29, no. 2–3, pp. 131–163, 1997, doi: 10.1023/a:1007465528199.

[10] J. Cheng and R. Greiner, "Comparing Bayesian Network Classifiers," 2013, [Online]. Available: http://arxiv.org/abs/1301.6684.

[11] J. E. Martín, T. Rivas, J. M. Matías, J. Taboada, and A. Argüelles, “A Bayesian network analysis of workplace accidents caused by falls from a height,” Saf. Sci., vol. 47, no. 2, pp. 206–214, 2009, doi: 10.1016/j.ssci.2008.03.004.
[12] S. García-Herrero, M. A. Mariscal, J. M. Gutiérrez, and D. O. Ritzel, “Using Bayesian networks to analyze occupational stress caused by work demands: Preventing stress through social support,” Accid. Anal. Prev., vol. 57, pp. 114–123, 2013, doi: 10.1016/j.aap.2013.04.009.
[13] H. Langseth and L. Portinale, “Bayesian networks in reliability,” Reliab. Eng. Syst. Saf., vol. 92, no. 1, pp. 92–108, 2007, doi: 10.1016/j.ress.2005.11.037.
[14] J. Y. Zhu and A. Deshmukh, “Application of Bayesian decision networks to life cycle engineering in Green design and manufacturing,” Eng. Appl. Artif. Intell., vol. 16, no. 2 SPEC., pp. 91–103, 2003, doi: 10.1016/S0952-1976(03)00057-5.

Biographies

Shivam Kumar received the bachelor's degree in Production engineering from Birla Institute of Technology, Mesra in 2022, and currently working as Graduate Engineer Trainee (Production) in Jindal Steel & Power Limited, Angul, Odisha, India. His research areas include Process safety management, Risk-analysis, Artificial intelligence and lean six sigma.

Arunjeet Chakraborty received the bachelor's degree in Production engineering from Birla Institute of Technology, Mesra in 2022, and currently working as a Business analyst in EXL service. His research areas include Machine learning, Statistics, Image processing, Computer vision and Blockchain technology.

Shatrudhan Pandey is pursuing a Doctorate of Philosophy degree in Production and Industrial engineering from Birla Institute of Technology, Mesra, Ranchi, India. His research areas include Occupational safety and health, Process safety, Hazard identification and analysis, and; Workplace accidents, severity & injury.

Dr. Abhishek Kumar Singh is an Assistant Professor in Production and Industrial engineering at Birla Institute of Technology Mesra, Ranchi, Jharkhand, India. He has over 13.9 years of teaching and research experience. He has published various articles in Peer-reviewed International Journals and authored one book. His research area includes Green manufacturing, Sustainability, Circular economy and Process safety.

Modeling and Simulation of Piezoelectric based Hybrid Energy Harvesting System

[1]Vikash Kumar, [2]Satish Kumar

Department of Applied Mechanics, Motilal Nehru National Institute of Technology Allahabad, Prayagraj, Uttar Pradesh, India
kumarvikashgyani1997@gmail.com, satistme@mnnit.ac.in

Abstract

Piezoelectric energy harvester reliable, environment-friendly, and needs much less maintenance when compared to conventional systems which work mainly by converting normally wasted vibration energy in the environment to usable electric energy. Energy harvesting using vibration will become tremendous technology in which the conversion of mechanical vibration into electricity is much more useful for micro-devices and it also reduced the need for continuous battery change or power cables. This paper is focused on harvesting wind energy using piezoelectric transduction. The geometrical configuration of proposed model is a cantilever beam, whose one end is fixed and another end is a bluff-body cross-section (rectangular). Lift forces are generated which cause strain across the cantilever beam by the vortex-induced vibration phenomena, and so the electrical power generated is directly related to the cross-section of the bluff body, speed of the wind, and angle of attack of the wind concerning the bluff body. The proposed model is simulated on COMSOL MULTIPHYSICS to obtain the frequency response, electrical resistance (load) dependence relation.

Keywords: Energy Harvester, Piezoelectric, Vortex-Induced Vibration.

1. INTRODUCTION

Electricity generation from alternative sources of energy has become a recent topic, especially in connection to Industry applications. A large amount of electrical energy is extracted by the conversion of solar, water, or wind power. In general, the energy obtained in such a way is called "green energy [1]. Different types of energy harvesting systems have been developed to store energy dissipated over roads, and railway stations such as solar energy from sunlight and kinetic energy from traffic and movements [2]. Since wind is an inexhaustible source of energy and it is also an omnipresent, rich, and most important environment friendly so energy source we focus on is wind energy harvesting which generates energy for low energy electronics [3]. Conversion of wind sources to electrical power sources is done by using different kinds of mechanisms, i.e., electromagnetic induction, piezoelectric, and electrostatic effect [4]. All three piezoelectric transducers have the benefit of greater power density, greater energy conversion, and ease of assembly and

maintenance. Continuous vibration is produced on piezoelectric cantilever beam by aerodynamic effect; this effect is vortex-induced vibration and galloping [5,6].
Vortex-induced vibration happens because of continuous vortex shedding from a non-streamlined bluff body like a rectangle and triangle when the wind flows over the bluff body. Vortex-induced vibration causes uneven vortex shedding patterns with very large amplitude and unstable frequency.

1.1 Shape and working operation of Piezoelectric Wind Energy Harvester

Figure 1 shows, that the beam has a rigid tip body with a rectangle-shaped cross-section. Piezoelectric sheets are bonded on the upper and lower surface of the cantilever beam and as this beam is cantilever it is fixed at one end with proof mass mounted on another end. From fluid dynamic, as wind flows across the rectangular section, the continuous vortices shedding from the edges of the section are in a wide range of Reynolds numbers [5,7]. The generated vortices induce a periodic lift force on the rectangular section and thus it is subjected to a longitudinal vibration and the attached proof mass will be subjected to vibrate upward and downwards sinusoidal motion.

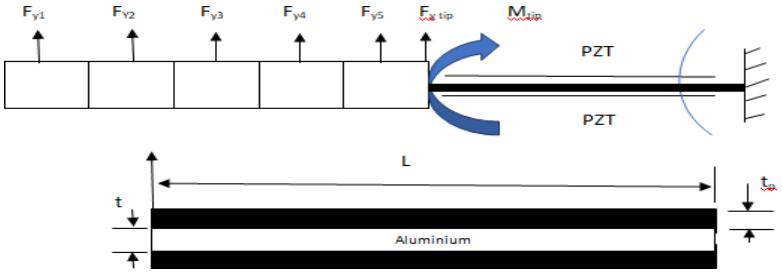

Figure 1. Schematic of the bean geometry[8]

Piezoelectric sheet elements (PZT) bonded to the top and bottom surface of the aluminum beam generate an alternating voltage in response to the bending induced by the upward and downward motion of the rectangular section [11-13]. Practically, electrical energy which is obtained from wind energy harvester will have two purposes it is either stored and power some devices, or the voltage obtained is discharged over a load resistance. For pure bending of the beam mechanical strain is given as

$$\in = -\frac{\partial^2 \omega}{\partial x^2}$$

The piezoelectric constitutive equations for uniaxial loading have the following form :

$$\begin{bmatrix} \in \\ D \end{bmatrix} = \begin{bmatrix} s^E & d \\ d^T & e^\sigma \end{bmatrix} \begin{bmatrix} \sigma \\ E \end{bmatrix}$$

Where $\in$ mechanical strain, electric displacement D, mechanical stress σ, electric field E, s^E is the compliance matrix, e^σ is the matrix of dielectric constants, and d is the piezoelectric coupling matrix[8].

2. METHODOLOGY

Simulation and Modeling- COMSOL Multiphysics 5.5 will be used to model the piezoelectric bimorph cantilever beam. Firstly, properties in solid mechanics like geometry, stress and boundary conditions should be given, and then in electrostatics properties, charge conservation, ground, and terminal voltage will be given. The following results were obtained.

- Frequency Response.
- Electrical Resistance (Load) dependence.
- Acceleration dependence.

2.1 Modeling and Simulation using COMSOL MULTIPHYSICS

The proposed model consists of two active layers of piezoelectric which are bonded on the upper and lower side of the base material. Given model is clamped on one side and at the free end, a cantilever mass is attached. This energy harvester using piezoelectric transduction is vibrated with the help of sinusoidal acceleration which generates electrical energy due to the direct effect of piezoelectric.

As this particular cantilever has two active layers (bimorph) in which the ground electrode is inserted withthe neutral plane and in this design there are two electrodes of the same voltage is situated at the exterior i.e.at the top and bottom of the cantilever despite that stress above the neutral plane is in compression and tension innature. Two piezoelectric sheets of the length of 21 mm, the width of 0.16 mm, and thickness of 0.06 mm are bonded on the upper and lower surfaces of aluminum sheets whose length and width are the same as piezoelectric but the thickness of 0.04 mm is selected as shown in Table 1.

Table 1. Materials and Geometry Specifications[9]

Material	Length (l) mm	Width (b) mm	Thickness (t) mm	Modulus of Elasticity (GPa)
PZT 5A	21	0.16	0.06	3
Aluminium	21	0.16	0.04	69

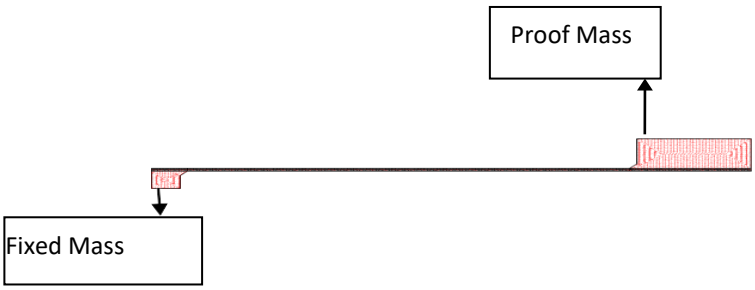

Figure 2. Major Components of Piezoelectric Bimorph.

3. RESULTS AND DISCUSSIONS

The mechanical performance of the energy harvester model is analyzed by obtaining three different graphs. The first resultshows a relationship between electrical power output with a frequency of vibration at a constant electrical load. In the second plot, a relationship between power output and electrical load impedance was obtained, and the last relationship between power output and acceleration is explored.

Results from figure 3 show that, at a fixed frequency of 80 Hz, which produces sinusoidal forces along thelength of the bimorph cantilever beam that shows the variation of Von-misses stress along the length of the bimorphcantilever beam.

And secondly, it is concluded that a ground boundary condition is provided which is a reference potential because of one electrode at the bottom and another at the top. Ground potential is provided at the bottom and another floating potential is to mimic a conducting material. Piezoelectric material is a dielectric material without any conductivity and there is a need to know the charge generation. So at a fixed frequency of 80 Hz the voltage generated across the bimorph cantilever beam energy harvester is obtained.

3.1 Effects of PZT 5A sensors utilizing the local variation in acceleration

1. The relationship between electrical voltage output, input mechanical power, and electrical power output obtained at a constant frequency of 70.5Hz as shown in Figure 4. It is concluded from this graph that voltage variation is linear and electrical power output is quadratic.

2. The Given results show the relationship between electrical power outputs and the voltage obtained concerning external load resistance as in Figure 5. From the obtained data it is clear that max output is at 6 kΩ obtained at a frequency of 70.5 Hz vibrating at 1g of acceleration.

3. This result shows the plot between input mechanical power, output electrical power, and the voltage induced on the piezoelectric beam to vibration frequency generated due to sinusoidal acceleration as shown in Figure 6. This result is computed at a fixed resistance load of 12 kΩ which also shows peak amplitude obtain at 70.5Hz which is near to the computed resonant frequency.

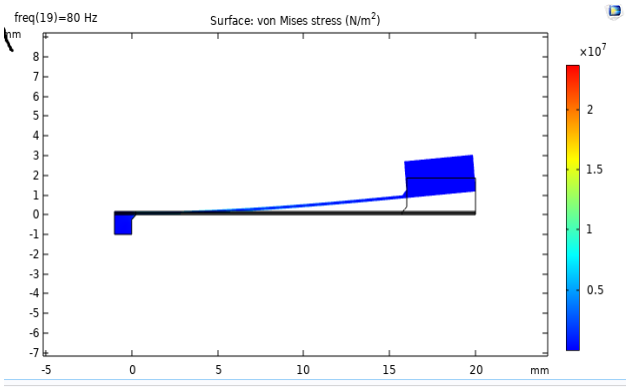

Figure 3. Von-misses stress generated along the length piezoelectric bimorph at Freq of 80 Hz

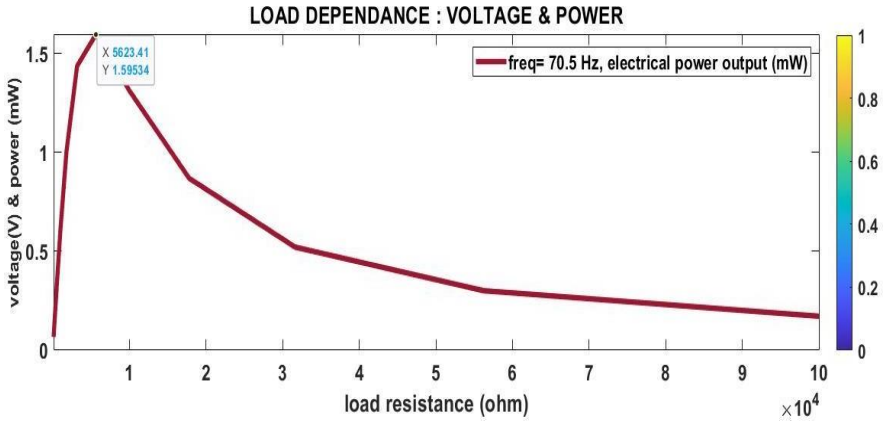

Figure 4. Effect of acceleration concerning dc voltage, mechanical and electrical power

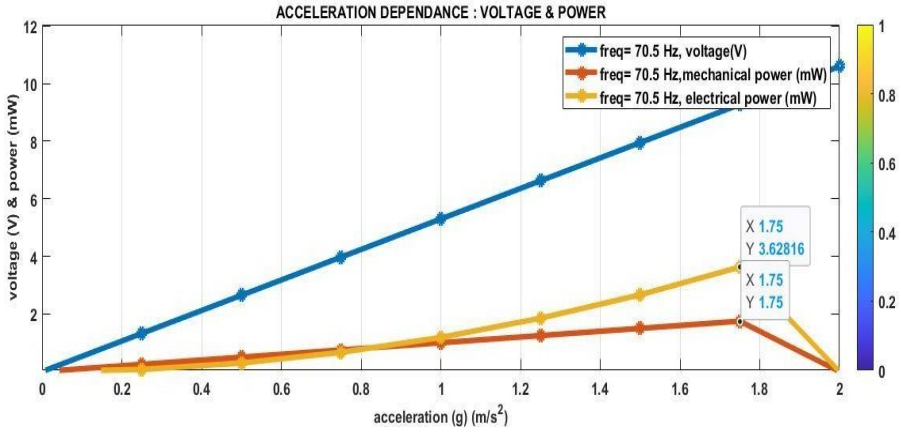

Figure 5. Relation between power output versus electrical load

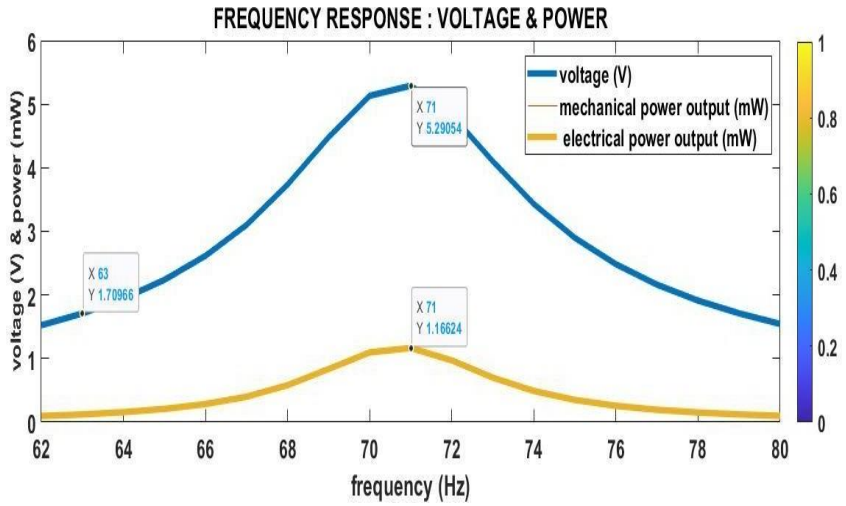

Figure 6. Relation between electrical power output versus excitation frequency

4. SUMMARY AND CONCLUSION

In this work, a device formed on vortex-induced vibration where a piezoelectric layer is established over a cantilever beam was developed which generates electrical power output from kinetic energy induced by wind and vibration induced by local variation in acceleration. The proposed model comprises two activelayers of piezoelectric which are bonded on the upper and lower side of the base material. Given model is clamped on one side and at a fixed end, a cantilever mass is attached.

A finite element solution using COMSOL MULTIPHYSICS of the device was performed. Three differenttypes of analysis were performed by this system which include Frequency Response, electrical load resistance dependence, and a function of acceleration. From the obtained data it is clear that max output electrical power is 1.145mW at 6 kΩ obtained at a frequency of 70.5 Hz vibrating at 1g of acceleration. To this end, although the power obtained was in mill watts but it is sufficient for many small power electronics, rechargeable batteries, and wireless communication.

REFERENCES

[1]. Machu, Z., Majer, Z., Seveček, O., Stegnerová, K. & Hadaš, Z. Electro-mechanical analysis of a multilayer piezoelectric cantilever energy harvester upon harmonic vibrations. *MATEC Web Conf.* **210**, 1–6 (2018).

[2]. Yan, Z., Abdelkefi, A. & Hajj, M. R. Piezoelectric energy harvesting from hybrid vibrations. doi:10.1088/0964-1726/23/2/025026.

[3]. Kim, S., Shen, J. & Ahad, M. Piezoelectric-Based Energy Harvesting Technology for Roadway Sustainability. *Int. J. Appl. Sci. Technol.* **5**, 20–25 (2015).

[4]. Alan Gonclaves Paulo e Silva, Jose Marques Basilio Sobrinho, Cicero da Rocha Souto,Andreas Ries, Alaxandre Cezar de Castro.Design, modelling and

experimental analysis of a piezoelectric wind energy generator for low-power applications.Sensors and Actuators A 317 (2021) 112462.

[5]. Shuyun Wang, Weilin Liao, Zhonghua Zhang, Yong Liao ,Mengjia Yan, Junwu Kan. Development of a novel non-contact piezoelectric wind energy harvester excited by vortex-induced vibration.Energy Conversion and Management 235 (2021) 113980.

[6]. Graak, P., Kaur, A. G. S., Chhabra, P., Kumar, D. & Shetty, A. Design & Simulation of Various Shapes of Cantilever Beam for Piezoelectric Power Generator. 560012 (2015).

[7]. Li, H., Tian, C. & Deng, Z. D. Energy harvesting from low frequency applications using piezoelectric materials. **041301**, (2019).

[8]. Sirohi, J. & Mahadik, R. Harvesting wind energy using a galloping piezoelectric beam. *J. Vib. Acoust. Trans. ASME* **134**, 1–8 (2012).

[9]. Malkin, M. C. & Davis, C. L. Multi-frequency piezoelectric energy harvester. *J. Acoust. Soc. Am.* **118**, 24 (2005).

Biographies

D Vikash Kumar is currently doing his M. Tech from Applied Mechanics Department, Motilal Nehru National Institute of Technology Allahabad, Prayagraj, India. He has completed his Btech from Gurukul Kangri Viswavidyalaya Haridwar. His M. Tech thesis was on “Design and Development of piezo-based hybrid Energy Harvesting System” and his Btech projects was on " Nozzle Testing Machine" His research interests lie in smart materials, Vibration of Structures and Internal Combustion Engines.

Dr. Satish Kumar is currently working as an Assistant Professor at Applied Mechanics Department, Motilal Nehru National Institute of Technology Allahabad, Prayagraj, India. He has completed his B. Tech from NIT Jalandhar, M. Tech, and Ph.D. from IIT Roorkee. His current research interests lie in the design, fabrication, and mechanical characterization of adaptive membrane-based lightweight structures for space applications, Hybrid Energy Harvesting Sytems, and Shape Memory-based Polymer Actuators, which he plans to study using a combined experimental and numerical approach.

Phase Change Materials for Solar Cooking: A Review

[1]Priyank Srivastava[*], [2]Bhupendra Koshti, [3]Rahul Dev, [4]Jitendra Narayan Gangwar, [5]Supriya Yadav

Motilal Nehru National Institute of Technology, Allahabad, Prayagraj, India

* priyank.srivastava25@gmail.com, bkpkoshti33@gmail.com, rahuldsurya@mnnit.ac.in, jgangwar@mnnit.ac.in, supriya@mnnit.ac.in

Abstract

Cooking with the help of solar energy using a solar cooker will provide colossal gap coverage for renewable energy. Solar can be classified mainly four types which can be stated as panel type cooker, box-type solar cooker, parabolic type solar cooker, and tube type cooker. The most widely used solar is the Box-type solar cookers and most modifications are done on the same. Solar cookers have a disadvantage due to the unavailability of solar energy in the evening and night time. However, this disadvantage can be removed by using thermal storage materials like Phase-change Material (PCM). Some developments have been done in different types of solar cookers in the last 25 years concerning different forms of glazing covers, booster mirrors, and cooking pots. In some recent advantages of solar cookers, thermal energy storage came into the picture. Various sensible and latent heat materials were used, which were placed in the form of encapsulation to the pot and storage tanks. This review covers various thermal storage materials, and a particular focus is on various types of PCM that can be used in solar cooking as thermal storage material [TSM]. Sensible TSM stores energy via increasing its temperature, while latent TSM stores energy via increasing its temperature as well as from its phase change. From the study, it was evident that organic thermal storage material is feasible. Fewer constraints come while using them, while eutectic PCM gives an advantage of including properties of both types of PCM i.e., organic and inorganic. PCM utilization is confined by its operating temperature range and storage container's material compatibility.

Keywords. Solar cooking, Thermal energy storage, Phase change materials, Sensible thermal energy storage, Latent thermal energy storage

1. INTRODUCTION

As per the Intergovernmental Panel on Climate Change (IPCC) report 2021, it is evident that quick and fast actions are required to correct the interventions and harms done to the planet. In the first part of the sixth test report, published in August and described as "code red for humanity," the IPCC showed that the world could hit 1.5 ℃ by early 2030 [1]. In COP26, India has set a target for meeting 50 percent of energy requirements from renewable energy (RE) by 2030 and achieving net-zero carbon by 2070. India, as a tropical country, has vast availability of solar energy. As the world's population increases, world energy demands and consumption are also increasing, which has led to a

variety of environmental impacts that are impacting the environment in a very harsh manner. Most of the energy demand, nearly 80%, is fulfilled with the help of fossil fuels only [2].

The footprint of non-renewable resources has created health issues, environmental issues, and socio-economic issues, especially in underdeveloped regions of the world [3]. With the limited supply of fossil fuels, one must use renewable resources for demand fulfillment. However, the selection of renewable resources comes with some cons: the availability of the energy sources, irregularity of the energy sources, and the storing of the excess energy. To use the alternative and renewable energy source, one must think about storing the energy for future use or when the source is not available in its peak form. The solar energy from the sun can be collected and converted into electricity which can be said as conversion of high-grade energy to low-grade energy.

In developing countries, domestic energy is consumed for different daily needs like water heating, cooking applications, and lighting. This energy demand and consumption are different in different developing countries. In India, 36% of the total primary consumption and 90% of the rural households depend on biofuel for cooking purposes [4]. In underdeveloped or rural or agrarian areas, biofuels such as wood, agricultural wastes, and animal dung cakes are few of the primary energy sources utilized for cooking purposes, whereas, in developed or non-rural areas, kerosene and LPG are the primary sources of energy. The demand for firewood is fulfilled by cutting trees, which causes deforestation, leading to desertification and dung cakes polluting the environment. Also, the supply-demand chain of fuel for cooking and some other factors have given a continuously increasing price of the fuel, which implies a dire need to utilize different renewable energy resources effectively for the purpose of cooking. For India, it is a blessing that a large amount of solar radiation occurs good potential for solar cooker practical usage in India [5]. However, the issue of irregularity or limited availability of solar radiation is the primary reason for the underutilization of solar radiation-based cooking. The use of energy storage systems can improve this drawback. To counterbalance the consumption and production of energy, it is obligatory to reserve excess energy for the short term or the long term. In today's time, storing electrical energy is not economic, but on the counterpart, it is significantly low if the cost of storing thermal energy is considered. The power supply grid cannot transfer thermal energy, but excess electric energy can be exported to the grid connection. This gives an area of utilization of thermal storage. Thermal energy storage may complement the electric utility grid whenever it is in not working condition or is under stress. Batteries or phase change materials can be used to store energy [6]. However, as the energy storage capacity of a kilowatt-hour battery is currently limited and to enhance its capacity and usage, research is going on. It is a viable and practical option for phase change material as an alternative [7]. Phase change materials are of various types out of these which is to be used for solar cooking depends on their application temperature, their application process, and compatibility with the storage container's material.

2. ENERGY STORAGE SYSTEMS

There are several types of energy storage systems. However, their utilization depends mainly on the application for which it will be used and its environment, including the equipment and working principles used. Figure 1 describes different energy storage systems based on their working principles.

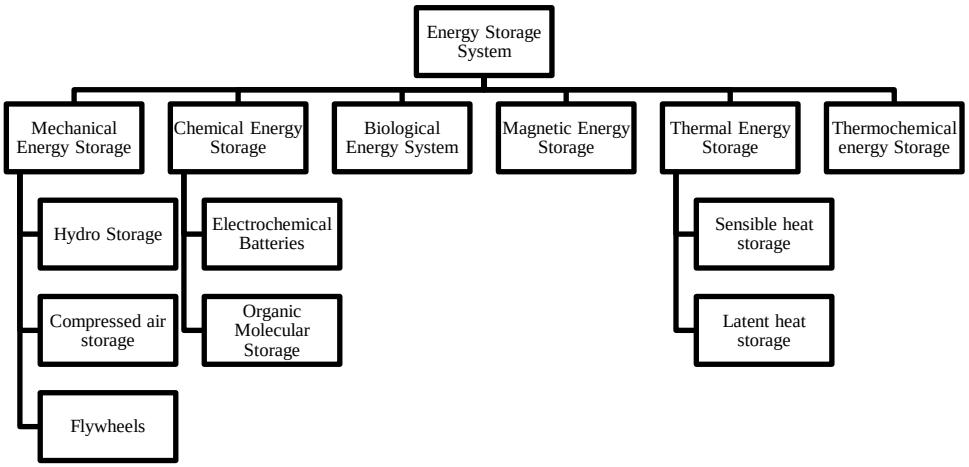

Figure 1. Types of Energy Storage Systems [8]

As mentioned earlier, thermal energy storage (TES) gives the highest efficiency of all the systems. TES systems can lessen the consumption of fossil fuels which will restrict CO_2 emissions. Utilization of the solar energy and excess energy generated during the daytime and stored for an extended or short period. This stored energy can be used to achieve an efficient system. One of the TES subcategories is PCM, a desired and valuable material because it stores a high energy density at a steady temperature.

3. CLASSIFICATION OF PCM

PCM is a viable option for solar heat storage due to its large energy storage capacity and property like a rapid supply of a large amount of heat to the application area. PCM's energy storage has many advantages over sound systems due to its low weight and volume. Energy is stored at a stable temperature which dissipates over time in which phase changes, and energy lost to the environment are smaller than in traditional arrangements.

3.1 Working Principle

As the temperature reaches a critical temperature, as the phase changes from solid phase to liquid phase, in this transition the chemical bonds of the PCM breaks down. The phase conversion process from solid to liquid is endothermic and PCM absorbs energy in the form of heat energy. When one keeps PCM in the area of storage, the PCM starts to melt when it detects the temperature change of critical value. The temperature then remains constant till the time the melting process is completely finished. The stored heat during PCM phase transition is called Latent heat. Latent heat retention can be defined via a high degree of energy density. When the temperature starts decreasing, the stored energy is again transferred to the critical area of interest with the help of sensible heat and latent heat from the exothermic process of solidification, which can be viewed in Figure 2. Figure 3 shows various types of heating, i.e., sensible and latent heating.

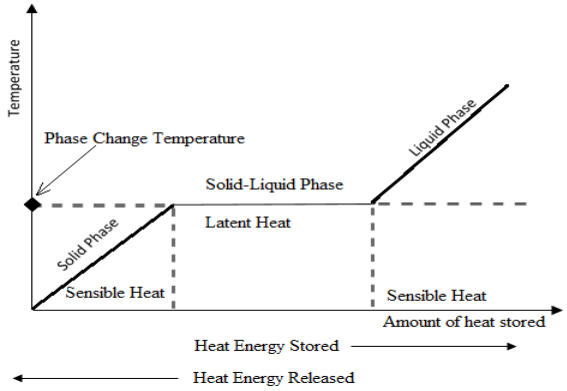

Figure 2. The Phase Transition of PCM [9]

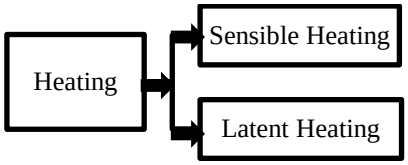

Figure 3. Classification of PCM based on heating

3.2 Sensible Heat Storage Materials:

Materials which are utilized in order to store heat by change in its temperature only are sensible heat storage devices. The widely used suitable heat-retaining materials are water, oil, and salt dissolved in alcohol. A list of solid and liquid thermal fluids used to maintain reasonable temperatures and their properties is shown in Table 1**.**

Table 1. Sensible heat storage materials with their properties [10]

S. No.	**Medium**	**Density (ρ) (kg/m^3)**	**Specific Heat Capacity (C) (J/kg K)**	**Heat Capacity $\rho \times C \times 10^{-6}$(J/m^3 K)**
1.	Calcium Chloride	2510	670	1.68
2.	Cast Iron	7900	837	6.61
3.	Clay	1458	879	1.28
4.	Aluminium	2707	896	2.43
5.	Steel, Limestone	2500	900	2.25
6.	Ethylene glycol	1116	2382	2.66
7.	Ethanol	790	2400	1.89
8.	Isobutanol	808	3000	2.42
9.	Lithium	510	4190	2.14
10.	Water	1000	4190	4.19

Water is an excellent choice for requirements in which a low temperature below 100 ℃ is required. Oil is used for medium temperatures applications varying from 100 ℃ to 300 ℃.

Soluble and inorganic salts are of use when installing large temperatures that require temperatures ranging over 250 ℃. Advantages of using melted salt are very high stability of the cost of the material, high density, high temperature, non-combustion, and low vapor pressure. Solids-liquids and solids-liquid mixtures can be utilized in sensible storage devices in the TES of solar cookers. Fuels that can be used as sensible liquids are Coconut oil and Engine oil. To maintain a reasonable temperature in high temperatures, such as energy production via solar power plants, a non-eutectic salt solution consists of 60 % by weight sodium nitrate ($NaNO_3$) and 40 % by weight potassium nitrate (KNO_3) is used. This composite is known as "sun salt" in layman's language. The resulting non-eutectic mixture possesses a melting point of 240 ℃ & maximum melting point temperature of about 550 ℃. Solid materials are stone, brick, brick/mortar, concrete, concrete, earth / dry and wet soil, metal, wood and concrete board. Very often solid materials show lower storage capacity than water. The use of rocks is acceptable on the basis of the per-unit cost of storage media of stored energy [11].

3.3 Latent Heat Storage Materials:

When a PCM for solar cookers is finalized, the operating temperature should be similar to PCM's critical temperature. The volumetric latent heat should be high to lessen the PCM's physical space/size required. Property such as high thermal conductivity would enhance in storing and dissipating power of PCM. Various types of materials are shown in table 2 with their properties.

Table 2. Latent heat storage materials with their properties.[10]

S.no.	PCM	Melting Point (℃)	Latent heat of fusion (kJ/kg)
1.	Stearic acid	55.8	160
2.	Acetamide	82	263
3.	$Mg(NO_3)_2.6H_2O$	89	134
4.	Paraffin	100	140
5.	$MgCl_2.6H_2O$	118	167
6.	Erythritol	118	339
7.	D-Mannitol	169	326.8
8.	Nitrate salts (KNO_3-$NaNO_3$)	220	146

PCM can also be classified based on its chemical structure, i.e., Organic, Inorganic, and eutectic, as mentioned in figure 4. Organic PCM includes Non-Paraffin and paraffin, and Inorganic PCM includes salt and metallic hydrates. Eutectic PCM includes inorganic-inorganic, organic-inorganic, and organic-organic, depending on what PCM types are being mixed.

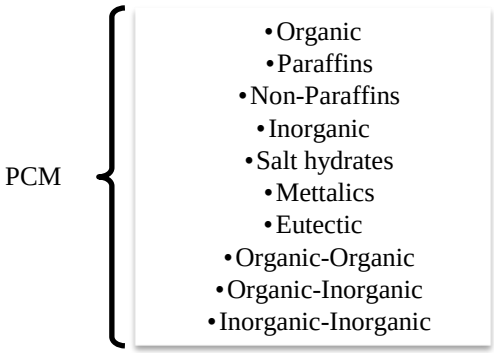

Figure 4. PCM classification based on chemical structure

Organic PCMs are hydrocarbons, primarily paraffin (C_2 H_{2n+n}), lipids, and sugar alcohols. Organic PCM freezes without showing significant supercoiling. They have a property to melt congruently. Organic PCMs are generally compatible with commonly used construction materials. They are chemically stable, which gives an advantage for usage, and are non-reactive. Organic PCMs generally show a phase change temperature range of -5 ℃ to 190 ℃. Organic PCM is behind due to its low thermal conductivity for solid structure, resulting in a high heat transfer rate during the phase conversion from liquid to solid. Its volumetric latent heat storage capacity is low compared to some inorganic PCMs.

Inorganic PCMs are generally Salt Hydrates ($M_xN_yH_2O$) type structures. The main advantage of using an inorganic PCM is its high volumetric latent heat storage capacity. Inorganic PCMs exhibit sharp melting points as well as high thermal conductivity. Most inorganic PCMs are readily available, and that too at low cost. Inorganic PCMs go through phase separation upon repeated process, which causes a considerable loss in latent heat enthalpy. Inorganic PCMs generally exhibit a phase change temperature range of -50 ℃ to 175 ℃. Water or oxygen in its chemical structure can cause corrosion to most metals of construction. There can be an issue with supercoiling in solid-liquid phase change, which should be considered in the design phase of the container only where PCM will be stored.

The eutectic mixture combines more than one type of PCM, which can be any organic or inorganic. It has a sharp melting point, High volumetric storage density. The issue with the eutectic mixture is that very little data is available, so using a eutectic mixture will require an experimental approach to some extent [12]. In many binary eutectics, different types of fatty acids may be incorporated into almost any melting point of TES systems according to climate requirements. Eutectic mixture PCMs generally have a phase change temperature range between -5 ℃ to 225 ℃, and this will depend on combining two mixed materials. Thermal properties and thermal reliability of pure or eutectic PCM should be examined for thermal cycling health tests to confirm the duration of the utilization of the TES system.

4. PCM PROPERTIES

PCM properties play an essential role in selecting PCM for solar cooking. Table 3 shows different properties of PCM Materials that are required if used as TES in solar cooking.

Table 3. PCM properties

S.NO.	PROPERTIES TYPE	PROPERTIES
1.	Thermophysical properties	• Melting temperatures lies in a fixed range. • Per unit volume high latent heat of fusion. • High specific heat so to have additional usable sensible storage. • High thermal conductivity in both phases, i.e., liquid and solid. • Small volume variation during transition and slight vapor pressure for working temperatures. • Befitting melting and freezing of PCM for a material storage capacity with both melting and freezing process. • Phase changing temperature conformable to use. • To minimize heat storage size, latent energy should be high. • Possess high enthalpy. • Fixed and mentioned transition temperature. • Density should be high during transition. • Small volume variation during phase transitions. • It should have high thermal conductivity.
2.	Kinetic properties	• High nucleation rate in order to elude supercooling in the liquid phase. • Crystal growth rate should be high that enables the system to fulfill the requirements of heat recovery from the material. • Undercooling crystallization rate should be pretty sufficient during the freezing process.
3.	Chemical properties	• Chemical stability throughout the working temperature. • Complete reversible for melting and freezing cycles. • No or minimum degradation even after a huge number of the working cycle. • Non-corrosive behaviour with the storage fabrication material. • Non-noxious, non-corrosive, non-combustible, and non-detonative material. • High chemical stability.
4.	Material characteristics	• The unit size should be small. • Desired low vapor pressure.
5.	Economic characteristics	• Cheap and large availability

5. PCM SELECTION CRITERIA FOR A BASIC SOLAR COOKER

When selecting PCM for a solar cooker, its properties and requirement both should be kept in mind. Some criteria are mentioned below:

- It should have critical temperatures within the required operating temperature (installation in solar cooker 60 ℃-120 ℃).
- It should acquire a high latent heat of fusion per unit mass in order to lessen the amount of PCM required.
- For maximum benefit, PCM must have a high specific temperature to maximize sensible heat retention.
- PCM materials must have high thermal conductivity to reduce charging and discharge duration.
- It should possess small volumetric expansion as well as small shrinking coefficients for phase changes.
- It must have little or no cooling during solidification.
- It must be chemically stable and non-corrosive for the containers used for storage.
- In addition, it should be non-toxic, inflammable, or non-explosive.
- PCM should be readily available at a low cost to improve cost optimization and mass production.

6. PROBLEMS WITH LATENT HEAT MATERIALS

The selection of latent thermal materials is based primarily on properties such as thermo-physical, which are the melting point, latent heat of fusion, specific heat, and thermal conductivity. However, the critical parameters limiting latent heat storage use are the number of repeatable processes without change in material properties and the valuable life of PCM-container setup. So the problem which has limited application of LHS (Latent Heat storage) is the requirement that it must last for a long time [13].

7. PROBLEMS WITH USAGE OF PCM MATERIAL IN SOLAR COOKER

PCMs, come with some disadvantages, which get highlighted when used in the solar cooker. Some common issues with PCM usage are as follows:

1. It increases the weight of the solar cooker as a whole setup which reduces its portability as using PCM increase weight of solar cooker by 10kg [14].
2. It increases the cost of a solar cooker setup.
3. Removing or refilling PCM from its storage tank is a heavy and challenging task.
4. The heat trapped inside the box increases due to the presence of PCM, which gives a condition like handling pots with gloves is a must condition.
5. The stability and lifecycle of some TES are very less for practical applications [15].

8. APPLICATIONS

Substantial efforts have been made to develop a latent energy thermal system in solar systems, where heat must be stored in the daytime for nighttime usage. Many PCMs possess

a low thermal conductivity which lowers the rate of heat transfer, making them infeasible for their applications. Therefore, PCM should be integrated in such a way as to limit a significant decrease in heat transfer rates that happens along the phase transition processes. PCM usually consists of small flat containers, such as plate-type heat exchangers [12]. The significant enhancement of rate of heat transfer was achieved via inserting PCM into small plastic parts to form a complete bed storage unit. Direct heat transfer by phase transition using hydrated salt provides significantly high temperatures. Storing thermal energy is essential for efficient solar energy in a building. PCM storage provides an extra edge for solar cooking purposes also. Solar ponds are one of examples for solar energy storage which happens naturally. Photosynthesis is a natural process in which solar energy is converted to other form of energy.

Similar to other applications, PCM will gain and store energy in day/sunshine time and store it, which can be used in night/off-sunshine time. Especially for solar cooking, latent heat comes forward as a better option for TES. PCM placement within the solar cooker setup is also a topic worth noting. The outer cover for the vessel can be co-cylindered [16], and PCM can be filled in that space which will act as the single-layer transmission of energy from PCM to food in the solar cooking vessel. Another area where PCM Materials can be stored will be the base of the solar cooker, where the solar cooking vessels are placed. However, there will be a two-layer energy transmission from PCM to food in the solar cooking vessel in this format. This drawback can be removed by providing holes of the same size as the vessel based on the cost of size and placing the solar cooking vessel.

9. CONCLUSION

This review paper can be concluded via the following points:

- Thermal storage materials are a viable option for better utilization of solar energy as it provide easy, convenient and practical application of energy storage.
- Organic, inorganic, and eutectic, all types are usable TES materials to utilize solar energy in the solar cooker. So, for a particular applications many options are there depending on type of application one can choose from them.
- Most salts are usable in the hydrated form, limiting the type of material used for storage tanks for TES.
- Organic PCMs generally have a low melting point, but it is short-range to cook food.
- The number of thermal cycles are higher when low or medium temperature range PCM are used compared to high temperature range PCM.
- Sunflower oil and many more edible oils also acts as a valuable material for TES.
- Stearic acid and paraffin wax are commonly used due to their easy availability and economically viable options.
- A sound approach is a must condition in area of solar cooking to promote its usage and affordability.

REFERENCES

[1] IPCC, Technical Summary. Contribution of Working Group I to the Sixth Assessment Report of the Intergovernmental Panel on Climate Change. 2021.

[2] P. Moodley and C. Trois, Lignocellulosic biorefineries: the path forward, Sustain. Biofuels, pp. 21–42, Jan. 2021.

[3] A. Saxena, V. Tirth, and S. Lath, Solar cooking by using pcm as a thermal heat storage Consultancy Project: Development of Modular Employable Skills-Training Curriculum in Brass Sector View project Development and Characterization of Low Cost Hybrid Metal Matrix Composites for Automotive Applications View project Solar Cooking by Using PCM as a Thermal Heat Storage, 2018.
[4] H. Sawarn, S. Kumar Shukla, and P. K. Singh Rathore, Development in Solar Cooking Technology in the Last Decade: A Comprehensive Review, IOP Conf. Ser. Mater. Sci. Eng., vol. 1116, no. 1, p. 012046, Apr. 2021.
[5] E. Cuce and P. M. Cuce, A comprehensive review on solar cookers, Appl. Energy, vol. 102, pp. 1399–1421, 2013.
[6] P. Sivasamy, A. Devaraju, S. Harikrishnan, and A. P. J. Abdul, Review on Heat Transfer Enhancement of Phase Change Materials (PCMs), 2018.
[7] P. A. Prabhu, N. N. Shinde, Prof, and P. S. Patil, Review of Phase Change Materials For Thermal Energy Storage Applications, IJERA, 2012.
[8] M. M. Farid, A. M. Khudhair, S. A. K. Razack, and S. Al-Hallaj, A review on phase change energy storage: materials and applications, Energy Convers. Manag., vol. 45, no. 9–10, pp. 1597–1615, Jun. 2004.
[9] B. Cárdenas and N. León, High temperature latent heat thermal energy storage: Phase change materials, design considerations and performance enhancement techniques, Renew. Sustain. Energy Rev., vol. 27, pp. 724–737, Nov. 2013.
[10] S. Sivalakshmi, A Review On Thermal Energy Storage Materials For Solar Cooking, IJRIET, 2019.
[11] G. Kumaresan, V. S. Vigneswaran, S. Esakkimuthu, and R. Velraj, Performance assessment of a solar domestic cooking unit integrated with thermal energy storage system, J. Energy Storage, vol. 6, pp. 70–79, May 2016.
[12] M. Mofijur et al., Phase change materials (PCM) for solar energy usages and storage: An overview, Energies, vol. 12, no. 16. MDPI AG, Aug. 17, 2019.
[13] B. Zalba, J. M. Marín, L. F. Cabeza, and H. Mehling, Review on thermal energy storage with phase change: materials, heat transfer analysis and applications, Appl. Therm. Eng., vol. 23, no. 3, pp. 251–283, Feb. 2003.
[14] P. M. Cuce, Box type solar cookers with sensible thermal energy storage medium: A comparative experimental investigation and thermodynamic analysis, Sol. Energy, vol. 166, pp. 432–440, May 2018.
[15] G. John, A. König-Haagen, C. K. King'ondu, D. Brüggemann, and L. Nkhonjera, Galactitol as phase change material for latent heat storage of solar cookers: Investigating thermal behavior in bulk cycling, Sol. Energy, vol. 119, pp. 415–421, Sep. 2015.
[16] S. M. Santhi Rekha and S. Sukchai, "Design of phase change material based domestic solar cooking system for both indoor and outdoor cooking applications," J. Sol. Energy Eng. Trans. ASME, vol. 140, no. 4, Aug. 2018, doi: 10.1115/1.4039605.
[15] S.Harshita, S.Shailendra, and R.Pushpendra, Development in Solar Cooking Technology in the Last Decade: A Comprehensive Review, OP Conf. Series: Materials Science and Engineering, 2020.
[16] C.Arunachala, J.Anuj, M.Sheikh, Design, Fabrication and Performance Analysis of Solar Cooker for Night Cooking, International Journal of Renewable Energy and Environmental Engineering, 2014.
[17] HMS. Hussein, H.H. El-Ghetany, S.A. Nada, Experimental investigation of the novel indirect solar cooker with indoor PCM thermal storage and cooking unit, ELSEVIER, 2008.

[18] R.Ajeet Kumar and S.Sanjay Kumar, Design and testing of cooking vessels of solar box cooker for evening cooking, International Journal of Mechanical Engineering and Technology (IJMET), 2019.

Biographies

Priyank Srivastava received the bachelor's degree in Mechanical engineering from DIT University Dehradun-248004, Uttarakhand, India. Currently pursuing the master's degree (M.Tech) in Thermal Engineering in the Department of Mechanical Engineering, MNNIT-A, U.P, India.

Bhupendra Koshti received the bachelor's degree in Mechanical engineering from RGPV University in 2009, the master's degree in Heat Power Engineering from RGPV University in 2011, and he is a Research scholar in the Department of Mechanical Engineering, MNNIT-A, Prayagraj, U.P, India.

Dr. Rahul Dev received the bachelor's degree in Mechanical engineering in 2004 from IET Lucknow in 2009, the master's degree in Energy Studies from IIT Delhi in 2007, and the philosophy of doctorate in Solar Distillation from IIT Delhi in 2012 respectively. He is Assistant Professor at the Department of Mechanical Engineering, MNNIT-A, Prayagraj, U.P, India. His research areas include Renewable Energy, Solar Energy Applications like Solar Energy Storage, Passive Buildings, Solar Stills, Daylighting, and Photovoltaics.

Dr. Jitendra Narayan Gangwar received the bachelor's degree in Mechanical engineering from UP Technical University, Lucknow, the master's degree in Fluid and Thermal Sciences from IIT Kanpur, and the philosophy of doctorate in Mechanical Engineering from MNNIT-A, respectively. He is an Assistant Professor at the Department of Mechanical Engineering, MNNIT Allahabad, Prayagraj-211004, and UP, INDIA. His research areas are internal combustion engines, Alternative fuels for IC engines, Combustion, Performance and emission characterization, Lubricating Oil Tribology, and Automobile Engineering.

Dr. Supriya Yadav received the bachelor's degree in Science (B.Sc.) from SPM, master's degree in Mathematics (M.Sc.), and have the philosophy of doctorate. She is an Assistant Professor in the Department of Mathematics, MNNIT-A, Prayagraj, U.P, India. Her research area includes Fluid dynamics, Differential equations, and Bio-Mechanics.

Design and Implementation of Solar Panel on E- Rickshaw

[1]Kapil kumar[*], [2]Rahul Dev, [3]Samir Saraswati, [4]Jitendra Narayan Gangwar,

[5]Navneet Kumar Singh

Motilal Nehru Institute of Technology, Allahabad, Prayagraj, India

* kapilkumar78910@gmail.com, rahuldsurya@mnnit.ac.in, samir@mnnit.ac.in, jgangwar@mnnit.ac.in, navneet@mnnit.ac.in

Abstract

In today's world, global warming is increasing at a tremendous level. There are several reasons like exhaust gases from vehicles, smoke from industries, deforestation and many more. Presently, most of the vehicles are running on internal combustion engines (ICEs) and producing exhaust gases. These exhaust gases are increasing the environmental pollution level and creating health problems. The best way to reduce the pollution from the automobile sector is to find an alternate way to fossil fuels. An alternate way can be the use of renewable energy in the automobile sector. These days electric vehicles (EVs) are in more demand and various research is also going on in this direction. Electric vehicles are the best substitute for fossil fuel-based vehicles. In recent days, EVs are very popular, and the main components of EVs are battery, DC motor, charge controllers, etc. Among these components, the battery is the most essential component of the EV because the battery helps to run the vehicle for a longer range. So, the use of the battery is an important parameter in EVs. With the help of solar energy in the EVs, the range of vehicles can be increased.

Keywords: Solar energy, Electric vehicles, Automobile: E- Rickshaw, Battery, DC motor

1. INTRODUCTION

Energy is one of the most important needs for the survival of human beings on earth and eventually on every planet of this universe. Humans are dependent on this type of energy to fulfil their all needs.[1] Humans are using fossil fuels for the smooth running of our vehicles for hundreds of years. Largely populated countries like India, China, U.S. are using a lot of fossil fuels for their transportation sector. But the main disadvantage of these fossil fuels is that they are not environment friendly and these are exhaustible. So, for the removal of such issues, we need to think of an alternate way, and the use of renewable energy is the option to tackle these problems.[2]

The solar electric vehicle is primarily powered by solar energy directly. Photovoltaic panels are used to collect solar energy, and this solar energy can easily be converted into electrical energy with the help of a photovoltaic cell. The PV cell collects a portion of the solar energy and stores it into the battery of the vehicle with help of the charge controller.[3] After storing the electrical energy in batteries, this energy is supplied to the DC motor to drive the vehicle continuously. The motor controller helps to control the amount of electrical energy to the motor corresponding to the throttle. The DC motor uses that controlled electrical energy to drive the vehicle.

1.1 Why we need Solar Electric Vehicles

When the combustion of fossil fuels takes place in automobiles, the engine produces a large amount of pollutants in their exhaust. These pollutants help to increase the rate of global warming and impact the environment. This is one of the biggest problems faced by the urban people throughout the world.

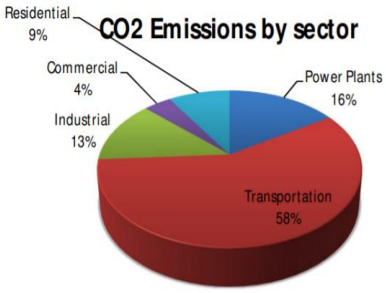

Figure 1. Different Sectors of CO2 Emissions [4]

The number of vehicles is increasing continuously with the increasing population and due to this, air pollution is also increasing. Figure 1 shows that the transportation sector is the main culprit for producing the CO_2 production. The earth has a limited amount of fossil fuels, and according to the consumption rate, fossil fuels are going to be eliminated in the near future. And these fossil fuels produce harmful gases during their combustion which impact the environment's health. Various actions and restrictions are taken to control the air pollution level but this is not sufficient. So, we have to shift towards the renewable energy side so that we can control the pollution level and can-do sustainable development.[5]

1.2 Working

A solar-powered electric vehicle is an electric vehicle that is powered by direct or indirect solar energy. The word "Solar Vehicle" directly shows that solar energy is used to perform all the functions of a vehicle. The solar-powered electric vehicle gets the energy from the solar energy it needs to move. The surface created by solar panels absorbs most of the light that falls on it with help of the photovoltaic effect.

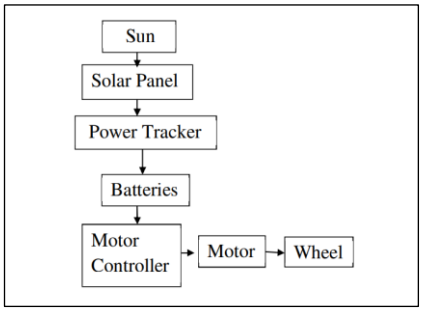

Figure 2. Energy flow diagram for solar-powered electric vehicle

The figure 2 gives an overview of the working of solar-powered electric vehicles. Sun is the main source of energy for the vehicle. Solar radiations are obtained on earth from the sun. Solar radiations are absorbed by the solar panel, and these solar radiations are converted into electricity by the photovoltaic effect in the solar panel. The electricity produced is being transferred to the batteries by the help of a power tracker which helps to charge the battery for future use. And then current flows from the battery to the motor via the motor controller for the movement of a vehicle. The motor controller helps to adjust the speed of a motor by its internal mechanism. The rest of the excess electricity is stored in the battery for future use during cloudy weather.[3] Solar panel helps to provide continuous current by photovoltaic effect to battery so that vehicle can cover a longer distance than its actual battery range.

2. CALCULATION

During the movement of a vehicle, there are certain resistant forces that act on a vehicle. These forces are rolling friction force, drag force, uphill resistance, and inertia force. With the increase in velocity, drag force increases rapidly.

The rolling resistance, aerodynamic drag, inertia force, and climbing force can be calculated using the below equations [2] –

$$Rolling\ force(Frolling) = mg \times \mu_{rolling} \times \cos\theta \quad (1)$$

$$Climbing\ resistance\ force(Fclimb) = mg \times \mathrm{Sin}\,\theta \quad (2)$$

$$Aerodynamic\ drag\ force(Fdrag) = (^1/_2) \times \rho \times C_D \times A \times V^2 \quad (3)$$

$$Acceleration\ force(Facc) = mass \times acceleration \quad (4)$$

$$Traction\ force(Ftrac) = Frolling + Fclimb + Fdrag + Facc \quad (5)$$

In these equations, ‘m’ is the Mass of the vehicle with load (Kg),

‘g’ is the Acceleration due to gravity (m/s^2),

‘C_D’ is Drag coefficient,

‘A’ is projected frontal area (m^2),

‘ρ’ is the air density (kg/m^3),

‘V’ represents the velocity of the solar-powered electric vehicle (m/s) and F_{trac} is the total force required to counterbalance the all forces which resist the motion of the vehicle.

The P_{trac} applied to the vehicle to move will be:

2.1 Estimation of DC Motor

The total power required by the vehicle to run on the road can be calculated using the equation number (6):

$$Traction\ power(Ptrac) = Ftrac \times V \quad (6)$$

where V represents the velocity of the solar-powered electric vehicle (m/s) and F_{trac} is the total force required to counterbalance the all forces which resist the motion of the vehicle [6],

where M is the total mass which includes the mass of the vehicle and mass of five passengers and mass of the battery and the mass of the solar panel.

Mass of vehicle = 200 kg

Mass of 1 passenger = 55 kg, (ICMR Report)

Mass of battery = 35 kg

Mass of solar panel = 25 kg

Total mass (M) = 200 + (55 x 5) + 35 + 25 =535 kg

Table 1. Specifications used during calculation

Total mass(M)	535 kg
Air Density(ρ) @ 27°	1.2 Kg/ m^3
Drag Coefficient (C_D)	0.44
Projected area(A)	1.8 m^2
Vehicle velocity (V)	25 km/h
Acceleration due to gravity(g)	9.81 m/s^2

Source: ARAI & Ministry of Road Transport and Highways

Vehicle is moving on a straight road with a velocity of 25km/h on a straight road. Here considering forces are rolling and drag forces only. Considering the data from Table 1 calculation of motor power is calculated as:

$$Rolling\ force(Frolling) = mg \times \mu_{rolling} \times \cos\theta = 535 \times 9.81 \times 0.011 = 57.73N$$

$$Aerodynamic\ drag\ force(Fdrag) = (1/2) \times \rho \times C_D \times A \times V^2$$

$$= (1/2) \times 1.2 \times 0.44 \times 1.8 \times (25 \times 5/18)^2$$

$$= 22.91\text{N}$$

$$Traction\ force(Ftrac) = Frolling + Fdrag$$

$$= 57.73 + 22.91 = 80.64\ N$$

The main aim is to determine the power of motor, so by multiplying the maximum velocity to our total traction force, we will get the total traction power. The power required to drive the vehicle will be calculated by using the equation number (2.6) as:

$$Traction\ power(Ptrac) = Ftrac \times Velocity$$
$$= 80.64 \times 25 \times \left(\frac{5}{18}\right) = 560\ W$$

Now, a DC Motor with a rating of 1000 W is sufficient and this used capacity is higher than the above calculated capacity. We decided to use a DC motor because of its long-life expectancy, low maintenance and operation cost .

2.2 Estimation of the Battery Capacity

Battery is the main component for continuous running of solar powered electric vehicle. Solar- powered electric vehicle can be used by the office staffs and college students. Consider the longest distance which will travel by our vehicle from Teachers colony to Yamuna gate, MNNIT, PRAYAGRAJ, UP, INDIA which is approximately equal to 1.5 km.

With 20 return trips in a day, the total distance will be:

Distance(D) = 20 (2 × 1.5) = 60 km.

The total distance to be travelled by solar- powered EV is 60 km then the total energy required by the DC motor during travel time is given by:

$$E_m = P \times \mathrm{T}$$

where T= (D/V)

$$E_m = 1\ KW \times (60/25)\ \mathrm{h} = 2.4\ \mathrm{kWh} = 2400\ \mathrm{Wh}$$

E_m is the capacity required by motor for smooth running of vehicle while E_b is the battery capacity required after considering the all loses.

Consider the efficiency of motor as 90%, then the maximum energy that should be supplied by the battery to the DC motor is:

$$E_b = \frac{2.4\ Wh}{0.9} = 2.6\ kWh = 2600\ Wh$$

2600 Wh battery capacity is required for the smooth flow of 1000 Watt DC Motor and this battery capacity helps to cover this distance without any problem with all conditions imparted. [6]

To know the battery capacity in Ampere Hour (Ah):

Now, 48-volt batteries are generally used in E – rickshaw vehicles.

Voltage(V) x Ampere Hour (Ah) = Watt Hour (Wh)

48 V x (Required Ah) = 2600 Wh

Required Ah = $\frac{2600}{48}$ = 54.16 Ah

The battery Ah measured here as 54.16 Ah, which will be acquired by considering 48 Volt 20 Ampere-hour in parallel connection of three batteries.

2.3 Estimation of Solar- Panel Size

To provide the continuous supply of current to battery, solar panel is required. The solar panel size can be determined by total energy requirement for battery and losses occur during supply.

Now, assume the efficiency of battery, the efficiency of charging the battery and the efficiency of charge controller as ηb , ηch, and ηcc respectively .

The total energy required from the solar panel is :

$$E_p = \frac{E_b}{\eta b \times \eta ch \times \eta cc}$$

$$= \frac{2.6}{0.9 \text{ x } 0.9 \text{ x } 0.9}$$

$$= 3.566 \text{ kWh}$$

where Ep is the total power required from the solar panel for continuous functionality of the vehicle without a stoppage. [6]

To run the vehicle at 25 Km/h, we required a battery of 2.6 kWh with a motor capacity of 1 KW.

The total energy required from the panel is 3.566 kWh for the continuous functionality of the vehicle.

For Solar panel power output:

Solar energy (Wh) = Solar panel power output (W) x (Average hour of sunlight) x (75% because of 25 % loss due to dust, pollution, weather, etc.)

- During Summer:

3566 Wh = Solar panel power output x 10 hour x (0.75)

Then, Solar panel output requirement $= \frac{3566}{(10 \, x \, 0.75)} = 475.46 \sim 475$ W

- During Winter :

3566 Wh = Solar panel power output x 5 hour x (0.75)

Then, Solar panel output requirement = $\frac{3566}{(5 \, x \, 0.75)} = 950.93 \sim 950$ W

Now, solar panel capacity will be considered by using the average method-

Average for solar panel = $\frac{Summer \ \ required \ capacity + Winter \ required \ capacity}{2}$

$$= \frac{475+950}{2} = 712.5 \text{ W} \sim 720 \text{ W}$$

So, the 720 W capacity of the solar panel is sufficient for the continuous running of the vehicle.

3. ADVANTAGES

As solar vehicle is the need of the future because it has a lot of advantages.[4] Some of the major advantages are –

- There is no need to refuel the solar electric vehicle.
- Maintenance required for a solar electric vehicle is very low.
- Solar electric vehicles are noise-free because of the use of an electric motor.
- Solar electric vehicles are environmentally friendly because they do not produce any harmful gases.
- The efficient solar panels can be used to obtain a large amount of electrical energy.
- Solar EVs can be easily produced because of their easy mechanism.

4. CHALLENGES

Despite the wide range of advantages, solar electric vehicles come with some challenges too. These are some of the major challenges of the solar electric vehicle –

- Solar panels available on the market are less efficient for the conversion of solar energy into electrical energy, so we need a large surface area of solar panels on the roof of vehicles.[3]
- It is not easy to fix the solar panel on the top of the vehicle to get the low value of wind resistance during the motion of the vehicle.
- Solar electric vehicles cannot be used during winter and cloudy weather.
- Highly efficient solar panels are required in solar electric vehicles and these are too expensive and this can increase the initial cost of the vehicle.
- Solar electric vehicles are not able to run at high speeds as compared to IC engines

5. CONCLUSION

Solar electric vehicle's future is quite bright and it will bring advancement in the automobile industry as it can help to reduce pollution.[3] It also helps to reduce the dependency on a single source. Other conclusions are like as :

- To charge the 3.5kWh battery, solar panel requirement during summer will be of 475-Watt capacity and for winter, solar panel capacity will increase to 950 Watt.
- Solar panel capacity will increase during winter because of less solar radiation intensity availability.
- Solar electric vehicle is the best option for controlling the pollution level.
- With the implementation of solar panel, the range of distance covered by the vehicle will increase due to continuous charging from the PV solar panel.

Solar electric vehicles also have some disadvantages, but the advantages are more and because of this, solar electric vehicles are the future of the automobile industry. So, we can use solar electric vehicle in the upcoming future.

REFERENCES

[1] A. R Jadhav & A. D. Bhoi., "Review Paper on Solar Powered Energy Management System for Electric Vehicle", International Journal of Engineering Research & Technology, 2016.

[2] M. M Rastegardoost, S. Heydari, P. Ahmadi, & K. Abrinia, "International Journal

of Automotive Engineering Simulation and Energy Performance Assessment of the Ghazal Solar-Electric Commercial vehicle in Tehran ", Iran. 9, 2019.
[3] I. Yves, Gonzales, "Solar Electric Vehicle Need Working Advantage,International Journal for Research in Applied Science & Engineering Technology",2020
[4] J. Connors,Solar vehicles and benefits of technologies,"International conference on clean electric power", 2007
[5] G. Shukla, K. Raval, D. Solanki & U. Patel, "A study on Campus-Friendly Solar Powered Electric Vehicle. Inernational Research Journal of Engineering and Technology", 2008.
[6] V. Khare & A. Bunglowala , "Design and assessment of solar-powered electric vehicle by different techniques. International Transactions on Electrical Energy Systems ", 2020.

Biographies

Mr Kapil Kumar received his bachelor's degree from UIET, Maharishi Dayanand University , Rohtak, Haryana in 2019 and pursuing his masters in Thermal Engineering from Department of Mechanical Engineering in MNNIT Allahabad, U.P., INDIA.

Dr. Rahul Dev received the bachelor's degree in Mechanical engineering from IET Lucknow, the master's degree in Energy Studies from IIT Delhi, and the philosophy of doctorate degree in Solar Distillation from IIT Delhi, respectively. He is currently working as an Assistant Professor at the Department of Mechanical Engineering, M.N.N.I.T. Allahabad, Prayagraj-211004, U.P, INDIA. His research areas include Renewable Energy, Solar Energy and its applications.

Dr Samir Saraswati received the bachelor's degree in Mechanical engineering from IIT Roorkee and did his master's degree in Design of process Machines from MNNIT Allahabad and the philosophy of doctorate degree in Mechanical engineering from MNNIT Allahabad. He is currently working as an Associate Professor at the Department of Mechanical Engineering, MNNIT. Allahabad, Prayagraj-211004, U.P, INDIA. His research areas are Internal Combustion Engines, alternative fuels, application of Artificial Intelligence in Engine Management, Energy and Thermal Management of Lithium-Ion Batteries.

Dr Jitendra N Gangwar received the bachelor's degree in Mechanical engineering from U.P Technical University, Lucknow and did his master's degree in Fluid and Thermal science from IIT Kanpur and the philosophy of doctorate degree in Mechanical engineering from MNNIT Allahabad. He is currently working as an Assistant Professor at the Department of Mechanical Engineering, MNNIT. Allahabad, Prayagraj-211004, U.P, INDIA. His research areas are Internal combustion Engines, Alternative Fuels for IC Engines, Combustion, Performance and Emission Characterization, Lubricating Oil Tribology, Automobile Engineering.

Dr Navneet Kumar Singh received the bachelor's degree in Electrical engineering and did his master's degree in Engineering systems and also received the philosophy of doctorate degree. He is currently working as an Assistant Professor at the Department of Electrical Engineering, MNNIT Allahabad, Prayagraj-211004, U.P, INDIA. His research areas are power system operations and planning, Artificial intelligence applications in power system.

Influence of Geometry Changes on the Radial Cooling Performance of Lithium-ion Battery

[1]Dwijendra Dubeya, [2]Ashutosh Mishraa*, [3]Taufeeq Ahmadb, [4]Ramesh Pandeya

[1,2,4]Department of Applied Mechanics, Motilal Nehru National Institute of Technology Allahabad, Prayagraj, Uttar Pradesh, India

[3]Sieger Robotek Electric Pvt. Ltd., Sonipat, Haryana, India
*dwijendrame0042@gmail.com, *amishra@mnnit.ac.in,*
taufeeq.nit@gmail.com, ramesh@mnnit.ac.in

Abstract

With the exponential rise of the electric vehicles in the field of automobile sector, the use of lithium-ion battery (LIB) has been increased to several folds. The performance and life cycle of LIBs is governed by its temperature during operation. Therefore, studies related to the prediction of thermal behavior of operating LIB is gaining worldwide attention nowadays. The thermal behavior of LIB under different charging and discharging rates are predicted experimentally and numerically. The present work includes the thermal analysis of cylindrical LIB at 1C rate of discharge using three-dimension (3D) multipartition thermal model. The influence of geometric changes on the cooling performance, using radial cooling approach, is analyzed for two convective heat transfer coefficients (h=20 and 50 W/m^2K).The numerical results are validated by the published experimental data. Present work compares the average surface temperature for three different geometries (datum geometry-DG i.e. 18650 LIB, large geometry-LG and small geometry-SG) of LIB subjected to radial convective cooling. Subsequently, the temperature heterogeneity in terms of radial temperature gradient for 1C discharge rate is compared. The results show that average surface temperature of DG is minimum, while radial temperature heterogeneity is minimum for LG.

Keywords: Lithium-ion battery, multipartition model, battery geometry, radial cooling, heat transfer coefficient, average surface temperature, radial temperature gradient.

1. INTRODUCTION

Lithium-ion cylindrical batteries (LIB) have been widely considered as an energy storage device for battery electric vehicles (BEV), hybrid electric vehicles (HEV), and plug-in hybrid electric vehicles (PHEV) etc, due to their high power density, high specific energy, high reliability, low self-discharge rate, as well as low cost [1,2]. However, LIB exhibit high sensitivity to temperature [3, 4]. As reported in some studies, the internal resistance of the battery will increase noticeably at low temperatures, which result in the reduction of battery specific energy and power significantly. In the charge/discharge process, considerable heat is generated in the battery[5,6]. Effect of temperature on the life of LIB is very crucial [7]

and some studies depicts that even a single degree increase in the temperature can reduce the life of battery significantly [8-10].

It is to be noted that, prediction of internal temperature variation of a battery for different rate of charging and discharging with the help of experiment is possible[11], but the real time situation of a battery during its operation when assembled as pack and module in an vehicle or device is difficult. Therefore, the numerical modelling is crucial to enhance the understanding of thermal aspects of battery. Finite element method, lumped analysis or electro chemical methods are some techniques which can be used for the simulation of battery thermal behaviour[11-14]. However, they have their own limitation and assumptions. Further, development of appropriate phenomenological models to simulate thermal behaviour of batteries can be battery electrode dependent that vary with different battery technologies [15, 16]. It is computationally expensive to have predictions of thermal behaviour accurately while battery is in operation. A comparatively less computational 3D model using the approach of equivalent circuit network (ECN) for thermal management is performed by coding on python[17]. However, to increase the accuracy level multi partition modelling using FEM for thermal analysis is an emerging approach[18-20].The 3D multi partition cylindrical model has been used and integrated with finite element method to investigate the internal temperature variation for different geometries.

In the present work, radial convective cooling is taken into the consideration with heat transfer coefficient equals to 20 W/m^2K (natural) and 50 W/m^2K (forced) and the effect of cooling is checked for three different types of geometry to find out the best geometry among the three with minimum average surface temperature and radial temperature gradient. The thermal behaviour of battery is different at different charging and discharging rate. The surface temperature and radial temperature gradient variation over the time for 1C discharge rate is numerically predicted and compared for the considered geometries. Discharge rate is taken into consideration rather than charging rate in the present work as, during charging, the endothermic reaction take place inside the battery. On the other hand, during the discharge process, exothermic reaction takes place, due to which the rise in temperature and temperature heterogeneity is high in battery[3, 11].

2. MATERIALS AND METHODS

Three different geometries considering multi partition model approach is designed to study the thermal behavior at 1C discharge rate. The multipartition model of a battery consist of five parts i.e. positive terminal, negative terminal, jelly roll, cell cap and cell steel can. Separately all parts are designed and assembled to carry out the thermal transient analysis using convective heat transfer cooling method in ANSYS platform.

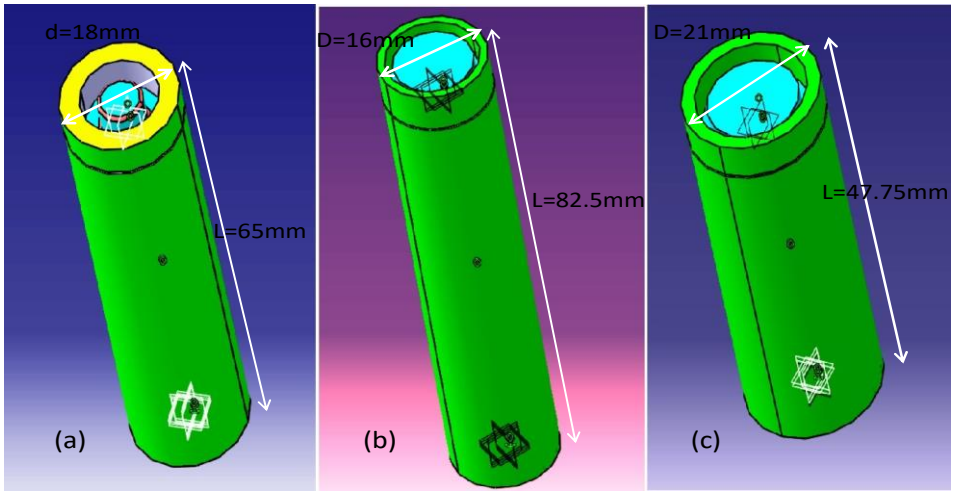

Figure 1. (a) Datum geometry (DG) i.e. 18650 LIB, (b) large geometry (LG) and (c) small geometry (SG).

In presented work three types of geometry is taken. The first one is Li-ion 18650 cylindrical battery with pre known dimensions of 18 mm diameter and 65 mm length and in paper this geometry is abbreviated as datum geometry (DG). In second geometry length has been increased and diameter has been decreased while keeping the volume constant and this geometry is abbreviated as large geometry (LG), in next geometry diameter has been increased and length has been decreased while keeping the volume constant and this geometry is abbreviated as small geometry (SG). The dimensions and data are tabulated in Table1.

Table 1. Diameter and length of different geometry

Geometries	Length (mm)	Diameter (mm)	Volume (mm^3)
DG	65	18	16520
LG	82.5	16	16520
SG	47.75	21	16520

From the above assembly design and dimensions table, it can be observed that different geometry has been found out by changing the dimensions while keeping the volume constant.

2.1 Thermo physical properties of different components of battery

As discussed earlier, three-dimensional (3D) multipartition model is considered, as compared to lumped model multipartition model give more accurate results[13]. Here a transient thermal analysis has been performed for 1C discharge rate (discharging in 3600 seconds). Mainly five components are taken to constitute multipartition model i.e. positive terminal, negative terminal, cap, jelly-roll and cell can. The orthotropic thermal conductivity has been taken for the jelly-roll as per cylindrical coordinate system and rest all other

components are provided with isotropic properties. The variation of temperature in jelly-roll is very crucial, jelly-roll plays the major contribution in radial temperature gradient.

Table 2. Thermo physical properties of all different component used in battery[13]

Components	Material	Density (kg/m^3)	Heat capacity (J/kg K)	Thermal conductivity (W/m K)
Positive terminal	Aluminum	2719	871	202.4
Negative Terminal	Nickel	8900	460.6	91.74
Jelly roll	Electrode &Separator	2440	1210	K_r=1.1, K_z=K_q=12.5
Cap	PTC	3455	565.5	30
Steel Can	Steel	8030	502.48	16.27

2.2 Heat generation for different component

Cap, positive terminal and negative terminal having a constant internal heat generation whereas internal heat generation for the jelly roll is dependent on rate of charging and discharging, it will give different value for different rate of charge/discharge[13]. Heat generation of jelly-roll mainly depends on its internal resistance and internal resistance of jelly-roll varies with state of charge and discharge. By tracking the variation of internal resistance, we can get the data related to internal heat generation for different rate of charge and discharge. Here the analysis is limited to 1C discharge rate. The plot of volumetric heat generation v/s time for 1C is given in Figure 2.

Table 3. Component wise heat generation [13]

Components	Heat generation(mW/mm^3) for 1C
Cap	0.147
Positive Terminal	0.214
Negative Terminal	0.671

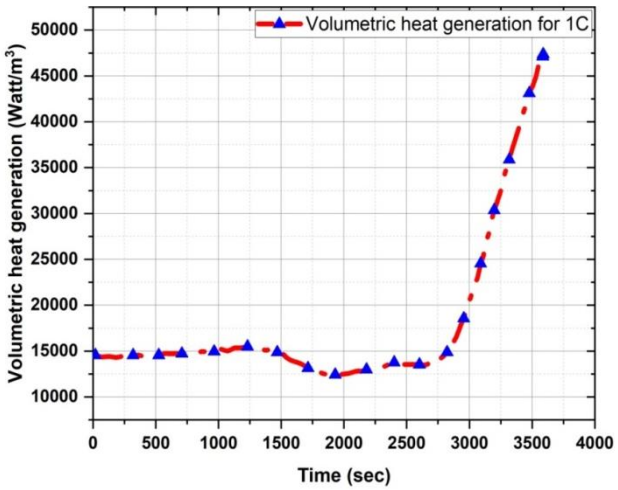

Figure 2. Volumetric heat generation of Jelly-roll at 1C discharge rate[13]

The volumetric heat generation for jelly-roll is plotted versus time, from the curve it can be observed that at the end of discharging i.e. in between 2500 to 3600 seconds the variation is large, from the above observation this can be said that at higher value of depth of discharge the heat generation is high. The variation heat generation with time can be seen in Figure 2.

2.3 Validation study

The thermal model is validated from the published experimental [13] cooling performace data for Li-ion 18650 battery which is also assumed as a datum geometry (DG). The percentage error in experimental and simulated result is less then 5 % the comparision graph is also ploted (Figure 3).

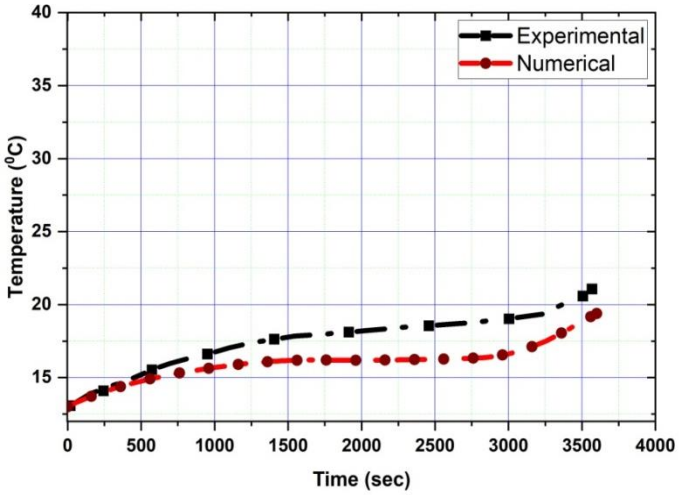

Figure 3. Numerical and experimental battery surface average temperature at 1C for DG i.e. LIB 18650. Experimental data are taken from the study Yang et al[13]

3. RESULTS AND DISCUSSION

After designing the battery model as per table 1 for DG, LG and SG, the multipartition heat generation transient thermal analysis is performed in ANSYS. The input parameters of table 2 and 3 and convective heat transfer values are provided to predict the average surface temperature. The results are shown in figure 3.

From the figure 4, it is observed that the average surface temperature for all the three geometry is different and it is maximum for SG at h=50 W/m^{2}K, which is 17.474 ℃. The maximum surface temperature for the LG and DG is 16.577℃ and 16.269℃ respectively. From the obtained results one can conclude that radial cooling approach for DG is good in terms of average surface temperature after 1 hour of cooling.

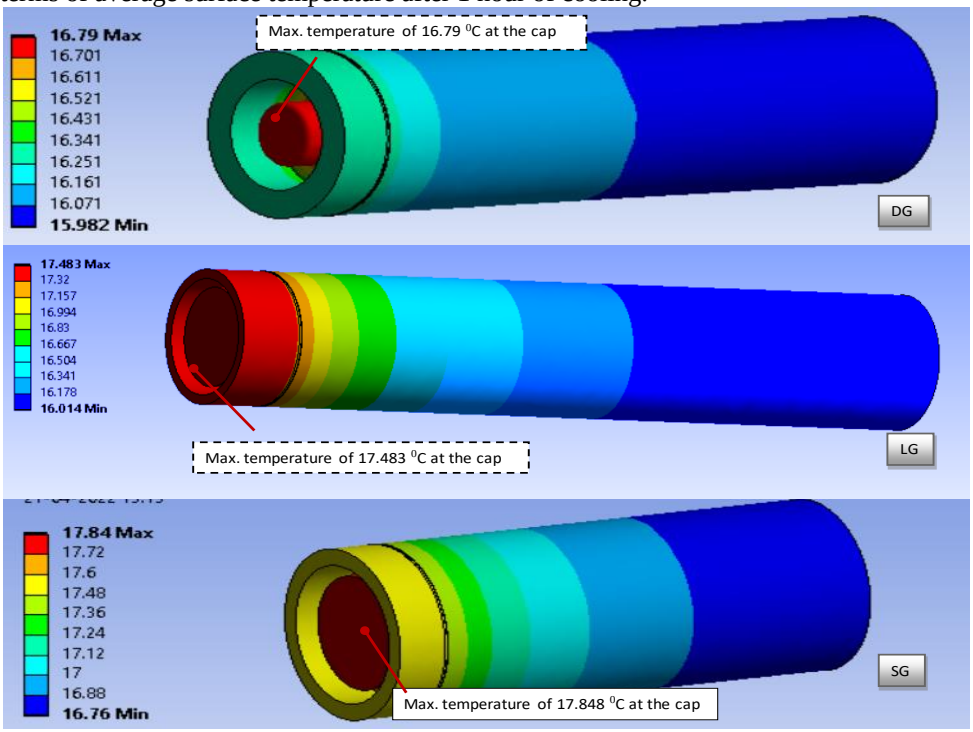

Figure 4. Average surface temperature contour for Datum geometry (DG), Large Geometry (LG), and Small Geometry (SG) at the end of 3600 seconds for 1C discharge rate at h= 50 W/m^{2}K (i.e. forced cooling).

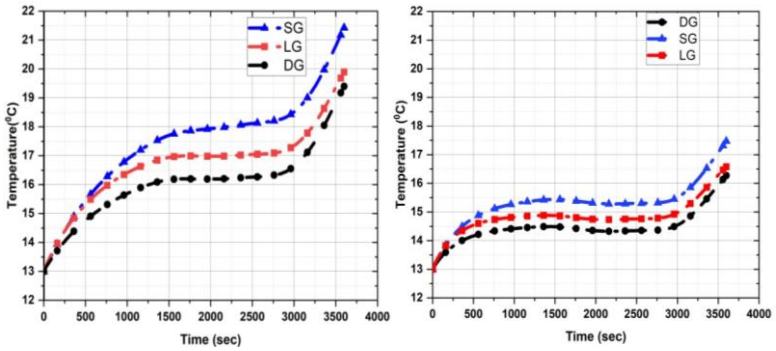

(a) (b)

Figure 5. Variation of average surface temperature with time for 1C discharge rate at (a) h= 20 W/m^{2}K, (b) h=50 W/m^{2}K

The average surface temperature of the considered geometries are predicted and the values are compared in figure 5 for h=20 Watt/m^{2}K and 50 W/m^{2}K, simulating the natural and forced convective cooling.

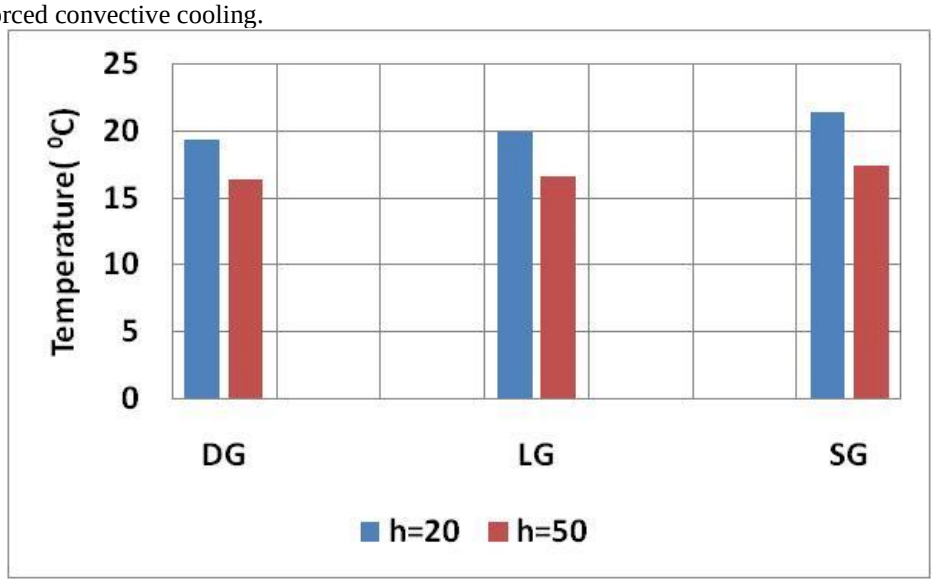

Figure 6. Maximum average surface temperature diffrance for DG, LG and SG for changing the heat transfer cofficient from 20 to 50 W/m^{2}K

As in the analysis when the convective heat transfer cofficient is chnaged from 20 to 50 W/m^{2}K the maximum surface average temperature fall is 2.954℃, 3.321℃ and 3.954℃ for DG, LG, and SG respectively, as shwon in Figure 6. The rate of cooling for the SG type battery on increasing the heat transfer cofficient is higher in comparision with DG and LG. This is because the difference between maximum average surface temperature and ambient temperature is high for SG type battery after natural cooling.

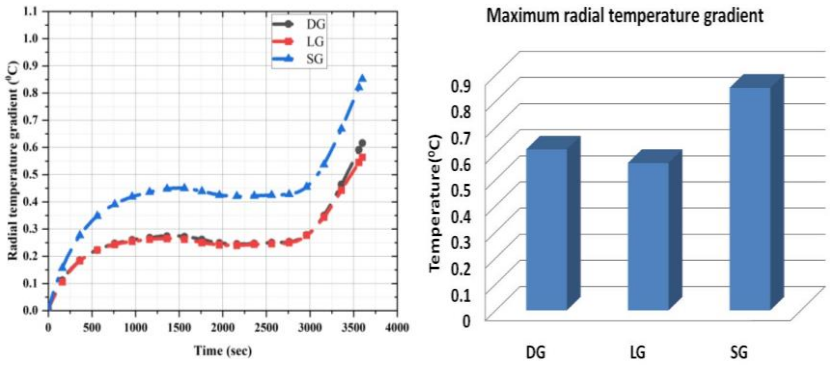

(a) (b)

Figure 7. (a) Variation of radial temperature gradient over the time for h=50W/m^{2}K and, (b) Maximum radial temperature gradient for different geometry for h=50W/m^{2}K.

Radial temperature gradient plot versus time at h=50 W/m^{2}K for radial cooling for all the three geometries is plotted in figure 7(a). This can observe that variation of radial temperature gradient for 1C rate for DG and LG is very close to each other. In figure 7 (b) this can be observed that maximum value of radial temperature gradient is minimum for LG and maximum for SG.

4. CONCLUSION

In the present work, the effect of geometry is clearly seen on radial convective cooling at different values of heat transfer coefficient. The cooling performance, in terms of average surface temperature, is most efficient for DG i.e. for 18650, intermediate for LG and least efficient for SG. It is also observed that, on increasing the value of heat transfer coefficient from 20 to 50 W/m^{2}K the average surface temperature decreases for all the geometries. This can be observed from the above analysis that on increasing the heat transfer coefficient the rate of cooling is increasing. The rate of cooling is highest for SG type batteries at elevated heat transfer coefficient due the high temperature difference between battery surface and ambient.

Radial temperature gradient is an important thermal parameter to analyze the life cycle and working conditions of cells. The non-uniform and high radial temperature gradient is dangerous and deteriorating. From the above analysis it has been observed that the radial temperature gradient is minimum for LG and highest for SG. The result can be different for different types of cooling process for different geometry.

It is inferred from the present approach of radial cooling strategy that by increasing the diameter and decreasing the length of LIB, both the average surface temperature and radial temperature gradient will increase. Conversely, decreasing the diameter and increasing the length of the LIB, the radial temperature gradient will decrease and a very minute rise in average surface temperature will take place. If it is important to keep the radial temperature gradient in limit then LG type geometry can be used and if it is required to keep the average surface temperature low, then DG type batteries is suggested in case of radial convective

cooling. Therefore, the present work gives a direction towards improving the cooling efficiency by using the optimum cell geometry.

REFERENCES

[1] T. Ahmad, A. Mishra, Energy Technology.2022, 10.2, 2100888.

[2] G. Zubi, R. Dufo-López, M. Carvalho, G. Pasaoglu, RenewableSustainable Energy Rev. 2018, 89, 292.

[3] M. S. Jo, S. Ghosh, S. M. Jeong, Y. C. Kang, J. S. Cho, Nano-Micro Lett.2019, 11, 3.

[4] M. Doyle, T. F. Fuller, J. Newman, J. Electrochem. Soc. 1993, 140, 1526.

[5] A. R. Baird, E. J. Archibald, K. C. Marr, O. A. Ezekoye, J. Power Sources2020, 446, 227257.

[6] V. G. Choudhari, A. S. Dhoble, S. Panchal, M. Fowler, R. Fraser,J. Energy Storage2021, 43, 103234.

[7] J. Hou, L. Lu, L. Wang, A. Ohma, D. Ren, X. Feng, Y. Li, Y. Li, I. Ootani,X. Han, W.Ren, X. He, Y. Nitta, M. Ouyang, Nat. Commun. 2020,11, 5100.

[8] P. Ahmad, S. Shriram, K. Gi-Heon, Large Format Li-Ion Batteries forVehicleApplications, 2013, http://www.nrel.gov/docs/fy13osti/58145.pdf.

[9] S. Ma, M. Jiang, P. Tao, C. Song, J. Wu, J. Wang, T. Deng, W. Shang,Prog. Nat. Sci.Mater. Int. 2018, 28, 653.

[10] C. Forgez, D. Vinh Do, G. Friedrich, M. Morcrette, C. Delacourt,J. Power Sources 2010, 195, 2961.

[11] S. Abada, G. Marlair, A. Lecocq, M. Petit, V. Sauvant-Moynot, F. Huet,J. Power Sources 2016, 306, 178.

[12] K. Makinejad, R. Arunachala, S. Arnold, H. Ennifar, H. Zhou, A. Jossen, W. Changyun, World Electr. Veh. J. 2015, 7, 1

[13] X. Yang, X. Hu, Z. Chen, Y. Chen, Appl. Therm. Eng. 2020, 178,115634.

[14] J. Newman, W. Tiedemann, AIChE J. 1975, 21, 25.

[15] S Kala, A Mishra, Materials Today: Proceedings 46,1543-1556.

[16] S Kala, A Mishra, V Shukla, Indian Chemical Society,2020

[17] S. Li, N. Kirkaldy, C. Zhang, K. Gopalakrishnan, T. Amietszajew,L. B. Diaz, J. V. Barreras, M. Shams, X. Hua, Y. Patel, G. J. Offer,M. Marinescu, J. Power Sources 2021, 492, 229594.

[18] S. D. Chitta, C. Akkaldevi, J. Jaidi, S. Panchal, M. Fowler, R. Fraser,Appl. Therm. Eng. 2021, 199, 117586.

[19] M.-K. Tran, A. DaCosta, A. Mevawalla, S. Panchal, M. Fowler, Batteries2021, 7, 51.

[20] D. Worwood, Q. Kellner, M. Wojtala, W. D. Widanage, R. McGlen,D. Greenwood, J. Marco, J. Power Sources 2017, 346, 151.

Biographies

Mr. Dwijendra Dubey received the bachelor's degree in Mechanical Engineering, the master's degree in, Engineering Mechanics and Design from Motilal Nehru National Institute of Technology Allahabad, Prayagraj, India, and currently pursuing the PhD from Motilal Nehru National Institute of Technology Allahabad, Prayagraj

Dr. Ashutosh Mishra received the bachelor's degree in Manufacturing Technology, the master's degree in Production Engineering from IIT BHU, Varanasi, India, and the philosophy of doctorate degree in Structural Mechanics, Mechanical Engineering from Indira Gandhi Centre for Atomic Research (IGCAR), Kalpakkam, Chennai, India. He is currently working as an Assistant Professor at the Department of Applied Mechanics, Motilal Nehru National Institute of Technology Allahabad, Prayagraj, UP, India. His research areas include Mechanics of composites and 3D printed parts, Battery modeling and battery abuse testing, Mechanical behavior of metals, Macro mechanics of bones and tissues under time dependent and radioactive load, Application of mechanics in multidisciplinary field.. He has been serving as a reviewer for many highly-respected journals - Latin American Journal of Solids and Structures (SCI-IF=1.289), Journal of Materials Engineering and Performance (SCI-IF=1.652).

Mr. Taufeeq Ahmad received the bachelor’s degree in Mechanical Engineering Dev Prayag Institute of Technical Studies, UP, India, have done M.Tech in Engineering Mechanics and Design from Motilal Nehru National Institute of Technology Allahabad, Prayagraj, India. He is currently working in the research and development (R&D) department (Battery modeling) of SiegerRobotek Electric Pvt. Ltd., Sonipat, Haryana.

Dr.Ramesh Pandey received the bachelor's degree in Civil Engineering from Motilal Nehru National Institute of Technology Allahabad, Prayagraj, Indiaand the master's degreein Structuresfrom Motilal Nehru National Institute of Technology Allahabad, Prayagraj.He has done PhD in Composite Structures from Motilal Nehru National Institute of Technology Allahabad, Prayagraj and currently working as an Associate Professor at the Department of Applied Mechanics, Motilal Nehru National Institute of Technology Allahabad, Prayagraj, UP, India. His research areas include Solid Mechanics and Smart Composite Structure.

Numerical Simulation of Shockwave/Boundary-Layer Interaction for Different Mach Numbers

[1]Prateek Kumar, [2]Shantanu Srivastava

Department of Mechanical Engineering, Motilal Nehru National Institute of Technology Allahabad, Prayagraj, Uttar Pradesh, India

prateek.2020TH15@mnnit.ac.in, shans@mnnit.ac.in

Abstract

This paper focuses on studying various sonic viscous flows in which the interaction of the shock wave and boundary layer dominates over the compression ramp corner. The interaction of the shockwave with the boundary layer is studied numerically by solving the Navier-Stokes system of equations for an unsteady flow using Mach numbers 1.5, 3.0, 7.0, and 10.30. The flow is modelled using the finite volume method with linear tetrahedral elements. Results include pressure coefficient and Mach number profiles. Dimensionless coefficient of pressure is calculated using a computational method and compared with experimentally obtained pressures for upstream and downstream surfaces for ramp angle 30°. The construction of a numerical grid, taking into account, the effect of pressure jumps associated with shock waves on the boundary layer has been discussed. Comparison with the experimental data for the coefficient of pressure depicts that the turbulence model is appropriate for the calculation of total pressure.

Keywords - Hypersonic, Supersonic, Boundary layer, Shockwave, Finite Volume Method

Abbreviations-

M	Mach number
SW	Shock wave
BL	Boundary Layer
M_∞	Freestream Mach number
Rex	Local Reynolds number
FVM	Finite Volume Method
SWBLI	Shockwave boundary layer interaction
P	Pressure
S	Source
u	Velocity in the x-direction
Cp	Coefficient of Pressure
t	Time

Greek letters-

τ	Shear stress
μ	Dynamic viscosity
ρ	Density
ϕ	Flux
Γ	Diffusion coefficient

1. INTRODUCTION

A shock front is a compression wave in supersonic flows that affects the flow properties across upstream and downstream locations. Typically, shock is a region where immense pressure, temperature, and momentum gradients occur.

The presence of any obstacle in the supersonic flow-field creates oblique shock, strength of which is dependent upon the local Mach number and the ramp angle. The oblique shock that appears to be in contact with the fore-front of the bow is called as attached bow-shock, and beyond the maximum deflection angle, the separated shock waves bend and locate themselves at a short distance away from the body.

The boundary layer (BL) is a thin region adjacent to the solid surface, where the viscous effects are under dominance. At the solid boundary, the fluid in contact assumes the velocity of the solid boundary. This is typically known as no-slip condition in the literature. The boundary layer develops in the region adjacent to the solid surface, in which the velocity gradients do exist. The velocity gradients are present due to the viscous nature of the fluid. A boundary layer may be laminar or turbulent in nature, which is strictly governed by the local Reynolds number. In supersonic flows, the boundary layers generated are turbulent in nature, exhibiting high dissipation.

In laminar flows the boundary laminar flow occurs when the flowing fluid comes into contact with a layer of solid material. The boundary layer is created by the interaction of the fluid and a solid surface. The BL can detach from the surface even if the pressure is too high or the surface is curved. Even if the Reynolds number is high, the boundary layer can separate off from the surface.

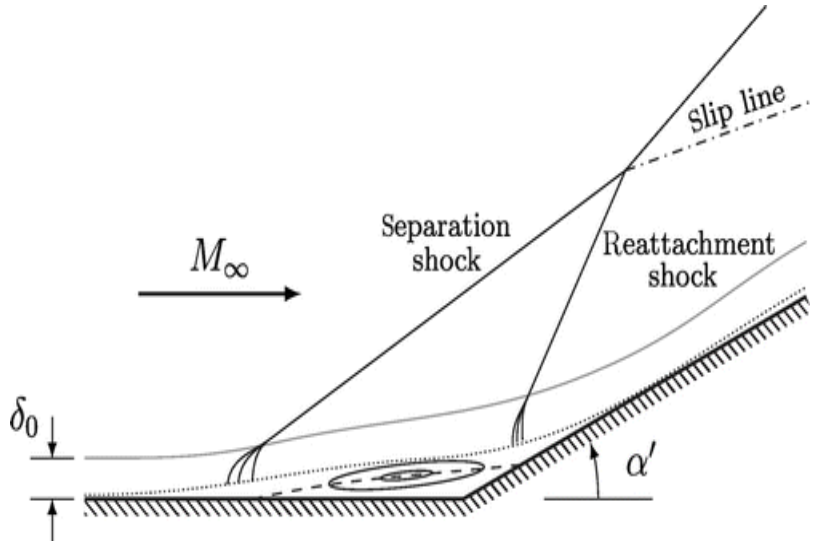

Figure 1. Shockwave-Boundary Layer Interaction over a compression ramp [1]

Oblique shock waves can be generated when the supersonic flow is turned into itself, results in the rise in pressure and temperature sharply. As the pressure rises, the boundary layer gradually thickens until it comes in contact with the shock and then quickly thins again. This property can lead to the separation and reattachment of the boundary layer. The interaction mechanism between the BL and SW depends upon several factors, including: ramp angle, Mach number, and the type of BL. In turbulent flow, the interaction region can extend up to the wall. Previous studies have shown that shock / BL interactions have a significant effect on the distribution of pressure, velocity, and heat transfer along the wall. The model developed by the ramp and the flat plate is a case of SWBLI. The shape is simple, but the phenomenon observed in this problem is complex. BL detachment is generated by the interaction of the SW/BL with the strong gradient developed in the compression zone. The major parameters affecting SWBLI [2] are Mach number, temperature, BL, inclination angle, Reynolds number and chemical state of the fluid.

The interaction between the SW and the BL produces a relatively weak shock on the compression front of the flat plate as shown in Figure 1. The shock wave caused by the ramp when comes in contact with the plate, the BL and upstream movement of pressure wave across the subsonic portion of the BL causes separation of flow which depends on the Mach number and ramp angle of the viscous fluid flow interaction parameters. There is a possibility that the presence of the bubbles causes detachment and reattachment shocks, the interaction of which creates a SW that comes in contact with the BL over the ramp based on the transfer of shock, shear layer, and the Mach number. Pressure and heat transfer increase rapidly downstream of reattachment due to flow recompression and peak occurs shortly after reattachment near the region where the boundary layer thickness is minimum.

The interaction of the shock wave with the boundary layer (SWBL) forms a recirculation zone and a large effect zone downstream and upstream of the shock point of the incident shock wave as shown in Figure 1. Numerical modelling by solving the first principles of conservation-law is a basic idea for evaluating SWBLs. The phenomenon of SWBLI for Mach number above 1.2 has been studied for the past 50 years. The shockwave- boundary layer interactions are essential for hypersonic problems. Neil D. Sandham [4] focused on the fundamental problems of shock waves caused by supersonic free currents and wedges in shear wave dynamics. Primarily focus was on the modelling the issues that arise when wedges create flow fields in supersonic free- flow. The ability to perform direct and large vortex simulations has made it possible to study the interaction between fluids and their dynamics. He further concluded that his work could also be used to study the physical mechanisms involved in the flow. SW/ BL interaction was frequently observed in high-speed currents by Ribhu Pal & Prince Raj Lawrence Raj [5] in which they observed large flow discontinuities and high heat transfer coefficient. The interaction between the BL and SW can cause blockages and increase flow rates. Numerical studies of the interaction between the BL and SW were performed at very high velocity concludes that the resulting separated bubbles were due to the strong interaction between the BL and SW. A detailed study of hypersonic currents governed by the interaction between SW and BL over the compression regime was conducted. The flow is investigated by the numerical simulation of the Navier-Stokes equation. The boundary layer interaction between the compressed corners and the shock wave was calculated using two explicit Taylor-Galerkin schemes [6] in which the temperature of the wall affects the condition of the BL in the form of wall

thickness, coefficient of viscosity, Reynolds number. This effect becomes more important as the separation region is increased.

2. NUMERICAL SIMULATION METHODOLOGY

This section provides a case for evaluating the accuracy, power, and performance of the Navier-Stokes equation in context of a mesh applied to a hypersonic flow solution for validation. This simulation ignores high temperature effect which leads to the chemical reactions.

In this study the simulation analysis has been done using a 2-D solver. The properties of fluid are taken as constant, with heat capacity ratio = 1.4 and Prandtl number = 0.74. In this study, the pressure coefficients and Mach no. downstream and upstream of the obtained corner is compared with the experimental results. The reason for the discrepancy between the experiment and the calculation is explained and will get the required turbulence model, numerical grid, and calculated parameters.

2.1 Hypersonic flow across a compression corner

In this study, a case study performed by Holden et al. (2006) [3] is examined for validation. This demonstration is extensively examined using computational and experimental techniques. The properties of fluid are provided with Mach number of 10.3. This validates the hypersonic flow scheme and explain to the understanding of the physical properties of the SW / laminar BL interaction problem. The boundary conditions for the flat plate problem are dimensions AB = 0.5, BC = L = 4.004, BD = 8.661, AF = 0.5, DE = 5.0, with a 30 ° tilted ramp. Entrance boundary conditions have been applied to AF and FE. Non-slip restrictions are imposed on BCG. At GE, boundary conditions are free and the free stream condition is assumed to be the initial condition.

Following is the detail of the boundary, along with the boundary conditions considered for simulation.

Table 1. Boundary with boundary conditions

Boundary	**Boundary condition**
Inlet	Velocity inlet
Far-field	Pressure far field
Outlet	Pressure outlet
Flat plate and ramp section	Wall (No slip)
Symmetry	Axis

FVM is a technique for expressing and calculating partial differential equations in terms of the algebraic equations. "Finite volume" refers to the tiny volume that surrounds every node on the mesh. This method is conservative because the flow that goes into a particular volume is similar to the flow that goes out of an adjacent volume. The advantage of FVM is that it

can easily be mapped to enable unstructured meshes. The conservation of a general flow variable is represented as a balance between different processes that likely to enhance or reduce it.

$$\frac{\partial(\rho\phi)}{\partial t} + div(\rho\phi u) = div(\Gamma grad\phi) + S\phi$$

The expression can be expressed as –

Rate of increase in flux of fluid element + Net rate of flow of flux out of fluid element
= Rate of increase of flux due to diffusion
+ Rate of increase of flux due to source

The CFD code is used to handle the most important transport phenomena: diffusion (transport by point-to-point variation of φ), convection (transport by fluid flow), and source terms (related to formation or the reduction of φ) and the rate of change over time. The SWBLI numerical model for slopes is based on ANSYS / FLUENT used finite-volume discretization for the generation of the grid. The selected viscosity model can be achieved with two equations. The viscosity is estimated with the help of 3-factor Sutherland equation accessible in Fluent-19.

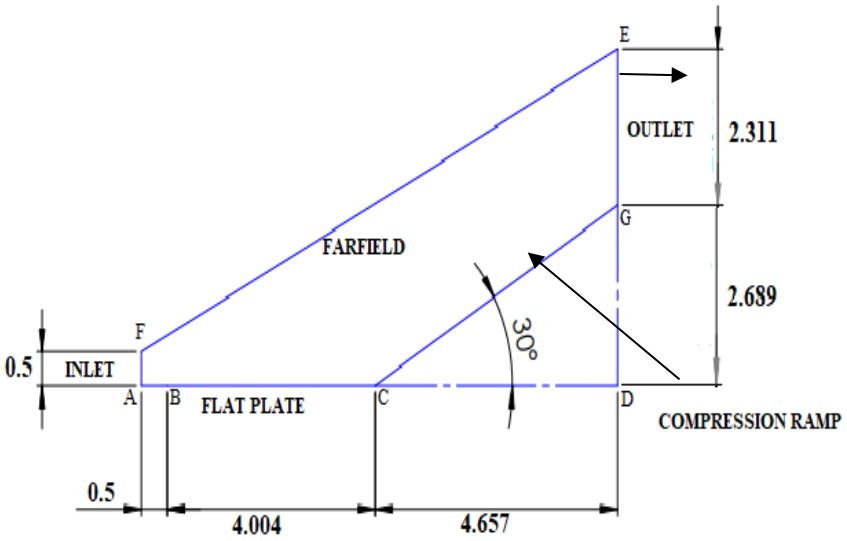

Figure 2 Computational domain with corresponding dimensions

The Fluent Handbook recommends a Sutherland formula with moderate temperature and pressure and is compared to the modelling of the flow field assuming a constant molecular viscosity (assumed at 273 K) with the results achieved by the Sutherland viscosity model accessible in Fluent-19 adopted for the entire flow field in the presented calculations. BL

separation depends primarily on the viscosity in the BL adjacent to ramp where the air temperature approaches the temperature of the wall at 290K.

3. RESULTS AND DISCUSSION

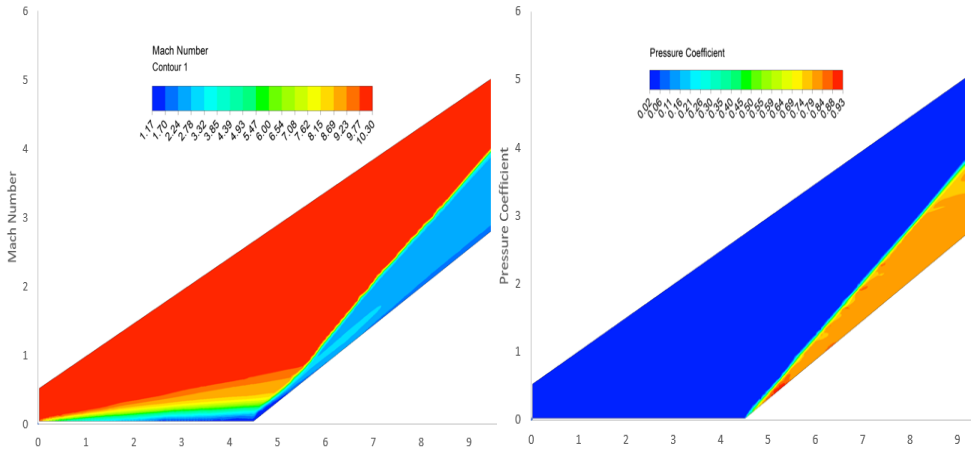

Figure 3. Mach number contour and Pressure Coefficient Contour obtained at M=10.3 using ANSYS-FLUENT 19.2

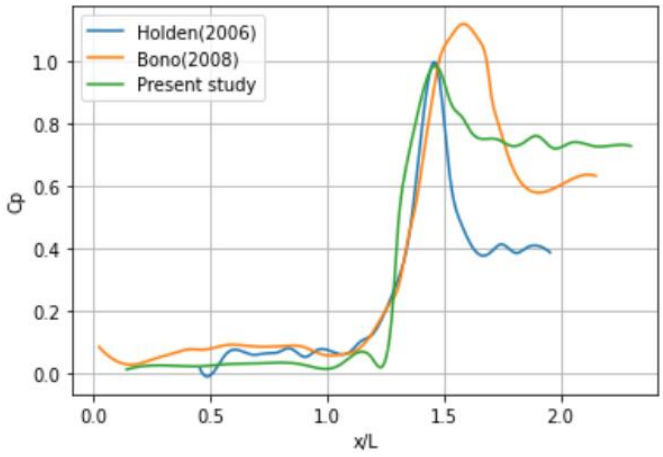

Figure 4. Variation of Coefficient (Cp) of pressure over the Flat plat and Compression Ramp arrangement.

From the above Mach number contour, it is clear that at Mach number 10.3, the shockwave and boundary layer interaction induce separation. A recirculation region is formed near the compression corner.

The coefficient of pressure (C_p) obtained after simulation shows a similar trend, and the value of the maximum coefficient of pressure (C_p) is identical to the result obtained by Holden (2006) and Bono (2008).

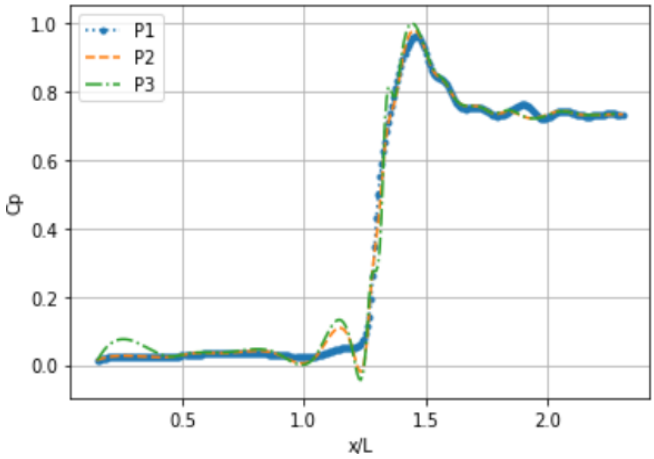

Figure 5 Grid Independence Study for variation of Coefficient of pressure along with the Flat plat and Ramp arrangement

In the Grid independence test P1, P2, and P3 are the curves obtained by computation at Mach number 10.3.

Table 2 Meshing Properties of Computational Domain for GIT

Properties	**Computational Domain**		
Element size (in mm)	(6 x 6)	(5 x 5)	(4 x 4)
No. of Grids (in millions)	0.61	0.80	1.25
Max. Aspect Ratio	5.31	7.12	9.54
Max. Orthogonality	0.998	0.998	0.999
Max. Skewness	0.80	0.82	0.84

It is observed after computation that there is no significant change in Coefficient of pressure (C_P). However, there is a slight variation in C_{Pmax}. The trend in the variation in Coefficient of Pressure (C_P) is similar in all three cases, which are compared and show good agreement with the result obtained [6]. This indicates that the solution obtained can be considered to be grid-independent.

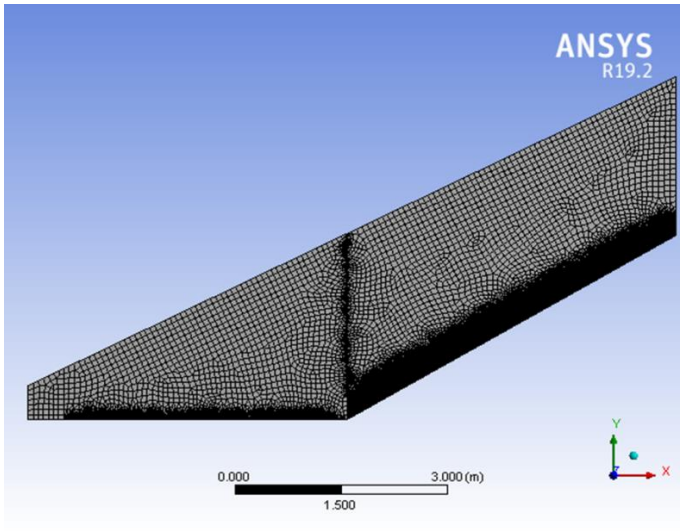

Figure 6. Mesh Generation in ANSYS Fluent 19.2

To study the boundary layer effects, the elements are dense over the flat plate and ramp section to get the enhanced and detailed output contour. In this present study the element size taken is 0.005 x 0.005, and the domain area is 18.931m^2. The present computation is carried out by providing boundary conditions as the inlet is considered velocity inlet, flat plat along with compression ramp is considered the wall, far-field is considered pressure far-field and outlet as pressure outlet.

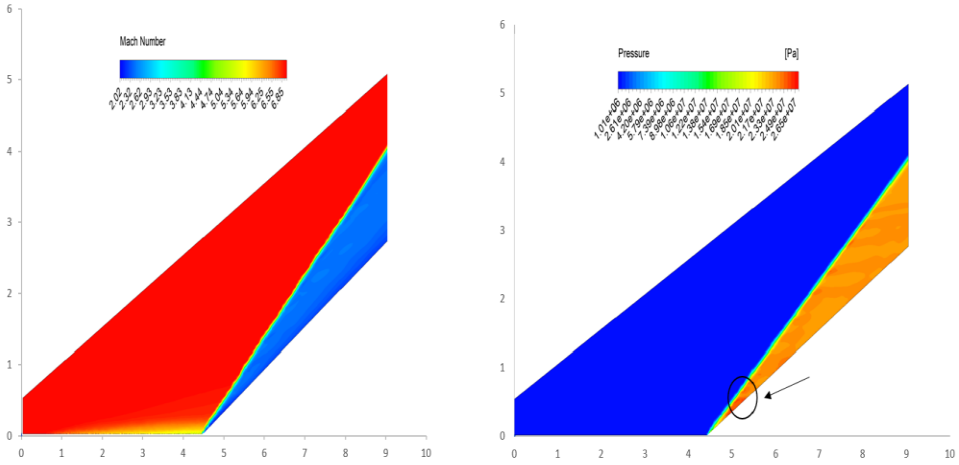

(i) (ii)

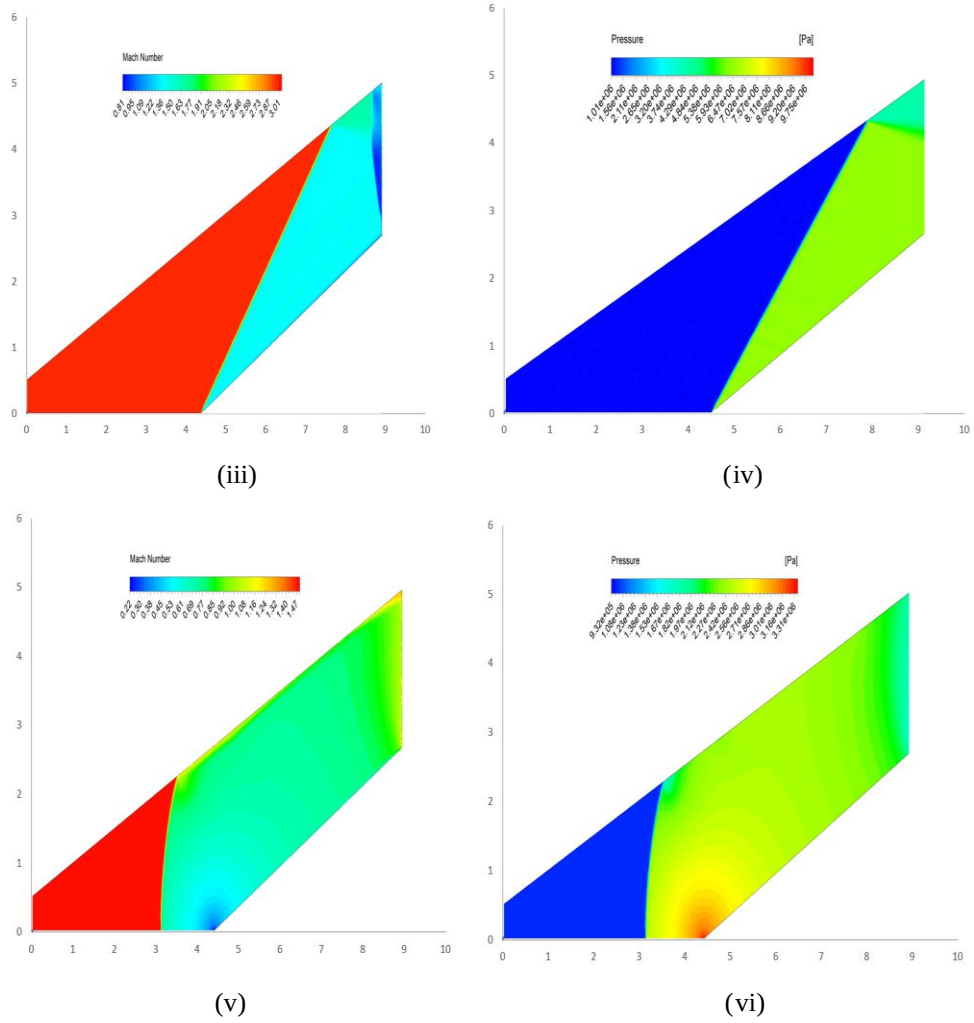

(iii) (iv)

(v) (vi)

Figure 7 Mach number contours for (i)M=7, (iii)M=3, (v)M=1.5, and Pressure contours for (ii)M=7, (iv)M=3, (vi)M=1.5 with tetrahedral elements computed in ANSYS-FLUENT 19.2

The different Mach numbers considered here from Supersonic to Hypersonic range are simulated for a contour comprising a flat plate and ramp section without a gap in the arrangement. At Mach number (M=7), strong oblique shock is observed over the compression ramp, whereas at Mach number (M=3), an oblique shock along with Mach reflection is obtained, but this oblique shock is not as strong as observed at M=7. At Mach number (M=1.5), near the transonic range, a shock that approaches the weak oblique shock is observed in front of the compression corner over the flat plate as the wave is turned into itself when it approaches the sharp compression corner.

For different Mach numbers considered, initially pressure at Inlet is provided as 10 bar for all the cases considered, Prandtl number considered is 0.74, and variation in pressure is obtained, which shows that at high Mach numbers, high-pressure gradient is obtained at

the sharp compression-corner. The separation and reattachment of shock are observed as the Mach number varies from Supersonic to Hypersonic for the computed domain.

4. CONCLUSION

- Variations of Mach number and Pressure are determined based on simulation. Good conformity is observed between the computational and experimental results.
- Significant pressure-rise and separation and reattachment of shock are seen at a high Mach number.
- This simulation gives the idea that a turbulent model (Realizable k- ε) provides better prediction of flow separation at adverse pressure gradient relieves the user from more time consuming for developing an appropriate mesh that leads to an optimal solution.
- Shock obtained over the compression corner shows that the angle between the ramp and shock decreases as the Mach number increases from 1.5 to 7.

REFERENCES

[1] S.B Verma, C. Manisankar & P. Akshara. Control of shock-wave boundary layer interaction using steady micro-jets. Shock Waves 25, 535–543 (2015). https://doi.org/10.1007/s00193-014-0508-5

[2] J.J. Bertin. Hypersonic Aerothermodynamics, AIAA Education Series, USA, 1994.

[3] M.S. Holden, T.P. Waldhams, J.K Harvey and G.V. Candler. Comparison between Measurements in Regions of Laminar Shock Wave Boundary Layer Interaction in Hypersonic Flows with Navier-Stokes and DSMC Solutions, OTAN RTO-TR-AVT-007-V3, 2006.

[4] Neil D. Sandham "Shock-Wave/Boundary-Layer Interaction" Aerodynamics and Flight Mechanics Research Group, University of Southampton, Southampton SO17 1BJ UK n.sandham@soton.ac.uk, 2011

[5] Ribhu Pal, Prince Raj Lawrence Raj, Proceedings of the 26th National and 4th International ISHMT-ASTFE Heat and Mass Transfer, IIT Madras, India Conference December 17-20, 2021

[6] Gustavo Bono, Armando M.Awruchb and Tales L. Popiolekc "Computational Study of Laminar Shock/Boundary Layer Interaction at Hypersonic Speeds", Asociación Argentina de Mecánica Computational, November 2008

[7] Duo Zhang, Weidong Liu, Bo Wang, Yi Su "Numerical simulation on the shock wave/boundary-layer interaction with heating/cooling effect," 7th International Conference on Fluid Mechanics, The Chinese Society of Theoretical and Applied Mechanics, ICFM7, 2015

[8] B. Chanetz, R. Benay, J.M. Bousquest, R. Bur, T. Pot, F. Grasso, J. Moss. Experimental and Numerical Study of the Laminar Separation in Hypersonic Flow, Aerosp. Scien. And Technology, 3, 205-218, 1998

[9] F. Grasso and M. Marini. Analysis of Hypersonic Shock-wave Laminar Boundary-layer Interaction Phenomena, Computer & Fluids, 25, 561-581, 1996

Biographies

Prateek Kumar received the bachelor's degree in Mechanical Engineering from Dr.APJ Abdul Kalam Technical University, Uttar Pradesh, in 2018 and currently pursuing the master's degree in Thermal Engineering from MNNIT Allahabad Prayagraj UP, India.

Shantanu Srivastava received the bachelor's degree in Mechanical Engineering from Uttar Pradesh Technical University, Lucknow, presently known as AKTU, and the master's degree in Thermal and Fluid Engineering from IIT BHU, and the philosophy of doctorate degree in Aerospace Engineering from IIT Kanpur, respectively. He is currently working as an Assistant Professor at the Department of Mechanical Engineering, MNNIT Allahabad, Prayagraj, UP. His research areas include Experimental and Numerical Study of Supersonic Free Shear Flows, Shockwave Boundary Layer Interaction, Supersonic Jet Control.

A Historical Review on the Efficiency of Perovskite Solar Cells

[1]Syed Mohd Azam, [2]Ajaya Bharti, [3]Naveen Kumar[*], [4]Rahul Dev

[1,2,3] Department of Applied Mechanics, Motilal Nehru National Institute of Technology Allahabad, Prayagraj, India-211004

[4]Department of Mechanical Engineering, Motilal Nehru National Institute of Technology Allahabad, Prayagraj, India-211004

[1]mohdazam177@gmail.com, [2]abharti@mnnit.ac.in, [3]chaudhary56naveen@gmail.com, [4]rahuldsurya@mnnit.ac.in

Abstract

Our dependency on the nonrenewable energy resources is increasing day by day, whereas the resources are scares. Therefore, it is the present need of humankind to look at some another sources of energies so that our future generation can also use the less available resources. Looking at renewable sources of energies, the most effective and abundant energy resource is solar energy. There are various generation of solar cells but among them 3rd generation solar cell shows greater efficiencies. One of most popular technology from 3rd generation solar cell is perovskite solar cell which has shown a tremendous increase in the efficiency in a decade period. Cost of fabrication is also very low and also it shows tremendous efficiency and various other properties. There is a stability issue related to perovskite solar cell which when reduced completely can make these solar cells a very good alternative for commercialization purposes as compared to Silicon Solar cell. Several obstacles need to be handled before it can be entered in the market of photovoltaics. Inspite of high PCE the instability of perovskite should be addressed and also it should be fabricated at lower processing temperature.

Keywords. Perovskite Solar Cell, Power Conversion efficiency, Open Circuit Voltage, Current Density.

1. INTRODUCTION

As the industrialization is growing day by day, and the fact that fossil fuels are nonrenewable sources of energy which pollute our environment and demand is increasing at very high rate, therefore this has put a pressure on humans to develop some sources which can be capable of meeting our demand. Fossil fuels has an adverse effect on the environment therefore to reduce this, people are seeking clean renewable energies to replace fossil fuels [1]. Basically, our energy resources are categorized as renewable resources of energy and nonrenewable resources of energy. As our population is tremendously increasing therefore use of nonrenewable resources

are increasing very rapidly. If we keep on consuming the nonrenewable energy resources at the same rate, then our future generation might not use it because they are on the verge of extinction. Therefore, among the various renewable energy resources we need to look at which energy resources are easily available and can be useful for providing a large amount of energy. Among various renewable energy resources solar energy is one the important source because it provides us a very large amount of energy continuously throughout the year. Sun is a very enormous source of energy and we are currently unavailable to use its energy properly. There are various technologies available for the generation of solar energy [2]. One of the most advanced and popular technique which researchers have found in previous decade is Perovskite solar cell which requires easy laboratory preparation methods and on the other hand it is very cost effective technology [3]. The increase in efficiency, fill factor, Open circuit Voltage, Current density, etc. has taken place very rapidly. As compared to Silicon solar cell in which the efficiency of 25% has reached in 60 years whereas it only took 10 years to reach to that level. Therefore, it plays a major role in generation of electricity in the upcoming years which will provide a great support in decreasing the use of nonrenewable energy resources which produces a lot of pollution and also, they are very scarcely available resources.

2. GENERATIONS OF SOLAR CELL

Different Generations of solar cells are shown in Figure 1. There are 3 generations of solar cell. Since the development of first solar cell a large number of researches started on solar cell and as the time progresses 3 generations are developed which have different advantages as well as disadvantages

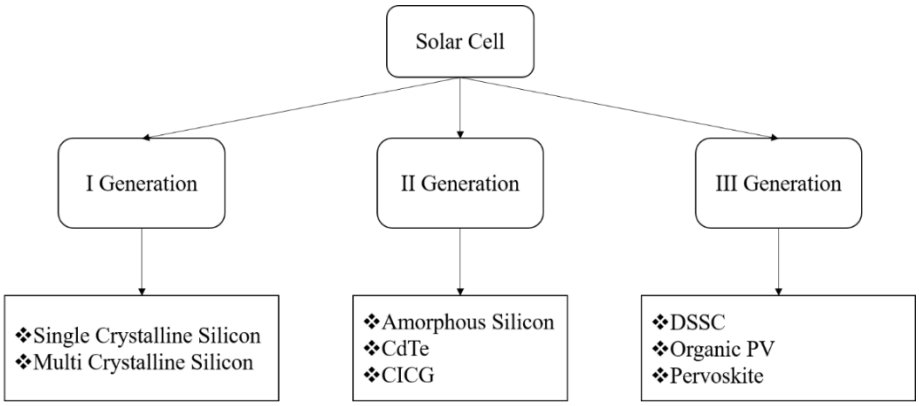

Figure 1. Generations of Solar Cell

2.1 First generation

These are based on Silicon wafers and it is playing a vital role in the photovoltaic market. Mostly these solar cells are made of crystalline silicon which can be either single-crystal or poly-crystal silicon wafers having a high purity. Although these have an efficiency in the range of 20 % but

they have a disadvantage that for the large scale production the manufacturing cost rises to very high level and also its method of production has a poor impact on environment.

2.2 Second Generation

These are based on thin film technology. A very thin film of active material is deposited on the substrate. Due to this reason the use of active material is reduced and also it helps in decreasing the weight and making the cell more flexible. Some of the active materials used are Cadmium Telluride (CdTe) or Copper Indium Gallium Selenide (CIGS). The efficiency of second generation solar cells is around 20 % but it still faces the difficulty of production at large scale and also the availability of the Te, In, and Ga is difficult.

2.3 Third Generation

These are the latest technology solar cells that aims at producing the solar cells which has a great efficiency and also it can be manufactured at low cost. Various efforts are made on this technology so that it can be used for industrial purposes which can solve the problem very easily since they are of low cost with a great efficiency. Organic solar cells, quantum dots solar cells, dye-sensitized solar cells (DSSCs), perovskite solar cells are some of the examples of third generation solar cell. As we can see from Figure 2 that the third generation solar cells are showing a great efficiency as well as the cost of the solar cells are also very less as compared to other generations. Therefore, various measures are taken by researchers to increase the efficiency and making low cost solar cells [4]. Perovskite solar cells are one of those types of solar cells that had taken a very rapid growth and the efficiency of these solar cells are increased in the upcoming years also.

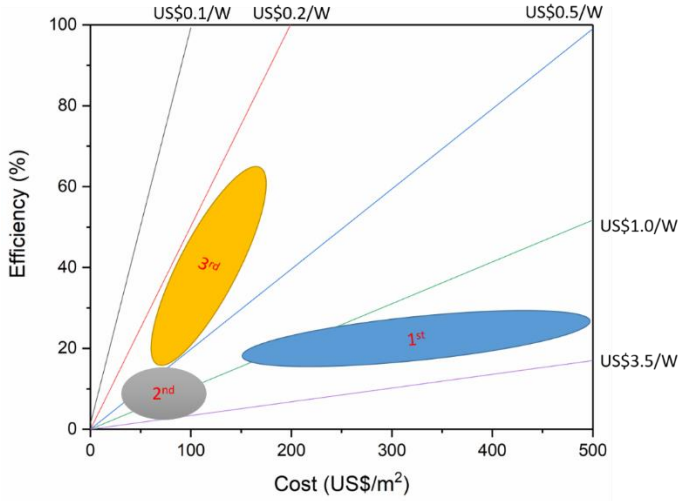

Figure 2. Efficiency and Cost Comparison of different Generations of Solar Cell[6]

3. PEROVSKITE

In 1939 Gustav Rose found this mineral in Ural mountain, Russia. Lev Alekseevich Perovski, a mineralogist had done the research and hence was named as 'Perovskite'. Mitzi et al. reviewed the optoelectronic properties of the perovskites in 1991 [5]. The report shows that the perovskites has strong excitation properties and therefore may be used in LEDs, transistors and solar cell. The process of Photovoltaic generation was firstly being observed in this material by Kojima et al. in 2009 [6]. First use of perovskite material in solar cells application was by using it as a liquid sensitizer in DSSC architecture [7]. Since first use of perovskite in solar cells, the efficiency of perovskite solar cells has increased from 3.81% to 25.8 %.

4. STRUCTURE OF PEROVSKITE

Compounds with perovskite structure have a chemical formula of ABX_3, where an A Cation is present at the eight corners of the cubic cell and the B Cation is present at the body center, surrounded by six X Anions (located at the face center), forming a BX6 octahedron [8]. Some of the examples of cation and anion are shown in Figure3.

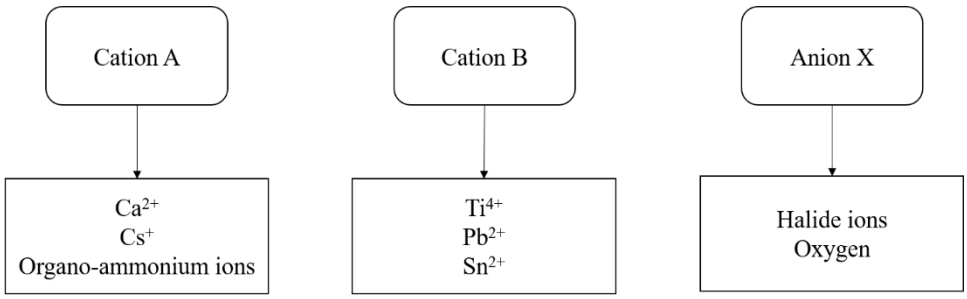

Figure 3. Examples of Cation and Anion

5. PEROVSKITE SOLAR CELL

Perovskite Solar cell was firstly developed in 2009 by Kojima et al. At the time of its development its model was taken from DSSC Structure with a slight modification in it. But due to the presence of liquid electrolyte it could not work for longer duration. [9].Therefore, after many years of hard work the PCE of perovskite solar cells is increased from 3.51 % to 25.8 %. The researchers working in the area of DSSC and Organic solar cells are mostly influenced by this technology because PSC consist of similar structure and components. [10]

5.1 Major Components of Perovskite Solar Cell

There are 4 major components of the Perovskite Solar cell as shown in Figure4. Main component of perovskite cells consists of absorber layer which is generally made up of MaPbX3, FaPbX3

and various others. Electron transport layer is generally made of TiO2, ZnO, Al2O3 [11]. Hole transport layer is generally made up of Spiro-OMetad, Pedot etc. and metal electrode is made up of silver or gold layer. [12]

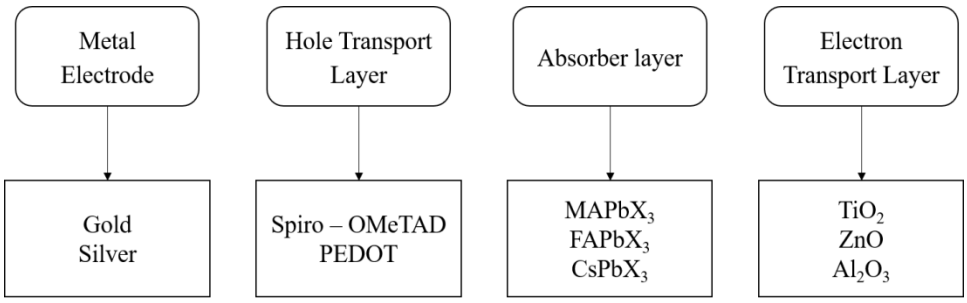

Figure 4. Components of Perovskite Solar Cell [8]

The Configuration of Solar cell is shown in Figure **Error! No text of specified style in document.**.. Various components of the Perovskite Solar cells such as metal Cathode, Hole Transport Layer, Perovskite Layer, Electron transport Layer, FTO glass are shown.

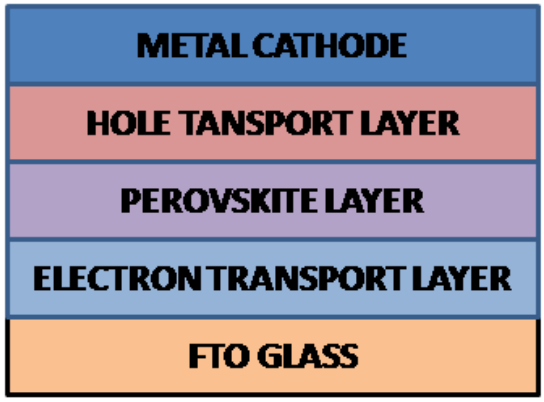

Figure **Error! No text of specified style in document.**. Structure of perovskite solar cell [12]

6. PROGRESS IN PEROVSKITE SOLAR CELLS

Kojima et al. discovered a new type of solar cell by doing some modifications in DSSC structure. The results obtained was great and they obtained the efficiency of 3.51%. The perovskite was used as a liquid sensitizer, but due to the presence of liquid electrolyte, the system was extremely unstable and it could not work for longer duration. The device configuration which was used was (Pt-FTO/Electrolyte solution/$CH_3NH_3PbI_3$/TiO2) [9].Park et al. make use of quantum dots of nano-crystalline material and used dye-sensitized method which in turn increases the cell efficiency from 3.8% to 6.54% and they found that still the device performs for only 10 min.

This is because of the dissolution of quantum dots in the electrolyte. Due to instability by liquid electrolytes, this architecture does not meet the expectation. The device configuration which was used is Pt/Liquid Electolyte/ $CH_3NH_3PbI_3$ (QD) / TiO2/FTO [13]. Kim et al. solve this problem of liquid electrolytes by developing solid-state Photovoltaic Solar cell. The Spiro-OMeTAD has been used as a HTL and hence the efficiency increased to 9.7%. The device configuration which was used is Au/spiroOMeTAD/ $CH_3NH_3PbI_3$/mTiO2/FTO. Due to this a tremendous change occured in the field of the PSCs which increases the PCE and also raised the stability. [14]. Also, in the same year Lee et al. developed a device efficiency of 10.9% with the open-circuit voltage higher than 1.1 V. [15]. Burschka et al. found the efficiency of 15% with the help of 2-step sequential deposition technique by making it in planar architecture. This is done through the sequential deposition method in which they firstly deposited PbI_2 layer and then deposition of CH_3NH_3I.The device configuration which was used is Au/spiroMeOTAD/TiO2/ $CH_3NH_3PbI_3$/Glass [16]. Im et al. manufactured solar cells with two-step solution processing in which MAPbI3 is used. Due to the regulated size of the MAPbI3 cuboid, which allowed good light harvesting and increased charge transportation, high performance is achieved. The solar cell's efficiency is therefore increased to 17.01 %. The device configuration which was used is Au/spiroMeOTAD/TiO2/CH3NH3PbI3/Glass [17]. A technique in which Yang et al. deposited improved quality FAPbI3 film with (1 1 1) crystallographic orientation, uniform, dense and large microstructures was developed. In place of $CH_3NH_3PbI_3$, they used FAPbI3 and achieved 20.2 % efficiency. The device configuration which was used is Au/PTAA/Perovskite/(bl/m-TiO2)/FTO [18]. Li et al. fabricated a perovskite film which has uniform morphology as well as crystalline behavior. They used VASP in which FA0.81MA0.15PbI2.51Br0.45 was used as an absorber layer. Due to this reason PCE of 20.5% was achieved. The device configuration which was used is Au/Spiro-OMeTAD/Perovskite/m-TiO2/ bl-TiO2/ FTO [19]. Bi et al. have reported a new technique to manufacture perovskite film in the same year and improved electronic properties due to polymer usage. Growth and nucleation processes are increased by the use of poly methyl methacrylate (PMMA) and 21.6 % efficiency. The device configuration used was Au/Spiro-OMeTAD/Perovskite/m-TiO2/ Perovskite/bl-TiO2/ FTO [20]. Many cations, such as FA and mixed halide anion, were used as an absorber layer by Yang et al. By adding iodide solutions to the organic cation solution, they reduce the concentration of deep-level defect states. This enables to reach uptoPCE of 22.1% for small scale and 19.7% in 1 cm^2cell.The device configuration which was used is FTO/TiO2/m-TiO2/perovskite composite layer/perovskite upper layer/PTAA/Au [21]. The Chinese Academy of Sciences researchers developed a solar cell device which has shown a great efficiency of 23.3%. Jung et al. developed a solar cell made of P3HT as a hole transport layer. In this a thin layer of halide perovskite is deposited which have very high bandgap. The PSC of the device came out to be 22.7%. The device configuration which was used is FTO/d-TiO2/mp-TiO2/NBH/P3HT/Au [22]. This type of perovskite solar cell is developed by Mingyu. Jeong et al. using isomeric HTM instead of normal HTM and therefore due to this reason the efficiency is increased upto 24.82%. Spiro-OMetad was used as hole transport material. Also, the stability of solar cell was increased upto a great extent [23]. Min et. al created an interlayer between SnO_2ETL and perovskite layers to minimize interfacial defects. This interlayer enhances charge extraction and transport from perovskite layer and efficiency is also maintained to about 90 % after 500 hours of light exposure [24].

6.1 Improvement in the Power Conversion Efficiency of PSC

As we can see from the Figure **Error! No text of specified style in document.** that the efficiency of PSC started from 3.8% in 2009 and in a very less amount of time the efficiency has come a long way to 25.8 %.This change occurs by developing various changes in the device configuration and by changing the materials required in the fabrication techniques of PSC [24]..In 2009 when it was firstly used by kojima et al. then the PCE was coming to be 3.8%. kojima fabricated their device by using DSSC structure but it doesn't have much stability therefore park et al. uses quantum dots so the efficiency is increased to 6.54%.Kim et al. solve this problem of liquid electrolytes by developing solid-state Photovoltaic Solar cell and the increased efficiency is found 9.7%.by changing the carrier transport material the efficiency is increased and also as the time progresses many researchers who have made their contributions and now the PSC stands at 25.8 %. The life of solar cell is increasing and in near future there is a scope of much more enhancement in the efficiency.

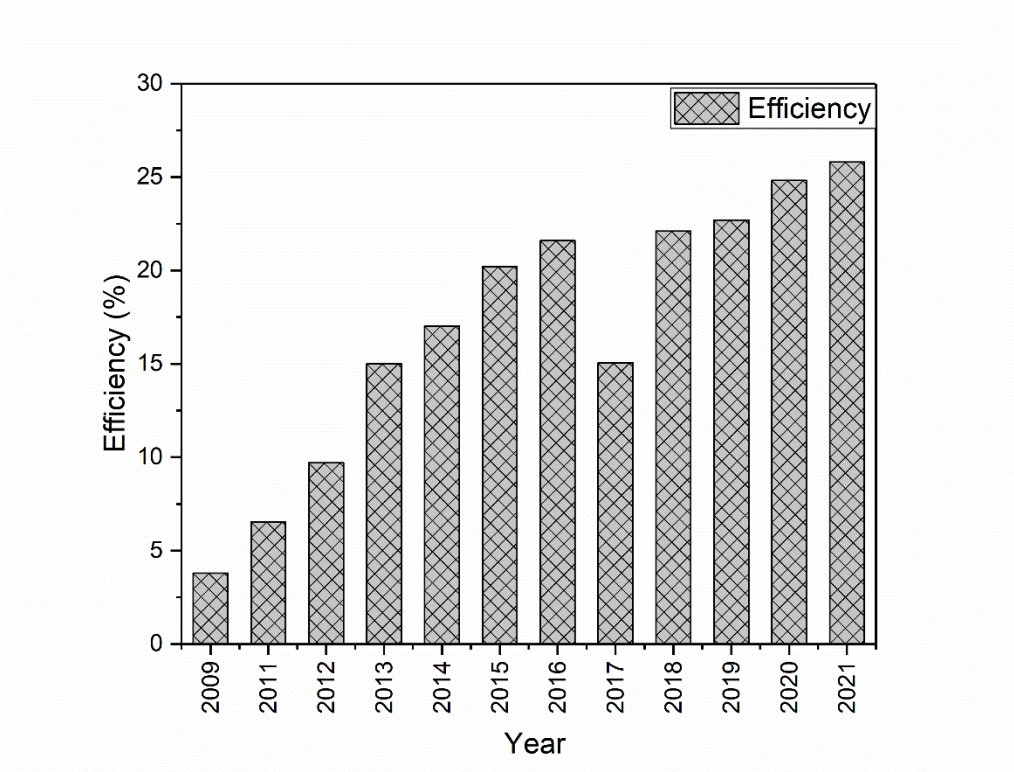

Figure **Error! No text of specified style in document.**. Power Conversion Efficiency

6.2 Improvement in the Fill Factor of PSC

The ratio of actual maximum available power to the product of the open circuit voltage and short circuit current is known as the fill factor. In assessing efficiency, this is a key parameter. The Fill Factor is a measure of the I-V curve's "squareness". As it is clear from the Figure 7 that the increase in the fill factor in case of perovskite solar cell is upto a great extent in the last decade.

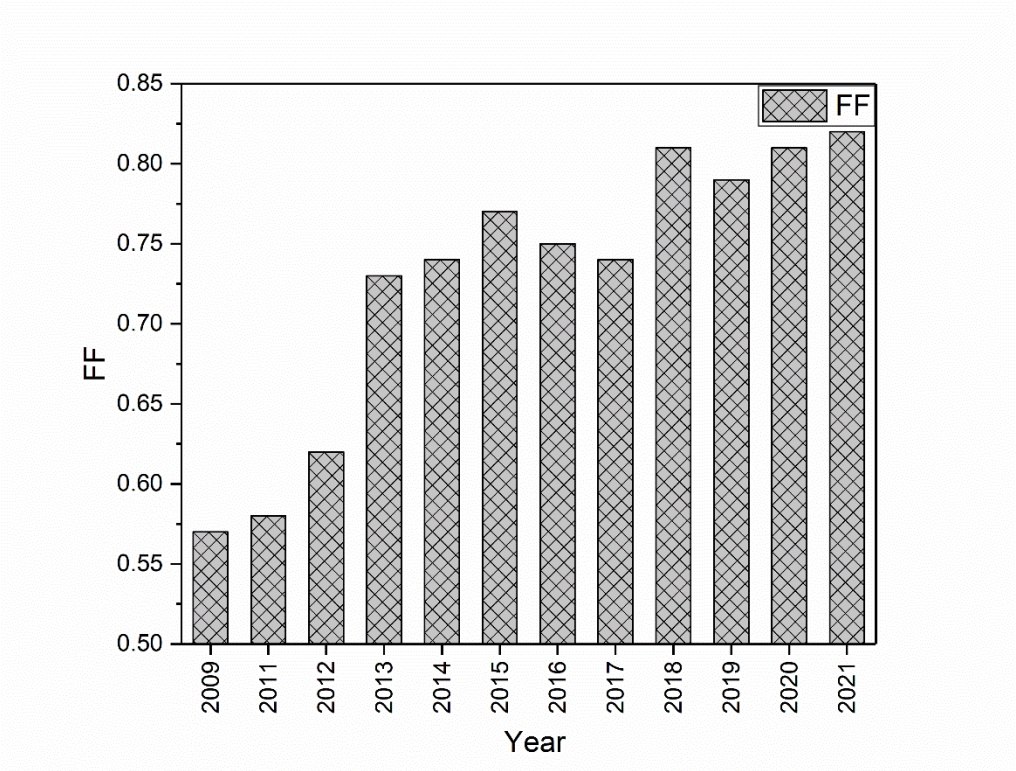

Figure 7. Increase in Fill Factor

6.3 Improvement in the Open Circuit Voltage of PSC

Open-circuit voltage is the electrical potential difference between two terminals of a device, when disconnected from any circuit. This is achieved if there is no attached external load and no external electric current flows between the terminals as well. From the year of development of PSC and till now there has been a continuous growth in the open circuit voltage because researchers are doing various modifications in the material and the fabrication techniques of the PSCs [25]. The growth rate is so fast that PSC has made a great impact in the field of solar energy and the number of researchers related to PSC is increased rapidly. It is shown in Figure8.

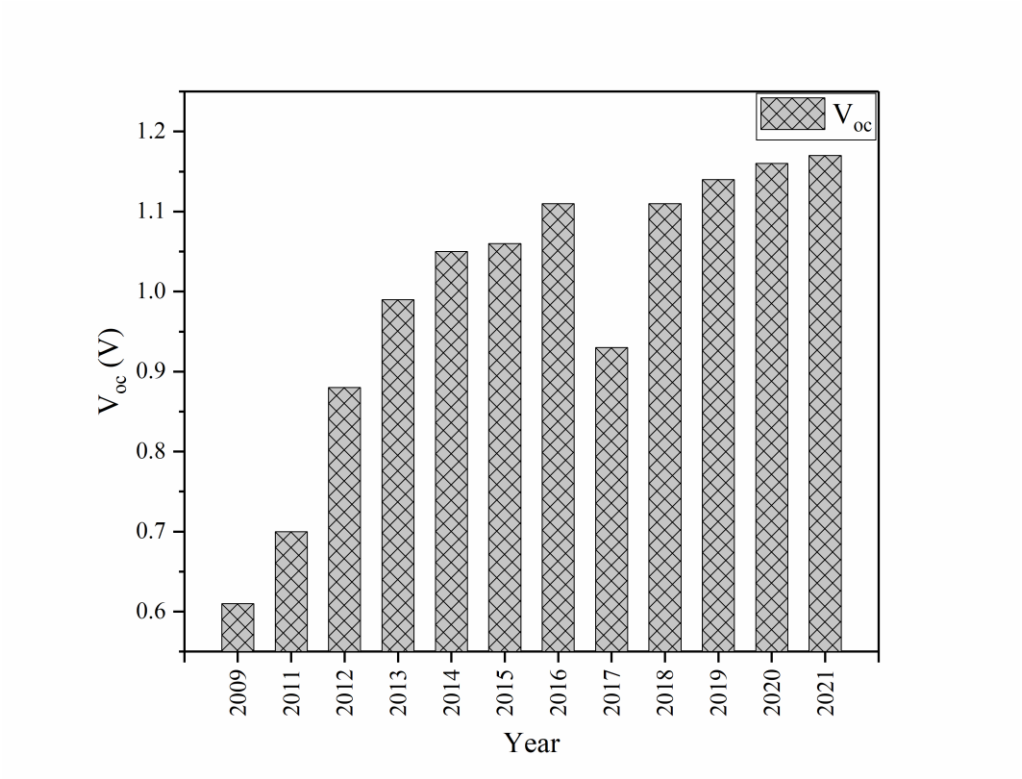

Figure 8. Improvement in Open circuit Voltage

6.4 Improvement in the Current Density of PSC

Current density is the amount of charge per unit time that flows through a unit area of a chosen cross section. A continuous growth in the current density is seen. In 2009 at the time of PSC development it was 11 mA/cm2 and now it has reached to 25.7 mA/cm2. Current density plays a important role in case of solar cells applications [26]. This increase in the current density of the perovskite solar cells make this solar cell a very advantageous for various solar energy applications. It is shown in Figure 99.

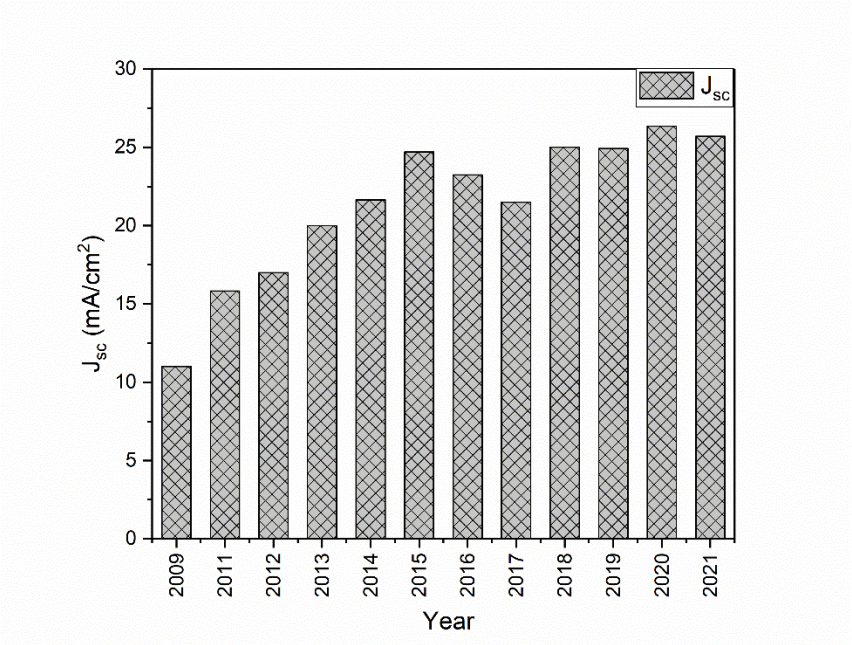

Figure 9. Improvement in Current Density

7. CONCLUSION

Renewable Resources of energy are capable of producing a large amount of power because its availability is very large and throughout the year. The only reason for a lesser consumption of these resources is that we are not having a great technology so that we can fulfill our needs from these renewable energy sources. Whereas many steps are taken in the recent years for enhancing the use of these resources. Perovskite solar cells shows a great result in producing the energy from the sun via photovoltaic effect. There is a tremendous increase in the efficiency, fill factor, open circuit voltage, current density etc. by changing the configuration of the device. The development was so quick that it gained interest of lot of researchers and various other methods were adopted in order to increase its performance. If some stability related issues are solved in the upcoming years then it can prove out to be one of the greatest techniques which can be used for commercialization purposes.

REFERENCES

[1] D. Chapin, C. S. Fuller and G. L. Pearson, "A new silicon p-n junction photocell for converting solar radiation into electrical power," Journal of Applied Physics, vol. 25, pp. 676-677, 1954.

[2] Back, Kim, G., K. Kim, T., H. Kang and J. Kong, "Interfacial modification of hole transport layers for efficient large-area perovskite solar cells achieved via blade-coating," Sol. Energy Mater, pp. 309-315, 2018.

[3] Barrows, Pearson, Kwak, C.K., Dunbar, Buckley, A.R., Lidzey and D.G., "Efficient planar heterojunction mixed-halide perovskite solar cells deposited via spray deposition," Energy Environ. Sci, pp. 2944-2950, 2014.

[4] B. Gao and J. Meng, "Flexible CH3NH3PbI3 perovskite solar cells with high stability based on all inkjet printing," Solar Energy, vol. 230, pp. 598-604, 2021.

[5] Chess, Guloy, Feild, C.A., Mitzi, D.B. and Wang, "Conducting layered organic-inorganic halides containing<110>-oriented perovskite sheets.," Science, pp. 1473-1476, 2004.

[6] Mitzi, D.B., Chondroudis, Kagan and C.R., "Design, structure, and optical properties of organic−inorganic perovskites containing an oligothiophene chromophore.," Inorganic Chemistry, pp. 6246-6256, 1999.

[7] S. Han, F. Wu, W. Qin and H. Cao, "Perovskite solar cell based on double-layer Ag/SnBi alloy as cathode," Journal of Alloys and Compounds, vol. 888, 2021.

[8] Jeon, Noh, J.H., Yang, W.S., Kim, Y.C., . and J. Seo, "Compositional engineering of perovskite materials for high-performance solar cells.," Nature 517, pp. 476-480, 2015.

[9] A. Kojima, K. Teshima, Y. Shirai and T.Miyasaka, "Organometal halide perovskites as visible-light sensitizers for photovoltaic cells," Journal of the American Chemical Society, vol. 131, pp. 6050-6051, 2009.

[10] Ismail, M. Boujnah, a. e. kenz, m. abatal and a. bassaml, "lead free perovskite based bismuth for solar cells absorber," Journal of Alloys and Compunds, pp. 796-801, 2019.

[11] N. Gamal, S. H. Sedky, A. Shaker and M. Fedawy, "Design of lead-free perovskite solar cell using Zn1-xMgxO as ETL: SCAPS device simulation," Optik, vol. 242, 2021.

[12] F. Bai, y. hu, Y. hu, T. qiu, X. miou and S. zhang, "lead free , air stable ultrathin Cs3BiI9 perovskite nanosheets for solar cell," Solar Energy Material and Solar cell, pp. 15-21, 2018.

[13] Im, Jeong-Hyeok, Chang-Ryul, Lee, Jin-Wook, Sang-Won, Park and Nam-Gyu, "6.5% efficient perovskite quantum-dot-sensitized solar cell," Nanoscale 3, 2011.

[14] H. Kim, C. Lee and J. Im, "Lead iodide perovskite sensitized all-solid-state submicron thin film mesoscopic solarcell with efficiency exceeding 9%," Scientific Reports, vol. 2, 2012.

[15] M. M. Lee, J. Teuscher, T. Miyasaka, T. N. Murakami and H. J. Snaith, "Efficient hybrid solar cells based on meso superstructuredsuperstructured," Science, vol. 338, p. 643–647, 2012.

[16] J. Burschka, N. Pellet and S. Moon, "Sequential deposition as a route to high-performance perovskite-sensitized solar cells," Nature, vol. 499, p. 316–319, 2013.

[17] Im, Jang, Pellet and Park, "Growth of CH3NH3PbI3 cuboids with controlled size for high-efficiency perovskite solar cells," Nature Nanotechnology, pp. 927-932, 2014.

[18] Yang, W.S., Noh, J.H., Jeon, N.J., Kim, Y.C., Ryu, J. Seo, Seok and S.I., "High performance photovoltaic perovskite layers fabricated through intramolecular exchange," Science, p. 1234–1237, 2015.

[19] Li, Xiong, Bi, Dongqin, Yi, Chenyi, Décoppet, Jean-David, Luo, Jingshan, Zakeeruddin, S. Mohammed, Hagfeldt, Anders, Grätzel and Michael, "A vacuum flash–assisted solution process for high-efficiency large-area perovskite solar cells," Science, p. 58–62., 2016.

[20] Bi, D., Yi, C., Luo, J., Décoppet, J.D., Zhang, F., Zakeeruddin, S.M., Li, Hagfeldt, Grätzel and M., "Polymer-templated nucleation and crystal growth of perovskite films for solar cells with efficiency greater than 21%.," Nat. Energy 1, pp. 1-5, 2016.

[21] Yang, W. Seok, Park, Byung-Wook, E. H. Jung, Jeon, N. Joong, Kim, Young, Chan, Lee, D. Uk, Shin, S. Sik, Seo, Jangwon, Kim, E. Kyu, Noh, J. Hong, Seok and Sang, "Iodide management in formamidinium-lead-halide–based perovskite layers for efficient solar cells," Science, p. 1376–1379, 2017.

[22] Jung, E.H., Jeon, N.J., Park, E.Y., Moon, C.S., Shin, T.J., Yang and T.Y., "Efficient stable and scalable perovskite solar cells using poly(3-hexylthiophene).," Nature, p. 511–515, 2019.

[23] M. Jeong, I. W. Choi, E. M. Go, Y. Cho, M. Kim, B. Lee, S. Jeong, Y. Jo, H. W. Choi, J. Lee, J. H. Bae, S. K. Kwak, D. S. Kim and C. Yang, "Stable perovskite solar cells with efficiency exceeding 24.8% and 0.3-V voltage loss," Science, 2020.

[24] H. Min, D. Y. Lee, J. Kim, G. Kim, K. S. Lee, J. Kim, M. J. Paik, Y. K. Kim, K. S. Kim, M. G. Kim, T. J. Shin and S. I. Seok, "Perovskite solar cells with atomically coherent interlayers on SnO2 electrodes," Nature, vol. 598, pp. 444-450, 2021.

[25] Yang, W.S., Noh, J.H., Jeon, N.J., Kim, Y.C., Ryu, Seo, J., Seok and S.I., "High performance photovoltaic perovskite layers fabricated through intramolecular exchange," Science 348, pp. 1234-1237, 2015.

[26] Zhu, Hao, Bin, S. T, Miller, C.E., Wasielewski and M.R., "Solution-processed air-stable mesoscopic selenium solar cells," ACS Energy Lett, pp. 469-473, 2016.

Biographies

Syed Mohd Azam received the bachelor's degree in Mechanical Engineering from SRMCEM Lucknow in 2015, the master's degree in Materials Science and Engineering from Motilal Nehru National Institute of Technology Allahabad in 2019. Currently, He is working on solar cells.

Ajaya Bharti is an Associate Professor in the Applied Mechanics Department, Motilal Nehru National Institute of Technology Allahabad, Prayagraj, India. He has guided more than 40 M. Tech. and PhD students. He has published so many research papers in various recognised international journals. His research area is powder metallurgy, severe plastic deformation, energy absorbing material, etc.

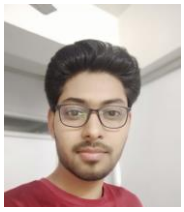

Naveen Kumar is a PhD research scholar at Motilal Nehru National Institute of Technology Allahabad, Prayagraj. He is working on metal matrix composites fabrication by powder metallurgy. He has more than 30 publications in various peer-reviewed international journals.

Rahul Dev is an Assistant Professor in the Mechanical Engineering Department, Motilal Nehru National Institute of Technology Allahabad, Prayagraj, India. He has guided various M. Tech. and PhD students. He has published so many research papers in various recognised international journals. His research area is energy absorbing material.

Experimental Analysis of the Photovoltaic Solar Panel Using Water Spray Cooling

[1]Manish Kumar Chauhan, [2]Ram Prakash Yadav and [3]Akhilesh Kumar Chauhan

Department of Mechanical Engineering, KNIT Sultanpur, Uttar Pradesh, India

[1]manishchauhan2849@gmail.com, [2]ram9289@gmail.com, [3]akc.knit@gmail.com

Abstract

This experiment gives an alternative cooling method of photovoltaic (PV) solar panel using water spray. The PV panel has a specific experimental setup at Sultanpur (India) explained in detail. This set up tested in a geographical location with different climate conditions. It was found that by spray cooling, the temperature of the panel decreases on average 53℃ to 23℃ in both case of up and bottom cooling and total power was increased by 15.3%.Apartfrom that effectiveness of the system also increased by its cleaning effects. The efficiency of this solar PV, as well as water-based crystalline, gets reduced with the increase of panel temperature. It was also observed from the experiment that the efficiency of PV cells dropped by 0.5% with anincreaseof1℃ofpaneltemperature.

Keywords. Experimental analysis, photovoltaic solar panel, cooling, water spray method, efficiency.

1. INTRODUCTION

Photo-voltaic (PV) cells are widely adopted as one of the most significant sources of renewable energy applications that can utilize solar energy by converting solar irradiance into direct current (DC) electricity [1,2]. According to the PV cells manufacturing materials, converting of solar irradiance into direct electricity can be achieved with various conversion efficiency atratingvaluesbetween7and40% [2,3].From the solar radiation incident on the surface of PV cells, a range of about 80% can be absorbed, however, only a small portion of the absorbed incident solar energy is converted into electrical energy based on the conversion efficiency of the PV cell manufacturing technology [4]. The remainder of absorbed energy is overheating the PV cells and according to many researchers, the operating temperature of the PV cells above the ambient atmospheric temperature byabout40°C [5–7].

The reason for overheating is since PV cells convert a certain band of the coming irradiance spectral wavelength that is responsible for light direct converting into electrical energy, while the

remaining spectral wavelength is overheated by the PV cells [8]. Elevated temperatures of the PV panels are considered one of the most critical issues especially in hot climatic regions causing a series drop in PV electrical conversion efficiency by about 0.5%/1 °C for every degree rise of the PV panel temperature and reducing the lifetime of the PV cells [9].

Thus, an integral cooling system of PV cells during operation is the task of great significance to enhance the performance of the PV cells with an efficient conversion process, particularly in sunbelt regions. Furthermore, the presence of the cooling system will help in decreasing the overall cost of solar cells, prolong the PV cell's lifetime, encourage solar cell industries, and ensure maximum output power from the installed PV cells [10]. The cooling method is water and air normally. Air takes less amount of energy compared to water cooling however the cooling capacity of water is more, water can be circulated for recoiling purposes and warm water can be used for domestic purposes like bathing washing, etc. It is experimented and checked out that the surface of the solar cell is not allowedabove46℃.Whenexplosivesperiod4hoursofthewater-basedcoolingsystem. Module constructed such that solar energy Impact on more area and cooling Medium also [11].

The main cooling system for reducing solar panel temperature is an active and passive cooling system. The case of active cooling requires coolant like air and water which is worked with a favor electric motor. Where in the case of passive cooling there cooling is divided into three main categories passive cooling of the air, passive cooling of water, and conductive cooling natural convection is done by heat exchange sink, heat pipe, etc. are used in passive cooling. Modern cooling technologies include phase change material (PCM) nanotechnology (nanofluid) sinks thermoelectric generators microchannel.

Previously different cooling techniques were discussed such as solar panel air cooling was invented when the panel was cooled by air then panel temperature decreases to 4℃ and its efficiency increases about 2.6% while in the case of water the temperature decreases to 8℃ and system efficiency increase up to 3% [12]. Shelby et al. [13] examined that the efficiency of solar panel water cooling is more than air cooling also it was also examined that the total power output of photovoltaic panels increases 33.3%, 25.9%, and 27.7% with the help of water spray cooling. The panel temperature falls from 57.1% to 24.7℃ and 26.4℃ by water spray cooling. While PCM absorbs or releases significant quantities when it is realized to change their physical state, PCM has high absorber capacity latent heat before phase change solidifies or melts [14]. Apart from this Lupu et al. [15] examined that heat pipe cooling improved the thermal efficiency of the PV panel by 13.9%. Apart from this heat pipe uses sealed pipe which should have a high value of thermal conductivity like as copper-silver etc. The heat pipe converted solar panel heat to air or water this lowered system heat and improved system efficiency. Apart from that other cooling techniques were discussed previously such micro-channel heat exchanger [16], solar panel nano fluid cooling [17], and solar panel evaporative cooling [18].

It was observed from the literature survey that various research was present on solar panel water spray cooling but only a few manual works achieved above 25% efficiency. The novelty of this study is to analyze the PV panel cooling system and its thermal aspect for Sultanpur (India). Effects of the number of the nozzle, the distance between nozzle and panel, angle of the spray

nozzle, and angle of the panel concerning the surface on system performance have been examined.

2. EXPERIMENTAL SETUP AND PROCEDURE

An experimental setup has been developed to study the performance of a photovoltaic panel with spray cooling. The main component soft his experiment area solar panel nozzle strainer, motor pump, and a tank. The solar panel is located at some angle from the earth's surface. It is situated on the four pillar tidewaters pulled from the tank by an electric motor which has some power after pulled arthritis sprayed by a nozzle on the surface of the solar panel. After's praying the cooled the panel temperature, therefore, panel t temperature falls from the rated temperature, water is full slides on the panel surface so that with cooling action, cleaning action also done. Water falls into the tank after sliding downs. This water, again and again, recalculates via a softer pipe. The water distribution system is located on a flexible pipe around 4 mm India meter on which the nozzle is fixed. The distance between the nozzle and panel surface is around 80mm from the front and back side150mm.

In general water spray cooling is more efficient than the other cooling media. Except for that water submerged method in which higher efficiency was obtained. Water spray also acts as a self-cleaning agent from a good cleaning action technique. The surface of the panel is made bless coefficient of reflex ion material. Less reflection means more light is observed by the surface and also it has low weight than other materials. When the solar light falls on the surface of a photovoltaic cell them most infra radiation is absorbed by the surface. The remaining light is generated into electricity by the photovoltaic cell. The solar panel water spray cooling system remains on the roof of hostel of KNIT Sultanpur India for several days during June 2021. The geographical location of this place is the latitude, longitude & altitude respectively, is 26.270 N& 82.070E and 95meters above the sea-level. The schematic diagram and photograph of setup are showninFigure1 and Figure 2 respectively.

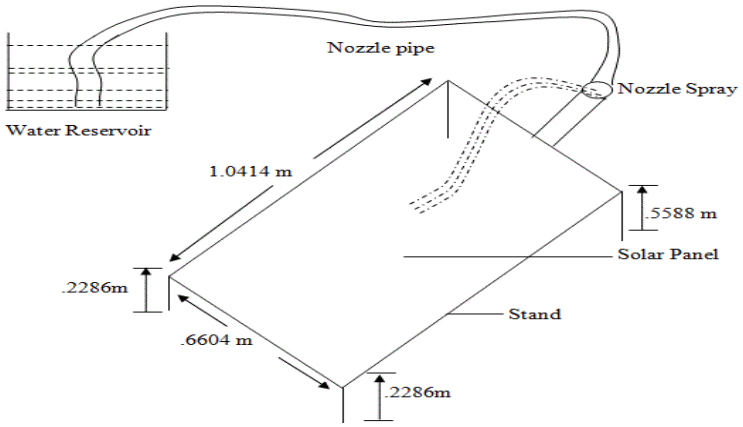

Figure 1. Schematic diagram of solar panel water spray cooling system

Figure 2. Photograph of Solar Panel Water Spray Cooling System

The main components used in the solar panel water spray cooling system and their specifications are described as

2.1 ***Solar panel stand****:* a stand is necessary for holding the panel. It has four legs in taper form. It is constructed by iron material and parts are welded having dimensions 1.0414m X0.6604m. The length of the small and bigger leg is 0.2286m and 0.5588m respectively. It has a nozzle mouth from bigger legs at height. The nozzle diameter mouth is 1.51mm as displayed in figure.

2.2 ***Nozzle pipe:*** A PVC material pipe is used for transferring water from the bucket to the nozzle mouth. It has a length of 1.5m and 1.38mm in diameter as shown in Figures 1 and 3. *Motor:* The motor is used for the conversion of mechanical energy into hydraulic energy. It generates flow with power and according to the load manages the pressure. An AC motor 18W, 165-230V/50Hzis used for pulling water from the reservoir and send to the nozzle pipe. Its photograph is shown *Nozzle:* for spraying water, a 1.38m diameter nozzle is used. It is made of steel materiality has many small holes for spraying to water. *Solar panel:* Photovoltaic modules use for the generation of electricity by use of light energy (photons) mast modules use thin-film cells or water-based crystalline silicon cells. All cells one electric cell is so connected that mechanical damage and vibration do not take place. A 12V power solar panel is used for cooling purposes.

Its length is 1.0414 m and its width is0.6604 m. This solar panel is fixed on the solar panel stand. The panel absorbs solar energy and converts it into electrical energy as illustrated in Figure (2.1) and (2.3).

2.3 Water reservoir: A water reservoir is used for the flow of water. It is used for the continuous supply of water. The motor is fully dipped inside it and pulled waterbrain.

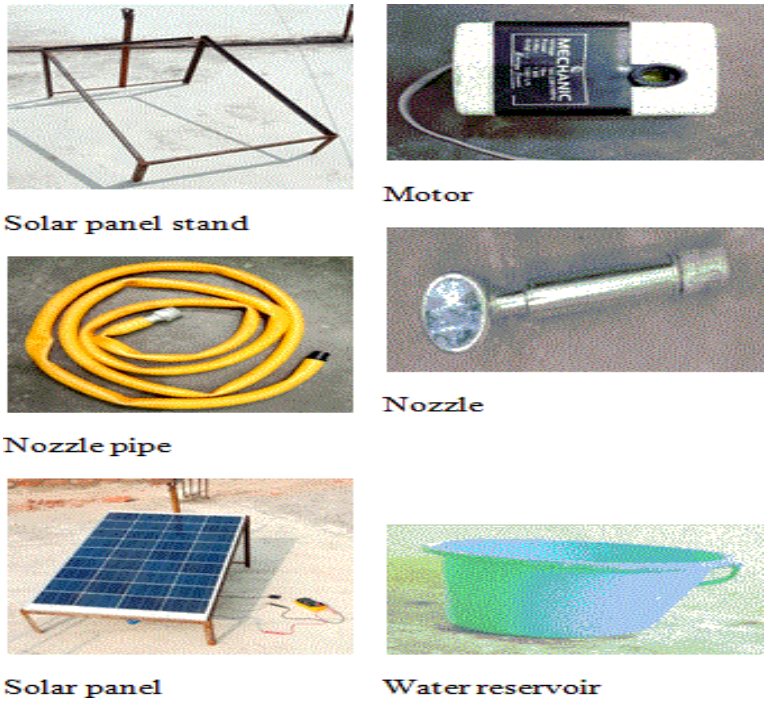

Figure 3. The Component Used in The Experimental Setup

Apart from this for calculating the performance and characteristics of the solar panel water cooling spray following instruments are used.

2.4 ***Temperature sensor:*** *the* temperature at the required places was measured by the digital sensor and shown by Figure 4. This sensor can be used to measure the temperature in the range of -50℃ to 110℃ with accuracy ± 1℃.

2.5 Whirling hygrometer: whirling hygrometer is used for measuring dry bulb temperature and wet bulb temperature. It can measure the dry bulb and wet bulb temperature to 20 Fahrenheit can be seen in Figure 4.

2.6 ***Anemometer:*** the wind velocity affects the temperature of the solar panel; its speed is measured by an anemometer as shown in Figure 4. The range of velocity of the anemometer is

0to 45 m/s with a range of operating temperature– 10℃ to 50℃ and humidity 40% RH – 85%RH respectively.

2.*7 Voltmeter:* voltmeter is used for measuring to voltage and the current value of the solar panel. It can measure the maximum voltage is 600V and the maximum currents 10A.It has three polls one is voltage, and another is current and in between to this neutral pole.

2.*8 Electronic digital caliper :*electronic digital calipers used for measuring the dimension of different sections. It can measure in both units like mm and inch. It can measure maximum dimensions int he ranges of 150mm. Its photograph can be configured 4.

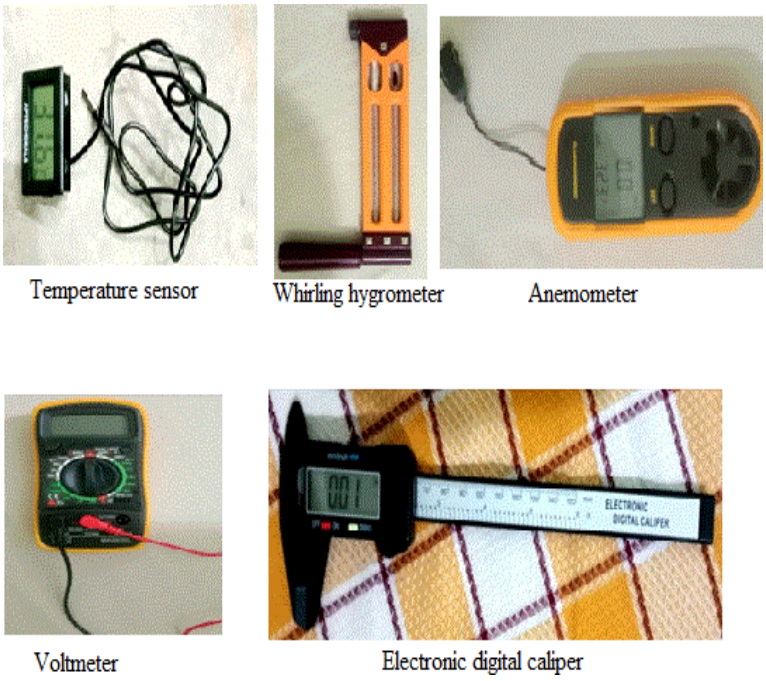

Figure 4. Instrument Used in The Experimental Setup

In summer conditions the temperature of solar panels generally gets very high consequently the value of power output becomes decreases. We are cooled to solar panel and getting reached to anormal temperature of the solar panel so in this way the efficiency of my system becomes improved.

2.9 Working Procedure

First, a water reservoir is taken, and solar panel put on a solar panel stand generally sliding on a panel and going out from panel surface for pulling to water from reservoir an AC motor issued which is pulled water from reservoir and water goes inside the nozzle and the water comes out from nozzle in the form of a spray. Become water expands during spray so its temperature

becomes down in some amount. The panel so in this way, cleared to the panel surface and cooled it. We have taken reading every 5 to 10-minute interval and noted voltage, current, DBT and WBT reading, and air velocity because velocity affects the panel temperature by the process of forced convection. The water spray cooling technique aim stoa cheval overtemperatures of solar panels in this way increasing the photovoltaic panel power output. If we wantto apply water spray on both sides of the panel front and backward both then suppose $G_S$is the incoming solar irradiation APis the total solar panel area. Now we are interested in convertinguse of full power output of this incoming solar radiation. Solar energy of this in radiation is wanted into uncreative solar.

According to this Figure 5, it can be seen Q is the total heat loss, in convection Q_C,$Q_E$is the total evaporation heat and $Q_R$is the radiation heat l loss.

Then the total solar irradiation is expressed as

$$Q_{SOLAR} = \alpha\, G_S A_P (1)$$

Where, α,$G_S$and$A_P$absorptive coefficient, solar irradiation, and panel area, respectively.

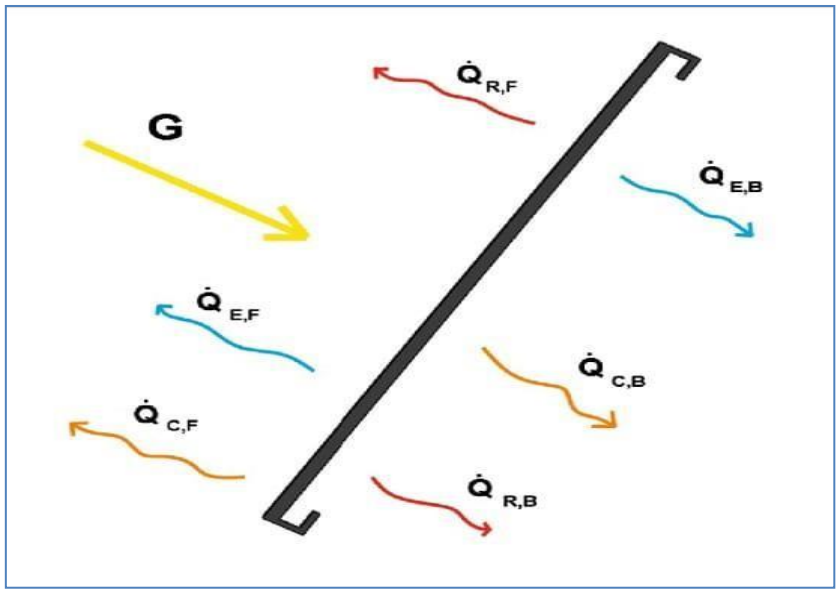

Figure 5.Net Heat

Loss from Solar Panel Overall photovoltaic heat loss Q_{LOSS} can be calculated by

$$Q_c + Q_R + Q_E = Qloss \qquad (2)$$

Where Q_C, Q_R, $Q_E$are convection heat loss, radiation heat loss, evaporation heat loss respectively

If we total heat loss considered the heat exchange by front and back side of the PV
Total convection heat loss is

$$Q_{CF} + Q_{CB} = Q_C \quad (3)$$

Convection heat loss from the front side isa also calculated by given below

$Q_{CF} = Front\ A_P\ (T_{PANEL\ FRONT}$ - $T_{PANEL\ FRONT}$) (4)

Same as from back side

$Q_{CB} = h_{back\ side}\ A_P\ (T_{PANEL\ BACKSIDE}$ - $T_{AIR\ BACKSIDE}$) (5)

Total radiant or heat loss is expressed as.

$$Q_{RF} + Q_{RB} = Q_R \quad (6)$$

Total heat radiation Q_{Rc} ana also be calculated by

$$Q_R = \sigma\ \varepsilon A_P F_{XY}\ (Tx^4 - Ty^4) \quad (7)$$

Where x subscription denoted that front side any description denoted that backside, and F_{xy}, T_X, Ty, σ, AP andε are view factor of both side, front side temperature, backside temperature, StefanBoltzmann Constant, panel area, emissivity respectively.

Thetotalevaporationheatlossdependsonbothrelativehumilityandsurroundingairtemperature and the velocity of air respectively. Total heat loss evaporation depends on applied water flow temperature i.e., the boundary layer of the photovoltaic panel this can be explained.

$$Q_E = Q_{EF} + Q_{EB} \quad (8)$$

The evaporation heat loss also can be written as.

$$Q_E = e\ A_P\ (P_S - P_R)r \quad (9)$$

P_S, P_d is the partial pressure the total evaporation heat loss depends on the relative humidityvelocity of the air and the temperature of the water spray and the purpose of the spray of water is to increase overall heat refection by evaporation it strongly depends on evaporation coefficient.

(e) (where evaporation coefficient greatly depends on the air velocity in case of turbulent flow it directly depends on the convection heat transfer coefficient).

Furthermore, depends on surrounding air temperature relative humidity as well as the temperature of the thin boundary layer.

Also following equations has been considered for the performance calculation During cooling of PV, panel water is sprayed forcefully by the pump. Hence it is clear that heat transfer via force convection.

According to Newton's cooling law

$$Q = h\ A_S(T_W - T_F) \quad (10)$$

Here T_W and T_f is the temperature difference between wall and fluid, Q is related to overall heat$_{transfer}$.

According the second energy balance

$$Q = m\ C_P(T_E - T_O) \quad (11)$$

First, we check that flows laminar or turbulent by the Reynolds Number

$$R_e = \frac{\rho v d}{\mu} \quad (12)$$

P is the density of the fluid, v is the velocity of the fluid and μ is the dynamic viscosity.

The velocity of fluid can be determined by

$$m = \rho AV \quad (13)$$

Nusselt number can be calculated as.

$N_U = 0.332\ Re^{1/2} Pr^{1/3}$ (laminar) (14)

$N_U = 0.0228\ Re^{4/5} Pr^{1/3}$ (turbulent) (15)

Heat transfer coefficient(h)can be determined by

$$N_U = \frac{h_d}{K}$$

Where, d is hydraulic length

Efficiency of the system can be calculated as.

$$\eta = \frac{output\ power}{A_P G_S}$$

3. RESULTS AND DISCUSSIONS

In this section performance of the system were discussed without cooling and with cooling on after the other.

3.1 Performance testing without cooling

The results of experiment were recorded without cooling of solar panel in the month of 10th July2021 as shown listed in Table 1. The wind velocity, DBT, WBT, module power has been recorded at some stage in the test and were used within the calculation of the efficiency of the PV module. The panel temperature initially at60.6℃ (1:00 PM) is increased and reaches the peak point of day 62.3℃ (2:00PM). During the experiment, the panel temperature was fluctuated, according to wind velocity and environmental conditions. The minimum temperature of the panel is 59.8℃ at 2:30 PM. After this time the temperature becomes down gradually. Here it can be seen that the value of voltage become decreases with temperature and the value of current also decrease with higher cell temperature. It has been observed that that the module efficiency slightly decreases with increase in temperatures. At 1:00 PM, initial temperature of the solar panel was 60.6℃ and corresponding efficiency was observed as

2.88%. When temperature slightly decreases to 60.1℃, then efficiency slightly improved to 2.919%. All variation were listed in Table 1

Table 1. Recorded data of solar panel without Cooling on10th-July-2021

Time	1:00PM	1:15PM	1:30 PM	1:45 PM	2:00PM	2:45 PM	3:00PM
Temp (℃)	60.6	60.1	60.8	61.2	62.3	61.8	59.8
Voltage(V)	19.08	19.30	19.24	19.11	19	19.03	19.28
Current (A)	1.04	1.06	0.98	0.93	0.63	0.58	0.08
DBT (℃)	89	89.1	90	90	91	89.9	88
WBT (℃)	82.5	82.4	83	83	83.5	03	82.9
Air velocity(m/s)	1.1	1.2	1.1	1.3	1.08	1.2	1.08
Output power(W)	19.84	20.458	18.85	17.77	12.92	11.03	20.822
Efficiency (%)	2.88	2.919	2.69	2.536	1.84	2.33	3.027

It was also observed that the current first increased with the voltage and after some value of the voltage, it decreased. Keeping constant all other parameters, the as the voltage increased corresponding temperature also decreased which leads to the decrease of the current. The maximum current was foundat1. 06Vofvoltage. It can also be seen in Figure 6, the dropping grate of the current was faster corresponding voltage from 0.58V to0.55V. As discussed previously in this reason rate of temperature drop was also sharp.

Figure 6 shows the temperature variation of solar panels with time. Itis observed that the maximum temperature is between 1:00 pm to 2:30 pm on July 10th, 2021. Because at this time the high amount of solar radiation was received in India. Therefore, energy transformation rate was also high. It can be observed that solar panel temperature fluctuated with the environmental condition and wind velocity also.

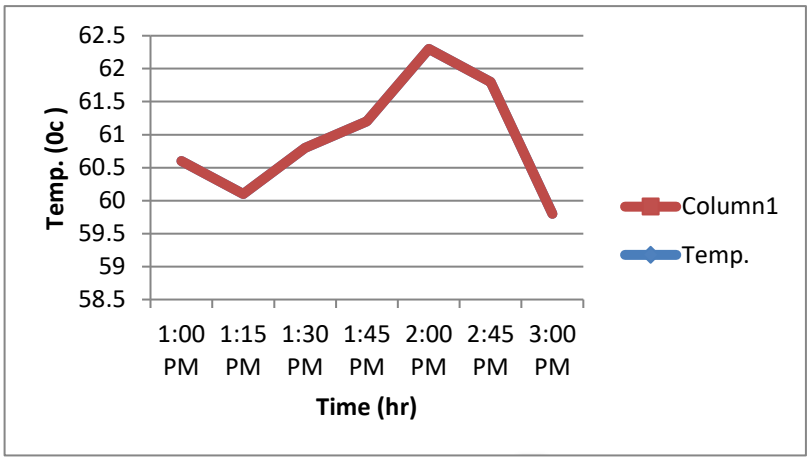

Figure 6. Variation of Temperature with Time

Figure 6 shows the relation between voltage and power output. The maximum power was achieved at the time 3:00PM, where minimum temperature was found. The maximum power was obtained as 20.822W at 59.8℃ of temperature. It can be seen from the Figure 6 that power out decreased with the voltage and found maximum a voltage of 19.28V. It is concluded that when the panel temperature tends to maximum then their power output becomes minimum.

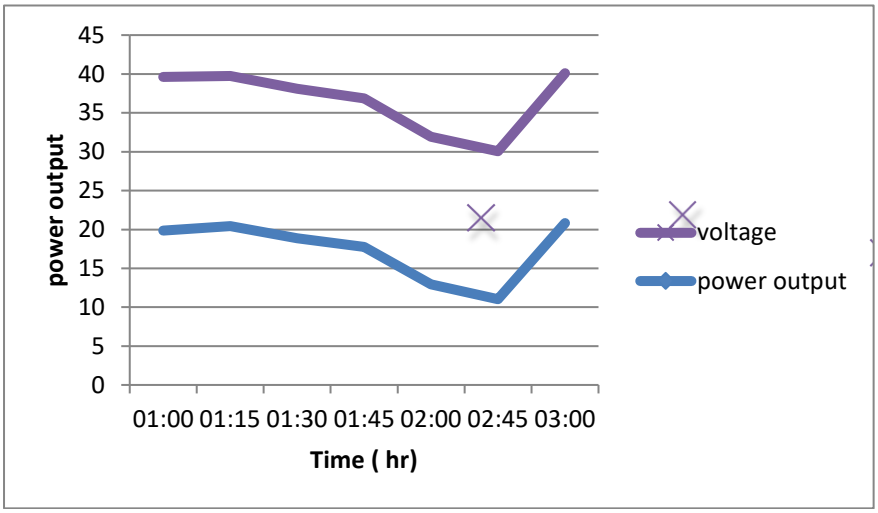

Figure 7. Variation of Power Output with Voltage

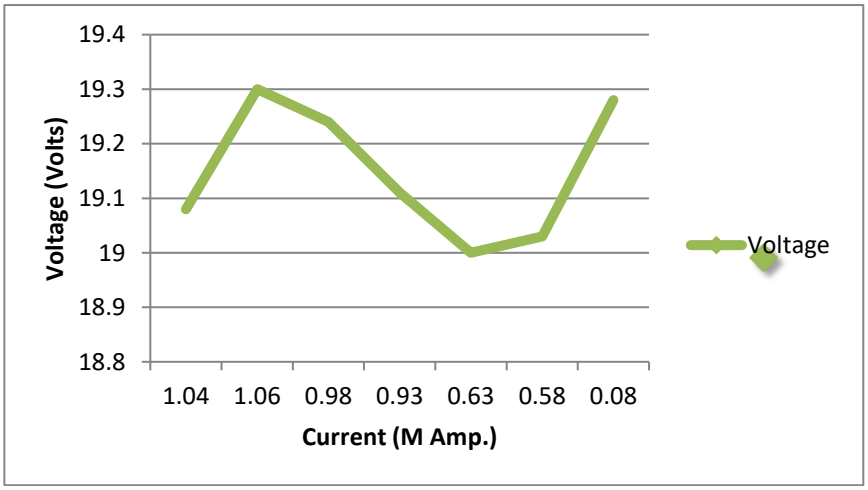

Figure 8. Variation of Current with Voltage

It was observed that when the panel temperature reached to maximum value corresponding electrical efficiency also obtained its maximum value as can been seen in Figure 9. In this experiment, the maximum efficiency occurred at the lowest temperature which is 59.8℃ at the maximum temperature 62.3℃ efficiency is the lowest value which is 1.84%.

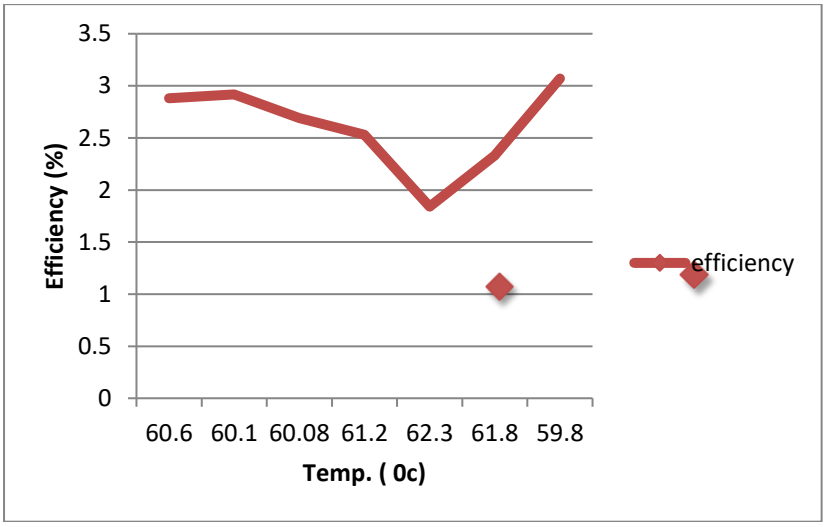

Figure 9. Variation of Electrical Efficiency with Temperature

3.2 Performance analysis of the system with cooling

In this section all measurements were taken with cooling of the solar panel on 12th July 2021 Sultanpur India. The wind velocity, DBT, Titmouse power has-beens recorded atmometer in the test and were used within the calculation of the efficiency of the PV module. The panel temperature initially at 45℃ (1:00 PM) is lowered and reaches the lowest point of day42.8℃ (3:15 PM). During the experiment, the panel temperature was fluctuated, according to wind velocity and environmental conditions. The minimum temperature of the panel is 42.8℃ at3:15 PM. After cooling the temperature become down gradually. Here It was seen that the value of voltage decreases with temperature and the value of current also decreases with higher cell temperature. After the experiment, It can also be seen that the module efficiency gradually increases with temperature. At 1:00 PM my initial temperature of a solar panel is 45℃and my efficiency is 13.5%. When the temperature slightly decreases to 42.8^{0}C, then efficiency slightly improved to 15.662%. At 1:15 PM my efficiency is 14.64% after 15-minute temperature become44.6℃temperature lowest by 0.2℃my and efficiency become improved to 15.2% from 14.64% another worthies when temperature become improved by 0.28% hence it can be said that the panel temperature should by a moderate temperature value at a higher temperature value its efficiency become lowered. Therefore, solar panel must be cooled for achieving better performance and efficiency.

Table 3.2 Recorded data of solar panel without cooling on 12th, July-2021

Time	1:00 PM	1:15 PM	1:30 PM	1:45 PM	2:00 PM	2:15 PM	2:30 PM	3:00 PM	3:15 PM
Temperature (℃)	45.0	44.9	44.6	44.5	44.3	46.3	46.3	43	42.8
Voltage(V)	20.6	21.9	21.2	20.9	21.9	19.6	20.6	22.1	22.3
Current(A)	4.54	4.75	4.96	4.84	4.90	4.75	4.58	4.80	4.83
DBT (℃)	80	79.9	79.8	79.7	79.8	80	80	79.9	79.9

WBT (℃)	74	73.9	73.8	73.8	73.7	74	74	73.9	73.9
Air Velocity (m/s)	1.1	1.09	1.33	1.08	1.45	1.06	1.3	1.09	1.8
Output Power (W)	93.5	100.7	105.152	101.156	107.31	91.14	95.264	106.08	107.709
Efficiency (%)	13.5	14.64	15.29	14.709	15.60	13.25	13.856	15.42	15.662

Figure 10. shows temperature variation with time. The maximum temperature was observed as46.23℃ between the whole test range i.e., between 1:00 PM to 3:15 PM on July 12th, 2021. The Figure 6andFigure cane compared and due to spray water cooling temperature of the panel decreased sharply. The minimum temperature was found as 42.8℃ at the 3:15 pm while in previous test i.e., without cooling it was 59. 75℃ at the same time. Apart from this panel temperature fluctuated with the environmental condition and wind velocity also as can be seen in Figure 10.

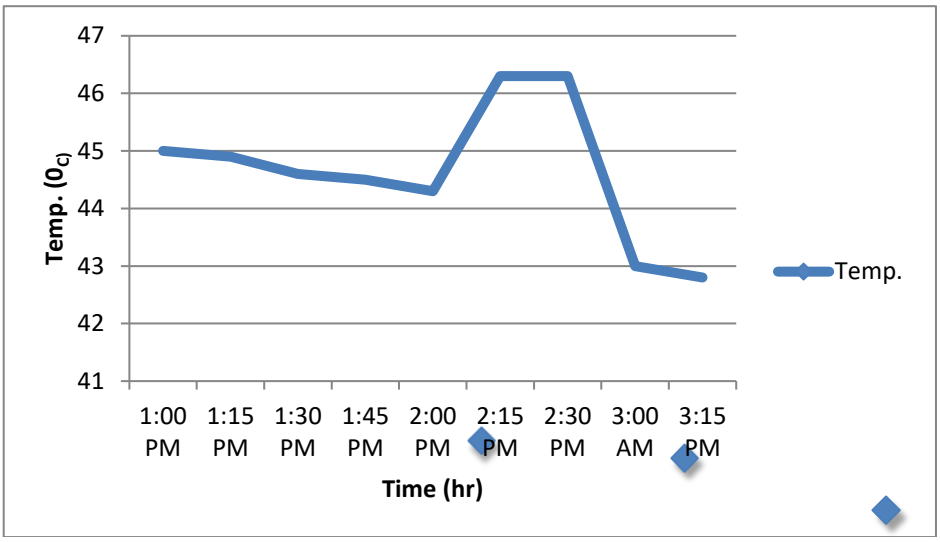

Figure 10. Variation of Temperature with Time

Figure 11 shows the variation of electrical power with voltage. Maximum was observed at the 3:15 PM when the temperature was minimum of all-temperature readings. It can see in the table 3.2 at 42.8℃ voltage is a maximum of 22.3 volts and here maximum power output was obtained as 107.709 W. It is concluded that when the panel temperature tends to maximization then their power output becomes minimized. Comparing the Figures 7 and 11, it was observed that due to cooling effect the efficiency was improved. As discussed above, the electrical efficiency decreased with panel surface temperature.

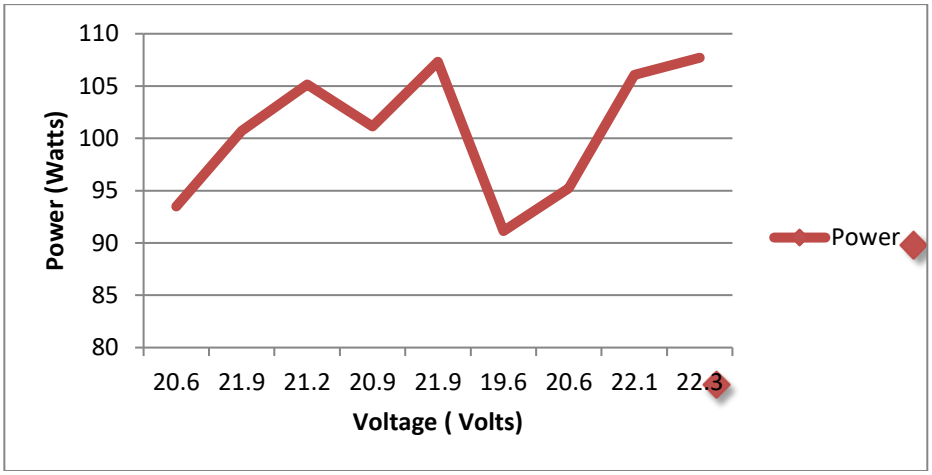

Figure 11. Variation of Power Output with Voltage

Further current variation with the voltage can be seen in the Figure 12. The pattern of variation was same as in without cooling conditions. It was observed that the maximum current value occurred at maximum value of the voltage. As the panel temperatures lowered then both temperature and voltage became maximum. As comparison to the figure 8, it was seen that with cooling the current was obtained more than the without cooling.

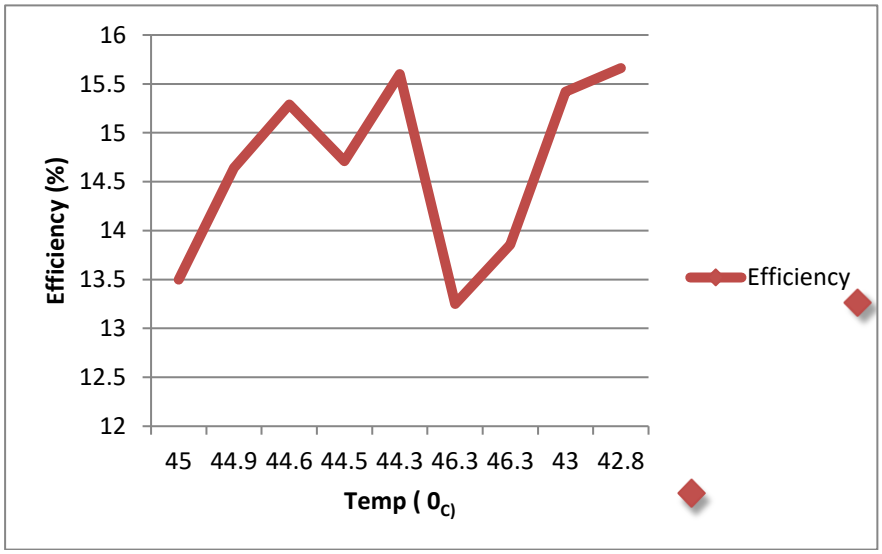

Figure 12. Variation of electrical efficiency with temperature

REFERENCES

[1] Solar electricity: T. Marquart (Ed.), seconded. John Wiley & Sons, Chichester,2000.

[2] E. Keith, The rating of photovoltaic performance, IEEE Trans. Electron Devices 46 (1999)1928–1931.

[3] S. Kurtz, Opportunities, and challenges for development of mature concentrating photovoltaic power industry, National Renewable Energy Laboratory, 2011, Technical Report (NREL/TP)520–43208.

[4] W.G.J. Van Helden, R.J.C.H. Van Zolingen, H.A.P.V. Zondag, Thermal systems: PV panels supply in grenewableelectricityandheat, Prog.PhotovoltaicsRes.Appl.12(2004)415–426.

[5] Z. Ye, A. Nobre, T. Reindl, J. Luther, C. Reise, On PV module temperatures in tropicalregions, Sol.Energy88(2013)80–87.

[6] M.M. Rahman, M. Hasanuzzaman, N.A. Rahim, Effects of various parameters on PV module power and efficiency, EnergyConvers.Manage.103(2015)348–358.

[7] M.S. Abd-Elhady, M. Fouad, T. Khalil, Improving the performance of photovoltaic panels bilocating, EnergyConvers.Manage.115(2016)1–7.

[8] A. Luque, S. Hegedus, Handbook of Photovoltaic Science and Engineering, second ed., JohnWiley&Sons, WestSussex,2011.

[9] E. Skoplaki, J.A. Palyvos, On the temperature dependence of photovoltaic module electrical performance: a review of efficiency/power correlations, Sol.Energy83 (2009)614–624.

[10] S. Chatterjee, G. Tamizh Mani, BAPV arrays: side-by-side comparison with and without fan cooling, IEEE Photovoltaic Specialists Conf. (PVSC)7(2011)537–542.

[11] Nabil A.S. Elminshawy, A.M.I. Mohamed, K. Morad, Y. Elhenawy, Abdulrahman A. Alrobaian, Performance of PV panel coupled with geothermal air cooling system subjected to hotclimatic, AppliedThermal Engineering148(2019)1–9.

[12] Zainal Arifin, Dominicus Danardono DwiPrija Tjahjana, Syamsul Hadi, Rendy Adhi Rachmanto, Gabriel Setyohandoko, and Bayu Sutanto, Numerical and Experimental Investigation of Air Cooling for Photovoltaic Panels Using Aluminum Heat Sinks, International Journal of Photoenergy Volume 2020, Article ID 1574274, 9 pages https://doi.org/10.1155/2020/1574274.

[13] S.M.ShalabyM.K.ElfakharanyB.M.MoharramH.F.Abosheiasha.Experimental study on the performance of PV with water cooling, Energy Reports Volume 8, Supplement 1, (2022),957-961.https://doi.org/10.1016/j.egyr.2021.11.155.

[14] M.Rajvikram,S.Leoponraj,S.Ramkumar,H.Akshaya,eA.Dheeraj.Experimenta linvestigation on the abasement of operating temperature in solar photovoltaic panel using PCMandaluminium,SolarEnergy,188(2019)327-338.

[15] A G Lupu et al 2018. A review of solar photovoltaic systems cooling

technologies. IOP Conf. Ser.: Mater.Sci.Eng.444082016.doi:10.1088/1757-899X/444/8/082016.

[16] Samson Shittu et al. Experimental study and exergy analysis of photovoltaic-thermoelectric with flat plate micro-channel heat pipe. *Energy Conversion and Management***,** 207, 2020,112515. https://doi.org/10.1016/j.enconman.2020.112515.

[17] Abdulrahman A. Arabian, Abdulrahman Saleh AlturkiInvestigation of numerical and optimization method in the new concept of solar panel cooling under the variable condition using nano fluid. *Journal of Thermal Analysis and Calorimetry*, volume 142,2173–2187(2020).

[18] P. Dwivedi I. Kirpichnikova, Advance cooling techniques of P.V.modules: A state of art, October 2020.

[19] A Hadipour, M.R. Zargarabadi, and S. Rashidi, An efficient pulsed-spray cooling for photovoltaic panels: Experimental study and cost analysis. *Renewable Energy* 164, (2021), 867-875.

Biographies

Manish Kumar Chauhan received the bachelor's degree in Mechanical Engineering from BIT, Muzaffarnagar (AKTU, Lucknow) in 2016, the master's degree in Thermal Engineering from KNIT, Sultanpur, in 2019, respectively. He is currently working as an Assistant Professor at the Department of Mechanical Engineering, at KNIT Sultanpur. His research areas include Solar Distillation System, Solar Energy, Thermal Engineering, Renewable Energy, Heat Transfer deep learning, and Thermal analysis.

Ram Prakash Yadav received his bachelor’s degree in mechanical engineering from Aktu Lucknow in 2013, Master degree in Thermal Engineering from Knit Sultanpur in 2021. Currently working as an assistant professor at the Kamla Nehru Institute of Physical and Social sciences in the Department of Mechanical engineering.

Dr. A K Chauhan is an Assistant Professor in the Department of Mechanical Engineering at Kamla Nehru Institute of Technology (KNIT), Sultanpur (U.P), INDIA. He did his M.Tech (2003) & Ph.D. (2008) from IITR, Roorkee. He has Published about 35 papers in International/National Journals, conferences, and seminars. He has more than 13 years of experience in Teaching & Research. He has done several courses on MOOCS / NPTEL/ SWAYAM.

Fuzzy Logic Based Hybrid Energy Storage System

[1]Arnab Jana, [2]Sukanya Roy, [3]Damodar Panigrahy

SRM Institute of Science and Technology, Kattankulathur, Tamil Nadu, India

[1]aj4527@srmist.edu.in, [2]sr9179@srmist.edu.in, [3]damodarn@srmist.edu.in

Abstract

The manuscript proposes the implementation of parallel full active topology of a Hybrid Energy Storage System (HESS). It includes combination of a lead-acid battery and super-capacitor on microgrid. An active topology has been simulated using four direct current/direct current (DC/DC) converters with switches controlled by Fuzzy Logic Controller. The proposed model is implemented to provide the additional power for the requirement of the load. The proposed model also minimizes the power fluctuation between the load and supply and maintain the power demand from the grid within limit. The Energy Management System (EMS) is designed with help of Fuzzy Logic Controller (FLC). The simulated EMS provides a dependable and continuous power supply to local loads while ensuring a stable supply condition.

Keywords. Energy Management System (EMS), Energy Storage Systems (ESSs), Fuzzy Logic Controller (FLC), Lead-Acid battery (LA Battery), Super-capacitor (SC).

1. INTRODUCTION

A microgrid is a distributed small-sized grid. It is often denoted as systems that are connected to the Distributed Generations units and usually consists of various renewable energy resources, power generators, Supercapacitors, Battery Energy Storage Systems (BESSs) and Load Demand (LD). This is normally capable of functioning in either stand-alone mode or grid-connected mode.

In a period for 24 hours, a grid faces various fluctuations like change in demands, change in power supply, electrical malfunctions, short circuits, etc. All these issues combined cause an increase in stress on the grid along with its EMS. An effective way to solve this is addition of localized energy storage systems, which can reduce the mismatch between consumption and power generation, ensuring system power balance [1]. Energy Storage Systems are classified based on various characteristics like energy density, power density, ramp rates, etc. Unfortunately, there is no single Energy Storage System, that fulfills all requirements [2]. Considering this fact, Hybrid Energy Storage Systems, which uses the benefits of all ESS emerge to be an effectual solution for solving economic and performance issues.

In recent times, research is being carried out in the field of Energy Management Systems including Hybrid Energy Storage Systems. In [3], a decoupled controlling strategy has been proposed for supercapacitors and batteries which is based on nonlinear PI controller (NPIC) and k - Type compensators respectively. In [4], the existing LPF has been replaced with single rate limiter, for ensuring proper battery discharge rate. This has resulted in solving

challenges like non-systematic selection of cut-off frequency at much ease. In [5], a new approach to energy management has been proposed. A two-level energy management strategy has been used, in order to optimize the operation cost and manage uncertainties. In [6], a novel power management strategy has been approached to solve the demand generation gap and maintain DC bus voltage, in addition to minimizing stress levels in the battery. In [7]-[8] a Fuzzy Logic based controlling is used in the functioning of a grid-tied MG and standalone MG. FLC controller for voltage and/or frequency control using flywheel ESS operation also presented in [9]. FLC for evening the variation in stand-alone wind power generation with BESS is given in [10].

The main intent of this work is to develop a controlling strategy for a HESS consisting of Lead-Acid battery and Super-capacitor to improve stability and efficacy of the microgrid while constantly considering SoC of both SC and LA battery at an acceptable limit. The SoC is being considered in order to prevent the damages of ESS due to excess charging and discharging of ESS. An FLC-based controlling algorithm has been proposed for energy management and distribution. The model is designed on MATLAB/Simulink platform.

The rest of the paper is organized as given: Section 2 provides a general overview and system configurations, Section 3 gives the proposed energy management system, Section 4 demonstrates the simulations and results obtained and the paper has been concluded with Section 5.

2. GENERAL OVERVIEW AND SYSTEM CONFIGURATION

The microgrid system considered in this simulation is shown in Figure 1. It shows configuration of microgrid with proposed energy management system. The model consists of seven parts: Lead-Acid battery, Super-capacitor, DC-DC boost converter, DC-DC buck converter, FLCs, DC supply, and DC Load. Lead-Acid battery and Super-capacitor (that constitutes the Hybrid Energy Storage System) have been connected in parallel to DC bus with the DC-DC converter. Two separate fuzzy logic controlling systems are being used for switching between charging and discharging modes for ESSs.

The main objective of proposed energy management system has been provided as to:

i) Decompose systems power demand into lower and higher frequency components.

ii) Power distribution among HESS for realizing power-sharing based on ESs' characteristics.

iii) Scheduling dynamic charging and discharging of the HESS with FLCs.

iv) Maintain a constant power drawn from the grid irrespective of the load.

Let P_{Total} be the active power flowing in the microgrid. P_{HESS} denotes the power output/input from/to the HESS, the power that is shortage/surplus is injected/absorbed by the HESS. P_{Supply} denotes the power supplied by the utility to the grid and P_{Load} refers to the power demand. The main objective is to reduce the fluctuation of power balance. The power balance equation can be given by:

$$P_{Total} = P_{Supply} + P_{Batt} + P_{SC} - P_{Load} = P_{Supply} + P_{HESS} - P_{Load} \quad (1)$$

$$P_{Total} = \begin{cases} P_{Total} < 0 if P_{load} > P_{HESS} + P_{Supply} \\ P_{Total} = 0 if P_{load} = P_{HESS} + P_{Supply} \\ P_{Total} > 0 if P_{load} < P_{HESS} + P_{Supply} \end{cases} \quad (2)$$

SoC is given by [16]:

$$SoC_{ess}(n) = (E_{ess}(n) / E_{ess,max}) \quad (3)$$

$SoC_{ess}(n)$ denotes current capacity of ESS, $E_{ess,max}$ denotes the maximum capacity and $E_{ess(n)}$ is current capacity of the ESS.

The state-of-charge of the HESS SOC_{HESS} is connected to the SOC of Lead-Acid battery and Super-Capacitor, which is given as [11]:

$$SOC_{HESS} = ((Q_{bat} \times SOC_{bat} + Q_{sc} \times SOC_{sc}) / (Q_{bat} + Q_{sc})) \quad (4)$$

Where Q_{bat} and Q_{sc} respectively denotes the rated-capacity of battery and supercapacitor. SOC_{HESS} tells the remaining capacity of the HESS.

A Low Pass Filter (LPF) has been used to divide power into high and low frequency components. P_{net} denotes difference between P_{load} and P_{supply} [1]

$$P_{low}(t) = (1/(1+T_s)) * P_{net}(t) \quad (5)$$

Here low-frequency component is denoted by P_{low}. T indicates reciprocal of the cut-off frequency. High-frequency component P_{high} is calculated by removing low-frequency component from the P_{net}. It is given as follows [1]:

$$P_{high}(t) = P_{net}(t) - P_{low}(t) = (T_s/(1+T_s)) * P_{net}(t) \quad (6)$$

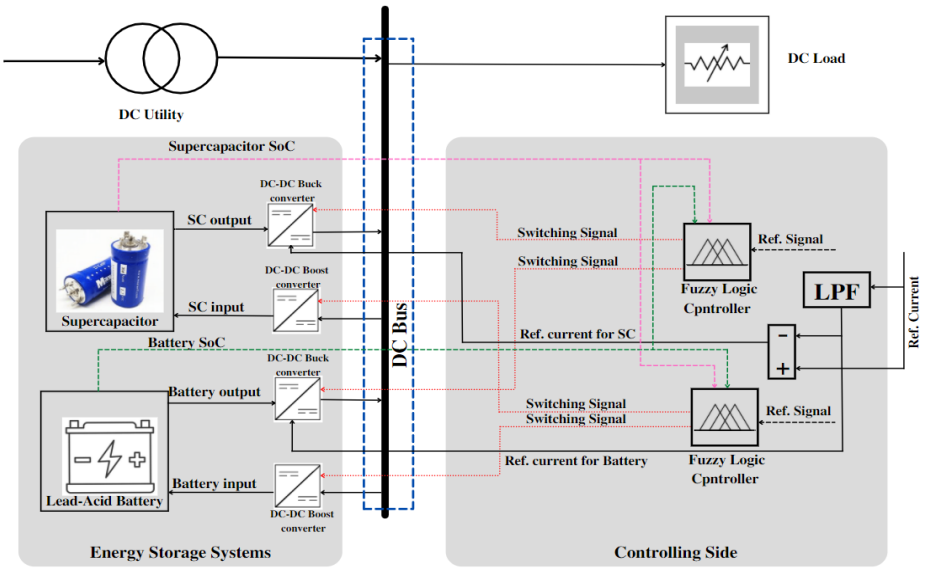

Figure 1. Configuration of the microgrid with proposed EMS

3. PROPOSED ENERGY MANAGEMENT SYSTEM

3.1 Fuzzy Logic Controlling:

By simulation of unreliable judgment and rational thinking, FLC has been used to manage with optimization problem that is strenuous to solve with old control methods [11].

A normal FLC consists of:

- *Fuzzification*: In this step, crisp inputs are converted into fuzzy values using membership functions.
- *Rule base*: This block stores the defining commands for the operation of FLC.
- *Fuzzy Interference Engine*: It is a process of simulation of human decisions which is built on fuzzy concepts. It is depicting from a given input(s) to an output(s) [12].
- *Defuzzification*: This process will evaluate a crisp output which is developed based on the output of inference. Mamdani − type FIS is used in this paper. A block diagram is exhibited in Fig 2

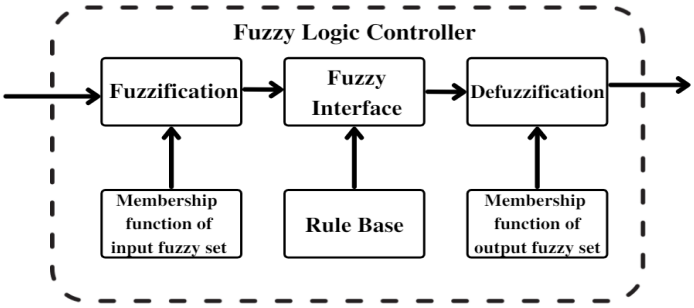

Figure 2. Mamdani type FLC

The EMS that has been proposed consists of Low Pass Filter (LPF) and two Fuzzy Logic Control (FLC). Two FLC have been used for scheduling of charging and discharging of HESS.

Fuzzy Logic Control-1 (FLC-1) is used to control the recharging of HESS. There are three inputs to the FLC: Battery State-of-Charge (*SoC_B*), Super-capacitor State-of-Charge (*SoC_SC*) and the difference between reference Supply Power and Load (*Value*). The *SoC_SC* and *SoC_B* are divided into three levels: High (H) Medium (M) and Low (L). The other component, *Value* is divided into two components, Neg (N) and Pos (P). The output of the FLC-1 gives two outputs that control two switches (*SW_Batt_Conv and SW_SC_Conv*). Separate switches are used for Battery and Super-capacitor to increase the system reliability. The input/output membership functions are given at figure 3(a) and 3(b) respectively.

$$\textit{Possible values of SOC states of Lead-Acid Battery} = \begin{Bmatrix} High\ if\ 90 \le SOC_B \le 100 \\ Medium\ if\ 30 \le SOC_B \le 90 \\ Low\ if\ 30 \le SOC_B \le 0 \end{Bmatrix} \quad (7)$$

$$\textit{Possible values of SOC states of Super-Capacitors} = \begin{Bmatrix} High\ if\ 90 \le SOC_{SC} \le 100 \\ Medium\ if\ 20 \le SOC_{SC} \le 90 \\ Low\ if\ 20 \le SOC_{SC} \le 0 \end{Bmatrix} \quad (8)$$

Fuzzy Logic Control-2 (FLC-2) is used to control discharging of the HESS into grid. There are three inputs to the FLC: difference between reference Supply Power and Load (*Difference*), Battery State-of-Charge (*SoC_Battery*) and Supercapacitor State-of-Charge (*SoC_SC*). *SoC_SC* and *SoC_Battery* are divided into two levels: High (H) and Low (L) both. The other component, *Difference* is divided into two components, Neg (N) and Pos (P). The output of the FLC-2 controls two switches (*Switch_B* and *Switch_SC*) which control the discharge of HESS into the grid according to the rule. Separate switches are used for Super-capacitor and Battery to increase the system reliability. The input/output membership functions are given in figure 3(c) and 3(d) respectively.

$$\textit{SOC states of Lead-Acid Battery} = \begin{Bmatrix} High\ if\ 30 \le SOC_{Battery} \le 100 \\ Low\ if\ 0 \le SOC_{Battery} \le 30 \end{Bmatrix} \quad (9)$$

$$\textit{SOC states of Super-Capacitors} = \begin{Bmatrix} High\ if\ 20 \le SOC_{SC} \le 100 \\ Low\ if\ 0 \le SOC_{SC} \le 20 \end{Bmatrix} \quad (10)$$

Charging and discha

$$\textit{rging scenarios of HESS} = \begin{Bmatrix} Discharge\ if\ P_{Total} \ge 0 \\ Charge\ if\ P_{Total} < 0 \end{Bmatrix} \quad (11)$$

3.2 Membership functions:

Membership functions engages in an important position in controlling operation of FLC. These MFs are defined with linguistic terms having specified boundaries [13]. The input membership functions are being used as transitions among different operating modes [14]. In the proposed EMS, Trapezoidal MFs are being used. Various membership functions that are used in this energy management are shown in figure 3(a), 3(b), 3(c) and 3(d).

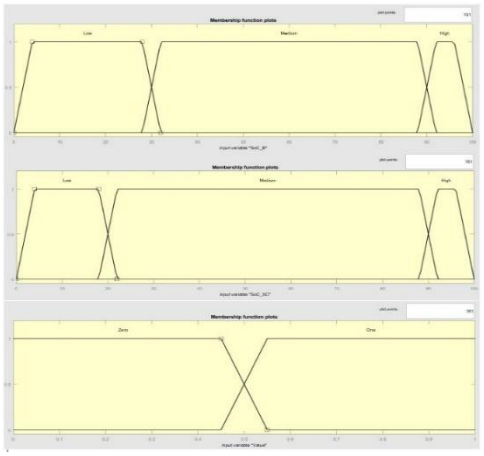

Figure 3(a): Input MFs for FLC-1

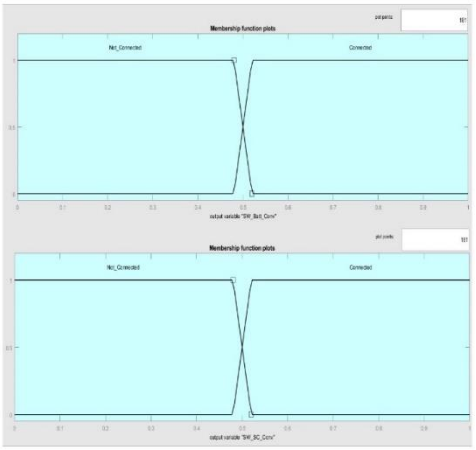

Figure 3(b): Output MFs for FLC-1

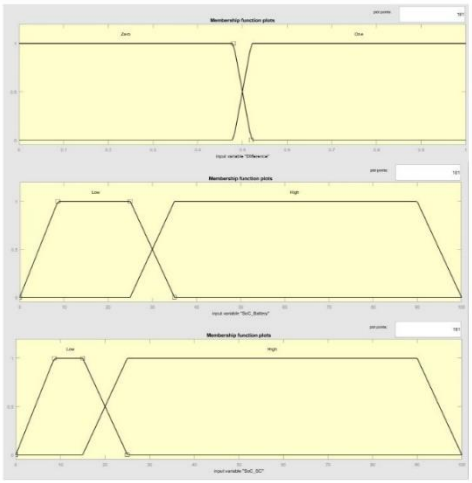

Figure 3(c): Input MFs for FLC-2

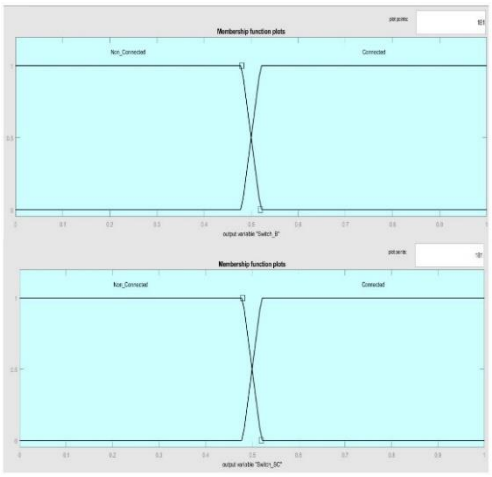

Figure 3(d): Output MFs for FLC-2

Overall system Specifications

Table 1: Overall system specification

System Specifications	
System Parameters	**Rating**
Capacity of the Microgrid	4KW
DC Bus voltage	72 V
Supercapacitor rating	29F
Lead-Acid Battery rating	250Ah
DC-DC buck converter input/output	100V/72V
DC-DC boost converter input/output	72V/100V
Number of Residential Houses considered	3 Nos
Number of FLCs considered	2 Nos
Simulation duration considered	24 Hours

3.3 Power allocation strategy:

The power allocation strategy used is this energy management system is achieved with the help of LPF. The LPF separates the High and low frequency components from the difference between supply and demand. The separated value then acts as an input to the PWM

generators, which generated a specific pulse for the DC-DC converters accordingly. Figure 4 gives a schematic for the power allocation strategy used.

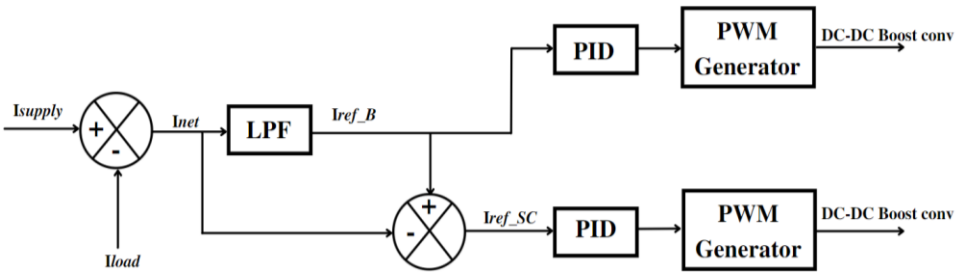

Figure 4. Controlling structure for power allocation strategy

3.4 Functioning of the EMS:

The value of the P_{Total} can be calculated by the formula given in eqn. 1. It reflects the power shortage or power surplus in the grid. The term P_{Load} refers to the load power demand at a specific time and is measured in KW. The value P_{Load} is compared to a predefined threshold value P_{Ref} (4000KW). Based on the comparison, three modes are possible:

(i) *Positive Value*: This result is observed when reference power demand is more than load power demand, which demonstrates that the supply is in excess and excess energy is used to charge the Energy Storage Elements.

(ii) *Negative Value*: This result is observed when reference power demand is less than load power demand, which shows that there is an outage of power and additional sources of energy is required to fulfill the requirements.

(iii) *Ideal*: This situation is seen when the power load demand and reference supply are equal, thus resulting in an ideal stage.

$$\textit{Possible outputs of the comparison} = \begin{Bmatrix} Positive\ if\ P_{Ref} > P_{Load} \\ Negative\ if\ P_{Ref} < P_{Load} \\ Ideal\ if\ P_{Ref} = P_{Load} \end{Bmatrix} \quad (12)$$

The proposed Energy Management System has been designed to operate in four states to manage the flow of energy in system which depends on power drawn by load [15] and SoCs. The states are briefly discussed in the paragraphs following:

- State 1: This state is operated when load power demand is more than the reference power and the SOC of ESS i.e., Lead-Acid Battery / Supercapacitor is in between 30% and 100% / 20% and 100% respectively. In this mode, the ESS is connected to the microgrid to fulfill the shortage of supply.
- State 2: This state is switched on when the load power demand is more than the reference power and the SOC of the Energy Storage Systems are not within the limits i.e., less than 30% for Lead-Acid Battery and less than 20% for Supercapacitor. In this situation, due to the non-availability of the ESSs, the DC supply is directly connected to the load without ESS.

- State 3: This state is switched on when load power demand is less than reference power denoting that the supply is excess than the demand and the SOC of both the Energy Storage Systems is below 90%. In this mode, the ESSs are connected to microgrid with the help of a DC-DC boost converter, and ESSs are charged till the SOC of both the Energy Storage Systems reaches 90%.
- State 4: This state is switched on when load power demand is less than the reference power denoting that supply is excess then the demand and the SOC of both the ESSs i.e., Lead-Acid Battery and Supercapacitor is 90% or above. In this mode, the ESSs are not connected to the microgrid and are kept in the same ideal state.

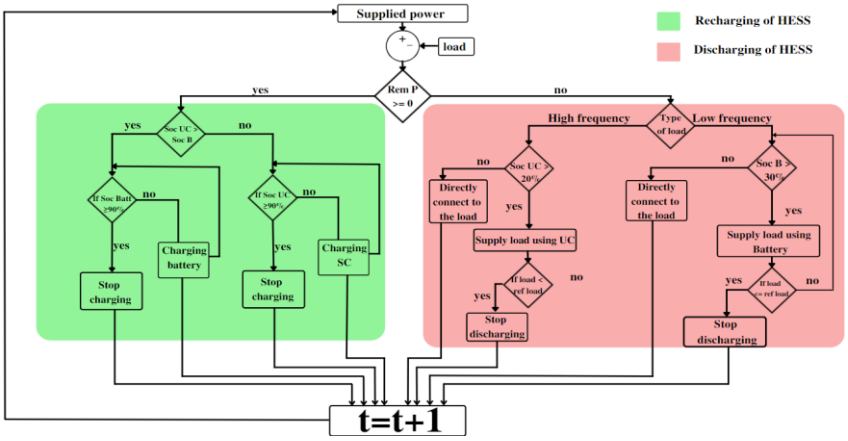

Figure 5. Various operation stages in proposed energy management system

4. SIMULATION RESULTS AND DISCUSSION

This simulation has been executed out in the MATLAB/Simulink software. A source-controlled Voltage source has been used as a supply from the microgrid. A uniform voltage of 72 V has been maintained for the DC bus utilizing a DC source. SoC of the ESSs have also been maintained in the limits.

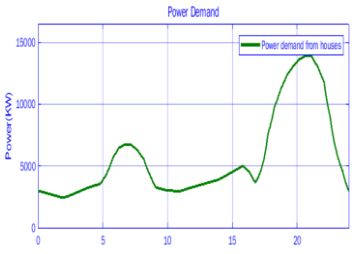

Figure 6(a). Load demand for 24 Hours

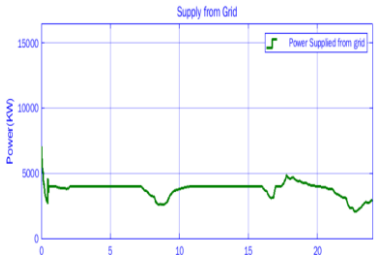

Figure 6(b). Power supplied from grid to load

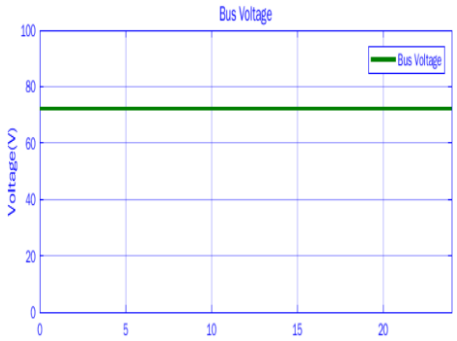

Figure 6(c). DC Bus voltage

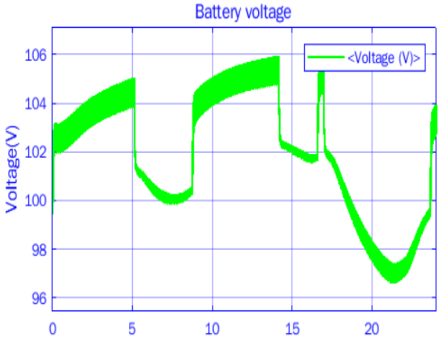

Figure 6(d). Battery Voltage levels

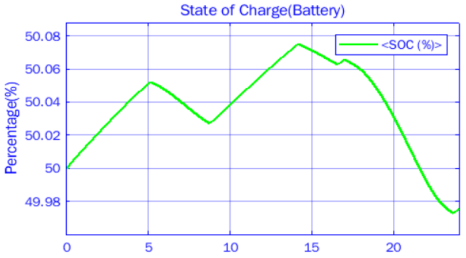

Figure 6(e). SoC levels of battery

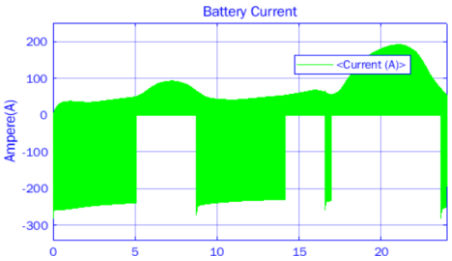

Figure 6(f). Battery current levels

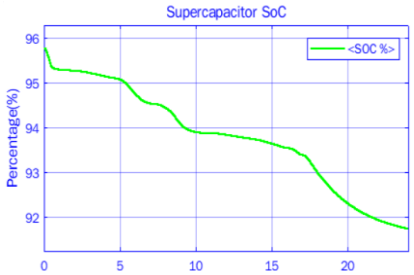

Figure 6(g). SoC level of SC

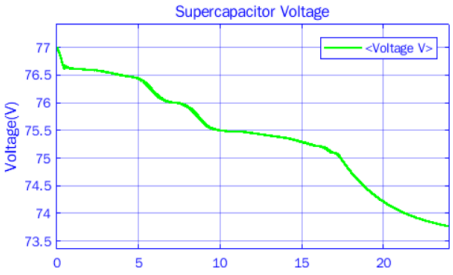

Figure 6(h). Voltage level of SC

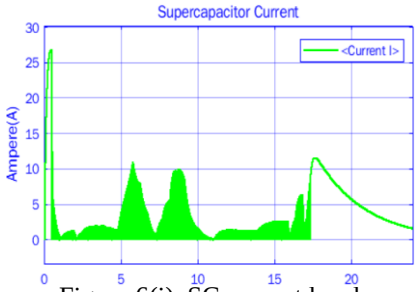

Figure 6(i). SC current levels

Three resistive loads have been considered, for three houses for a period of 24 hours. In the presented simulation, a grid has been designed to supply a power of 4KW. The purpose of the proposed EMS is to connect ESSs to the grid, whenever the load exceeds the capacity limit of the grid, it feeds the excess load demand and the other purpose of EMS is to recharge the ESS to the predefined values when there is excess power in grid. The microgrid system presented in this simulation has been tested for 24 hours. Overall parameters of the model have been mentioned in Table 1.

A LPF has been used to distribute demand according to the frequency at τ = 0.3 sec. The initial SoC of the Battery and SC was considered 50% and 95.8%. Fig 7(e) and Fig 7(f) show SoC capacity of ESSs in the simulation. Figure 7(a) represents the load demand from three houses for 24 hours. The graph shows us two peaks around 7:00 hrs and 21.00 hrs.

From the demand graph (Fig. 7(a)), it can be observed that the presented grid is insufficient to supply the load and needs more energy. At t= 5 to t=8.55; t=14.15to t=16.66; t=17to t=23.65, it is noticed that the load demand is exceeding the capacity of the grid which resulted in the activation of the EMS and connecting ESS to the system. The graph response that is being shown in Fig 7(b) gives us the data about how much power is being taken from the grid. It shows us that there has been stability in the power taken from the grid, irrespective of the load being increased in 24 hours. The additional demand is being stabilized to a limit of around 4KW with the help of the proposed EMS.

The controller is mainly responsible for balancing the power taken from the grid by using energy being stored in the ESSs. The proposed Energy Management System Successfully reduces the demand on the grid within the predicted range (4KW) as shown in Fig. 7(b), reducing the load on the grid, reducing the prices, and prolonging the lifespan of the critical devices in the grid.

A fall in the SoC levels of LA-Battery and SC has also been noticed, proving the fact that the ESS power is being utilized. For the period, when the load demand is less than the grid capacity, the EMS directs the additional power to recharge the ESS. In the Lead-Acid Battery, for a duration of t=0.00 to t=5.10; t=8.75 to t=14.15; t=16.58 to t=16.96 and t=23.65 to t=0.00 a rise in SoC level has been noticed confirming the recharge of the battery. Whereas, in the case of SC, no rise in SoC has been observed as the ESSs are recharged only if the SoC is below 90%.

The graphs show a remarkable improvement in grid system after the implementation of localized ESSs. The use of Fuzzy Logic Systems has made the system more reliable and functional.

5. CONCLUSION

In this paper, a new Fuzzy Logic based Energy Management has been developed and proposed for a HESS connected microgrid. It is exhibited that the presented EMS is dependable and ensures continuous power supply without increasing power draw from the grid irrespective of the load demand. Stable DC bus voltage, maintained SoCs of the ESS, smooth transition between charging and discharging modes and fast response are a few other pros of the proposed EMS that have been observed. Simulation of the model has been carried

out in MATLAB/Simulink. Results with varying values of loads and smooth transition between modes prove the effectiveness of the proposed EMS.

REFERENCES

[1] P. Wang, J. Xiao, L. Setyawan, C. Jin, and C. F. Hoong, "Hierarchical control of active hybrid energy storage system (HESS) in DC microgrids," in *Proceedings of the 2014 9th IEEE Conference on Industrial Electronics and Applications, ICIEA 2014*, 2014, pp. 569–574. doi: 10.1109/ICIEA.2014.6931229.

[2] M. C. Romer, G. H. Miley, N. Luo, and R. J. Gimlin, "Ragone plot comparison of radioisotope cells and the direct sodium borohydride/hydrogen peroxide fuel cell with chemical batteries," *IEEE Trans. Energy Convers.*, vol. 23, no. 1, pp. 171–178, 2008, doi: 10.1109/TEC.2007.914159.

[3] K. A. Khan and M. Khalid, "Improving the Transient Response of Hybrid Energy Storage System for Voltage Stability in DC Microgrids Using an Autonomous Control Strategy," *IEEE Access*, vol. 9, pp. 10460–10472, 2021, doi: 10.1109/ACCESS.2021.3051144.

[4] A. J. Abianeh and F. Ferdowsi, "Sliding Mode Control Enabled Hybrid Energy Storage System for Islanded DC Microgrids with Pulsing Loads," *Sustain. Cities Soc.*, vol. 73, 2021, doi: 10.1016/j.scs.2021.103117.

[5] A. Jani, H. Karimi, and S. Jadid, "Hybrid energy management for islanded networked microgrids considering battery energy storage and wasted energy," *J. Energy Storage*, vol. 40, 2021, doi: 10.1016/j.est.2021.102700.

[6] P. Singh and J. S. Lather, "Power management and control of a grid-independent DC microgrid with hybrid energy storage system," *Sustain. Energy Technol. Assessments*, vol. 43, 2021, doi: 10.1016/j.seta.2020.100924.

[7] L. Roine, K. Therani, Y. Sahraei Manjili, and M. Jamshidi, "Microgrid energy management system using fuzzy logic control," in *World Automation Congress Proceedings*, 2014, pp. 462–467. doi: 10.1109/WAC.2014.6936001.

[8] D. Arcos-Aviles, J. Pascual, L. Marroyo, P. Sanchis, and F. Guinjoan, "Fuzzy logic-based energy management system design for residential grid-connected microgrids," *IEEE Trans. Smart Grid*, vol. 9, no. 2, pp. 530–543, 2018, doi: 10.1109/TSG.2016.2555245.

[9] X. D. Sun, K. H. Koh, B. G. Yu, and M. Matsui, "Fuzzy-logic-based V/f control of an induction motor for a DC grid power-leveling system using flywheel energy storage equipment," *IEEE Trans. Ind. Electron.*, vol. 56, no. 8, pp. 3161–3168, 2009, doi: 10.1109/TIE.2009.2021679.

[10] S. Zhang, Y. Mishra, and M. Shahidehpour, "Fuzzy-Logic Based Frequency Controller for Wind Farms Augmented with Energy Storage Systems," *IEEE Trans. Power Syst.*, vol. 31, no. 2, pp. 1595–1603, 2016, doi: 10.1109/TPWRS.2015.2432113.

[11] H. Shao, Y. Wang, H. M. Li, L. D. Qin, and H. S. Zhao, "A Novel Design of Fuzzy Logic Control Algorithm for Hybrid Energy Storage System," 2018. doi: 10.1109/EI2.2018.8582002.

[12] B. P. Singh, A. Dubey, N. K. Verma, and S. Chakrabarti, "Modeling and simulation of fuzzy expert system for mitigation of power fluctuation in AC-DC hybrid microgrid connected to a distribution network," 2020. doi: 10.1109/NPSC49263.2020.9331857.

[13] S. T. Kim, S. H. Bae, Y. C. Kang, and J. W. Park, "Energy Management Based on the Photovoltaic HPCS With an Energy Storage Device," *IEEE Trans. Ind. Electron.*, vol. 62, no. 7, pp. 4608–4617, 2015, doi: 10.1109/TIE.2014.2370941.

[14] Z. Cabrane, M. Ouassaid, and M. Maaroufi, "Battery and supercapacitor for photovoltaic energy storage: A fuzzy logic management," *IET Renew. Power Gener.*, vol. 11, no. 8, pp. 1157–1165, 2017, doi: 10.1049/iet-rpg.2016.0455.

[15] T. N. Reddy, M. K. Mishra, and S. Srinivas, "Grid interactive combined supercapacitor/battery energy storage system with power quality features," in *Proceedings of the IEEE International Conference on Industrial Technology*, 2015, vol. 2015-June, no. June, pp. 2600–2605. doi: 10.1109/ICIT.2015.7125481.

[16] T. T. Teo, T. Logenthiran, W. L. Woo, and K. Abidi, "Fuzzy logic control of energy storage system in microgrid operation," in *IEEE PES Innovative Smart Grid Technologies Conference Europe*, 2016, pp. 65–70. doi: 10.1109/ISGT-Asia.2016.7796362.

Biographies

Arnab Jana is currently an Undergraduate student at SRM Institute of Science and Technology, Kattankulathur, Tamil Nadu. He is pursuing his Bachelor in Technology in the field of Electronics and Communication engineering. He is deeply interested in the field of Microgrids and Smart Systems. His research interests are Power Electronics, Electronics devices, and Fuzzy Logic.

Sukanya Roy is currently an Undergraduate student at SRM Institute of Science and Technology, Kattankulathur, Tamil Nadu. She is pursuing her Bachelor in Technology in the field of Electronics and Communication engineering. She is interested in Electromagnetic theory and Smart Sensors. Her research interests are Smart System Management, Power Electronics, and Digital Electronics.

Dr. Damodar Panigrahy had received his PhD degree in Electrical Engineering from the NIT, Rourkela, in 2018. He is presently working as assistant professor in electronics and communication engineering department, SRM Institute of Science & Technology, Kattankulathur, Tamil Nadu. His research area is FPGA programming and biomedical signal processing.

Energy Optimization of High Concentration Fly Ash Slurry Disposal through Pipelines in Laminar Regime

[1]Ankit Prakash[*], [2]Y.S.A. Venkataram, [3]Kuldeep Singh, [4]Anubhav Rawat,

[5]Ashutosh Kumar Upadhyay

[1,2,4,5]Department of Applied Mechanics, Motilal Nehru National Institute of Technology Allahabad, Prayagraj, UP, India

[3] Gas Turbine and Transmissions Research Centre, University of Nottingham, Nottingham,UK

**ankit.prakash.994@gmail.com, venkataram1997@gmail.com, kuldeepdagar@gmail.com, anubhav-r@mnnit.ac.in, ashutosh@mnnit.ac.in*

Abstract

Safe disposal of coal ash is a major concern for the thermal power industry, as the coal ash is to be transported to ash pond, which are situated at some distance from the ash generation unit. It can be transported through various modes of transport viz. trucks, trolleys including the pipeline transportation in slurry convey mode. As the energy required for transportation of coal ash with the help of hydraulic conveying is substantially less in comparison to other transportation modes, present study has been focussed on the optimization of power requirement for the transportation of high concentration coal ash slurry disposal (HCSD) system under laminar flow regime. In current work various parameters like pipe diameter, flow velocity and solid weight concentration have been considered to evaluate their effect on the optimum energy requirement (specific) for slurry transportation using computational Fluid Dynamics (CFD) in laminar regime, with the help of commercially available CFD software Ansys FLUENT 16. It is found that the effect of the selected parameters is substantial.

Keywords. Slurry flow, Bingham plastic fluid, specific energy consumption, CFD

1. INTRODUCTION

The demand of energy is increasing day by day in today's modern world, which is fulfilled through renewable and non-renewable source of energy. Although there are many advantages of renewable energies both in terms of environment protection and their ease of handling, their high initial cost makes it unaffordable to many countries like India and they have to depend more on non-renewable sources of energy including coal based thermal power. The major challenge in such thermal systems is its residue which is fly ash. Although the utilization of ash been substantially increased in last decade, still tonnes of ash needs to be transported to the dumping sites/Ash ponds including their pipeline transportation to the nearby utilization industries like brick manufacturing plants etc. Among various transportation modes pipeline transportation of coal ash is more prevalent due to its low

operating cost and less wear to the pipeline systems. That too the energy required for high concentration slurry transportation is lesser in comparison to low concentration slurry [1].

The slurry transportation can be classified into three types: low (5-20% approx.), medium (20-45% approx.), and high (50-70% approx.) (all concentrations mentioned are in terms of by weight) [2]. High concentration slurry behaves like Bingham plastic fluid and its rheological behaviour may be modelled as Herschel-Bulkley model [3]. Based on the available rheological data fly ash slurry could be suitably modelled using Bingham plastic fluid having concentration by weight in the range of 40-70% [4]. Pressure drop, for high concentration fly ash slurry can be accurately evaluated using CFD for both laminar and turbulent flow regime for the calculation of friction factor along with the effect of particle size on head loss [5-7]. The energy required for the transportation of both fine and coarse particle will be less when the ratio between fine and coarse particle is not more than 30% also the particle size ratio will be in the range of 4:1 to 3:2 [8,9]. There are many other studies available in literature which generally relates to very limited aspects of slurry transportation that too without giving due weightage to flow regime of the slurry [10-14]

Therefore, the objective of the current study is set to optimize the energy requirement for the high concentration slurry transportation with respect to various operating parameters viz. pipe diameter (D), flow velocity (V) and solid weight concentration (C_w), with the help of commercially available CFD tool ANSYS FLUENT 16, in laminar regime. The current study mainly focuses on the energy consumed for high concentration slurry disposal systems which is calculated in terms of Specific Energy Consumption (SEC) [15]. It is the amount of energy required for the transportation of unit mass to a unit distance and is given as

$$SEC = \frac{2.726\ X\ i}{C\ X\ \delta_S} \tag{1}$$

Where, i = hydraulic gradients of slurry (mm W/m),

C = Volumetric concentration of slurry (%),

δ_s = Specific gravity of solids

SEC is expressed in kW.h/t.km.

2. COMPUTATIONAL METHODOLOGY

Following are the various step wise computational strategies adopted in current work.

2.1. Geometry

In the current work, the study is of conducted for different pipe geometries having pipe sizes 75 mm, 100 mm, 125 mm, 150 mm, and 200 mm and pipe lengths of 6, 8, 8, 9, and 12m respectively. Figure 1 shows the straight pipe considered for computational study having variable diameter and length. For structured meshing the shown pipe is divided into five parts where the inner square is of dimension a, where a = 0.2D (D = pipe diameter). The solid cylinder is representing the fluid (slurry) domain used for computational study. The

shown geometry is drawn in Design Modular, of a commercially available CFD software, ANSYS Fluent 16.

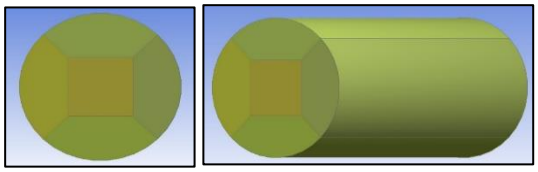

Figure 1. Cross-section and profile view of the cylindrical pipe

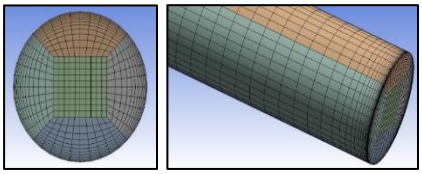

Figure 2. Cross-sectional and profile view of meshing

2.2. Meshing

Once the geometry i.e., computational domain is modelled, it is then discretized into small grids, known as elements. A structured hexahedral mesh is generated, using multizone mesh method as shown in figure 2. Edge sizing is used to control the number of elements. Inflation layer is used to capture the wall phenomenon by keeping the Y+ value equal to 1, for finding the first layer height. The governing equations are solved for each element.

2.3. Boundary conditions, solution controls, and slurry properties

For the present study the boundary condition taken into consideration are Inlet: the flow velocity Outlet: the outflow, wall: no slip having wall roughness as constant.

The first order upwind scheme is used for discretization, whereas the under-relaxation parameters are set to the default values.

The slurry rheological properties changes with respect to change in particle size, and concentrations. The slurry experimental properties are taken from Rawat et al. [16] as shown in Table 1 where displayed values are used for simulation.

Table 1 Rheological properties of slurry having d_{wm}=34.5 µm [16]

Sl. No.	**C_w (% by weight)**	**Density (kg/m^3)**	**Yield Stress (Pa)**	**Bingham Viscosity (Pa.s)**
1	55	1394.72	0.173	0.007
2	60	1446.63	0.317	0.0136
3	62	1468.49	0.484	0.0282
4	65	1502.63	0.736	0.0502
5	68	1538.23	1.6730.	0.1388

Table 2 Particle size Distribution (PSD)

Size (µm)	300	200	100	74	53	43	38	25	18	13	9	7	5	3
PSD (%)	100	97.8	88.9	84.4	75.1	69.1	67.2	53.6	45.8	36.1	24.4	16.7	7	3.1

2.4. Models and governing equations

From literature review it is clear that High concentration slurry flow behaves like homogeneous Bingham plastic fluid and can be modelled using Herschel-Bulkley equation. The current study is conducted for laminar flow regime and thus the governing equation are the continuity and momentum equation and are written in equation 2 and 3 below respectively.

$$\nabla.(\rho\vec{v}) = 0 \tag{2}$$

$$\nabla.(\rho\vec{v}\vec{v}) = -\nabla p + \nabla.(\tau) + \rho g \tag{3}$$

where, ρ is density, p is static pressure, and τ is stress tensor. The rheological equation for the Bingham plastic fluid can be written as

$$\tau = \tau_o + \mu_B D \tag{4}$$

where μ_B is Bingham viscosity, τ_o is yield stress and $D = (\frac{\partial U_j}{\partial x_i} + \frac{\partial U_i}{\partial x_j})$.

2.5. Grid Independency Test (GIT) and Validation

For the selection of optimum mesh, the GIT for 75 mm diameter pipe is shown in Fig. 3. It is observed from Fig. 3 that after the mesh M* (having 2.88 x 10^5 elements) there is no substantial change in the values of pressure drop and therefore M* is selected as the optimum mesh for the current study. Similarly, GIT is done for all pipes having diameter 75 mm to 200 mm.

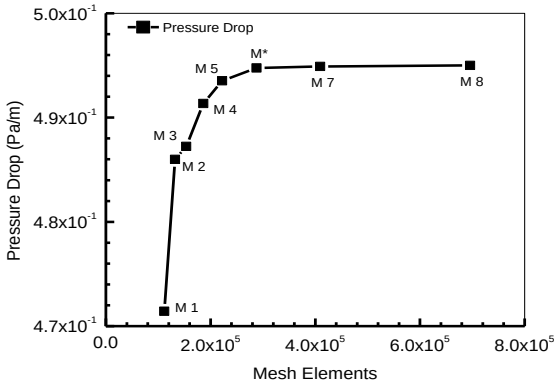

Figure 3 Pressure Drop vs No. of Mesh elements
for pipe diameter, D=0.075m

For validation the pressure drop obtained computationally is compared with the pressure drop obtained from experimental data and Buckingham-Reiner equation. Both the obtained results show close precision having very less deviation within the acceptable limits of ±1%.

3. RESULTS AND DISCUSSIONS

Various results obtained are discussed in the subsequent sections.

3.1. Effect of solid concentration on energy consumption (specific)

A graph between SEC and solid concentration (by weight) (C_w) of fly ash particles is shown in Fig. 4. Fig. 4 (a) shows that for constant Pipe diameter, the amount of energy consumed increases non-linearly with the increase in C_w for a fixed velocity. Whereas, the increase in velocity causes a related increase in energy. Fig. 4(b) depicts that the SEC increases non-linearly with the increases in C_w for a fixed pipe diameter at constant velocity. The figure also reveals that the value of SEC reduces with the increase in pipe size at a constant velocity of flow.

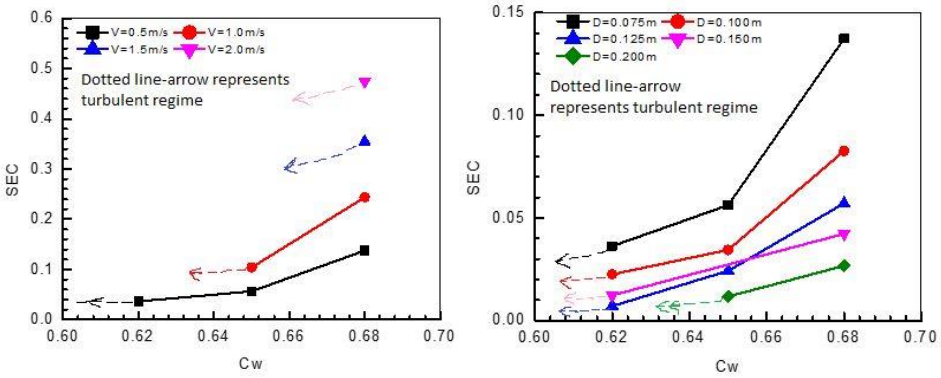

(a) D = 0.075m

(b) V = 0.5m/s

Figure 4 SEC vs C_w

3.2. Effect of Pipe Diameter on energy consumption (specific)

Ash shown in Fig. 5 (a) with the increase in pipe diameter the specific energy consumption will decrease at constant velocity for a given C_w. Whereas, the increase in C_w causes a related increase in SEC values. Fig. 5 (b) depicts that increment in Pipe diameter causes a decrement in SEC at constant flow velocity and given C_w. Whereas, the increase in flow velocity for a given C_w brings a related increment in the values of SEC. This can be explained based on the fact that pressure drop is inversely proportional to the pipe diameter, whereas the SEC is directly proportional to the pressure drop. Thus with the increase in pipe diameter the pressure drop decreases which in turn causes a lesser corresponding value of the SEC.

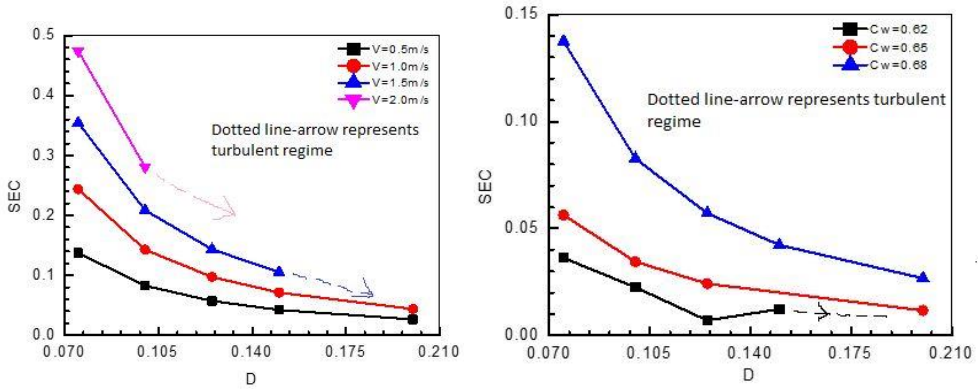

(a) C_w = 0.68 (b) V = 0.5m/s

Figure 5 SEC vs D

3.3. Effect of flow velocity on energy consumption (specific)

In this section the effect of flow velocity on SEC is evaluated with respect to constant pipe size and C_w values. Fig. 6(a) revels that for constant Pipe sizes the SEC increases almost linearly with respect to flow velocity for a given C_w. Whereas, a related increase in flow velocity for a given pipe size brings a related increment. Similar effect is seen in Figure 6 (b) where variation of SEC w.r.t. slurry flow velocity is seen at fixed C_w and given pipe size.

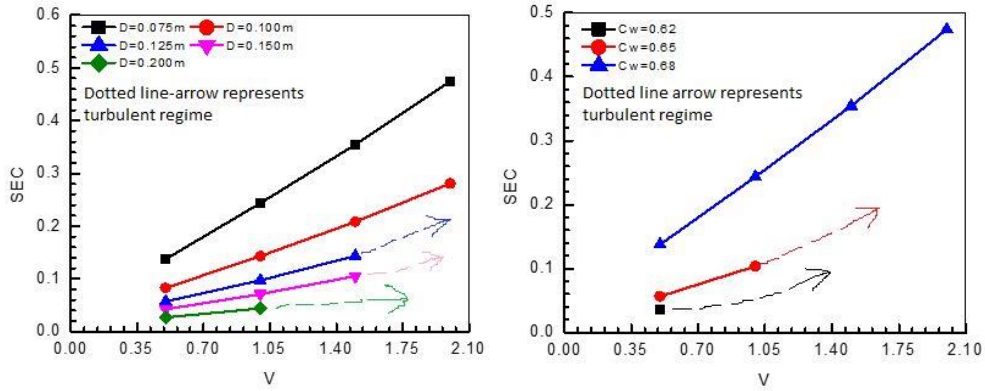

(a) C_w= 0.68 (b) D = 0.075m

Figure 6 SEC vs V

4. CONCLUSIONS

The current study i.e., optimization of HCSD flow in laminar regime by using computational method is taken up with the help of commercially available CFD tool Ansys FLUENT 16.

Herschel-Bulkley model is used for modelling of the rheological properties of HSCD system whereas the viscous model is set to be laminar. The effect of various operating parameters like flow velocity, pipe diameter, and concentration (by weight) on the energy required (specific) is studied. The following conclusion may be drawn out of the study for the flow of high concentration fly ash slurries through pipelines in laminar regime:

- With the increase in concentration and flow velocity, the SEC increases non-linearly.
- With the increase in pipe diameter, the SEC decreases non-linearly.

REFERENCES

[1] Kaushal DR, Navneet K. Optimum design of high concentration fly ash slurry disposal pipeline. Electronic Journal of Polish Agricultural Universities. 2013;16(4).

[2] Rawat A, Singh SN, Seshadri V. Computational methodology for determination of head loss in both laminar and turbulent regimes for the flow of high concentration coal ash slurries through pipeline. Particulate Science and Technology. 2016 May 3;34(3):289-300.

[3] Singh MK, Ratha D, Kumar S, Kumar D. Influence of particle-size distribution and temperature on rheological behavior of coal slurry. International Journal of Coal Preparation and Utilization. 2016 Jan 2;36(1):44-54.

[4] Verma AK, Singh SN, Seshadri V. Pressure drop prediction for the flow of fly ash slurries through pipes at high concentrations. International Journal of Fluid Mechanics Research. 2010;37(4).

[5] Rawat A, Singh SN, Seshadri V. Computational methodology for determination of head loss in both laminar and turbulent regimes for the flow of high concentration coal ash slurries through pipeline. Particulate Science and Technology. 2016 May 3;34(3):289-300.

[6] Rawat A, Singh SN, Seshadri V. Variation of physical and rheological properties of fly ash slurries with particle size and its effect on hydraulic transportation at high concentrations. Particulate Science and Technology. 2019 Feb 17;37(2):151-60.

[7] Rawat A, Singh SN, Seshadri V. Computational investigation on the flow of high concentration fly ash slurries through converging-diverging bends. International Journal of Coal Preparation and Utilization. 2019 Jul 15:1-21.

[8] Mishra R, Singh S, Seshadri V. Velocity distribution in horizontal pipes conveying non-uniform particles. International Journal of Fluid Mechanics Research. 2002;29(6).

[9] Kumar U, Mishra R, Singh SN, Seshadri V. Effect of particle gradation on flow characteristics of ash disposal pipelines. Powder technology. 2003 May 29;132(1):39-51.

[10] Hashemi SA, Wilson KC, Sanders RS. Specific energy consumption and optimum operating condition for coarse-particle slurries. Powder technology. 2014 Aug 1;262:183-7.

[11] Hegde R. Specific Energy Consumption (SEC) for pipeline transport of liquid CO 2 slurries. University of Alberta (Canada); 2013.

[12] Singh MK, Kumar S, Ratha D, Kaur H. Design of slurry transportation pipeline for the flow of muti-particulate coal ash suspension. International journal of hydrogen energy. 2017 Jul 27;42(30):19135-8.

[13] Wu J, Graham L, Wang S, Parthasarathy R. Energy efficient slurry holding and transport. Minerals Engineering. 2010 Aug 1;23(9):705-12.

[14] Li M, He Y, Jiang R, Zhang J, Zhang H, Liu W, Liu Y. Analysis of minimum specific energy consumption and optimal transport concentration of slurry pipeline transport systems. Particuology. 2022 Jul 1;66:38-47.

[15] Seitshiro I, Sato I, Sato H. Verification and Application of Design Model for Settling Slurry Transport in Pipes. International Journal of the Society of Materials Engineering for Resources. 2012;18(2):44-50.

[16] Rawat A, Singh SN, Seshadri V. CFD analysis of the performance of elbow-meter with high concentration coal ash slurries. Flow Measurement and Instrumentation. 2020 Apr 1;72:101724.

Biographies

Ankit Prakash received the bachelor's degree in mechanical engineering from IIST-Indore in 2017, the master's degree in fluids engineering from MNNIT Allahabad in 2021, respectively. He is currently pursuing Ph.D. at the Department of Applied Mechanics, MNNIT Allahabad.

Y.S.A. Venkataram received the bachelor's degree in mechanical engineering from GMRIT-Vizianagaram in 2019 and currently pursuing master's degree in fluids engineering from MNNIT Allahabad respectively.

Dr. Kuldeep Singh received the master's and Ph.D. degree in mechanical engineering from IIT-New Delhi in 2011 and 2016 respectively. He is currently working as a senior CFD research fellow at Nottingham university. His research areas include mechanical, aeronautical and aerospace engineering.

Dr. Anubhav Rawat received his master’s degree in pipeline engineering from UPES Dehradun and Ph.D. degree in fluids engineering from IIT- New Delhi in 2010 and 2016 respectively. He currently working as an assistant professor at Applied Mechanics Department at MNNIT Allahabad. His research areas include multiphase flows, CFD, fluid mechanics, complex fluids, Bio fluids, machine learning in fluids and energy engineering.

Dr. Ashutosh kr. Upadhyay received his master’s and Ph.D. degree in applied mechanics from MNNIT Allahabad. He is currently working as an associate professor at Applied Mechanics Department at MNNIT Allahabad. His research areas include composite structures, impact mechanics, vehicle crashworthiness, energy absorbers.

A Novel Design of Low Power and High Speed 1-Bit and 4-Bit Magnitude Comparator

[1]Yasmine Begum. A, [2]M. Balaji, [3]M. Tharun Kumar Reddy, [4]G. Namratha

Sree Vidyanikethan Engineering College, Tirupati, India

[1]anwaralyyasmine@gmail.com,[2]balajichaitra3@gmail.com,

[3]tharunmallela143@gmail.com, [4]namrathanaidu12@gmail.com

Abstract

In order to boost speed, reduce space for compactness, and minimise power consumption, numerous innovative circuit designs must be developed. Comparators are a fundamental design module that can be used in VLSI, digital signal processors, and data processing application-specific integrated circuits. In this research, we suggested four distinct models of one-bit comparators and used model-4 to develop a four-bit comparator. The performance of these four different comparators was compared to that of an existing comparator, and it was determined that the proposed model 4 outperforms the existing comparator in terms of speed, power consumption, and area. The DSCH-3.1 software programme is used to develop and simulate the schematics. Then, using Microwind 3.1 software, they simulated Verilog files and examined the performance of different design comparators at 90nm and 120nm technologies. From the results we can conclude that designing a magnitude comparator using proposed model 4 design style we can reduce all parameters of transistor count, logic gates count, power consumption and delay by 30%, 40%, 58.38%, 38.688 % respectively for 1 bit comparator and 19.5%, 14.05%, 13.21%, 28.088% respectively for four-bit comparator.

Keywords. Magnitude Comparator, Area, Power Consumption, Delay, VerilogHDL

1. INTRODUCTION

The magnitude of two binary values, say X and Y, is compared using a digital magnitude comparator, which is a logic circuit. As depicted in Figure 1, the logic circuit will have three outputs that indicate if XY, X=Y, or X>Y is true. Table-1 depicts the truth table.

Conventional comparator consumes more area and delay due to it requires more transistors in CMOS design. In CMOS AND gate itself requires 6 MOS transistors and NOR requires 4 MOS transistors. Conventional one magnitude comparator requires 2 NOT, 2 AND and 1 NOR gate shown in Figure 2. All it takes 20 MOS transistors to implement in CMOS design. In a 4-bit magnitude comparator shown in Figure 3 have two binary numbers in which each of the binary number consists of four bits. The logic circuit of Four Bit Comparator consists of 8 NOT gates, 23 two input AND gates and 6 two input OR gates4 two input NOR gates. Here also we have three outputs X<Y, X=Y and X>Y. It requires 178 MOS transistors to implement in CMOS [1- 2].

Previously described works have been focused on designing comparator in transistor level using different design techniques. In this paper comparator is designed using 2 NOR gates and 1 XNOR gate where it requires only 14 MOS transistors to implement it in CMOS. This makes circuit simple, less area, low power and less delay. Using proposed model 4 designed four-bit comparator then simulated and compared results with existing comparator in both 90nm and 120nm technologies [3- 4].

The paper is organized as follows. The section 2 clearly explained different models of one bit magnitude comparator. This section clearly explains the designing of all four proposed models 1, 2, 3 and 4 and redundant Boolean expressions for every model and their logic diagrams. Simulation results of one bit and four-bit existing magnitude comparator and proposed model-4 comparator in 90nm and 120nm technologies are analyzed and discussed in Section 3. And finally, Section 4 concludes that designing a magnitude comparator using proposed model-4 have better performances than existing magnitude comparator.

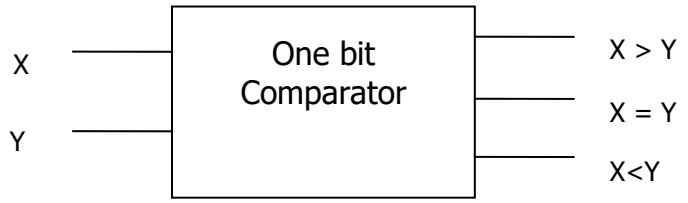

Figure 1. Block of one-bit Magnitude Comparator

Table1: Truth Table of one- Bit Magnitude Comparator

Input		Output		
X	Y	F (X>Y)	F (X=Y)	F (X<Y)
0	0	0	1	0
0	1	0	0	1
1	0	1	0	0
1	1	0	1	0

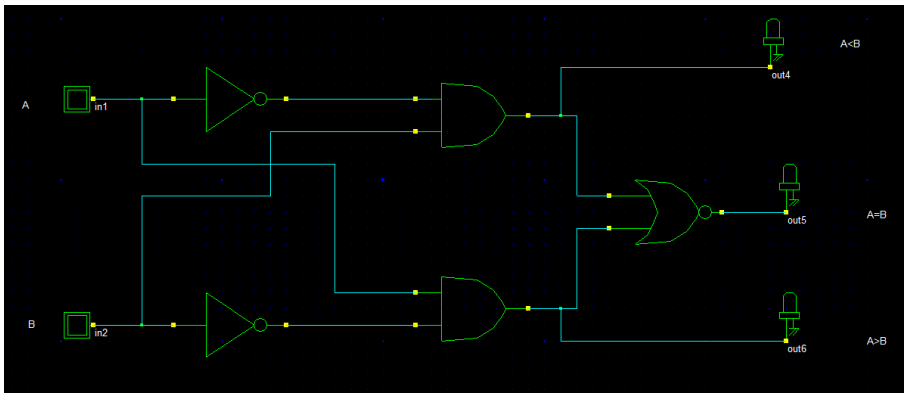

Figure 2. Implementation of existing one-bit Magnitude comparator

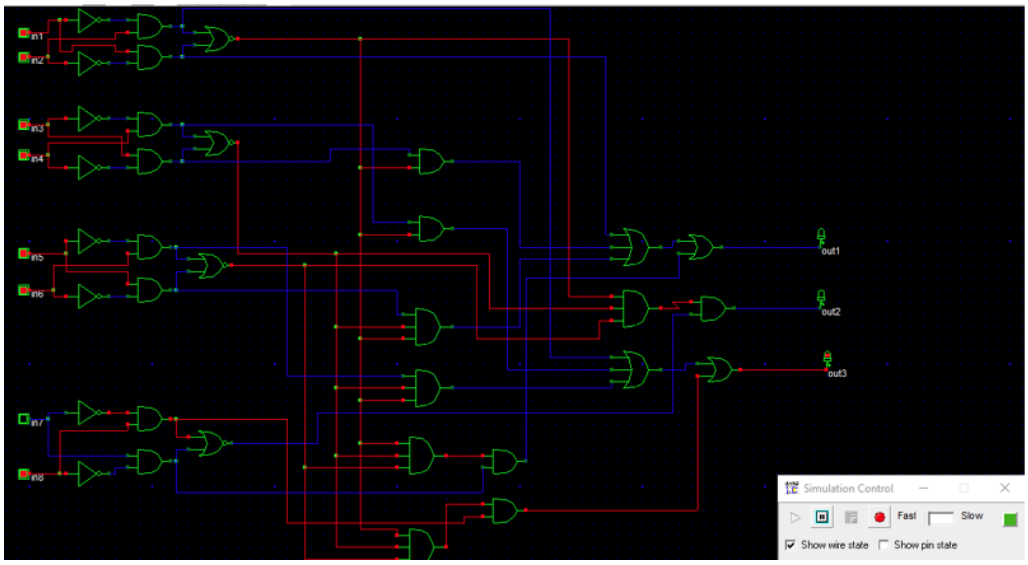

Figure 3. Implementation of existing 4-bit Magnitude comparator

2. PROPOSED MODELS

The proposed models are designed in terms of logic gates. The first two proposed models are designed using half subtractor logic. The proposed model 3 is modified version of proposed model 2 where it reduces one gate compare to proposed model 2 and also with existing comparator. Proposed model 4 is designed only using one XNOR and two NOR gates, this model requires only 3 gates and this model have better performance interms of area, power, delay when compared with existing comparator and also all proposed models [5- 6].

2.1. Proposed Model -1

As said above this model is designed by using half subtractor logic. The truth table in Table-2 shows that borrow of half subtractor is high if and only if the input Y is greater than X. And also, the Difference of half subtractor is low if and only if the both inputs are similar. The compliment of difference output of half subtractor gives X equals to Y output. The outputs Difference and Borrow of half subtractor fed to XOR gate to get X greater than Y [7- 9].

By adding one XOR and one NOT gate to half subtractor one bit magnitude comparator is realized in proposed model-1 as shown in Figure 4.The logical expressions for every output is realized below. The difference output of Half Subtractor is given to a NOT gate to get X equals to Y. Difference and Borrow is given to a XOR gate to get X Greater than Y. And Borrow of Half Subtractor equals to X Less than Y. This Proposed model 1 needs 2 XOR gates, 2 NOT gates and 1 AND gate [9- 11].

Table2: Truth Table of Half Subtractor

Input		Output	
X	Y	Difference	Borrow
0	0	0	0
0	1	1	1
1	0	1	0
1	1	0	0

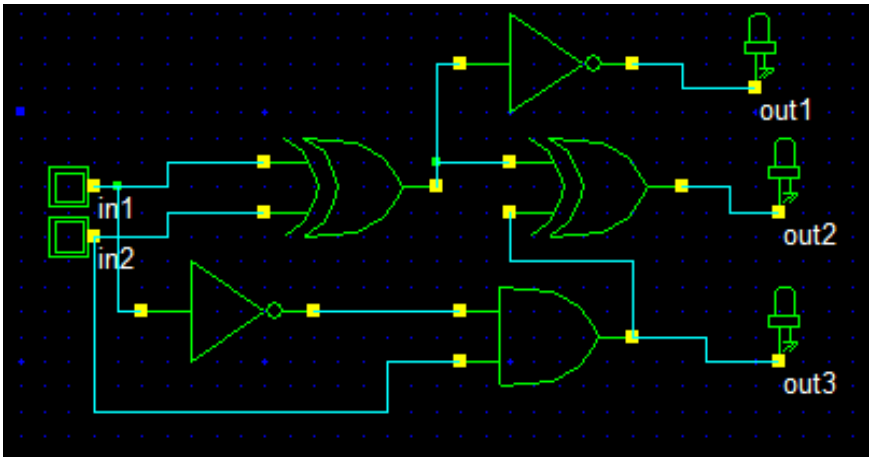

Figure 4. Implementation of Proposed-1one-bit Magnitude comparator

$$X<Y = \overline{X}Y$$

$$X = Y = \overline{\overline{X}Y + X\overline{Y}}$$

$$= \overline{\overline{X}Y}.\overline{X\overline{Y}}$$

$$= (X+\overline{Y})(\overline{X}+Y)$$

$$= XY + \overline{X}\overline{Y}$$

$$X > Y = (\overline{X}Y + X\overline{Y})\square\ (\overline{X}Y)$$

$$= (\overline{\overline{X}Y + X\overline{Y}}\ .X\overline{Y} + \overline{X\overline{Y}}\ )(\overline{X}Y + X\overline{Y})$$

$$= (XY+\overline{X}\overline{Y})X\overline{Y} + (X+\overline{Y})(\overline{X}Y + X\overline{Y}\ )$$

$$= X\overline{Y}$$

2.2. Proposed Model-2

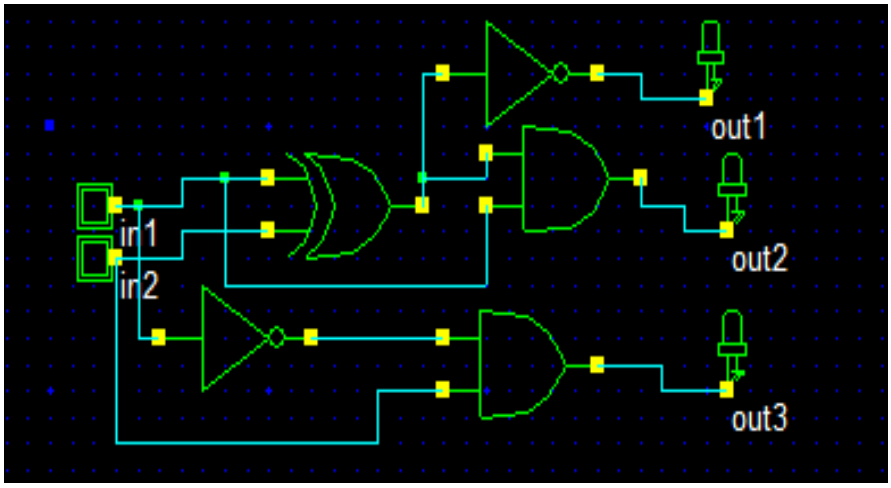

Figure 5. Implementation of Proposed-2 one-bit Magnitude comparator

The proposed model 2 shown in Figure 5 is a slight modification of proposed model-1 in Figure 4.This model is realized by replacing XOR gate by AND gate to get X greater than Y. The input X and difference output of half subtractor is given to AND gate to get X greater than Y. The logical expressions for every output is realized below. The difference of Half Subtractor is given to a NOT gate to get X equals to Y. Difference and input X is given to a AND gate to get X Greater than Y. And Borrow of Half Subtractor is equals to X Less than Y. This Proposed 2 model needs 2 AND gates, 2 NOT gates and 1 AND gate [12-15].

$$X<Y = \overline{X}Y$$

$$X = Y = \overline{\overline{X}Y + X\overline{Y}}$$

$$= \overline{\overline{X}Y}.\overline{X\overline{Y}}$$

$$= (X+\overline{Y})(\overline{X}+Y)$$

$$= XY + \overline{X}\overline{Y}$$

$$X>Y = (\overline{X}Y + X\overline{Y})A$$

$$= X\overline{Y}$$

2.3. Proposed Model-3

The proposed model 1, 2 and existing comparator have same number of logic gates. Proposed model-3 requires 4 logic gates shown in Figure 6.The output X greater than Y and the output X equals to Y both realization is similar to proposed model 2. In this model the input X and Difference output of Half Subtractor is given to AND gate to get X Less than Y. By modifying a circuit like this the number of gates required to design is reduced to 4 (as conventional comparator requires 5 gates).The logical expressions for every output is given below [16- 19].

The inputs X and Y are given to a XOR gate. The XOR output is given to a NOT gate to get X equals to Y. Input X and output of XOR is given to an AND gate to get X Greater than Y. Input B and output of XOR is given to an AND gate to get X Less than Y. This Proposed 3 model requires 2 AND gates, 1 NOT gate and 1 XOR gate [20- 22].

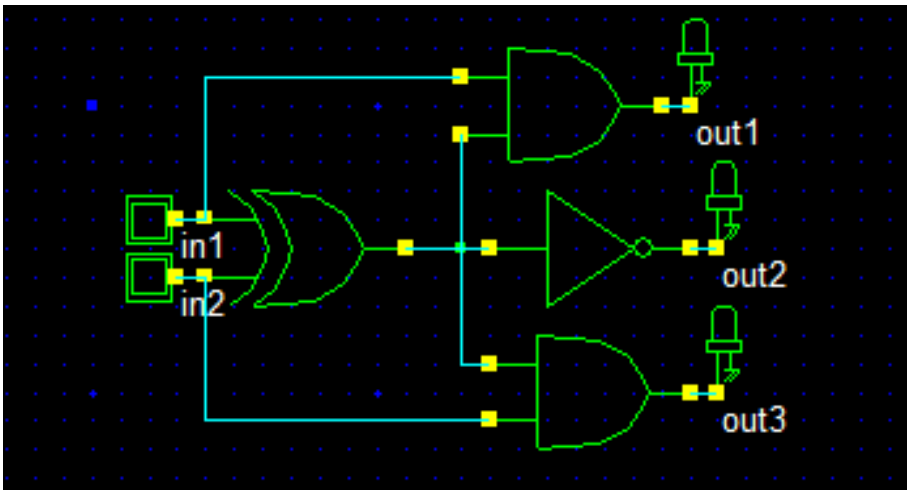

Figure 6. Implementation of Proposed-3 one-bit Magnitude comparator

$$X<Y = (\overline{X}Y + X\overline{Y})B$$

$$= \overline{X}Y$$

$$X = Y = \overline{\overline{X}Y + X\overline{Y}}$$

$$= \overline{\overline{X}Y}.\overline{X\overline{Y}}$$

$$= (X+\overline{Y})(\overline{X}+Y)$$

$$= XY + \overline{X}\overline{Y}$$

$$X>Y = (\overline{X}Y + X\overline{Y})X$$

$$= X\overline{Y}$$

2.4. Proposed Model-4

This model requires only 3 gates shown in Figure 7 and very simple to design and also the performance of this comparator is better interms of area, delay and power consumption compared to existing comparator. The input X and Y is given to XNOR gate to get X equals to Y output. The remaining two outputs are realized by using two NOR gates. To get X greater than Y output high the input Y and output of XNOR gate is given to NOR gate. The input X and output of XNOR gate is given as inputs to NOR gate to get X Less than Y. The logical expression for every output is given below [23-25]. The inputs X and Y is given to a XNOR to get X equals to Y. Input X and output of XNOR is given to a NOR gate to get X Greater than Y. Input A and output of XNOR is given to a NOR gate to get X Less than Y. This Proposed model-4 needs only XNOR gate and two NOR Gates [23-24].

$$\mathbf{X<Y} = \overline{XY + \overline{X\overline{Y}} + X}$$

$$= \overline{XY + \overline{X\overline{Y}}.\overline{X}}$$

$$=\overline{\overline{X\overline{Y}}}.\overline{XY}.\overline{X}$$

$$=(X+Y)(\overline{X}+\overline{Y})\overline{X}$$

$$=(\overline{X}Y)(\overline{X}+\overline{Y})$$

$$=\overline{X}Y$$

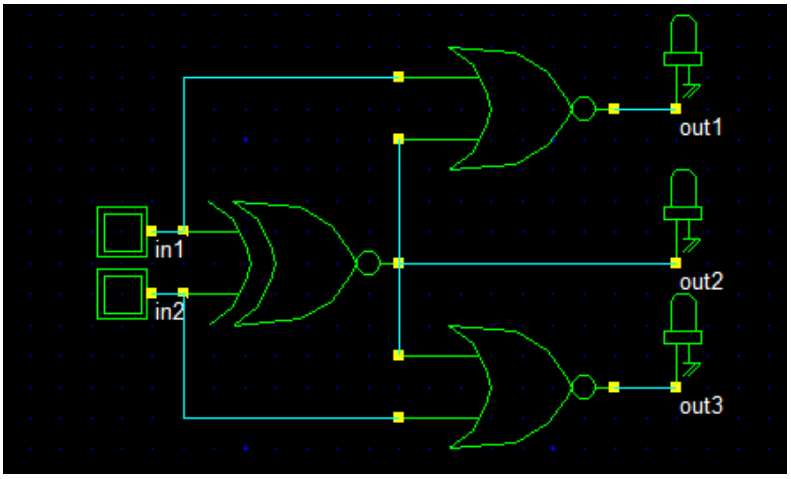

Figure 7. Implementation of Proposed Model-4 one-bit Magnitude comparator

$$X=Y = XY + \overline{XY}$$

$$X>Y = \overline{XY + \overline{X\overline{Y}} + Y}$$

$$= \overline{XY + \overline{XY}.\overline{Y}}$$

$$= \overline{\overline{XY}}.\overline{\overline{XY}}.\overline{Y}$$

$$= (X+Y)(\overline{X}+\overline{Y})\overline{Y}$$

$$= (X\overline{Y})(\overline{X}+\overline{Y}) = X\overline{Y}$$

3. RESULTS AND DISCUSSION

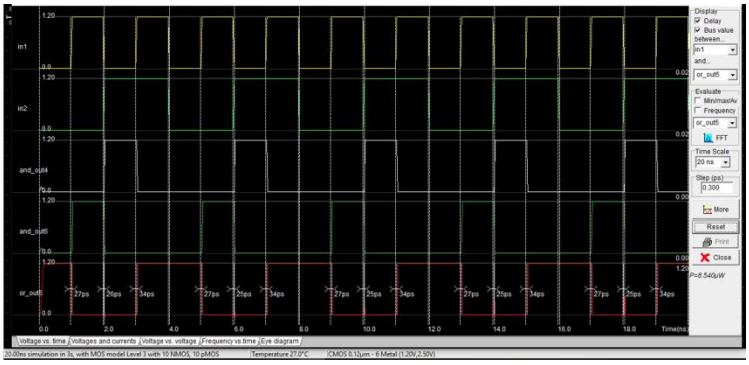

Figure 8. Timing Diagram of One Bit Comparator Existing Model in 120 nm Technology

The timing diagram shown in Figure 8 reveals that the average delay of existing one bit magnitude comparator is 25.7ps, power consumption 8.54µW and also it requires 20 transistors to implement in CMOS 120nm technology.

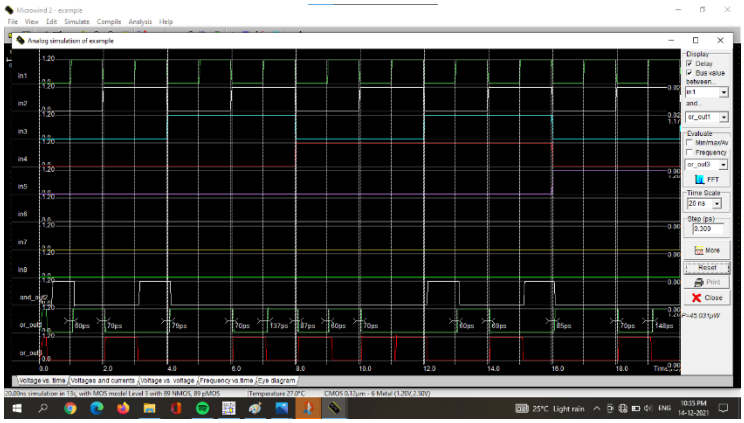

Figure 9. Timing Diagram of Four-Bit Comparator existing model in 120nm Technology.

The timing diagram shown in Figure 9 reveals that the average delay of existing four bit magnitude comparator is 117.83ps, power consumption is 45.03µW and it requires 178 transistors to implement in CMOS 120nm technology.

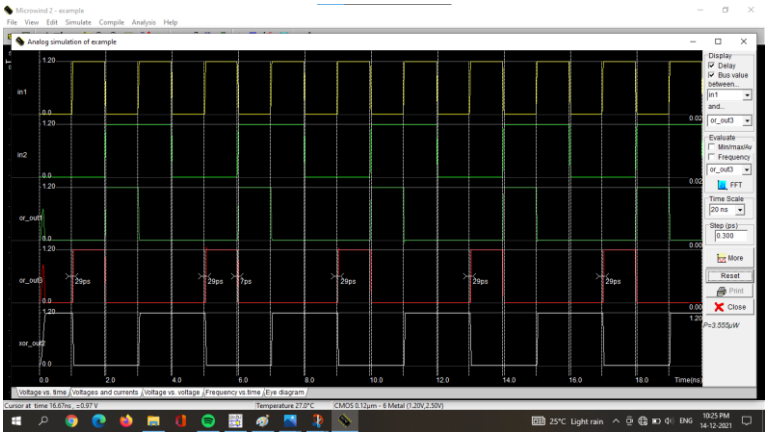

Figure 10. Timing Diagram of One Bit Comparator Proposed 4 Model in 120nm Technology

The timing diagram shown in Figure 10 reveals that the average delay of proposed model-4 one bit magnitude comparator is 15.5ps, power consumption is 3.55µW and it requires 14 transistors to implement in CMOS 120nm technology. The above results have better performance in terms of transistor count, power, delay than existing one bit magnitude comparator.

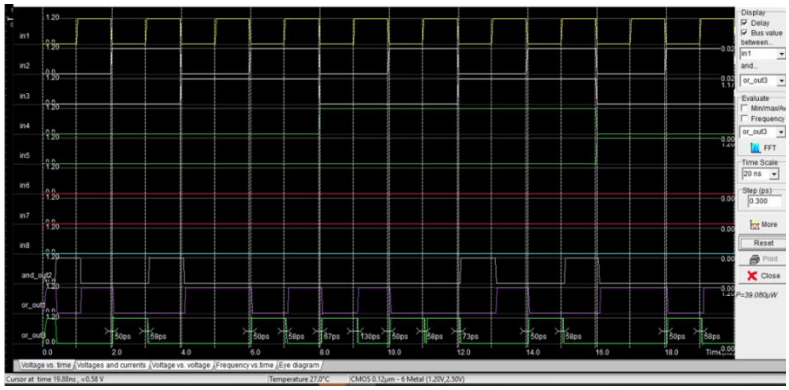

Figure 11 Timing Diagram of Four Bit Comparator proposed 4 Model in 120 nm Technology

The timing diagram shown in Figure 11 reveals that the average delay of proposed model-4 one bit magnitude comparator is 84.1ps, power consumption is 39.08µW and it requires 153 transistors to implement in CMOS 120nm technology. The above results have better performance interms of transistor count, power, delay than existing four-bit magnitude comparator.

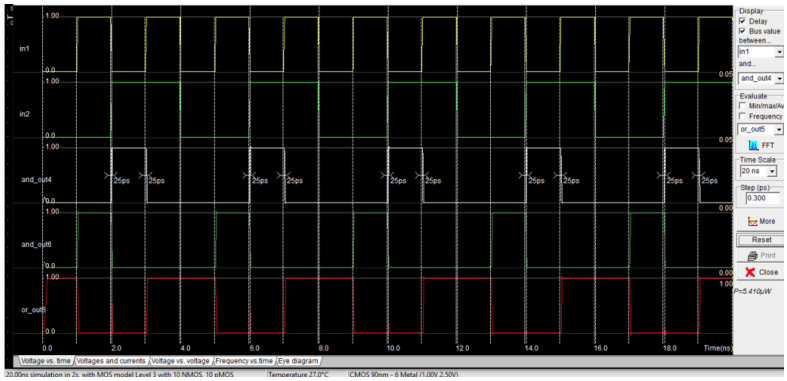

Figure 12. Timing Diagram of One Bit Comparator Existing Model in 90 nm Technology

The timing diagram shown in Figure 12 reveals that the average delay of existing one bit magnitude comparator is 23.16ps, power consumption 5.41µW and it requires 20 transistors to implement in CMOS 90nm technology.

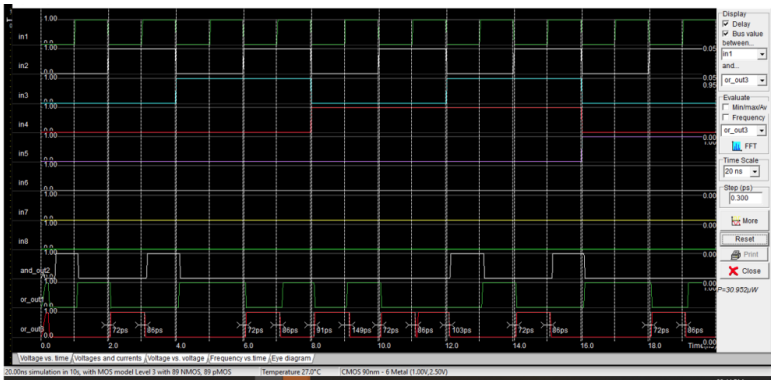

Figure 13. Timing Diagram of Four Bit Comparator Existing Model in 90 nm Technology

The timing diagram shown in Fig.13 reveals that the average delay of existing four bit magnitude comparator is 89.83ps, power consumption 30.95µW and it requires 178 transistors to implement in CMOS 90nm technology.

The timing diagram shown in Figure 14 reveals that the average delay of proposed model-4 one bit magnitude comparator is 14ps, power consumption is 2.37µW and it requires 14 transistors to implement in CMOS 90nm technology. The above results have better performance interms of transistor count, power, and delay than existing one bit magnitude comparator.

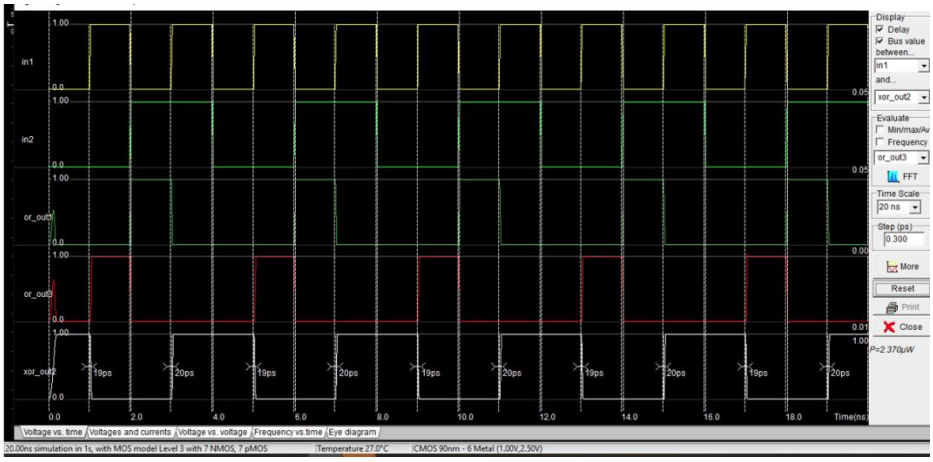

Figure 14. Timing Diagram of One Bit Comparator Proposed 4 Model in 90 nm Technology

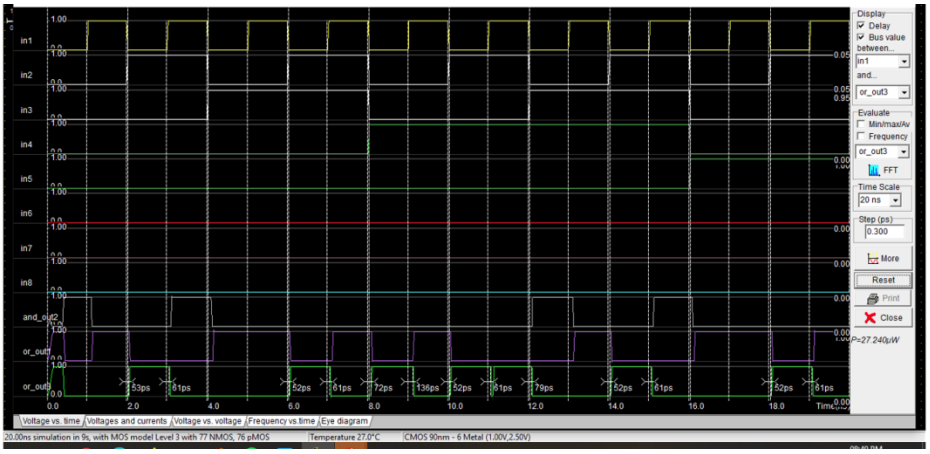

Figure 15. Timing Diagram of Four Bit Comparator Proposed 4 Model in 90 nm Technology

The timing diagram shown in Fig.15 reveals that the average delay of proposed model-4 four- bit magnitude comparator is 80.33ps, power consumption is 27.24µW and it requires 153 transistors to implement in CMOS 90nm technology. The above results have better performance interms of transistor count, power, delay than existing four- bit magnitude comparator.

The results shown in Table-3 and Table-4 shows that implementing proposed model-4 shown in Figure 7 in CMOS design have better performances in terms of transistor count, delay, power than the existing comparator in both 90nm and 120nm technologies. And also, it shows that implementing in 90nm technology have better results compared to 120nm technology.

Table 3. Comparison of one bit Magnitude Comparator with proposed model- 4 in 90nm and 120nm Technology

Technology used	**90nm**		**120nm**	
Parameters	**Existing Model**	**Proposed model- 4**	**Existing Model**	**Proposed model- 4**
No. of transistors	20	14	20	14
No. of logic gates	5	3	5	3
Power consumption (µW)	5.410	2.37	8.540	3.555
Delay (ps)	23.16	14	25.7	15.5

Table 4. Comparison of Four- bit Magnitude Comparator with proposed model- 4 in 90nm and 120nm Technology

Technology used	**90nm**		**120nm**	
Parameters	**Existing Model**	**Proposed model- 4**	**Existing Model**	**Proposed model- 4**
No. of transistors	178	153	178	153
No. of logic gates	41	33	41	33
Power consumption (µW)	30.952	27.240	45.031	39.080
Delay (ps)	89.83	80.33	117.83	84.1

4. CONCLUSION

The final results in terms of number of logic gates, transistor count, power consumption and delay have been obtained at 90nm and 120nm technologies. From the results designing a magnitude comparator using proposed model-4 design style reduce all parameters of transistor count, logic gates count, power consumption and delay of the comparator by 30% ,40%, 58.38%,38.688 % respectively for 1 bit comparator and 19.5%,14.05%,13.21%,28.088% respectively for four-bit comparator. And also implementing in 90nm technology have better performance than implementing in 120nm technology. All this simulation results have done in DSCH and microwind tools. Based on the following advantages in area, power and delay of the proposed model-4 magnitude comparator can be used for various applications such as scientific computations, VLSI designs, Test circuits etc. As per the results, the proposed model- 4 magnitude comparator is quite suitable for present day works.

REFERENCES

[1]. K. Ilamathi et al. 2021. “High-Speed And Area-Efficient 16, 64 -Bit Digital Comparator High-Speed and Area-Efficient 16, 64 -Bit Digital Comparator.” 12(11): 2649–61.

[2]. V. Satyanarayana, M. Balaji, M. & K. Neelima “Optimal of 1-bit Comparator design and Energy Estimation using Quantum Dot Cellular

Automata". International Journal of Engineering and Applied Physics, 1(2), 103-110, 2021

[3]. A. Sorwar et al. "Design of a High-Performance 2-Bit Magnitude Comparator Using Hybrid Logic Style." *2020 11th International Conference on Computing, Communication and Networking Technologies, ICCCNT 2020*: 2–6, 2020.

[4]. D. Bhaskara Rao, K. Geethanjali, and S. Babu Palli. 2020. "Design Of Hybrid Logic 4-Bit Comparator With Efficient Vlsi Design Constraints." 16(10): 478–86.

[5]. D., Bhaskara Rao et al. 2019. "Optimized VLSI Design of 2-Bit Magnitude Comparator Using GDI Technique." *International Journal of Recent Technology and Engineering* 7(6): 933–97.

[6]. D.M., Mahitha, G. Mohan, and K Aneesh. 2019. "A Novel Design of Hybrid 2 Bit Magnitude Comparator." (May): 8122–27.

[7]. H. Kishore. et al. 2018. "Area, Power and Delay Efficient 2-Bit Magnitude Comparator Using Modified Gdi Technique in Tanner 180nm Technology." *International Journal of Engineering and Technology(UAE)* 7(2.8 Special Issue 8): 222–26.

[8]. S. Chiwandea, M. L. Keote, Shilpa S. Katre, and Shruti H. Bhagwate. 2018. "VLSI Design of Low Power 4 Bit Magnitude Comparator Using GDI Technique." *SSRN Electronic Journal*: 224–28.

[9]. V. Krishna Boppana, N. V., and Saiyu Ren. 2016. "A Low-Power and Area-Efficient 64-Bit Digital Comparator." *Journal of Circuits, Systems and Computers* 25(12).

[10]. S. Tripathy, "Low Power, High Speed 8-Bit Magnitude Comparator in 45nm Technology for Signal Processing Application." *Indian Journal of Science and Technology* 8(1): 1–10, 2015

[11]. M. Balaji, and N. Padmaja, Design of Low Power Johnson Counter using Lector Technique Using 50nm Technology. Indian Journal of Public Health Research & Development, 9(11), 2018.

[12]. S. Rani, "Design and Analysis of Low Power 2-Bit and 4-Bit Digital Comparators in 45nm and 90nm CMOS Technologies." (5): 278–84, 2015.

[13]. K.C. Rout, S. Rath, and A. Belal. "Design of High Performance Magnitude Comparator." 3(25): 1–5, 2015.

[14]. R. Kumar. 2014 "Design of 8-Bit Comparator Using 45nm CMOS Technology." *Ijmer* 4(6): 59–64. http://www.ijmer.com/papers/Vol4_Issue6/Version-1/IJMER-46015964.pdf.

[15]. B Shruthi, K R Ashwini, "2-BIT MAGNITUDE COMPARATOR DESIGN USING DIFFERENT LOGIC STYLES", International Journal of Emerging Technologies and Innovative Research (www.jetir.org), ISSN:2349-5162, Vol.4, Issue 11, page no.113-117, November-2017, Available: http://www.jetir.org/papers/JETIR1711019.pdf

[16]. V. Shekhawat, T. Sharma, and K. G. Sharma. 2014. "Low Power Magnitude Comparator Circuit Design." *International Journal of Computer Applications* 94(1): 22–24.

[17]. G. Sharma, U. Nirmal, and Y. Misra. 2011. "A Low Power 8-Bit Magnitude Comparator with Small Transistor Count Using Hybrid PTL / CMOS Logic." *International Journal* 12(April): 110–15.

[18]. P., Kishore, Prof Prabhandhakam, and Sangameswara Raju. 1989. "An Implementation of 32 bit CMOS Comparator in Mentor EDA Tools" : 372–77.

[19]. D.N. Mukherjee, S. Panda, and B. Maji. 2021. "Design and Optimization of Reversible Logic Based Magnitude Comparator Using Gate Diffusion Input Technique." *IETE Journal of Research*. https://doi.org/10.1080/03772063.2021.1912658.
[20]. R.K. Mistri, R. Ranjan, A. Kumari Choudhari, and B. Kumari. 2017. "IC Layout Design of 4-Bit Magnitude Comparator Using Electric VLSI Design System." *IOSR Journal of VLSI and Signal Processing* 07(02): 67–73.
[21]. D. Kumar, and M. Kumar. 2017. "Design of Low Power Two Bit Magnitude Comparator Using Adiabatic Logic." *2016 International Symposium on Intelligent Signal Processing and Communication Systems, ISPACS 2016* (1): 3–8.
[22]. Reshma B Chougale, V. Agarwal "Design of Suitable Magnitude Comparator Architecture for Big Data Analytics." : 486–89.
[23]. S. Bhuvaneswari, and R Prabakaran. 2017. "Efficient Implementation of 2-Bit Magnitude Comparator Using PTL." 3: 140–44.
[24]. M. Aggarwal, and R. Mehra. 2015. "Performance Analysis of Magnitude Comparator Using Different Design Techniques." *International Journal of Computer Applications* 115(14): 12–15.

Biographies

Dr. A. Yasmine Begum is working as Associate Professor in the Department of Electronics and Instrumentation Engineering, SreeVidyanikethan Engineering College, A.Rangampet. She has completed Ph. D from Jawaharlal Nehru Technological University, Anantapur, Andhra Pradesh, India in the specialization on Process Control. Her Research Interests include Process Control, Sensors and Networks, Low power VLSI design.

M. Balaji completed the Bachelor's degree in Electronics and Communication Engineering in Sree Vidyanikethan Engineering College, Tirupati and M. Tech degree in Embedded Systems from Hasvitha Institute of Engineering and Technology, Jawaharlal Nehru Technological University, Hyderabad, India. He is pursuing Ph. D degree in Jawaharlal Nehru Technological University Anantapur, in the specialization of VLSI Signal Processing. His areas of interests are filter designs and DSP applications.

Mr. M. Tharun Kumar Reddy Pursuing Bachelor's degree in Electronics and Communication Engineering in SreeVidyanikethan Engineering College, Tirupati. His areas of interest are Digital VLSI Design and signal processing.

Ms. G. Namratha Pursuing Bachelor's degree in Electrical and Electronics Engineering in SreeVidyanikethan Engineering College, Tirupati. Her areas of interest are Digital Electronics and Power Electronics.

Categorization of Vaccine in Adolescent Implementing by the Chi − Square (χ^2) Test

[1]Rupa Rani Sharma*, [2]Paras Bhatnagar

[1,2]G. L. Bajaj Institute of Technology and Management, Greater Noida, UP, India

rupa.sharma@glbitm.ac.in, paras.bhatnagar@glbitm.ac.in

Abstract

When the dependent variable is recorded at a specific level, the χ^2 a statistical is essentially a non-parametric technique used to explore group differences. The χ^2 is powerful in regard to the distribution associated with information like all data being non-parametric. Particularly, it does not need equivalence of variances a few of the analyze this is research classes or homoscedasticity with the particular information. It allows analysis of both dichotomous variables is split along with numerous group studies. The computations required to determine the χ^2 provide a lot of information about how all of the teams fared in the research, as well as a variety of non-parametric and parametric statistics. This vast amount of information helps the researcher to acquire the result and so gain more specific info about this statistic than from other kinds. The χ^2 is an important statistic, and may get used by way of the power statistic. When a significant $\chi^2$the final result has been received, the Cramer's V is the ultimate greatest power that is commonly used to examine the information. Benefits of the χ^2 consist of value to circulation to its robustness associated at that the data, their simplicity of calculation, the step-by-step content which may become based on the test, it is used in studies which is why parametric assumptions can't be fulfilled, and its freedom in dealing with information at every two classes and several classes' studies. Limits contain their sample or test dimensions needs, the problem of explanation if there will be more and more categories into the separate aspects, and inclination of this Cramer's V to make general the correlation in which is reduced, also for very significant or considerable results.

Keywords. Categorical information; Chi-square formula; Assumptions; Non-parametric; Analytical analysis.

1. INTRODUCTION

The test this is certainly χ^2 (chi-square) of very important helpful statistics for examining hypotheses as soon as the variables are moderate, normally occurs in medical research. The Chi-square χ^2can provide information not merely from the importance about any noticed variations, however, usually gives step-by-step info on exactly which groups take into account any variations found, unlike most statistics. Therefore, the extent and information of data this statistic can offer render it probably one of the most of good use resources into the variety that is researchers of evaluation resources. As with every statistic, you can find

demands because of its usage that proper tends to be known as “assumptions” from the statistic. Furthermore, the χ^2is a value test, and may forever be paired at the test this is certainly appropriate of power. The χ^2 (Chi-square) test is the non-parametric statistic, also named a distribution test this is certainly no-cost. Non-parametric examinations should always be utilized when anybody is associated with the problems that are after towards the information:

1. The measuring quantity of the facets is nominal.

2. But some parametric tests need equal categories, the sample sizes from the identified categories are uncompilable; for the χ^2 (Chi-square), the categories are of the equal attribute or dissimilar dimensions, although other parametric tests require equal categories.

3.The initial data are assessed at a proportion level, however violate one of the after presumptions to the test this is certainly parametric.

i) The distribution regarding the information was seriously skewed or kurtotic and therefore the specialist should use a distribution for free statistic instead of a statistic that is parametric.

ii)The data change the assumptions of alike homoscedasticity or variance.

iii) For some of several aspects (1), the continuous facts were flattened as a quantity this is certainly tiny of, and therefore the info is not any more interval or proportion

2. PRESUMPTION ASSOCIATED WITH χ^2 TEST

The non-parametric examinations, like the χ^2assume the data had been gotten through random selection as with parametric tests. However, it is not uncommon to locate data that are inferential whenever information comes from convenience examples in the place of random examples. (to possess self-confidence within the outcomes as soon as the sampling this is certainly random is violated, a few duplication tests should be pre-created at basically the same outcome received). All test that is non-parametric its particular inference too. The presumptions for χ^2 test offer:

1) instead of percentage or a few other information transformations, the information within the cells must be frequencies or problems of cases.

2) The understood levels of these variables are collectively special. That is, a subject this is certainly certain into only one amount of each of the factors.

3) Each topic might add information to one and just one cellular in the χ^2.Then $\chi^2$is almost certainly not utilized if, for instance, the same topics are tested over moment in a way that the evaluations are of the same subjects at moment 1, moment 2, moment 3, etc.

4) Separate groups for academic analysis should be formed. If two teams are relevant, this suggests that a separate test should be used. For example, if the professor's data consists of independent variables and dependent variables, such as in investigations involving a mother or father and their kid, a different test should be used.

5) We may discover two factors, which are both calculated as classes, and which are frequently used throughout the minimal degree. Data, on the other hand, might be quantitative information. Additionally, percentage data that has been crumpled into ordinal types can be used. Although chi2 does not have a law limiting the number of cells, an actual

number this large (over 10) makes it difficult to satisfy the presumption not equal to 6 below, as well as to comprehend the significance of the results.

6) In a minimum of 80% of cells, the appropriateness for the cell expected is five or higher, with no cell having an expected of less than one (3). This assumption is almost definitely fulfilled if the sample size is at least the number of cells multiplied by five. This assumption, in essence, determines the number of instances necessary to utilize the $\chi^2$for any other number of cells since χ^2. This need will be easily specified in the example of statistic calculation when you look at the entire example instance.

3. ILLUSTRATION

In [1] authors created a number of versions to predict the cases' security and opportunities of recuperation in MERS-COV contaminated situations. The files on COVID-19 suggested that it is actually a pneumonia like SARS, in which 26 to 33 per cent of individuals called for extensive treatment and the mortality rate 4 to 15 % [2], [3] China [4], [5], Lombardy, Italy [6] as well as New York City, USA [7] has described clinical discussion and early outcomes on the attributes of COVID-19 clients. On 11th March, the infection outbreak was proclaimed a widespread due to the Planet Health Association [8] Far, it has actually been actually stated that 13.8-- 19.1% of COVID-19-infected clients in Wuhan, China, became drastically sick [9], [10] The first case of Coronavirus CoVID-19 illness in India was announced on 30th January 2020 [11] India is actually thought about as the largest country having affirmed situations in Asia. Since 11th June 2020, the Department of Health and also Family Well Being [12] have affirmed an overall of 286,579 scenarios, 141,029 rehabilitations and also 8,102 deaths in India [Thirteen], while the worldwide lot of afflicted instances is 7255960 as well as variety of confirmed deaths is 412583, describing Globe Wellness Company (WHO) [14] In India, 1024 validated cases as well as 27 varieties of confirmed deaths were stated by 29th March, 2020. Due to the opportunity, the amount of confirmed afflicted cases has been actually rapidly boosted in India. The growth rate of verified cases was actually rapid till 29th May, 2020, while India's casualty cost is actually relatively lower at 2.80%, against the global 6.13% as of 3rd June 2020 [15]. India is looked at as the biggest country having confirmed situations in Asia. In India, 1024 confirmed scenarios and 27 amounts of verified fatalities were mentioned through 29th March, 2020. Through the time, the amount of confirmed afflicted instances has actually been rapidly boosted in India [15].

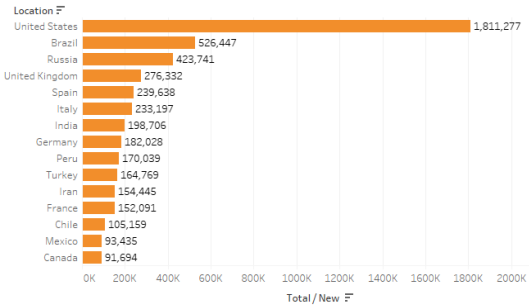

Figure 1. Top 15 Countries with COVID Cases [16,17]

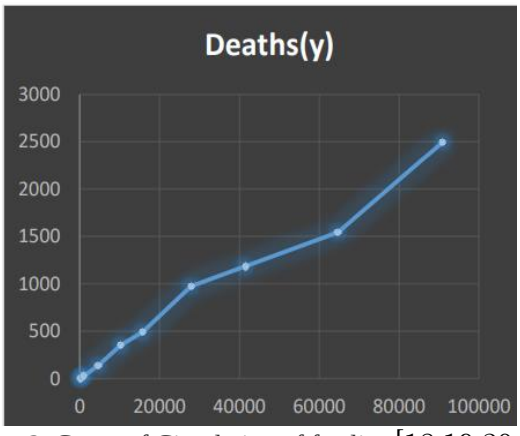

Figure 2. Curve of Circulation of fatality [18,19,20,21]

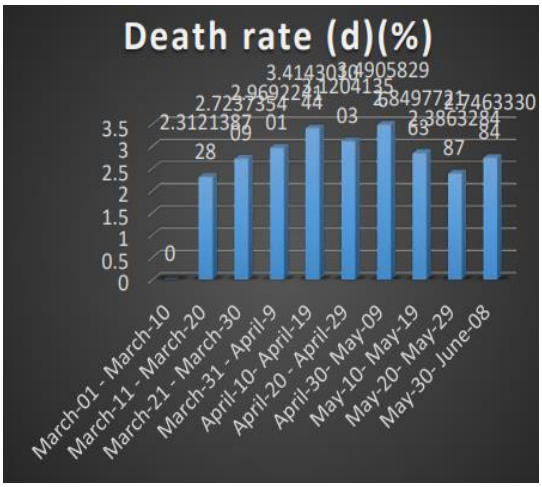

Figure 3. Mortality rate in India for various scenarios [23,24, 25]

The following case example can be used to explain how to calculate and explain the χ^2statistic. The Chairman of an Institute would like to hold keep this is certainly sick reasonable that you can by continuing to keep students healthier through illness avoidance programs. Many students have developed diseases ultimately causing output problems due to go out of that is ill the illness. Generally, there is a vaccine for bacterial disease, while the Chairman feels it is usually crucial to obtaining as numerous students vaccinated as you can Because of to difficulty with offline classes at the institute that makes the vaccine, there was only one vaccination that was sufficient for half of the students. Essentially, there are two groups of students: those who received the vaccine and those who did not receive the vaccine. Each student who hired illness received a questionnaire helper from the institute, and they were also required to accept a sputum test for culture to find the causative representative. They kept track of the true number of students who contracted sickness and what sort of ailment each of them had. The following is how the data was organized:

Category 1: The vaccination may not be provided with this class. (N=52)

Category 2: provided in conjunction with the vaccination. (N=52)

In conditions like these, the vaccination status is a distinct variable. The variable that is reliant Three degrees of overall health outcome:

- established a bacterial disease
- established non-bacterial disease and
- did not establish disease.

The organization needs to recognize whether or not providing the vaccination made much difference. To resolve this, they must each select a fact that will be utilized to test for differences when all of the variables are moderate. To evaluate the relevant question, the χ^2 statistical was utilized. "Was there a difference in the occurrence of disease between the two classes?" Table 1 was created over the summer months to represent the incident of disease in one of the students**.**

Table 1. The outcome of the vaccination model.

Overall health Impact	Non vaccinated	Vaccinated
Unwell with bacterial disease	21	12
Unwell with non-bacterial disease	8	10
No disease	23	30

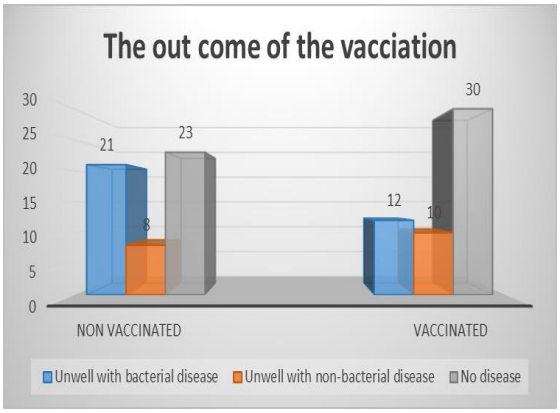

Figure 4. The outcome of the Vaccination

4. COMPUTING χ^2 TEST

To extend the problem posed by [1],[2],[3],[4], [5] the researcher can use the χ^2analysis to see if the vaccination program had any effect on the students' health and well-being. The following is the formula for obtaining a χ^2 *i*s:

$$\sum \chi^2_{i-k} = \frac{(Fo - Fe)^2}{Fe} \qquad (1.1)$$

Therefore:

F_0 = Observed value

F_e = Expected value

χ^2 = Calculate chi-square value
$\sum\chi^2$ =Technique studies to add up each cell's χ^2values

χ^2_{i-k} = i − k is the correct notation to represent all the cells

Adding the sums of all the rows and columns is the first step in computing χ^2 . These sums are referred to as the "borderline," and we may also discover row borderline values $B_R$and column borderline values B_C, which are borderline calculations. Table 2 usually contains values that are on the edge of the case study data. Second is the method for computing the expected values (F_e) for each cell. The "expected" values (F_e) represent a calculation of how the conditions would be distributed if the Chi-square statistic did not include a vaccination impact. Expected values(F_e) must represent both the incidence of cases in each group as well as the circulation when there is no vaccination effect. Because the total N is not equal to the expected number in each cell, the expected number (F_e) in each cell cannot be divided by 6. That will not explain the well-known fact that more people remained healthy whether or not they were vaccinated. (see Table 2, 3,4).

Table 2. Evaluation of Borderlines

Overall health Impact	**Non vaccinated**	**Vaccinated**	**Row borderlines (Row Sum)**
Unwell with bacterial disease	21	12	33
Unwell with non-bacterial disease	8	10	18
No disease	23	30	53
Column borderlines (Column Sum)	52	52	(N) = 104

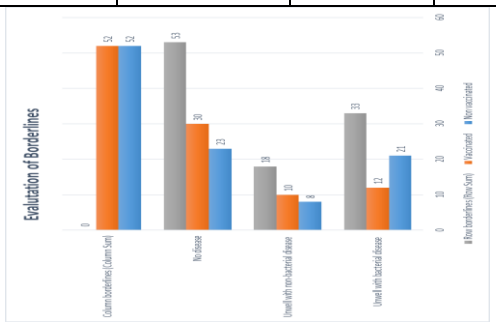

Figure 5. Evaluation of Borderlines

$$F_e = \frac{B_R \times B_C}{N}$$

Where:

$F_e =$ Denotes the expected value of something like the cell

$B_R =$ The rows borderlines for such a cell are represented by this symbol.

$B_C =$ The column borderlines for that cell are represented by this symbol.

$N =$ The total sample size is

Table 3. Compute Expected values F_e

Overall health Impact	Non vaccinated	Vaccinated
Unwell/Suffering with bacterial disease	21(16.5)	12(17.01)
Unwell/Suffering with non-bacterial disease	8(8.95)	10(9.05)
No disease	23(26.5)	30(27)

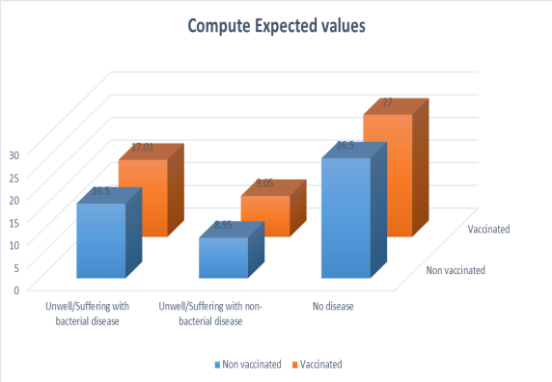

Figure 6. Compute Expected values

The following formula is used to determine the cell χ^2 values:

$$\chi^2 = \frac{(F_o - F_e)^2}{F_e}$$

The cellχ^2 value by each cell the value using parentheses for each cell. (see Table 4)

Table 4: Compute Cell Chi-Square Values $\chi^2 = \frac{(F_o - F_e)^2}{F_e}$

Overall health Impact	Non vaccinated	Vaccinated
Unwell with bacterial disease	21(1.227)	12(1.475)
Unwell with non-bacterial disease	8(.1008)	10(.099)
No disease	23(.4622)	30(.3333)

Following that, the cell chi2 values are computed and then totaled to produce the table's χ^2 statistic. In this condition, χ^2 is 3.697. The χ^2 the table uses the degrees of freedom of

the table to determine the significant level of the fact. The df for a $\chi^2 the$ table is determined with all the formulas: (R_s-1) x (C_s-1). Where R_s is several rows and C_s is the number of columns.

If the calculated value of χ^2 (3.679) differs for each of these df (1, 4, and 12), the significance level from the tabulated of χ^2 values tends to be: df = 1, P > 0.10(α), df = 4, P 0.025(α), and df = 12, P > 0.10(α), Observe that as df rises, the P-level becomes less significant; for example, at the.05 (α) degree, the computed value χ^2 (3.679) is no longer statistically significant because P was larger than 0.10. df =2, when working with a sample table with three rows and two columns. Many important statistics literature, as well as different web resources, provide a chi-square χ^2 of table. The significance of the value is chi-square χ^2 of with 2 df P < 0.005using a tabular value of χ^2. This number might be rounded to P < 0.01. for simplicity. When the Chi-square χ^2 is computed using the mathematical system, the significance is determined to be P = 0.0011.

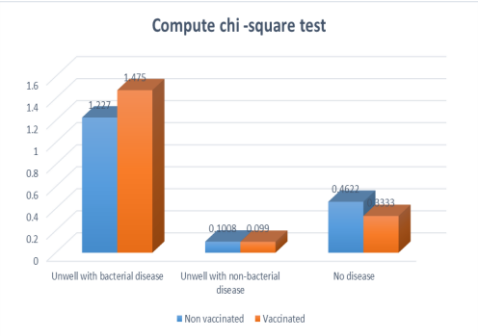

Figure 7. Compute chi square test

The null hypothesis (H_0) is rejected, whereas the alternative hypothesis (H_1) is accepted: when the table's P-value is considerably lower than P < 0.05. "There is indeed a difference in the number of bacterial disease incidents between the vaccinated and non-vaccinated groups." This overall conclusion, however, does not describe the difference could be. Examine the cell Chi-square χ^2 values to fully comprehend the overall result.

5. INTERPRETATION OF CHI-SQUARE X^2 VALUES

Table 4 may contain the fact that the cell with the largest value of 1.227is Cell 1. Here is the complete result of the value, which is observed 21 whereas only 16.5 was expected. As a result, these cells contain much more observed instances than may be expected with a chance. Cell 1 represents the number of non-vaccinated students who contracted the disease. Bacterial disease infection is most likely. This implies exactly how many not people that are vaccinated contracted disease that is bacterial disease significantly greater than anticipated. Cell 2 has the second cell with the highest χ2value of 1.475. However, we find that the number of observed instances in this cell is much lower than predicted (Observed =12, Expected =47.01). If the vaccination had no effect, there would be a significantly smaller number of vaccinated patients who had a bacterial disease. A cell with a χ2value larger than 99% is rare in any other cell.

Table 5. Compute Cell Expected value F_e and Chi-Square Values $\chi^2 = \frac{(F_o - F_e)^2}{F_e}$

Overall health Impact	Non vaccinated	Vaccinated
Unwell with bacterial disease	16.5(1.227)	17.01(1.475)
Unwell/Suffering with non-bacterial disease	8.95(.1008)	9.05(.099)
No disease	26.5(.4622)	27(.3333)

A cell χ^2 with a value less than 1.0 should be regarded as an exact number of observed cases roughly equaling the number of expected circumstances, implying that the vaccination has no impact on a few other cells. In the case study example, all of the cells had cell χ^2 values less than 1.0. As a result of the ongoing lessons, it can be concluded that there was no difference in the occurrence of non-bacterial sickness between the two teams. It was clear that virtually all workers stayed healthy in both merged groups. It's worth noting that vaccinated staff had far fewer occurrences of bacterial disease than non-vaccinated students. As a consequence, the institution should be able to establish if the vaccination program has consistently reduced the incidence of bacterial disease. Several statistical applications generate cell expected and cell χ^2 value tables as part of the basic processing. The cell χ^2 values must be checked using choice since certain applications build those tables as a choice. The method of this χ^2 price gives data if the indicates that having you print just the cell χ^2 value (or whichever cell they choose). A positive cell value denotes that the observed value surpasses the expected value, whereas a negative cell value denotes that the observed cases are less than the expected number. For convenience, researchers may choose to manually calculate the cell expected and cell 2 values. Whenever the application does not present either option, most experts can determine what it is: the general table shows that the two groups are either separate. The majority of studies examine the dinner table to see whether cells are overrepresented with a large number of scenarios against those with only a few. Nonetheless, the interpretation of the path for team variations is less accurate without the inclusion of cell expected or cell $\chi 2$ values. Researchers may wish to manually determine the cell expected and cell $\chi 2$ values to better interpretation due to the convenience of finding such values.

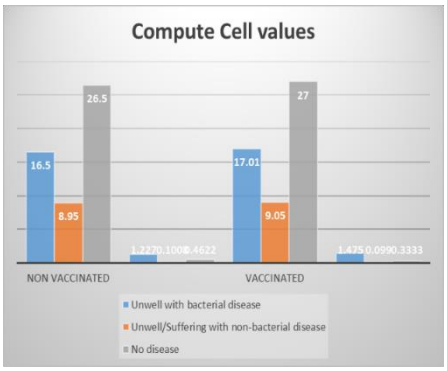

Figure 8. Compute cell values

6. CHI-SQUARE AND MANY OTHER TESTS THAT SEEM TO BE CLOSELY CONNECTED

One could ask if the Chi-square was the best or only test available to the researcher in this case. For nominal variables, non-parametric tests are necessary, and there are three commonly used significance tests for this type of nominal data. The Chi-square is the simplest basic and commonly used. Fisher's exact test is the second test, which is more precise than the Chi-square but only works with 2 x 2 tables (6).

The table would have two rows and two columns, and Fisher's exact test would be used if the case study's only options were Bacterial illness or Non-Bacterial disease. Because the case study example requires a 2 x 3 table, the data is insufficient. If the case study's sole alternatives were Bacterial illness or Non-Bacterial disease, for example, the table would have two rows and two columns, and Fisher's exact test would be employed. The data are unsuitable for Fisher's exact test since the case study example suggests a 2 x 3 table. Assume the sample size was significantly less. If the sample size was lower and the results presented In table 6 were in the table.

Table 6. A table that violates the expected cell values is shown below.

Impact on overall health	**Un-vaccinated**	**Not Vaccinated**
Bacterial disease	4(2.226)/1.42	0(1.75)/1.78
Non-bacterial disease	2(1.67)/.07	1(1.33)/.08
Stayed healthy	14(16.11)/.028	15(12.89)/.35

7. CONCLUSION

The Chi-square is a useful test that provides a lot of information on the type of study results. That's a helpful statistic for researchers to utilize when they want to test hypotheses about nominally measured variables. As with any inferential data, the best results are produced when information is gathered from arbitrarily selected topics, and when test sizes are large enough, they attain excellent analytical power. The Chi-square is a useful tool to use when the assumptions of equal variances and homoscedasticity are broken, and parametric data (Figure 2.3.1 Compute cell values, Table 5) such as the t-test [6] and ANOVA cannot provide trustworthy findings. Hence there is indeed a difference in the number of bacterial disease incidence between the vaccinated and non-vaccinated groups.

REFERENCES

[1] E. Mahdi, V. Maryam, A. Ali, A. Afsoon, O. Sepideh, J. Katayoun, S. Jila, F. Faranak, M. Farzaneh, M. Ali. Prevalence of tobacco consumption: Iranian health perception survey. Payesh (Health Monitor), 2011, 10(3):365-372. Available from: https://www.sid.ir/en/journal/ViewPaper.aspx?id=200649

[2] I. Turaiki, M. Alshahrani, T. Almutairi, “Building predictive models for Mers-CoV infections using data mining techniques”. Journal of Infection and Public Health 2016: 9,744-748.

[3] P. Tungjiratthitikan, “Accidents in Thai Industry between 2001 and 2017”, Evergreen Joint Journal of Novel Carbon Resource Sciences & Green Asia Strategy, Vol. 05, Issue 02, pp.86-92, June 2018.

[4] M. Rahman, A. Pal, K. Uddin, T. Kyaw, B.B. Saha, “Statistical Analysis of Optimized Isotherm Model for Maxsorb III/Ethanol and Silica Gel/Water Pairs”, Evergreen Joint Journal of Novel Carbon Resource Sciences & Green Asia Strategy, Vol. 05, Issue 04, pp.1-12, December 2018.

[5] S. Kitjanukit, “Attitude toward Bio remediation Related Technology and Relation with Company Social Responsibility”, Evergreen Joint Journal of Novel Carbon Resource Sciences & Green Asia Strategy, Vol. 06, Issue 03, pp240-245, September, 2019.

[6] F. Zhou, T. Yu, R. Du, G. Fan, Y. Liu, Z. Liu, J. Xiang, Y. Wang, B. Song, X. Gu, et al. Clinical course and risk factors for mortality of adult inpatients with covid-19 in Wuhan, China: a retrospective cohort study. The Lancet, 395(10229): 1054–1062, 2020.

[7] J. Zhang, X. Dong, Y. Cao, Y. Yuan, Y. Yang, Y. Yan, C.A. Akdis, and Y. Gao. Clinical characteristics of 140 patients infected with sars-Nov-2 in Wuhan, China. Allergy, 75(7):1730–1741, 2020.

[8] W. Guan, Z. Ni, Y. Hu, W. Liang, C Ou, J. He, L. Liu, H. Shan, C. Lei, D. Hui, et al. Clinical characteristics of coronavirus disease 2019 in china. New England journal of medicine, 382(18):1708–1720, 2020

[9] P. Bhatnagar, S. Kaura, S. Rajan, Predictive Models and Analysis of Peak and Flatten Curve Values of CoVID-19 Cases in India: vol.07.issue 04, pp458-467 November 2020.

[10] G.D. Nugraha, B. Sudiarto, R. Kalamullah, “Machine Learning-based Energy Management System for Prosumer”, Evergreen Joint Journal of Novel Carbon Resource Sciences & Green Asia Strategy, Vol. 07, Issue 02, pp309-313, June, 2020.

[11] N. Zhu, D. Zhang, W. Wang, X. Li, B. Yang, J. Song, “China novel coronavirus investigating and research team”. A novel coronavirus from patients with pneumonia in China, 2019. N Engl J Med 382: 727-33 2020.

[12] D. Wang, B. Hu, C. Hu, F. Zhu, X. Liu X, J. Zhang, “Clinical characteristics of 138 hospitalized patients with 2019 novel coronavirus-infected pneumonia in Wuhan”, China. JAMA, 323: 1061-9 2020.

[13] Z. Wu, J.M. McGoogan, “Characteristics of and important lessons from the coronavirus disease 2019 (COVID-19) outbreak in China: Summary of a report of 72314 cases from the Chinese center for Disease Control and Prevention”. JAMA, 323: 1239-42 ,2020.

[14] W.J. Guan, Z.Y. Ni, Y. Hu, W.H. Liang, “Clinical characteristics of coronavirus disease 2019 in China”. N Engl J Med ,382: 1708-20, 2020.

[15] G. Grassell, A. Zangrillo, M. Antonelli, L. Cabrini, A. Castelli, “Baseline characteristics and outcomes of 1591 patients infected with SARS-CoV-2 admitted to ICUs of the Lombardy region, Italy”. JAMA ,323: 1574-81, 2020.

[16] S. Richardson, J.S. Hirsch, M. Narasimhan, J.M. Crawford, T. McGinn, K.W. Davidson, “Presenting characteristics, co-morbidities and outcomes among 5700 patients hospitalized with COVID-19 in the New York city area”. JAMA ,323: 2052-9, 2020.

[17] World Health Organization. Coronavirus Disease 2019 (COVID-19) Situation Report 68,28thMarch-2020. [Online], Available: https://www.who.int/docs/default-source/coronavirus/situation-reports/20200328-sitrep-68-covid-19.pdf
[18] C. Huang, “Clinical features of patients infected with 2019 novel coronavirus in Wuhan”, China. Lancet ,395, 497–506, 2020.
[19] L. Zhonghua, B. Xing, Z. Xue. “Novel Coronavirus Pneumonia Emergency Response Epidemiolog Team The epidemiological characteristics of an outbreak of 2019 novel coronavirus diseases (COVID-19) in China,: 41, 145–151, 2020.
[20] M.A. Andrews, B. Areekal, K.R. Rajesh, J. Krishnan, R. Suryakala, B. Krishnan, “First confirmed case of COVID-19 infection in India”: A case report. Indian J Med Res ,151: 490-2, 2020.
[21] "India most infected by Covid-19 among Asian countries, leaves Turkey behind". Hindustan Times. 29th May 2020. Retrieved 30th May 2020.
[23] "Home | Ministry of Health and Family Welfare | GOI". [Online], Available: mohfw.gov.in. Retrieved 30 May 2020.
[24] World Health Organization (WHO) Coronavirus Disease (COVID-19) Dashboard Data [Online], Available: https://covid19.who.int., last updated: 2020/5/29, 7:02pm
[25] "Coronavirus pandemic (COVID-19) in India". Our World in Data. [Online], Available: https://ourworldindata.org/coronavirus/country/india, Retrieved 20th May 2020.
[26] J.H. Yoo, S.T. Hong, “The outbreak cases with the novel coronavirus suggest upgraded quarantine and isolation in Korea”. Journal of Korean Medical Science, 35(5) 2020.
[27] Korea Centers for Disease Control and Prevention 2020, [Online], Available: http://ghdx.healthdata.org/organizations/korea-cnters-disease-control-and-prevention-kcdc
[28] S. Bagheri Nezhad, N. Mozayani, Elham Abdi, and Setareh Rostami. Smoking data of hospitalized covid-19 patients, Jun -2021.
[29] New COVID-19 cases in India by state and union territory, [Online], Available: https://en.wikipedia.org/wiki/COVID-19_pandemic_in_India#Escaping_of_suspected_people

Biographies

Dr. Rupa Rani Sharma completed the bachelor's degree in Mathematics from CCS University in 2002, the master's degree in Mathematics from CCS University in 2004, and the philosophy of doctorate degree in Approximation Theory of linear positive operators from Chhattisgarh University in 2017, respectively. She is currently working as an

Associate Professor at the Department of Mathematics, G. L. Bajaj Institute of Technology and Management, Greater Noida, UP, India, AKTU University. Her research areas include Approximation Theory of linear positive operators. She has more than 6 research papers published in international peer reviewed journals and 5 scoups indexing. She has been serving as a reviewer for many highly-respected journals.

Dr. Paras Bhatnagar has completed M.Sc. (Mathematics) in 2000 and Ph.D. in Operational Research in 2006 and working as Associate Professor in Department of Mathematics, G. L. Bajaj Institute of Technology and Management, Greater Noida, UP, India. He has more than 19 research papers published in international peer reviewed journals. He is a member of International Association of Engineers.

The Recent Additive Manufacturing Efforts against the COVID-19 Pandemic

[1]Hari Narayan Singh and [2]Sanat Agrawal

Mechanical Engineering Department, National Institute of Technology, Uttarakhand, India,

[1]harinarayan.phd2020@nituk.ac.in, [2]sanata@nituk.ac.in

Abstract

COVID-19, a global pandemic, has caused a rapid increase in the demand of several medical devices and parts like testing swabs, face masks, emergency ventilator parts, and personal protective equipment (PPE). Filling this sudden increase in the demand of medical devices and PPEs has become a prime concern of the medical industry. Additive manufacturing which is extensively used for medical devices and other medical applications has been used to make such medical devices and PPE parts. In this work, several medical devices and parts like nasopharyngeal swab (NP swab), face mask, face shield, ventilator parts, and hands-free door opener fabricated by additive manufacturing technology have been reviewed. The additive manufacturing is found very helpful to combat with the COVID-19 pandemic by providing the customised face mask for frontline medical personal.

Keywords. Additive manufacturing, COVID-19 pandemic, 3D printing, rapid prototyping, and medical AM.

1. INTRODUCTION

The term additive manufacturing (AM) is referred to a group of technologies like rapid prototyping, 3D printing, layered manufacturing, free-form manufacturing and net-shaping. The ASTM International defines additive manufacturing, as "a process of joining the materials to make objects from 3D model data, usually layer upon layer, as opposed to subtractive manufacturing methodologies" [1]. The AM fabricates 3D object directly from the virtual CAD model. The CAD model is converted into STL file format. The STL file is obtained by tessellating the surface of the CAD model and is a closed volume. The STL file is checked for possible errors in translation and rectified with the help of a correction software tool. The STL file is then sliced in several layers and transferred to AM system for additive fabrication. The AM system builds the physical model by depositing or curing material layer-by-layer on to the build platform. Once the fabrication is complete, the part is removed from the build chamber. Post-processing operations such as cleaning, post-curing, surface finishing operations and removal of support structure is done, as required, in the last step of additive fabrication. The major stages of additive manufacturing are shown in the flow diagram in Figure 1.

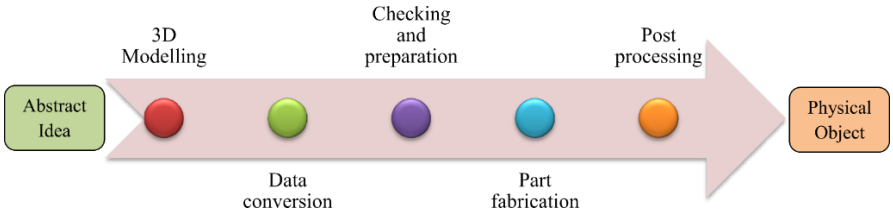

Figure 1. AM process chain to develop product from abstract idea.

The first human cases of COVID-19, the coronavirus disease caused by novel coronaviruses, SARS-CoV-2, were first reported in December 2019 from Wuhan City in China. The World Health Organization announced COVID-19 as a global pandemic on March 11, 2020 [2]. The patients suffer from a severe acute respiratory syndrome caused by the virus, SARS-CoV-2. A critical shortage of medical parts, devices and protective equipment is observed during a pandemic. Personal protective equipment (PPE), face shields and face masks for frontier health worker, and nasopharyngeal swab (NP swab) for collecting the patient samples are some of medical devices and equipment that are necessary to combat with COVID-19. Due to rapid increase in the counting of patients of COVID-19. The hospitals also face shortages of the emergency respirators and oxygen ventilators. It is a global challenge to fulfil the acute supply of medical parts and devices. The additive manufacturing comes in front to meet this challenge by fabricating the necessary medical parts. In this study, the endeavours made by the innovators and the organizations in helping the humanity fight the COVID-19 pandemic using additive manufacturing is reviewed.

2. AM TECHNIQUES APPLIED FOR FIGHTING AGAINST COVID-19 PANDEMIC

During COVID-19 pandemic, mainly polymeric materials were used to additively fabricate the medical devices and parts. Major AM techniques and polymeric medical parts and PPE that were fabricated to meet COVID-19 challenges are listed in Figure 2.

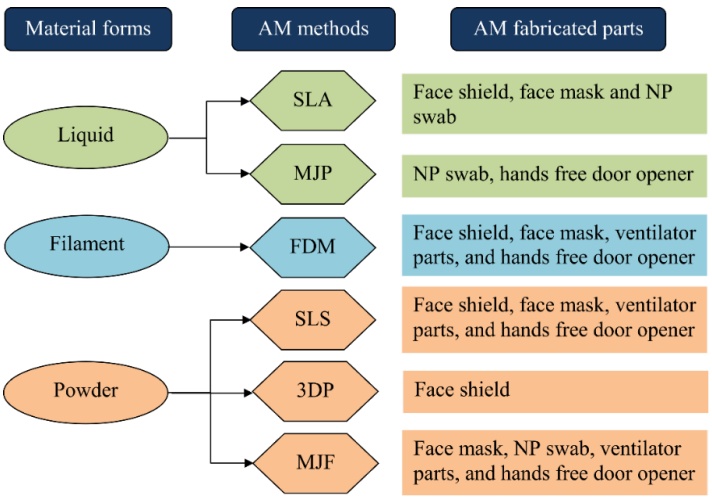

Figure 2. Additively fabricated medical parts in COVID-19 pandemic.

Photo-curing, laser sintering, and thermal melting are the primary manufacturing processes used by various technologies. The polymeric materials have been used in the following three states or forms: powder, filament and liquid, depending on AM technique used [3]. The AM technologies which are extensively being used to meet the acute demand of medical parts and devices in this COVID-19 pandemic situation are as follows:

- Stereolithography Apparatus (SLA)
- Multi Jet Printing (MJP)
- Fused Deposition Modelling (FDM)
- Selective Laser Sintering (SLS)
- 3D Printing (3DP)
- Multi Jet Fusion (MJF)

3. AM CONTRIBUTION TO FIGHT AGAINST COVID-19

To meet the acute demand of PPE parts, protective face-mask, NP swab, testing sticks and several medical parts necessary to combat COVID-19 are being fabricated with additive manufacturing. See Figure 3(a) and (b). The part design and development time is reduced significantly using 3D printing technologies to fabricate emergency respirator valve and ventilator parts as shown in Figure 4. Many other innovative ideas have also been additively manufactured to abate the expansion of SARS-CoV-2 virus, like the hands-free door opener shown in Figure 5. This hands-free door opener hand is designed and developed by Materialise Inc., Belgium, using MJF, SLS and FDM 3D printing technologies [4]. Many 3D printing industries have installed mass production units using several additive manufacturing technologies to fulfil the acute demand of medical parts and devices. The additively manufactured medical parts with production capacity of the AM system is summarized in Table 1 with the names of AM technologies, materials used, company, and country.

Figure 3(a) 3D printed emergency respirator valve by Isinnova and Weerg [5], reproduced with permission from Isinnova, and (b) NP swabs additively fabricated by Origin using SLA method [6].

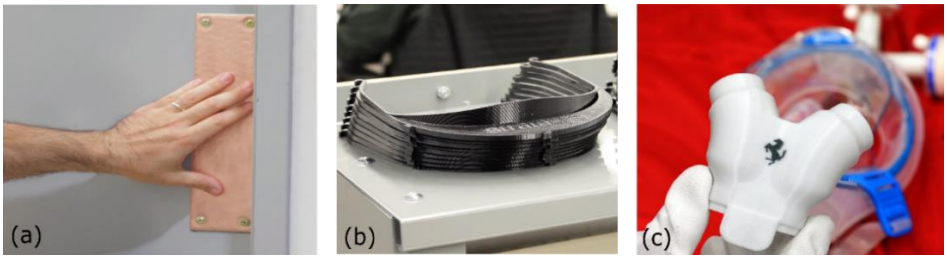

Figure 4 (a) Activated copper plate screwed on the face of door [7] reproduced with permission from SPEE3D (b) 3D printed face shield frame [8] (c) Respirator valve printed by Ferrari [9].

The Photocentric Ltd., UK, fabricates the large quantity of face shields using 45 Magna printers. The printing capacity of the Magna printer farm is 50,000 face shields per day. The face shields fabricated by Photocentric is customizable and the face screens with inclined surfaces provide space at the front and give protection at the sides [10]. The imakr® has installed a production unit at Guy's & St Thomas' supply-chain center for rapid production of eye shields, PPE parts and NP swabs by establishing a 3D printing farm of 200 3D printers to achieve production capacity of 1000 units/day. Nexa3D is producing 10,000 face-shields per week and 500,000 NP swabs per week, using NXE400 SLA 3D printers. Honda uses indirect rapid tooling technique of additive manufacturing for mass production of face shields and has donated 70,000 shields to frontline health personnel in the United States of America. Honda initially used 3D printing to fabricate face shields at five manufacturing facilities. Later on due rapid increase in the demand, they scaled up the production with plastic injection moulding up to 3,000 face shields per hour [11]. 3D Systems Inc. produced 2,880 emergency ventilator parts on demand using SLS method of additive fabrication in the United Kingdom. 3D systems Inc. is also producing several medical parts to help the COVID-19 patients and health worker like PPEs, face shield frames without visors and with visors, stopgap face masks, surgical N95 respirators and NP swabs [8]. See Figure 4. Stratasys is producing nasal testing swabs and face shield frames in the USA. Azul 3D and its partners are fabricating 1000 face shields per day per printer using high-area rapid printing (HARP). Copper3D (2020) produced NanoHack masks as a last resort device for protection against airborne particles. They used polypropylene material in surgical masks. The NanoHack masks achieved an efficiency of filtration approximately 96% for microorganisms of 1 µ and 90% for microorganisms of 0.02 µ.

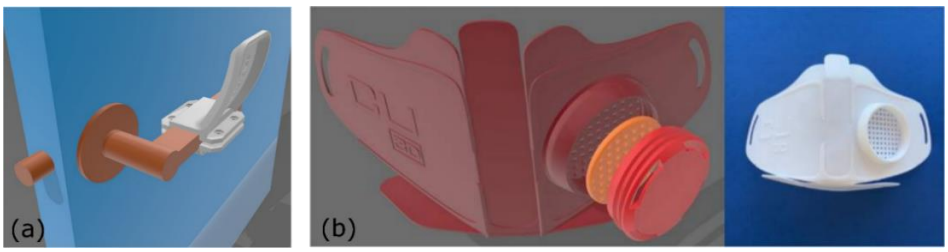

Figure 5(a) Hands free door opener designed by Materialise, Inc [4] and (b) NanoHack mask designed and fabricated by Copper3D [12].

To meet the shortage of face masks during the current pandemic, Filament Innovations in collaboration with St. Luke's University Health Network has designed and fabricated reusable 3D printed masks. The full mask is an assembly of four 3D printed parts: 3D printed guard, Laser cut acrylic plate, HEPA (High-Efficiency-Particulate-Air) filter, and mask frame. The parts have been fabricated using Filament Innovations' BFP-ICARUS-TP High Flow FDM 3D Printer. TPC (or PETG) material is used to print the parts and up to four (4) parts can be printed per build in three (3) hours [13]. Huaxiang Group designed and produced medical safety goggles using Farsoon 403P system. They used SLS, FDM and SLA method for fabrication of various parts of the safety goggles [14].

Table 1. AM contribution to meet the COVID-19 pandemic challenges.

Medical parts	Manufacturer/AM System	Material used	Production capacity	Country	Citation
Face shield	Photocentric Group Model: LC Magna Printer	Photopolymer resin	50,000/day	UK	[10]
	iMakr Model: SLS and FDM	PLA & PETG (Poly Ethylene Terephthalate Glycol)	1000/day	USA	[11]
	Nexa3D Model: NXE400 SLA 3D printer	proprietary material	10,000/ week	USA	
	Honda AM system: 3D printing, injection moulding.	NA	3000/hour	USA	
	3D Systems Model: ProX SLS 6100 Printer	Medical grade nylon	100/day	UK	[8]
	Stratasys Model: FDM	ABS	Total: 275,000 units	Israel	[15]
	Azul3D Model: High-Area Rapid Printing	Proprietary material	20,000/ week	USA	[16]
Face masks and fitting s	Filament Innovations Model: BFP-ICARUS-TP High Flow FDM 3D Printer	TPC/TPU & PETG	35/day	USA	[13]
	Farsoon Technologies AM system: Polymer Laser Sintering	Farsoon FS3300PA	1000/day	USA	[14]
	Pneumask Model: NA	PLA & ABS	Total: 23,534 units	California	[17]
	3D Systems, Inc. Model: Multi-Jet Fusion (MJF)	Powder Bed Fusion Nylon	NA	UK	[18]
	CIIRU CTU & CARDAM Model: HP MJF 540 Printer	PA 12	10,000/day	Czech Republic	[19]
	Copper3D AM system: FDM	PLACTIVE® and MDflex®, Nanocomposites developed by Copper3D	NA	Canada	[12]
Nasopharyngeal (NP) swabs	EnvisionTEC Model: Envision One cDLM Printer	Soft C-29C resin	112,000/ day	USA	[20]
	Origin and Stratasys AM system: Origin One Printer	Proprietary material	190,000/ day	Israel	[8]
	Forecast 3D and Abigenix, Inc. AM system: HP's MJF Printer	Proprietary material	100,000/ day	USA	[21]
	Markforged Model: Markforged Industrial Series Printer	Nylon base and Rayon	10,000/day	USA	[11]
	Hospital virtual Valdecilla AM system: Form 2 SLA Printer	Surgical Guide resin	324/print	Spain	[22]
	Nexa3D Model: NXE 400	Nexa3D material	500,000/ week	USA	[11]
	Formlabs Model: Formlabs SLA Printer	Surgical Guide resin	112,000/ day	USA	[23]
	Carbon3D Model: Carbon DLS™	KeySplint Soft®	1000,000/ week	USA	[24]
Emergency valves, respiratory masks, and Ventilator parts	Weerg with Isinnova and FabLab Brescia AM system: HP's MJF 5210 Printer	PA 11 and PA 12 Nylon	500/day	Italy	[25]
	Materialise, Inc.	Materialise Passive NIP	NA	Belgium	[26]
	CRP Technology Model: High Speed Sintering	Windform® P1 isotropic material	NA	Italy	[27]
	Ferrari AM system: FDM	ABS	NA	Italy	[9]
	Isinnova, Lonati Model: FDM, SLS	PLA	100/day	Italy	[5]

	3D Systems Model: SLS	Medical Grade Nylon	720 sets (total: 2,880 parts)	UK	[8]
Hands-free door opener	Materialise, Inc. AM system: MJF, SLS, and FDM	PLA	NA	Belgium	[4]
	Sintratec Model: Sintratec S2 SLS 3D printer	Sintratec TPE powder	NA	Switzerland	[28]
Anti-microbial copper	SPEE3D 3D Model: Light SPEE3D machine	ACTIVAT3D (Anti-microbial) copper	NA	Australia	[7]
Diagnostic platform (lab-on-a-chip)	3D Systems Inc. Model: Standalone 3D printer MED-AMB 10	MED-AMB 10, PRO-BLK-10, and RUBBER-65A BLK	NA	UK	[29]

Novak and Loy (2020a) have reviewed several projects initiated prior to April 01, 2020, utilizing various AM technologies. There were 91 such projects. These projects were aimed at fabricating a range of health and medical products for combating COVID-19 on-demand and close to the point of need. They declared that 65% of the products were for PPEs out of that 60% were face shields. FDM technology was mostly used to fabricate medical products to combat COVID-19 [30]. Novak and Loy (2020b) have performed an analysis of face shields and face masks fabricated by various AM technologies during COVID-19. They have investigated fabrication of 37 types of face shields and 30 types of facemasks varying in the company or institution producing them or AM machine being used. The timeline for the design of these face shields and face-masks is May-June 2020. They have demonstrated a range of considerations in fabricating PPE parts using AM such as the type of AM technology used, the quality of products to be fabricated, the amount of material required and the cost of manufacturing. They found that the face shields take almost half the time to additively fabricate compared to the face masks and require approximately half the filament material. They have concluded that printing face-shields is cheaper than printing face masks. The authors have also found that the AM technologies allowed use of distributed manufacturing for producing PPE parts during COVID-19 [31].

A diagnostic platform has been developed by Dr. Pantelis Georgiou using 3D Systems, Inc. This lab-in-a-chip rapid testing device can give the test report within 30 minutes [11]. Taking an initiative to help patients in this pandemic situation, Ferrari S.p.A. has started fabricating respiratory valves and other devices for protective masks from thermoplastic materials. See Figure 4. They use 3D printers at its car prototyping department in the Maranello plant [9]. Charlotte valve and Dave valve have been designed and developed to turn a normal mask into C-PAP mask by Isinnova and Weerg. These valves shown in Figure 3 connects the mask to the oxygen dispenser [5]. SPEE3D has developed a antimicrobial copper plate. The existing metal part is coated with copper by SPEE3D printers. This ACTIVAT3D copper push plate is mounted on doors to reduce the spread of virus as shown in Figure 4. The clinical trial results showed that 99.2% of SARS-CoV-2 virus killed within five hours whereas 96% of SARS-CoV-2 viruses were found dead within two hours with this antimicrobial copper plate while there is no reduction of virus presence with stainless steel plate [7].

4. CONCLUSIONS

In the present work several medical parts and devices fabricated by additive manufacturing technologies to help combat COVID-19 have been discussed. The manufacturing process of six AM methods, which were mainly used to fabricate the medical parts in this pandemic situation, are also explained. The effort by different manufacturers of AM systems all over

the world is tabulated to summarize how AM has helped humanity during this pandemic. The list is not exhaustive. However, it gives a fairly good idea of how the AM technology has been useful in responding to the COVID-19 needs. The suitable AM technique and material used by AM industries for mass production of medical parts with their production capacity have also reviewed. Certainly, the additive manufacturing played very important role to save the lives of many frontline heath-workers and patients by readily providing the customized face-masks, face-shields, emergency respirator valves, and other testing parts and devices.

REFERENCES

[1] C.K. Chua, K.F. Leong, C.S. Lim, "3D Printing and Additive Manufacturing: Principles and Applications", World Scientific Publishing Co. Pte. Ltd, 5th ed. Singapore, 2019.

[2] D. Cucinotta, and M. Vanelli, "WHO Declares COVID-19 a Pandemic", Acta Biomedica, vol. 91 (1), pp. 157-160. Italy, 2020.

[3] M.S. Tareq, , T. Rahman, , M. Hossain, and P. Dorrington, "Additive manufacturing and the COVID-19 challenges: An in-depth study", Journal of Manufacturing Systems, 2021.

[4] Materialise Inc., "Hands-free 3D-printed door openers to help against the spread of coronavirus", 2021.

[5] Isinnova, "Easy COVID", Mar., 2021, from https://isinnova.it/archivio-progetti/easy-covid-19/.

[6] Origin, "Origin 3D-printed COVID-19 test swabs clinical trial and validation completed with Beth Israel Deaconess Medical Center", 2021.

[7] SPEE3D, "3D printing a metallic coating of antimicrobial copper to fight the spread of COVID-19", 2020, from https://spee3d.com/activat3d-copper/.

[8] 3D Systems Inc., "COVID-19 Call to Action", UK, 2021.

[9] Ferrari S.p.A., "Ferrari continues its efforts to fight the COVID-19 pandemic" 2020.

[10] Photocentric, "The Creation of Magna Printer Farm", 2020.

[11] S. Davies, D. O'Connor, and L. Griffiths, "The latest 3D printing efforts against COVID-19", TCT Magazine: 3D printing and additive manufacturing intelligence, 2020.

[12] Copper3D, "NanoHack, the open source face mask", 2020.

[13] St. Luke's University Health Network and Filament Innovations, "3D Mask - SLUHN and Filament Innovations", 2020.

[14] Farsoon, "Farsoon Technologies – Open for industry", 2020.

[15] Stratasys, "Stratasys helps: Responding to the COVID-19 crisis", 2020.

[16] Azul3D, "Azul 3D Protects Healthcare Workers Facing COVID-19 Crisis-Printing 1,000 Face Shields Per Day Per Printer", 2021.

[17] T. Amenabar, "Stanford has made a reusable mask from scuba gear-and it's shipping it to the front lines of the pandemic", The Washington Post, 2021.

[18] C. Richburg, "Stopgap Surgical Face Mask (SFM)", 2020.

[19] A. Novakova, "Mass production of original Czech mask with the highest degree of protection", 2020.

[20] EnvisionTEC, "EnvisionTEC to 3D print mass quantities of nasopharyngeal swabs for COVID-19 testing based on successful clinical trial", 2020.

[21] Forecast 3D, "Forecast 3D now producing nasopharyngeal swabs for COVID-19 test kits", 2020.

[22] Hospital Virtual Valdecilla, “Sample collection – Swabs”, 2021.
[23] Formlabs, “3D printed COVID-19 test swabs”, 2020.
[24] Carbon, “Resolution medical using Carbon DLS™ technology to 3D print nasopharyngeal swabs for COVID-19 testing”, 2020.
[25] Weerg, “Weerg 3D prints valves for emergency respiratory masks”, 2020.
[26] V. Brigitte, “Materialise 3D-Printed non-invasive PEEP masks aim to alleviate ventilator shortage”, 2020.
[27] CRP Technology, “CRP Technology on the front line in the fight against COVID-19”, 2020.
[28] Sintratec, “Door opener against COVID-19 spread”, 2020.
[29] 3D Systems Inc., “Rapid Diagnostics Device Developed Using Figure 4® Standalone”, 2020.
[30] J.I. Novak and J. Loy, “A critical review of initial 3D printed products responding to COVID-19 health and supply chain challenges”, Emerald Open Res., 2020.
[31] J.I. Novak and J. Loy, “A quantitative analysis of 3D printed face shields and masks during COVID-19”, Emerald Open Res., 2020.

Biographies

Hari Narayan Singh received the bachelor's degree in mechanical engineering from Uttar Pradesh Technical University in 2013, the master's degree in computer aided design and manufacturing from Motilal Nehru National Institute of Technology in 2019, and pursuing the philosophy of doctorate degree in mechanical engineering from National Institute of Technology Uttarakhand, respectively. His research areas include application of additive manufacturing in fabrication of patient-specifics medical implants.

Dr. Sanat Agrawal received the bachelor’s degree in Mechanical Engineering from IIT Kanpur in 1988, the master’s degree in Mechanical Engineering with specialization in Machine Design Engineering from University of Roorkee in 1990 and PhD in Mechanical Engineering from IIT Kanpur in 2002. He is currently working as the Associate Professor and Head, Mechanical Engineering Department, NIT Uttarakhand. His research areas are computer-aided design and additive manufacturing.

Thermal Ablation of Tumour with Biocompatible Gold Nanorods: A Numerical Study

Vishal Bhalla, Rashmika Patole

College of Engineering Pune, Wellesley Rd, Maharashtra, India.

vbhalla.mech@coep.ac.in, rkp.extc@coep.ac.in

Abstract

Cancer is a life-threatening disease in which a lump is formed due to the growth of cells which starts damaging the healthy cells of the body. Removing the lump with hyperthermia is a technique where the lump is heated in the range of 50-60 °C with an electromagnetic wave (EMW). The absorptivity of the lump (tumour) is very low, due to which it cannot absorb the irradiation alone. To absorb the absorptivity of EMW nanoparticles have been added to the tumour, then nanoparticles absorb the irradiation, get heated and transfer the heat to the tumour. In the present study, gold nanorods have been used for absorption purposes, having a diameter of 25 nm and aspect ratios of 1.5, 3.5 and 5.5. The results show that with these aspect ratios broadband spectrum (400-1300 nm) has been covered. The volume fraction of the nanoparticles plays a crucial role in the ablation of the tumour at an optimum volume fraction. The study shows that the absorption coefficient of 40 cm-1 is an optimum value where the maximum temperature of the tumour has been found. Furthermore, the irradiation intensity and irradiation time also play an important role in the ablation of the tumour. In the current manuscript, numerically the effect of irradiation intensity, irradiation time, and volume fraction has been studied.

Keywords: Cardiovascular Fitness Recommendations, personalised recommendations.

1. INTRODUCTION

Cancer is a life-threatening disease in which a lump is formed due to the growth of cells which starts damaging the healthy cells of the body. There are certain techniques (chemotherapy, laser ablation, electroporation, surgery, and radiation therapy) used for the treatment of cancer (Jamil and Ng, 2013). These conventional techniques have limitations for example in cases when the tumour is deep inside the body and out of reach or in many such scenarios these techniques might be very cumbersome (Ashikbayeva *et al.*, 2019). Hyperthermia or thermal ablation technique uses laser or electromagnetic waves to damage the tumour by heating it for a certain period. The electromagnetic waves are incident in the near-infrared region. The ablation temperature in the range of 50-60 °C is sufficient for the complete mutilation of the tumour (Ahmed *et al.*, 2011). The tissue is damaged due to low levels of oxygen, nutrients and pH level. The hyperthermia causes focal hyperthermic injury to the ablated cell, which affects the tumour microenvironment and damages the cell at the membrane and subcellular level. This technique can be applied to the local cell and the whole body. It has been mentioned that the hyperthermia technique alone is not enough to replace one of the established therapy modalities when they have been applied alone, but, the hyperthermia technique is without any doubt enhances the effect of cell killing drug. The

main benefit of hyperthermia is that it is flexible, less expensive and involves less invasiveness as compared to other conventional cancer treatment methods (Carrafiello *et al.*, 2008).

The drawback of this technique is that the absorptivity of the tissue is very less which results in low-temperature rise, thus very low heating takes place. A more promising hyperthermia technique involves the usage of nanoparticles which enhances the optical properties. When the electromagnetic wave (in the range of near-infrared wavelength) is incident on nanoparticles embedded in the tumour, the nanoparticles absorb the irradiation, get heated and help in damaging the breast tumour which is surrounded by healthy tissue as shown in Fig. 1. This method selectively destructs the tumour and the localized hyperthermia provides better-targeted treatment (Manthe *et al.*, 2010).

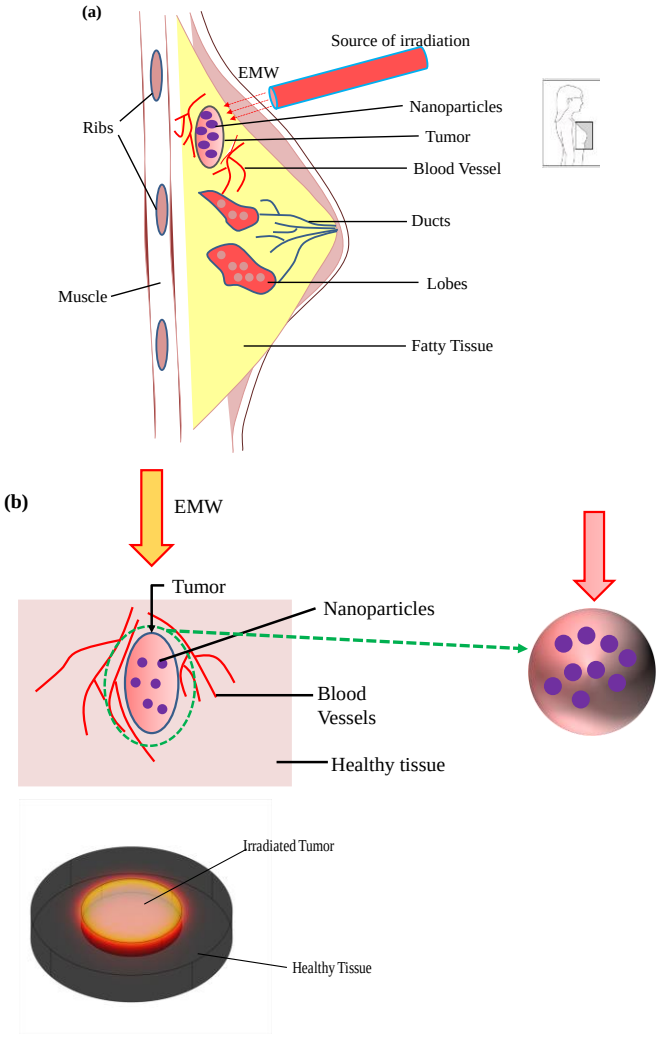

Figure 1 (a) Schematic of the breast tumour irradiated with electromagnetic wave (EMW) and (b) the description of tumour surrounded by blood vessels and healthy tissue.

The nanoparticles used in the hyperthermia treatment mostly are iron oxide, doped iron oxide, superparamagnetic iron oxide, carbon nanotubes and various polymer-based technologies are used (van Landeghem *et al.*, 2009; Lee *et al.*, 2011; Kaur *et al.*, 2016). For the thermal ablation of the tumour, as the optical properties of the nanoparticles play a crucial role, so for the hyperthermia biocompatible gold nanoparticles have been used (Monga *et al.*, 2020). These nanoparticles have been used to achieve the thermal ablation temperature for denaturation of tissue proteins and apoptosis is preferred. The main aim of the present study is to predict the effect of irradiation, irradiation time and volume fraction of the nanoparticles of the ablation of the tumour.

2. NUMERICAL MODELLING OF NANOPARTICLES ASSISTED TUMOUR

2.1 Optical properties of nanoparticles

In the ablation of the tumour, the nanoparticles and their optical properties play an important role. The literature suggests that gold nanorods are more beneficial to use than nanospheres, due to which gold nanorods have been considered in this study. The metallic nanorods show plasmonic peaks at different wavelengths (depending on the diameter and the aspect ratio), due to which the absorption at the plasmonic wavelength happens. These nanorods show two plasmonic peaks, radially and axially (i.e. it has transverse and longitudinal oscillation). In the current study, for the calculation of optical coefficients, Mie scattering has been used. As $\lambda > 10D$, the nanoparticles experience polarization (Ξ) and the induced polarization can be evaluated as

$$\Xi = 4\pi D^2 L \left(\frac{\varepsilon_{gold} - \varepsilon_{tissue}}{3\varsigma_i \left(\varepsilon_{gold} - \varepsilon_{tissue} \right) + 3\varepsilon_{tissue}} \right) \tag{1}$$

where D is the diameter of the nanorod, L is the length of the nanorod, $\varepsilon_{\text{gold}}$ is the dielectric constant for gold, $\varepsilon_{\text{tissue}}$ is the dielectric constant of tissue and ς is the geometric factor, where i = 1, 2 and 3.

The geometric factor (ς) is calculated by using equation 2

$$\varsigma = \frac{1-f2}{f2}\left[\frac{1}{2f} \ln\left(\frac{1+f}{1-f} \right) - 1 \right]$$
$$\text{where } f = \left(1 - \frac{D}{L} \right)^{0.5}, \varsigma_2 = \varsigma_3 = \frac{1-\varsigma_1}{2} \tag{2}$$

Further, the absorption and scattering coefficients are calculated by using equation 3

$$\alpha_{abs} = \frac{2\pi\varphi}{3\lambda V_{np}} img\left(\Xi_1 + \Xi_2 + \Xi_3 \right)$$
$$s_{scat} = \frac{16\pi^3\phi}{18\lambda 4 V_{np}} \left(\left|\Xi_1\right|^2 + \left|\Xi_2\right|^2 + \left|\Xi_3\right|^2 \right) \tag{3}$$

where ϕ is the volume fraction, V_{np} is the volume of nanorods, λ incident wavelength.

2.2 Spatial temperature distribution in the tumour

As we know that the bare tumour is unable to absorb the irradiation due to less absorptivity. For a bare tissue the absorption and scattering values are 0.062 mm^{-1} @ 725-325 nm and 0.95 mm^{-1} @ 925 nm respectively (Soni *et al.*, 2015). Further, the scattering and absorption values for the nanorod are around 10 mm^{-1} and 0.375 mm^{-1} respectively. These results show that with the gold nanorods, absorption is more dominant than the scattering. So, in the absorption dominating media, the attenuation of the irradiation is found by the Beer Lambert's law, which states that the extinction of the irradiation happens exponentially in the absorption dominated media and mathematically it is given by equation 4

$$I = I_o \exp\left(-K_{e\lambda}.Z\right) \tag{4}$$

where I_o is the incident radiation, $K_{e\lambda}$ is the spectral extinction coefficient and Z is the depth of the tumour. The absorption of irradiation by the nanorods generates the temperature rise and thus damages the tissue. The initial temperature of the tumour is 35 °C and the outer boundary of the healthy tissue has been considered isothermal. The spatial temperature rise in the tissue has been evaluated by Penne's equation, which is represented by equation 5.

$$\rho_t C_t \frac{\partial T\left(r,z,t\right)}{\partial t} = K_t\left(\nabla^2 T\left(r,z,t\right)\right) + w_b \rho_b C_b\left(T_c - T\left(r,z,t\right)\right) + Q_{met} + Q_{ab} \tag{5}$$

where Q_{met} is heat generation due to metabolism of the body, Q_{ab} is the amount of heat absorbed by nanoparticles due to intensity attenuation within the tissue, $T(r,z,t)$ is the tissue temperature as a function of r,z co-ordinates, T_c is the core body temperature, C_t is the specific heat of the tissue, C_b is the specific heat of the blood, ρ_t is the density of the tissue and ρ_b is the density of the blood.

The thermophysical properties of the healthy tissue and the tumour are presented in table 1.

Table 1. Thermophysical properties of healthy tissue

For Healthy tissue	
Thermal conductivity (K_t)	0.5 $W.m^{-1}.K^{-1}$
Density (ρ_t)	1000 $kg.m^{-3}$
Heat capacity (C_{pt})	4200 $J.kg^{-1}K^{-1}$
Absorption coefficient (α_t)	0.02 m^{-1}
Arterial blood temperature	37 °C
Heat capacity of blood (C_{pb})	4200 $J.kg^{-1}K^{-1}$
Blood perfusion rate (s^{-1})	1×10^{-3}
Density of blood (ρ_b)	1000 $kg.m^{-3}$

Table 2. Thermophysical properties of tumour

For Tumour	
Thermal conductivity (K_t)	0.55 $W.m^{-1}.K^{-1}$
Density (ρ_t)	1100 $kg.m^{-3}$
Heat capacity (C_{pt})	4200 $J.kg^{-1}K^{-1}$
Absorption coefficient (α_t)	0.06 m^{-1}
Blood perfusion rate (s^{-1})	9.1×10^{-3}
Density of blood (ρ_b)	1000 $kg.m^{-3}$

2.3 Skin Tumour and distribution of nanoparticles

The skin tumour case in the 3D module has been selected for the study. For the study, both healthy tissue and tumour have been considered cylindrical (as shown in figure 2).

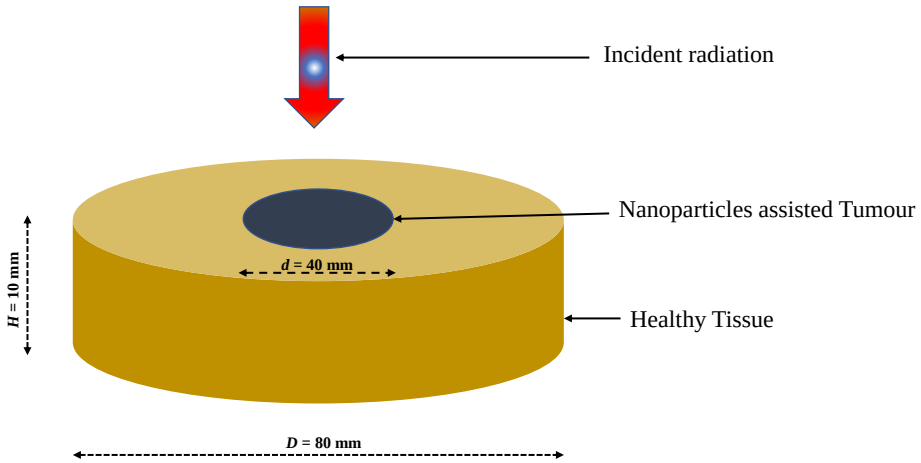

Figure 2. Schematic of the healthy tissue and the tumour irradiated with electromagnetic waves.

For the numerical analysis, it has been assumed that the tumour has a diameter of 40 mm and the height of the tumour is 5 mm. This tumour is surrounded by healthy tissue having a diameter of 80 mm and a height is 10 mm. Further, it has been assumed that gold nanorods have impinged on the tissue. The irradiation is normal to the tumour and gets absorbed by the nanoparticles.

3. RESULTS AND DISCUSSIONS

3.1 Optical properties of nanorods

The absorption coefficient for the gold nanorods has been shown in Fig. 3. For the absorption coefficient, a diameter of 25 nm and aspect ratio (AR) of 1.5, 3.5 and 5.5 has been considered. To understand the effect of volume fraction, two different volume fractions have

been considered i.e. 0.001 and 0.002% respectively (see Fig. 3a and 3b). From these figures, we found that the absorption increases with the increase of volume fraction. Further, the aspect ratio shows there are three peaks, and the highest peak has been achieved with AR of 3.5. At AR 3.5, the absorption peak is at the wavelength of 725 nm and this maximum peak is because of the local surface plasmon resonance (LSPR) effect. To ablate the tumour, the incident radiation will be at the wavelength of 725 nm and maximum irradiation will get absorbed by the nanoparticles. Maximum absorption results in more heating and thus ablation of the tumour takes place.

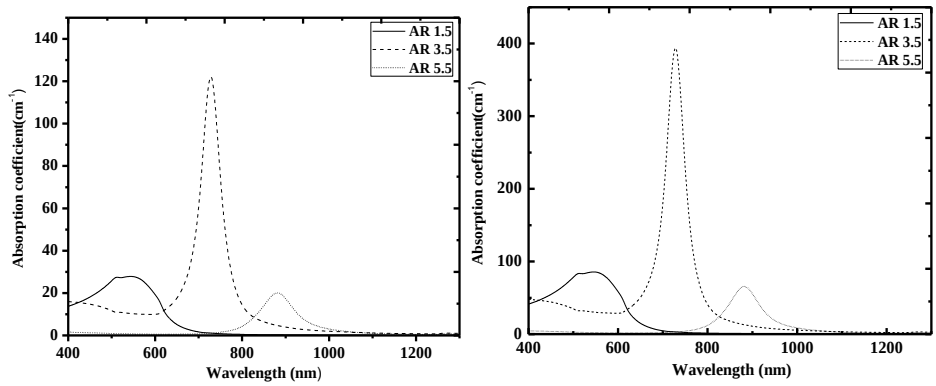

Figure 3. Optical signature of the gold nanorods at different aspect ratio (a) for volume fraction of 0.001% and (b) 0.002%.

3.2 Effect of volume fraction on the ablation of tumour

Figure 4 shows the effect of volume fraction on the temperature rise of the tumour. It shows that with the increase of absorption coefficient (which depends on the volume fraction), the average temperature in the tumour increases, reaches a stagnant point and with further increase of absorption coefficient, the temperature starts decreasing. This is because, at a low volume fraction, the whole irradiation is not absorbed by the nanorods. On the other hand, at a higher volume fraction, the irradiation is absorbed by nanorods in the top layer, thus the irradiation does not reach the whole volume of the tumour, thus there will be no complete damage to the tumour. Due to this fact, the optimum volume fraction of the nanoparticles needs to be added to the tumour for complete ablation of the tumour.

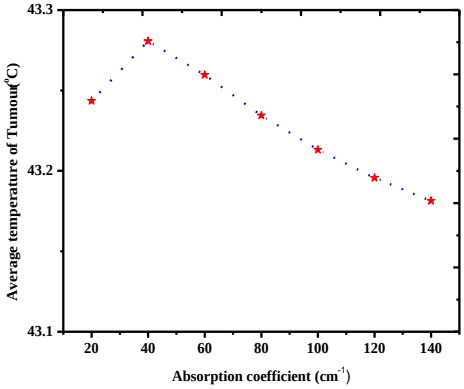

Figure 4. Effect of absorption coefficient on the average temperature of the Tumor

3.3 Effect of irradiation time and irradiation intensity

The effect of irradiation intensity and irradiation time on the damage of the tumour has been shown in Fig. 5. From figure 5 it can be seen that the average temperature rise of the tumour directly depends on the irradiation intensity. So, according to the size of the tumour, the intensity needs to select. Further, the ablation temperature also increases with irradiation time. As we know, for complete damage to the tumour, the temperature should be in the range of 50-60 ºC. So, this temperature can be achieved with an irradiation intensity of 5000 Wm-2 (see Figures 6a and 6b). Further, to illustrate the effect of irradiation intensity on the damage to the tumour, isosurfaces have been shown in figure 6b, which confirms that the tumour ablated with the irradiation time. Further, care is needed when selecting the irradiation intensity because more irradiation time and irradiation intensity damage the healthy tissue.

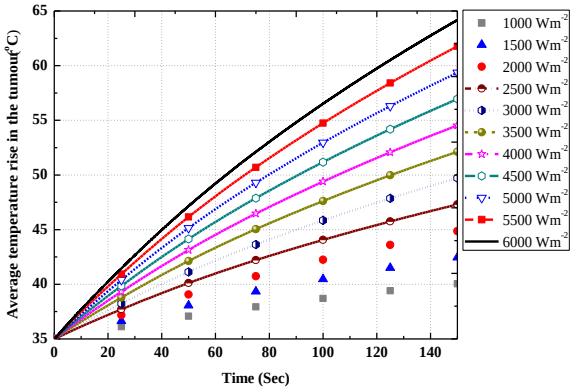

Figure 5. Effect of irradiation intensity on the temperature rise in the tumour

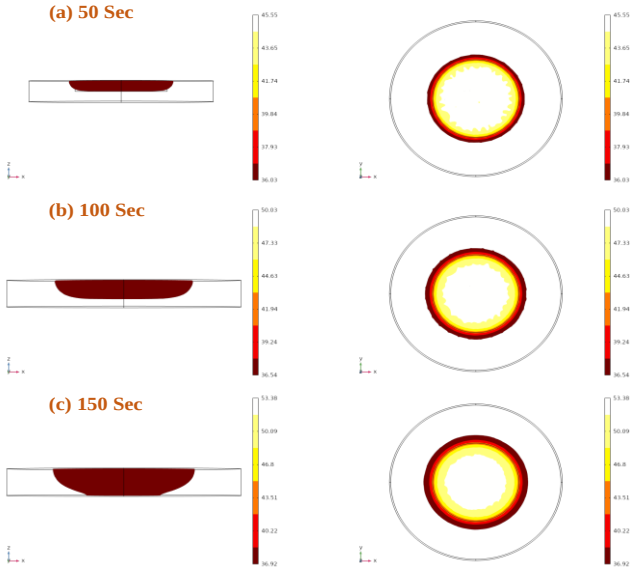

Figure 6(a)

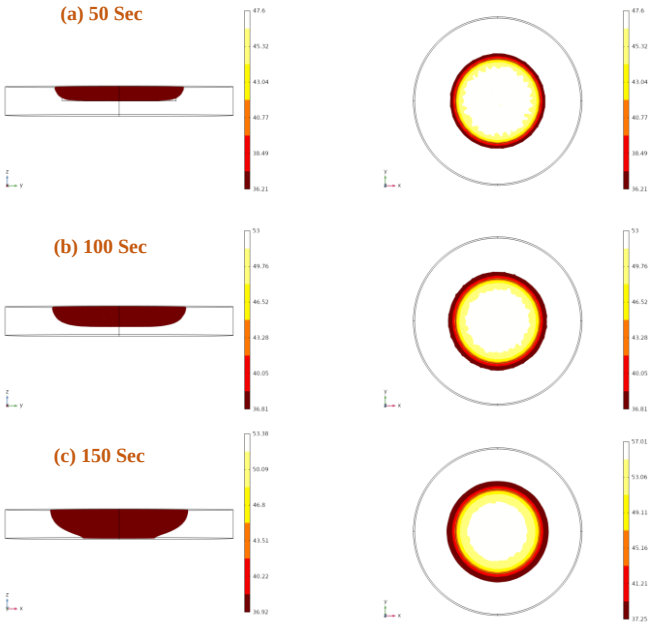

Figure 6(b)

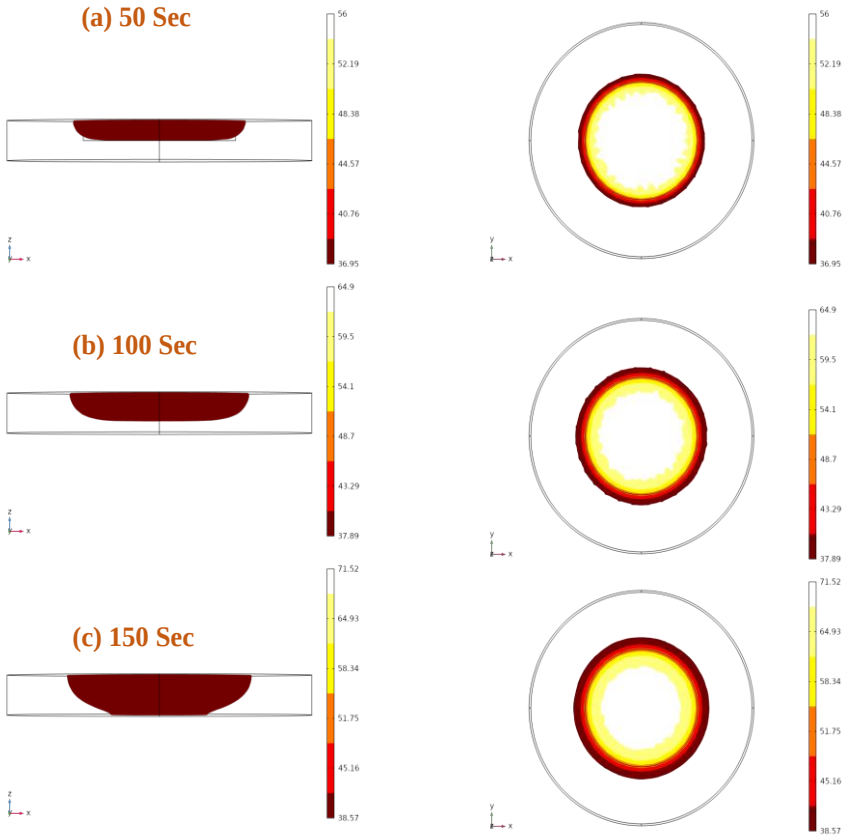

Figure 6(c)

Figure 6. Temperature contours for the ablation of the tumour at different intensities (a) 2500 Wm^{-2} (b) 3000 Wm^{-2} and (c) 5000 Wm^{-2}

3.4 Effect of temperature along the diameter of the tumor

The temperature variation along the radius of the tumour has been shown in Fig. 3.4. From the figure, it can be seen that the temperature is maximum in the centre of the tissue and decreases at the outer periphery. This is because the flowing blood in the healthy tissue near the tumour takes away the heat, which cools it down. Further, the same trend has been seen at different depths along with the tumour.

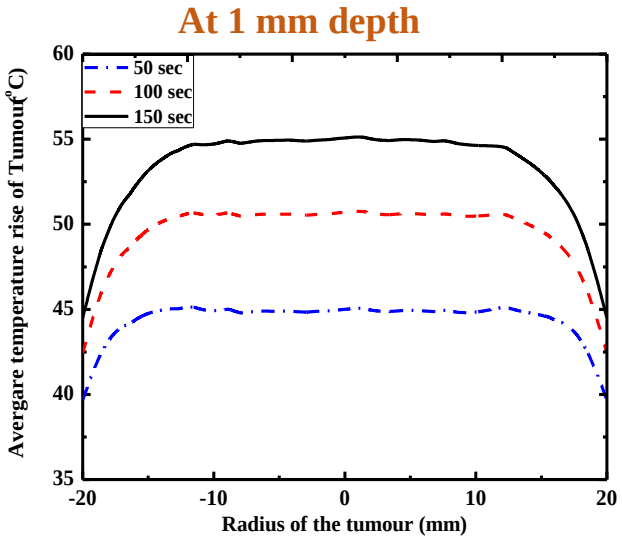

Figure 7(c)

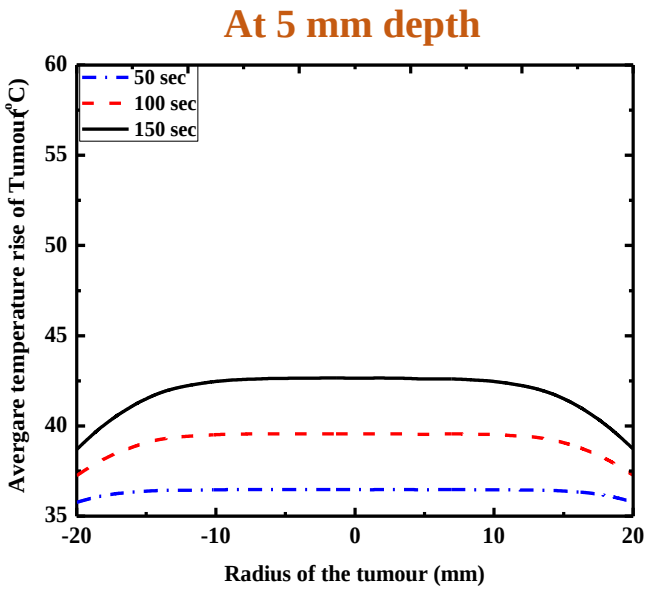

Figure 7(b)

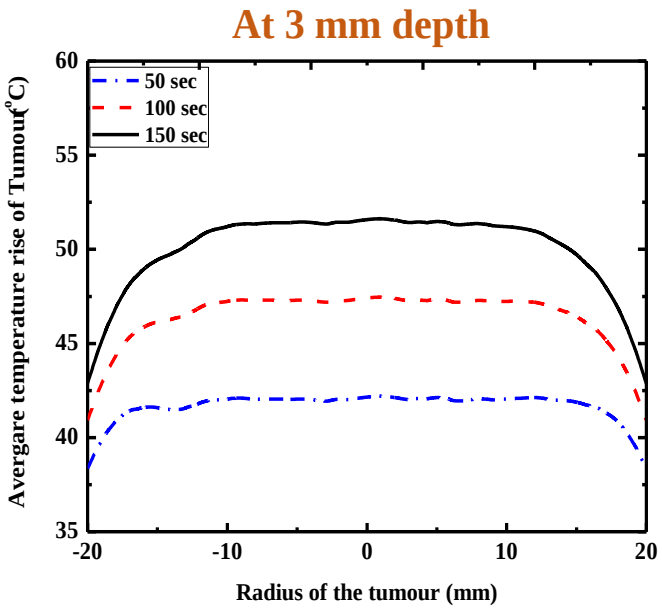

Figure 7(c)

Figure 7. The temperature rise in the tumour along the radius of the tumour at different depths (a) 1 mm (b) 3 mm and (c) 5 mm

4. CONCLUSION

From the results, it has been found that for the damage to the tumour, the temperature required is around 50-60 ºC. The ablation temperature depends on various factors like volume fraction of the nanoparticles, irradiation time and irradiation intensity. From the study, it has been found that the absorption coefficient depends on the volume fraction and it increases with the increase of volume fraction. Further, an intensity of 5000 Wm-2 is required for ablation of the tumour in 50-60 sec. The temperature in the outer periphery of the tumour is less than the inner part because due to blood perfusion, the heat is lost from the tumour to the healthy tissue. It is very important to maintain the optimum irradiation time and irradiation intensity, otherwise, it can damage the healthy tissue.

ACKNOWLEDGMENT

V.B. acknowledges the support provided by the Department of Mechanical Engineering at College of Engineering Pune, India.

REFERENCES

[1]. Ahmed, M. *et al.* (2011) 'Principles of and advances in percutaneous ablation', *Radiology*, 258(2), pp. 351–369. doi: 10.1148/radiol.10081634.

[2]. Ashikbayeva, Z. *et al.* (2019) 'Application of nanoparticles and nanomaterials in

thermal ablation therapy of cancer', *Nanomaterials*, 9(9). doi: 10.3390/nano9091195.
[3]. Carrafiello, G. *et al.* (2008) 'Microwave tumors ablation: Principles, clinical applications and review of preliminary experiences', *International Journal of Surgery*, 6(SUPPL. 1), pp. 65–69. doi: 10.1016/j.ijsu.2008.12.028.
[4]. Jamil, M. and Ng, E. Y. K. (2013) 'To optimize the efficacy of bioheat transfer in capacitive hyperthermia: A physical perspective', *Journal of Thermal Biology*, 38(5), pp. 272–279. doi: 10.1016/j.jtherbio.2013.03.007.
[5]. Kaur, P. *et al.* (2016) 'Hyperthermia using nanoparticles - Promises and pitfalls', *International Journal of Hyperthermia*, 32(1), pp. 76–88. doi: 10.3109/02656736.2015.1120889.
[6]. van Landeghem, F. K. H. *et al.* (2009) 'Post-mortem studies in glioblastoma patients treated with thermotherapy using magnetic nanoparticles', *Biomaterials*, 30(1), pp. 52–57. doi: 10.1016/j.biomaterials.2008.09.044.
[7]. Lee, J. H. *et al.* (2011) 'Exchange-coupled magnetic nanoparticles for efficient heat induction', *Nature Nanotechnology*, 6(7), pp. 418–422. doi: 10.1038/nnano.2011.95.
[8]. Manthe, R. L. *et al.* (2010) 'Tumor ablation and nanotechnology', *Molecular Pharmaceutics*, 7(6), pp. 1880–1898. doi: 10.1021/mp1001944.
[9]. Monga, D. *et al.* (2020) 'Optimization of tumor ablation volume for nanoparticle-mediated thermal therapy', *International Journal of Thermal Sciences*, 157(June), p. 106515. doi: 10.1016/j.ijthermalsci.2020.106515.
[10]. Soni, S. *et al.* (2015) 'Experimental and numerical investigation of heat confinement during nanoparticle-assisted thermal therapy', *International Communications in Heat and Mass Transfer*, 69, pp. 11–17. doi: 10.1016/j.icheatmasstransfer.2015.10.001.

Biographies

Dr. Vishal Bhalla holds B.Tech degree in Mechanical Engineering from P.T.U, M.E degree in Thermal Engineering from Thapar University, and a PhD in Mechanical Engineering from IIT Ropar (2018). His interests are in the field of heat transfer and thermal analysis. After completing his PhD he worked at NIT Hamirpur, and later at Brunel University London, U.K. as a Post-Doctoral research scholar. Currently he is working as Assistant Professor at College of Engineering Pune, Maharashtra, India. He is the reviewer of many reputed research papers.

Rashmika Patole received a B.Tech. degree in Electronics and Telecommunication Engineering from the College of Engineering, Pune, India, in 2010, and M.Tech. degree in Signal Processing from the same institute. She received her Ph.D. from the Savitribai Phule Pune University, Pune, India in 2021. She has been working with the Department of Electronics and Telecommunication, College of Engineering, Pune, India, as an Assistant Professor since 2013. Her research interests include speech processing, audio authentication, audio forensics, and machine learning.

Cardiovascular Fitness Recommendations

Vijay Verma, Mohit Rohilla, Anuj Sharma, Mohit Gupta

National Institute of Technology, Kurukshetra, India

vermavijay1986@gmail.com, mrmohit4000@gmail.com, anujsharma11599@gmail.com, mkgmohit20@gmail.com

Abstract

Cardiovascular disorders are one of the prevalent causes of acute fatalities in sportspersons. Regular physical activity helps maintain cardiovascular fitness and lowers the risk of cardiac disease. However, under intense physical exertion, a sportsperson may succumb to sudden cardiac death. People, with the evolution of intelligent devices, have the opportunity to track and measure their heart rate during physical activities. That's why data collected from these devices is a promising source. Though it is challenging to model such data because this kind of data has a high level of heterogeneity, diversity in scale, and complex interdependencies. Therefore, it is necessary to handle such data using some machine learning approaches for personalized recommendations. Specifically, this work focuses on the prediction of the heart rate of the user for the next moment. We have designed a model that can learn the heart rate profile of the user during exercise and can predict the short-term profile of heart rate so that users can effectively manage the maximum or minimum heart rate. Here, a Long Short Term Memory based model with dual attention has been used to predict the heart rate for the next moment of a user.

Keywords: Cardiovascular Fitness Recommendations, personalised recommendations.

1. INTRODUCTION

Living a sedentary and poor lifestyle is one of the major causes of numerous health problems. But in recent years, humans have developed technology in the form of wearable devices that have given us the ability to keep track of daily activities by only wearing smart bands or by just carrying our mobile phones. With this, we can measure various activities such as heart rate, location, altitude, activity type, calories burnt ,and much more. This type of sequential data can be harnessed for a lot of useful information and can predict heart rate and other parameters, but the collected data is often heterogeneous and consist of interdependencies that are hard to capture. Another reason is the changing activity patterns and the health fluctuation of the user. Also, data has high variance from user to user. This type of data can easily be calculated, whereas getting lots of data about a particular user is far more complicated than the former. Our target is to adopt a model to capture features in workouts or activities done by the user. We propose a method based on the Recurrent Neural Network [1], [2] model to capture gathered sequential data, which has shown significant performance [3]. An extensive dataset of activities is explored in order to build a predictive model. Here, the suggested model is based on LSTM, which takes attributes of the person and several session parameters. The model can be used to predict (1) Quantitative tasks, such as predicting workout parameters that will change simultaneously as the session goes

ahead; (2) Qualitative metrics, like finding significant features that affect performance more in comparison to others.

1.1. Motivation

The impact of the famous quote 'health is wealth' on people is increasing tremendously. Below are some points behind motivation.

- Health is the foremost requirement for doing anything. If we are unhealthy means losing out precious time from our life for getting treatment and lacking energy and confidence in every task we do.
- Campaigns like International Yoga Day, Swastha Bharat, etc., also add to our motivation (motivate people to stay healthy).
- The spread of new diseases like COVID-19 can only be tackled with a sound immunity system. Further, people with cardiovascular diseases are more vulnerable to these diseases, and that's why we use heart rate profile forecasting and prediction for the short term.
- Due to such a busy life, we tend to do a good workout in limited time and also acc to our health factors.

Therefore, this work will help users to predict their workout profile (speed and heart rate) and also suggest workouts for better immunity in individuals. The overall contribution of this work is summarized as follows:

- To study different techniques/algorithms and find the best one based on accuracy.
- To provide the personalized prediction of the workout profile (speed and heart rate) of a user.
- Implement the model in real-time by giving a prediction for the short term.

2. LITERATURE REVIEW

Table 1 summarizes a few different paradigms associated with fitness recommendations. In particular, each paradigm's methodology has been illustrated using some representative research articles. Further, we have listed a few limitations, in terms of the pros and cons, of these techniques.

Table 1: Different methods for fitness recommendations

Paradigm	Brief Methodology	Pros	Cons
Mining Sensor Data. [4][5][6]	This category falls into pervasive computing and studies about the collection and handling of data from wearable and mobile devices like smartwatches and fitness bands. Here data can be related to the various types of behaviour of a person like sleep order, health, exercise and many more. To model a person's wellness by using some sensor data is a present-day growing trend.	Users' exercise data can be collected easily and can be combined with social network details/statistics to forecast his/her fitness trends [7]. Limited training data can be used to detect exercise types like walking, running, aerobics, etc. [7] specifically focused on the Body Mass Index (BMI) for the same.	Prediction and recommendation tasks are not satisfactory as they are not using sequence prediction (sequential modelling).

Context-aware modelling.[8][9]	A system or its components can collect information about its environment at any given time and accordingly adapt behaviours; this is known as context awareness. Fitness and exercise data have heterogeneity in the input structure naturally (contextual data and sequential information), and hence context-aware modelling can be used.	Recommender systems, clinical predictions, social networks with contextual information, etc., are some of the applications which can be fulfilled by context-aware modelling. RNN models can be used with the context-aware layer [8].	An LSTM layer with contextual embedding modules performs better than context-aware modelling as it also learns from historical sequences. Measurement within each activity does not consider in context-aware modelling.
RNN-based sequential modelling.[10][11]	RNN (Recurrent Neural Networks) recently has shown exceptional efficacy in modelling sequential data such as clinical data, text, and audio. These are a type of neural network where the input to the current unit is fed through the output of the previous unit along with the new input of the current unit.	RNN-based models can be combined with convolution layers (CNN) to show short as well as long-term dependencies both. This model performs better than Linear SVM and other RNNs.	Measurement within each activity does not consider in RNN-based sequential modelling.
Personalized Recommendation. [7][12]	User behaviour is a crucial point of personalized recommendations. Also, these are based on a large amount of historical data of the user and then recommend some products in static scenarios like e-commerce. Personalized recommendations incorporate content like item attributes and contexts like user clicks or purchases. Now, researchers from these industries are trying to evolve such systems for personalized recommendations.	Various targets, such as user's goals, desirable performance and environment, can be considered for personalized running route recommendations [12]. A combination of workout information and social network information can be used to conduct wellness predictions [9].	These works don't centre around the modelling of sequential fitness data like the heart rate/speed sequences of a user. A few works in personalised recommendation provide hand-crafted statistics instead of providing the whole sequential information of each activity/task.

3. BACKGROUND

3.1. Recurrent Neural Network(RNN)

It is a general feedforward neural network with internal memory. RNN performs the identical function for each input of data, and that's why recurrent in nature. The current input's result relies on the previous unit computation. The output is copied after producing from the previous step and then sent back into the recurrent network. These are gaining popularity in today's world very drastically from advances in network designs and also by increasing the computational power of Tensor Processing Unit (TPU) and Graphic processing units(GPU). These networks give the best result in the case of sequential data because the RNN unit is easily able to maintain information about the previous unit result by using its internal memory. To process the sequence of data, RNNs can use internal memory, which distinguishes RNNs from feedforward neural networks. That's why, with all these features, tasks such as handwriting recognition, speech recognition, time series prediction etc., can be easily performed by RNN. Unlike other neural networks, all the inputs are related to each other in RNNs.

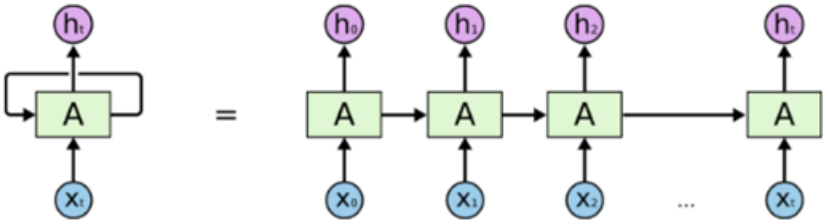

Figure 1. Unfold Recurrent Neural Network

The drawback of the RNN is that it can't be used with a very long sequence, and it has a problem of vanishing gradient. Also, it is a very difficult task to train an RNN. In figure 1, Xt is an input, A is an activation function, and ht is the output corresponding to each cell.

3.2. Long Short Term Memory (LSTM)

The LSTM has an architecture similar to the RNN, but it has overcome the limitations of RNN (like it is fully capable of remembering the past values of the context). These values will not change over the entire training period of the model. Basically, an LSTM contains four components, which are LSTM Recurrent Components, Gates, Blocks, and LSTM units. LSTM units are capable of storing the values for short as well as for a long time. An LSTM Block contains a lot of similar units. LSTMs come under deep neural networks. So, well known for their better results. LSTMs are implemented in parallel/stacked systems to minimize the workload of large-scale computing systems. To control the overall flow of information, LSTM has three gates. Different logistic functions are used for implementing these gates, for having a result between 0 and 1. The name of the gates are Output gate, Input gate and Forget gate. For the entry of information inside or outside the memory, these logistic functions are multiplied. The input gate plays a pivotal role in controlling the entry of new values into memory. The Forget gate controls the amount of time till a value will remain inside of memory. We can forget the old value when a new value is available. This functionality is controlled by the update gate. The combining effects of input and forget gates are represented by the update gate. Following is the basic information of all the gates of a Long short term memory (LSTM) unit.

- Input gate – input gate plays a pivotal role in controlling the entry of new values into memory. Through [0,1], which values to enter, are decided by a sigmoid function. Further, these values pass through a tanh function to determine their significance ([-1,1]).
- Forget gate – It discovers the details which need to be abducted from the unit. This is done using a sigmoid function or some other activation function. A number between 0 and 1 is given as output (i.e. omit this or keep this).
- Output gate – This gate is used to decide the output. Like the input gate, here also through [0,1], which values to enter, are decided by a sigmoid function. Further, these values pass through a tanh function to determine their significance ([-1,1]).

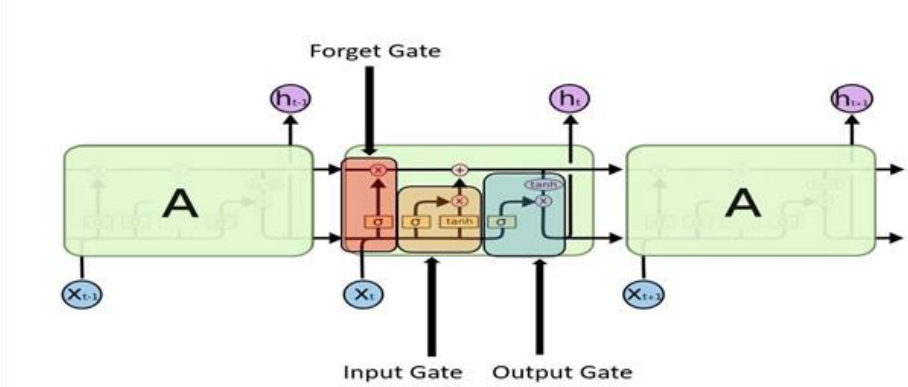

Figure 2. Typical DataCenter Infrastructure [18, 19]

4. PROPOSED APPROACH

We have taken two kinds of sequential data problems, i.e., prediction for the short term and prediction of workout profile [13].

Prediction of workout profile: This module takes contextual sequences, attributes of a user's workout, historical sequences, and the total time of a workout and predicts the target. This task can be considered as a case when the user has given his intended route and desired the whole time, i.e., how much the user wants to perform the intended task so that the system predicts or forecast what would be the heart rate profile of the user.

Prediction for the short term: This module takes contextual sequences, attributes of a user's workout, historical sequences, along with total duration. These inputs can be referred to as estimates for a particular period of time corresponding to a fixed duration of a single activity session. This allows us to predict the heart rate for a short term during the activity session.

The interrelationship between tasks: Basically, both the tasks differ in inputs and outputs and application scenarios. Short term prediction module aims to predict sequential parameters during the activity session. It is like traditional time-based models used to predict the parameters at a particular instant of time. This is useful in cases of anomaly detection and real-time prediction; e.g., this can advise the user to slow down the pace of a workout in case his heart rate is going to exceed the next moment.

Whereas predicting of workout profile module aims to predict the performance of the user on being provided route and time as input. It will predict trends for a complete session like maxima, minima and average of the parameter, i.e., heart rate, and it also predicts the speed of the workout in the same manner before the user starts doing the activity. From this model, the user can formulate his plan for the workout that can meet his expectations, i.e., how many calories she/he wants to burn and also judge if the workout is according to the ability of his body or not. Moreover, the model helps to formulate a plan which is according to her/his expectations of performance, and it can also be used to find alternate routes for the workout. In other words, this model can predict a few suggestions, and the user can check these against his/her expectation.

4.1. Modules Split-Up

Figure 4.1 depicts the overall architecture of the system along with the different modules, and a sequence of data flow is shown in Figure 4.2.

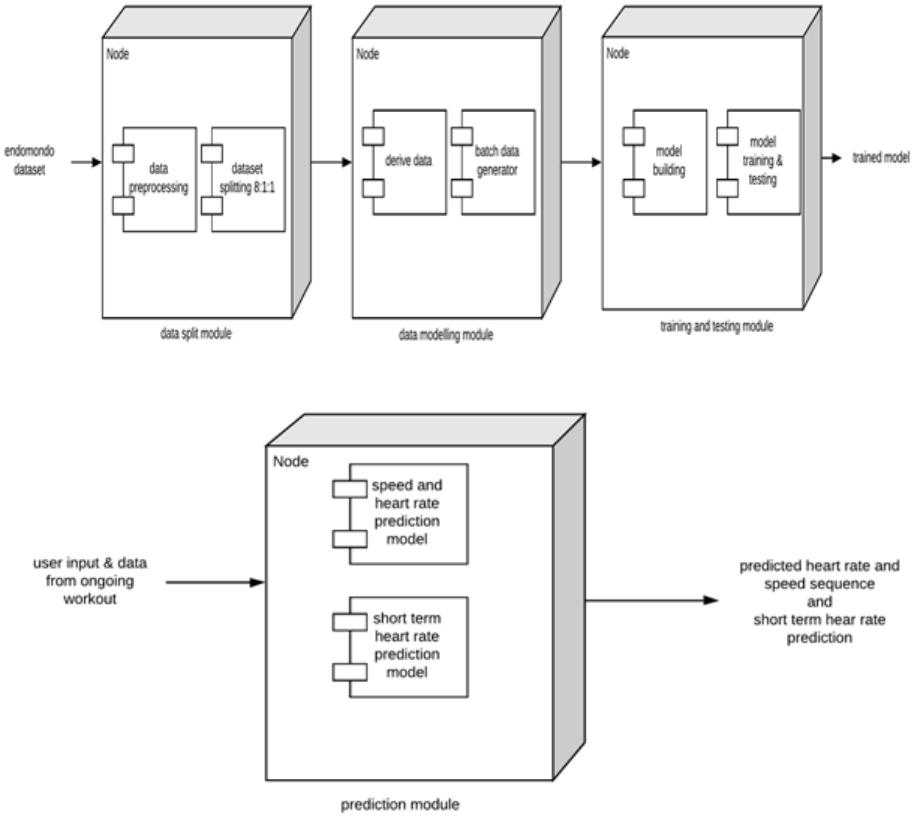

Figure 3. System Architecture of the proposed approach

- Data Split Module – This module does preprocessing and test train splitting of data. After that, data is in a usable form.
- Data Modeling module – This module derives some additional attributes like distance, speed, etc., for dividing the whole dataset into batches of small size.
- Training and testing module – Here, we apply LSTM to train and test our model and finally get the trained model.
- Prediction Module – This module takes inputs like route as the sequence of longitude, latitude and altitude, time etc. and predicts the heart rate and speed and also makes predictions for the short term.

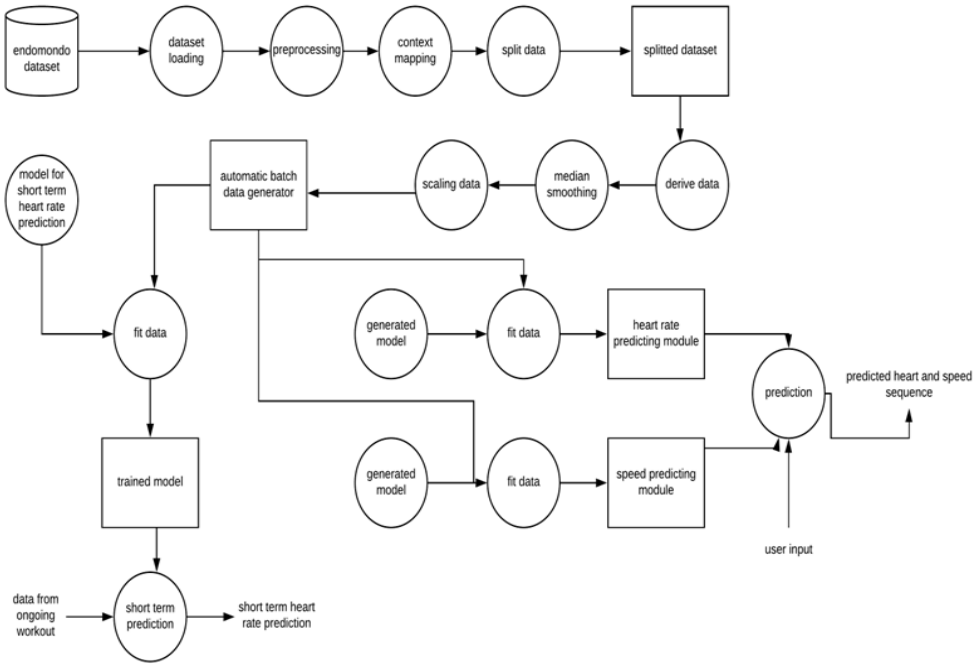

Figure 4. The flow of data in the system

5. EXPERIMENTS & RESULTS

The experiments are designed to forecast the profiles of workouts, i.e., the speed and heart rate profile of the user. A user can use this profile forecast to find a workout plan which can meet the expectation of the user on performing a particular task. Further, prediction for the short term will be helpful to detect any kind of anomaly in his/her heart rate and also helpful for real-time decision making. For example, the user can be advised that he/she ought to slow down in the next moment so that his/her heart rate will not exceed the maximum desired rate.

5.1. Dataset

The dataset from a popular website called endomodo.com [13] is used for all the experiments. The dataset consists of measurements and contextual data. Measurements include 1)timestamps 2)heart rate 3)speed 4)distance and contextual data include 1)latitude 2) longitude 3)gender 4) altitude 5)user 6) sport 7)user identity.

The dataset has a massive missing rate since not all devices like smart bands provide all the attributes mentioned above, and that's why we preprocess the data and add a few derived attributes like distance and derived speed for training our model. The dataset contains more than 2,00,000 records of workouts spread across more than 900 users.

5.2. Workout Profile Forecasting

Due to the large dataset and each instance of the dataset containing a huge amount of continuous sequential data having altitude, longitude, latitude, timestamps, heartbeat, and data from other sensors, we took a slice of 15000 workout records of 90 unique users. Firstly,

we partitioned the dataset into training, testing, and validation sets into the ratio of 8:1:1. We have used 50 epoch/iterations to train the model for heart rate prediction, and the score(loss) decreased from 10364.802 to 259.49. Table 2 shows the details of the best scores for workout profile forecasting.

Table 2. Scores And Errors In Workout Profile Forecasting

Profile	Dataset (Training/Testing)	Best Score	Mean Absolute Error(MAE)	Root Mean Squared Error(RMSE)
Heart Rate	Training	259.49	12.95	17.216
	Testing	291.96	12.98	16.82
Speed	Training	15.89	2.73	4.40
	Testing	25.39	2.62	5.104

The score can further be improved by increasing the number of epochs/iterations, as shown in Figure 5.

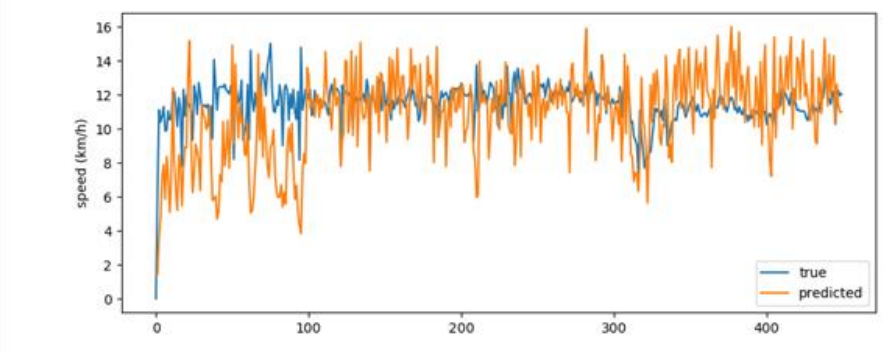

Figure 5. Speed Profile Forecasting

5.3. The Prediction of Short-Term

As shown in Figure 5.2, it is clearly visible that with an increasing number of iterations, the loss reduces significantly up to a point.

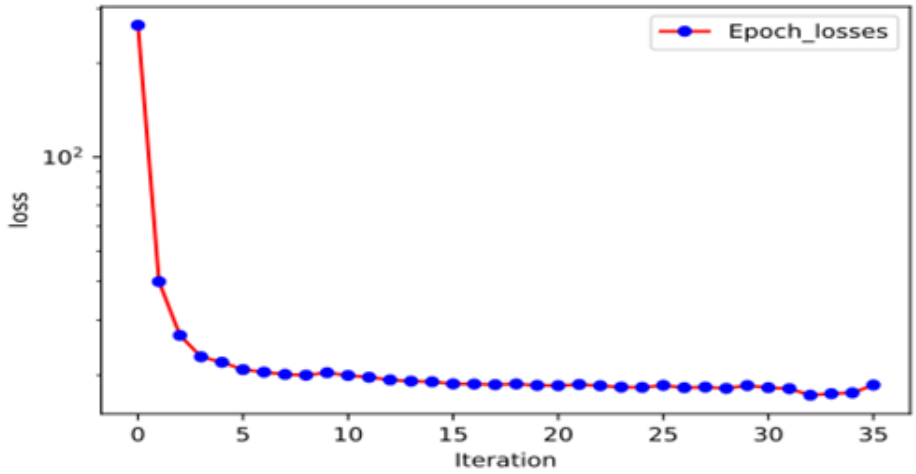

Figure 6. Iteration v/s Loss for prediction of short term

Further, the prediction of short-term heart rate (in BPM) is evaluated against the number of epochs/iterations. Results in Figure 7 show promising values for a sports person's short-term prediction of heart rate and can be used in real-time for decision-making.

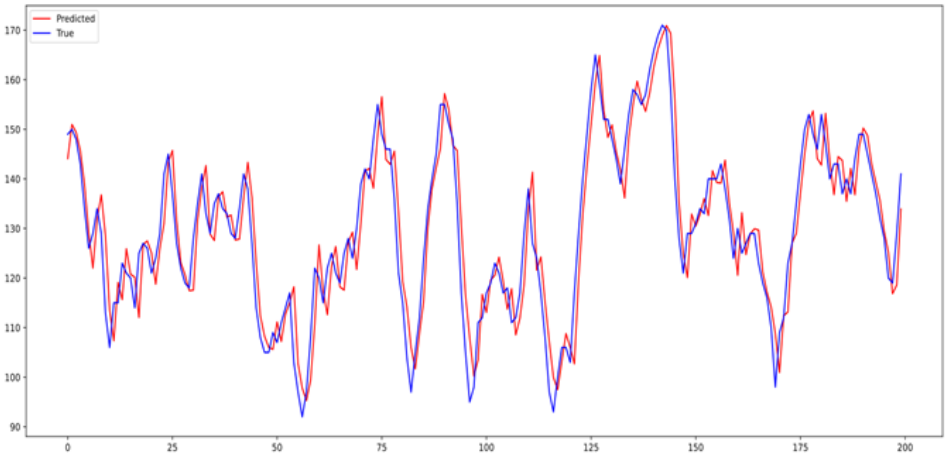

Figure 7. Prediction of short-term Heart rate(real-time)

6. CONCLUSION AND FUTURE WORK

We have presented a system that solves problems of sequential forecasting in exercising and fitness-related data and can be used as an elementary unit for improving personalized fitness recommendation applications. From the supplementary information like user ID, sport/activity type and historical sequences of the workout, embedded description/presentation can be learned. Each of this embedded information is comprised of a sequential modelling framework (Long short-term memory) to achieve high accuracy of prediction.

We have tried to provide very high-quality predictions (short-term predictions) with promising results. Furthermore, interactive recommendations and some other recommendations like route recommendations (which fulfilled the user performance preferences and goals) can also be implemented by further studies.

REFERENCES

[1] K. Cho *et al.*, "Learning phrase representations using RNN encoder-decoder for statistical machine translation," in *EMNLP 2014 - 2014 Conference on Empirical Methods in Natural Language Processing, Proceedings of the Conference*, 2014.

[2] S. Hochreiter and J. Schmidhuber, "LSTM 1997," *Neural Comput.*, 1997.

[3] Z. Che, X. He, K. Xu, and Y. Liu, "DECADE: A Deep Metric Learning Model for Multivariate Time Series," in *KDD Mining and Learning from Time Series Workshop*, 2017.

[4] T. Kurashima, T. Althoff, and J. Leskovec, "Modeling Interdependent and Periodic Real-World Action Sequences," 2018.

[5] H. Banaee, M. U. Ahmed, and A. Loutfi, "Data mining for wearable sensors in health monitoring systems: A review of recent trends and challenges," *Sensors (Switzerland)*. 2013.

[6] A. K. Chowdhury, A. Farseev, P. R. Chakraborty, D. Tjondronegoro, and V. Chandran, "Automatic classification of physical exercises from wearable sensors using small dataset from non-laboratory settings," in *2017 IEEE Life Sciences Conference, LSC 2017*, 2018.

[7] A. Farseev and T. S. Chua, "TweetFit: Fusing multiple social media and sensor data for wellness profile learning," in *31st AAAI Conference on Artificial Intelligence, AAAI 2017*, 2017.

[8] M. R. De Araujo, P. M. P. Ribeiro, and C. Faloutsos, "Tensorcast: Forecasting with context using coupled tensors (best paper award)," in *Proceedings - IEEE International Conference on Data Mining, ICDM*, 2017.

[9] X. Li, S. Wu, and L. Wang, "Blood pressure prediction via recurrent models with contextual layer," in *26th International World Wide Web Conference, WWW 2017*, 2017.

[10] G. Lai, W. C. Chang, Y. Yang, and H. Liu, "Modeling long- and short-term temporal patterns with deep neural networks," in *41st International ACM SIGIR Conference on Research and Development in Information Retrieval, SIGIR 2018*, 2018.

[11] Y. Qin, D. Song, H. Cheng, W. Cheng, G. Jiang, and G. W. Cottrell, "A dual-stage attention-based recurrent neural network for time series prediction," in *IJCAI International Joint Conference on Artificial Intelligence*, 2017.

[12] B. Loepp, T. Donkers, T. Kleemann, and J. Ziegler, "Impact of item consumption on assessment of recommendations in user studies," in *RecSys 2018 - 12th ACM Conference on Recommender Systems*, 2018.

[13] J. Ni, L. Muhlstein, and J. McAuley, "Modeling heart rate and activity data for personalized fitness recommendation," in *The Web Conference 2019 - Proceedings of the World Wide Web Conference, WWW 2019*, 2019.

Biographies

Vijay Verma is currently working as an assistant professor at Computer Engineering Department, National Institute of Technology (NIT), Kurukshetra, India. He holds MTech. degree from Indian Institute of Technology (IIT) Roorkee and PhD degree from NIT Kurukshetra, Haryana, India. His research interest includes Data Mining, Recommender Systems, Personalization, and related areas.

Mohit Rohilla received bachelor's degree (B.Tech.) in Information Technology from NIT Kurukshetra in 2020 and currently working as a software engineer in SAP Labs India.

Anuj Sharma received bachelor's degree (B.Tech.) in Information Technology from IIIT Sonepat (Mentor: NIT Kurukshetra) in 2020 and currently working as a software engineer in ServiceNow Software Development India Private Limited.

Mohit Gupta received bachelor's degree (B.Tech.) in Information Technology from IIIT Sonepat(Mentor: NIT Kurukshetra) in 2020 and currently working as a software engineer in Delhivery India.

.

A 3D Finite Element Analysis of Splinted and Non-Splinted Mandibular Incisors with Reduced Periodontal Tissue Support

Mariam Maroof, R. Sujithra, R. P. Tewari

Department of Applied Mechanics, Motilal Nehru National Institute of Technology, Allahabad, Prayagraj, Uttar Pradesh, India
mariammaroof09@gmail.com, rsujithra@mnnit.ac.in, rptewari@mnnit.ac.in

Abstract

Tooth mobility is an extremely discomfort situation that is caused by periodontitis, occlusal trauma, or even a loss of an adjacent tooth. This article describes the use of Stainless-steel (SS) and Superelastic (SE) Ni-Ti to develop a dental splint for periodontally compromised mandibular anterior teeth. FEA is carried out to evaluate the changes in displacement and stress distribution of mandibular anterior teeth and supporting tissue during small biting force (30N) when splinted by SS and SE Ni-Ti splint. Both the dental splints are observed to be equally functional at distributing the stresses from the loaded incisors to the unloaded canines. When splinted by SS, the stress level sufficiently decreases on the central incisors by 50% (L1-48%, R1-52%) and lateral incisors by 60% (R2, L2). SE Ni-Ti dental splint resulted in a decrease of the stress on the central incisors by 46% (L1-45%, R1-48%) and lateral incisors by 55% (L2-55%, R2-56%), showing an almost equal amount of reduction in stress. The labial displacement reduces by an average of 63% and 60% for the incisors when splinted by SS and SE Ni-Ti dental splints, respectively. There is 48% and 44% reduction in the displacement of the incisor's vertical gingival direction when splinted with SS and SE Ni-Ti, respectively. The splint effect is higher for SS which leads to higher clinical failure rate due to its higher rigidity than SE Ni-Ti. This study shows that both types of dental splints SS (rigid) and SE Ni-Ti (flexible), reduces stress level around periodontally comprised teeth.

Keywords. Dental splint, periodontal splint, periodontitis, tooth mobility, superelastic, Ni-Ti, splint effect.

1. INTRODUCTION

Periodontitis, is a disease of the periodontal tissues resulting in attachment loss or pocket formation of varying depth around the tooth due to the destruction of alveolar tissue and widened periodontal ligament. It is induced by bacterial biofilms that accumulate in the gingival margin, characterized by gingival inflammation [1, 2]. One of the unwanted effects of periodontal disease is tooth mobility [3]. Besides periodontitis, primary or secondary occlusal trauma, re-implantation of missing teeth, and orthodontic reposition can also lead to tooth mobility [4]. Even a single anterior tooth loss may cause an adjacent tooth to be mobile. Such tooth mobility usually refrains patients from brushing and even altering their feeding or masticatory habits [5].

The mechanoreceptors of the periodontal ligament and alveolar bone control the normal physiological function, such as masticatory forces during chewing or food/drink intake. Reduced periodontal tissue support can lower their threshold level [6]. Depending on the clinical situation, such teeth are typically extracted and re-implanted in case of severe dislocation [7]. But to regain periodontal health, one of the non-invasive and effective practices in restorative dentistry is dental splinting which allows the patient to keep their natural teeth longer. Splint is a device that maintains hard/soft tissues in a predetermined position [8]. A dental splint should be firm enough to allow the fixation of teeth in their anatomical position during the masticatory forces. Moreover, it should be flexible enough to enable periodontal and alveolar tissue healing by allowing physiologic tooth movement [7,9]. Dental Splinting is usually done on the 'injured' teeth by attaching them with as few 'uninjured' adjacent teeth as possible. Various authors have evaluated a variety of rigid, semi-rigid, and flexible dental splints such as orthodontic-wire, wire-composite, resin, fiber-glass, button-bracket, Titanium Trauma Splint (TTS), etc. Among these, the alloy-based periodontal splints are usually in wire form which causes high rate of discomfort to the patient especially during speech or mastication. The dental splints require at least 14 days to heal the PDL, so there is a need to investigate dental splint in form of thin strip rather than protruding wires. The dental splints so far developed are made of conventional materials such as stainless-steel and woven fibers. Superelastic Ni-Ti is an emerging smart alloy in the field of dentistry as it has been used as orthodontic archwires and endodontic files. In this work, the authors have utilized the property of superelastic Ni-Ti by analyzing its function in the form of dental splint which is not yet practiced.

The objectives of this study were to utilize finite element analysis (FEA) to analyze the changes in displacement and stress distribution of anterior teeth and supporting tissue periodontal ligament (PDL) of the mandible during small biting force (30N), when splinted by alloy-based Superelastic Ni-Ti (SE Ni-Ti) and conventional stainless-steel (SS) periodontal splint as thin strip. The anterior teeth considered were left and right central and lateral incisors (injured teeth) splinted with left and right canines (uninjured teeth). An effort is also made to analyze the influence of splint material by occlusal and bite forces during mastication. The authors have assumed that the tooth does not possess inherent mobility but the reduction of bone level around incisors is the primary cause of tooth mobility.

2. MATERIAL AND METHODS

In this study, only the incisors and canines are used for determining the effect of splinting because tooth mobility due to periodontitis or occlusal trauma is primarily prevalent in the mandibular incisor region [10]. Stereolithography (.stl) files are obtained from [11] to evaluate the proposed objectives. The .stl file consists of the mandibular anterior and posterior teeth (incisors, canines, premolars, and molars). Hence, only the anterior teeth are extracted for the analysis as shown in Figure 1 The anterior teeth are assigned the notation as LC (left canine), L2 (left lateral incisor), L1 (left central incisor), R1 (right central incisor), R2 (right lateral incisor) and RC (right canine).

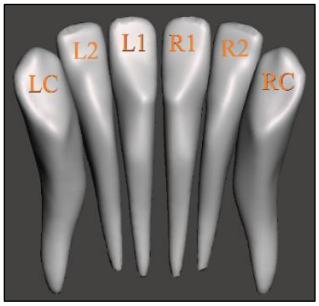

Figure 1. Mandibular anterior teeth

The .stl file is then imported in ANSYS SpaceClaim (3D CAD Modelling Software) and it is converted to a 3D finite element model. Altogether three models are designed by constructing a supportive structure (PDL and mandibular jaw) around the extracted anterior teeth for non-splinted and splinted applications. A 0.25 mm thick periodontal ligament layer (PDL) is modeled around the rooted portion of each tooth as shown in Figure 2(a). The mandibular jaw is designed (Figure 2(b)) to mimic the dental arch with approximately 40% bone reduction level around the central and lateral incisors [12]. In contrast, the canines are healthy with no jaw abnormality around them. From the patient's perspective, the dental splint should not traumatize or interfere with the teeth, surrounding tissues, occlusion, or speech [7, 13], for which 2-3mm width of the dental splint is recommended [14]. Thus, to model splinted teeth, 2mm wide and 0.2mm thick SS and SE Ni-Ti periodontal splints are bonded on the lingual surface of the anterior teeth splinted from left canine to right canine as shown in Figure 2(c).

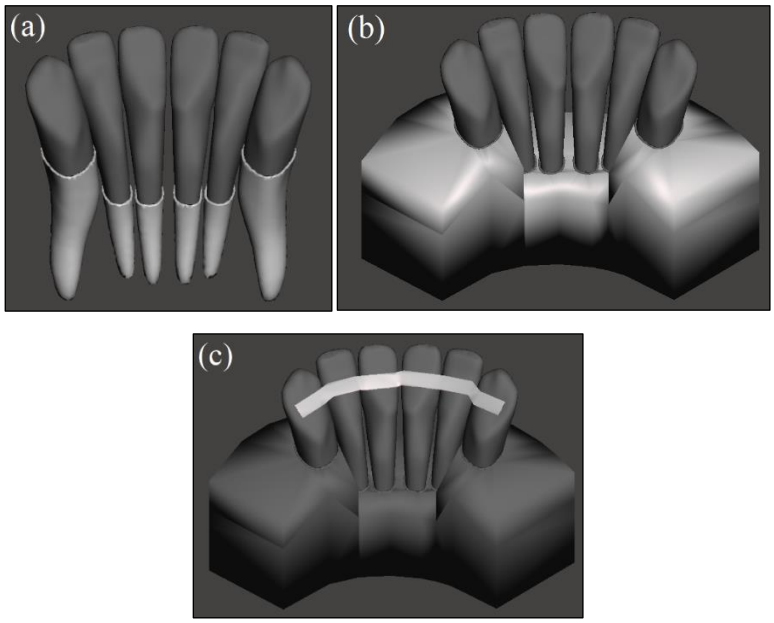

Figure 2. 3D model (a) PDL, (b) Mandible jaw (c) dental splint, around anterior teeth

The isotropic material properties are considered for tissues and dental splint. The mandibular jaw is created as cortical bone. The dental splints are assigned the properties of stainless steel (SS) and superelastic Ni-Ti (SE Ni-Ti) as given in Table 1 and Table 2. After the model is precisely developed in ANSYS SpaceClaim, it is exported to ANSYS Workbench Ver. 19.2 (ANSYS, Inc., Canonsburg PA, USA) for displacement and stress distribution analysis. Models are meshed with 90126-92195 tetrahedral 3D elements connected by 163428-167799 nodes.

Table 1. Isotropic Elastic Properties

	Young's Modulus (MPa)	Poisson's Ratio
PDL [12]	0.667	0.49
Tooth [12]	20300	0.26
Cortical Bone [12]	34000	0.26
Stainless-steel [21]	90,000	0.3
Superelastic Ni-Ti [22]	44000	0.33

Table 2. Superelastic Properties

	Start of transformation loading (MPa)	End of transformation loading (MPa)	Start of transformation unloading (MPa)	End of transformation unloading (MPa)	Transformation strain
Superelastic Ni-Ti [22]	377	430	200	140	0.06

Since the physiological masticatory forces are exerted primarily in a vertical direction and are usually found to be in the range of 40-200N. But for the soft foods, 10-20N are utilized [13, 15] so vertical load of 30N is chosen to replicate the forces applied on the teeth for biting small and soft foods. As shown in Figure 3, force is applied on the incisal edge of all the four incisors by gradually increasing the load intensity from 0-30N. For static analysis, fixed support is provided to constrain the mandibular regions with the boundary condition similar to the actual jaw. The contacts between the teeth-PDL, PDL-bone, and splint-teeth are defined as bonded to prevent slippage or separation. Bonded condition is taken as the contact among the teeth, PDL and mandible as it is assumed that the tooth does not possess inherent mobility but the reduction of bone level around incisors is the primary cause of tooth mobility [16]. Altogether, three analyses are performed to evaluate the effect of splinting on mandibular anterior teeth.

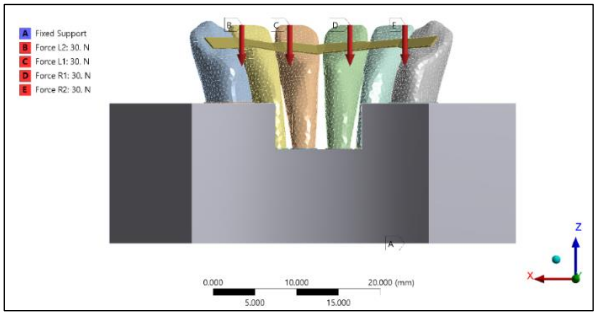

Figure 3. Boundary Conditions of the model

Displacements are evaluated in each incisor's labial/lingual and vertical gingival direction by considering one of the nodes of each incisal edge. To analyse the changes of tooth mobility, a splint effect is calculated as Horizontal and Vertical Splint effects (HSE and VSE, respectively). The HSE and VSE are defined as the difference in horizontal and vertical displacement (HD and VD, respectively) for Non-Splinted (NS) and Splinted (S) teeth as given in Equations 1 and 2. The stress distribution pattern is analysed by evaluating changes in stress values in incisors due to the distribution of forces over to the canines.

$$\Delta HSE = HD_{NS} - HD_S \quad (1)$$

$$\Delta VSE = VD_{NS} - VD_S \quad (2)$$

3. RESULTS AND DISCUSSION

3.1. Stress distribution analysis of anterior teeth

Due to the masticatory load on the incisors as given in Figure 4(a), the average stress generated were high (18-19.5 MPa), whereas the average stress on the canine is found to be very small (0.4-0.5MPa) as it is transferred through the mandible. The high stress on the incisors is predominantly because of the reduced mandible bone (almost 40%) around them thereby exposing the root directly to the vertically applied load. The canines in this case show negligible stress. When splinted by SS, the stress level was sufficiently distributed over to the canines thereby decreasing the stress on the central incisors by almost 50% (L1-48%, R1-52%) and lateral incisors by 60% (R2, L2). Almost equal amount of reduction in stress is shown when SE Ni-Ti is used as dental splint material. SE Ni-Ti dental splint results in decreased stress on the central incisors by 46% (L1-45%, R1-48%) and lateral incisors by 55% (L2-55%, R2-56%), as it distributes the masticatory and perioral muscle forces over to the canines through its surface attachment. When splinted by SS, maximum stress is generated at the canines (144-170MPa) whereas when splinted by SE Ni-Ti, lateral incisors show the maximum stress value (L2-107MPa, R2-126MPa) which can be due to the contact with the splint as well as with the canines. SE Ni-Ti dental splint develops the stress on the canines around 88-118MPa.

Due to the collateral effect of splinting, the stress increases in the canine by almost 1740% for SS and 1630% for SE Ni-Ti dental splint. But this stress level can be accepted as the canines are optimally supported by the mandible jaw. The stress distribution pattern among the anterior teeth of mandible before splinting and following placement of dental splints is shown in Figure 5. For non-splinted model (Figure 5a)), the highest stress is observed around

the apical region of the incisors with a value of almost 158MPa. Figure 5(b) and 5(c) shows stress generation on the canines due to load transfer through dental splint. Higher amount of stress distribution is observed when splinted by SE Ni-Ti at the contact of splint and teeth.

Stress distribution around PDL of each tooth is equally important to evaluate the transmission of load from the teeth to the jaw. The average stress variation in each tooth PDL can be seen in the Figure 4(b). When teeth are not splinted, the stress is developed around the cervical region of incisors only in the range of 0.6-0.8 MPa. Under both the splinting material, the highest stress is around the cervical region of the incisors. The average stress varies as 0.18-0.46MPa and 0.16-0.51MPa when splinted by SS and SE Ni-Ti, respectively. This indicates that mild load is applied to the healing tissues (PDL) as compared to the stress developed in the teeth. The sections of high stress are the contact areas of tooth-PDL (2.4MPa and 2.65MPa at central incisors when splinted by SS and SE Ni-Ti, respectively). Figure 6 represents changes in the stress distribution pattern among the anterior teeth PDL. Figure. 6(a) shows stress in incisors PDL only, whereas Figure 6(b) and 6(c) shows stress around all anterior teeth PDL by placement of dental splints.

Although, there is almost no significant difference in the average stress distribution by the two kind of dental splints, but the stiffness of the material usually plays a significant role in the healing of PDL by not completely restricting the tooth displacement but allowing small mobility. The stress developed on the canine and dental splint indirectly through splinting is equally important and it is less in case of SE Ni-Ti as compared to SS dental splint as discussed earlier. Thus, SE Ni-Ti can provide better tooth splinting capability with less damage to teeth as well as dental splint and providing higher amount of stress distribution among the teeth.

Both SE Ni-Ti and SS dental splint are observed to be equally functional at distributing the stresses from the loaded incisors to the unloaded canines. This might be because SS possesses comparably higher elastic modulus (rigidity) that leads to lower stresses under vertical loading conditions. Similarly, SE Ni-Ti lacks sufficient rigidity (low austenitic stiffness), leading to comparable reduction in stresses. Thus, both types of dental splints, rigid (SS) and flexible (SE Ni-Ti), reduces stress level around periodontally comprised teeth when compared with non-splinted teeth. This is due to the functional advantage of load distribution onto the adjacent healthy teeth via thin strip dental splint.

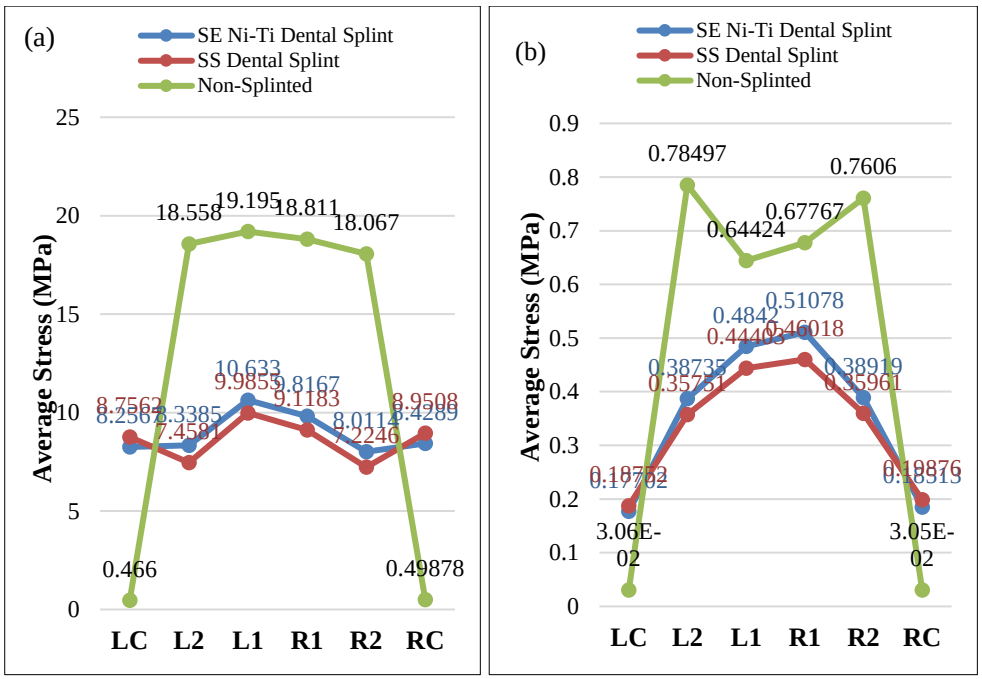

Figure 4. Average stress distribution in (a) anterior teeth, and (b) PDL under vertical load of 30N

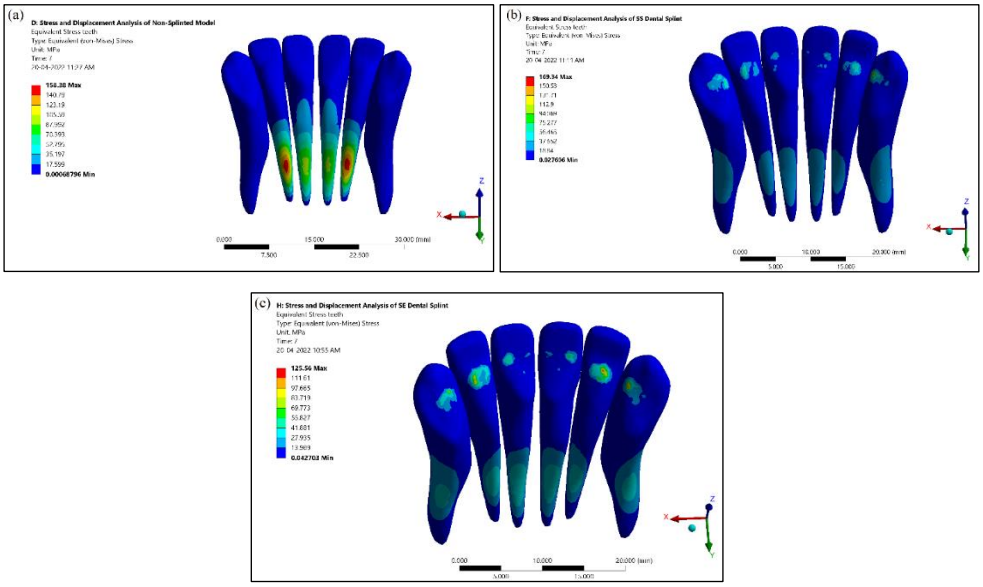

Figure 5. Stress distribution pattern in anterior teeth (a) without splint, and with (b) SS and (c) SE Ni-Ti dental splint

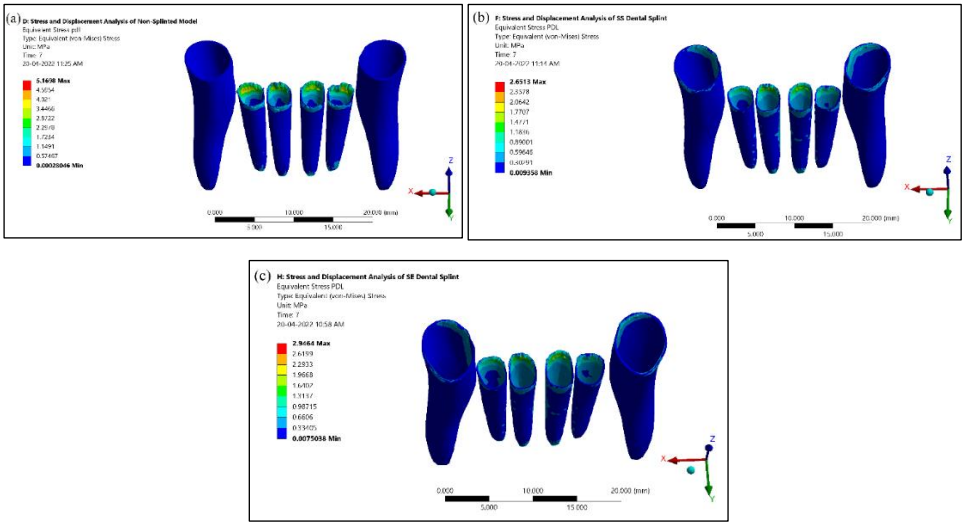

Figure 6. Stress distribution pattern in anterior teeth PDL (a) without splint, and with (b) SS and (c) SE Ni-Ti dental splint

3.2. Displacement of incisors

Although stress redistribution is beneficial, the displacements are also important as they inform about retaining the splint for a long duration in patients with reduced bone thickness [12]. The displacements of the labial/lingual and vertical gingival direction for the four incisors is shown in Table 3. Lateral incisors are found to be displaced the most (1.4 mm) in the labial direction whereas central incisors are found to be displaced the least (1.15mm) in the downward vertical gingival direction.

Dental splinting results in change in the displacement of the incisors for the two different materials of splint. The labial displacement reduces by an average of 63% and 60% for the incisors when splinted by SS and SE Ni-Ti dental splints, respectively. There is 48% and 44% reduction in the displacement of the incisor's vertical gingival direction when splinted with SS and SE Ni-Ti, respectively. SE Ni-Ti dental splints possess high elastic strain recovery capability (6-7%) as compared to SS dental splints, so it shows slightly higher degree of displacement. SE Ni-Ti dental splint can be taken as an appropriate choice in reducing displacement of the incisal edge as it does provide result equivalent to SS dental splint but qualitatively it provides higher flexibility which has clinical implications as they allow PDL healing along with patient comfort in the lingual region.

Table 3. Average Displacement of incisors

	Labial/lingual direction (mm)				Vertical gingival direction (mm)			
	L2	L1	R1	R2	L2	L1	R1	R2
Non-Splinted	-1.400	-1.214	-1.230	-1.427	-1.199	-1.149	-1.181	-1.238
Stainless-steel splint	-0.396	-0.575	-0.556	-0.378	-0.507	-0.720	-0.716	-0.502

Superelastic Ni-Ti splint	-0.440	-0.621	-0.603	-0.415	-0.549	-0.776	-0.781	-0.541

*Negative value gives the labial/downward gingival displacement

3.3. Splint effect on incisors

Dental splinting is considered beneficial as physiological tooth mobility is permitted to aid healing and reduce ankylosis [17]. In this study, such changes in tooth mobility is measured through the parameter called 'Splint effect' [18]. The interpretation of splint effect depends on the interactions between the teeth and dental splint.

The splint effect of each incisors is tabulated in Table 4. Lateral incisors show higher HSE and VSE than central incisors for the same value of load (30N). This shows that lateral incisors are more affected by splints. The splint effect is similar for both SS and SE Ni-Ti dental splint with higher reduction in horizontal tooth mobility as compared to vertical one. The higher splint effect of SS is because of its higher rigidity as compared to SE Ni-Ti. But higher rigidity can contribute to a higher clinical failure rate thereby giving SE Ni-Ti as a better substitute with similar mobility and higher flexibility. This indicates that material of dental splint is an adequate task to choose such that it ensures labial/lingual teeth stabilization, while allowing for vertical physiological tooth mobility.

Table 4. Splint effect of incisors

	HSE (mm)				VSE (mm)			
	L2	L1	R1	R2	L2	L1	R1	R2
Stainless-steel splint	-1.004	-0.639	-0.674	-1.049	-0.692	-0.429	-0.465	-0.736
Superelastic Ni-Ti splint	-0.96	-0.593	-0.627	-1.012	-0.65	-0.373	-0.4	-0.697

4. CONCLUSION

FEA is a valuable technique for indicating the mechanical aspects of newly developed biomechanical devices and their interaction with human tissues, which are difficult to measure in vivo. The FEA done in this study states the benefit of splinted teeth through stress redistribution and displacement analysis in biting small and soft food particles. The connection between the teeth through splinting must be strong enough to resist the forces of mastication [19]. In this context, the SS and SE splints have proved beneficial in distributing stresses over to the canines. Maintaining a certain degree of tooth mobility is appreciated for periodontal healing [20]. Thus, the greatest HSE and VSE is found in lateral incisor splinted by SS and SE Ni-Ti dental splints.

Based on the results, both SS and SE Ni-Ti can be used for splinting depending on the amount of rigidity required. For example, flexible SE Ni-Ti can be used for trauma involving the PDL, whereas for hard-tissue injuries such as alveolar fracture, rigid SS can be used. In general, both SS and SE Ni-Ti can be chosen as suitable splint as they allow vertical flexibility but maintains adequate lateral support. The highly flexible SE Ni-Ti dental splints

are expected to be more durable than other one in terms of failure rate. Various kinds of light-curing resins are usually used to fix dental splints on teeth. The amount of these resins influences the rigidity of the dental splint, reducing the unrestricted and deformable splint section. Future investigations will be focused on the effect of proposed thin strip dental splints when the teeth will possess inherent mobility and the effect of resin that attaches the splint.

REFERENCES

[1] J. Highfield, 'Diagnosis and classification of periodontal disease', Australian Dental J, S11-S26, 2009.

[2] B.L. Pihlstrom, B.S. Michalowicz, N.W. Johnson, 'Periodontal diseases' Lancet, pp. 1809-1820, 2005.

[3] H.O. Heymann, A.V. Ritter, 'Resin-bonded splints and bridges', In Sturdevant's Art and Science of Operative Dentistry Elsevier, e52-e68, 2018.

[4] O. Kumbuloglu, A. Saracoglu, M. O¨zcan, 'Pilot study of unidirectional E-glass fibre-reinforced composite resin splints: Up to 4.5-year clinical follow-up', J. of dentistry, pp. 871-877, 2011.

[5] K.A. Ebeleseder, K. Clockner, C. Pertl, P. Stadtler, 'Splints made of wire and composite: an investigation of lateral tooth mobility in vivo' Endodontics and Dental Traumatology, pp. 288-293, 1995.

[6] J.W. Kleinfelder, K. Ludwig, 'Maximal Bite Force in Patients with Reduced Periodontal Tissue Support with and Without Splinting', J. Periodontology, 2002.

[7] A. Thomas von, F. Andreas, L. Adrian, 'Comparison of a new dental trauma splint device (TTS) with three commonly used splinting techniques', Dental Traumatology, pp. 266-274, 2001.

[8] A.V. Ritter, 'Periodontal splinting', J Esthet Dent., 2004.

[9] B. Christine, A.J. Friedrich, P. Sergej, P. Anselm, 'Rigidity evaluation of quartz-fiber splints compared with wire-composite splints', Dental Traumatology, pp. 65-74, 2012.

[10] S. Kurgan, H. Terzioglu, B. Yilmaz, 'Stress distribution in reduced periodontal supporting tissues surrounding splinted teeth', The Int. J. of Periodontics and Restorative Dentistry, 2014.

[11] https://www.thingiverse.com

[12] A. Geramy, J.M. Retrouvey, F. Sobuti, H. Salehi, 'Anterior teeth splinting after orthodontic treatment: 3D analysis using finite element method', J Dent (Tehran) Spring, pp. 90-98, 2012.

[13] D. Farhan, A. Galohda, S.K. Rai, N.K. Singh, R. Verma, D.S. Yadav, S.M. Karthickraj, 'Evaluation and Comparison of Stress Distribution around Periodontally Compromised Mobile Teeth Splinted with Different Materials: Three-dimensional Finite Element Analysis', Indian J. of Dental Research, 2019.

[14] H.E. Strassler, F.G. Serio, 'Stabilization of the natural dentition in periodontal cases using adhesive restorative material' Periodontal Insights, pp. 1-10, 1997.

[15] M. Sergio, M. Guglielmo, C. Raffaello, B. Eriberto, T. Cristiano, F. Roberto, S. Edoardo, 'In vitro comparison of the flexibility of different splint systems used in dental traumatology', Dental Traumatology, pp. 30-36, 2010.

[16] H. Hussein, Ammar, P. Ngan, R. J. Crout, V. H. Mucino, O. M. Mukdadi, 'Three-dimensional modeling and finite element analysis in treatment planning for

orthodontic tooth movement', American J. of Orthodontics and Dentofacial Orthopedics, e59-e71, 2011.
[17] I. Mackie, S. Ghrebi, H. Worthington, 'Measurement of tooth mobility in children using the periotest', Endodontics and Dental Traumatology, pp. 120-123, 1996.
[18] H. Sobczak-Zagalska, K. Emerich, 'Assessment of a Power Chain as a New Dental Trauma Splint and Its Comparison with Two Commonly Used Splinting Materials, Appl. Sci., 2020.
[19] E.S. Howard, C. L. Serio, 'Esthetic Considerations when Splinting with Fiber-Reinforced Composites', Dent Clin N Am., pp. 507-524, 2007.
[20] Thomas von A., F. Andreas, B. Danial, 'Splinting of traumatized teeth with a new device: TTS (Titanium Trauma Splint)', Dental Traumatology, pp. 180-184, 2001.
[21] A. Gerami, S. Dadgar, V. Rakhshan, P. Jannati, F. Sobouti, 'Displacement and force distribution of splinted and tilted mandibular anterior teeth under occlusal loads: An in-silico 3D finite element analysis', Prog Orthod., 2016.
[22] M.F. Razali, A.S. Mahmud, 'Mechanical Deformation of Superelastic NiTi Wire at Different Deflections in an Orthodontic Bracket System', Malaysian J. of Medicine and Health Sciences, pp. 13-17, 2020.

Biographies

Mariam Maroof received the bachelor's degree in mechanical engineering from A.P.J Abdul Kalam Technical University (AKTU), India in 2018 and the master's degree in material science and engineering from Motilal Nehru National Institute of Technology Allahabad (MNNIT-A), India in 2020. She is currently pursuing doctorate of philosophy from (MNNIT-A) in the area smart composites. Her area of interest is experiment, characterization and modelling of smart materials and smart composites.

R. Sujithra received the doctorate of philosophy degree from Indian Institute of Technology, Madras in 2016 in the area of shape memory polymer. She is currently working as an Assistant Professor at the Department of Applied Mechanics in Motilal Nehru National Institute of Technology Allahabad (MNNIT-A), India. Her area of research includes smart materials, polymers and composites, biomaterials, material modeling, and additive manufacturing.

R. P. Tewari received the doctorate of philosophy degree from Indian Institute of Technology, B.H.U., Varanasi in 1999 in the area of design and analysis of below knee lower limb model. He is currently working as a Professor at the Department of Applied Mechanics in Motilal Nehru National Institute of Technology Allahabad (MNNIT-A), India. His area of research includes biomechanics, robotics, rehabilitation engineering and biomaterials.

Prediction of Wear Rate of Polyethylene Bearing in Total Hip Replacement Implants using Linear Regression Model

Vipin Kumar, Sajal Kumar Babu Degla, Anubhav Rawat, R P Tewari

Department of Applied Mechanics, Motilal Nehru National Institute of Technology Allahabad, Prayagraj, Uttar Pradesh, India

vipinkumar10me@gmail.com, sajal.kumar3@gmail.com, anubhav-r@mnnit.ac.in, rptewari@mnnit.ac.in

Abstract

For total hip replacement implant bearings, pin-on-disc (PoD) studies are commonly performed to quantify wear of different bearing material. However, it is difficult to compare polyethylene wear results from multiple PoD trials, which may lead to knowledge being lost. In the present work, a machine learning based linear regression model is trained by quantifying the error encountered during model training. The linear regression model is able to predict the wear rate of polyethylene bearing material with the accuracy of 95% when compared with the actual wear rate of polyethylene bearing material taken from literature.

Keywords. Total hip replacement, artificial intelligence, linear regression, polyethylene wear rate, Pin-on-disk test.

1. INTRODUCTION

The bones present in human body are made up of strongest material, but bone fractures come into existence as external forces are applied or the individuals suffer from osteoporosis and femur necrosis. Despite the ability of the associated tissues to mend themselves, some bone injuries are permanent and irreversible [1-3]. Hip injury is a significant and regular occurrence that can be extremely debilitating, resulting in permanent disability. Hip fracture related injuries are anticipated to grow to about 6.26 million worldwide by 2050 [4]. As many person with hip joint related illness struggle to even do daily chores, hip replacement surgery has gained its popularities. In 'total hip replacement surgeries', the hip joint is replaced by an artificial metallic and polymer based joint, which transfer bodyweight to the femur [5]. The primary goal of hip replacement is to alleviate discomfort and increase mobility. The total hip replacement implants are composed of metallic femoral and polymer bearing cup component which are intended to restore the function and relieve pain of hip joint [6]. The most prevalent bearing material in total hip replacement implants [7] is metal-on-polyethylene (MoP), which typically pairs a metallic femoral head with a polymer based acetabular cup. Polyethylene wear debris has the potential to promote osteolysis (bone weakening) [8], which may make the implant loosemechanically unstable [9]. Several

attempts were made by researchers all across the world to enhance the mechanical and tribological properties of polyethylene liners viz. crosslinking and vitamin E blending to the polyethylene. In vitro and in vivo show that high crosslinking of polyethylene and blending of vitamin E produce less wear as compared to conventional ultrahigh molecular weight polyethylene (UHMWPE) [10, 11].

Pin-on-disc (PoD) wear studies are prevalent approaches for quantifying, comparing, and ranking wear of various polymer based bearing materials [12]. On the other hand, computational wear modelling could be a remedy to the POD tests shortcomings. Many mathematical wear models have been formulate d and available in the literature, and are used to assess the wear of polyethylene based bearing materials. Machine learning-based algorithm is another major modelling approach that scientists, engineers, and researchers in the field of wear modelling are considering these days. It may also be used to estimate the mechanical and tribological properties of composites and medical-graded polymers [13-16]. Materials scientists, on the other hand, have made strides in recent years by having used machine learning approaches in conjunction with experimental dataset to make it easier to model complex material connections, components structure, and the mechanical attributes that go with them [17]. These data-driven models allow the comparison of exisitng datasets with the newly developed ones. Prediction of new outcomes based on previously learned information, which would be difficult or time-consuming to gather otherwise using conventional research procedures(@vipin please revise this sentence) [18]. One of the advantages of machine learning is that some models can be trained on massive amounts of data, also known as "big data." The more data the underlying model is trained on, the more accurate its predictions get [19], which improves the usage of these models in decision making. Decision trees, support vector machines, regression analysis, and Bayesian networks are among the ML models employed [20, 21]. In addition, a subset of machine learning known as "deep learning" has been developed, which comprises models based on artificial neural networks (ANNs) for evaluation of wear performance of total knee replacement implants. These models have the advantage of not requiring humans to preprocess the data; instead, they can evaluate raw inputs and determine which attributes are most significant for a study. Thus, the aim of the current study is to use machine learning based linear regression method to create a model which should be able to make predictions of wear rate of polyethylene based bearing materials. A model similar to this may be used to enhance PoD wear tests and discover previously unknown correlations between polyethylene wear rate and PoD operation parameters.

2. MATERIALS AND METHOD

2.1. Linear regression model

The relationship between the feature and actual dependent values can be given as

$$y = b_0 + b_1 x_1 + e \qquad (1)$$

The estimated regression model takes the following form:

$$y = b0 + b_1 x_1 \qquad (2)$$

and the following relationship is used to compute the regression error:

$$e = y - y \qquad (3)$$

where, y and y are the actual dependent value and estimated dependent variable, x_1 and b_0 are the explanatory factor and intercept term, b_1 and e are the sensitivity of y to factor x and regression error terms respectively. Figure 1 depicts the entire flow chart of the methods used to train and test the network. The training and testing of this network entails multiple processes, including the data collection, data split into training and testing datasets, definition of machine learning model, error computations, and ultimately testing the network with a new input dataset.

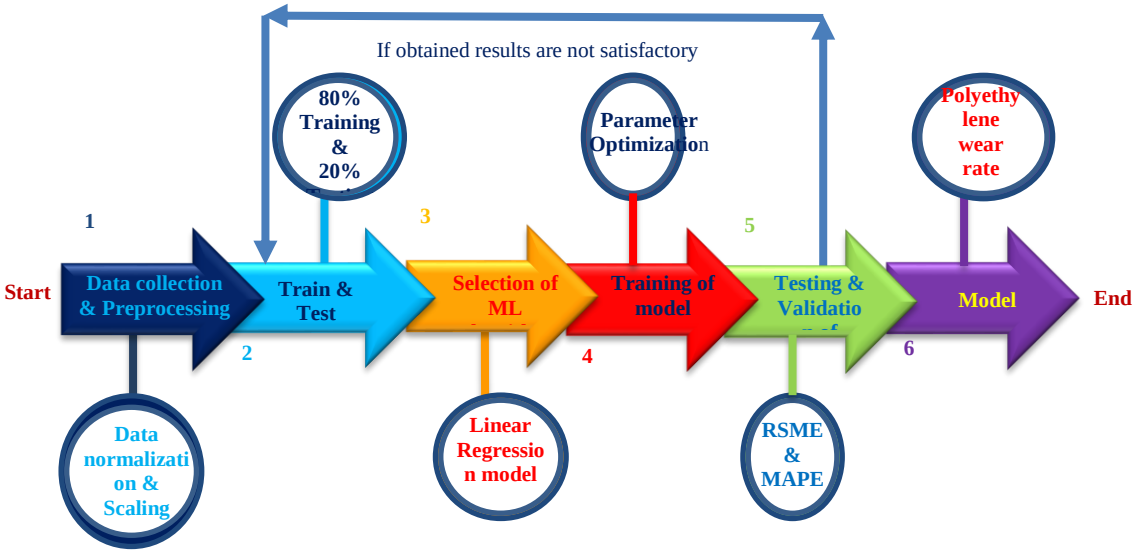

Figure 1. A flowchart showing the process of developing a linear regression algorithm

2.2. Modelling Performance Criteria

A) Mean Square Error

The root mean square error is defined as

$$MSE = \frac{1}{N}\sum_{i=1}^{N}(y_i - y_i)^2$$

where,symbols have the same meaning as explained earlier in section 2.1.

2.3. Data Collection and Preprocessing

The experimental raw dataset, based on POD test, of all parameters and polyethylene wear rate is collected from available literature. After acquired dataset is scaled and normalized to ease the linear regression model training, normalized dataset is split into training and testing dataset. The 80% of available dataset is used for training and 20% for testing of linear regression model respectively.

The kernel density estimate plots are used to observe the probability distribution of variables. These have been s in Fig. 2. Kernel density estimation (KDE) is a non-parametric method of estimating a probability density function of a random variable. Kernel density estimation is fundamentally data smoothening problem in which statistical predictions are obtained from a discrete dataset. The statistical properties viz: minimum (min), maximum (max) and standard deviation (std) of all wear parameters that affects the wear of polyethylene acetabular cup in total hip replacement are summarized in Table 1.

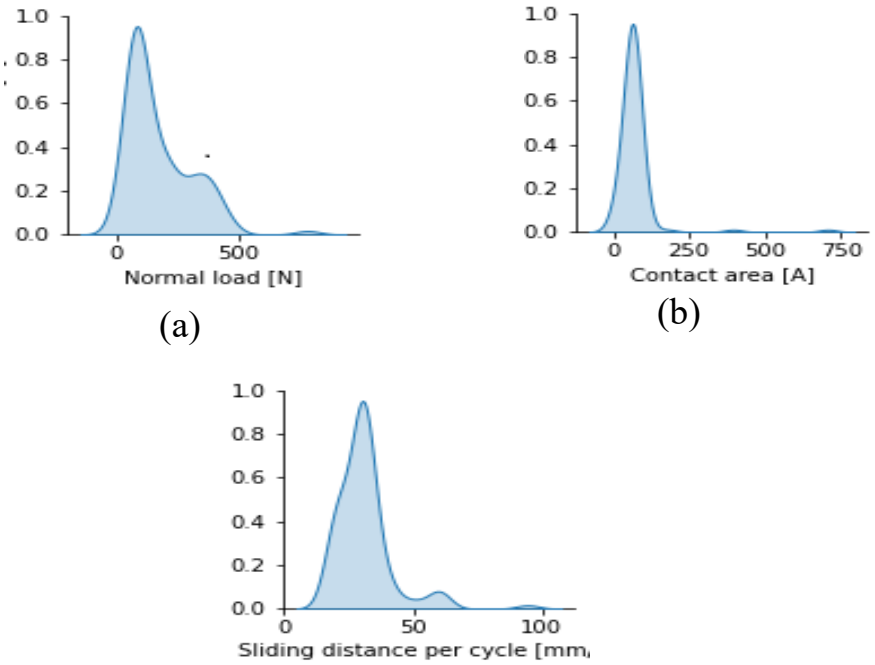

Figure 2. Schematic diagram of kde distribution of variable

Table. 1 Statistical parameters of wear variable and Polyethylene wear rate

	count	mean	std	min	max
Normal load [N]	103.0	168.915495	132.329401	7.00	777.546
Contact area [A]	103.0	69.954466	74.238209	7.07	706.860
Sliding distance per cycle [mm/C]	103.0	30.899320	11.088335	17.76	94.250

The linear regression model was trained by considering mean square error and ‘Adam' as loss function and optimization function respectively. The value of learning rate was taken 0.1 during whole model training.

3. RESULTS AND DISCUSSION

The training and validation losses obtained during dataset training are shown in Figure 3. The regression model can fit the training dataset accurately when there are only a few instances, say two or three. However, when more new instances are added to the model, it begins to fit incorrectly. The ultimate purpose of a regression model is to reduce the error that it produces while comparing predictions with real time data. The learning curve descends smoothly and steeply for each epoch before flattening out at the end. As the number of instances and epochs progresses, both training and validation curves matches closely.

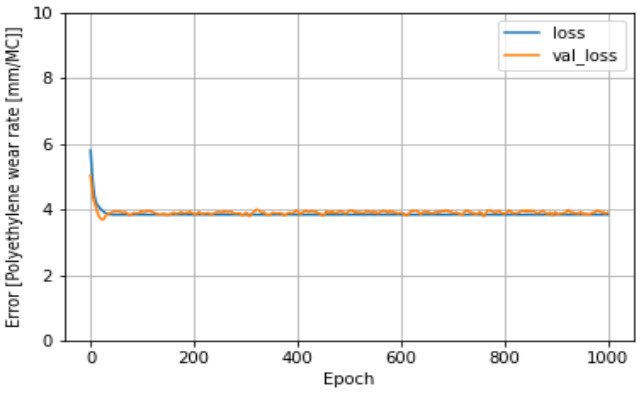

Figure 3. The schematic diagram of regression vs number of epochs (@vipin please make this figure in origin)

The actual and predicted values of polyethylene wear rate using linear regression model have been shown in Fig. 4. As explained earlier, for a few starting instances, the model has the capability to predict a data accurately but as training of model proceeds, the model starts to manifest over-fitting and under-fitting of input dataset. Upon further training of regression model, it starts to fit the data accurately and manifests good convergence. This behaviour of model is just because of training data may have some noise. Therefore, before training of regression model, all the noise and the irregularities present in the input dataset should be removed by applying scaling and data filtering procedures.

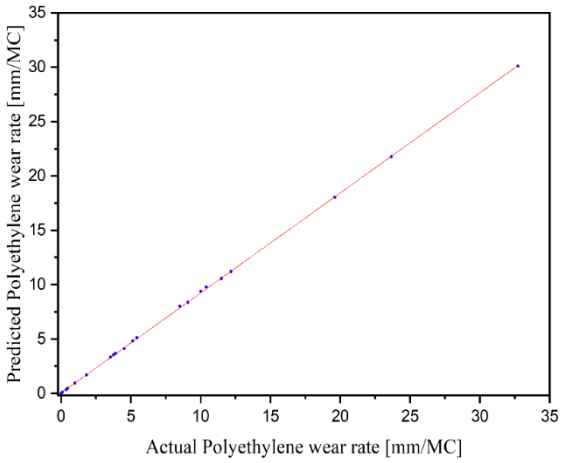

Figure 4. Scattering diagrams between predicted polyethylene wear rate and actual polyethylene with linear regression model with normal load as input variable. (Please prepare this graph in better way in origin, increase the data point size to visibly big)

In the current work only one variable i.e. normal load is considered on hip wear. In practical applications the effect of other variables viz., contact area, also exists. Therefore, to enhance the prediction capabilities of the current model more variables should be incorporated in this linear regression model. Further, the experimental dataset used for training of the model is also very small, therefor a large dataset should be used for better prediction of polyethylene wear rate in total hip replacements implants.

4. CONCLUSION

The polyethylene wear rate is estimated using a linear regression model technique with normal load as an input variable in this study. The aim of this study is to see how effective a linear regression model may be in tribological analysis in the setting of total hip replacement. When compared to standard polyethylene wear rate, it is established that the proposed model has a prediction accuracy of 95%. Thelinear regression model is suitable for obtaining perfect tuning between input variables and target values.

REFERENCES

[1] Koons, G.L., M. Diba, and A.G. Mikos, *Materials design for bone-tissue engineering.* Nature Reviews Materials, 2020. **5**(8): p. 584-603.

[2] Frost, H.M., *Skeletal structural adaptations to mechanical usage (SATMU): 1. Redefining Wolff's law: the bone modeling problem.* The Anatomical Record, 1990. **226**(4): p. 403-413.

[3] Mi, Z.R., et al., *Problem of stress shielding and improvement to the hip Implat designs: a review.* J. Med. Sci, 2007. **7**(3): p. 460-467.

[4] Cooper, C., G. Campion, and L. Melton, 3rd, *Hip fractures in the elderly: a world-wide projection.* Osteoporosis international, 1992. **2**(6): p. 285-289.

[5] Terrier, A., *Adaptation of bone to mechanical stress: theoretical model, experimental identification and orthopedic applications*. 1999, Verlag nicht ermittelbar.

[6] López-López, J.A., et al., *Choice of implant combinations in total hip replacement: systematic review and network meta-analysis.* bmj, 2017. **359**.

[7] Parsons, C., et al., *Clinical outcomes assessment of three similar hip arthroplasty bearing surfaces.* Orthopedic Reviews, 2014. **6**(2).

[8] Sadoghi, P., et al., *Revision surgery after total joint arthroplasty: a complication-based analysis using worldwide arthroplasty registers.* The Journal of arthroplasty, 2013. **28**(8): p. 1329-1332.

[9] Ulrich, S.D., et al., *Total hip arthroplasties: what are the reasons for revision?* International orthopaedics, 2008. **32**(5): p. 597-604.

[10] Kurtz, S.M., H.A. Gawel, and J.D. Patel, *History and systematic review of wear and osteolysis outcomes for first-generation highly crosslinked polyethylene.* Clinical Orthopaedics and Related Research®, 2011. **469**(8): p. 2262-2277.

[11] Baykal, D., et al., *Advances in tribological testing of artificial joint biomaterials using multidirectional pin-on-disk testers.* Journal of the mechanical behavior of biomedical materials, 2014. **31**: p. 117-134.

[12] Borjali, A., K. Monson, and B. Raeymaekers, *Predicting the polyethylene wear rate in pin-on-disc experiments in the context of prosthetic hip implants: Deriving a data-driven model using machine learning methods.* Tribology international, 2019. **133**: p. 101-110.

[13] El Kadi, H., *Modeling the mechanical behavior of fiber-reinforced polymeric composite materials using artificial neural networks—A review.* Composite structures, 2006. **73**(1): p. 1-23.

[14] Zakaulla, M. and S. kesarmadu Siddalingappa, *Prediction of mechanical properties for polyetheretherketone composite reinforced with graphene and titanium powder using artificial neural network.* Materials Today: Proceedings, 2022. **49**: p. 1268-1274.

[15] Esmaeili, R. and M. Dashtbayazi, *Modeling and optimization for microstructural properties of Al/SiC nanocomposite by artificial neural network and genetic algorithm.* Expert systems with applications, 2014. **41**(13): p. 5817-5831.

[16] Altarazi, S., M. Ammouri, and A. Hijazi, *Artificial neural network modeling to evaluate polyvinylchloride composites' properties.* Computational Materials Science, 2018. **153**: p. 1-9.

[17] Han, J., J. Pei, and M. Kamber, *Data mining: concepts and techniques*. 2011: Elsevier.

[18] Ramprasad, R., et al., *Machine learning in materials informatics: recent applications and prospects.* npj Computational Materials, 2017. **3**(1): p. 1-13.

[19] Bini, S.A., *Artificial intelligence, machine learning, deep learning, and cognitive computing: what do these terms mean and how will they impact health care?* The Journal of arthroplasty, 2018. **33**(8): p. 2358-2361.

[20] Shameer, K., et al., *Machine learning in cardiovascular medicine: are we there yet?* Heart, 2018. **104**(14): p. 1156-1164.

[21] Lopez, C.D., et al., *Artificial Learning and Machine Learning Decision Guidance Applications in Total Hip and Knee Arthroplasty: A Systematic Review.* Arthroplast Today, 2021. **11**: p. 103-112.

Biographies

Vipin Kumar received the bachelor's degree in Mechanical Engineering from Engineering Dr. B. R. Ambedkar University, Agra and currently doing the philosophy of doctorate degree in Biomedical Engineering from MNNIT Allahabad since 2018, respectively. His research areas include Tribological analysis of medical implants and machine learning.

Dr Anubhav Rawat received the bachelor's degree in Mechanical Engineering Dr. B. R. Ambedkar University, Agra, master's degree in Pipeline Engineering, University of Petroleum and Energy Studies, Dehradun, and Ph.D. in Fluids Engineering from Indian Institute of Technology Delhi respectively. His research areas include multiphase flows, fluid mechanics, complex, fluids, machine learning in fluids engineering, bio-fluids, and machine learning in energy engineering.

Prof. R.P. Tewari received the bachelor's degree in Mechanical Engineering from M. M. M. Engineering. College, Gorakhpur, the master's degree in Biomedical Engineering from IIT BHU, and the philosophy of doctorate degree in Biomedical Engineering from IIT BHU respectively. His research areas include Biomechanics, Robotics, Rehabilitation Engineering and Biomaterials.

Biomimetic Soft Hyper-Redundant Robotic Gripper: A Comprehensive Review

Shubhashis Sanyal, Anuj Kumar Shukla*, Hrishi Sharad Pinjan, Piyush Tailor, Pyla Pavan Kumar, Suman Saurav, Surjeet Kumar Bhargav

Department of Mechanical Engineering, NIT Raipur

ssanyal.mech@nitrr.ac.in, akshukla.me@nitrr.ac.in, hrishi662000@gmail.com, piyush1062000@gmail.com, pylapavan72@gmail.com, firebendersuman@gmail.com, bhargavsurjeetkumar@gmail.com*

Abstract

Engineers have traditionally used rigid materials (such as hard plastics and metals) to build precise robotic systems that may be represented as a combination of rigid components joined at discrete points. However, designing robots inspired by natural systems consisting of continuous deformable materials should be equivalent to or even surpass the functionality of rigid robotic systems. These robots possess almost infinite degrees of freedom (DOF) and high levels of kinematic redundancy and are hence called hyper redundant robots. This paper describes the various types of soft hyper redundant robots, respective features, actuation mechanisms, sensors used in their control, and the future scope of hyper redundant robots in the field of robotics. We have shortlisted 200 papers based on keyword searching, namely soft robotics, pneumatic actuation, elastomers, bio-inspiration, bio-mimicry, universal gripper, etc. Further, the papers have been shortlisted using the paper's title, abstract, conclusions, and other details such as mathematical modelling, etc. This paper presents a comprehensive review of 116 articles covering the evolution of the topic, including the details of methodologies, design and analysis performed. This paper gives an overview of recent developments in soft robotics inspired from nature and their applications in gripping, inspection, medical field, etc. Challenges in designing soft robots include material modelling methods, incorporation of sensors and control.

Keywords. Hyper Redundant Robots, Soft Robotics, Gripper, Bio-mimetics.

1. INTRODUCTION

Soft robotics is a relatively new and under-researched field. Earlier, robots were always constructed using rigid components. The term "soft robot" was at the outset used in the 1950s to describe a rigid pneumatic hand with a degree of flexibility utilizing gas inside that could be compressed to offer compliance. The upcoming years saw more and more efforts being put into the soft robotics field because everyone soon realized the importance of flexibility.

Engineers have long been motivated by nature's beauty, and efficiency, and this fascination led to the development of bioinspired robots [1]. Such an attraction to nature has given birth to the development of soft hyper redundant robots. These robots have an almost infinite number of actuable degrees of freedom and possess high levels of kinematic redundancy.

These robots, morphologically and functionally similar to snakes, tendrils, elephant trunks, and tentacles, play a valuable role in tasks where reaching difficult places and interaction with delicate objects are required. Compared with rigid grippers, these grippers can grip/manipulate various objects from different directions where accessibility is a constraint [2], e.g., gripping an object placed inside a narrow passage.

Green plant vines covering huge land parts are a fascinating inspiration for soft hyper redundant robots used in inspection and exploration purposes. Such robots have numerous applications and can be used in the study of the environment. This can be done by attaching a camera on the tip of the tendril or vine-like modelled robots. Robots inspired by octopus tentacles like the octarm robots are used to move traffic divider cones from one location to another. These robots, also used by NASA, have found their application in inspection, lifting small objects and reaching restricted places [3]. Inspiration from plant root growth has also helped in the development of innovative hyper redundant actuators [4, 5].

The construction of soft robots has led to an increment in demand for alternative materials. These materials are highly deformable and stretchable, enabling the interaction of soft robots with delicate objects. These materials need to be checked for their tensile strength, strain and failure under different loading. For further development, additional knowledge of material behaviour is necessary and also a unified database of material constitutive models and experimental characterizations is of significant importance.

Actuation of these soft robots requires different actuators than those used in rigid link robots like pneumatic actuation [6, 7, 8], tendon-driven actuation [9] and actuation based on shape memory alloy (SMA) [10]. Most popular systems are based on pneumatic action using compressed gas. They provide significant mechanical output on little input energy while providing considerable flexibility, adaptability, cost effectiveness, lightweight, and safe human-robot interactions. Soft pneumatic robots based on flexible elastomers can consistently transfer pressure over broad areas without complicated controls, allowing them to operate fragile and irregular objects. Soft pneumatic actuators are being employed from space applications to medical applications, resulting from the breakthrough in material sciences and rapid prototyping [11]. A brief timeline of development in soft robotics can be seen in figure 1. Motor-based tendon-driven mechanisms are associated with unwieldy attachments resulting in the making of small and lightweight autonomous robotic systems difficult, and hence they have found little application. Meanwhile, the inherent softness of SMA actuators results in low actuation force and hence limits their application. They also require constant energy usage to keep the SMA at a certain temperature to maintain the appropriate deformation [12].

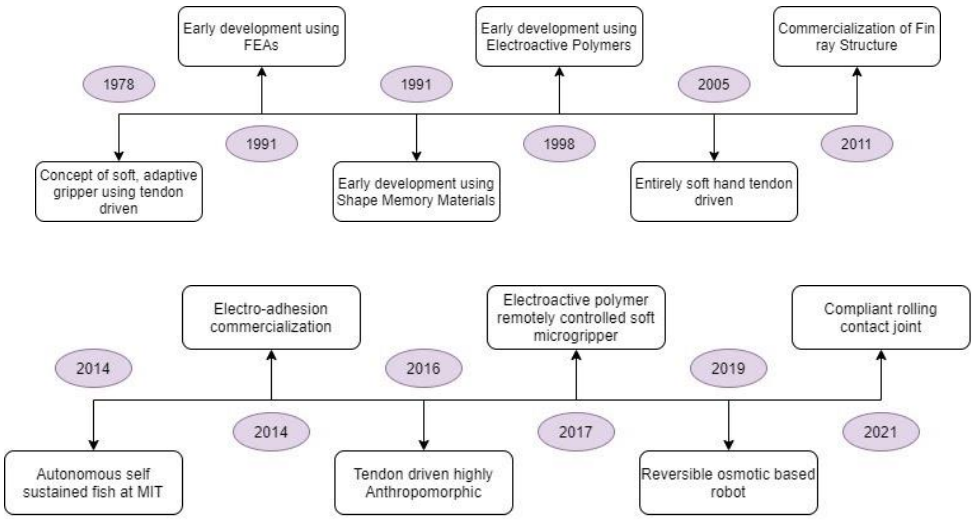

Figure 1. Timeline of developments in soft robotics

2. DESIGN

Engineers have traditionally looked to biology for inspiration when creating more sophisticated machines. The beauty and efficiency of nature greatly motivated engineers essayed at transferring ideas from biology to technology and specified it as biomimetics. There are several organisms from which the inspiration has been taken to mimic them in soft robotics, namely climbers, elephant's trunk, octopus tentacles, human fingers, fins of fishes, worms like caterpillars, Oligochaetes etc. as shown in figure 2, a brief summary of which is mentioned in Table 1.

Figure 2. Natural things from which inspirations have been taken, (i) octopus tentacles, (ii) elephant trunk (iii) caterpillar, (iv) tendril

Table 1. Various inspiration of soft robotic grippers and their applications

S. No.	Inspiration	Applications
1.	Octopus Tentacles	Holding different size object, inspection [3, 7, 16]
2.	Snake	Inspection, locomotion, cleaning clogged tubes [29, 30, 31]
3.	Elephant Trunk	Gripping heavy objects [32]
4.	Human Finger	Compliant fingers to handle delicate objects [15, 26]
5.	Climber	Inspection, exploration, gripping [20, 21]
6.	Worms (caterpillar)	Locomotion, exploration [3, 17]
7.	Plant roots	Soil penetration, search and rescue [5, 11]

2.1. A 2-finger Gripper for grasping an unknown object

Dexterous gripping is a recent difficulty in the field of robotics and automation. These grippers should be capable of grabbing various objects of varying sizes and forms. The shape of the gripper can also be put in as a restrain in the process of grasping. The associated hand configuration can be investigated using a probabilistic model to evaluate the inverse kinematics of the hand. To govern the locations and forces of joints and fingertips during task execution, grip synthesis algorithms must be used to control the grasping fingers. The process of developing a gripping configuration that fits a set of attributes important to the grasping action is referred to as grasp synthesis.

To construct this type of soft robotic gripper for two output port topology synthesis of compliant mechanism, a soft add scheme and an energy-based function are combined. The suggested gripper has two underactuated fingers, each of which is synthesized with the help of the recommended topology optimization method and designed using thermoplastic elastomer 3D printing. A general topologically optimized two-finger gripper has been made, which can hold objects of different shapes and sizes varying from a length of 42 mm to 141 mm and a limiting weight of 2.1 kg [3]. A similar type of gripper has been modelled and fabricated which deals with holding different types of fruits having a maximum payload capacity of 1.4 kg [5]. The detailed modelling of the gripper, which is supposed to hold unknown or irregular objects, has been described in [13, 14] . Universal grippers are also used to grasp unknown objects, and also new techniques are used to increase their application in different fields [15].

2.2. Octopus Tentacles inspired gripper

Octopuses utilize their tapering tentacles to grasp their meal; inspired by this, a soft robotic tentacles gripper with suckers attached has been developed to grip the object tightly. Changing the taper angle of the conical shaped actuators gives a range of bending curves for the soft tentacle gripper. The conical-shaped actuators are also more flexible than the cylindrical actuators.

The variable bending curvature along the length of the tentacle is a curious and possibly beneficial phenomenon since it allows for the grabbing of much smaller items than those generally managed using non-tapered geometry. The pneumatic actuation plays a great role in actuating these grippers while having suction cups on the gripper ensures a proper hold of the gripper on the object. The whole design and their simulations along with the mathematical support, have been given in [3, 7, 16].

2.3. Worm, caterpillar, inspired soft robot

Unlike other soft robots in development which require pneumatic or fluid actuation, these use shape-memory alloy micro coils or motor tendons for actuation. Different designs may be swiftly and cheaply created using elastomeric polymers or direct 3D printing because of the technology's versatility. Softworms can be constructed in any shape, but the emphasis is given to designs that don't require cumbersome assembly. In research paper [3, 17], the worm caterpillar's biology is discussed and their robotic models have been prepared and tested.

Research paper [18] suggests the usage of several modes of deformation and depicts a crawling robot with high deformability that employs deformation using compression and bending simultaneously. Inspired by the silkworm’s crawling gait motion, a compressive or bendable beam was proposed, further developed into a crawling robot. The simulation and prototype’s experimental results show that combining multiple deformation modes can help boost locomotion speed.

Origami has recently gained popularity as a way of creating compliant reconfigurable robots [19]. Using the programmable origami backbone, an open triangular spring model has been designed to provide stability and customizable elasticity that can be magnetically actuated to get the desired mobility. Its locomotion mechanism was similar to that of a caterpillar, in that it achieves directional motion by controlling body tension, which produces compressive stresses on the travelling surface. An extensive range of motion for travelling through varied terrains can be achieved by actuation based on the interaction between external and internal permanent magnets.

2.4. Bio-robotic tendril

Climbing plants, with their fascinating intricacy and functional views, can be a substantial source of inspiration for biomimetic purposes. Climbing tendril-bear plants, for example, have an exciting technique of searching for grasping and climbing support, which can be explored and applied in future bio-inspired technologies. They can wrap around support to grasp, enabling it to obtain vertical displacement by single tendrils, which are filiform, irritable and lengthy organs. Tendrils characterize three primary motions; (i) Circumnutation: a natural movement that enhances the likelihood of finding support. (ii) Contact coiling: Curling of the tendril to grasp support, (iii) Free coiling: helical coiling of the tendril along its axis [20, 21]. The different phases in coiling are shown in figure 3. The tendril structure develops into two helical springs with opposite rotations starting from the linear configuration. The contraction or the evolution of the helical structure begins after the free coiling stage. Furthermore, the pulling effect is accomplished by forming an elastic spring-like attachment between the grabbed support, which can withstand highly strained situations like wind and loads. The tendril body is made up partially of G cells, a particular

type of cells, which can dehydrate and increase the stiffness of the body, preventing uncoiling and this process is called lignification.

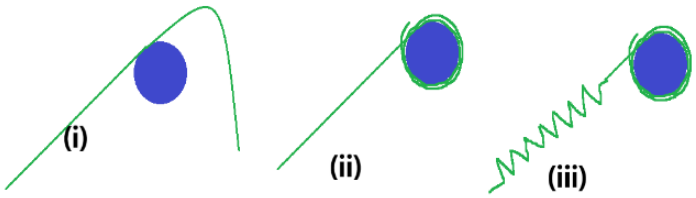

Figure 3. Phases in coiling (i) Circumnutation (ii) contact coiling (iii) free coiling.

The model for the vine-inspired continuum robot is adopted from computational biology in which circumnutation was interpreted as a kinematic model. The relation between the curvature change, orientation and longitudinal length along the perimeter is established [22]. The modelling of the tendril is done in two phases: the grasping part and the free coiling part. The free coiling part has been modelled as a helical spring, and the grasping part has been modelled as a continuum robot as a collection of 'n' linkages. Also, this model has been simulated in stimulation software, showing that free coiling and grasping are achieved. A detailed explanation has been given in [21].

The kinematic model was conceptualized and summarized using two main parts: (a) the Free coiling part, which is primarily dedicated to the free-coiling and pulling phase, (b) Grasping-Coiling part, which is primarily dedicated to the coiling and grasping phase. The GC component can be divided into separate pieces that move and bend when activated. The FC component that pulls can be thought of as an actuator that transforms a linear model to attain helical spring-like deformation [20]. Each sub-section of the GC portion was kinematically modelled and characterized using primary joints and the Denavit-Hartenberg (DH) parameters for modelling. The tendril's grasping coiling can then be characterized using closed-form equations [21]. By relating actuator inputs like pneumatic pressure or tendon length to cartesian coordinates with the help of robot configuration coordinates, an approach for kinematic relationship is developed. This approach provides real-time shape and task control. It could be applied to a vast variety of continuum robots, also for bending individual sections [23, 24].

Tendril perversion was investigated on elastic rods using static Kirchoff equations. The model represents an elastic rod as a curve in the space with specific physical properties. The curve represents the axis and the rod's parameters including orientation in space, stiffness, twist, and spin. The rod's external stresses, pressures, and moments are averaged over the filament's cross-sections. Differential growth has been used for intrinsic curvature in physical systems like tendril perversion. Kinematics of differential growth and the static solution for helix has been discussed in [25].

2.5. Finger type gripper

Relative stiffness allows the gripper to turn in the desired direction of the stiffer material. One hemispherical side is made more rigid and a cloth is stuffed to make it inextensible. This makes the inner part along which the finger curves. The model is being prototyped and tested with different weights. Increasing actuation pressure gives higher lifting force and grasping force. For a particular activation pressure, an increase in the finger's length decreases the generated pressure [15, 26].

Soft robotic gloves are also made to strengthen and support the muscles of the finger [27, 28]. Research is being done on soft robotic gloves that can be used to help people with functional grasp disorders with hand rehabilitation. These gloves are made from soft elastomers having great twisting and bending abilities.

2.6. Continuum Robotics in medical surgery

The current robotic systems and manipulators for medical applications are inspired by octopus tentacles, elephant trunks, snakes and many other creatures that can navigate limited areas, operate things in complicated settings, and follow curved trajectories in space. They can be used in different types of precision surgery because their small size and compliance are advantageous from a medical standpoint. Still, a lot of technological advancement in the field of sensing, control, and human-machine interaction is required [29, 30, 31].

2.7. Elephant trunk inspired robots

A manipulator with four sections using a hybrid cable and spring servo system actuation has been developed inspired by elephant trunks where it was assumed that an elephant trunk manipulator's sections bend into a circular arc with continuous curvature and an inextensible backbone. Similar trunk-like robots named 'snake-arm robots' have been made using cable tendon actuators with alternating stiff and soft discs to produce a bending backbone. Another elephant trunk-type manipulator was designed that consisted of a spiral tube looped around the manipulator backbone like a coil [32].

2.8. Root inspired soil penetration robotic mechanism

A kinematic model for growing robots was designed by inspiration from plant growth strategies. A 3D printer-like mechanism or tool were installed in the robot's tip, allows it to construct its body shape by using a sensor placed on the tip and a deposition head. It grows similarly to how a plant's root or shoot tip moves forward. Later, the simulation was done using simulation software and the positional and curvature errors were calculated between simulation results and practical results [11]. Also, another inspiration from root penetration is a working prototype design made up of a hollow cylinder, 3D-track (flexible cylindrical skin) and motor tendon skin actuation mechanism. It was observed in experiments that the use of this mechanism reduced the axial penetration force [5].

3. SOFT GRIPPING

Soft gripping is divided into three mechanisms: (i) actuation, (ii) variable stiffness, and (iii) variable adhesion. These three categories are not independent of each other, and many gadgets combine two or more classes to achieve greater performance.

3.1. Actuation

3.1.1. Thermal responsive actuation (SMAs/ SMPs)

Some polymers and alloys exhibit a shape memory attribute, where the material being temporarily deformed returns to an initial shape in response to a stimulus (typically heat). These materials are called Shape Memory Polymers (SMPs) or Shape Memory Alloys (SMAs) [33, 34]. These materials have found varied applications in the field of aerospace, medicine and robotics [35, 36, 37].

SMPs are made up of a polymer arrangement consisting of transition domains (TD) and elastic domains (ED). The TD softens (low stiffness) when the temperature is above the transition temperature, allowing the deformation of ED in response to force applied. As the temperature goes down, the TD gets stiff and averts the ED from deforming. When the material is heated again, the ED is released, and the object returns to its original state. This transition in SMPs happens due to a material phase change, in which crystallization-melting or vitrification-glass play a part. SMPs are frequently blended with other materials to increase properties such as strength, recovery force, and additional stimulus effects such as magnetic-active and electro-active effects [38]. Working cycle of SMA is shown in figure 4.

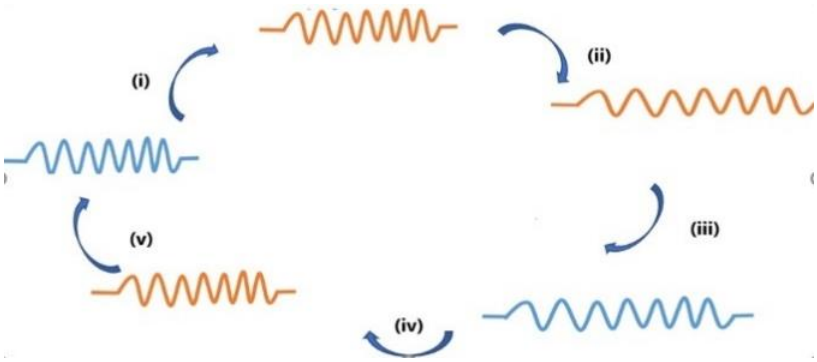

Figure 4. Working of SMA material(spring) (i) heating, (ii) deformation due to stress (iii) cooling in deformed state (iv) stress removal (v) repetition

Temperature-induced crystallographic changes cause the SMAs to exhibit form memory. During these changes, the material transforms from martensite to austenite structure. The alloy takes on a martensitic structure with low stiffness at low temperatures, and external stress can plastically deform it. Reaching above the transition temperature converts it to an austenitic form with high stiffness, recovering the material to its initial undeformed shape. These alloys can be employed as actuators by taking advantage of the contraction of up to 5% achieved when heated from martensite to austenite phases.

Latest developments include the incorporation of SMAs with compliant materials like silicone elastomers to improve object adaptability [39, 40, 41]. SMA microgrippers were created using stiff materials and flexural joints. In these micro-grippers, softness can be improved by using super-elastic SMAs by reducing the thickness of the structure [42].

3.1.2. Magnetic Responsive Actuation

These actuators work by controlling the magnetic field magnitude and direction. They are used in places with high magnetic susceptibility [43]. Magnetic stimulation is appealing due to the ease with which it is possible to regulate the magnetic field's direction and magnitude quickly and precisely and its capacity to permeate most materials. Magnetic particles and fillers are blended with polymers, gels, papers, and fluids so that they could operate on applying magnetic fields externally. When discrete magnetic fillers are inserted into soft materials, a magnetic profile with varying amplitude and direction is generated [44].

3.1.3. Photo Responsive Actuation

This type of actuation can be achieved in the Visible light-driven and the Near Infrared (NIR) light actuator. Because of the potential of long-wavelength NIR light to permeate biomaterials with low losses, NIR has emerged as the most biocompatible way of wireless actuation for biomedical devices. Visible light-driven actuators can actuate in sunlight, saving a lot of excess energy when working in an open or natural environment [44].

3.1.4. Electrically responsive actuators (EAPs)

For this type of actuation, specific kinds of materials are needed which can show deformation whenever there is a fluctuation in electrical conditions like dielectric elastomers, piezoelectric materials, and mechanical servo motors. While hydraulic or pneumatic actuation has been used in many soft robot designs, a lot of work has gone into developing electrically activated soft actuators made of EAPs. Developing electrically actuated soft actuators comprised of electroactive polymers has taken a lot of time. Some of them are even prototyped. Because energy is more easily reserved in electrical form and computation is commonly performed on electronic circuits, actuating soft robotics directly using electrical potential may be more efficient. Piezoelectric, ferroelectric polymers, mechanical or servo motors, ionic EAPs, dielectric EAPs are some examples of EAPs [11].

a. Dielectric Elastomer Actuators (DEA)

A thin elastomer membrane (thickness 3–500 μm) [45] is sandwiched between two compliant electrodes in a DEA. An electric attraction (known as Maxwekk stress) between the electrodes is created by applying high voltage, resulting in compression of the elastomer membrane and expansion of its area. Soft elastomers having an elastic modulus of 1MPa are used to makes DEAs, as they have a quick reaction time and may create massive actuation strokes.

Furthermore, their electromechanical efficiency is capable of reaching 90%. Multilayer stacking is required when high output forces are demanded due to the long actuation stroke and low generated stress of DEAs, resulting in a more complicated fabrication method. Due to their inherent simplicity, they can be shaped in any configuration. Recent developments and commercial availability of the kV thin-film transistors [46] and miniaturized high voltage components have enabled the designing of more compact systems.

The first demonstration of the usage of DEAs for gripping was having a design known as self-organized dielectric elastomer minimal energy structures (DEMESs) [47]. The main problem in this type of system is to overcome the low generated stress. For this particular problem, other than multilayer stacking, different techniques like incorporating variable stiffness functionality [48], implementation of controllable adhesion [49] are being explored.

b. Ionic Polymer Metal Composites (IPMCs)

IPMCs comprises an expandable membrane of electrolyte polymer (usually thickness of 100-300μm) wedged between two thin metallic layers. Cations and anions in the electrolyte are evenly dispersed when the voltage applied is zero. The concentration of cations increases at the cathode and anions at the anode when voltage is applied, causing non-uniform swelling resulting in the entire structure bending towards the positive side [50]. Thus, the device can be curved bi-directional depending on the applied polarity.

IPMCs have stiffness ranging between 0.60 to 21.0 GPa, influenced by electrode and polymer membrane materials. This actuator technology allows for broad bending strokes for the applied small actuation voltages in the range of 1-5V. Using the electrolyte frequently necessitates the aqueous solution submerging of actuators, but encasement allows for functioning in the dry setting [51]. IPMCs, like DEAs, are capable of self-sensing however their response time is slow [50]. IPMCs have the benefit of being easily made at a millimetre scale. IPMCs have certain disadvantages, like low generated stress and slow actuation response. Exploiting this technology's capacity to work in aquatic conditions could be one way to get it closer to applications.

3.1.5. Fluidic Elastomer Actuators (FEAs)

These actuators are among the oldest and still widely used in soft robotics because of their advantages, such as ease of production, resilience, and low-cost elastomer materials [52]. The fluid applies pressure on the walls of elastic material and provides actuation. FEAs structures often have asymmetric geometry or are made of anisotropic materials, resulting in the chamber's inflation being transformed into bending of the entire actuator. High forces can be generated by FEAs depending on the pressure applied and active surface area.

For FEAs, there are a variety of architectures to choose from. Some of the most prevalent are bellows-like structures, tube-like tentacles, elongated elastomeric chambers with reinforcing layers and fibres etc. The moulding process that makes up the chamber is commonly used in the fabrication of FEAs. Fibres, adhesion, nonprotractile layers textiles and papers, origamis, strain sensors, porous materials and variable stiffness elements can all be incorporated into the actuator using the moulding process (during the molten state of material) [53, 54].

Fibre reinforcement in FEAs resulted in the creation of bioinspired soft hands that can replicate various human movements and manage ordinary things like flasks, pencils, and eyeglasses. Silicone elastomers structurally reinforced with polyaramid fibres are used to achieve properties like self-healing of minor punctures and boosted tear resistance.

Researchers used 3D printing to demonstrate the quick manufacture of FEA-based grippers. Researchers have inserted functional aspects into the grippers' structure to increase their

functionality, taking advantage of the diversity given by the moulding process. Resistive strain sensors composed of expandable or pliable electrodes, stretchable optical waveguides, and force sensors employing a piezoresistive fabric component were used to accomplish curvature sensing. Increased holding weight can be achieved by incorporating variable stiffness parts.

Using compressors and external pumps to pressurize fluid for actuation is one possible issue of FEA grippers. These components are frequently big and hefty, compromising the device's portability. Efforts to combine and miniaturize the production of pressurized fluids have yielded hopeful results in the past [55]. Response time can be a problem since, for the full actuation with the required flow rate and given the channel's fluidic impedance, crossing 1 Hz frequency can be challenging.

3.2. Variable Stiffness

3.2.1. Low melting point alloy (LMPA)

The alloy that undergoes a phase change in response to heat, typically at low temperatures, generally determined by alloy composition, is termed LMPA. Synthetic elastomeric composites have fixed internal structures and defined properties. Unlike natural composites, these materials cannot alter their structure and mechanical properties depending on environmental conditions. For example, the structure of bone changes upon induced mechanical stresses. LMPA inclusions in the elastomeric composites induce a change in stiffness upon phase change. These molten alloys can flow in the pneumatic channels or may be mixed up with the molten elastomer during the fabrication of the structure [56, 57].

A high variation in stiffness can be observed when the alloyed elastomer is heated above the LMPA melting temperature [58, 59]. Soft dielectric materials usually have poor heat conduction as the thermal conductivity is directly proportional to the elastic modulus. This constraint can be overcome with LMPAs added in the elastomer composites resulting in an unrivalled combination having thermal conductivity as high as metals, elastic modulus similar to elastomers and the ability to experience large deformation having strain greater than 600 percent [60].

Further developments include reducing the phase transformation period of LMPAs. Based on geometry and size, melting time can range from 1 to 30 seconds while solidification time can be double. This timing can be an issue when there is a need for quick manipulation [61]; melting time can be reduced by the increment of heat addition while the time to solidify can be reduced using the metal of high thermal conductivity [60] or integration of additional cooling devices like electrocaloric effect based device [61], water circulating system, increase in heat transfer area [62] and fractal channel design [63]. Relative stiffness doesn't change upon scaling the design. However, having a high proportion of PDMS materials and LMPA will increase the power required for the required melting speed. Therefore, the different designs need to be considered (when scaling is done) having low melting time, power requirements and high stiffness [57].

3.2.2. Magneto-rheological fluids (MRF) and Electro-rheological fluids (ERF)

MRF and ERF are the class of suspended particles in fluids that undergo a large reversible variation in the rheological properties (viscosity related properties) when imposed to magnetic and electric fields, respectively [64, 65]. The change in rheological properties when subjected is indicated by flow resistance increment depending on fluid flow direction and constitution. These smart materials are implemented in smart structures, shock absorbers, clutches and brakes [66, 67]. Under an electric field, the particles convert into long fibrous chains aligning in flux lines direction due to molecular dipoles' orientation and dielectric polarization. These chains develop resilience to the deformation of fluid, resulting in increased stiffness of application.

Similarly, MR fluids convert into long chains of ferromagnetic particles aligning in the direction of magnetic flux lines [68, 69]. To initiate viscoelastic behaviour, magnetic field of up to 500mT and an electric field of about 5 kilovolts per mm need to be applied. The response time is relatively short, less than 10 milliseconds and the relative stiffness increases tens of times [70, 71]. ER fluid generally requires low energy as an electric field is proportional to the applied voltage and no steady-state flow of current is needed, while for MR fluid, the magnetic field intensity depends on the electric current. The fluid can be added with elastomeric composites to produce variable stiffness models upon applying the respective actuating fields [72].

3.2.3. Granular Jamming

This is a handy process for constructing changing stiffness media, which is commonly used in robotics applications for gripping complicated and fragile items. Granular jamming is a mechanism that allows granular material to change reversibly from fluidic to solid-state and vice versa. During the fluidic state, granular material can move freely, hence the object feels soft and pliable. Application and removal of vacuum on the bladder containing the grains result in the transition of states [73].

Jamming actuators have a simple structure and use pressure to modulate stiffness. This technique is said to be capable of changing stiffness by nearly 24 times [74]. The stiffness change rate is relatively rapid; for the solidification state, it takes 0.1-1.1s whereas for the fluidic state, it takes 0.1-1seconds [14, 75]. The transition time is typically on the flow rate & pressure differential obtained from the pump and the volume of the granule-filled bladder. When portability is necessary, the pump required to generate a relatively high-pressure differential becomes a limitation. Nonetheless, granular jamming has demonstrated its utilization in mobile manipulators and robots [76, 77].

Once the gripper goes into the solidified state, it is difficult to accommodate object deformation therefore unsuitable for deformable objects. This universal jamming gripper has been employed in some industry setups and has also proved its utility in research applications like assembly tasks, prosthetics, human cooperation and learning algorithm integration [78]. Future granular jamming research could focus on expanding the flexibility of object kinds. Jamming grippers, for example, might be outfitted with adhesive technology to allow them to grasp deformable and flat objects which are difficult as of now. Layer jamming is a technology that uses a variable stiffness method and is dependent on inter-

layer friction. Because of its low thickness, it has potential future utilization in lightweight fingered grippers with adjustable stiffness [79].

3.3. Variable Adhesion

Adhesion is the attraction between two surfaces at their common interface, which causes shear stress to be a direct function of the normal pressure generated. Soft gripper having adhesive techniques generate greater grasping forces because of the considerable shear friction force. Simultaneously, the closure force normal to the object's surface is significantly less than the forces in other grasping techniques, allowing the handling of delicate or fragile objects. Low power need, high ratio of shear force to closing force are some of the attributes needed for having a lightweight and easily transportable gripper. Controlled adhesion can primarily be done by electro and gecko adhesion (dry adhesion).

3.3.1. Electrostatic Adhesion

The electrostatic force is the attraction force between opposite electric charges. Electro adhesion takes advantage of this nature of attraction by adjusting the electric charges on both sides of the gripper-object common surface [49]. Charge polarization in dielectric models and electrostatic charge induction in the conductive models is an implication of the applied electric field. The electric fields are generated by the interdigitated electrodes with a thin layer of passivation coating. On both smooth and uneven surfaces, electro adhesion has been successful. High electric fields are required for this adhesion method, which necessitates voltages on the order of a few kilovolts current. World technology uses electro-adhesion in different types of rigid and flexible grippers, vertical climbing, water handling etc. [80, 81, 82]. An eight-leaf flexible, electrostatic adhesive gripper has been fabricated and thoroughly discussed in [83].

Electro adhesion is electrically controlled and may be utilized with dielectric objects, and metallic objects with any kind of surfaces in most cases [82]. It eliminates the need for extra actuators to grasp or leave an object. After the voltage is removed, there is a little residual adhesive force. However, residual forces are exceedingly low for dielectric objects and persist barely for some seconds [84, 85, 86]. Using AC voltage instead of DC for conductive objects is a good solution. Electro adhesion performance is also affected by surface conditions for example presence of unwanted materials like dust and moisture will result in a lower holding force. A solution to this problem is in implementing techniques like self-cleaning [87].

3.3.2. Gecko Adhesion

Geckos can climb up tilted surfaces using the van der Waals forces to attract surface molecules, generating shear forces. Gecko adhesion was inspired by the surface adhesion developed by microfibres of geckos [88, 89, 90]. The adhesion is done by the microfibers on their bottom foot surface and triggered by pressing them normally to the object surface (preloading) and disengaged by eliminating the preloaded force. Directional shear force during adhesion can also be feasible by adjusting the angle of setal-fibres [91]. Gecko adhesive adheres to both rough and smooth surfaces, although it struggles to stick to low-surface-energy materials [92]. In this form of adhesive technology, self-cleaning is a unique

feature [93, 94]. It has also been demonstrated that applying a surface coating on gecko-inspired pillars allows them to stick to damp surfaces.

A new convex object gripping approach that relies almost entirely on shear forces has been discussed in [95]. Also, the gripper uses gecko-inspired-film fibrillar adhesives that conform to the object's curvature. The model has been proposed & validated for grasping a variety of curvatures. Also, inspired by gecko, adhesion microfibres are replicated by angled micropillars made from elastomers with round or flat tips introduced as compliant micromanipulators for pick and place operations [96].

The adaptability of soft grippers with gecko adhesion was demonstrated by their ability to adhere to various objects, among which most were rigid and smooth surfaces. Handling rough-surfaced things and manipulating soft, malleable objects are two examples of potential obstacles. Shape optimizations and microfibres material could be a possible solution for the former. Enhanced adhesion performance on rough surfaces has been achieved by enhancing the bending behaviour of gecko adhesion pillars [97]. Microspines are another promising candidate, as they demonstrated extraordinary grabbing abilities on hard surfaces like concrete and rubble.

4. SENSORS

The development of sensors for soft robotic applications has evolved into a research trend over the past few years. This is because of: a) increase in demand for more intelligent systems, b) interests in developing soft robots and other applications that require confirmation to different shapes. Sensors are described as devices that “convert physical quantities such as pressure, temperature, force, acceleration, deformations into electrical signals being input to the control system”. Implanting stretchable sensors on soft grippers would vastly intensify how they can interact with the object and simultaneously obtain information about the manipulated object's characteristics.

Pressure sensors can be used to monitor grasping force. Rubber encapsulated MEMS pressure sensor can be incorporated with a gripper, allowing real-time grasping force monitoring. Force information can be indicated with the help of LED lights, which changes colour when pressure exceeds a predefined threshold [98]. Pressure sensors are mostly based on the capacitive or resistive structures, and these were developed from soft matter and attached to the silicone skin of the palm and fingertips [99] of the robot's hand to obtain the pre touch perception. With the help of these sensors and an algorithm, the robotic hand could determine the suitable closing pattern from the capacitive sensor data [100, 101]. Soft robotic and wearable systems experience large deformation and require sensors to measure this deformation. Graphene materials provide magnificent properties that integrate several flexible and stretchable characteristics into electronic devices. Resistive sensors embedded in the material change its resistance on bending, which is converted into voltage and interpreted by the Arduino. The data obtained from the pressure sensor (Honeywell-ASDX AVX100 PGA A5) is also utilized in computing bending angles corresponding to the pressure. The above data correlates with the actual bending angle observed from the developed vision system for better accuracy and feedback [102]. Highly stretchable strain sensors are conventionally made of carbon black (CB)- filled elastomer composites (up-to 500%) [54]. Recent advances in stretchable electronic materials are discussed in [103, 104] and applications in [105].

Tactile sensing is necessary to have safe contact with surrounding humans and objects. Tactile sensing is done with a permanent magnet embedded in a soft elastomer placed over a hall sensor to compute total force vectors (both shear and normal forces). This sensing is also used for palpation and diagnosis of tissues [106, 107, 108]. Several tactile sensors perform better using micro-electro-mechanical systems (MEMS) technology. Some practical problems during the application of MEMS in systems include endurance, wiring difficulties and corrosion. One of the best alternatives to MEMS is fibre optic sensors which are appealing due to their performance capability and resilience to several environmental disturbances, especially electromagnetic and electrostatic fields. Human skin touch sensors are incorporated into devices like grippers or robot hands to pursue human fingers' equivalent skill and adaptability. Having these on our prototypes or robots will eventually give us a large set of information that can be backtracked for design evolution. These sensors can detect the distributed force using micro-bending of optical fibres and are used for artificial skins [99, 109, 110, 111, 112, 113] and reflective heartbeat sensors based on optical fibres [114].

Depending on the type of work to be carried out, various types of soft actuators are applicable in the medical and surgery field. The actuators in the surgery field need to be precise and provide accurate data. For collecting different kinds of data, the actuators are fitted with proprioception sensors [35] like fibre bragg grating (FBG), stretchable resistance or conductance sensor, environmental perception sensors like flexible optical fibre and interactive perception sensors. The screen-printed sensors were printed on elastomeric substrates and incorporated with soft pneumatic actuators in a single process [115]. With the help of these sensors, the true curvature of an actuator can be known within the sensor hysteresis and creep limits. The key advantages of these sensors are: a) need less time to manufacture b) need a small amount of additional effort in the actuator manufacturing, and c) are made with readily available equipment and materials. Measurement of small fluctuating or variable parameters is vital in any robotic application that includes interaction with the environment because it enables the robot to identify encounters early and respond appropriately. Taking inspiration from the ciliary structure found in nature, a Miniaturized Light force sensor has been developed, designed, and simulated [116].

5. CONCLUSION AND FUTURE SCOPE

This paper discusses how the advent of technologies has impacted robot structures. Since performing jobs with delicacy has been demanded for a long time and rigid robots have been unable to fulfil that idea, the soft robots have outdone them in this field. The hyper redundant robots somehow stand on the line with structural strength from the rigid robot’s point of view and abilities to stretch, squeeze and morph from their soft counterparts. The different hyper redundant robots that are developed are a sort of inspiration from nature. To achieve desirable robotic behaviour in real-world situations, an insight of characteristics, interface with control systems and environment of soft materials is also required. Advanced materials are the heart of these types of robots as they play a vital role in deciding the system's speed, force, adhesion, and kinematics. Different materials like silicone elastomer, hydrogels, shape memory alloy, electroactive polymer etc., are used to get the desired deformation of the system. However, the peak of commercializing these specific robots have not reached. So, it becomes important that these potential robots are continuously evolved with upcoming technologies so that they don’t become obsolete. There is a need to look upon the properties

of materials like self-healing and room temperature actuation of SMAs. Combining advanced materials and processes definitely increases the system's complexity, but it will undoubtedly be a topic of discussion in the near future if the performance is enhanced. Enhancement of interaction of soft robots with objects can be greatly done with the implementation of stretchable sensors. Ongoingly, research is being done to develop sensors that measure and sense various parameters like pressure, temperature, force, strain, proximity and shear. Some problems may be encountered during the practical application of tactile sensing using MEMS technology and the best alternative to them is fibre optic sensors. These are attractive due to their performance capability and resilience to environmental disruptions. The overall rapid rate of advancements in optical fibre-based sensors suggests a bright future for them. Systems such as soft robots that undergo large deformations require sensors that can withstand these large deformations. Future works include manufacturing graphene films possessing high conductivity, chemically stable in air, good uniformity and the ability to adhere to device substrates. This will enhance the performance and longevity of the resulting devices.

REFERENCES

[1] I. Fiorello, E. Del Dottore, F. Tramacere, and B. Mazzolai, 'Taking inspiration from climbing plants: methodologies and benchmarks—a review,' Bioinspir. Biomim., vol. 15, no. 3, p. 031001, May 2020, doi: 10.1088/1748-3190/ab7416.

[2] J. Shintake, V. Cacucciolo, D. Floreano, and H. Shea, 'Soft Robotic Grippers,' Adv. Mater., vol. 30, no. 29, p. 1707035, Jul. 2018, doi: 10.1002/adma.201707035.

[3] S. Kim, C. Laschi, and B. Trimmer, 'Soft robotics: a bioinspired evolution in robotics,' Trends Biotechnol., vol. 31, no. 5, pp. 287–294, May 2013, doi: 10.1016/j.tibtech.2013.03.002.

[4] A. Souhail and P. Vassakosol, 'Low cost soft robotic grippers for reliable grasping,' J. Mech. Eng. Res. Dev., vol. 41, no. 4, pp. 88–95, 2018, doi: 10.26480/jmerd.04.2018.88.95.

[5] C. H. Liu and C. H. Chiu, 'Optimal design of a soft robotic gripper with high mechanical advantage for grasping irregular objects,' Proc. - IEEE Int. Conf. Robot. Autom., pp. 2846–2851, 2017, doi: 10.1109/ICRA.2017.7989332.

[6] J. Paek, I. Cho, and J. Kim, 'Microrobotic tentacles with spiral bending capability based on shape-engineered elastomeric microtubes,' Sci. Rep., vol. 5, no. March, pp. 1–11, 2015, doi: 10.1038/srep10768.

[7] R. V. Martinez et al., 'Robotic tentacles with three-dimensional mobility based on flexible elastomers,' Adv. Mater., vol. 25, no. 2, pp. 205–212, 2013, doi: 10.1002/adma.201203002.

[8] Y. Sun et al., 'Stiffness Customization and Patterning for Property Modulation of Silicone-Based Soft Pneumatic Actuators,' Soft Robot., vol. 4, no. 3, pp. 251–260, 2017, doi: 10.1089/soro.2016.0047.

[9] M. Calisti et al., 'An octopus-bioinspired solution to movement and manipulation for soft robots,' Bioinspiration and Biomimetics, vol. 6, no. 3, 2011, doi: 10.1088/1748-3182/6/3/036002.

[10] M. Cianchetti, M. Calisti, L. Margheri, M. Kuba, and C. Laschi, 'Bioinspired locomotion and grasping in water: The soft eight-arm OCTOPUS robot,' Bioinspiration and Biomimetics, vol. 10, no. 3, pp. 1–19, 2015, doi: 10.1088/1748-3190/10/3/035003.

[11] D. Rus and M. T. Tolley, ‘Design, fabrication and control of soft robots,’ Nature, vol. 521, no. 7553, pp. 467–475, 2015, doi: 10.1038/nature14543.

[12] W. Wang, C. Li, M. Cho, and S. H. Ahn, ‘Soft Tendril-Inspired Grippers: Shape Morphing of Programmable Polymer-Paper Bilayer Composites,’ ACS Appl. Mater. Interfaces, vol. 10, no. 12, pp. 10419–10427, 2018, doi: 10.1021/acsami.7b18079.

[13] A. Sadeghi, A. Tonazzini, L. Popova, and B. Mazzolai, ‘Robotic mechanism for soil penetration inspired by plant root,’ Proc. - IEEE Int. Conf. Robot. Autom., pp. 3457–3462, 2013, doi: 10.1109/ICRA.2013.6631060.

[14] H. M. J. and H. L. J.R. amend, E.brown, N.rodernberg, ‘a positive pressure universal gripper based on yhe jamming of granular material,’ IEEE Trans. Robot., vol. 28, no. 2, pp. 341–350, 2012, doi: 10.31812/apd.v0i14.1833.

[15] F. Ongaro et al., ‘Autonomous planning and control of soft untethered grippers in unstructured environments,’ J. Micro-Bio Robot., vol. 12, no. 1–4, pp. 45–52, 2017, doi: 10.1007/s12213-016-0091-1.

[16] Z. Xie et al., ‘Octopus Arm-Inspired Tapered Soft Actuators with Suckers for Improved Grasping,’ Soft Robot., vol. 7, no. 5, pp. 639–648, 2020, doi: 10.1089/soro.2019.0082.

[17] T. Umedachi, V. Vikas, and B. A. Trimmer, ‘Softworms: The design and control of non-pneumatic, 3D-printed, deformable robots,’ Bioinspiration and Biomimetics, vol. 11, no. 2, p. 0, 2016, doi: 10.1088/1748-3190/11/2/025001.

[18] T. Umedachi, M. Shimizu, and Y. Kawahara, ‘Caterpillar-Inspired Crawling Robot Using Both Compression and Bending Deformations,’ IEEE Robot. Autom. Lett., vol. 4, no. 2, pp. 670–676, 2019, doi: 10.1109/LRA.2019.2893438.

[19] C. J. Cai et al., ‘Diversified and Untethered Motion Generation Via Crease Patterning from Magnetically Actuated Caterpillar-Inspired Origami Robot,’ IEEE/ASME Trans. Mechatronics, vol. 26, no. 3, pp. 1678–1688, 2021, doi: 10.1109/TMECH.2020.3028746.

[20] L. Cortese, S. Milanovic, and R. Vidoni, ‘A FEM-Experimental Approach for the Development of a Conceptual Linear Actuator Based on Tendril’s Free Coiling,’ Appl. Bionics Biomech., vol. 2017, 2017, doi: 10.1155/2017/6450949.

[21] R. Vidoni, T. Mimmo, and C. Pandolfi, ‘Tendril-Based Climbing Plants to Model, Simulate and Create Bio-Inspired Robotic Systems,’ J. Bionic Eng., vol. 12, no. 2, pp. 250–262, 2015, doi: 10.1016/S1672-6529(14)60117-7.

[22] M. Wooten, C. Frazelle, I. D. Walker, A. Kapadia, and J. H. Lee, ‘Exploration and inspection with vine-inspired continuum robots,’ Proc. - IEEE Int. Conf. Robot. Autom., pp. 5526–5533, 2018, doi: 10.1109/ICRA.2018.8461132.

[23] B. A. Jones and I. D. Walker, ‘Kinematics for multisection continuum robots,’ IEEE Trans. Robot., vol. 22, no. 1, pp. 43–55, 2006, doi: 10.1109/TRO.2005.861458.

[24] B. A. Jones, W. McMahan, and I. D. Walker, ‘Practical kinematics for real-time implementation of continuum robots,’ Proc. - IEEE Int. Conf. Robot. Autom., vol. 2006, no. 6, pp. 1840–1847, 2006, doi: 10.1109/ROBOT.2006.1641974.

[25] T. McMillen and A. Goriely, ‘Tendril perversion in intrinsically curved rods,’ J. Nonlinear Sci., vol. 12, no. 3, pp. 241–281, 2002, doi: 10.1007/s00332-002-0493-1.

[26] J. Fraś, M. Maciaś, F. Czubaczyński, P. Salek, and J. Glówka, ‘Soft flexible gripper design, characterization and application,’ Adv. Intell. Syst. Comput., vol. 543, pp. 368–377, 2017, doi: 10.1007/978-3-319-48923-0_40.

[27] P. Polygerinos, Z. Wang, K. C. Galloway, R. J. Wood, and C. J. Walsh, ‘Soft robotic glove for combined assistance and at-home rehabilitation,’ Rob. Auton. Syst., vol. 73, pp. 135–143, 2015, doi: 10.1016/j.robot.2014.08.014.

[28] S. Ueki et al., ‘Development of a hand-assist robot with multi-degrees-of-freedom for rehabilitation therapy,’ IEEE/ASME Trans. Mechatronics, vol. 17, no. 1, pp. 136–146, 2012, doi: 10.1109/TMECH.2010.2090353.

[29] J. Zhao, X. Zheng, M. Zheng, A. J. Shih, and K. Xu, ‘An endoscopic continuum testbed for finalizing system characteristics of a surgical robot for NOTES procedures,’ 2013 IEEE/ASME Int. Conf. Adv. Intell. Mechatronics Mechatronics Hum. Wellbeing, AIM 2013, pp. 63–70, 2013, doi: 10.1109/AIM.2013.6584069.

[30] A. Bajo, R. E. Goldman, L. Wang, D. Fowler, and N. Simaan, ‘Integration and preliminary evaluation of an Insertable Robotic Effectors Platform for Single Port Access Surgery,’ Proc. - IEEE Int. Conf. Robot. Autom., pp. 3381–3387, 2012, doi: 10.1109/ICRA.2012.6224986.

[31] D. C. R. and H. C. J.Burgner-kahrs, ‘Continuum robots for medical application: a survey,’ IEEE tansactions Robot., vol. 31, no. 6, pp. 1261–1280, 2015.

[32] P. Taylor, D. Trivedi, C. D. Rahn, W. M. Kier, and I. D. Walker, ‘Applied Bionics and Biomechanics Soft robotics : Biological inspiration , state of the art , and future research,’ no. October 2014, pp. 37–41, doi: 10.1080/11762320802557865.

[33] G. J. Monkman, ‘Controllable Retention,’ vol. 5, no. July 1994, pp. 567–575, 2015.

[34] C. W. K.Otsuka, shape memory materials. 1998.

[35] J. Zhu et al., ‘Intelligent Soft Surgical Robots for Next-Generation Minimally Invasive Surgery,’ Adv. Intell. Syst., vol. 3, no. 5, p. 2100011, 2021, doi: 10.1002/aisy.202100011.

[36] M. D. Hager, S. Bode, C. Weber, and U. S. Schubert, ‘Shape memory polymers: Past, present and future developments,’ Prog. Polym. Sci., vol. 49–50, pp. 3–33, 2015, doi: 10.1016/j.progpolymsci.2015.04.002.

[37] L. Sun et al., ‘Stimulus-responsive shape memory materials: A review,’ Mater. Des., vol. 33, no. 1, pp. 577–640, 2012, doi: 10.1016/j.matdes.2011.04.065.

[38] H. Meng and G. Li, ‘A review of stimuli-responsive shape memory polymer composites,’ Polymer (Guildf)., vol. 54, no. 9, pp. 2199–2221, 2013, doi: 10.1016/j.polymer.2013.02.023.

[39] W. Wang, H. Rodrigue, H. Il Kim, M. W. Han, and S. H. Ahn, ‘Soft composite hinge actuator and application to compliant robotic gripper,’ Compos. Part B Eng., vol. 98, pp. 397–405, 2016, doi: 10.1016/j.compositesb.2016.05.030.

[40] H. Rodrigue, W. Wang, D. R. Kim, and S. H. Ahn, ‘Curved shape memory alloy-based soft actuators and application to soft gripper,’ Compos. Struct., vol. 176, pp. 398–406, 2017, doi: 10.1016/j.compstruct.2017.05.056.

[41] Y. Zhou, H. Jin, C. Liu, E. Dong, M. Xu, and J. Yang, ‘A novel biomimetic jellyfish robot based on a soft and smart modular structure (SMS),’ 2016 IEEE Int. Conf. Robot. Biomimetics, ROBIO 2016, pp. 708–713, 2016, doi: 10.1109/ROBIO.2016.7866406.

[42] C. C. Lan, C. M. Lin, and C. H. Fan, ‘A self-sensing microgripper module with wide handling ranges,’ IEEE/ASME Trans. Mechatronics, vol. 16, no. 1, pp. 141–150, Feb. 2011, doi: 10.1109/TMECH.2009.2037495.

[43] S. Kaluvan, C. Y. Park, and S. B. Choi, ‘Bio-inspired device: A novel smart MR spring featuring tendril structure,’ Smart Mater. Struct., vol. 25, no. 1, p. 01LT01, 2015, doi: 10.1088/0964-1726/25/1/01LT01.

[44] N. El-Atab et al., ‘Soft Actuators for Soft Robotic Applications: A Review,’ Adv. Intell. Syst., vol. 2, no. 10, p. 2000128, 2020, doi: 10.1002/aisy.202000128.

[45] A. Poulin, S. Rosset, and H. R. Shea, ‘Printing low-voltage dielectric elastomer actuators,’ Appl. Phys. Lett., vol. 107, no. 24, 2015, doi: 10.1063/1.4937735.

[46] A. Marette, A. Poulin, N. Besse, S. Rosset, D. Briand, and H. Shea, ‘Flexible Zinc–Tin Oxide Thin Film Transistors Operating at 1 kV for Integrated Switching of Dielectric Elastomer Actuators Arrays,’ Adv. Mater., vol. 29, no. 30, pp. 1–6, 2017, doi: 10.1002/adma.201700880.

[47] G. Kofod, M. Paajanen, and S. Bauer, ‘Self-organized minimum-energy structures for dielectric elastomer actuators,’ Appl. Phys. A Mater. Sci. Process., vol. 85, no. 2, pp. 141–143, 2006, doi: 10.1007/s00339-006-3680-3.

[48] H. Imamura, K. Kadooka, and M. Taya, ‘A variable stiffness dielectric elastomer actuator based on electrostatic chucking,’ Soft Matter, vol. 13, no. 18, pp. 3440–3448, 2017, doi: 10.1039/c7sm00546f.

[49] J. Shintake, S. Rosset, B. Schubert, D. Floreano, and H. Shea, ‘Versatile Soft Grippers with Intrinsic Electroadhesion Based on Multifunctional Polymer Actuators,’ Adv. Mater., vol. 28, no. 2, pp. 231–238, 2016, doi: 10.1002/adma.201504264.

[50] S. Nemat-Nasser and Y. Wu, ‘Comparative experimental study of ionic polymer-metal composites with different backbone ionomers and in various cation forms,’ J. Appl. Phys., vol. 93, no. 9, pp. 5255–5267, 2003, doi: 10.1063/1.1563300.

[51] J. Barramba, J. Silva, and P. J. Costa Branco, ‘Evaluation of dielectric gel coating for encapsulation of ionic polymer-metal composite (IPMC) actuators,’ Sensors Actuators, A Phys., vol. 140, no. 2, pp. 232–238, 2007, doi: 10.1016/j.sna.2007.06.035.

[52] B. Gorissen, D. Reynaerts, S. Konishi, K. Yoshida, J. W. Kim, and M. De Volder, ‘Elastic Inflatable Actuators for Soft Robotic Applications,’ Adv. Mater., vol. 29, no. 43, pp. 1–14, 2017, doi: 10.1002/adma.201604977.

[53] F. Connolly, P. Polygerinos, C. J. Walsh, and K. Bertoldi, ‘Mechanical programming of soft actuators by varying fiber angle,’ Soft Robot., vol. 2, no. 1, pp. 26–32, 2015, doi: 10.1089/soro.2015.0001.

[54] F. Connolly, C. J. Walsh, and K. Bertoldi, ‘Automatic design of fiber-reinforced soft actuators for trajectory matching,’ Proc. Natl. Acad. Sci. U. S. A., vol. 114, no. 1, pp. 51–56, 2017, doi: 10.1073/pnas.1615140114.

[55] A. Yamaguchi, K. Takemura, S. Yokota, and K. Edamura, ‘Ii. Electro-Conjugate Fluid,’ 2011.

[56] A. C. Siegel, D. A. Bruzewicz, D. B. Weibel, and G. M. Whitesides, ‘Microsolidics: Fabrication of three-dimensional metallic microstructures in poly(dimethylsiloxane),’ Adv. Mater., vol. 19, no. 5, pp. 727–733, 2007, doi: 10.1002/adma.200601787.

[57] B. E. Schubert and D. Floreano, ‘Variable stiffness material based on rigid low-melting-point-alloy microstructures embedded in soft poly(dimethylsiloxane) (PDMS),’ RSC Adv., vol. 3, no. 46, pp. 24671–24679, 2013, doi: 10.1039/c3ra44412k.

[58] A. Tonazzini, S. Mintchev, B. Schubert, B. Mazzolai, J. Shintake, and D. Floreano, ‘Variable Stiffness Fiber with Self-Healing Capability,’ Adv. Mater., vol. 28, no. 46, pp. 10142–10148, 2016, doi: 10.1002/adma.201602580.

[59] W. Shan, T. Lu, and C. Majidi, ‘Soft-matter composites with electrically tunable elastic rigidity,’ Smart Mater. Struct., vol. 22, no. 8, 2013, doi: 10.1088/0964-1726/22/8/085005.

[60] S. H. Jeong et al., ‘Mechanically Stretchable and Electrically Insulating Thermal Elastomer Composite by Liquid Alloy Droplet Embedment,’ Sci. Rep., vol. 5, no. December, pp. 1–10, 2015, doi: 10.1038/srep18257.

[61] J. Shintake, B. Schubert, S. Rosset, H. Shea, and D. Floreano, ‘Variable stiffness actuator for soft robotics using dielectric elastomer and low-melting-point alloy,’ IEEE Int. Conf. Intell. Robot. Syst., vol. 2015-Decem, pp. 1097–1102, 2015, doi: 10.1109/IROS.2015.7353507.

[62] S. Launay, A. G. Fedorov, Y. Joshi, A. Cao, and P. M. Ajayan, ‘Hybrid micro-nano structured thermal interfaces for pool boiling heat transfer enhancement,’ Microelectronics J., vol. 37, no. 11, pp. 1158–1164, 2006, doi: 10.1016/j.mejo.2005.07.016.

[63] Y. Chen and P. Cheng, ‘Heat transfer and pressure drop in fractal tree-like microchannel nets,’ Int. J. Heat Mass Transf., vol. 45, no. 13, pp. 2643–2648, 2002, doi: 10.1016/S0017-9310(02)00013-3.

[64] J. W. Sohn, G. W. Kim, and S. B. Choi, ‘A state-of-the-art review on robots and medical devices using smart fluids and shape memory alloys,’ Appl. Sci., vol. 8, no. 10, 2018, doi: 10.3390/app8101928.

[65] T. Hao, ‘Electrorheological Fluids.’

[66] J. P. Coulter, K. D. Weiss, and J. D. Carlson, ‘Engineering applications of electrorheological materials,’ J. Intell. Mater. Syst. Struct., vol. 4, no. 2, pp. 248–259, 1993, doi: 10.1177/1045389X9300400215.

[67] J. D. Carlson, D. M. Catanzarite, and K. A. St. Clair, ‘COMMERCIAL MAGNETO-RHEOLOGICAL FLUID DEVICES,’ Int. J. Mod. Phys. B, vol. 10, no. 23n24, pp. 2857–2865, Oct. 1996, doi: 10.1142/S0217979296001306.

[68] P. Sheng and W. Wen, ‘Electrorheological fluids: Mechanisms, dynamics, and microfluidics applications,’ Annu. Rev. Fluid Mech., vol. 44, pp. 143–174, 2011, doi: 10.1146/annurev-fluid-120710-101024.

[69] J. De Vicente, D. J. Klingenberg, and R. Hidalgo-Alvarez, ‘Magnetorheological fluids: A review,’ Soft Matter, vol. 7, no. 8, pp. 3701–3710, 2011, doi: 10.1039/c0sm01221a.

[70] S. Sun et al., ‘A Compact Variable Stiffness and Damping Shock Absorber for Vehicle Suspension,’ IEEE/ASME Trans. Mechatronics, vol. 20, no. 5, pp. 2621–2629, 2015, doi: 10.1109/TMECH.2015.2406319.

[71] M. Eshaghi, R. Sedaghati, and S. Rakheja, ‘Dynamic characteristics and control of magnetorheological/electrorheological sandwich structures: A state-of-the-art review,’ J. Intell. Mater. Syst. Struct., vol. 27, no. 15, pp. 2003–2037, 2016, doi: 10.1177/1045389X15620041.

[72] M. Kallio, T. Lindroos, S. Aalto, E. Järvinen, T. Kärnä, and T. Meinander, ‘Dynamic compression testing of a tunable spring element consisting of a magnetorheological elastomer,’ Smart Mater. Struct., vol. 16, no. 2, pp. 506–514, 2007, doi: 10.1088/0964-1726/16/2/032.

[73] H. M. Jaeger, ‘Celebrating Soft Matter’s 10th Anniversary: Toward jamming by design,’ Soft Matter, vol. 11, no. 1, pp. 12–27, 2015, doi: 10.1039/c4sm01923g.

[74] A. Jiang et al., ‘Robotic Granular Jamming: Does the Membrane Matter?,’ Soft Robot., vol. 1, no. 3, pp. 192–201, 2014, doi: 10.1089/soro.2014.0002.

[75] J. Amend, N. Cheng, S. Fakhouri, and B. Culley, ‘Soft Robotics Commercialization: Jamming Grippers from Research to Product,’ Soft Robot., vol. 3, no. 4, pp. 213–222, 2016, doi: 10.1089/soro.2016.0021.

[76] E. Steltz, A. Mozeika, J. Rembisz, N. Corson, and H. M. Jaeger, ‘Jamming as an enabling technology for soft robotics,’ Electroact. Polym. Actuators Devices 2010, vol. 7642, p. 764225, 2010, doi: 10.1117/12.853182.

[77] S. G. Fitzgerald, G. W. Delaney, and D. Howard, ‘A review of jamming actuation in soft robotics,’ Actuators, vol. 9, no. 4, pp. 1–31, 2020, doi: 10.3390/act9040104.

[78] S. Reitelshofer, C. Ramer, D. Graf, F. Matern, and J. Franke, ‘Combining a collaborative robot and a lightweight Jamming-Gripper to realize an intuitively to use and flexible co-worker,’ 2014 IEEE/SICE Int. Symp. Syst. Integr. SII 2014, no. 0, pp. 1–5, 2014, doi: 10.1109/SII.2014.7028001.

[79] Y. J. Kim, S. Cheng, S. Kim, and K. Iagnemma, ‘A novel layer jamming mechanism with tunable stiffness capability for minimally invasive surgery,’ IEEE Trans. Robot., vol. 29, no. 4, pp. 1031–1042, 2013, doi: 10.1109/TRO.2013.2256313.

[80] K. Asano, F. Hatakeyama, and K. Yatsuzuka, ‘Fundamental study of an electrostatic chuck for silicon wafer handling,’ IEEE Trans. Ind. Appl., vol. 38, no. 3, pp. 840–845, 2002, doi: 10.1109/TIA.2002.1003438.

[81] H. Wang, A. Yamamoto, and T. Higuchi, ‘A crawler climbing robot integrating electroadhesion and electrostatic actuation,’ Int. J. Adv. Robot. Syst., vol. 11, pp. 1–11, 2014, doi: 10.5772/59118.

[82] H. Prahlad, R. Pelrine, S. Stanford, J. Marlow, and R. Kornbluh, ‘Electroadhesive robots - Wall climbing robots enabled by a novel, robust, and electrically controllable adhesion technology,’ Proc. - IEEE Int. Conf. Robot. Autom., pp. 3028–3033, 2008, doi: 10.1109/ROBOT.2008.4543670.

[83] E. W. Schaler, D. Ruffatto, P. Glick, V. White, and A. Parness, ‘An electrostatic gripper for flexible objects,’ IEEE Int. Conf. Intell. Robot. Syst., vol. 2017-Septe, pp. 1172–1179, 2017, doi: 10.1109/IROS.2017.8202289.

[84] P. M. Taylor, G. J. Monkman, and G. J. F. Farnworth, ‘Principles of electroadhesion in clothing robotics,’ Int. J. Cloth. Sci. Technol., vol. 1, no. 3, pp. 14–20, 1989, doi: 10.1108/eb002951.

[85] J. Singh, ‘Electro-Adhesive Gripper Component Selection for Pick and Place of Commonly Used Materials,’ 2019.

[86] K. Yatsuzuka, F. Hatakeyama, K. Asano, and S. Aonuma, ‘Fundamental characteristics of electrostatic wafer chuck with insulating sealant,’ IEEE Trans. Ind. Appl., vol. 36, no. 2, pp. 510–516, 2000, doi: 10.1109/28.833768.

[87] Y. Lu, S. Sathasivam, J. Song, C. R. Crick, C. J. Carmalt, I. P. Parkin, ‘Robust self-cleaning surfaces that function when exposed to either air or oil,’ Science (80-.)., vol. 347, no. 6226, 2015.

[88] L. F. Boesel, C. Cremer, E. Arzt, and A. Del Campo, ‘Gecko-inspired surfaces: A path to strong and reversible dry adhesives,’ Adv. Mater., vol. 22, no. 19, pp. 2125–2137, 2010, doi: 10.1002/adma.200903200.

[89] M. Zhou, N. Pesika, H. Zeng, Y. Tian, and J. Israelachvili, ‘Recent advances in gecko adhesion and friction mechanisms and development of gecko-inspired dry adhesive surfaces,’ Friction, vol. 1, no. 2, pp. 114–129, 2013, doi: 10.1007/s40544-013-0011-5.

[90] Y. Li, J. Krahn, and C. Menon, ‘Bioinspired Dry Adhesive Materials and Their Application in Robotics: A Review,’ J. Bionic Eng., vol. 13, no. 2, pp. 181–199, 2016, doi: 10.1016/S1672-6529(16)60293-7.

[91] D. S. and M. R. C. S. Kim, M. Spenko, S. Trujillo, B. Heyneman, ‘Smooth Vertical Surface Climbing With Directional Adhesion,’ IEEE Trans. Robot., vol. 24, no. 1, pp. 65–74, 2008.

[92] K. Autumn and A. M. Peattie, ‘Mechanisms of adhesion in geckos,’ Integr. Comp. Biol., vol. 42, no. 6, pp. 1081–1090, 2002, doi: 10.1093/icb/42.6.1081.

[93] J. Lee and R. S. Fearing, ‘Contact self-cleaning of synthetic gecko adhesive from polymer microfibers,’ Langmuir, vol. 24, no. 19, pp. 10587–10591, 2008, doi: 10.1021/la8021485.

[94] Y. Mengüç, M. Röhrig, U. Abusomwan, H. Hölscher, and M. Sitti, ‘Staying sticky: Contact self-cleaning of gecko-inspired adhesives,’ J. R. Soc. Interface, vol. 11, no. 94, 2014, doi: 10.1098/rsif.2013.1205.

[95] E. W. Hawkes, D. L. Christensen, A. K. Han, H. Jiang, and M. R. Cutkosky, ‘Grasping without squeezing: Shear adhesion gripper with fibrillar thin film,’ Proc. - IEEE Int. Conf. Robot. Autom., vol. 2015-June, no. June, pp. 2305–2312, 2015, doi: 10.1109/ICRA.2015.7139505.

[96] Y. Mengüç, S. Y. Yang, S. Kim, J. A. Rogers, and M. Sitti, ‘Gecko-inspired controllable adhesive structures applied to micromanipulation,’ Adv. Funct. Mater., vol. 22, no. 6, pp. 1246–1254, 2012, doi: 10.1002/adfm.201101783.

[97] H. Hu et al., ‘Discretely Supported Dry Adhesive Film Inspired by Biological Bending Behavior for Enhanced Performance on a Rough Surface,’ ACS Appl. Mater. Interfaces, vol. 9, no. 8, pp. 7752–7760, 2017, doi: 10.1021/acsami.6b14951.

[98] J. Gafford et al., ‘Shape deposition manufacturing of a soft, atraumatic, deployable surgical grasper,’ J. Med. Devices, Trans. ASME, vol. 8, no. 3, 2014, doi: 10.1115/1.4027048.

[99] H. Huang, J. Lin, L. Wu, Z. Wen, and M. Dong, ‘Trigger-based dexterous operation with multimodal sensors for soft robotic hand,’ Appl. Sci., vol. 11, no. 19, 2021, doi: 10.3390/app11198978.

[100] M. Tavakoli et al., ‘Autonomous Selection of Closing Posture of a Robotic Hand Through Embodied Soft Matter Capacitive Sensors,’ IEEE Sens. J., vol. 17, no. 17, pp. 5669–5677, 2017, doi: 10.1109/JSEN.2017.2726348.

[101] H. Vandeparre, D. Watson, and S. P. Lacour, ‘Extremely robust and conformable capacitive pressure sensors based on flexible polyurethane foams and stretchable metallization,’ Appl. Phys. Lett., vol. 103, no. 20, 2013, doi: 10.1063/1.4832416.

[102] K. Elgeneidy, N. Lohse, and M. Jackson, ‘Bending angle prediction and control of soft pneumatic actuators with embedded flex sensors – A data-driven approach,’ Mechatronics, vol. 50, no. October, pp. 234–247, 2018, doi: 10.1016/j.mechatronics.2017.10.005.

[103] D. McCoul, W. Hu, M. Gao, V. Mehta, and Q. Pei, ‘Recent Advances in Stretchable and Transparent Electronic Materials,’ Adv. Electron. Mater., vol. 2, no. 5, pp. 1–51, 2016, doi: 10.1002/aelm.201500407.

[104] H. Jang, Y. J. Park, X. Chen, T. Das, M. S. Kim, and J. H. Ahn, ‘Graphene-Based Flexible and Stretchable Electronics,’ Adv. Mater., vol. 28, no. 22, pp. 4184–4202, 2016, doi: 10.1002/adma.201504245.

[105] M. Amjadi, K. U. Kyung, I. Park, and M. Sitti, 'Stretchable, Skin-Mountable, and Wearable Strain Sensors and Their Potential Applications: A Review,' Adv. Funct. Mater., vol. 26, no. 11, pp. 1678–1698, 2016, doi: 10.1002/adfm.201504755.

[106] D. S. Chathuranga, Z. Wang, Y. Noh, T. Nanayakkara, and S. Hirai, 'Magnetic and Mechanical Modeling of a Soft Three-Axis Force Sensor,' IEEE Sens. J., vol. 16, no. 13, pp. 5298–5307, 2016, doi: 10.1109/JSEN.2016.2550605.

[107] T. Paulino et al., 'Low-cost 3-axis soft tactile sensors for the human-friendly robot Vizzy,' Proc. - IEEE Int. Conf. Robot. Autom., pp. 966–971, 2017, doi: 10.1109/ICRA.2017.7989118.

[108] Institute of Electrical and Electronics Engineers., 'INES 2013 : proceedings : IEEE 17th International Conference on Intelligent Engineering Systems : June 19-21, 2013, Costa Rica.,' p. 364, 2013.

[109] J. S. Heo, K. Y. Kim, and J. J. Lee, 'Development of a distributed force detectable artificial skin using microbending optical fiber sensors,' J. Intell. Mater. Syst. Struct., vol. 20, no. 17, pp. 2029–2036, 2009, doi: 10.1177/1045389X09348256.

[110] S. Bauer, S. Bauer-Gogonea, I. Graz, M. Kaltenbrunner, C. Keplinger, and R. Schwödiauer, '25th anniversary article: A soft future: From robots and sensor skin to energy harvesters,' Adv. Mater., vol. 26, no. 1, pp. 149–162, 2014, doi: 10.1002/adma.201303349.

[111] M. L. Hammock, A. Chortos, B. C. K. Tee, J. B. H. Tok, and Z. Bao, '25th anniversary article: The evolution of electronic skin (E-Skin): A brief history, design considerations, and recent progress,' Adv. Mater., vol. 25, no. 42, pp. 5997–6038, 2013, doi: 10.1002/adma.201302240.

[112] V. A. Ho, H. Yamashita, Z. Wang, S. Hirai, and K. Shibuya, 'Wrin'Tac: Tactile Sensing System with Wrinkle's Morphological Change,' IEEE Trans. Ind. Informatics, vol. 13, no. 5, pp. 2496–2506, 2017, doi: 10.1109/TII.2017.2718660.

[113] R. M. R. F. Spano, A. Dabrowska, B.M. Quandt, L. Boesel, Empa, A. Massaro, and A. Lay-Ekuakille, 'IEEE NANO 2015 15th International Conference on Nanotechnology : July 27-30, 2015, Rome,' Flex. touch sensors based nanocomposites Embed. Polym. Opt. fibers Artif. Ski. Appl., pp. 27–30, 2015.

[114] B. M. Quandt et al., 'Body-monitoring with photonic textiles: A reflective heartbeat sensor based on polymer optical fibres,' J. R. Soc. Interface, vol. 14, no. 128, 2017, doi: 10.1098/rsif.2017.0060.

[115] A. Koivikko, E. S. Raei, M. Mosallaei, M. Mäntysalo, and V. Sariola, 'Screen-printed curvature sensors for soft robots,' IEEE Sens. J., vol. 18, no. 1, pp. 223–230, 2018, doi: 10.1109/JSEN.2017.2765745.

[116] P. Ribeiro et al., 'A Miniaturized Force Sensor Based on Hair-Like Flexible Magnetized Cylinders Deposited over a Giant Magnetoresistive Sensor,' IEEE Trans. Magn., vol. 53, no. 11, pp. 1–5, 2017, doi: 10.1109/TMAG.2017.2714625.

Biographies

Dr. Shubhashis Sanyal received Master of Technology in Machine Design from IIT Roorkee, philosophy of doctorate degree in Mechanical Engineering at Rani Durgavati Vishwavidyalaya, Jabalpur (M.P.). He has worked at many administrative positions, including Dean Faculty Welfare, Dean R&C etc., and currently working as a professor in Department of Mechanical Engineering at National Institute of Technology, Raipur. His area of interest includes Synthesis

of Mechanisms, Stress Analysis, Stress Concentration Factor, Biomechanics, Comfort Analysis.

Dr. Anuj Kumar Shukla received Master of Technology in Engineering Mechanics from IIT Delhi, philosophy of doctorate degree in Mechanical Engineering at IIT Delhi. He is currently working as assistant professor in Department of Mechanical Engineering at National Institute of Technology, Raipur. His area of interest includes Computational Fluid Dynamics (CFD), Convective Heat Transfer, Thermal Engineering, Turbulence Modelling, Simulation, RANS, LES, Filtration and Clean Air.

Hrishi Sharad Pinjan currently 4th year student in Department of Mechanical Engineering at National Institute of Technology, Raipur pursuing bachelor of technology degree. His area of interest includes Design, Soft Robotics, Automation,

Piyush Tailor currently 4th year student in Department of Mechanical Engineering at National Institute of Technology, Raipur pursuing bachelor of technology degree. His area of interest includes Soft Robotics, Automation, Design.

Pyla Pavan Kumar currently 4th year student in Department of Mechanical Engineering at National Institute of Technology, Raipur pursuing bachelor of technology degree. His area of interest includes Soft Robotics, Design, Automation

Surjeet Kumar Bhargav currently 4th year student in Department of Mechanical Engineering at National Institute of Technology, Raipur pursuing bachelor of technology degree. His area of interest includes Design, Soft Robotics, Automation,

Suman Saurav currently 4th year student in Department of Mechanical Engineering at National Institute of Technology, Raipur pursuing bachelor of technology degree. His area of interest includes Design, Soft Robotics, Automation,

Light Fidelity (LiFi) Based Medical Networking for Secure and Anti-Theft Data Transfer with Protection for Radio Frequency Devices

Hoimanti Dutta[1*], Abhinandan Sarkar[2], and Rajdeep Chakraborty[3]

[1, 3]*Dept. of CSE, Netaji Subhash Engineering College, Kolkata, India.*

[2]*Dept. of ETCE, Shree Ramkrishna Institute of Science & Technology, Kolkata, India.*

[1]*hoimantidutta.nsec@gmail.com ORCiD: 0000-0002-2232-0852*

[2]*abhinandansarkar12@gmail.com ORCiD: 0000-0002-5527-7301*

[3]*rajdeep_chak@yahoo.co.in, ORCiD: 0000-0001-6641-0860*

Abstract.

Light-Fidelity (LiFi) is a new way of data communication through the visible light spectrum (4.3×10^{14} Hz to 7.5×10^{14} Hz) coined by Prof. Harald Haas in 2011. Since, in the span of ten years a lot of work being carried out, recently it is claimed that a 26Gbps speed of data transfer being achieved. In this paper, we propose a representation of medical networking using LiFi. LiFi is also considered one of the secure physical layer data transfers and thus it can be effectively used as an anti-theft data transfer. The other advantage of LiFi-based networking is that it doesn't interfere with many radiofrequency devices such as MRI Scanner whereas the conventional Wireless Fidelity (WiFi) based network does. The only disadvantage of LiFi is that it works on line-of-sight. In this paper, we first give a brief introduction of LiFi and then describe LiFi in detail with architecture and mathematical equations. Then we give a detailed literature survey stating why LiFi is important for medical networking. We give a scheme of a proposed model thereafter and then we discuss the probable implementation and its features.

Keywords. Light Fidelity (LiFi), Light Fidelity (LiFi) based medical network, Light Fidelity (LiFi) based anti-theft data transfer, Secure networking, Radiofrequency devices

1. INTRODUCTION

With the development of communication systems, the necessity and dependency on networking have also increased. If we look around two to three decades back, long-distance communication was a difficult task for people. But it has become so cheap and inevitable now. We can see the development of a generation of networks from 1G to 5G which is further stepping toward 6G. With this increase in the necessity, congestion of networks, theft of data, loss of speed, and interference of signal has all got included in the network and communication system. In 2011, Professor Harald Haas, University of Edinburgh, coined the term 'Li-fi', due to which the whole outlook of the networking and communication system changed. He showed the use of visible light as a data carrier and named it Li-Fi – Light Fidelity. As the radio wave spectrum is congested due to the increase in demand for

mobile communication, the visible light spectrum is vacant and still not commercially introduced. The wavelength of visible light communication ranges from 350 nm to 750 nm, with frequencies ranging from 4.3 x 10^{14} Hz to 7.5 x 10^{14} Hz. Making it an excellent mechanism for data transfer.[1] This band is readily available in all indoor environments and does not interfere with other waves in the specified space. A commonly used solid-state device, LED, transmits the data from the transmitter to the receiver. As LED is a current-driven device, the modulation technique is also simplified. An LED is a p-n junction semiconductor device, whose current intensity can be controlled or regulated. The lifetime of the light-emitting diode is comparatively longer when compared with the other sources. If we consider fluorescent light as a source, the durability and efficiency of the LED are much better [2]. To send and receive data, the transmitter has to modulate the signal and the receiver has to demodulate the signal received. When we use led as a source, with only intensity modulation the data becomes suitable for transmission, we do not have to include phase and frequency modulation techniques. For transferring 1 bit of data at a time the on-off keying technique is used. So, it can be said that led proves to be a good transmitter point.

Though radio waves have a long-range, can be communicated to distant places, it becomes a disadvantage for it when we consider it from a data loss or theft point of view. There is attenuation in radio waves and theft of data, while using visible light, it cannot pass through any opaque object, keeping the range very secure to nearby places and known persons. Considering VLC as communication illumination is a factor for proper data transfer, so from this point of view also if we study, the range of visible light from a led will be constricted to an indoor space only. So, data theft can be minimized or eliminated, if we use VLC for our local networking. Furthermore, it is surveyed that the maximum of the traffic generated is in an indoor environment, so visible light communication can serve as a good source of wireless connectivity [3]. VLC is a low power consumption system, with uncontrolled bandwidth allocation. The future is predictive of a hybrid model for RF and VLC, which will impart a much faster communication model [4].

Section 2 gives details about LiFi Technology with The OOK modulation in Section 2.1, Section 3 gives the literature review and motivation, Section 4 illustrates the scheme of the proposed LiFi-based networking model in medical hospitals, Section 5 gives a probable implementation and its features. Finally, Section 6 draws the conclusion. References are listed at last.

2. THE LIGHT FIDELITY (LIFI) TECHNOLOGY

Data transmission through light fidelity will be a life-changing prospect in near future. This is a subset under VLC, developed and tested in the indoor environment when invented, but conquering many of its misconceptions, like Li-Fi is Los technology, it does not work on sunlight, dimming is not advisable, lights flicker a lot, no uplinking is possible, [5] it has emerged to be a technology for versatile applications. It has gained its control in the field of smart cities, healthcare, delicate industrial sectors, airlines, defence, underwater data transfers, and many more [6]. Though there is some restriction to using Li-Fi or visible light for communication like attenuation, interference, or noise [1], using some advanced modulation techniques like OFDM and adaptive modulation with coding, the loss of data can be minimized.

Let us now understand the architecture of light fidelity. As Li-Fi comes under visible light communication, we can easily understand the architectural flow between the transmitter and receiver. The architecture consists of a physical layer, medium access control layer, and the application layer, for more security purposes in mobile communication we can use a security layer before the implementation of the application layer. The below diagram shows the layered architecture of Li-Fi (Fig 1.)

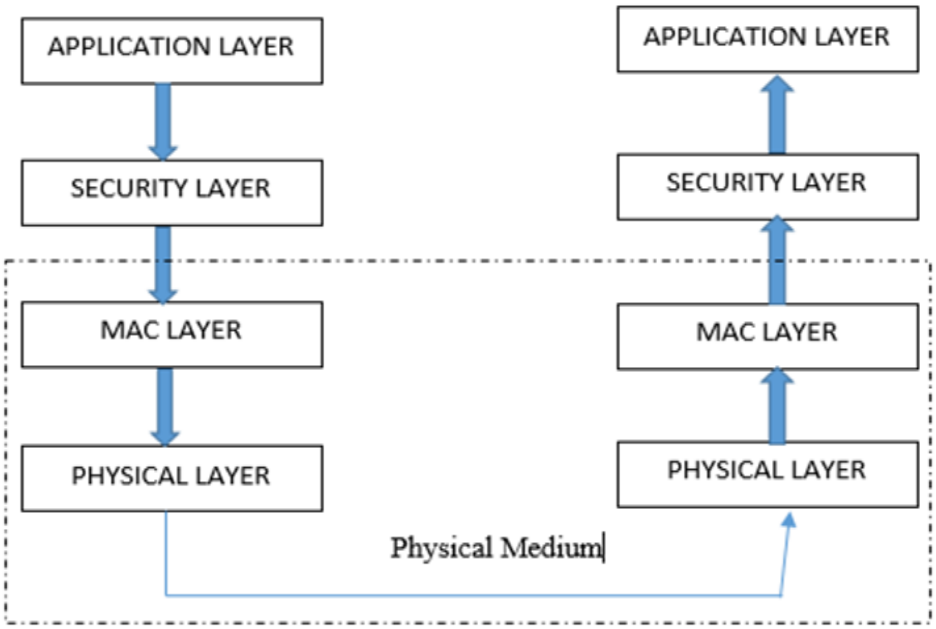

Figure 1. The layered architecture of LiFi

Discussing the physical system, we can design it for three sections: the transmitter module, channel, and receiver module. The transmitter module consists of the modulator and the light source, the channel is the distance between the transmitter and the receiver, the channel gain can be given by the equation 1 –

$$CC(f) = CL + CD(f), \qquad (1)$$

where CL is the path loss and CD is the channel gain [18], and the receiver section consists of the demodulator, signal conditioning and finally, we receive the data [7]. The data received in Li-Fi is non-coherent, positive, and real [1]. The received signal can be given by the relation $z = Lx + n$, where L is the multiple input LED channels.[12] Fig 2. Shows a physical system of visible light communication.

So, studying the complexity of systems, designs, and networking layers, it is understood that it can be established and used in many core application areas. Visible light communication or more specifically light fidelity will give a step forward towards the development of 6G communication. In Fig. 2, Blue arrows signify the outer channel of the communication and black arrows portray the inner channel of communication for both sender and receiver sections.

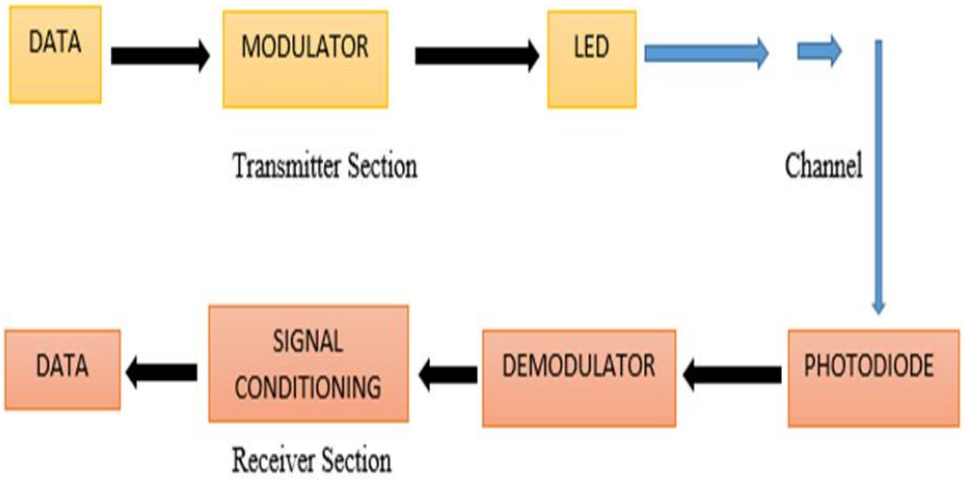

Figure 2. The physical system of visible light communication

While we develop some applications from new technology, understanding contemporary technology is very important, and in this article, as we propose to establish a complementary technology of RF spectrum, let us know some disadvantages of RF in the case of medical fields. Not only inside the medical premises, using radio wave spectrum for communication outside the medical buildings has a severe effect on the patients as well as the medical equipment of the Medical [8]. The equipment in the Medicals that are used for imaging or scanning of the human body, uses electromagnetic spectrum, frequency ranging in MHz, which interferes with the mobile networks near the building, and tends to give faulty results [9]. They imbibe noise within the signal and hamper the machine. Continuous propagation of radio waves inside the premises also has an adverse effect on the human body. The machines used in ICU get affected when the people inside the medical carry a mobile communication device with him/her. Not only on the machines, radiofrequency has a long-term effect on the human body, a study shows that when rodents are exposed to radio waves they mimic the lifetime human exposure, it also has an increased rate of schwannomas, malignant gliomas as well as chromosomal DNA damage. The brain development of children also decreases with exposure to mobile networks [10]. But knowing the effects on machines and human health, networking is also an integral part of life, without which a Medical cannot run. Proper communication between building floors, different wards, and laboratories is very important. Proper transmission of data is needed for prompt response and service deliveries in the healthcare sector. Li-Fi can be a stable alternative to these factors. The frequency used is very high in terms of 10^{14} Hz, and interference and signal fading are very minimal in Li-Fi. Due to the use of the current-driven solid-state device as transmitter output, modulation becomes easy, so the lagging of data is less, and the noise becomes very minimal when orthogonal modulation techniques are implied. Li-Fi can also be used for easy transmission of sensor data, making it suitable for use as patient monitoring device transmitters. The data can be easily received and plotted at respective storage areas [11]. As discussed previously, visible light cannot cross thick walls, and theft of data can also be neglected. With the use of optical filters and expressing automatic gain control

algorithms, Li-Fi can be used in outdoor communication systems, as the effect of sunlight and shot noise can be reduced [5].

Though the mobile network radio waves are fast and deployed in each corner of the world. Within a few years, a massive change will be noticed, when commercially Li-Fi will be implemented for indoor and outdoor networking, edge computing, and many modern tech applications. Making a radiation-free space for treatment at medical centres or Medicals.

2.1. The On-Off Keying (OOK) Modulation

The primary method used in this technology is On-Off Keying of OOK. In this technique, the LEDs are turned off to represent the logic value 0, and LEDs are turned on to represent the logic value 1. Let the Phl is the error probability of receiving 1 as 0 and also Let Plh is the error probability of receiving 0 as 1. This condition is also known as the coherent receiver. Then this probability is calculated as equation 2

$$Phl = Plh = \tfrac{1}{2}\, f(\sqrt{((E/N) * 1/4)}) \qquad (2)$$

Where, E/N is the Energy to Noise Ratio and function, f represents the complementary error function.

There are few important advantages of OOK modulation than other modulations in LiFi technology are:-

- OOK modulation is the closest digital modulation with analog modulation so, the conversion time from Analog to Digital and vice versa is very less, hence data transfer is fastest and bandwidth is also increased.
- The LIFi with OOK modulation also enhanced data security as encryption and decryption can be done right in transmission and receiving modules along with the signal itself.
- OOK modulation is very susceptible to distortion, noises, non-linearities and cross talk.
- OOK modulation provides the highest signal strengthen in a quite large distance.
- OOK modulation is cheapest to implement.

3. PREVIOUS WORK AND MOTIVATION

In this section of the article, we will be discussing some of the previous development with the thrust on the following and the primary motivating factor in writing this paper: -

Protection from Radiofrequency device interferences.

- Li-Fi can be used for real-time tracking of important prescribed and aseptic drugs e.g., cytotoxic drugs
- LiFi for remote monitoring
- LiFi for doctors, staff, and patients
- Li-Fi enabled tracking and relocation of the positions of key medical devices

As discussed earlier in this article's introduction section, the exposure to radio waves in a long term causes critical diseases, as well as it is studied to have interference with the medical instruments in the clinical areas. Li-Fi tends to be a better solution when establishing a network system in Medical and critical care units.

From the article [16], we can see that remote monitoring and a radiation-free environment can be created by using light fidelity, as the medium of data transmission. Through some embedded system designed on the concept of the internet of things, monitoring ECG, heart rate, blood oxygen level, non–invasive blood pressure, and overall health can be sensed. A device equipped with light fidelity can transmit this data fetched from the different sensors. This helps doctors and health workers to know about the health condition of the patient.

Interference of radio waves with the precision devices in the Medical is a crucial issue, in getting the proper result from the devices. Light fidelity plays an important role to eliminate this interference. Protection against radio waves is very much needed, as it may also cause heart stress, and insomnia and may reduce brain activity. When multiple Li-Fi transmitters are installed, they can transfer around 224 gigabits of data per second, which are much faster than Wi-Fi or a cellular network. So, networking in the Medical becomes very easy for doctors and other staff, as it can be noticed that medical illumination is very bright and at every corner, so fading or noise absorption also becomes very less [12].

Tracking the medication on a real-time basis for remote patients is very important. The sensitive patients treated at home needs, proper care, location update, and health parameter updates, from [11], it is studied that with the use of multiple sensors not only the parameters of the body but also the medication timing, injection timings can be monitored and checked. The use of respiration sensors and glucose sensors will help in getting the variable levels of glucose and inhale-exhale level while taking the medicines. When injected or orally taking any cytotoxic drugs, the glucose level varies in the body, so more this kind of critical medical also, Li-Fi serves a good purpose. The patients taking cytotoxic drugs are very weak, so exposure to radio waves mainly the cellular waves or wi-fi would harm their health condition in an adverse situation. So, communication through visible light prevents the worsening [10].

Multiple Li-Fi transmitters can be attached to a variety of places, to detect the movement of a patient, relocation of beds, and medical devices can be traced using network handover in inter LED communication module. While using multiple transmitters, inter–LED mitigation can be seen, which on using a technique known as channel inversion precoding can be minimized [12].

The Li-Fi technology is covering the whole world wherever there is a problem with the radio waves. Though much development and research are needed to establish a fully commercial system, it has been tested and introduced in many fields, other than healthcare sectors. Li-Fi plays a huge role in the development of smart cities, IoT devices, traffic lights, airlines, underwater data transmission, disaster management, defence as well as educational institutions also [17].

4. THE PROPOSED MEDICAL NETWORK SYSTEM

The proposed model is a scheme or representation of a Li-Fi-based patient monitoring system that uses white LEDs to transfer data through a VLC-based data transmission system in the medical network. In this proposed system, the illumination and the communication sources are provided by several LEDs that might be utilized and used as data transmission of sensors located in the static patients in bed. The usage of the illumination values in the LED lamps and a built-in transmitter that is connected with the medical database in turn will

allow downlink in a controlled manner. Since a typical patient kept in the ICU monitoring is static in time, so, a static proposed model is chosen here. The Installation of data transmission with LEDs is done for each of the sensors through a precision-based transmission module which makes the proposed system different from the existing system. In this model, the receiver is placed on the top of the patient i.e., the ceiling, and the transmission module points upward to the receiver at the ceiling [13]. The electronic medical database that just discussed transfers medical data to the Li-Fi transmitting module and this is a point-to-point connection. Photodetectors (PDs) are used as a receiver and placed on desktops, tablets, or user devices [12]. Moreover, transmission modules that are placed on the patient with LOS are also connected to the PDs that are placed on the ceiling. The other implementation perspectives are: -

- Multiple detectors minimize the diversity effects.
- Photodetectors spacing achieves robustness.
- This is an obstacles-free environment model in the ICU [14].

Fig. 3 illustrates the proposed scheme of LiFi-based medical network system.

The various biomedical signals collected in the proposed system are: -

- ECG
- Photoplethysmogram (PPG)
- Body Temperature
- Pulse rate
- SPO_2 Value

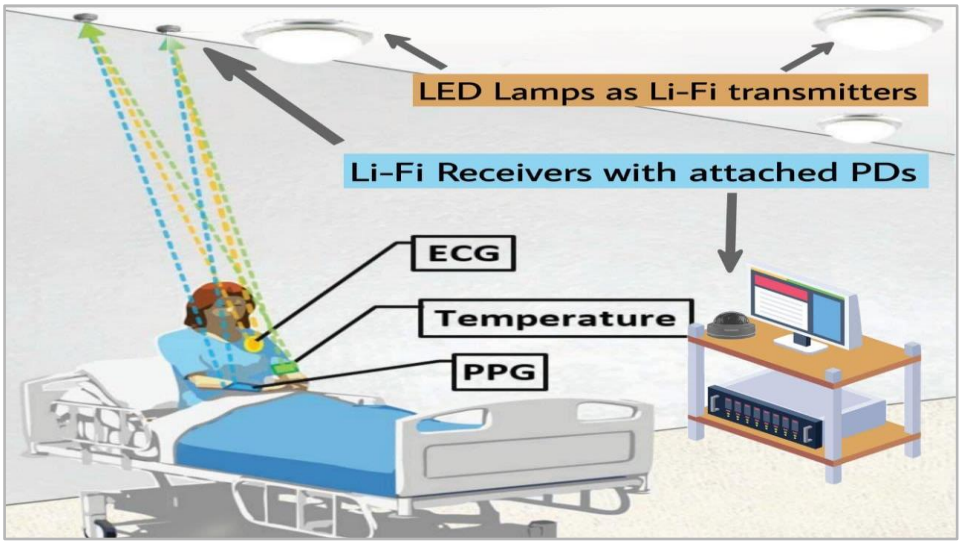

Figure 3. The Representation of Proposed Li-Fi based Medical Network System

We used here the OOK modulation because it provides both accuracy and reliability in this system [13]. We also achieved a very low bit error rate (BER), which is less than 10-5, at considerable SNR values in that service area [14]. Therefore, Li-Fi based system in medical communication is indeed a novel use as discussed in this section.

5. IMPLEMENTATION AND DISCUSSION

In Medicals, a patient's current medical condition is monitored by critical care equipment. Doctors, nurses, technicians, and caregivers use their smartphones, tablets, smartwatches, or desktop computers to monitor the same via data communication. van der R. Togt performed an electromagnetic interference test with several medical equipments. 20% of the incidents were classified as hazardous as a result of this test. To avoid such potentially hazardous equipment malfunctioning due to electromagnetic interference, only wired communication channels are used in Intensive Care Units (ICUs) instead of Wi-Fi. Hence, Li-Fi which permits high-speed data communication via Visible Light Communication (VLC) could be safely used to avoid such limitations of Wi-Fi in corridors, waiting rooms, patient rooms, and operating theatres. Nowadays, the security and reliability of data transmission are playing key roles in patient monitoring. However, all related technologies operate in the radiofrequency spectrum which not only jeopardizes patients' health but is also responsively congested and highly susceptible to hacking. Li-Fi is secure against hacking and data theft as light cannot penetrate through walls. Li-Fi is also used in the transference of curative text data and analog physiological signals can be used. Moreover, patients could connect to the internet to check emails, and news, listen to songs, play video games, access social media platforms, and watch movies and web series on OTT platforms to avoid feeling homesick during their medical stay. Hence, Li-Fi could monitor and report the movements and vital signs of patients on their beds in real-time without using wired communication channels. Li-Fi could assist the medical staff by tracking and relocating of crucial positions, as these devices are shared between various departments. Fig 4. Shows a summary of Li-Fi implementation between patients and caregivers.

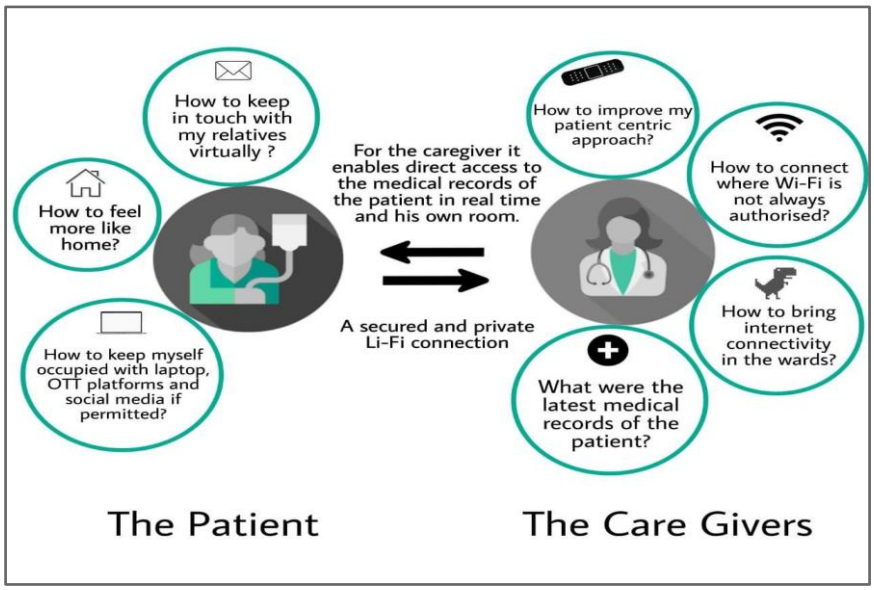

Figure 4. Summary of Li-Fi implementation between patients and caregivers

Li-Fi could be implemented using light-emitting diodes (LEDs) in medical environments to enhance comfortability for sufferers and carers which prevents the risk of disturbance that

can arise from electromagnetic waves interference disturbing the precision medical device. Indoor wireless communication could be achieved at a much faster rate by using LED bulbs as a data transmission medium instead of Wi-Fi. As the flickering rate is faster than the human eye can realize, people could still use the same light source in each room without interfering with medical equipment operation. The real-time tracking of advised aseptic drugs like cytotoxic drugs can also be performed from medical pharmacies. Li-Fi can aid pharmacists in receiving and screening electronically approved prescriptions directly in the unit. Healthcare professionals can access, monitor, and share the real-time status of patients' records in a suitable, rapid, and very safe manner on their smartphones without the necessity to make a call, go directly to the unit, or wait to collect their reports at the pharmacy terminals. Li-Fi could be implemented in data collection from any device enabled with Li-Fi technology using a secure network by data loggers to remotely observe a situation with data uploading periodically without the need of being collected from a desktop [15].

6. CONCLUSION

Thus, in this paper, we have successfully given the representation of LiFi-based medical networking and its probable implementation by discussing it. We also provided the architecture of this technology with the OOK method of transferring data with equations. The main advantage of this model is security and anti-theft transferring of data. It also protects radiofrequency devices such as MRI scanners. The other applications of this proposed model are Li-Fi for concurrent tracking of advised aseptic drugs like cytotoxic drugs, LiFi for remote monitoring, LiFi for doctors, staff, and patients, and Li-Fi for not only keeping in sight but also resettlement of the positions of crucial medical gadgets. In future work, we will insert machine learning into the model to implement some more applicability in smart computing. We will also incorporate Optical OFDM where a baseband signal is used to modulate the LED intensity.

REFERENCES

[1] J.G., Webster, A.R Ndjiongue, H.C. Ferreira, and T.M.N Ngatched, Visible Light Communications (VLC) Technology. In Wiley Encyclopedia of Electrical and Electronics Engineering, J.G. Webster (Ed.). 2015 doi: 10.1002/047134608X.W8267

[2] J. Gancarz, H. Elgala and T. D. C. Little, "Impact of lighting requirements on VLC systems," in IEEE Communications Magazine, vol. 51, no. 12, pp. 34-41, December 2013, DOI: 10.1109/MCOM.2013.6685755.

[3] H. Burchardt, N. Serafimovski, D. Tsonev, S. Videv, and H. Haas, "VLC: Beyond point-to-point communication," in IEEE Communications Magazine, vol. 52, no. 7, pp. 98-105, July 2014, doi: 10.1109/MCOM.2014.6852089.

[4] H. Abuella et al., "Hybrid RF/VLC Systems: A Comprehensive Survey on Network Topologies, Performance Analyses, Applications, and Future Directions," in IEEE Access, vol. 9, pp. 160402-160436, 2021, doi: 10.1109/ACCESS.2021.3129154.

[5] H. Haas, LiFi is a paradigm-shifting 5G technology,Reviews in Physics,Volume 3,2018,Pages 26-31,ISSN 2405-4283, doi:10.1016/j.revip.2017.10.001.

[6] D. Khandal, and S. Jain. "Li-fi (light fidelity): The future technology in wireless communication." International Journal of Information & Computation Technology 4.16 (2014): 1687-1694.

[7] L. Ullah Khan, Visible light communication: Applications, architecture, standardization and research challenges, Digital Communications and Networks, Volume 3, Issue 2,2017, Pages 78-88, ISSN 2352-8648, doi: 10.1016/j.dcan.2016.07.004

[8] E. Hanada. The electromagnetic environment of Medicals: how it is affected by the strength of electromagnetic fields generated both inside and outside the Medical. Ann Ist Super Sanita. 2007;43(3):208-17. PMID: 17938450.

[9] E. Hanada, K. Kodama, K. Takano, Y. Watanabe, Y. Nose. Possible electromagnetic interference with electronic medical equipment by radio waves coming from outside the Medical. J Med Syst. 2001 Aug;25(4):257-67. DOI: 10.1023/a:1010727220929. PMID: 11463202.

[10] B. Miller Anthony, E. Sears Margaret, L.L. Morgan, L.D. Devra, H. Lennart, O. Mark, S. Colin L., Risks to Health and Well-Being From Radio-Frequency Radiation Emitted by Cell Phones and Other Wireless Devices, Frontiers in Public Health, VOLUME=7,2019,10.3389/fpubh.2019.00223, ISSN=2296-2565

[11] S. Sudha, D. Indumathy, A. Lavanya, M. Nishanthi, D. M. Sheeba and V. Anand, "Patient monitoring in the Medical management using Li-Fi," 2016 IEEE Technological Innovations in ICT for Agriculture and Rural Development (TIAR), 2016, pp. 93-96, DOI: 10.1109/TIAR.2016.7801220.

[12] T. Ardi Nugraha, Y. Ardiyanto, "Li-Fi Technology for Transmitting Data in Medical Environments", 2020 IEEE 1st International Conference on Information Technology, Advanced Mechanical and Electrical Engineering (ICITAMEE) | DOI: 10.1109/ICITAMEE50454.2020.9398406

[13] W. Anugrah Cahyadi, T. Jeong, Y-H Kim, Y-H Chung, T. Adiono, "Patient Monitoring Using Visible Light Uplink Data Transmission", 2015 International Symposium on Intelligent Signal Processing and Communication Systems (ISPACS) November 9-12, 2015, 978-1-4673-6499-7/15/$31.00 ©2015 IEEE

[14] S. Singh, S. Mishra, P. Asthana, S. Kumar, "Comprehensive Visible Light Communication System for Healthcare", IOSR Journal of Computer Engineering (IOSR-JCE) e-ISSN: 2278-0661,p-ISSN: 2278-8727, Volume 19, Issue 3, Ver. II (May.-June. 2017), pp 08-11 www.iosrjournals.org

[15] Chukwuemeka Livinus, "Top 5 Applications of Li-Fi Technology", September 3, 2018 Available: https://www.lifitn.com/blog/2018/8/30/5-applications-of-li-fi-technology

[16] T. Ananth Kumar, et al. "LIFI-Based Radiation-Free Monitoring and Transmission Device for Medicals/Public Places." Multimedia and Sensory Input for Augmented, Mixed, and Virtual Reality, edited by Amit Kumar Tyagi, IGI Global, 2021, pp. 195-205. doi: 10.4018/978-1-7998-4703-8.ch010

[17] Kuppusamy, S. Muthuraj, and S. Gopinath, "Survey and challenges of Li-Fi with comparison of Wi-Fi," 2016 International Conference on Wireless Communications, Signal Processing and Networking (WiSPNET), 2016, pp. 896-899, DOI: 10.1109/WiSPNET.2016.7566262.

[18] Y. Wang, D. A. Basnayaka, X. Wu and H. Haas, "Optimization of Load Balancing in Hybrid LiFi/RF Networks," in IEEE Transactions on Communications, vol. 65, no. 4, pp. 1708-1720, April 2017, doi: 10.1109/TCOMM.2017.2654249.

Biographies

"A teacher by profession and a learner by passion."

Abinandan Sarkar has completed his Bachelor of Technology in Electronics & Instrumentation from Greater Kolkata College of Engineering and Management, M.Tech in VLSI from Techno India University. He is trained in multiple domains especially IoT, Circuit Designing and Curriculum Development, and Academic Leadership from the National Institute of Technical Teachers Training and Research Kolkata, Chandigarh. With a keen interest in administrative and managerial skills, he is undergoing MBA in Project Management from Jaipur National University and has undertaken professional certification from IIM, Bangalore. He is a registered Innovation Ambassador for MIC, AICTE, facilitating and cultivating an innovative and entrepreneurial mindset among the youth. He has mentored more than 5 projects at the National level for National Innovation Contest, MIC. He has been selected among the top 5 Innovation Ambassadors (2019 - 2020) in the Eastern Region. He has also performed as an Observer of the School Innovation Ambassador training Program conducted by MIC and has been honored as an invited reviewer for the World Journal of Engineering, Emerald Publications. He has successfully published a patent at IPO. He started his professional career in 2015 as an academician, presently he is working as an Assistant Professor at Shree Ramkrishna Institute of Science & Technology, Kolkata.

Hoimanti Dutta is currently pursuing a B. Tech degree in Computer Science from Netaji Subhash Engineering College, India. She is the Secretary of the IEEE Computer Society Student Branch Chapter at Netaji Subhash Engineering College. Her current research interests are Cloud Computing, Data Mining, Machine Learning, and Li-Fi technology. She has already published two conference papers and one book chapter in Springer's publication. Most Notably, she got Best Paper Award, for the article titled "An Approach Towards Near-Field Communication (NFC) with Light Fidelity (Li-Fi)" in the International Conference on "Current Research in Engineering and Technology (ICCRET-2021)", organized by Department of Computer Science & Engineering, Brainware University, in association with Institution's Innovation Cell (IIC) and technically sponsored by CSI, BWU student Chapter during November 26 – 27, 2021.

Rajdeep Chakraborty, Ph.D., working as an assistant professor last fifteen years. He has got several publications in international journals and conferences covering SCI - indexing, Scopus indexed, IEEE, Springer, Scrivener Wiley, CRC Press, and other major indexing/publications. He has got six Indian patents published and one research copyright grant/registration. He is a guest editor & reviewer in some international and national journals. He gave several guest lectures, keynote talks, and invited talks at various academic events. He has been associated with many international conferences in the capacity of organizer, session chair, and reviewer. He is a member of IEEE and many other professional societies. He has got many awards and appreciation letters and e-contents are available on YouTube. He is now guiding two Ph.D. research scholars at MAKAUT, West Bengal, India, and also guided several UG students and PG research scholars in his teaching career so far.

Performance Analysis of $Si_{1-x}Ge_x$ Channel Based Double Gate Junctionless Transistor

[1]Achinta Baidya, [2]Rajesh Saha, [3]Amarnath Gaini, [4]Niladri Pratap Maity

[1]Department of Electronics and Communication Engineering, Mizoram University, Aizawl, India, 796004, achintabaidya@yahoo.com

[2]Department of Electronics and Communication Engineering, Malaviya National Institute of Technology Jaipur, Jaipur 302017, India, rajeshsaha93@gmail.com

[3]Department of Electronics and Communication Engineering, Marri Laxman Reddy Institute of Technology and Management, Hyderabad, India, amaranth.nits@gmail.com

[4]Department of Electronics and Communication Engineering, Mizoram University, Aizawl, India, 796004, maity_niladri@rediffmail.com

Abstract

A Silicon-Germanium channel based double gate junctionless transistor is demonstrated with 20 nm gate length. Mole fraction of germanium in SiGe channel is varied to understand the effect of germanium percentage in the device characteristics and opportunity of device performance optimization. Different characteristic like transfer characteristics, drain characteristics, transconductance, gate leakage current is evaluated for the junctionless transistor structures. Junctionless transistor with increasing germanium mole fraction demonstrated improvement in the device performance in all respect except the gate leakage current. To achieve appropriate threshold voltage the mole fraction of germanium in the SiGe can be adjusted. Performance of the $Si_{1-x}Ge_x$ channel junctionless device with gate dielectrics GeO_2 are compared for different mole fraction.

Keywords. Junctionless, mole fraction, transconductance, gate leakage current, TCAD, $Si_{1-x}Ge_x$.

1. INTRODUCTION

For decades researchers are involved in continuous improvement of semiconductor technology. In the race of down scaling of physical dimensions many critical issues are faced. These challenges need to be addressed to keep up the increment in switching speed and reduce power consumption [1-2]. Requirement of the ultra- shallow junction brings a challenge to the fabrication process [3]. In such context Junctionless transistor (JLT) was conceptualized and demonstrated by J. P. colinge et al. as a uniformly doped drain, channel and source region [4-6]. Ease of fabrication, absence of junction, and immunity to short channel effects made JLT attractive to the researchers. The Junctionless transistor conducts in accumulation mode and acts like a gated register. Study of SCEs [7-8], temperature effect [9-10], analytical modelling [11-12] of parameters for junctionless transistor was performed. Junctionless transistors have been tested for sensors and circuit applications [13-16]. Due to

developments in recent years, JLT been projected as an alternative of conventional MOSFET for future technology.

Still, some of the research has shown the inferior on-state current of junctionless transistor compare to the conventional MOSFETs [17]. Many techniques like use of high-k dielectric, multi-gate structure and gate stack are also employed to improve the on state current level of JLT. Use of group III-V compound or Ge in channel material can be an alternative to overcome the fundamental limitation of silicon technology [18-19]. But due to the lower quality of Ge epitaxy and fabrication difficulties, use of Ge channel has not become popular. Further inferior interface and unstable dielectric on the Ge epitaxy is also inherited. Due use of SiGe will be more suitable to get the advantages of high mobility and dielectric constant along with less interface trap problem of Ge. With merger of the advantages of Si and Ge, use of SiGe channel in junctionless transistor can play a big role in future technology. As SiGe properties changes with the percentage of the Ge, the requirement of study related to the mole fraction effect in junctionless characteristics is also inevitable. In this paper, performance of $Si_{1-x}Ge_x$ channel based junctionless transistor with double gate structure is studies for different mole fraction (x) of Ge.

2. DEVICE STRUCTURE AND SIMULATION ENVIRONMENT

The side view or cross-sectional view of the double gate junctionless transistor is shown in Figure 1. The terminals are named and marked in the figure. This symmetrical double gate structure is used for all the device simulations. As semiconductor wire thickness is kept low and double gate structure is used, the whole wire under gate will act like a channel. $Si_{1-x}Ge_x$ is used as a channel material and 1nm thick GeO_2 gate oxide is used in the device. The channel, source and drain regions are uniformly doped with 1.5×10^{19} atoms/cm^3. A thin gate oxide layer of 1 nm and semiconductor wire of 10 nm was considered to ensure the full depletion of the channel at the time of off condition. As the device works in accumulation mode, conduction will be done in bulk. In double gate structure entire semiconductor wire will act like a channel during its on-state. All the structural details are listed in the Table 1.

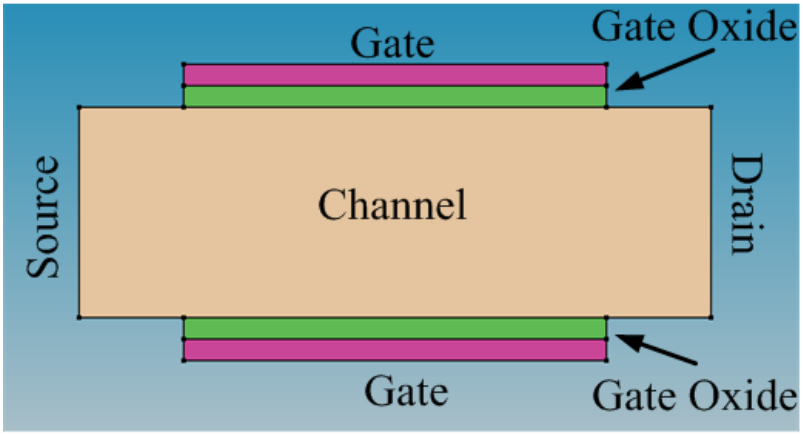

Figure 1. SiGe channel double gate junctionless transistor structure.

The thin body double gate junctionless transistors are simulated in the Synopsys Technology Computer Aided Design (TCAD). Structure editor is used to design the 3D structure. S device tool is used to simulate the structure for different condition with the help of carrier transport models, generation-recombination models, mobility models and tunnelling models. Further the results of the simulation are viewed with the help of S visual and inspect tool. Proper material parameters are also been included at the time of simulations. Work function of the gate material polysilicon (4.4eV) is specifically mentioned in the device physics section. Leakage current model also been included in the physics section of the simulator to estimate the gate leakage for the structure.

Table 1. Structural parameters of SiGe channel DGJLT

Sl. No	Parameter	Material Type	values
1	Channel length	$Si_{1-x}Ge_x$	20 nm
2	Channel Width	$Si_{1-x}Ge_x$	12 nm
3	Channel thickness	$Si_{1-x}Ge_x$	10 nm
4	Doping	Arsenic	1.5×10^{19} atoms/cm^3
5	Gate oxide Thickness	GeO_2	1 nm
6	Gate Contact	Polysilicon	4.4eV
7	Mole fraction (x)	$Si_{1-x}Ge_x$	1 to 0

3. RESULTS AND DISCUSSION

The proposed thin-body double gate structured SiGe channel junctionless transistor is simulated for gate voltage from -0.6V to 2 V. The mole fraction (x) of $Si_{1-x}Ge_x$ is changed from 0 to 1. With the change in quantity of Ge in SiGe the junctionless transistor characteristics also changes. It is observed that the DGJLT with germanium channel (x=1) shows better characteristics compare to DGJLT with Si channel (x=0). The transfer characteristics of DGJLTs are shown in Figure 2. With increment in mole fraction(x) of Ge the overall drain current increases and it also affect the threshold voltage. The threshold voltage moves towards the positive side with the increment in mole fraction of Ge. So increase in mole fraction of Ge makes the device more suitable for CMOS circuit applications.

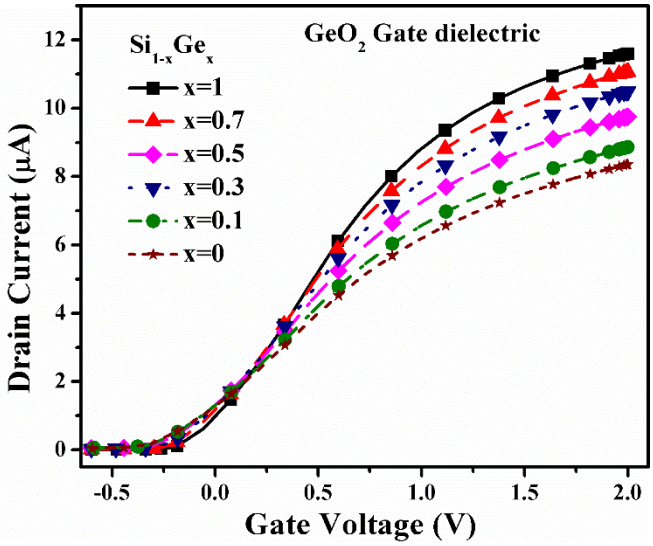

Figure 2. Transfer characteristics of $Si_{1-x}Ge_x$ channel DGJLT with GeO_2 gate oxide.

The transfer characteristics of DGJLTs in log scale are shown in Figure 3. It clearly shows the effect of mole fraction of Ge in the steepness of the curve in the subthreshold region. Degree of more steepness in the curve is better for analog and digital circuit applications. Device with higher steepness in the subthreshold region will require less gate voltage to sweep the device from off to on-state. Thus $Si_{1-x}Ge_x$ channel DGJLT with higher x value gives better subthreshold swing. Further increase in x value also shows improvement in Ion/Ioff ratio for the $Si_{1-x}Ge_x$ channel DGJLT.

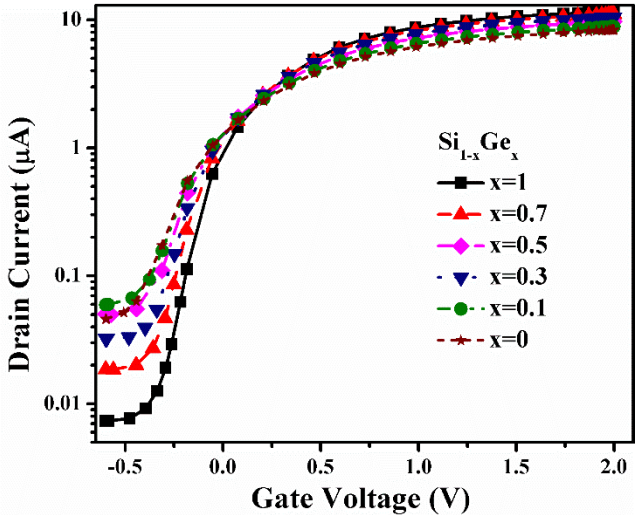

Figure 3. Steepness of transfer characteristics of $Si_{1-x}Ge_x$ channel DGJLT with GeO_2 gate oxide.

The drain characteristics of $Si_{1-x}Ge_x$ channel DGJLT with GeO_2 gate oxide is shown Figure 4. It shows that the mole fraction have effect in drain saturation current also. In saturation

region the drain current for higher x value changes less with change in drain voltage. As the results shows drain characteristics is more independent of drain voltage at the saturation, it is obvious that the $Si_{1-x}Ge_x$ channel DGJLT with higher x value will show better drain induced barrier lowering.

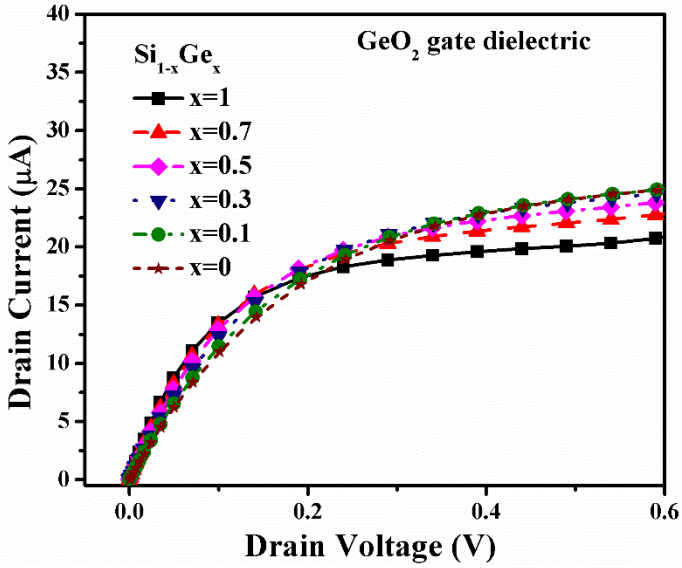

Figure 4. Drain characteristics of $Si_{1-x}Ge_x$ channel DGJLT with GeO_2 gate oxide.

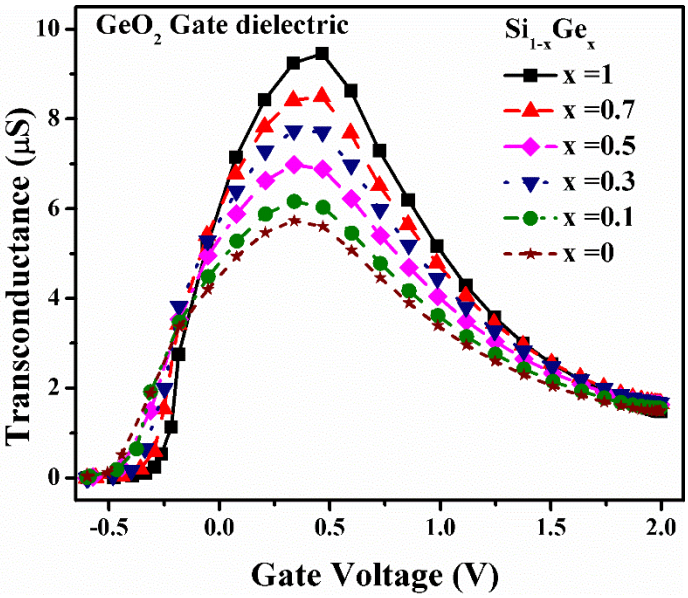

Figure 5. Transconductance of $Si_{1-x}Ge_x$ channel DGJLT with GeO_2 gate oxide.

As transconductance is a very important parameter for the device performance, it was evaluated for $Si_{1-x}Ge_x$ channel DGJLT with GeO_2 gate oxide. Figure 5 shows the transconductance of $Si_{1-x}Ge_x$ channel DGJLT as a function of gate voltage. High Ge

percentage in $Si_{1-x}Ge_x$ exhibits better transconductance. The details of the transconductance, threshold voltage, and on current are shown in Table 2. For mole fraction x=1, $Si_{1-x}Ge_x$ channel DGJLT showed maximum on current of 11.59 µA at V_{GS}= 2 V. Change in the threshold voltage of the devices with the change in germanium mole fraction shows that threshold voltage can be tailored with the help of mole fraction adjustment. Overall it helps the designer to optimize the junctionless transistor performance for future applications. Desired threshold voltage and current characteristics can be achieved with proper adjustment in mole fraction of the $Si_{1-x}Ge_x$ semiconductor material.

Table 2. Parameters of $Si_{1-x}Ge_x$ channel DGJLT with GeO_2 gate oxide.

Sl. No.	Mole fraction of $Si_{1-x}Ge_x$	Threshold Voltage, Vth (V)	Ion at V_{gs}=2V (µA)	g_m (µS)	V_{gm} (V)
1	x=1	-0.052	11.59	9.458	0.464
2	x=0.7	-0.099	11.07	8.503	0.463
3	x=0.5	-0.1293	10.49	7.743	0.336
4	x=0.3	-0.156	9.75	6.984	0.338
5	x=0.1	-0.183	8.85	6.162	0.339
6	x=0	-0.197	8.35	5.731	0.337

Figure 6 shows the gate leakage current of $Si_{1-x}Ge_x$ channel DGJLT for different mole fraction variation. With increased gate voltage gate leakage current also increases in all the junctionless devices. As germanium has lower energy bandgap compare to silicon, increasing mole fraction of Ge in $Si_{1-x}Ge_x$ channel leads to increase in gate leakage current. It is observed that the on-state gate leakage current increases in SiGe channel JLT compare to Si JLT. But the gate leakage current for all these devices are quite low with respect to the off state drain current, observed in Figure 3.

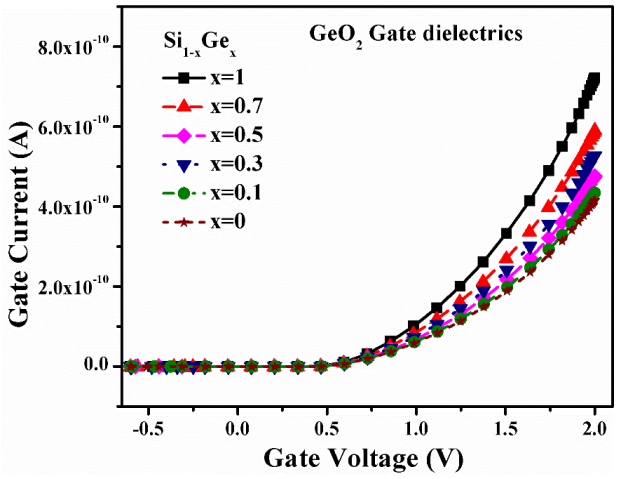

Figure 6. Gate leakage current of $Si_{1-x}Ge_x$ channel DGJLT with GeO_2 gate oxide.

4. CONCLUSION

This paper demonstrates a detailed device performance analysis of $Si_{1-x}Ge_x$ channel DGJLT with GeO_2 gate oxide. Simulation and analysis of different characteristics of the JLT with

different mole fraction of Ge were performed. $Si_{1-x}Ge_x$ channel JLT shows typical MOSFET characteristics. Change in mole fraction in $Si_{1-x}Ge_x$ has affect in all the device characteristics. Higher Ge percentage improves the threshold voltage, gives higher on-state current and transconductance. As increase in on-state gate leakage current stays under permissible limit, $Si_{1-x}Ge_x$ channel can be used in JLT with proper optimized performance to meet the future requirements of CMOS technology.

REFERENCES

[1] K. J. Kuhn, 'Moore's crystal ball: Device physics and technology past the 15 nm generation', Microelectron. Eng., vol. 88, no. 7, pp. 1044–1049, Jul., 2011.

[2] C. Hu, 'Device challenges and opportunities', in VLSI Symp. Tech. Dig., pp. 4–5, Jun., 2004.

[3] R. H. Dennard, F. H. Gaensslen, V. L. Rideout, E. Bassous, and A. R. LeBlanc, 'Design of ion-implanted MOSFET's with very small physical dimensions', IEEE J. Solid-State Circuits, vol. 9, no. 5, pp. 256–268, Oct., 1974.

[4] C. W. Lee et al., 'Junctionless multigate field-effect transistor', Appl. Phys. Lett., vol. 94, no. 5, pp. 053511–053512, Feb., 2009.

[5] J. P. Colinge et al., 'Nanowire transistors without junctions', Nat. Nanotech., vol. 5, no. 3, pp. 225–229, Feb., 2010.

[6] J. P. Colinge et al., 'Junctionless nanowire transistor (JNT): Properties and design guidelines', Solid-State Electron., vol. 65–66, pp. 33–37, Nov.–Dec., 2011.

[7] C.W. Lee, I. Ferain, A. Afzalian, et al., 'Performance estimation of junctionless multigate transistors', Solid-State Electron., vol. 54, 2010.

[8] H. Lou, et al., 'A junctionless nanowire transistor with a dual-material gate', IEEE Trans. Electron Devices, vol. 59, no. 7, July 2012.

[9] C.W. Lee, A. Borne, I. Ferain, et al., 'High-temperature performance of silicon junctionless nanowires', IEEE Trans. Electron Devices, vol. 57, no. 3, Mar. 2010.

[10] M.D. Souza, M.A. Pavanello, R.D. Trevisoli, R.T. Doria, J.P. Colinge, 'Cryogenic operation of junctionless nanowire transistors', IEEE Electron Device Lett., vol. 32, no.10, Oct., 2011.

[11] F. Jazaeri, L. Barbut, J.M. Sallese, 'Generalized charge-based model of double-gate junctionless FETs, including inversion', IEEE Transaction on Electron Devices, vol. 61, no.10, Oct., 2014.

[12] F. Jazaeri, L. Barbut, J.M. Sallese, 'Trans-capacitance modeling in junctionless gate-all-around nanowire FETs', Solid-State Electron, June 2014.

[13] Singh P, Miao J, Pott V, Park W-T, Kwong D-L 'Piezoresistive sensing performance of Junctionless nanowire FET', IEEE Electron Device Letters, vol. 33, no. 12, pp.1759–1761, Dec., 2012.

[14] Choi S-J, Moon D-I, Kim S, Ahn J-H, Lee J-S, Kim J-Y, Choi Y-K, 'Nonvolatile memory by all-around-gate Junctionless transistor composed of silicon nanowire on bulk substrate', IEEE Electron Device Letters, vol. 32, no.5, pp. 602–604, May 2011.

[15] A. Baidya, T. R. Lenka & S. Baishya, '3D Double-Gate Junctionless Nanowire Transistor-Based Pass Transistor Logic Circuits for Digital Applications', IETE Journal of Research, 2019.

[16] A. Baidya, T. R. Lenka, and S. Baishya, 'Mixed-mode simulation and analysis of 3D double gate junctionless transistor for circuit applications', Superlattices and Microstructure, vol. 100, pp. 14–23, Dec. 2016.

[17] J. Wang, G. Du, K. Wei, et al., 'Mixed-mode analysis of different mode silicon nanowire transistors-based inverter', IEEE Trans. Nanotechnol., vol. 13, no. 2, Mar., 2014.

[18] R. Yu et al., 'Device design and estimated performance for p-type junctionless transistors on bulk germanium substrates', IEEE Trans. Electron Devices, vol. 59, no. 9, pp. 2308–2313, Sep. 2012.

[19] M. F. M. Rasol, F. K. A. Hamid, Z. Johari, R. Arsat and M. F. M. Yusoff, 'Performance Analysis of Silicon and III-V Channel Material for Junctionless-Gate-All-Around Field Effect Transistor', 2020 IEEE Student Conference on Research and Development (SCOReD), pp. 1-5, 2020.

Biographies

Achinta Baidya received his B.Tech. in Electronics and Communication Engg. from Guru Nanak Institute Of Technology, India, in 2009. M.Tech in Microelectronics and VLSI Design form NIT Silchar, India, in 2011 and the PhD from National Institute of Technology, Silchar. He is currently working as an Assistant Professor at the department of Electronics and Communication Engineering, Mizoram University, Aizawl, India. His research areas include microelectronics, VLSI, high speed solid state devices. He has been serving as a reviewer for many highly-respected journals.

Rajesh Saha has received B.E. with honours in Electronics and Telecommunication Engineering from Assam Engineering College, Guwahati, Assam in 2012. M.Tech in Microelectronics and VLSI Design form NIT Arunachal Pradesh, India, in 2014 and the PhD from National Institute of Technology, Silchar in 2018. He is currently working as an Assistant Professor at the department of Electronics and Communication Engineering, Malaviya National Institute of Technology Jaipur, India. He has worked as Junior Research Fellow in IIT Guwahati, Assam from September 2012 to April 2013

Amarnath Gaini received his B.Tech. in Electronics and Communication Engg.. M.Tech in VLSI System Design and the PhD from National Institute of Technology, Silchar. He is currently working as an Assistant Professor at the department of Electronics and Communication Engineering, Marri Laxman Reddy Institute of Technology and Management.

Niladri Pratap Maity received M.Tech in Electronics Design & Technology form Tezpur University and the PhD from National Institute of Technology, Silchar. He is currently working as a professor at the department of Electronics and Communication Engineering, Mizoram University, Aizawl, India. His research areas include microelectronics, VLSI, high-speed solid-state devices. Published more than hundred sixty research papers in International and National Journals/Conferences of repute. He has been serving as a reviewer for many highly-respected journals.

Uber for Ambulances, Emergency Health Response, and Blood Inventory

[1]Vipul Patil, [2]Ayush Kadam, [3]Kushal Khadtare, [4]Vijayalaxmi Kadroli

Terna Engineering College, TEC, Universityof Mumbai, Mumbai, India

[1] vipulpatil1999@gmail.com, [2] kadamayush35@gmail.com,

[3] kushal.khadtare25@gmail.com, [4] vijayalaxmikadroli@ternaengg.ac.in

Abstract

In today's society having an effective and efficient healthcare service is of at most importance. Ambulances are important part of medical services. Ambulance helps patience's reach hospitals and avail medical services faster but due to the shortage of ambulances, its becomes difficult for the patients to reach the hospital, so a small step has been taken towards filling this gap by developing an application that would enable the user to book an ambulance to reach the hospital quickly. The user can upload their current location and destination through the map in the application. The application would then show the available ambulances near the patient's location and the user can choose the appropriate ambulance. Once a particular ambulance is booked by the user the ambulance driver would receive a message. Once the booking is confirmed by the ambulance driver, they will be provided the location of the user.

Keywords. Ambulance, Health, Blood Inventory, Patient.

1. INTRODUCTION

In today's society having an effective and efficient healthcare service is of at most importance. The ambulance has proved to be very helpful as it helps the patient to reach the hospital faster. Italso to helps avail the medical services quickly, but due to the shortage of ambulances, it becomes difficult for the patients to reach the hospital. Existing System - Effective Ambulance Service Advantages - Helps the ambulance driver find the patient's location.Disadvantages - Less feature available. A small step has been taken towards filling this gap by developing an application that would enable a person to book an ambulance for a patient so that they reach the hospital faster. The patient can upload their current location and destination through the map in the application. The application would then show the available ambulances nearthe patient's location and the user can choose the appropriate rides.

Functional Requirements

- Administrator should have access to all details of Users, Ambulances, and ` hospitals.
- End devices must be in network to get details.

- No user could access any details without being a register.

2. LITERATURE SURVEY

A survey done on the various Users and taking their Opinions on the Online Cab Services on the two of the most popular cab rental applications Ola and Uber and the data collected from their customers is presented in [1]. The data is collected from professionals in this field. It is found that customers favor Uber over Olawhen it comes to billing. Whereas when safety is the concern ola is preferred more than uber [2]. A general thesis on the ambulance Service has developed a way for saving lives more efficiently. With the help of this application, the ambulance can reach the patient quickly,the user's location is traced or delivered by the application. This can also accommodate important equipment and services that will ensure the well-being of thepatient [3] It can be done by collecting the surveillance of the streets in real-time by using IGA. Ambulances interact with each other using IGA. Ambulance gets information on othercars with the help of IGA [4]. Global positioning system GPS Based Shortest Path for Ambulances makes sense of GPSas a lattice of the shuttle, that sends case. Data about the fluctuating area of the gadget to andfrom the satellite the back to the planet. GPS handsets, for example, exploring objects are used to gauge the area, speed, and length at the position of the transporter [5]. Location-based push service with clustering method. It is a position-based push administration structure. This applies the grouping technique works on the transmission intricacy of crisis information with the assistance of Push and Pull LBS. Traditionally, where crisis reactions were finished physically with call focuses, dormancy inside reaction was upward keeping human existence in question. Later all manual reactions framework was supplanted with a computerized framework with calculations on independent gadgets either in rescue vehicle or handsets. Crisis Medical System Services is a calculation that diminishes the delay to dispatch emergency vehicle administrations within 10 to 15 minutes in urban communities and 20 to 30 minutes in local regions. EMSSguarantees clear data from the patient, whether it be the area, infection, or charging. Consequently, with EMSS the patient can get early development care [6]. RIS for Ambulance Services given GPS and GIS innovation gives a Route Construction Algorithm. The rescue vehicle appraises the street information gathered by IGA and characterizes the briefest way by RCA. RCA utilizes the Dijkstra technique where an intersection implies one vertex, a road inside a junction implies an edge, a way involves the heading, an unremarkable passageway of each intersection turns into the force of the edge,and a guide is a marked outline. For intersections where there is traffic and vehicle are amazed, information isn't gathered, henceforth further boundaries are not identified. Subsequently, street information was dissected before traffic is finished and shippedoff to the rescue vehicle. On the off chance that the current way needs a more drawn-out length than the new course, the rescue vehicle assesses the new course.[7] It is an application made by the Delhi police. Client requirements to enlist at the Delhi Police site. After fruitful enlistment, the client gets an enrollment key (OTP) which should be placed to finish the application design. When the client of the Himmat application raises the SOS alert fromthe Himmat App, the area data and sound video is sent to the Delhi Police control room. DelhiPolice can then quickly send the closest Police help to the person in question [8]. It is an application that is made by the Mumbai police which gives fundamental tips onprivate security and digital dangers and the utilization GPS for finding an individual in trouble. Some of the related systems are presented in Table 1, along with

their limitations.

Table 1. Summary of Related Systems

Work	Method	Features	Limitations
Collection Of Data From Uber And OlaConsumers [1]	Data collection	Determine which cab rental is preferred bycustomers	Low availability in Rural areas. High charges in peak hours
Effective Ambulance Service [2]	Location detection	Helps the ambulance driver findthe patient's location.	Less features available.
Dynamic Routing For Emergency Vehicle [3]	Dynamic Routing	The cars in the ambulancepath get notified about the ambulance behind them.	The notification can be distracting and dangerous for the driver especially if they are on a busy road

3. PROPOSED SYSTEM

In the proposed system, Administrator will be provided with the Web application for managing users, maintaining their details. Also admin can add the ambulance and manage their details, and can track the ambulances as shown in Figure 1.

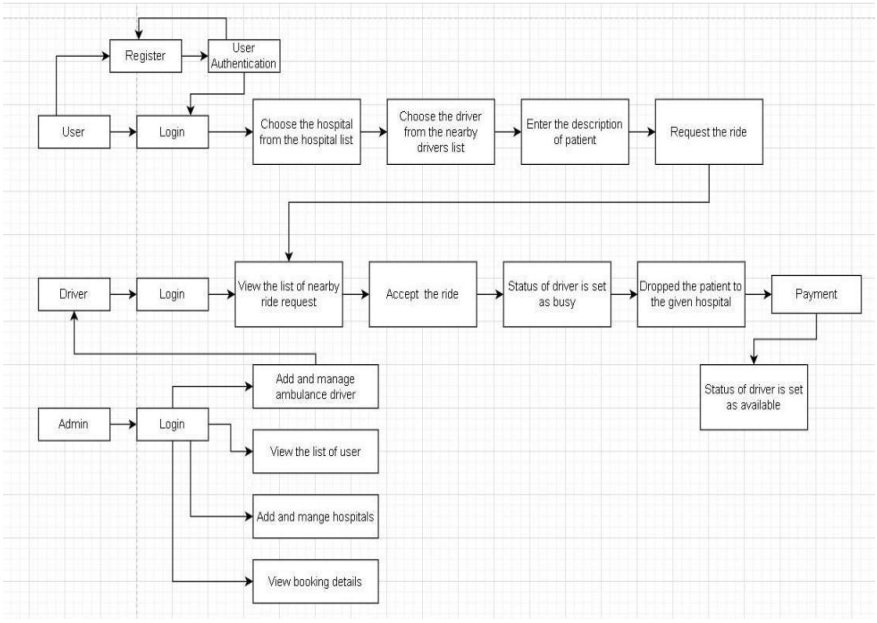

Figure 1. System Architecture

The proposed system is divided into two parts. First is the user's side which is basically a smart phone owned by the person/user. Internet connection is required by the user to request for an ambulance. Thus, it is essential for the user to have telephone and internet services enabled for the system to function. The second is the ambulance side. The ambulance ride

is an android application used by the driver. It uses internet and maps. Google Maps will be used to locate the user. When the request for an ambulance made by the user, the request will be sent to the server first. The server then will look for available ambulances around the user's location. Then a request is sent to the nearest available ambulance. Once the request is accepted the driver is provided with the person's location, name and phone number At the same time user will be able to see the driver's location. If the driver rejects the request, the server will look for another nearby ambulance and the request is sent.

4. RESULTS

Various results obtained during the development of the prototype are presented in this section. The initial screen and the user authentication process in the proposed framework is presented in Figure 2, where if a user can register as a new member and then can successfully use the application.

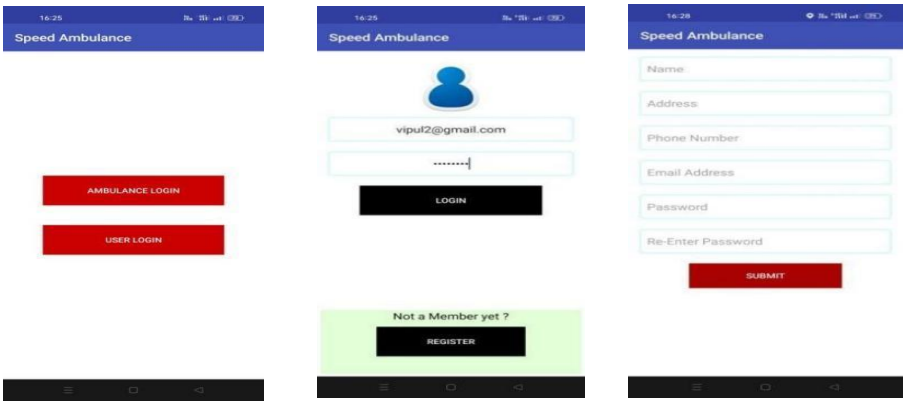

Figure 2. Home page and User Authentication in Proposed System

Furthermore, the list of hospitals will be populated in the application ad the user can select a hospital from the list, which will then ask for the confirmation from the user to book an ambulance and to add the details of the medical emergency as presented in Figure 3.

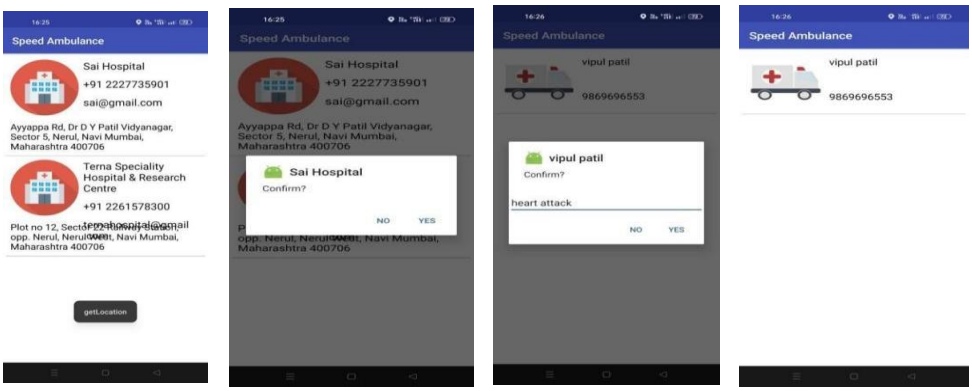

Figure 3. Display of Hospitals List and Ambulance Booking Process

The user can track the ambulance through the application and can pay the bill as presented in Figure 4.

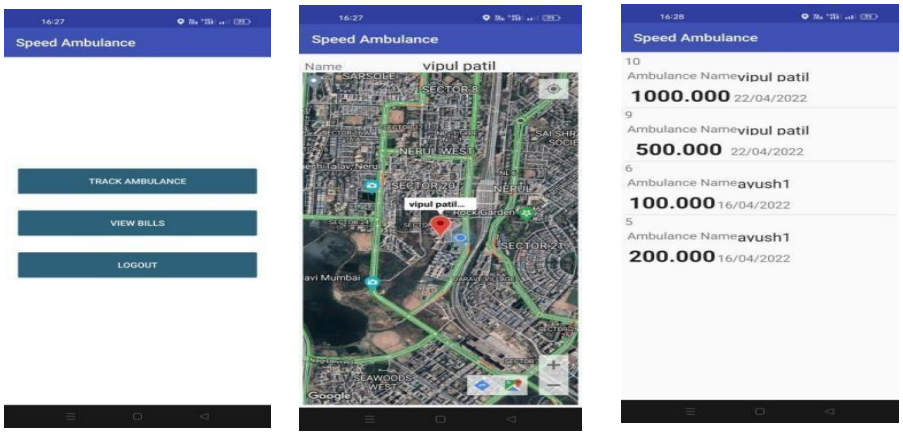

Figure 4. Ambulance Tracking and Bill Payment through App

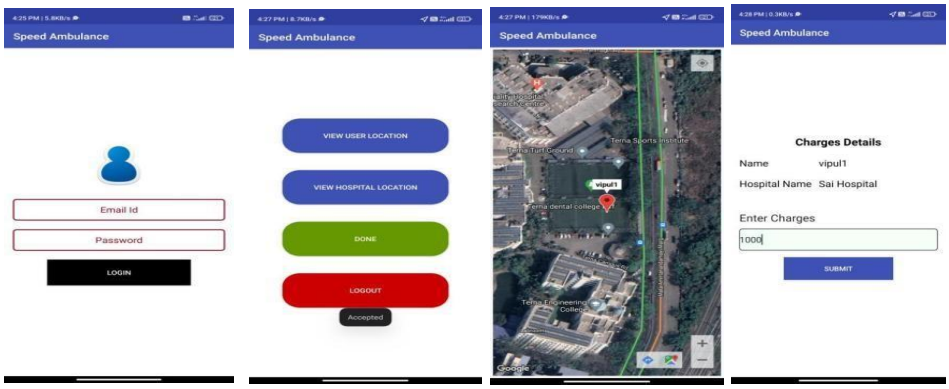

Figure 5. Driver side interface and booking related information

The driver side interface of the proposed application is presented in Figure 5, where the driver can log in to the interface and can see the user's details to check the destination.

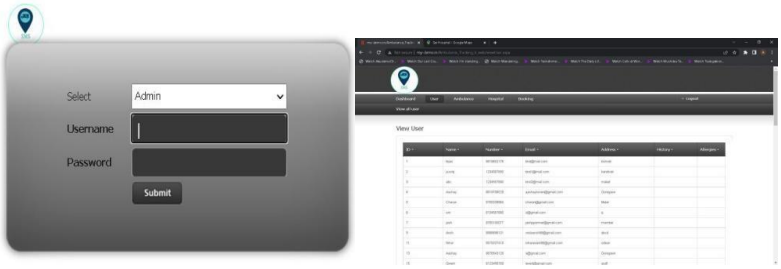

Figure 5. Admin side interface for Admin login and user details

The admin side interface of the proposed application will be able to check the existing ambulances and to add the new ambulance through the portal as shown in Figure 6. Existing hospitals and the addition of new hospital can also be done at the admin side as presented in Figure 7. Furthermore, all the booking details and the location of the user will also be available at the admin side as shown in Figure 8.

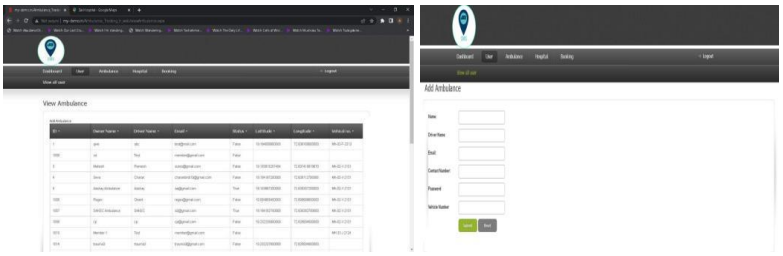

Figure 6. Admin side interface with ambulance details and addition of new ambulance

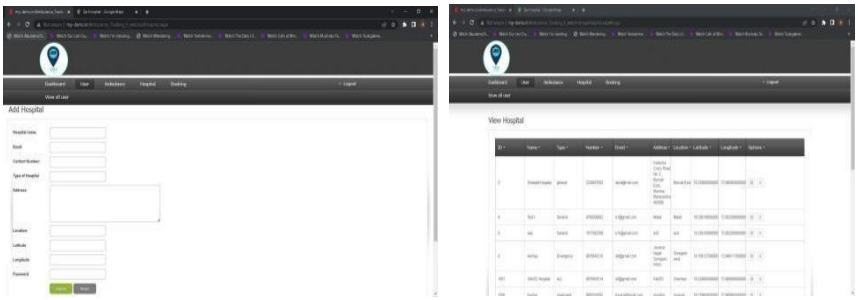

Figure 7. Hospital addition and checking at Admin Login

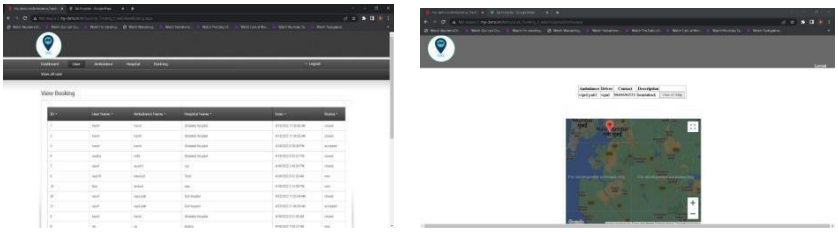

Figure 8. User Booking Details and Location Checking at Admin Side

5. CONCLUSION

This proposed project can provide a safe, secure and efficient way of ambulance tracking for users. An approach will be made towards rescuing a patients life quickly. Final demo will be an app similar to that of an online taxi service provider app , but the services we will be providing will be different , as mentioned above . We will try to incorporate all the mentioned features with proper designing making it very much user friendly and easy to use. The overhead of calling is eliminated. Even if the route is not known to the driver, still he can reach the patients location.

REFERENCES

[1] Dr. S. M. Yamuna, “A Progressive Study on Users Perception and Satisfaction towards Online Cab Service with Reference to Coimbatore,” International Journal for Research in Applied Science and Engineering Technology, vol. 7, no. 4, pp. 1561–1570, Apr. 2019, doi: 10.22214/ijraset.2019.4283.

[2] I.K. Adusei, K. Kyamakya and F. Erbas, "Location-based services: advances and challenges," *Canadian Conference on Electrical and Computer Engineering 2004 (IEEE Cat. No.04CH37513)*, 2004, pp. 1-7 Vol.1, doi: 10.1109/CCECE.2004.1344944.

[3] R. Katsuma and S. Yoshida, “Dynamic Routing for Emergency Vehicle by Collecting Real-Time Road Conditions,” International Journal of Communications, Network and System Sciences, vol. 11, no. 02, pp. 27–44, 2018, doi: 10.4236/ijcns.2018.112003.

[4] A.Blome, J. Rosenbaum, N. Lucas, and K. Schreyer, “Ridesharing as an Alternative to Ambulance Transport for Voluntary Psychiatric Patients in the Emergency Department,” WestJEM 21.3 May Issue, vol. 21, no. 3, Apr. 2020, doi: 10.5811/westjem.2020.2.45526.

[5] L. Samuel. For a trip to the ER, some are opting for Uber over an ambulance. https://www.statnews.com/2017/04/05/uber-lyft-emergency-room-ride/ (04.05.2021).

[6] M. Kekatos Rise in passengers using Uber over ambulance to go to the hospital. http://www.dailymail.co.uk/~/article-4383990/index.html (04.05.2021).

[7] P. Kumar, L. Priya, A. Sathya. Smart Traffic Light System for Emergency Ambulance Using IoT. Annals of the Romanian Society for Cell Biology, 8655–8662, 2021. Retrieved from http://annalsofrscb.ro/index.php/journal/article/view/2410

[8] S. Magar, V. Jadhav, O. Raut, Ambuitec: Ambulance Booking Application for Emergency Health Response, Blood Inventory. Test Engineering and Management. 83. 12068-12075, 2020

[9] M. Eshtayah, J. Morrar, A. Baghdadi, and A. Hawash, “Reducing Ambulances Arrival Time to Patients,” 2019 2nd International Conference on new Trends in Computing Sciences (ICTCS), Oct. 2019, doi: 10.1109/ictcs.2019.8923066.

[10] B. Isong, N. Dladlu, and T. Magogodi, “Mobile-Based Medical Emergency Ambulance Scheduling System,” International Journal of Computer Network and Information Security, vol. 8, no. 11, pp. 14–22, Nov. 2016, doi: 10.5815/ijcnis.2016.11.02.

[11] B. Almadani, M. Bin-Yahya, and E. M. Shakshuki, “E-AMBULANCE: Real-Time Integration Platform for Heterogeneous Medical Telemetry System,” Procedia Computer Science, vol. 63, pp. 400–407, 2015, doi: 10.1016/j.procs.2015.08.359.

[12] Peng Zhou, T. Nadeem, Porlin Kang, C. Borcea, and L. Iftode, “EZCab: A Cab Booking Application Using Short-Range Wireless Communication,” Third IEEE International Conference on Pervasive Computing and Communications, doi: 10.1109/percom.2005.21.

[13] V. Goud, V. Padmaja, "Vehicle Accident Automatic Detection and Remote Alarm Device ", International Journal of Reconfigurable and Embedded Systems, Vol. 1, No. 2, July 2012, pages 2089-4864.

[14] S. Singh Patwal, R. Kumar, R. Mishra, " Smart Band Ambulance System", International Journal of Advanced Research in Computer Engineering and Technology, Vol-06, Issue-05, May 2017, pages 2278 -1323

[15] V. Rajesh Kumar & P. Benedict.P. Development of Route Information System for Ambulance Services using GPS and GIS. International Journal of Geomatics and Geosciences, ISSN 0976-4380. 2. 147- 156, 2011.

[16] B. Smitha Shekar, G. Narendra Kumar, H.V. Usha Rani, C.K. Divyashree, G. George and A. Murali, "GPS Based Shortest Path for Ambulances using VANETs," International Conference on Wireless Networks (ICWN2012) IPCSIT vol.4910.7763/I PCSIT, 2012

Biographies

Vipul Patil is a final year student of Terna Engineering College pursuing bachelor'sdegree in information technology. His research area includes interactive systems and Back end development.

Ayush Kadam is a final year student of Terna Engineering College pursuing bachelor's degree in information technology. His research area includes interactivesystems and Front end development.

Kushal Khadtare is a final year student of Terna Engineering College pursuing bachelor's degree in information technology. Her research area includes Back enddevelopment.

Dr. Vijayalaxmi K is currently Associate Professor at Terna Engg College in InformationTechnology.She completed Ph.D in Computer and Information Science at Poojya Doddappa Appa (PDA) colleg, VTU, an autonomous institute affiliated to Visvesvaraya Technological University (VTU) , Belagavi, Karnataka, Indian. She has obtained M.Tech in Computer Science and engineering in 2004 from PDA college of Engineering from VTU. she has published many papers in international conferences and journals. Her main research areas are in Wireless sensor network, Artificial Intelligence, Soft computing.

Blockchain Based Remote Patient Monitoring system for Healthcare Data Security

Vishal Sharma, Anand Sharma

Mody University of Science and Technology, Lakshmangarh, Sikar, Rajasthan, India
er.vishu1983@gmail.com; anand_glee@yahoo.co.in

Abstract

In the field of digital health system, Remote Patient Monitoring (RPM) is strengthens the online healthcare services and it permits to deliver the healthcare services to patient remotely doctors can get real-time health updates of their patients. Presently, RPM is widely used in smart healthcare system to remotely monitor the vital signs of patients. Remote patient monitoring (RPM) have also become more popular and demanded than ever in the critical situation of COVID-19 pandemic. RPM is one of the considerable fields that widely use IoT infrastructures. In this system various body sensors and wearable devices collects the vital signs of patients and the actuator processes and analysed them and sends them to the central storage such as the cloud. Aforesaid centralization and unsecure transmission of heath information can be challenging, as it can be a single point of failure, manipulation of data and tampering with information, and leak of privacy. Blockchain can be a potential solution to solve these problems due to its distributed and tamper proof structure. However, due to the expansive mathematical calculations in the blockchain technology it comprises the overhead of high bandwidth and delay; it may not fit perfectly into the energy efficient and time critical RPM system. In this paper we have proposed a design for integration of modified blockchain approach and RPM systems to obliterate the overhead of the conventional blockchain technology and its benefits for security and privacy preservation of patient's critical healthcare data. The amalgamation of these two approaches will be highly favourable not only for the patient but also for the doctors and other healthcare providers.

Keywords. IoT, Blockchain, RPM, Healthcare System, Privacy, Security.

1. INTRODUCTION

The report from the Ministry of Home Affairs, Government of India showed that 68.84% of the population are staying in rural areas [1]. The doctor and patient ratio is very low in these areas. The non-availability of doctor's services in these areas is also a big problem in the crucial time of COVID-19 Pandemic. RPM can become an effective solution to overcome these barriers of healthcare services. Through the RPM system, doctors can monitor the patient's health condition from anywhere at any time. In the era of digital health system RPM is a field in which key architecture is IoT. An Internet of Things network is a network of many physical objects; even human beings behave like a thing in it which can communicate with each other. All these things which are available in this network are embedded with different types of sensors and software. All these things and devices are in this network; they can communicate and collect data among themselves without any human intervention, as shown in Figure 1. These sensors might be a moisture sensors, pressure sensors, light

sensors, motion sensors and temperature sensor etc. The concept of "Internet of Things" was first introduced by Kevin Ashton in his presentation, which he presented in P&G (Proctor & Gamble) in 1999 [2].

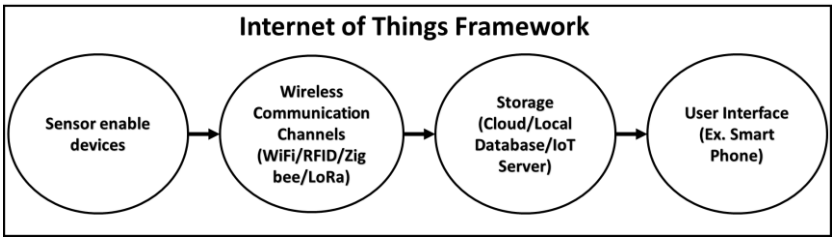

Figure 1: Structure of IoT framework

As shown in Figure 2, the architecture of an IoT network is divided into three tiers, i.e. Cloud layer, Gateway or Fog layer and Sensor layer. Subsequent, we briefly discussed each and every layer [3].

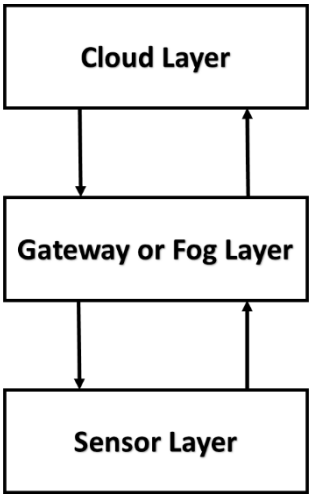

Figure 2: Layered architecture of IoT

- **Cloud Layer:** This is the uppermost layer of the IoT layered architecture. To provide the needed data information and required services to meet the necessary requirement of the user is the principal responsibility of this layer. Data information storage, different types of services and backup are also offered by this layer. This layer also provides different analysis services to estimate the future state of the devices [4].
- **Gateway or Fog Layer**: This is the middle layer of IoT layered architecture. By interconnecting many different physical infrastructure network and network devices (Bluetooth, RFID, Zigbee, Wi-Fi, etc.), this layer provides an integrated and heterogeneous network. This layer works to route and transmit the collected

data from the sensor layer through a secure channel to central control or cloud storage. This layer also provides the services like processing of data, computation and decision making. Gateways, hubs, switches, cloud etc. networking devices are parts of this layer [5].

- **Sensor Layer**: This layer is the lowermost layer of this architecture and it is liable for interacting with a number of actuator, different types of sensors, RFID enabled devices and other physical devices. Therefore this layer is also known as sensor layer. The main responsibility of this layer are sensing of data, measuring of sensed data and also data processing sometimes. This layer is responsible for connecting all the things to the Internet [6].

Remote Patient Monitoring system integrated with body sensor or wearable devices to collect the vital signs of patients and store these health data on the central storage such as cloud and also send the health alert in the suspicious situations. In addition to the vital signs, other information such as demographic data, geographic location of the patient can also be there. The top most priority of any RPM system is the security and privacy preservation of patient health data. Privacy of patient's health data also includes the capacity to have control over data and determine access levels to be granted to others. Blockchain technology can prove to be a revolution for the security and privacy of patient health data in RPM systems. Since Blockchain possesses the advantages of distributed, tamper proof and access control architecture [7].

This paper proposed an integrated architecture of RPM and Blockchain for securing and preserve the privacy of critical healthcare data. This proposed design contain three layers architecture: Sensor layer, Blockchain layer and cloud layer. Rest of the paper includes the general architecture and challenges of general RPM architecture, outlines the existing literature related to the use of blockchain in the digital healthcare field, Blockchain and its integration with RPM system architecture, Presents the detail about our proposed framework and finally concludes the paper and sets a road map for future research [8].

2. RELATED WORKS

Remote patient monitoring system is a demanding field of healthcare system that contains sensors for collecting biomedical data of the patients and by which healthcare professionals can remotely monitor the patient's vital signs outside the traditional healthcare locations such as the healthcare places viz. hospital, clinic etc. Consequently, when storing, sharing, and retrieving these remotely collected healthcare data, it might be possible to tamper with these critical data.

Alexandru Archip et al. in [8] have developed a prototype using mobile sensors and gateway. The functionality of this system can be accessed by RESTful API on any mobile device of the physician. They have analyzed their work based on power consumption test and feasibility test and they found system performed well in both the result.

Rui Guo et al. inm [9] have proposed a blockchain based on demand access policy changed ABE model for maintaining the integrity and privacy of patient's sensitive data in smart healthcare system. They have also proved prevention of collusion attack. They have proved their work by analyzed the security and performance comparison with other related works in different phases.

Sandi Rahmadika et al. in [10] have proposed a model for storing the patient health data on to the blockchain which are coming from various sources. They have also analyzed their work against various attacks.
Md Ashraf Uddin et al. in [11] have proposed a two tier based model based on many layers of interfacing for storing the required and non-required data. They have discussed the optimized and secure communication between various layers. They have also analyzed their work for energy consumption; delay in data processing and against various types of attacks.
Kristen N. Griggs et al. in [12] have proposed a model for storing the all events on the blockchain using smart contract. They have also analyzed their work against various security aspects and compared their work with traditional system.
Aiqing Zhang et al. in [13] have proposed a model for sharing patient's data using the combination of private and consortium blockchain architecture using public key encryption with keyword search. They have evaluated the performance of their work on JUICE platform.
Md Ashraf Uddin et al. in [14] have proposed a three level patient centric model for storing patient health data on the blockchain implemented at Fog and Cloud level. They have also proposed a modified PoS consensus mechanism. They have analyzed the energy consumption in block generation.
Gautam Srivastava et al. in [15] have proposed a blockchain integrated network with various lightweight cryptographic services like ARX and ring signature to enhance security and privacy and smart contract for IoT enabled healthcare network security.
Bashayer Al-Ahmadi et al. in [16] have proposed a three layers blockchain enabled model for storing the patient's health data.
Jigna Hathaliya et al. in [17] have proposed a blockchain and machine learning integrated RPM model for classify the patient according to symptoms of health data.
Lei Hang et al. in [18] have proposed a permissioned smart contract enabled blockchain and IoT integration model for securing sensing healthcare data integrity using web interface. They have analyzed their work by various performance analysis analysis.
Muhammad Salek Ali et al. in [19] have proposed a combination of on-chain and off-chain system model for record keeping and securely transfer the health data between patient and healthcare provider respectively. Their proposed model preserve the privacy of health data and anonymously and securely transfer the data using Tor network. They have used Ethereum's Rinkeby testnet for analysis of their framework.
Partha Pratim Ray et al. in [20] have proposed a blockchain enabled IoT based healthcare model for storing the healthcare data on chain. They have compared various blockchain platform and consensus algorithm those are suitable for IoT based healthcare system.
Hoe Tung Yew et al. in [21] have proposed a model for real time sensed health data sending via MQTT broker on the database in both public and private network from where healthcare provider can view the real-time data via Android mobile application (App).
Lei Ru et al. in [22] have proposed a model which builds around the six different modules as a data gathering module, a data receiving module, a data transmission module, a data processing module, and a display and alarm module for a health monitoring project. They have analyzed their work by observing the pulse readings, body temperature readings, ECG readings, and physiological data gathering
M. Dhinakaran et al. in [23] have proposed a machine learning enabled IoT based health monitoring system.

Bessem Zaabar et al. in [24] have proposed a three layer blockchain enabled IoT based model for storing and communicating the patient's private data between patient and healthcare providers and RESTful API is used for the creation of web services.

3. REMOTE PATIENT MONITORING (RPM) ARCHITECTURE

In-home monitoring or remote patient monitoring is a type of system such that by which healthcare professional can track the real-time healthcare data of patient remotely and use it in various treatment plans. Remote Patient Monitoring (RPM) is one of the areas where IoT technology is being used. It is a fundamental component of the e-health domain. It can become an alternative to hospital visits, increasing the number of people monitored without increasing workloads for healthcare providers [9]. RPM focuses on rural area's patients, patients of chronic diseases, post-operative patients, senior citizen patients, and where healthcare facilities are limited. RPM devices capture a masses of health data, from heart rate to blood pressure, without any surveillance by any healthcare provider. They can be either sensors enabled user-friendly wearable or implanted devices in a body or stationary devices having physical location and transmission of these health readings for further diagnosis and treatment [10].

Figure 3: General RPM Architecture

Thus, a remote patient monitoring system may comprise the following components as shown in Figure 3:

- **Health Data acquisition:** This module is responsible for acquiring health data (Such as Blood Pressure, Temperature, ECG.etc) through the various sensors or sensor embedded wearable devices and then sending of these collected data to central storage for further analysis through a smart device [10].
- **IoT Gateway:** IoT Gateway is responsible for connecting smart devices to the cloud either physically or virtually. Though, IoT gateway provides preprocessing, normalization of data and the connectivity of network. It translates the diversified data set which is obtained from various sensors in a common format by data normalization [11].
- **Cloud repository:** The storage of massive and ever changing health data array and retrieval servers is an important module of these systems. It also plays a very important role for the identification and testing of abnormal healthcare data. It also aggregate and analyzed crucial health data from various sources and process it to

gain a real-time view of health state, as well as promptly alert the doctors and patients about potential issues [12].

4. ISSUES OF RPM

4.1. Security and Privacy

A lot of data is stored on the central cloud where it is handled by third parties, due to this there is a full risk of data stolen. The Integrating a third-party system that can be hacked puts patients' privacy and security at risk as a result. Subsequently RPM systems have to be ensured proper security and privacy of stored and processed sensitive and private data like electronic health records, various diagnostic results, etc. There are some risks related to track the location of a patients and use their private data to harm the patient. There is no such provision that the healthcare provider should take the consent for data collection and to review and access their private information. And no any explicit consideration are there for what information will be shared; with whom; and for how long time. There is also no transparency about how privacy and security will be managed. Although there are no universally agreed standards for health the privacy and confidentiality of data, still it is essential to achieve compliance with all the necessary standards, such as HIPAA and HITECH in the USA, as well as GDPR in the Europe [13].

4.2. Integrity

In RPM systems, a lot of data is transferred from sensor devices and wearables across the cloud and from the cloud to the healthcare provider. Any intruder can integrate the data, and the data that has been integrated can put the patient's life at risk. And also the healthcare data of the patient aggregated from various sources can be obtained in several formats, including unstructured or semi-structured data formats. Apart from this, there are many vendors who do not use the same data format for sensor and wearable devices [14].

4.3. Real-time Access to Data

Timely transfer of health data information in RPM system is a long and tedious process as it involves multiple transfers. Healthcare data of the patient is collected and uploaded from various sensors and wearable devices. Now if this device is on the mobile network, then this data reaches the healthcare provider through many networks and RPM network. If there is an interrupt or outage at any of these hops, then the data sending will either fail or it will reach late to the healthcare providers. Because there is no guarantee that the mobile network will always be available. Because due to this the question of patient's life and death remains, so it is very important for the data to reach reliably and timely [21].

4.4. Accuracy of Data

The data quality is also matter in the case of RPM system. The results of the diagnostic practitioner always depend on the accuracy of the data, Even if the system, the sensors, and the network are running fine, the reached data must be accurate [22].

4.5. Storing and processing massive arrays of data

A very large amount of data is generated from the RPM system. So it takes a lot of time to process, analyze and respond [23].

4.6. Scalability and high availability

Scalability also a big issue in the RPM system. If the system is not scalable, then it will take a lot of time for the patient's information to be processed and response, due to which the life of the patient can also be at stake [24].

5. BLOCKCHAIN ARCHITECTURE

An anonymous researcher Satoshi Nakamoto first time presented that concept in a white paper in 2009 [25]. The blockchain concept is built on the linked list premise. So similarly there is a series of blocks in a blockchain, all these blocks are linked to their previous block with a unique numerical value. Each and every block in this contain hash value, set of transactions, timestamp and one time varying value, nonce. In this, each block keeps the hash value of its previous block, resulting in a chain of cryptographically secure blocks. This concept was raised for bitcoin, a digital currency. Blockchain technology was introduced so as to eliminate the need for a central authority and trust can be developed for the transaction between two entities without the involvement of any third party. So, thus, the blockchain is a trusted, distributed and decentralized digital ledger. In a point-to-point network, this technology operates, and each and this network's blocks are all tamper-proof and unchangeable. Blockchain technology plays an important role in securing various applications because of its properties (tamperproof, Immutability, cryptographically secure etc.) [26]. Figure 4 shows the working of the blockchain network. The first block in this network is called the generic block and rest of the blocks are called miner or validator blocks. Miner peers add newly constructed blocks to this chain of blocks, for this they solve a complex mathematical puzzle and whoever miner solves the puzzle named as proof of work called consensus algorithm, he adds the new block to the previous chain. As a result, over the untrusted participants, all of the participating nodes can establish a trusted network. [27].

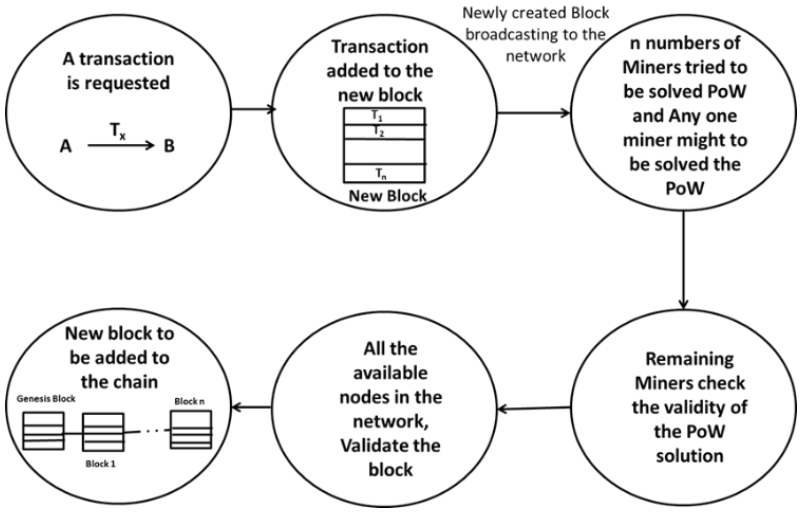

Figure 4: Working architecture of Blockchain

5.1. Blockchain's Types

Blockchain can be categorized into following three types based on peer's permissions:

1. **Public (Permissionless) Blockchain:** This is a category of blockchain which is also called permissionless blockchain because anyone can join it whenever they want. In this, any participant can see the ledger and can take part in the consensus process. [26]. Example; Bitcoin, Ethereum.
2. **Private (Permissioned) Blockchain:** This category of blockchain is also called permissioned Blockchain. Any participant who wants to join in this has to take permission. In this there is a limited decentralized system. In which only a single organization can access and control the system [26]. Example; Hyperledger.
3. **Consortium blockchain:** this is a type of semi-private blockchain network. In this, several organizations work together to run the platform. [26]. Example; Corda, Quorum and Hyperledger.

5.2. Components of Blockchain

- **Consensus mechanisms:** Consensus Mechanism in Blockchain is a procedure by which at least 51% peers to validate the global state of the distributed ledger by achieving a single data value agreement. In this way double spending attack can be prevented. In this way trust can be developed among unknown peers in a distributed environment through consensus mechanism. [27].
- **Smart Contract:** In blockchain network smart contract works as a self-executing program that automatically executes business logics set by peers in a distributed ledger. It is an interface to interact with the data in the blockchain. It is available for each of the participating peers in the network [3]. Smart contracts are added to each block of the blockchain. [12]. If any of the transactions make changes in it, then that too gets updated in the ledger like the transaction. Therefore, like transactions, smart contracts are also immutable. [27].

6. PROBLEM STATEMENT

A lot of data is generated day by day in RPM system. Storage of this big data is also a big problem, because complete health data is not important but it is useful for medical research. When the data collected by the sensor is sent to the gateway and cloud, then that data can also be tampered by the attacker. Adequate medical facilities do not reach the patients living in remote areas and rural areas. That's why we need such an approach so that the healthcare provider can take care of the patient from afar without being physically present and simultaneously, the problem of storage of large volume data and the problem of privacy and security of data should also be solved. On the basis of studied some existing applications and architectures in healthcare systems, we found some research finding as specified below in the existing systems that encourage us to work in the integration of blockchain and RPM in the digital medical system.

- No efficient and effective light weight cryptographic algorithm has been used in the Resource Constrained RPM system.
- A scalable and less computational power blockchain framework is needed that can integrate with energy efficient RPM applications in an efficient manner.

- Better security is required between every hop from the patient's healthcare data gathering to the data reaching the healthcare provider.
- There is a need for a smart contract based healthcare system that maintains critical healthcare data privacy and also verify the identity of the user..
- An efficient mechanism is required which can efficiently collect real time accurate data without any delay.

7. PROPOSED REMOTE PATIENT MONITORING (RPM) HEALTHCARE SYSTEM FRAMEWORK

Amalgamation of blockchain technology with smart healthcare system might be an excellent solution due to its features as cryptographic security, decentralization, immutability and transparency, for above discussed challenges for RPM. This future changing technology was conceptualized for the first time by an anonymous person Satoshi Nakamoto in his white paper in 2009 [25]. She/he introduced a digital currency as bitcoin in the distributed ledger. At the present time, several researchers, academician, industry professional and government are showing concern in this potential technology for securing the various applications. Although this technology can resolve the above discussed challenges of RPM, but this technology is founded on rich computation and cryptographic techniques, such that, It entails a significant bandwidth and delay overhead. Consequently, it is not totally fit in its original form for the IoT devices those are resource-constrained. Integration of Healthcare and Blockchain technology comes with some serious risks, because the logs of all the transactions are updated in the distributed ledger, due to this the privacy of the user can be leaked, the risk of privacy and security increases. [26]. Even due to process delay and due to privacy leaks, the life of the patient can also come to the fore.

Three layered architecture of proposed integrated RPM - Blockchain platform is represent in the Figure 5. In this proposed architecture all the medical sensors and wearable devices can sense patient's vital signs and transmit these data via Bluetooth or Wi-Fi to a mobile device. The mobile device sends this data to the gateway and the gateway sends this data in an encrypted form to the blockchain. Blockchain execute the master smart contract and it executes specific smart contract according to the threshold value of data [12]. If there is uneventful data then it is stored on the cloud and if there is eventful data then the event gets stored in the blockchain and the data is stored on the cloud and a hash of that data is created and that hash value is stored in the form of a transaction in the blockchain. And also an alert signal is sent to the healthcare provider and patient and his/her relative [12]. In this way, the security and privacy of the patient's data is not compromised.

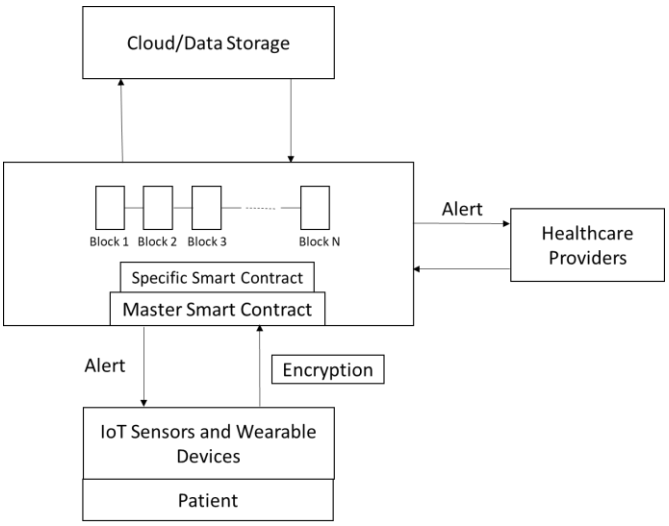

Figure 5: Blockchain in RPM based digital healthcare System

8. CONCLUSION

This paper proposed a three layer blockchain enabled RPM system for the healthcare data security and privacy preservation. This proposed model provides a solution to the majority of security and privacy issues while deal with the resource constraint aspect of the RPM system and ensures all information security constraints confidentiality, integrity and availability. In this paper, we proposed a novel hybrid approach that combines the benefits of blockchain, IPFS and lightweight cryptographic primitives to evolve a patient-centric access control for electronic health records and providing effective security and privacy to critical health information. Since in this model only metadata will be stored in the blockchain, it is also scalable. As our proposed model is resolving almost all RPM issues against the rest of the state of the art solution. Hence, it can become an efficient RPM solution that can secure the health information of the patient. In the future, we will practically test this proposed architecture in different IoT networks.

REFERENCES

[1] https://censusindia.gov.in/2011-prov-results/paper2/data_files/india/paper2_1.pdf

[2] Sandro N. et al., "Internet of Things (IoT): Opportunities, issues and challenges towards a smart and sustainable future", Journ. of Cleaner Prod., Vol. 274, 2020.

[3] Sharma V., Lal N. (2022) Role of Blockchain in IoT Enabled Power and Energy Related Healthcare System-Platform for the Development of IoT Security. In: Malik H., Ahmad M.W., Kothari D. (eds) Intelligent Data Analytics for Power and Energy Systems. Lecture Notes in Electrical Engineering, vol 802. Springer, Singapore. https://doi.org/10.1007/978-981-16-6081-8_27

[4] Aakriti Singla, Anand Sharma "IoT Crypt–An Intelligent System for Securing IoT Devices Using Artificial Intelligence and Machine Learning" Artificial Intelligence and Global Society: Impact and Practices, Pages 161-174, CRC Press

[5] Anand Sharma, Alekha Parimal Bhatt “Quantum Cryptography for Securing IoT-Based Healthcare Systems” Limitations and Future Applications of Quantum Cryptography, Pages 124-147, IGI Global
[6] Raju, Joel et al. “Cyber Security in IoT Devices using Blockchain Concept.” (2020).
[7] Daniel M. and Benedict O. “Blockchain mechanisms for IoT security”, IoT,Vol.1, pp. 1-13, 2018.
[8] A. Archip et al.,"An IoT based system for remote patient monitoring," 17th ICCC, 2016, pp. 1-6, 2016.
[9] R. Guo et al., "Flexible and Efficient Blockchain-Based ABE Scheme With Multi-Authority for Medical on Demand in Telemedicine System," in IEEE Access, pp. 88012-88025, 2019.
[10] Rahmadika S and Rhee K-H, “Blockchain technology for providing an architecture model of decentralized personal health information,” Int. Jrnl. of Engg. Business Mgmt., 2018.
[11] M. A. Uddin et al., "Continuous Patient Monitoring With a Patient Centric Agent: A Block Architecture," in IEEE Access, pp. 32700-32726, 2018.
[12] Griggs, K.N. et al. Healthcare Blockchain System Using Smart Contracts for Secure Automated Remote Patient Monitoring. J Med. Syst. (2018).
[13] Zhang, A., and Lin, X. Towards Secure and Privacy-Preserving Data Sharing in e-Health Systems via Consortium Blockchain. J Med. Syst. (2018).
[14]M. A. Uddin et al., "A Decentralized Patient Agent Controlled Blockchain for Remote Patient Monitoring," Int. Conf. on WiMob, pp. 1-8, 2019.
[15] G. Srivastava et al., "A Light and Secure Healthcare Blockchain for IoT Medical Devices," IEEE CCECE, pp. 1-5, 2019.
[16] Bashayer Al-Ahmadi and Sanaa Sharaf, “Blockchain Based Remote Patient Monitoring System”, JKAU: Comp. IT. Sci., pp: 111 – 118, 2019.
[17] J. Hathaliya et al., "Blockchain-Based Remote Patient Monitoring in Healthcare 4.0," IEEE 9th IACC, pp. 87-91, 2019.
[18] Hang, L. and Kim, D.-H. Design and Implementation of an Integrated IoT Blockchain Platform for Sensing Data Integrity. Sensors 2019.
[19] Ali, M.S. et al. A Decentralized Peer-to-Peer Remote Health Monitoring System. Sensors, 2020.
[20] P. P. Ray et al., "Blockchain for IoT-Based Healthcare: Background, Consensus, Platforms, and Use Cases," in IEEE Sys. Jrnl., pp. 85-94, 2021.
[21] H. T. Yew et al., "IoT Based Real-Time Remote Patient Monitoring System," 16th IEEE Int. CSPA, pp. 176-179, 2020.
[22] Lei Ru et al., "A Detailed Research on Human Health Monitoring System Based on Internet of Things", WCMC, 9 pages, 2021.
[23] M. Dhinakaran et al. "A System of Remote Patients’ Monitoring and Alerting Using the Machine Learning Technique", JFC, 7 pages, 2022.
[24] Zaabar et al., "Secure and Privacy-aware Blockchain-based Remote Patient Monitoring System for Internet of Healthcare Things," 17th Int. Conf. on WiMob, pp. 200-205, 2021.
[25] Nakamoto, Satoshi. (2009). Bitcoin: A Peer-to-Peer Electronic Cash System. Cryptography Mailing list at https://metzdowd.com.
[26] V. Sharma et al., “A Detail Dominant Approach for IoT and Blockchain with their Research Challenges,” ICONC3, India, pp. 1-6, 2020.
[27] V. Sharma et al., "A Novel comparison of Consensus Algorithms in Blockchain," AAMS, Vol. 19, 2020.

Biographies

Vishal Sharma received his bachelor's degree in computer engineering from Rajasthan University, Jaipur in 2006 and master degree from Jagannath University, Jaipur in 2012 and pursuing Ph.D. degree from Mody University of Science and Technology, Sikar. His research areas include Network Security, Information Security and Blockchain. He has a total teaching experience of 13 years. He has published and reviewed several articles in journals of repute. Currently he is working as Assistant Professor in CSE Department of School of Engineering and Technology at Mody University of Science and Technology, Lakshmangarh, Sikar, Rajasthan, India.

Dr. Anand Sharma, received his Ph.D. degree in Engineering from MUST, Lakshmangarh, M.Tech from ABV-IIITM, Gwalior and B.E. from RGPV, Bhopal. He has been working with Mody University of Science and Technology, Lakshmangarh for last 12 years. He has more than 14 years of experience of teaching and research. He has been invited to several reputed institutions like ISI-Kolkata, IIT-Mumbai, IIT-Jodhpur, IIT-Delhi, RTU-Kota etc. He has pioneered research in areas of Information Engineering, Information Security, IoT, Knowledge Management and Machine Learning. He is a member of IEEE, IET, ACM, IE(India), Life Member of CSI and ISTE. He is serving as Vice-Chairman of CSI-Lakshmangarh Chapter and Student Branch Coordinator of CSI-MUST Student branch. He has authored / edited 10 books of national/international publishers. He has more than 90 papers in reputed International Journals and conferences. He has organized more than 15 conferences / seminars and workshops. He is serving on advisory capacity in several international journals as Editorial Member and in International Conferences as Technical Programme committee / organizing committee.

Speech to Text Conversion with Multiple Indian Languages

Arthat Arora, Gouri Sankar Mishra, Parma Nand, Rani Astya, Pradeep Kumar Mishra, Nikhil Sharma, Anubha Sah, Abhinav Srivastava

Department of Computer Science and Engineering, SET, Sharda University, India

arthatarora@gmail.com, nikhil.k2524@gmail.com, sahanubha12@gmail.com, abhi.s007ea@gmail.com, gourisankar.mishra@sharda.ac.in, parma.nand@sharda.ac.in, rani.astya@sharda.ac.in, pradeepkumar.mishra@sharda.ac.in

Abstract

Communication is one of the vital components to pass on any kind of information and communicate with individuals. Various applications are used for speech recognition, speech to text conversion, language interpretation, and so on. SPEECH TO-TEXT recognition is a product that allows the client to enhance the cognition capacity and directs text by voice. This paper focuses on the speech to text conversion of English to multiple Indian languages by using the methodologies of natural language processing and machine learning. Since a large number of the issues emerging in speech recognition are appropriate for algorithmic examinations, we present them in wording recognizable to algorithm designers.

Keywords: Speech Recognition, Speech to text, Automatic Speech Recognition, Interpretation

1. INTRODUCTION

Natural language processing (NLP) is a branch of artificial intelligence in the computer technological that makes the assisting computers to recognize the manner that human beings write and talk. This is a tough undertaking as it includes numerous unstructured statistics. The fashion in which human beings communicate and write (referred to as 'tone of voice') is unique to individuals, and constantly evolving.

Understanding context is also a difficult task – something that requires semantic analysis for system gaining knowledge of to get a deal with on it. Natural language understanding (NLU) is a sub-branch of NLP and deals with those nuances via gadget analyzing comprehension in preference to without a doubt knowledge literal meaning. The goal of NLP and NLU is to assist computer systems recognize human language properly enough that they can communicate in a natural manner. Some of the common applications of NLP are : Voice Assistants, Different service based chatbots, Language Translation, Voice based application

1.1. Working of NLP

The working of NLP is divided into 5 steps; starting from the lexical analyzer to the pragmatic analyzer. The input speech is sub-divided at each step for the simplification of the speech and converted to small blocks of information that can be processed and understood by the machine to perform the specific task. The 5 stages of analyzing sentence are represented in Fig.1.

The initial step involves lexical analyzer which helps in the simplification of the huge text into small blocks called lexicons, it divides or classify the text into words, sentence, phrases or paragraphs. The processed classification is then moved to syntactic analyzer which checks and arranges the text into correct grammar format and forms a meaning of the sentence that is understood by the user. Syntactic analyzer arranges the words and phrases in such a format that in form a correct readable sentence. The text is moved further to semantic analyzer which perform the task of converting the formed sentence to show case the actual meaning of the sentence i.e checking if the formed sentence is having the same meaning as it is intend to make. Once the

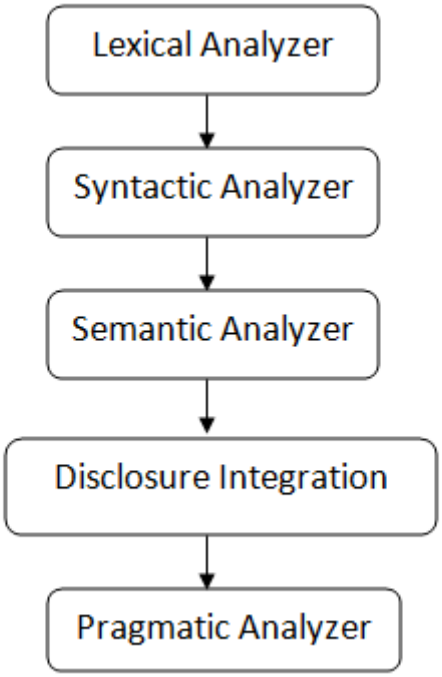

Figure 1: Working Flow of NLP

sentence is verified for its meaning then it moves to the next phase of disclosure integration, which helps in a formation of group of sentences without losing the meaning of each line and converting them into a meaning paragraph. The Disclosure Integration checks for each sentence meaning with the sentence just before it to check if the correct meaningful sentence is maintained. The final stage is the pragmatic analyzer in which the whole output is checked

is it correct and have some relation with the real-world knowledge. After all the successful processing of all the phases the system processes the desired output.

1.2. Automated Speech Recognition (ASR)

Automatic Speech Recognition (ASR) is an innovation or a technology that grants individuals to utilize their voices to talk and have conversation with a PC interface in a way like a typical human discussion. The most progressive adaptation of at present created ASR innovations spins around what is called Natural Language Processing, or NLP. This variation of ASR comes the nearest to permitting genuine discussion among individuals and machine intelligence.

Lately, ASR has become famous in the customer care divisions of huge corporation. It is additionally utilized by a few government offices and different associations. Some of the ASR frameworks perceive the input in a single word like yes/no or numeral which makes it feasible for people to manage computerized options without typing numerals and has no capacity to bear any kind of error. In a manual-section circumstance, a client could hit some unacceptable key subsequent to having entered 20 or 30 numerals at stretches already in the menu, and surrender as opposed to bringing again and beginning once again. ASR for all intents and purposes disposes of this issue. Refined ASR frameworks permit the client to enter direct questions or reactions, for example, a request for driving direction or the phone number of a lodging in a specific town. It likewise decreases the quantity of directions that the client should get and comprehend.

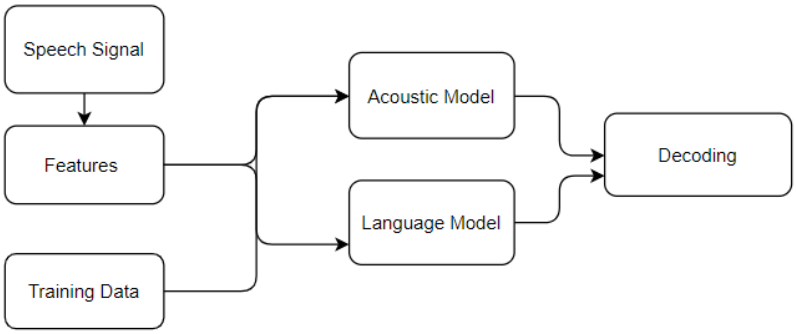

Figure 2: Working of ASR

In the easiest terms, speech recognition happens when a PC gets audio input from an individual talking, processes the input by separating the different parts of speech, & afterward translates that speech to message.

Some ASR frameworks are speaker-dependent and should be prepared to perceive specific words and speech pattern. These are basically the voice-recognition frameworks utilized in your smart devices. You need to say explicit words and expressions into your telephone

before the ASR-powered voice assistant begins working for it to figure out how to recognize your voice.

Other ASR frameworks are speaker-independent. These frameworks don't need any preparation or training. Speak independent frameworks can perceive verbally expressed words regardless of the speaker.

2. SPEECH RECOGNITION-A STATE OF ART

This mixture strategy helps application that requires brief outline of extended speeches which is very valuable for documentation. One of the most important step while working with NLP is to extricate the components of speech having few qualities. It turns into a kind of obstruction to summarization process by supposing a word or a sentence is perceived as negligible. Even punctuation assumes an indispensable part in synopsis as semantics is significant while summing up the content. The methodology proposed by the team was to summarize the text extracted through the input with respect to the rank of the sentences. The frequency of occurrence of words can be used to determine the rank of the sentences. And to find the frequency of words, they used the sentence tokenize and word tokenize techniques are available in python NLTK packages. Using Google API, text is extracted and then the sentences are obtained using sentence tokenize and words are extracted using word tokenize. This input received through the user is converted into signals and then converted into text format.

This aricle on “Speech to Text Conversion Methods” explained varieties of the speech signal and their significance in automatic speech recognition. A database has been made from the different words and syllables. The ideal speech is delivered by the Concatenative speech synthesis methodology. The framework gives the input information as voice, then, preprocessed that information and changed over into text showed on PC. The client types the input string and the framework peruses it from the database or information store where the words, telephones, diaphones, triphones are put away. This system had a speech to text system with the vocabulary of ten words i.e. digits 0 to 9 and statistical modelling (HMM). HMM was used for machine speech recognition. This system builds an HMM model using C programs for each word present in vocabulary. This is done during the training phase. However, during the recognition phase, speech is acquired and stored in FPGA's memory to preprocess and calculate the probability of observation sequence.

The authors proposed a framework named “ScribeBot” to help the visually impaired students to pro their assessments and exams. SCRIBEBOT is a Raspberry Pi 3 coordinated with a headset with Microphone, a Monitor and a printer. The framework they've made uses the advanced deep learning algorithms and neural organizations which have been carried out in the Google speech API. The two principle measures associated with their work is the speech to text transformation and furthermore the way toward changing the content over to speech so the students can think about the question that has been asked in the paper. The framework has been executed utilizing python programming language which imports the Google Speech API package alongside the Google Text To Speech package.

This study had talked regarding the strategies of dynamic time traveling and mel scale repeat cepstral constant within the confined talk affirmation. Unique elements of the

communicated word have been freed from the information talk. Associate degree illustration of five speakers has been assembled and each one of them had spoken ten digits. A information set is formed on this premise. Then, at that time highlight has been separated utilizing MFCC. DTW is used for adequately overseeing entirely unexpected talking speed. It is used for closeness assessment between 2 plans that shifts in speed & time.

Table 1. A comparative summary of existing related surveys

Author(s)	Year	Technique
"Vinnarasu A., Deepa V. Jose"	2019	Use of NLP and text summarization by neglecting repeated words.
"Dhanush Kumar S, Lavanya S, Madhumita G and Mercy Rajaselvi V"	2018	ScribeBot: Made with Raspberry Pie and Google API
"Mittal et al."	2018	ASR framework for Punjabi language under various acoustic conditions(created explicitly for mobile phones)
"Sagar Patil, Mayuri Phonde, Siddharth Prajapati, Saranga Rane and Anita Lahane"	2016	ASR framework for Punjabi language under various acoustic conditions(created explicitly for mobile phones)
"Miss. Prachi Khilari and Prof. Bhope V. P."	2015	Database of different words and syllables for conversion of speech to show text on monitor by concentrating on string rather than information.
"Geeta Nijhawan, Poonam Pandit and Shivanker Dev Dhingra"	2013	Strategies of dynamic time traveling and mel scale repeat cepstral constant(Sub band centroid)
"Puneet Kaur, Bhupender Singh and Neha Kapur"	2012	Recognizing speech by Hidden Markov Model
"Jingdong Chen and et al"	2004	mel-recurrence cepstral coefficients (MFCCs) in clean discourse, while passing preferred execution over MFCC in boisterous conditions.

The author examined that notwithstanding their boundless fame as frontend boundaries for discourse acknowledgment, the cepstral coefficients which has been received from either

direct assumption examination or a channel bank are found to be tricky to added substance clamor. Here in this letter, we examine the utilization of ghastly sub band centroids for good discourse acknowledgment. We show that centroids, assuming appropriately chosen, can achieve acknowledgment execution tantamount to that of the mel-recurrence cepstral coefficients (MFCCs) in clean discourse, while passing preferred execution over MFCC in boisterous conditions. A technique is proposed to assemble the unique centroid highlight vector that essentially typifies the temporary apparition information.

The author proposed and executed an ASR framework for Punjabi language under various acoustic conditions. The significant limit of setting subordinate unfastened model is the necessity of higher memory space. This framework is explicitly created for cell phones.

The author had discussed a way to use Hidden Markov Model in the method of popularity of speech. The crucial 3 steps that are important to broaden an 'Automatic Speech Recognition' machine are pre-processing, characteristic Extraction and popularity and subsequently hidden markov version is used to get the required end result. Since there are already huge amount of improvements inside the discipline of virtual sign processing, research persons are trying their best to broaden a ideal ASR device. However, the overall performance of PCs within identical timings aren't that high in terms of matching speed and accuracy.

The author proposed a framework named "Multilingual Speech and Text Recognition and Translation using Image" to robotize the application to defeat from the language boundary in between the nations & furthermore states inside the country. They carried out framework for client who staging issues of language obstruction and furthermore its user interface is additionally easy to use so that the client can undoubtedly collaborate with this framework. So due to this framework, users don't need to utilize word reference for knowing the importance of word, hence it naturally decreases the client task for knowing the language for communication.

3. PROPOSED METHODOLOGY

The system works with the understanding or the audio signal of stream or audio input through the microphone jack and interpretation of the signals into the data is done by pre-requisite audio files which can understand the audio inputs and act upon them. There is a database same as on which Google API works which can understand the spoken words and get the correct grammar and meaning and form the correct meaningful sentence.

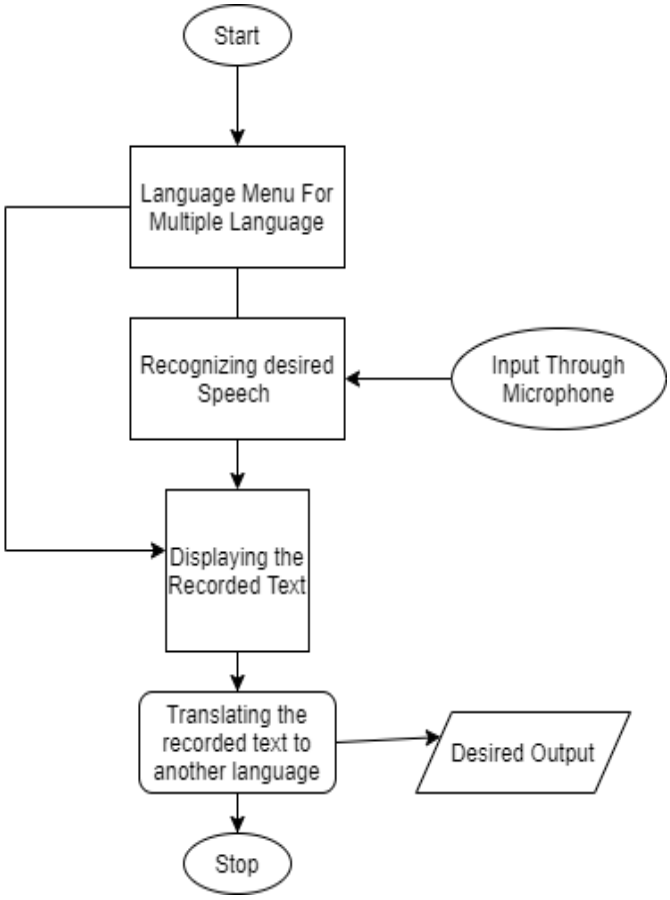

Figure 3: Process Flowchart

The successful sentence formed is then processed for further evaluation and conversion, the system work both for multi-language support to remove to banner of knowledge of all the language for the communication around the globe. The processed data in the user language is then converted to desired client language for understanding of what another user is saying. The working is as follow:

- There is a menu of multiple language support for conversion which user can use to translate its text and record in the selected desired language.
- After the selection the user inputs the data as an audio signal through the microphone.
- The recorded input text is showing to the user for verification if it is actual correct to what is being said.
- The menu is again shown to the user to convert the recorded text to desired language that he wants to translate.
- After successful processing, the desired output is given of the screen after conversion for further use.

The main advantage of this system is the simplicity of communication and speedy document turnaround. It helps us to perform multiple tasks while dictating and can create records in under a fraction of the time it takes to type. It provides us the adaptability to work in or out of the workplace. Also, the time is saved with expanded productivity and has less desk work.

The main disadvantage of this system is the absence of accuracy and misinterpretation. In the event that you talk excessively quick or vaguely, you'll increment spelling and punctuation blunders. It will most likely be unable to separate between your speech, others talking and other surrounding noise, prompting record misunderstandings and mistakes.

he functions of system is to provide the language option for the user in the language menu, receive audio stream through microphone in the form of speech, classify audio signal addressee at the run time, provide the desired output in the preferred language selected by the user, map applicable signal to word series and then to action request, and user feedback.

4. CONCLUSION

Speech Recognition is a vast area to explore. Speech recognition framework permits PCs to take spoken sound, interpret it and create text from it. The speech to text conversion might appear to be compelling and effective to its clients in the event that it produces regular speech and by making a few alterations to it. Our proposed system allows the user to recognize their speech and convert them into text in English as well as some Indian Languages provided in the option. This helps the user who find themselves uncomfortable in English language and provides leverage to have their text converted into their preferable language.

REFERENCES

[1] Vinnarasu A., Deepa V. Jose, “Speech to text conversion and summarization for effective understanding and documentation”, IOSR Journal of Computer Engineering (IOSR-JCE), Vol. 9, No. 5, October 2019.

[2] Miss.Prachi Khilari, Prof. Bhope V. P., “A REVIEW ON SPEECH TO TEXT CONVERSION METHODS”, IJARIIT, Vol. 4, July 2015.

[3] Dhanush Kumar S, Lavanya S, Madhumita G, Mercy Rajaselvi, “Journal of Speech to Text Conversion”, IJARCET, Vol. 4.

[4] Shivanker Dev Dhingra, Geeta Nijhawan, Poonam Pandit, “Isolated Speech Recognition using MFCC and DTW” International Journal of Advance Research in Electrical, Electronics and Instrumentation Engineering, Vol.2, Issue 8, August 2013.

[5] Jingdong Chen, Member, Yiteng (Arden) Huang, Qi Li, Kuldip K. Paliwal “Recognition of Noisy Speech Using Dynamic Spectral Subband Centroids” in IEEE SIGNAL PROCESSING LETTERS, VOL. 11, NO. 2, FEBRUARY 2004

[6] Ayushi Trivedi,Navya Pant, Pinal Shah,Simran Sonik and Supriya Agrawal, “Speech to text and text to speech recognition systems-Areview”, IOSR Journal of Computer Engineering (IOSR-JCE), Volume 20, Issue 2, Ver. I (Mar.- Apr. 2018)

[7] Bhupinder Singh, Neha Kapur, Puneet Kaur “Sppech Recognition with Hidden Markov Model:A Review” International Journal of Advanced Research in Computer and Software Engineering, Vol. 2, Issue 3, March 2012.

[8] Sagar Patil, Mayuri Phonde, Siddharth Prajapati, Saranga Rane and Anita Lahane, "Multilingual Speech and Text Recognition and Translation using Image", International Journal of Engineering Research & Technology (IJERT), Vol. 5 Issue 04, April-2016

[9] Shaikh Naziya S.1*, R.R. Deshmukh2, "Speech Recognition System – A Review", IOSR Journal of Computer Engineering (IOSR-JCE), Volume 18, Issue 4, Ver. II (Jul.-Aug. 2016)

[10] Anchal Katyal, Amanpreet Kaur, Jasmeen Gill, "Automatic Speech Recognition: A Review", International Journal of Engineering and Advanced Technology (IJEAT), Volume-3, Issue-3, February 2014

[11] Manjutha M, Gracy J, Dr P Subhashini, Dr M Krishnaveni, "Automated Speech Recognition System – A Literature Review", International Journal of Engineering Trends and Applications (IJETA) – Volume 4 Issue 2, Mar-Apr 2017

[12] T.Y.G, "Development and Comparison of ASR Models using Kaldi for Noisy and Enhanced Kannada Speech Data," pp. 1832–1838, 2017.

[13] P. Mittal and N. Singh, "Development and analysis of Punjabi ASR system for mobile phones under different acoustic models," Int. J. Speech Technol., vol. 0, no. 0, p. , 2019.

[14] S. Huang and S. Renals, "Hierarchical Bayesian Language Models for Conversational Speech Recognition," vol. 18, no. 8, pp. 1941–1954, 2010.

[15] Sarika Hegde ,K K Achary,Surendra Shetty- Analysis of Isolated Word Recognition for Kannada Language using Pattern Recognition Approach-International Journal of Information Processing , 7(1), 73 - 80. -2013.

[16] Sai Prasad P. S. V. S, . Girija P. N Speech Recognition of Isolated Telugu Vowels Using Neural Networks. Proceedings of the 1st Indian International Conference on Artificial Intelligence, IICAI 2003, Hyderabad, India, 28-34 December 18-20, 2003.

[17] Hegde, R.M., Murthy, H.A., Gadde, V.R.R., 2004. Continuous speech recognition using joint features derived from the modified group delay function and MFCC. In: Proceedings of ICSLP, Jeju, Korea, pp. 905–908.

[18] Hegde, R.M., Murthy, H.A., Rao, G.V.R., 2005. Speech processing using joint features derived from the modified group delay function. In:Proceedings of ICASSP, vol. I. Philadelphia, PA, pp. 541–544.

[19] Sunitha .K.V.N & Kalyani.N (2009). Syllable analysis to build a dictation system in Telugu language. International Journal of Computer Science and Information Security. Vol 30. No 30.

[20] Sunitha K V N, Kalyani N. Isolated Word Recognition using Morph Knowledge for Telugu Language. International Journal of Computer Applications 38(12):47-54, February 2012. Published by Foundation of Computer Science, New York, USA.

[21] Vijai Bhaskar P , Rama Mohan Rao S , Gopi A - "HTK Based Telugu Speech Recognition" International Journal of Advanced Research in Computer Science and Software Engineering - Volume 2, Issue 12, December 2012.

[22] Usha Rani N, Girija P N "Error analysis to improve the speech recognition accuracy on Telugu language" Sadhana Vol. 37, Part 6, December 2012, pp. 747–761. Indian Academy of Sciences.

[23] Himanshu N. Patel, P.V. Virparia - "A Small Vocabulary Speech Recognition for Gujarati"- International Journal of Advanced Research in Computer Science Volume 2, Issue 1, Jan-Feb 2011. ISSN 0976-5697.

[24] Patel Pravin, Harikrishna Jethva -" Neural Network Based Gujarati Language Speech Recognition " International Journal of Computer Science and Management Research Vol 2 Issue 5 May 2013.

[25] M.K.Deka , C.K.Nath , S.K.Sarma , P.H. Talukdar - "An Approach to Noise Robust Speech Recognition using LPC-Cepstral Coefficient and MLP based Artificial Neural Network with respect to Assamese and Bodo Language" International Symposium on Devices MEMS, Intelligent Systems & Communication (ISDMISC) 2011.

[26] Utpal Bhattacharjee-"Recognition of the Tonal Words of BODO Language"- International Journal of Recent Technology and Engineering (IJRTE) ISSN: 2277-3878, Volume-1, Issue-6, January 2013.

[27] Syama R, Suma Mary Idikkula (2008) "HMM Based Speech Recognition System for Malayalam", ICAI'08 – The 2008 International Conference on Artificial Intelligence, Monte Carlo Resort, Las Vegas, Nevada, USA (July 14-17, 2008) .

[28] Krishnan, V.R.V. Jayakumar A, Anto P B (2008) , "Speech Recognition of isolated Malayalam Words Using Wavlet features and Artificial Neural Network". DELTA2008. 4th IEEE International Symposium on Electronic Design, Test and Applications, 2008.Volume,Issue, 23-25 Jan. 2008 Page(s):240 – 243.

[29] A.R. Sukumar, A.F. Shah, and P.B. Anto, "Isolated question words recognition from speech queries by using Artificial Neural Networks", in proc. of IEEE 2nd International conference on Computing, Communication and Networking Technologies(ICCCNT), Karur, India, 2010, pp. 1-4.

[30] Anuj Mohamed, K. N. Ramachandran Nair-Continuous Malayalam speech recognition using Hidden Markov Models. Proceedings of the 1st Amrita ACM-W Celebration on Women in Computing in India, September 16-17, 2010, Tamilnadu, India; 01/2010.

[31] Sonia Sunny, David Peter S , and K Poulose Jacob -A Comparative Study of Wavelet Based Feature Extraction Techniques in Recognizing Isolated Spoken Words," International Journal of Signal Processing Systems, Vol.1, No.1, pp.49-53,June 2013.

[32] Kavita Sharma, Prateek Hakar "Speech Denoising Using Different Types of Filters" International journal of Engineering Research and Applications Vol. 2, Issue 1, Jan-Feb 2012

[33] Om Prakash Prabhakar, Navneet Kumar Sahu,"A Survey on Voice Command Recognition Technique" International Journal of Advanced Research in Computer and Software Engineering, Vol 3,Issue 5,May 2013.

[34] Shivanker Dev Dhingra, Geeta Nijhawan, Poonam Pandit, "Isolated Speech Recognition using MFCC and DTW" International Journal of Advance Research in Electrical, Electronics and Instrumentation Engineering, Vol.2, Issue 8, August 2013.

[35] Hakan Erdogan, Ruhi Sarikaya, Yuqing Gao, "Using semantic analysis to improve speech recognition performance" Computer Speech and Language, ELSEVIER 2005.

[36] Ibrahim Patel, Dr. Y. Srinivas Rao, "Speech Recognition using HMM with MFCC-an analysis using Frequency Spectral Decomposition Technique" Signal and Image Processing:An International Journal(SIPIJ),s Vol.1, Number.2, December 2010.

Design & Development of Vehicle Theft Detection System

Geervani Bandi, Shiva Prasanna Kumar Pillalamarri, Krishna Chaithanya Janapati

Vardhaman College of Engineering, Affiliated to JNTU, Hyderabad, India

geervani463@gmail.com, shivaprasannakumar321@gmail.com, j.krishnachaitanya@vardhaman.org

Abstract

Nowadays, it is not difficult to duplicate vehicle keys and the use of such keys increases the risk of theft. We hereby suggest an efficient and reliable solution to such problems. Our system uses a facial recognition system to identify the authorized users of the vehicles. This allows for a fast and easy-to-use authentication system. The system uses a ESP32Cam for facial recognition. Whenever the registered user tries to unlock the vehicle, the motor starts. When an unauthorized user tries to use the car, the system scans the person's face and checks if the face matches the authorized face, if it does not match, the system sends a notification to the registered user using Blynk app and GSM. The registered user can control the motor based on the person who is trying to unlock it. In this way the system helps to protect the vehicles.

Keywords: Speech Recognition, Speech to text, Automatic Speech Recognition, Interpretation

1. INTRODUCTION

According to the 2013 Car Theft and Robbery Census, car theft has increased by almost 8.47% in India. On average, in this situation, vehicle anti-theft technology, microcontrollers also need to be increased. Real-time vehicle theft detection and prevention systems provide a solution to this problem. Global system Mobile (GSM) communication is the globally recognized standard for cellular communication. The owner of the vehicle inserts Subscriber Identification Module (SIM) into the GSM module to send messages. A system that is a part of an anti-theft system is installed in a vehicle. This system is used by everyone Cheap for vehicles such as buses, bicycles and cars.

The main aim of the system is to send alert messages to the owner whenever an unauthorized person tries to start the engine. This project includes a GSM modem, ESP32 Cam module, relay module and blynk app to send notifications whenever theft is about to happen.

2. RELATED WORK

Kaushik [1] has developed a security vehicle security system that starts with fingerprints vehicle. The thumbprints of authorized persons are stored in the system's database. The vehicle will start If the database fingerprints match. If someone tries to access the vehicle, the system has relay module connected to fuel, the alarm that the vehicle was stolen is also emptied at the same time. Unauthorized person cannot refill empty fuel tank.
S S Pethakar [2] uses GSM, GPS & RFID security system for taxi like a car. To launch a vehicle, workers need to use an RFID card with an identification number. Numbers are

provided such that they have already been biased in the system database. FITS, GPS, GSM will be submitted to send SMS in locations like the owner, latitude and longitude of the vehicle. If the owner recognizes his feet, he sends SMS to GSM to lock the doors of the vehicles.

Nagaraja [3] used a GSM module, a microcontroller, and a relay module for the ignition system. Theft when detected, the microcontroller activates the GSM system and sends SMS to the owner when the owner responds. SMS then activates the relay switch and deactivates the ignition system.

Alkheder [4] uses GPS ,GSM module, the Google Earth application. This system includes an in-vehicle GPS module that replaces this GPS module Information about the GSM system for sending SMS to the owner. After receiving the SMS, the owner can know the latitude, longitude and speed using the Google Earth application.

3. SYSTEM DESCRIPTION

The components in the system are turned on as soon as the power supply is provided. The vehicle owner would be given an application. The notification about the theft can be sent to a maximum of 5 electronic devices provided that the devices have installed Blynk app and are connected to the same Local Area Network. Firstly, the owner's face is enrolled in ESP32 Cam module for facial recognition. The DC motor requires 12V power supply and ESP32 Cam module requires a power supply of 5V so step down transformer is used to convert AC power supply to two different DC power supplies.

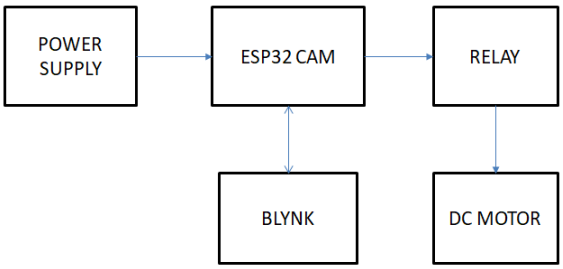

Figure 1. Block Diagram of the project

3.1 ESP32-CAM

ESP32-CAM is a development board module with a size of 27x40mm. It can be integrated into a camera system with an ESP32 module and a camera. ESP32-CAM can be widely used in various IoT applications. Suitable for smart appliances, industrial wireless control, wireless monitoring, wireless QR identification, wireless positioning system signals and other IoT applications. An ideal solution for IoT applications.

- Input Voltage: 3.3V /5V
- Digital I/O Pins (DIO): 10
- Input Voltage: 3.3V /5V
- Digital I/O Pins (DIO): 10

Figure 2. ESP32-CAM

3.2 GSM Module

A GSM module is an electronic hardware device that uses GSM mobile phone technology to provide a data connection to a remote network. From a cellular network point of view, it is same as a regular cell phone, but we need to insert a SIM card.

Figure 3. GSM Module

3.3 FTDI Programmer

The FTDI USB to TTL serial converter module is used for common serial applications. It is generally used to communicate with microcontroller development boards such as the ESP32Cam and Arduino Micros, which do not have a USB interface.

Figure 4. FTDI Programmer

3.4 Relay Module

A Relay module is an electric switch operated by an electromagnet that is activated by low power signal from the microcontroller like ESP32 Cam. When the electromagnet is activated, it is pulled to open and close the circuit.

Figure 5. Relay Module

Other components like DC motor, connectors, breadboard, step down transformer are also required.

4. EXECUTION FLOW

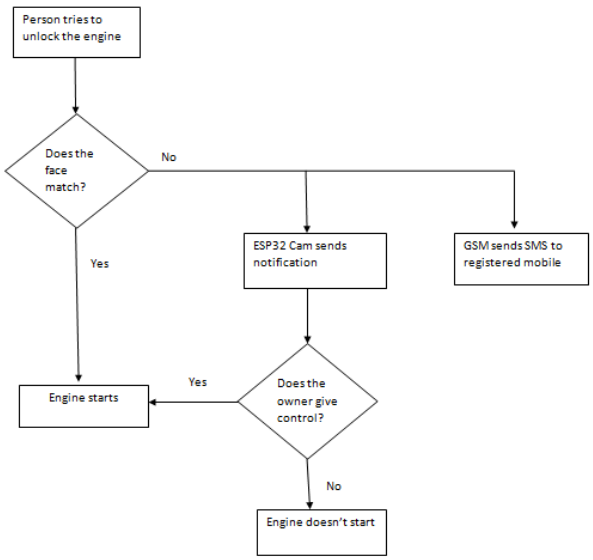

Figure 6. Execution Flow

The system can send notification up to 5 electronic devices provided that the devices are installed with Blynk app and are connected to the same Local Area Network. The GSM module included in the system sends an SMS to the registered mobile. The system would

turn on as soon as it is provided with power supply. Firstly, owner's face is enrolled in ESP32-Cam module with the inbuilt feature for facial recognition. So if any one tries to unlock the engine it compares with the enrolled face. If the face matches then the engine starts.

If the face doesn't match with the enrolled face, then ESP32-Cam module sends notification via Blynk app and the owner can control the engine with the help of Blynk app. The SMS notification is also sent by GSM module to the registered mobile number.

4.1 Data Push on ESP32-Cam

For pushing data into the ESP32-Cam module we use FTDI programmer because we there is no inbuilt USB interface available for ESP32-Cam module. We write code in Arduino IDE software and with the help of FTDI programmer we push data into ESP32-Cam module.

4.2. Software Implementation

In this project, Arduino IDE is used to program and deploy the code in to ESP32-Cam board. Blynk is used as the platform for sending notification and controlling DC motor, which is a free source for building apps.

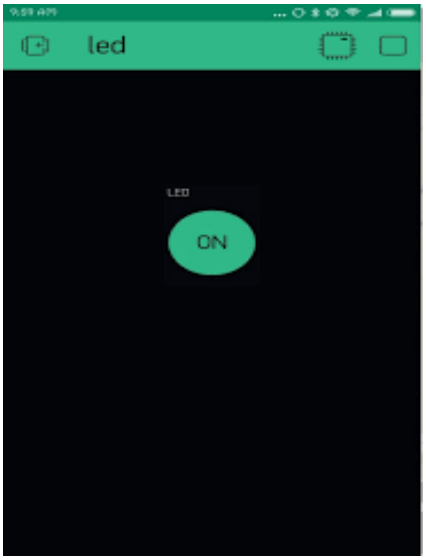

Figure 7. Blynk platform for controlling DC motor

5. RESULTS AND DISCUSSIONS

As soon as the device is plugged on the step down transformer supplies ESP32-Cam board with 5V and DC motor with 12V power supply.

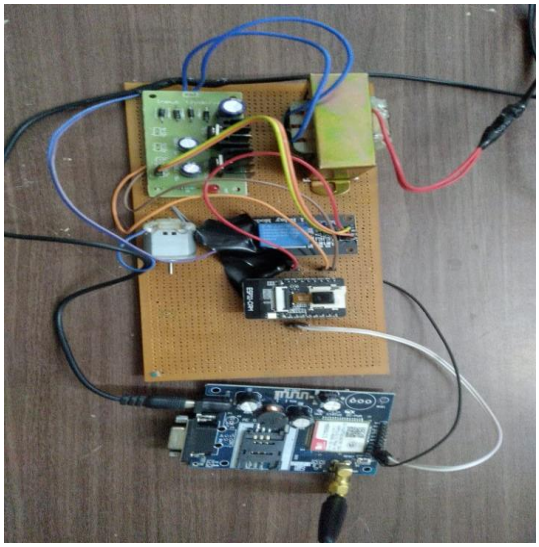

Figure 8. Prototype

VI. ADVANTAGES

- Owner can keep track of the status of the vehicle.
- Upto 5 persons can keep track of the status.
- Inexpensive.
- GSM is also included to send SMS so evenif WiFi is not available, he/she can keep track of the status .

6. FUTURE SCOPE AND CONCLUSIONS

The proposed system may be extended in such a way that it can be able to send picture of the person, who is trying to unlock the engine, to the owner so that the owner can be able to give control to the people whom he knows otherwise blocks the engine. The proposed system has been developed and tested effectively. The system is able to enroll faces and starts engine only for authorized users and if unauthorized person is detected it is able to send notifications and also able to control the DC motor.

ACKNOWLEDGEMENT

We sincerely thank, faculty of ECE at Vardhaman College of Engineering, Hyderabad for their guidance in reviewing of the manuscript and suggestions at different levels of the work and also grateful for the management for providing necessary facilities to carry out our project work at Center of Excellence for Intelligent Systems (#3021) in Physical & Remote environment.

REFERENCES

[1] N. Kaushik, M. Veralkar, Pranab. P, k. Nandkarny, “Anti-theft vehicle security system”, International journal for scientific research and development, vol. 1, no.12, pp. 2845-2848, March 2014.

[2] S. S. Pethakar, S. D. Suryavanshi, N. Srivastava, “RFID, GPS and GSM based vehicle tracing and employee security system”, International Journal of Advanced Research in Computer Science and Electronics Engineering, vol. 1, no. 10, pp. 91-96, Dec. 2012.

[3] B. G. Nagaraja, Mahesh. M, R. Rayappa, C. M. Patil, “Design and development of a GSM based vehicle theft control system”, presented at the International Conference on Advanced Computer Control, Singapore, January 2009.

[4] M. A. Khedher, “Hybrid GPS-GSM localization of automobile tracking system”, International journal of computer science and technology, Vol. 3, no. 6, pp. 75-85, December 2011.

[5] Pham Hoang DAT,MICHEAL DRIEBERG, Nguyen chi CUONG, “development of vehicle tracking system using GPS and GSM modem”, 2013 IEEE conference on open system (ICOS), December 2-4, 2013, Sarawak , Malaysia.

[6] Sayma Shammi, Sayeed Islam, Hafiz Abdur Rahman, and Hasan U. Zaman. “An Automated Way of Vehicle Theft Detection in Parking Facilities by Identifying Moving Vehicles in CCTV Video Stream”. In: 2018 International Conference on Communication, Computing and Internet of Things (IC3IoT). 2018, pp. 36–41. doi: 10.1109/IC3IoT.2018.8668135.

[7] S. Mohanasundaram, V. Krishnan, and V. Madhubala. “Vehicle Theft Tracking, Detecting And Locking System Using Open CV”. In: 2019 5th International Conference on Advanced Computing Communication Systems (ICACCS). 2019, pp. 1075–1078. doi: 10.1109/ICACCS.2019.8728460.

[8] Syed fasiuddin, Syed Omer, Khan Sohelrana, Amena Tamkeen, and Mohammed Abdul Rasheed. “Real Time Application of Vehicle Anti Theft Detection and Protection with Shock Using Facial Recognition and IoT Notification”. In: 2020 Fourth International Conference on Computing Methodologies and Communication (ICCMC). 2020, pp. 1039–1044. doi: 10.1109/ICCMC48092.2020.ICCMC-000194.

[9] Hoang Dat Pham, Micheal Drieberg, and Chi Cuong Nguyen. “Development of vehicle tracking system using GPS and GSM modem”. In: 2013 IEEE conference on open systems (ICOS). IEEE. 2013, pp. 89–94.

[10] A. Hadi Fikri A. Hamid, Kah Weng Chang, Rozeha A. Rashid, Alias Mohd, Mohd. Abdullah, Mohd Adib Sarijari, and Mazlan Abbas. “Smart Vehicle Monitoring and Analysis System with IOT Technology”. In: International Journal of Integrated Engineering (2019).

i-Kitab: An Interactive Textbooks Platform

[1]Kanupriya Ishu, [2]Gayatri Bangar, [3]Jigar Chawda, [4]Vaishali Khairnar

Department of Information Technology, TEC, University of Mumbai, Mumbai, India

[1] kanupriyaishu@ternaengg.ac.in, [2] gayatribangar@ternaengg.ac.in,
[3] jigarchawda@ternaengg.ac.in, [4] vaishalikhairnar@ternaengg.ac.in

Abstract

Use of digital mode for learning has proliferated significantly in past few years. However, digital learning is not as effective as interactive learning, since it is one way unlike the later which engages user for better experience and improved learning process. Interactive textbooks are one of the most popular tools used for interactive learning, they are easy to use and highly engaging. There are many platforms available on the internet that contain a plethora of interactive textbooks, however there are meagre platforms that let user create and share interactives textbooks. Therefore, the proposed system enables user to create and share interactive textbooks with other users. Users will be able to experience immersive learning by using these interactive textbooks and learning can become interesting experience in and of itself as a result of the interactive aspect.

Keywords. Interactive learning, Interactive textbook, Online learning, Book creator, Online textbook

1. INTRODUCTION

Nowadays, due to the rise in technology, traditional learning methods incorporate some sort of digital learning methods to achieve better understanding of concepts. Digital learning is the type of learning that involves the use of technology which is supposed to make the learning process more personalized and effective. However, to make learning experience more engaging and enriching, interactive elements should be incorporated in the existing digital learning methods. Interactive learning is the type of learning that actively involves the student in the learning process. Interactive textbooks are one of the best ways of incorporating interactive learning into students' curriculum.

An interactive textbook is a digital version of a textbook that includes interactive components. After all, when it comes to online learning, becoming digital isn't enough. It is remarkably convenient because it is equivalent of having both your study materials and visual elements under one roof. Various computer programming courses, and science courses can be made immensely easy to learn using interactive platforms. Many interactive learning platforms available do not provide user the freedom of creating their own textbooks as per their needs. While designing this website, one of the most important factors was to let user create their own textbooks and share them with others. The user can create textbooks without having to pay subscription fee. For the textbook creation purpose, an editor with many interactive functionalities was developed.

2. LITERATURE SURVEY

Smith et al. [1] provided comprehensive research on student's involvement using interactive computer textbooks. They created an interactive textbook based on Jupyter-notebook for the students who have newly enrolled for computer-related courses. There were three levels of engagement, change frequency, reading time, and response frequency. Change frequency refers to the number of times new cells were created by the students apart from solving the given problems. Reading time refers to the time the notebook was kept open in the browser. Response frequency is the number of times the cells consisting of given code were executed. The response frequency and change frequency were the key parameters in determining the active interaction. The major findings of the study were, the reading time spent on the textbook does not completely relate to the active interaction and active interaction was more efficacious than reading time in determining students' progress. The main aim of Weng et al [2] was to scrutinize the interactive online textbooks' impact on the methods of active learning, performance and cognitive load of students of 7th grade. The class was divided into two groups consisting of an equal number of candidates. Each group was handed a static PDF e-textbook and an interactive e-textbook. The interactive e-textbook group outperformed the static PDF e-textbook group in terms of cognitive and affective learning, as well as willingness to use an online textbook. However, the static PDF e-textbook group outperformed the interactive e-textbook group on the final exam. The findings also revealed that neither group's cognitive load differed considerably. D. Bikowski and J. Casal [3] conducted research among 13 students of a large U.S. University to explore their engagement towards interactive digital textbooks. An iBook was used for this study which acted as the digital textbook. The study employed a phased analysis design. All participants took an expected involvement survey during Phase I (Weeks 1–2), and six took part in the first round of TAP. Students' reflective journals and training in Phase II (Weeks 3–10) were informed by this information. The survey of actual participation, the final TAP, and member checking was all part of Phase III (Weeks 11–15). Students were mostly pleased with the interactive textbook and strongly suggested that it should be included in future classes. This interaction helped students stay motivated during training and gave them more time with the digital textbook to learn new techniques and processes, as well as decide which current strategies should be transferred or changed for this setting. A. Edgcomb et al. [4] researched whether incorporating an interactive textbook into preliminary STEM classes would help students increase their grades. The interactive textbook was characterized as having significantly lesser text in comparison to a traditional textbook, as well as various integrated problem, sets built for learning rather than quizzing, as well as multiple illustrations of core ideas and built-in tools. The University of California at Davis, the University of Michigan, and the University of Arizona all offered four preliminary computer programming courses: MATLAB, C++, and C/C++ respectively. Two-course offerings, one with a traditional textbook or static online tools and the other with an interactive textbook, were compared. Final course grades as well as results on individual course pieces were examined. From static to an interactive textbook, course grades increased by 0.28 points on a scale of 0-4 points for all 1,945 students. More notably, students in the course's lowest quartile gained 0.38 points. From static to interactive textbooks, exam scores increased by 13.6 per cent and project scores by 7.4 percent. The interactive textbook was subscribed to by 98 percent of the students, and they completed a few of the activities on it. An average student

accomplished about 87 percent of the assigned tasks in the specified interactive textbook. Chen [5] briefed about the effects in engagement, implications and features of visual representation in different science textbook formats. He compared conventional, digitized and interactive science textbooks based on the visuals present in them and corroborated that the digitized and interactive textbooks have many more emerging features that can be beneficial in engaging students and expanding their comprehension, investigation and analysis of content-related queries. B. Nansen et al. [6] did a detailed study Mathletics, an online application for learning mathematics interactively. The results are based on an ethnographic study of children's technology usage in Melbourne, Australia. They analysed the governance, commerce, and experience of children using Mathletics, as well as the growing opportunities and difficulties that have emerged as a result of the use of online apps for education and learning. According to the findings, websites provide different modes of learning, including intuitive, enjoyable, and temporary methods of appropriating online applications, for instance modes of play, or counter-play. Such collaborations make use of technology to achieve alternative and collaborative solutions. The study also underscores the importance of using conceptual and theoretical methodologies to evaluate digital education critically, taking into account the software's performance as well as the material's potential and the ways in which children's digital learning, play, and culture are influenced by the relationships they develop with and through software. R. Spencer et al. [7] looked into the effects of Top Hat on student experience, especially belonging, commitment, and self-confidence. To find out how students felt about using Top Hat, a convergent parallel mixed methods system was employed by the researchers. Engagement, and Self-Confidence Scale, Demographic surveys, the Student Belongingness, the Autonomous Learning Scale, and sub-scales associated more directly to the Top Hat’s usage were used to gather quantitative results. The results show that students' experiences with digital media technologies in the classroom are varied. Top Hat was seen as encouraging as well as hampering students' ability to communicate with one another, the professors, and the course content. Top Hat technology brings students closer together through interactivity, simplicity, and connectivity, but by limiting human interaction, it also alienates them from course teachers and peers.

3. RELATED WORK

Table 1. Performance Analysis of Existing and Related Applications

WEBSITE	TECHNOLOGIES USED	ADVANTAGES	DISADVANTAGES
Mathletics [11]	○ Javascipt Libraries: Isotope, Lightbox, jQuery, Modernizr ○ Programming Language: PHP ○ UI frameworks: Bootstrap ○ Databases: MySQL ○ SEO: YoastSEO	○ Students are interested in learning and are encouraged to do so. ○ Mathletics is adaptive, it responds to the child's individual strengths and weaknesses. ○ Students instinctively know whether they are on the correct track and can proceed at their own speed through the program.	○ Students responses aren't adaptive to questions which are rote

Tophat [12]	○ PaaS: WP Engine, AWS ○ Javascipt Libraries: jQuery, Slick ○ Programming Language: PHP ○ Databases: MySQL ○ SEO: YoastSEO	○ It tracks participation in the classroom ○ Task automation ○ Improved student assessment. ○ Better student engagement	○ The format of the grade book needs to be improved. ○ Website Charges a lot.
PathFinder [8]	○ CMS: Wordpress ○ CDN: Cloudflare ○ Database: MySQL ○ Programming language: PHP ○ Analytics: Facebook Pixel, Google Analytics ○ Tage manager: Google tag manager ○ Video Player: Plyr. Youtube ○ UI framework: animate.css, Bootstrap ○ Front scripts: Google front API, font awesome, Twitter Emoji ○ Security: reCAPTCHA	○ User friendly ○ Platform Independent ○ Job opportunities (as the name of website) ○ Emergency contact	○ The main focus is on academic books and marks. ○ Target audience is exclusively students appearing for entrance exams.
Mathigon [9]	○ Analytics: Cloudflare Browser Insights, Google Analytics ○ Font scripts: Google Font API ○ Video players: Youtube ○ CDN: Google cloud, cloudflare	○ User friendly ○ Platform Independent ○ Paid version is not necessary	○ The lack of a teacher dashboard and a limited course catalogue
Brilliant [10]	○ Analytics: Facebook pixel, Quantcast measure, Profitwell, google analytics ○ Javascripts framework: Vue.js ○ CDN: Cloudflare ○ Cookie: Quantcast choice ○ Miscellaneous: webpack ○ Widgets: Facebook	○ Users can experience endless entertainment while watching, solving interactively. ○ Clean and elegant user interface. ○ Light colours are used in the interface as more focus is on contents on the website.	○ Only STEM subjects are covered. ○ The monthly payment plan is pricey.

After scrutinizing various platforms, it was clear that many applications provided users to browse and use interactive textbooks to a certain limit, after crossing the limit users are compelled to take up subscription by paying a certain fee. Also, there were a handful of free platforms that let user to create their own textbooks. Keeping in mind, all of the above reasons we developed a platform where users can create as well as share interactive textbooks for free.

4. METHODOLOGY

As compared to the existing system, for some websites the process of content creation and teacher approval takes an intensive amount of time, which results in less material availability, and for some websites only textbooks from the author are available to users.

We are proposing a web application where anyone can create an interactive textbook or learning material and share it with others. The block diagram of the system is shown in Figure 1.

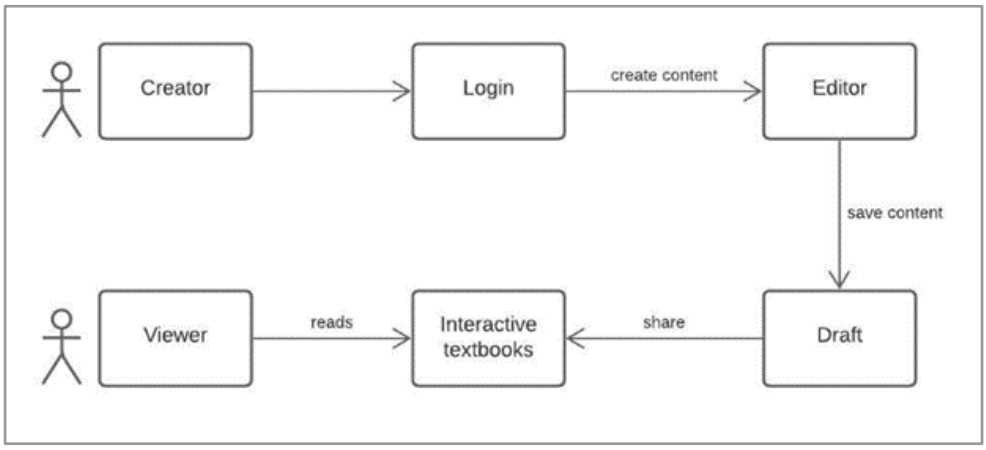

Figure 1. Systems block diagram.

There are following parts in our system:

- Creator: The creator is the person who will create the interactive textbook. They will be able to the content of their choice which will be interactive for the viewers.
- Login: Create will have to create an account on the website. They have to login to start editing the interactive textbook.
- Editor: An editor will be provided on the website where the creator will edit the interactive textbook. The editor will contain different functionalities to make the textbook interactive.
- Draft: Creator can save their work and come to edit it later by logging in to the website.
- Interactive Textbooks: After the creator finishes with the editing they will publish the interactive textbook and share it with the public.
- Viewer: Anyone can view the interactive textbooks without logging in after it is being shared by the creator.

Creating a web application that users will find useful and usable is challenging, and to avoid wasting time on flawed ideas, programmers should be involved early in the process. In order to get a glimpse of the final product early in the development process, low fidelity [13] and high fidelity mock-ups [14] are viable strategies.

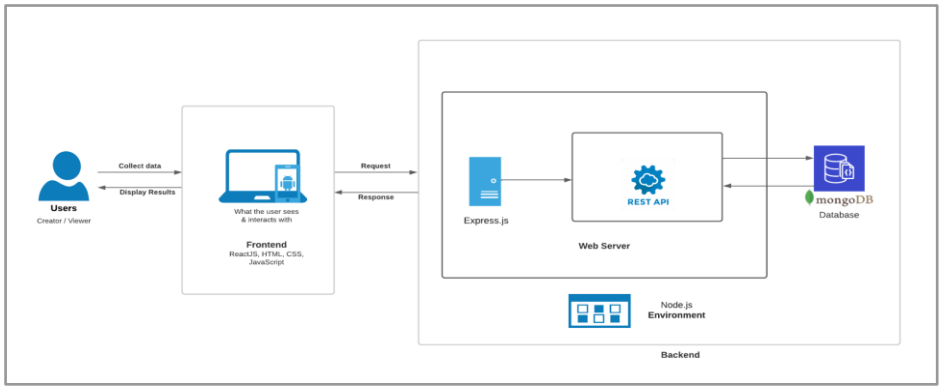

Figure 2. Web Application Architecture.

5. RESULTS

The use of interactive textbooks can bring a revolutionary change in education. This analysis of various systems reveals that interactive textbook significantly improves the performance of the user in the subject. When compared to traditional textbooks, it helps the user learn the contents better and retain them for a longer period.

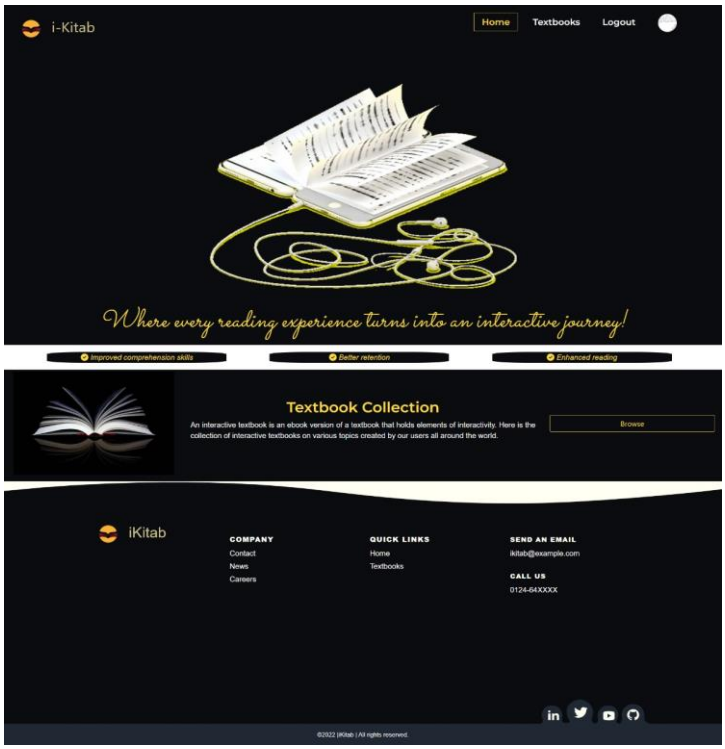

Figure 3. Home Page: This is the Home page that shows an overview of the website as well as shows how to use the website.

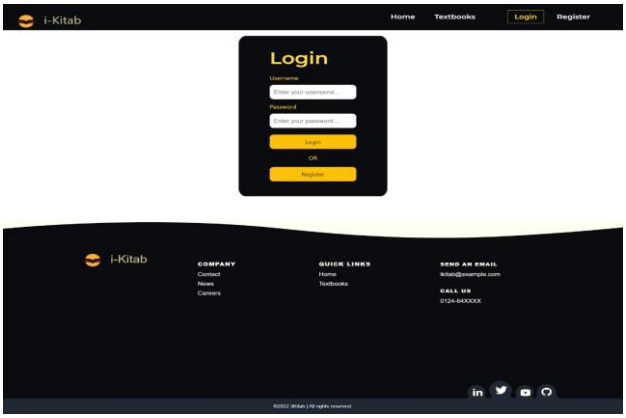

Figure 4. Login Page: This is the login page that lets the user to login the website.

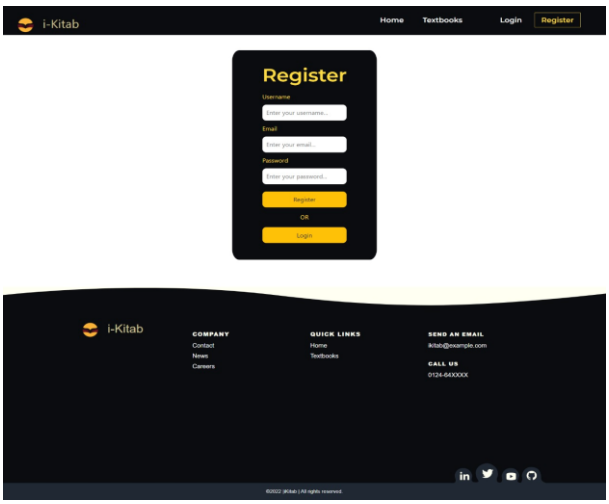

Figure 5. Register Page: This a registration page for the website which lets the user to register as a creator or a viewer.

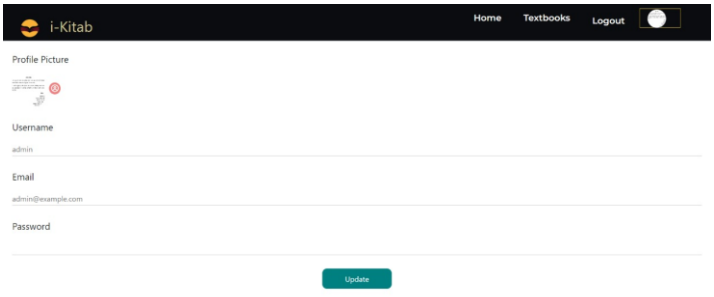

Figure 6. Account Information page: Account information page displays the information of user like their Username, Email address, Profile Picture and Password.

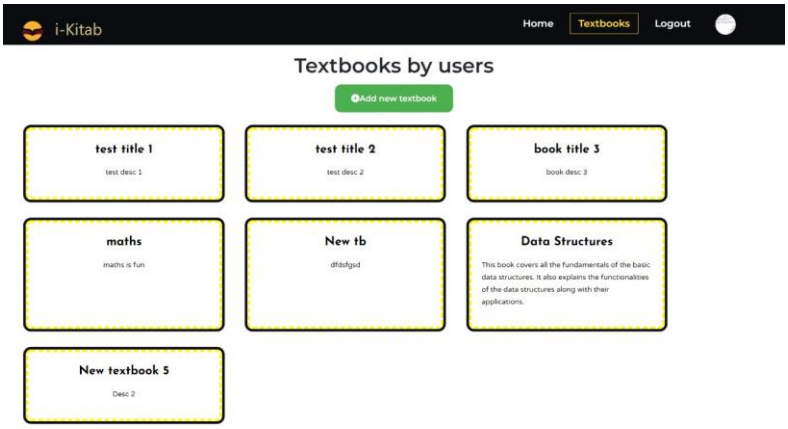

Figure 7. Textbook Page: This page shows the textbooks uploaded by the users.

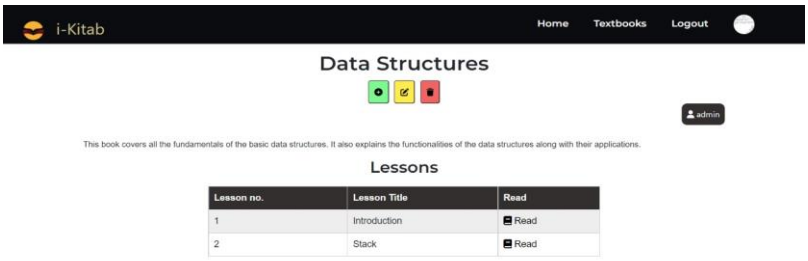

Figure 8. Individual Textbook: This page gives a brief overview of the textbook

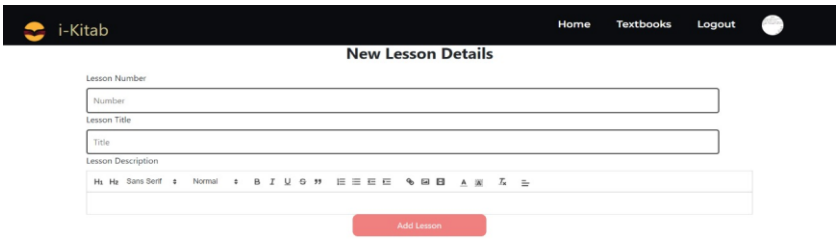

Figure 9. Create Page: This page is essentially an editor which lets the user create interactive textbooks using different elements provided.

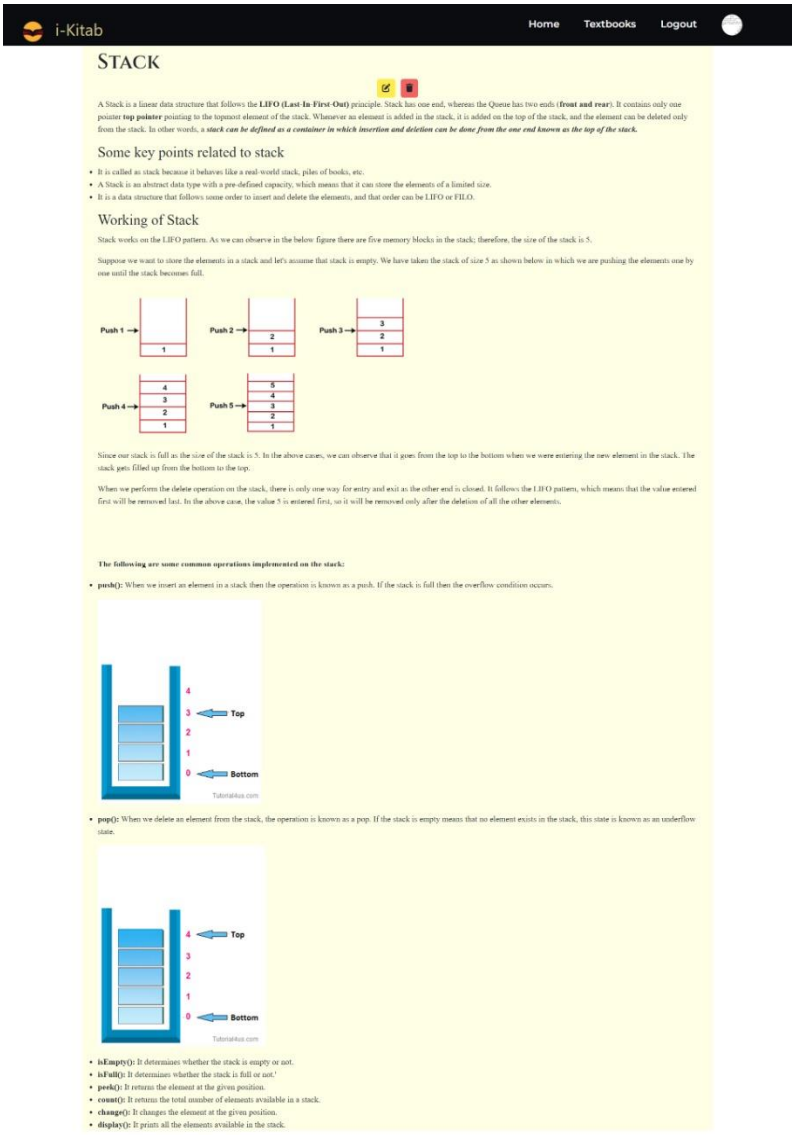

Figure 10. Individual Lesson: This an example of a user textbook.

6. CONCLUSION

Use of interactive textbooks can bring a revolutionary change in education. Through the analysis of various systems, it can be concluded that interactive textbook significantly improves the performance of the user in the subject. When compared to traditional textbooks, it helps the user learn the contents better and retain them for a longer period. The proposed system successfully allows users to not only create interactive textbooks but also share them with other users. Some of the improvements that can be added in future are, quizzes at the end of every lesson, a chatbot can be integrated for better user interaction, and

a few more interactive components can be added to the editor to make the textbooks even more interactive.

REFERENCES

[1] D. Smith, Q. Hao, C. Hundhausen, F. Jagodzinski, J. Myers-Dean and K. Jaeger, "Towards Modeling Student Engagement with Interactive Computing Textbooks", Proceedings of the 52nd ACM Technical Symposium on Computer Science Education, 2021. Available: 10.1145/3408877.3432361.

[2] C. Weng, S. Otanga, A. Weng and J. Cox, "Effects of interactivity in E-textbooks on 7th graders science learning and cognitive load", Computers & Education, vol. 120, pp. 172-184, 2018. Available: 10.1016/j.compedu.2018.02.008.

[3] D. Bikowski and E. Casal, "Interactive digital textbooks and engagement: A learning strategies framework", Dx.doi.org, 2021. [Online]. Available: http://dx.doi.org/10125/44584.

[4] A. Edgcomb, F. Vahid, R. Lysecky, A. Knoesen, R. Amirtharajah and M. Dorf, "Student Performance Improvement using Interactive Textbooks: A Three-University Cross-Semester Analysis", Static.cs.ucr.edu, 2021. [Online]. Available: http://static.cs.ucr.edu/store/techreports/UCR-CSE-2014-10030.pdf.

[5] X. Chen, "A comparative study of visual representations in conventional, digitized and interactive high school science textbooks", Journal of Visual Literacy, vol. 36, no. 2, pp. 104-122, 2017. Available: 10.1080/1051144x.2017.1386388.

[6] B. Nansen, K. Chakraborty, L. Gibbs, F. Vetere and C. MacDougall, "'You do the math': Mathletics and the play of online learning", New Media & Society, vol. 14, no. 7, pp. 1216-1235, 2012. Available: 10.1177/1461444812442926.

[7] R. Spencer, J. Sinno, K. Hatfield, M. Biderman, N. Doria and M. Numer, "Exploring Top Hat's Impact on Undergraduate Students' Belongingness, Engagement, and Self-Confidence: A Mixed Methods Study", Journal of Research on Technology in Education, vol. 52, no. 2, pp. 197-215, 2020. Available: 10.1080/15391523.2020.1722977.

[8] "Pathfinder – JEE, NEET-UG, WBJEE, KVPY Exam Training Institute", Pathfinder.edu.in, 2021. [Online]. Available: https://pathfinder.edu.in/.

[9] "Mathigon – Textbook of the Future", Mathigon, 2021. [Online]. Available: https://mathigon.org/.

[10] "Brilliant | Learn to think", Brilliant.org, 2021. [Online]. Available: https://brilliant.org/.

[11] "Mathletics India | Empowering Mathematics Learning Online", Mathletics India, 2021. [Online]. Available: https://www.mathletics.com/in/.

[12] "The Active Learning Platform for Online, In-Person and Blended Courses | Top Hat", Top Hat, 2021. [Online]. Available: https://tophat.com/

[13] Ishu, K., Bangar, G. & Chawda, J., Lo-fi Mockup. Google Docs. Available at: https://bit.ly/3pMpoMx.

[14] Ishu, K., Bangar, G. & Chawda, J., Hi-fi Mockup. Google Docs. Available at: https://bit.ly/3tuM8kY.

Biographies

Kanupriya Ishu is a final year student of Terna Engineering College pursuing bachelor's degree in information technology. Her research area includes interactive systems and Internet of Things. She has been serving as an author for many highly-respected journals.

Gayatri Bangar is a final year student of Terna Engineering College pursuing bachelor's degree in information technology. Her research area includes interactive systems, machine learning, deep learning and Internet of Things. She has been serving as an author for many highly-respected journals.

Jigar Chawda is a final year student of Terna Engineering College pursuing bachelor's degree in information technology. His research area includes interactive systems.

Vaishali Khairnar received the bachelor's degree in computer engineering from North Maharashtra University in 1997, the master's degree in information technology from Mumbai University in 2006, and the philosophy of doctorate degree in Vehicular ad hoc networks from Nirma Institue of Technology in 2015, respectively. She is currently working as Head of Department at the Department of Information Technology, Terna Engineeing College. Her research areas include interactive systems, machine learning, deep learning and Internet of Things. She has been serving as an author for many highly-respected journals.

Leveraging Facial Recognition Technology in Criminal Identification

Arjun Menon, Kumari Shivani Singh, Raushan Kumar, Ritvik Sethi, Abha Kiran Rajpoot

Sharda University, Greater Noida, India

arjunmnn7@gmail.com, *kumarishivanisingh14@gmail.com*, *raushankumar606@gmail.com*, *ritviksethi56@gmail.com*, *abhakiran.rajpoot@sharda.ac.in*

Abstract

Detecting and identifying a criminal is a time-consuming and complex task. Criminals have become more astute in recent years, leaving no genetic evidence or fingerprint traces at the crime site. Using state-of-the-art facial identification technology is a quick and simple option. Surveillance cameras are being deployed at most buildings and traffic signals for monitoring reasons, thanks to advancements in security technology. Perpetrators, offenders, runaways, and lost individuals can all be identified using the camera's video recordings. This article aims to provide a brief survey of current improvements in face recognition, as well as a complete overview of several approaches to incorporating face detection in criminal identification based on various application scenarios. We also look at the evolution of facial recognition and where it is now in this study. It gives an overview of the internal architecture of a typical face detection system. It also highlights the obstacles that will be faced in instilling facial recognition as well as approaches to improve it while taking various trade-offs into account. It also identifies areas for future research in the incorporation of facial identification in a variety of sectors.

Keywords. Machine Learning, face recognition, neural networks, criminal identification, CCTV.

1. INTRODUCTION

Finding a criminal has proven to be a challenging task over the years. Previously, the whole approach was predicated on leads derived from evidence discovered at the incident site. Genetic evidence is simple to locate. Perpetrators, on the other hand, have developed and are now more skilled than ever at hiding their tracks and avoiding leaving any detectable trace. Facial recognition and surveillance are used in this case. The face is vital for social identity because each face is distinct owing to its distinctive features. Facial recognition for crime detection is a one-of-a-kind bio - metric approach that boasts excellent accuracy while being minimally invasive. It's a technique for naturally recognizing and checking an individual's distinguishing proof from video groupings or photographs utilizing the individual's face. The facial recognition system described in this article is a unique blend of the best facial recognition, classification, and feature extraction algorithms currently

available. MTCNN for recognition and FaceNet for embeddings have already been shown to be effective and state-of-the-art deep learning approaches.

Automated facial recognition is a technique in which a computer extracts important facial characteristics like the width of the nose or jawline, the space between both the eyes, the colour of the eyes, and so on. These traits come in handy when it comes to categorization and record matching. In this system, there are two important processes: detection and recognition. Facial recognition sets in motion two primary processes: training and assessment. The algorithm is fed a sample of pictures model trained on the training set. The facial recognition assessment phase compares the freshly obtained test image to the database [1].

The face is a crucial aspect of humans that reveals their distinct character, feelings, and age, as well as allowing for social interaction [2]. In recent years, biometric-based technologies, such as face recognition, have surfaced as being the most effective and reliable means of recognizing faces. Biometrics is a field that looks at a person's natural characteristics that are specific to the person, and this knowledge gathered might be beneficial in identification of a person [3]. While it is possible for individuals to deny the truth, biometric technologies – that is, inherent biological attributes such as fingerprints, faces and eyes – are relatively more reliable and incredibly hard to thieve since "the body never lies," and changing biometric features is incredibly challenging [4].

2. LITERATURE REVIEW

Nurul et al. [5] use CCTV video and compare the photos from the film with a police database if they don't uncover any fingerprints from the crime site. This technique is divided into five parts, the first of which is planning, wherein the why and how of the technique are examined. The prerequisite to design the system was considered in the second step of requirement analysis. The third step was design, in which they specified the system's workflow. The system is developed and tested using the Principal Component Analysis (PCA) Algorithm in the fourth and last significant stage. Maintenance is the final stage; this phase was skipped because the system was built in a controlled setting. The authors employed the PCA Technique to detect comparable features of photos accessible in the database with acquired images of CCTV for identifying criminals. The system will access a database containing the person's details in order to show the person's information if FRCI recognizes a face. Visual Studio Code is used to create the system interface, while MATLAB R2013b is used for database and code. Using the suggested approach, they were able to attain an accuracy of 80%.

Apoorva et al. [6] employed four phases, the first of which is real-time training using images, and the second of which is face identification using a Haar-classifier. The matching of surveillance camera captured photos with real-time images is the third phase, followed by the outcome section based on the comparison. For face detection, the authors use a Haar-classifier in OpenCV; Haar-cascading is one of the techniques for facial recognition. This algorithm

recognises many people and may be used to locate the suspects we're looking for. In comparison to the existing model, the suggested system has a very high accuracy. They also assured us that by using our Adhar database, we would be able to quickly identify Indians

and foreigners, as well as determine whether or not a person is a perpetrator. We may apply this approach by utilising the currently existing citizen database.

Rupali et al. [7] utilised the database containing passport information to determine if the passenger was an authorised passport holder. They're doing this with computer vision techniques and LBPH statistical models. For airport security purposes, this approach consists of six steps. First, capture a picture using a camera. Second, send the image to the Django server. Third, extract the LBPH feature set from the picture. Fourth, compare the image to a database using a classifier. Fifth, If a match is found, retrieve the user's information from the database. Lastly, email the user's predicted information to the administrator. They process LBPH pictures with webcam photos before applying classifiers and compare them to database images. This will also aid in catching offenders who travel from one nation to another, as well as detecting if the passenger has taken a bank loan, in which case the passenger's comprehensive information will be submitted to the police precinct for authentication.

Mohanty et al. [8] developed a web-based tool called Photo Sleuthing to identify soldiers from the American Civil War, which took place between 1861 and 1865. They said that locating a needle in a haystack is akin to this identifying mechanism. It contains a haystack structure, a narrowed haystack, and a needle in the haystack is found. Using a combination of automatic facial recognition and human knowledge, the team is able to complete their work. When the approach was first introduced, it assisted in the identification of unknown pictures, and the authors highlighted the ramifications for person identification pipelines. They demonstrate how the Photo Sleuthing pipeline has assisted in the identification of thousands of previously unknown photos while also encouraging long-term voluntary participation. Pate et al. [9] published an article in 2016 in which they employed the LEM method for facial identification to locate disappeared persons. The system’s productivity was 85 percent. Muyambo developed a face identification system in his work [10] in 2018 to discover missing individuals in Zimbabwe, which employed the LBPH approach to identify faces. The suggested technique achieved a 67.5 percent facial recognition rate. The LBPH algorithm is not affected by changes in brightness. Qasim et al. [11] have demonstrated a quick algorithm-based facial recognition system. Two datasets are used in this model: Unrestricted Facial Images (UFI) and Olivetti Research Laboratory (ORL). ORL comprises four hundred 92X92 pixel pictures, nine of which are used for training and one image is used for assessing each person. UFI has four hundred and one 128X128 pixel pictures, seven of which are utilized for training and one for assessing each individual. The captured picture is transformed to the HSV format, and then force field characteristics are retrieved. The three distance approaches used for classification are Manhattan, Euclidean, and Cosine. They obtained the best resolution and 99.9% accuracy for the datasets ORL and UFI by comparing these approaches.

A similar investigation of existing work by various creators has been summarised in Table 1.

Table 1. A comparative summary of existing related surveys.

Reference	Contribution
Nurul et al. [5]	Used CCTV footage to identify felons if fingerprints are not available and achieved 80% accuracy.
Apoorva et al. [6]	Used Haar-classifier in OpenCV for facial identification. This technology is capable of detecting many people.
Umbare et al. [7]	Used the passport database to determine whether or not the passenger was a verified passport holder.
Mohanty et al. [12]	Developed Photo Sleuthing to identify unknown portraits.
Pate et al. [13]	Used LEM method for face recognition to locate disappeared persons.
Muyambo et al. [14]	Used LBPH method to track down disappeared individuals in Zimbabwe. The LBPH algorithm is not affected by changes in brightness.
Qasim et al. [15]	Developed an algorithm that achieved an accuracy of 99%.

3. BASICS OF FACIAL RECOGNITION

Facial identification is a method for perceiving or approving a singular's ID by looking at their face. Facial acknowledgment programming can distinguish people in photos and recordings continuously. Police officials might use cell phones to distinguish people. Face identification softwares uses techniques to identify particular, distinguishing features on a being's face. These elements, for example, eye distance or jawline shape, are then changed into a numerical model and investigated with information from different countenances in a facial ID data set. The information about a specific face is in many cases called a face layout and is unmistakable from a photo since it's intended to recognize one face from multiple faces by just incorporating specific subtleties.

3.1. History of Facial Recognition

Facial recognition applications have been emerging since the 1960s, according to [12], which invented the idea of utilising a RAND tablet to coordinate facial characteristics. A gadget called as a RAND tablet was used because it gave the feature to input coordinates using a stylus. The stylus transmitted electromagnetic signals. RAND tablet was used to physically record the coordinates of nose, hair, eyes, mouth etc. facial features.

Goldstein et al. [13] took facial identification to a different level by using 22 specific facial traits such as hair colour, chin, nose elevation, skin colour, and so on. A vast amount of data on the human-assigned values of human faces was acquired. The original 34 features were

whittled down to 22 for which the data is reliable and consistent in terms of the participants who allotted the evaluation metrics. [14] & [15] introduced the world to eigenfaces and statistical techniques to face recognition in the late 1980s. Eigenfaces decrease dimensionality by projecting a sample/training data onto tiny feature faces using Eigenvalues and Eigenvectors. Principal Component Analysis is based on this concept (PCA). Face recognition was used for law enforcement for the first time in 2002. Since then, criminal identification has grown in importance as a facial identification application. [16] Creates a criminal identification system called "FRCI" using the dimensionality reduction approach Principal component analysis. The Haar-Features approach is used in [17], [18], and [19], as mentioned in [20]. The recognition time-frame in a Haar highlights framework is comprised of strong square shapes at the areas of specific elements. In a detection window at a certain position, a Haar-like feature evaluates neighbouring rectangular sections. Adriana et al. suggested a method in [21] that employs eighteen aspects, one of which being RGB, which is used in [22]. Le et al. [23] discusses the use of AdaBoost and ANN together to develop a hybrid model "ABANN" after neural networks became effective in dealing with computer vision tasks like facial identification in 2010. Many deep learning models have been used particularly for facial identification.

Table 2. History of Facial Recognition.

Year	Brief History
1960	Bledsoe coined the approach of using a RAND tablet for coordinating features on the face.
1971	Goldstein, Harmon and Lesk used 22 special facial features like the colour of hair, chin, nose elevation, skin colour etc.
1987	Sirovich and Kirby introduced the world to eigenfaces and statistical approaches to face recognition.
2001	For quick object identification, Viola and Jones employed a boosted cascade of basic characteristics.
2011	Le explains the usage of AdaBoost and ANN together to create a hybrid model "ABANN"
2015	Adriana Kovashka, Margaret Martonosi proposed a system which uses 18 features, one of them being RGB.
2017	Abdullah, Saidi and Rehman used dimensionality reduction technique Principal component analysis for creating a criminal identification system known as "FRCI"

3.2. Workflow of facial recognition system

Figure 1 depicts the fundamental stages required in face identification, which are discussed below:

- Taking an image: The picture that is taken is known as the test picture. With or without the subject's awareness, a closed-circuit camera might be used to capture the image.
- Face detection: The subject's features are detected from the whole picture collected in this stage.
- Features extraction: In this stage, the particular and unique features of the identified face are extracted in for the matching process between them with the matching photographs in this dataset.
- Matching: The resultant image is compared to the database pictures.
- Verification/identification: The final stage is to recognize the individual. A 1:N and 1:1 match is made for identification and verification respectively.

In face-acknowledgment frameworks, the distinguishing proof of the individual is the concluding phase after face recognition, and face to face matching is utilized to work with individual discerning. A face-recognition system was presented in one research as a way to identify a person. The technology worked by communicating between a stationary server and a mobile device, and it had a 95 percent accuracy rate. For the face detection identification, OpenCV Library techniques were employed. The face-detection skills of the utilised recognition algorithms are used to identify people.

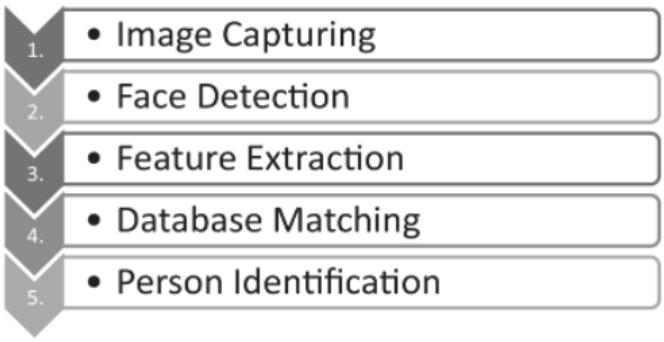

Figure 1. Workflow of facial identification.

4. APPLYING MTCNN AND FACENET FOR FACIAL RECOGNITION

To create a reliable facial recognition system, several strategies for detection, embedding, and recognition must be applied one after the other.

A. Multi-task Cascaded Convolutional Networks (MTCNN) - MTCNN demonstrates a method for detecting and aligning faces in photographs. It comprises a three-part CNN that can distinguish facial landmarks such as the nose, forehead, and eyes. MTCNN is divided into three phases. The image is first enlarged to build a pyramid of images so that detection for all sizes may be done, and then it is processed through a neural network known as P Net,

which outputs face coordinates and bounding box. Faces that are only partially visible are handled within the second step, and bounding boxes are produced using an R net. The P and R net results are quite close. In the third and final stage, an O net is used to provide three outputs: coordinates, landmarks on the face, and bounding box confidence levels. After each step, bounding boxes with low confidence are removed using a non-max suppression approach.

B. FaceNet - FaceNet was introduced in 2015 by a group of Google researchers. The job of face recognition, verification, and clustering was dealt with separately. FaceNet achieves very accurate results by using neural networks and a "triple loss function." The identified face is fed into the model, and the result is a face embedding, which is a vector with 128 components that reflect unique features in this face. A triplet loss function was utilised to train the deep CNN. It's based on the idea that feature vectors of similar faces are more similar than feature vectors of dissimilar faces. Machine learning techniques such as k-NN and SVM can be utilised for identification once the embeddings have been simplified.

4.1. Applying facial recognition in criminal identification

Criminal identification is the most vital responsibility for officers searching for criminals, but it is also the most complex and time-consuming because they must look for it everywhere. It will be more challenging in densely populated cities or public spaces. In certain circumstances, manual identification allows for the gathering of additional information about offenders. As a result, this study develops an automated criminal recognition system that detects offenders' faces. This will aid police in identifying and apprehending offenders in public areas. There are two methods for identifying criminals. Police personnel searching them in public locations use the Manual Identification System (MIS) to identify them. It takes a long time to offer sufficient attention, and it also has the potential to miss criminals since they will be warned by noticing officers and quickly flee the scene. Because the MIS is taking longer than expected, we will not be able to adequately pivot on every being. Talking about an automatic identification system (AIS), however, public inspection is not required. All of the processes in this system are automated here. The following are some key features of an automated criminal recognition surveillance system:

1. Criminal Enrolment: Criminal photographs with names attached to them are put to the criminal database so that the collected images may be compared to those in the database.
2. CCTV Interconnectivity: Cameras should be linked to the system that houses a criminal database and the application that runs on it.
3. Criminal Confirmation: If a person is located in a public location using this method, the criminal database may be used to determine who the culprit was.

4.2. Future scope of facial recognition in crime

Through the use of CCTV cameras located in several locations, an elegant face identification system may be automated to identify thieves. This technique may also be used to locate missing persons after natural disasters and other mishaps. This method may be enhanced to recognise many faces at once and to recognise faces in hazy or cropped photos. A criminal recognition system can also provide information about where the offender was seen utilising

camera locations. To offer extra facts about the offender, the database can include additional details such as age, crimes committed, linked persons last seen, and so on.

5. CONCLUSION

This article tackles the difficulty of using face recognition to detect criminals, which is a significant issue. In terms of data integrity, security, and traceability, traditional criminal identification has a number of flaws. Facial recognition automates the process, and it overcomes all of the disadvantages of traditional criminal identification. Because artificial intelligence powers face recognition technology, it may deliver outstanding results in detecting criminals. Even with the fact that most individuals strive to conceal their identities when engaging in illegal conduct by disguising their faces or covering their identities with scarves, masks, or other means. In these situations, AI uses deep learning techniques to identify the individual. Especially in comparison to other criminal systems such as biometrics or DNA, which require the criminal to leave a physical trace, facial identification may be able to issue a prompt more quickly (both in terms of detection and analysis of various image sources), making an increasing number of police departments around the world to adopt it.

REFERENCES

[1] P. M. and C. Iancu, "Automatic Face Recognition System for Hidden Markov Model Techniques," New Approaches to Characterization and Recognition of Faces, Aug. 2011, doi: 10.5772/17694.

[2] A. K. Agrawal and Y. N. Singh, "Evaluation of Face Recognition Methods in Unconstrained Environments," Procedia Computer Science, vol. 48, pp. 644–651, 2015, doi: 10.1016/j.procs.2015.04.147.

[3] R. Jafri and H. R. Arabnia, "A Survey of Face Recognition Techniques," Journal of Information Processing Systems, vol. 5, no. 2, pp. 41–68, Jun. 2009, doi: 10.3745/jips.2009.5.2.041.

[4] L. Introna and H. Nissenbaum, "Facial Recognition Technology A Survey of Policy and Implementation Issues," eprints.lancs.ac.uk, 2010. https://eprints.lancs.ac.uk/id/eprint/49012 (accessed Sep. 17, 2022).

[5] N. A. Abdullah, Md. J. Saidi, N. H. A. Rahman, C. C. Wen, and I. R. A. Hamid, "Face recognition for criminal identification: An implementation of principal component analysis for face recognition," 2017, doi: 10.1063/1.5005335.

[6] Apoorva P, Impana HC, Siri SL, Varshitha MR, Ramesh B. Automated criminal identification by face recognition using open computer vision classifiers. In2019 3rd International Conference on Computing Methodologies and Communication (ICCMC) 2019 Mar 27 (pp. 775-778). IEEE.

[7] Umbare, Janhavi, Yadav, Pruthvi. 2020. Airport security using face-recognition. International Journal of Future Generation Communication and Networking. vol. 13, No. 3.

[8] Mohanty, Thames, Mehta, and Luther. 2019. Photo Sleuth: Combining Human Expertise and Face Recognition to Identify Historical Portraits. Conference: the 24th International Conference.

[9] Sumeet Pate. 2016. Robust Face Recognition System for E-Crime Alert. In International Journal for Research in Engineering Application and Management, Issue 1.

[10] Muyambo. 2018. An Investigation on the Use of LBPH Algorithm for Face Recognition to Find Missing People in Zimbabwe, International Journal Of Engineering Research & Technology (IJERT) Volume 07, Issue 07 (July 2018)

[11] Kian and Sara, "Force Field Feature Extraction Using Fast Algorithm for Face Recognition Performance", Iraqi Syndicate International Conference for Pure and Applied Sciences.

[12] Bledsoe.1960. Manual measurements.

[13] A.J. Goldstein, L.D. Harmon and A.B. Lesk, "Identification of human faces,"in proceedings of the IEEE, vol 59, pp. 748-760, May 1971.

[14] L.Sirovich and M.Kirby, "Low dimensional procedure for the characterisation of human faces," in Journal of the Optical Society of America A, vol 4, pp. 519-524, 1987.

[15] M. Turk and A. Pentland, "Eigenfaces for Recognition," in Journal of cognitive neuroscience, vol 3, pp. 71-86, Jan 1991.

[16] N. A. Abdullah, Md. J. Saidi, N. H. A. Rahman, C. C. Wen, and I. R. A. Hamid, "Face recognition for criminal Identification: An implementation of principal component analysis for face recognition," AIP Conference Proceedings 1891:1, Oct 2017.

[17] P. Kakkar and V. Sharma, "Criminal identification system using face detection and recognition," in International Journal of Advanced Research in Computer and Communication Engineering, vol 7, pp. 238-243, March 2018

[18] P.Apoorva, H.C. Impana, S.L. Siri., M.R.Varshitha and B.Ramesh, "Automated criminal identification by face recognition using open computer vision classifiers, " in 2019 3rd International Conference on Computing Methodologies and Communication (ICCMC), pp. 775- 778, 2019

[19] P. Chhoriya, "Automated criminal identification system using face detection and recognition", in International Research Journal of Engineering and Technology (IRJET) , vol 6, pp. 910-914, Oct 2019.

[20] P. Viola and M. Jones, "Rapid object detection using a boosted cascade of simple features," in Computer Vision And Pattern Recognition, vol 1,pp. 511-519, Feb 2001.

[21] A. Kovashka and M. Martonosi, "Feature-based face recognition for identification of criminals vs. identification for cashless purchase".

[22] A. Chevelwalla, A. Gurav, S. Desai and S. Sadhukhan, “Criminal face recognition system,” in International Journal Of Engineering Research & Technology (IJERT), vol 4, pp. 47-50, March 2015

[23] T. H. Le. 2011. Applying artificial neural networks for face recognition. Hindawi Publishing Corporation Advances in Artificial Neural Systems, vol 2011, pp. 1-16, 2011

Biographies

Arjun Menon is a final year student of B.Tech Computer Science at Sharda University. Currently he is working as a software engineer intern. His areas of interest are Machine Learning, Web development and Android Development.

Kumari Shivani Singh is a final year student of B.Tech Computer Science at Sharda University. Currently she is working as a software engineer intern. Her areas of interest are Machine Learning, Web development and Android Development.

Raushan Kumar is a final year student of B.Tech Computer Science at Sharda University. Currently he is working as a software engineer intern. His areas of interest are Machine Learning, Web development and Android Development.

Ritvik Sethi is a final year student of B.Tech Computer Science at Sharda University. Currently he is working as a software engineer intern. Her areas of interest are Machine Learning, Web development and Android Development.

Abha Kiran Rajpoot is an M.tech Graduate. Currently working as an Associate Professor in the department of Computer Science and Engineering at Sharda University. Her areas of interest are wireless sensor networks, soft computing and computer networks.

Handwriting Authorship Recognition using Convolutional Neural Networks

Shravani Patel, Daanish Baig*, Dasi Sanjay, Ashwin Kothari

Department of Electronics and Communications Engineering, Visvesvaraya National Institute of Technology, Nagpur, India

**shravanipatel9@gmail.com, daanishbaig@hotmail.com, thesanjayoffl@gmail.com, ashwinkothari@ece.vnit.ac.in*

Abstract

With the advent of imaging and communication technology, files consisting of high-quality images of handwritten text grow increasingly common in academia, business, education, medical sciences, forensic sciences and various other fields. It is often necessary to ascertain the authorship of such data, especially in the cases of education and forensics. Human-based authorship recognition is fairly reliable, but time-consuming and tedious. In this paper, we explore the possibility of using pre-existing convolutional neural network architectures like ResNet50 as well as data augmentation and image pre-processing to accurately identify authorship of a given page of handwritten text. As a result of this work, we were able to train the model and achieve an accuracy of over 80% on a subset of the Firemaker dataset. Overall, we conclude that neural networks have strong potential for rapid and accurate author identification, however, long training times and the large networks required for this level of accuracy somewhat hamper the system.

Keywords. Convolutional neural networks, authorship recognition, handwriting, residual neural networks, ResNet50, machine learning.

1. INTRODUCTION

The rapid growth and combination of old methods of data saving (handwriting) with more modern techniques (digital files) has resulted in a situation where handwritten data is being broadcast as an image, with the intent of it being read as handwritten data. This differs from pure textual data as a person's handwriting is dependent on various criteria such as personality, age, upbringing, education, parents, surface and scribing tool, nervous system health etc. [1-2]. Generally, we consider the case of a generic ballpoint pen on paper. As there are a large number of factors that could potentially affect an individual's handwriting, and these factors could not all be the same across every individual, it is possible to identify individuals based on the unique style of their handwriting, similar to how fingerprints are different for every person and uniquely identify them.

Handwriting identification is a lengthy and time-consuming process. First and foremost, one needs examples of handwriting from known individuals — the more available, the better, as it covers more of the fringe and edge cases that could reasonably be expected from natural variations in an individual's handwriting. One also needs a diverse database with as many samples from different sources as possible. Additionally, the data should be uniform so that

the analysis takes place without needing to consider variations in scribing tool, surface, noise, damage to text etc. Due to the complexity and intricacy of these techniques, they present a suitable target for automation using convolutional neural networks (CNN), support vector machines (SVM) and other automated machine learning (ML) based approaches [3].

This paper uses an existing architecture (ResNet50) which has previously been used for signature verification by various parties [4]. The accuracy of over 90% in this use case was a strong suggestion that it might be suit-able for usage in a broader authorship-recognition environment. The aim of our work is to develop a system that achieves a reasonably high degree of consistent accuracy (80%) over a suitably challenging training and testing dataset. Additionally, only a single page of handwriting is used for training, and the testing and training datasets consist of different texts. The images are segmented, thresholder and resized before being used to train the CNN, which greatly improves accuracy of the results. Further, data augmentation in terms of angle and noise are performed to simultaneously add resistance to rotation and noise, and also to increase the amount of effective training data available.

The applications of the proposed method range across a variety of fields — for example, in academia, it could be used to verify that students are submitting their own work. In forensics, it could suggest connections between writings and people. In medical science, it might work as a diagnostic tool to detect degradation of fine motor skills or neurological issues.

The rest of the paper is structured as follows - Section 2 consists of an explanation of CNNs and ResNet50. Section 3 pertains to the dataset used, as well as the processing applied to it. Section 4 covers the implementation of the machine learning aspect, and various choices made with regards to parameters, learning rate, etc. Section 5 covers the results of the training, and Section 6 concludes the paper.

2. CONVOLUTIONAL NEURAL NETWORKS

A convolutional neural network is a specialized form of an artificial neural network (ANN). As stated by O'Shea et al. in [5], The key difference be-tween ANN and CNN is the neuron organization. In a CNN, the neurons are organized into three dimensions, which consist of height and width of input along with depth i.e. activation volume of the ANN. Neurons of any layer may only connect to a reduced subset of the layers neighbouring, unlike the behaviour of ANNs.

These operations can be represented by convolutions, and can quickly and easily be performed using modern computing technology. Apart from that, they are similar in nature to ANNs i.e. the kernels involved are updated based on the cost function (difference between the expected result and the actual result.)

As a result of these changes, the CNN is much more suitable to image-based applications, especially in cases where a large number of layers are required for complex operations as the problem of overfitting is greatly reduced. In this case, we require the high number of layers and complexity in order to perform the task of identifying the author of a particular

handwritten text based purely on images of the text, as the only information available is image-based i.e. no online stroke or path information is given.

2.1. Residual Networks (ResNet)

CNNs are powerful and exceedingly useful for many applications. Adding additional layers to a CNN would logically improve performance, as the model gains more flexibility and ability to adapt to a particular dataset. However, in practical applications, after a certain level of depth is reached, performance actually starts to degrade. This is due to the 'vanishing gradient problem', wherein gradients from the loss function shrink to zero and the system is no longer able to update any values, effectively stopping the learning process. Residual networks or ResNets are a further specialized form of CNNs, designed to resolve this problem, developed by He et al. [6]. The primary feature of ResNets is the skip-connection feature spanning across layers, al-lowing gradients to flow through them or for inputs to skip past layers of low importance, as seen in Figure 1. Further, it should be noted that the skips occur over intervals of 2 layers in the case of ResNet34, however, this is instead over 3-layer intervals in ResNet50. As a result of this modification, significantly deeper and more powerful neural networks can be used in order to extract features and generate meaningful information from the provided data. In this paper, we have selected ResNet50 as it provides a good balance between nuance and accuracy, and time taken for training and testing.

3. DATA USED

The Firemaker dataset [7] was used for both training and testing the proposed model. Firemaker consists of 4 sets of handwritten text collected from 250 writers. The 4 sets of text are - P1 (sentence case, fixed text), P2 (uppercase, fixed text), P3 (attempted disguising of handwriting) and P4 (description of a cartoon image). Of these, P1 and P4 were selected for training and testing sets respectively, following [8]. This was done so as to simplify the training process, since the handwriting was standardized to some extent. Further, a testing set completely disjoint from the training set was used to mimic practical applications where exact handwriting samples of identical text for comparison would not be available.

3.1. Image Pre-processing

The pre-processing pipeline consisted of the following steps, taken sequentially.

1. 25 writers out of the whole dataset were arbitrarily chosen. Images from set P1 were manually segmented into five paragraphs of roughly equal length.
2. The adaptive thresholding method proposed by N. Otsu [9] was used to improve contrast between the actual text and the background.
3. Data augmentation techniques were used to increase the amount of data available as well as add rotation and noise resistance. This step consisted of two substeps -
    a. Angle augmentation, wherein the data was rotated in increments of 2 degrees, from -10° to +10° offset from the given sample. This boosted the five samples per writer to fifty-five.

b. Next, noise augmentation was performed. Various forms of noise (speckle, salt-and-pepper, Gaussian) were randomly added to the image, based on the findings of Joshua et al. [10] This resulted in the generation of 330 images per writer.

4. The resultants were resized into a standard, uniform shape that was identical for all samples.

5. Similar steps were followed for the P4 set that was used for testing, with the primary difference being that the text was segmented into only two paragraphs.

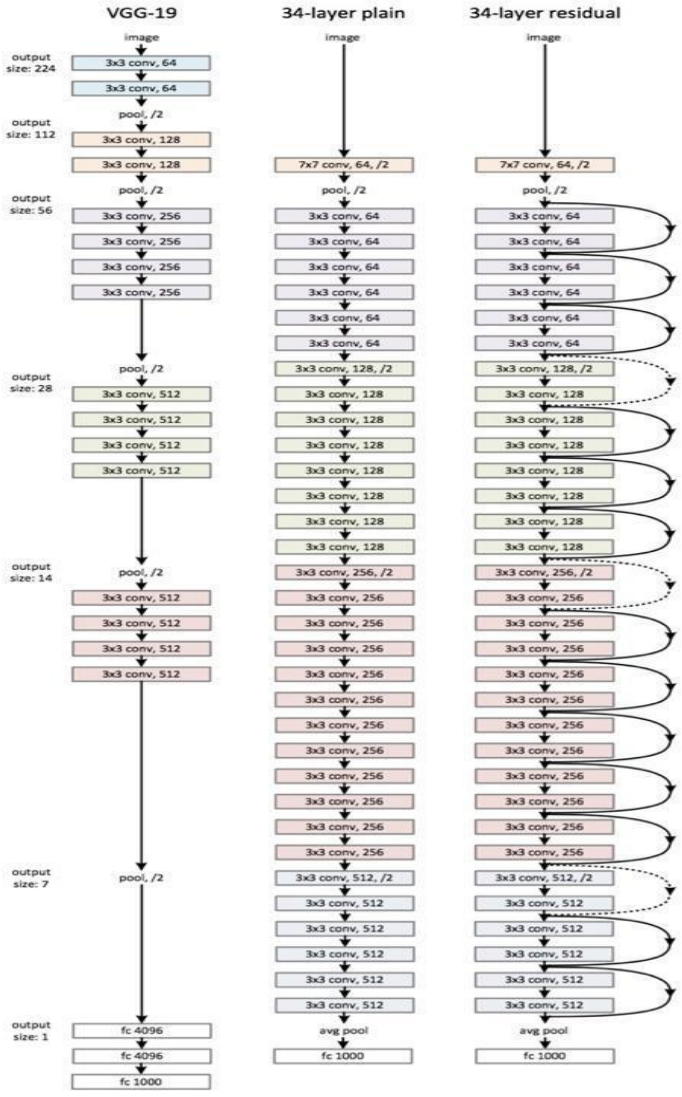

Figure 1. A comparison between a normal 19-layer neural network (VGG-19), a plain 34-layer neural network, and a 34-layer ResNet [3].

4. IMPLEMENTATION

The ResetNet50 model was used to create the proposed model. Of the 23,761,953 trainable parameters, approximately 23,708,833 parameters were used for training, while the remainder were left untrained. The starting weights used in this model were based on those acquired from the ImageNet dataset [11].

This pre-trained model is flattened and sent to a dense layer. Tanh is the activation unit in the fully linked layer, which includes 84 filters. Be-cause our dataset comprises less samples per writer, the dropout layer is employed to avoid overfitting. Softmax is employed as the activation unit for the final linked output. Kernel regularization hyperparameters are also incorporated to make the model less prone to overfitting. The following are the hyperparameters used during the training phase.

Table 1. Parameters used for training the model.

Subset	Learning Rate	L1	Epochs	Validation Split
5 Writer Classification	0.00005	0.001	10	0.10
25 Writer Classification	0.000061	0.00001	15	0.10

The pre-processed images were associated to the corresponding writers and converted into categorical data for use with a CNN. The Adam optimizer [12] was used to increase the rate of convergence towards cost minima as compared to other optimizers. Training was then performed for fifteen epochs, which was the point at which severely diminishing returns per epoch was noted.

5. RESULTS

The model was able to achieve an accuracy of 92% for a set of 5 writers and 82% for a set of 25 writers. This was compared to some other works in terms of Top-1 accuracy on the Firemaker dataset as shown in Table 2.

Table 2. A comparison between various other works and the results of this paper.

Author	Details	Accuracy (%)
Lai et al. [13]	Path signatures	91
Bulacu et al. [14]	Hybrids	83
He et al. [15]	Junclets	80.6
Wu et al. [16]	SDS+SOH	92.4

Khan et al. [17]	DCT features	89.47
He et al. [18]	Quad-hinge	92.2
Proposed method	ResNet50V2 (5 writers)	92
Proposed method	ResNet50V2 (25 writers)	82

The results are on par with the mentioned models, indicating that the proposed model does have the ability to accurately identify writers based only on a training set of one page per writer.

6. CONCLUSION

In this paper, we have introduced a novel data-augmentation and transfer-learning based approach to author identification using existing residual neural network frameworks. The advantages of this proposal are that it uses a pre-trained ResNet as a starting point, greatly cutting down on the length of time required for training to reach a reasonably high level of accuracy. Further, the approach is greatly simplified and easily modifiable to include various other forms of data augmentation, pre-processing or redesigning of the neural network itself. Thus, it is able to be used by individuals with somewhat less experience with machine learning, neural networks or image processing, providing an accessible point of entry for laypersons, academics, students, etc. Limitations of the method include the need for manual data segmentation, which increases the human-time requirement. In future work, the proposed method could be coupled with more extensive data augmentation techniques, enhancing robustness of the input data, as well as automated segmentation of the testing and training data and also training with increased numbers of potential writers.

REFERENCES

[1] O'Shea, Keiron & Nash, Ryan. An Introduction to Convolutional Neural Networks. ArXiv e-prints (2015).

[2] K. He, X. Zhang, S. Ren and J. Sun, Deep Residual Learning for Image Recognition, 2016 IEEE Conference on Computer Vision and Pattern Recognition (CVPR), Las Vegas, NV, USA, 2016 pp. 770-778. doi: 10.1109/CVPR.2016.90

[3] S. Lai and L. Jin, Offline Writer Identification Based on the Path Signature Feature 2019 International Conference on Document Analysis and Recognition (ICDAR), 2019, pp. 1137-1142, doi: 10.1109/ICDAR.2019.00184.

[4] M. Bulacu and L. Schomaker, Text-independent writer identification and verification us-ing textural and allographic features IEEE transactions on pattern analysis and machine intelligence, vol. 29, no. 4, pp. 701-717, 2007.

[5] M. Bulacu, L. Schomaker & L. Vuurpijl Writer identification using edge-based di-rectional features. ICDAR '03: Proceedings of the 7th International Conference on Document Analysis and Recognition, pp. 937-941 Piscataway: IEEE Computer, ISBN 0-7695-1960-1

[6] Hemlata, & Sachan, Manoj & Singh, Shailendra. Personality Detection using Handwrit-ing Analysis:Review. The Seventh International Conference on Advances in Computing, Electronics and Communication - ACEC 2018 10.15224/978-1-63248-157-3-33.

[7] S. He and L. Schomaker, ”Beyond OCR: Multi-faceted understanding of handwritten document characteristics”, Pattern Recognition, vol. 63, pp. 321-333, 2017.

[8] X. Wu, Y. Tang and W. Bu, ”Offline text-independent writer identification based on scale invariant feature transform”, IEEE Transactions on Information Forensics and Security, vol. 9, no. 3, pp. 526-536, 2014.

[9] N. Otsu, A Threshold Selection Method from Gray-Level Histograms IEEE Transactions on Systems, Man, and Cybernetics, vol. 9, no. 1, pp. 62-66, Jan. 1979, doi: 10.1109/TSMC.1979.4310076.

[10] Joshua, Owotogbe & Ibiyemi, T & Adu, B. A Comprehensive Review On Various Types of Noise in Image Processing. International Journal of Scientific and Engineering Research (2019). 10. 388-393.

[11] S. He, M. Wiering and L. Schomaker, ”Junction detection in handwritten documents and its application to writer identification”, Pattern Recognition, vol. 48, no. 12, pp. 4036-4048, 2015.

[12] Irjes, Saini Aishwarya Srinivasan Monika and Anup Kumar Kapoor. Inheritance of Handwriting Features.” International Refereed Journal of Engineering and Science (IRJES). ISSN (Online) 2319-183X, (Print) 2319-1821. Volume 4, Issue 4 (April 2015).

[13] Mr. Nikhil R Shrivastva, Dr. Seema. V. Kedar Author Identification of Handwritten Text: A Review International Journal of Management Technology and Engineering. Page No: 493-499. DOI:16.10089.IJMTE.2019.V9I3.19.27486.

[14] F. A. Khan, M. A. Tahir, F. Khelifi, A. Bouridane and R. Almotaeryi, ”Robust off-line text independent writer identification using bagged discrete cosine transform features”, Expert Systems with Applications, vol. 71, pp. 404-415, 2017.

[15] S. Lai and L. Jin, ”Offline Writer Identification Based on the Path Signature Feature,” 2019 International Conference on Document Analysis and Recognition (ICDAR), 2019, pp. 1137-1142, doi: 10.1109/ICDAR.2019.00184.

[16] J. Deng, W. Dong, R. Socher, L. -J. Li, Kai Li and Li Fei-Fei, ”ImageNet: A large-scale hierarchical image database,” 2009 IEEE Conference on Computer Vision and Pattern Recognition, 2009, pp. 248-255, doi: 10.1109/CVPR.2009.5206848.

[17] Diederik P. Kingma and Jimmy Lei Ba. Adam : A method for stochastic optimization. 2014. arXiv:1412.6980v9

[18] Deshpande, Santosh & Kulkarni, Mukul. . Writer Identification using Neural Network. Test Engineering and Management. 83. 10529 - 10533. 2020.

Biographies

Shravani Patel. Completed a B.Tech (Electronics and Communications Engineering) at Visvesvaraya National Institute of Technology. General interests include digital image processing, embedded systems, and digital logic.

Daanish Baig. Completed a B.Tech (Electronics and Communications Engineering) at Visvesvaraya National Institute of Technology. General interests include data analysis and visualization, digital image processing and digital logic.

Dasi Sanjay. Completed a B.Tech (Electronics and Communications Engineering) at Visvesvaraya National Institute of Technology. Academic interests consist of broadband communication systems and radar engineering.

Dr. Ashwin Kothari, received a PhD from Visvesvaraya National Institute of Technology in 2010, where he now works as an Associate Professor in the Electronics and Communications Engineering Department. Fields of interest include commbedded systems, signal processing and antennas, with a special interest in applications of rough sets.

A Study on building a Video Sharing Website (PlayTube)

[1]Rahul Lokare, [2]Sarvesh Mahadik, [3]Sana Mulani, [4]Smita Deshmukh

Department of Information Technology, TEC, University of Mumbai, Mumbai, India

[1]rahullokare@ternaengg.ac.in, [2]sarveshmahadik@ternaengg.ac.in, [3]sanamulani@ternaengg.ac.in, [4]smitadeshmukh@ternaengg.ac.in

Abstract

In this era, Due to the internet there is a continuous rise in Video sharing websites like YouTube, as it is accessible for all categories of age group. With the approach of Web 2.0, various video sharing sites utilizing different storage and also content conveyance models have become well known. Video sharing sites are a powerful technique to grow in online social networks. Nowadays, Internet is a combination of online social networks (such as Facebook and Google) and film sharing websites (such as YouTube), where the use of video sharing websites is increasing day by day since it provides value to individuals of all ages. People used ICTs solutions for a variety of reasons, including entertainment, education (scientifical), and even business. Videos on video-sharing websites can be a valuable source of information and can be used to improve the efficiency of learning processes. People visit these sites for a variety of reasons, including content consumption, educational objectives, and news. This study aims to develop a site which is scalable to handle high load of files from the server and also define the architecture for streaming files in the system.

Keywords. Video sharing website, short videos, Video recommendation, Online Social Networks (OSNs).

1. INTRODUCTION

In OSNs, video sharing has become increasingly popular, allowing users to upload individual recordings or interesting recordings they've found with their companions. An OSN is a useful tool for forming social relationships as well as sharing, organizing, and discovering content. The traditional client-server design of OSNs video sharing website stymies further advancement because it isn't just exorbitant with regards to server capacity and transfer speed, yet additionally as far as adaptability as the number of clients and video content in OSNs develops.

An internet based informal community is arising as a possible choice for people who need fast access to video content. Users of the online social network have access to a large number of videos because they can import and yet again share them through friendly associations. The growing quantity of user-generated video gives viewers a lot of options for finding ones that they're fascinated in, and it is now possible to combine online social network services via the internet video sharing services. do so. recommendation based on both social and content considerations.

With the advancement of Internet technology, users may now watch and share videos that others have uploaded. People can learn new things, view videos for pleasure, listen to music, and do a lot more on this website. People can also rate it, dislike it, leave comments, and share it with others. Video-sharing services can also be used to bring together like-minded people around a common cause and raise awareness about a problem. This website will serve as a platform for people of all ages.

Not only the online social network changing the way videos are created, but on the other hand, it's changing how video content is seen by crowds Users can track down recordings that interest them on the web-based interpersonal organization because of the enormous amount of recordings accessible. Clients are mentally inspired to import and yet again share motion pictures on the web-based informal community, but choosing which recordings to import or re-share from the gigantic measure of recordings accessible may be troublesome, bringing about appealing ideas for the two activities. We're looking for video suggestions for two fundamental social demonstrations in the web-based informal community to completely use the capability of social video sharing.

Video resources are today used for more than just entertainment; they are also being used to improve knowledge and skills, as well as to promote positive attitudes. The video is preserved on the multimedia host's server, and users can share it with others by using various embedded codes or links. The website is commonly referred to as a video streaming website because it is mostly utilized for video hosting.

2. LITERATURE SURVEY

The project panel analyzed literature from a variety of sources, including research papers, books, current bibliographic information, and recommendations. These figures have yielded a wealth of information.

They offered the SNACS (social network-aware cloud assistance for video sharing), architecture to help the OSN improve its video viewing experience at a lower cost by utilizing content cloud services. They showed that typical In SNACS, cache replacement schemes may be ineffective. They devised the best action replacement algorithm possible. in this novel condition this novel condition, they designed an optimal offline substitution

algorithm that produces the fewest misses. In addition, the method was improved to keep substitutions to a minimum among the solutions with the fewest misses. The finest digital methods are used not just as a reference, but also as inspirations for developing an online replacement algorithm.[3]

The following concerns and challenges confront current video recommendations in the case of digital social networks. (1) They are the result of a misinterpretation of how information spreads through social connections [11], an online social network's distinctive feature. (2) Clients generally give explicit assessments to recordings they've imported as well as re-shared, as opposed to other existing suggestion calculations. (3) Cold-beginning is considerably more troublesome with the present client produced content proposals for two reasons: (a) Because current recommendation algorithms are dependent on users' historical preferences, Users who had recently joined the system had only sometimes uploaded or shared movies., making it impossible to provide content to them. (b) A high percentage of

videos imported by users with few friends have essentially no viewers. It's also difficult to figure out who these contents should be recommended to.

The establishment of YouTube. Its various Features like link generated after uploading the video, Video Format Quality, YouTube Crawler, media servers, Metadata video category generated on a video and social networking aspects. The author created a YouTube Spider and used a combo of YouTube API's employing the breadth first search (BFS) approach to scrape YouTube video web pages to collect information about YouTube videos.

The author also shared some preliminary results from a social media network on how mentoring technology can be used for large-scale live-streaming and how it can be difficult for YouTube.[2] They unveiled SocialTube, a new learning video-sharing, sharing technology that looks at peer social interactions, the similarity of interests, and physical closeness in OSNs. A P2P overlay creation approach based on social networks (SNs), a fragment prefetch mechanism based on SNs, and a buffer strategic approach are all included in SocialTube..[1]

This article demonstrates how the degree to which Depending on how members share data about themselves and the substance they produce, a media circuit is of the "public" sort. They concentrate on two aspects: Making connections with a large number of people while being relatively private in terms of disclosing personal information is what it means to be "privately public." While fostering their companion and endorser records and transferring films with broadly accessible substance, clients in this part keep a few parts of their characters hidden. YouTube like website users and non-famous volunteers who preferred to remain anonymous were among those interviewed in a private setting. One guy, for example, did not want his identity known for fear of compromising his professional credibility with clients and coworkers. Others expressed safety worries and a desire to avoid stalkers [4].

Our recommendation is for user-generated content and re-posts, which means we recommend videos that users like to import or re-share on the web-based informal community. Coming up next are the distinctions between the two social exercises.

Various objectives. Clients work as providers of video material While bringing in recordings to the internet-based informal organization, they are anxious to give recordings that will intrigue their web-based interpersonal organization amigos. At the point when clients re-share films, they are assisting with advancing recordings that have recently been shared via virtual entertainment. network.

A variety of scales. According to our Tencent Weibo data, the number of buys given by clients is multiple times more than the number of re-shares given by clients. On Weibo, clients are more able to create recordings than to re-share old recordings. Different viewpoints impact the proposal. While bringing in a video, a client essentially thinks about the actual video, for example, deciding if the video will bear some significance with his companions; be that as it may while re-sharing a video, the client additionally considers the client who initially shared the video, for example, whether the client will help their companions in appropriating the video. We construct a broad Before offering videos for downloads and re-shares, a model - based approach based on multiple features from the internet network and online streaming sharing network was used for both activities.[11]

The video playback innovation utilized by YouTube is Adobe Flash Player. This strategy empowers YouTube to show recordings in a comparative quality to notable video playing frameworks (like Windows Media Player, QuickTime, and Real player). YouTube permits recordings in an assortment of codecs, including WMV, AVI, MOV, MPEG, MKV, MP4, SWF, FLV, and 3GP, which are then changed over to FLV (Adobe Flash Video) after being posted [8]. It is generally recognized that the utilization of a normalized and effectively playable arrangement is vital to YouTube's prosperity.[6]

Users can request the latest video playing experiences from the MMOD server using the Web Controller, which connects to the MMOD system. Users can also join sessions that have been in progress. Basic tools like VIC and vat can be used to inspect the material.[7]

Drawbacks of client/server architecture in scalability and cost and how Peer-to-peer technology can overcome these issues. They presented video watch data from one of the most popular online social networking (OSNs) sites, Facebook, in this research.[1]

The most firmly related examination can be isolated into two classes: web traffic investigation and video access examination for video-on-request frameworks, without any past reviews of online video access. Demands from a gathering of clients or straightforwardly from the server can be inspected in web traffic examinations. Access patterns at specific servers were explored by Mogul and Kwan [9]

Because video content is sent across a high-bandwidth network, this VOW experiment is unusual. As a result, Users to make selections concerning access without bothering to think about the network. Similarly, the video data that is stored is optimized for a high-speed network. Soam Acharya Brian's research yielded the following results:

Between appearance times: With a middle between appearance term of about 400 seconds, video inquiries are not even close as normal as HTML archive demands. Video browsing habits: consumers frequently watch the first few minutes of videos to see if they are interested. They keep watching if they like what they see. Otherwise, they will come to a halt. In our research, we discovered that around 55% of all playbacks were completed. The majority of the remaining 45 percent stopped watching the video relatively early in the process. Temporal Locality: Video accesses have a strong sense of temporal proximity A video that has previously been viewed is likely to be viewed again soon.

Patterns in document size: As more organization data transmission opens up and low-bitrate streaming turns out to be progressively well known, innovations are carried out in video conveyance, and recordings are expanding. The middle document size at the Lulea University video server was 110 MBytes, because of an expanded organization and a multicast design in view of H.261The average time spent was 77 minutes. [10]

Because of the absence of a simple to-utilize coordinated stage, downloading, putting away, and sharing made distributing, making due, having the option to share, and watching recordings transferring, making due, sharing, and watching recordings very awkward. All the more urgently, the recordings given by standard streaming media servers or distributed document moves, for example, BitTorrent were single pieces of content without any linkages to other video cuts. Web 2.0 capacities are being remembered for the following flood of video-sharing stages. The videos are no longer reliable of one as the clients explore the videos and click on the links. As a result, popular videos may naturally rise to the top. With

320 x 240 resolution display and mono MP3 audio, YouTube employed the Macromedia Spark H.263 video codec. YouTube later added the "mobile" format for viewing on cellular telephones, and also the "top - notch" format for better viewing quality [6]

Moreover, our tracing analysis revealed the highest dynamic localized factor, implying that adding a cache to increase video brand performance could be quite beneficial. With discoveries in mind, Intermediary, a video caching remote server solution, was created. Based on the first studies, the architectural encouraging results. [8]

3. PROBLEM STATEMENT

Sharing video's is an effective and powerful technique to grow in social media networks. A website that allows users to publish and share YouTube videos with the general public or invited guests.

While uploading their videos they face some problems such as reduced quality, lack of flexibility, privacy, website down Low Bandwidth issue. Some issues like Video buffering, loss over data when they watch the videos on site.

So, we are building a website which can overcome all problems faced by the users. In this website people can upload, download and share their videos with flexibility and good quality assurance.

- Logged-in users can create their channel and upload their videos.
- Logged-in users/Guest users can browse, share, like and dislike videos.
- Logged-in users can download the videos from this site if the creator allows.
- Logged-in users can comment on a particular video and can subscribe to the channel.
- Logged-in users can save a particular video for viewing later.
- Logged-in users can create a playlist.

4. METHODOLOGY

Technology used for development is MERN Stack which includes languages like MongoDB, Express, React and Nodejs. For designing front-end React is used. It is a JavaScript library used to create User-Interfaces, usually single page apps as it is quick and scalable. Backend is designed using Express and Nodejs. Nodejs is a server side language designed to run the JavaScript code outside the web browser. Express is Node js framework that aids in the development of web applications. MongoDB is used for database storage. React will send information to the express and node js and then node js will process the user request and it will be saved to the MongoDB database. Express will have the middleware routes which will help to authenticate and validate the user permissions. Mongoose is the package used to create a data model for MongoDB.

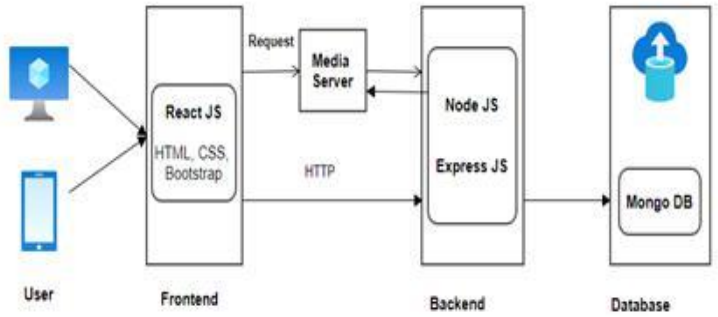

Figure. 1 Block diagram of video sharing website

The above block diagram shows, the user watches the videos on the website and searches for particular videos the request goes to the media server to backend and return to the frontend. Here we use the red5 media server. In this ,media server Automated connection speed optimization Available in a variety of formats, including FLV, F4V, MP4, 3GP, and others. On the PC and mobile devices, live events are streamed. Remote sensing is supported for a variety of protocols. Without buffering, you can play from any region of the screen. Deliver advanced interactive material, such as a video conference or a chat. The client's systems do not store physical data.

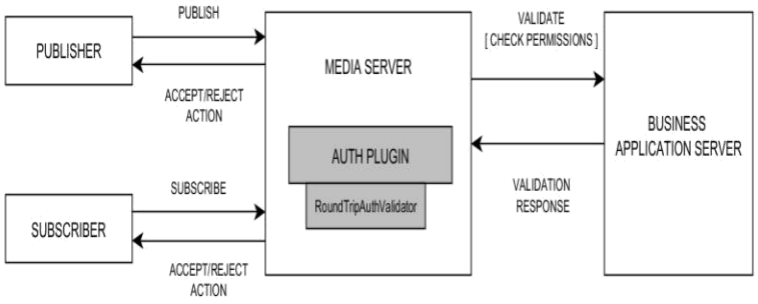

Figure. 2 Architecture Diagram of Video Sharing website

As you can see in the architecture, the media server will take the request from the server and then send that to the backend system for validation after validation backend will again send back the response and then the media server will display the video user requested for. For storing and sharing the media source Red5 media server is used. Red5 is an open-source media server for live streaming arrangements executed in java, for all class of media. It is intended to be adaptable with a straightforward module architecture that considers customization of essentially any Video On Demand and live streaming situation. Red5 has been and is being utilized by great many organizations from Amazon to Facebook. Red5 Media Server is presently utilized for live streaming over Flash, including HLS, WebSocket's, and RTSP. RTMP is used by the Red5 media server. The Real-Time Messaging Protocol (RTMP) stands for Real-Time Messaging Protocol. It's built on the TCP protocol, which is used to transmit music, video, and data over the Internet. Low-latency and high-rate streaming are provided by RTMP.

Data Models as Follows:-

The Backend Design of this website consists of various sections like models, category, controllers, auth, playlist, video, Thumbnail, user, authentication , comments. The app backend consists of models like user, video, category, thumbnail comment and playlist. The authentication process like sign in, signup, sign out. The video model consists of like, dislike, save, delete, update, create videos options.

The isAdmin, isAuthenticated are the middlewares. Middleware functions are the functions that have access to request to objects, response objects. The middleware executes the code, makes changes to the access and response objects, completes the request-response cycle, and calls the next middleware on the stack. The primary keys are getCommentById, getPlayListById, getUserById, categoryById, getVideoById These primary keys are used to fetch the data from the backend.

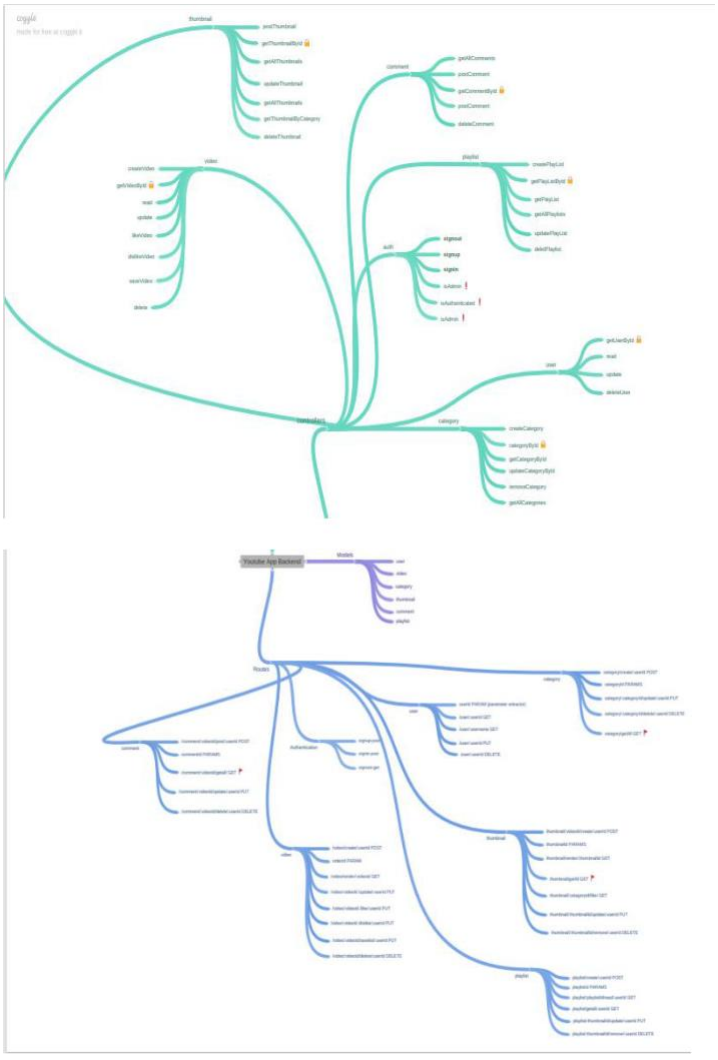

Figure. - 3 Backend Design

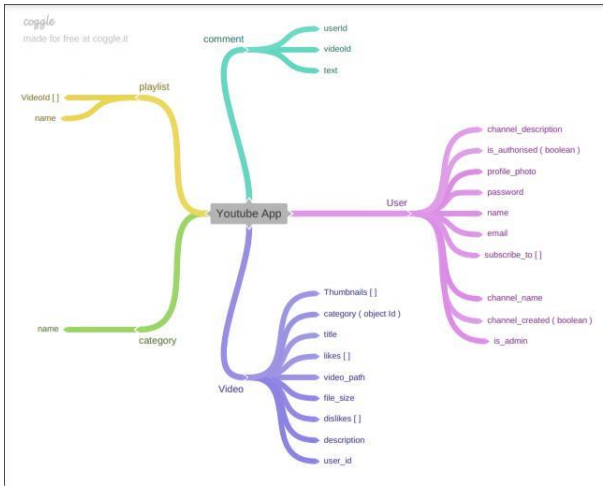

Figure. 4 Database Design

The database design has various subsections like playlist, comment, Thumbnails, User, category and video section. The User section has various parts like name, email, password, profile photo, is_admin . If the user creates the channel then the user allows the options like channel_created, subscribers. If the user is watching videos and the user wants to like and dislike videos then the user needs to sign in or sign up using gmail id. The user is authenticated successfully then only allows for further options. The middleware functions are the functions that have access to request to objects, response objects. In data modelling, dealing with the demands of the application, the database engine's technical specifications, and data retrieval patterns is a big difficulty. When building data models, take into account the data's application usage (i.e. queries, updates, and processing) as well as the data's intrinsic structure. The mapping of documents to entities or objects is made easier by flexibility. Every document in the collection is unique. differs in some manner from the others. The structure of documents and how the application displays data interconnections are the most essential factors to consider when creating database systems for MongoDB. MongoDB makes it possible to combine important data into a single document.

5. RESULTS

The screenshots of the PlayTube video sharing website.

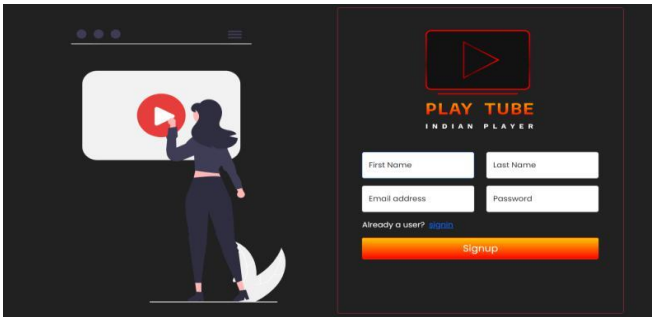

Figure. 4 Sign up page

The above screenshots shows the sign up page where the user have to fill the details like First name, last name email address and password.

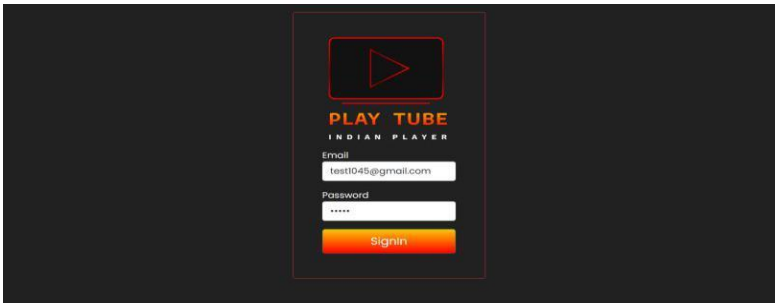

Figure. 5 Sign in page

The above screenshot represents the user sign in page.

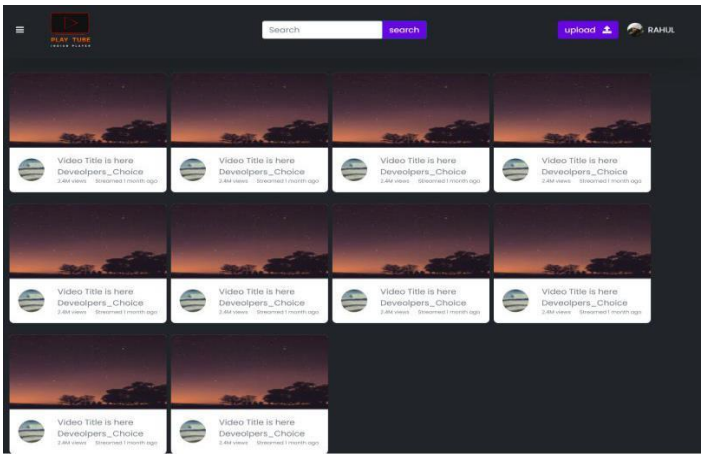

Figure 6. Home page

The result shows the home page of the website. In this, each video show with video title with views and subscribe button to subscribe the channel.

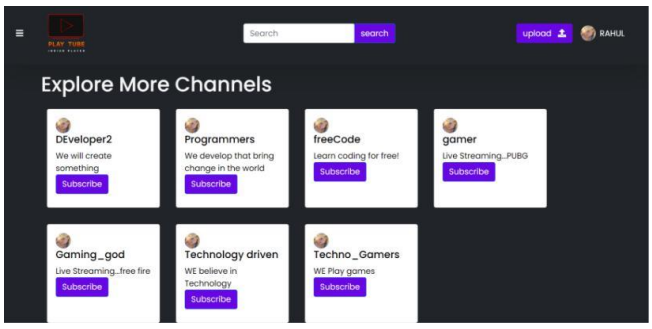

Figure 7. Explore page

The Explore page shows the various channels to subscribe to.

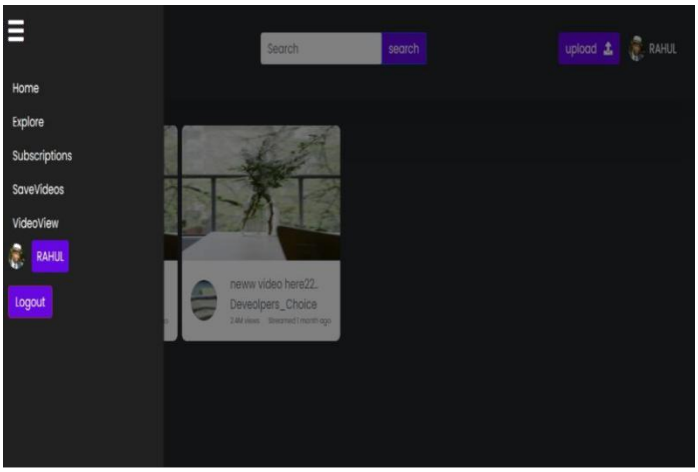

Fig no. 8. Navigation Bar page

This has functionalities like Home, Explore, Subscription, Saved Videos, Profile and Logout options.

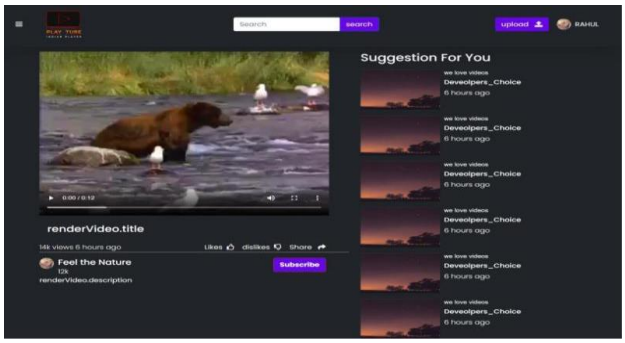

Figure. 9 Video View Page

The above result shows the specific video in zoom in or zoom out mode. The user also sees the related videos to the right side of the videos. The user like, dislike, comment and subscribe to the video or channel on this page.

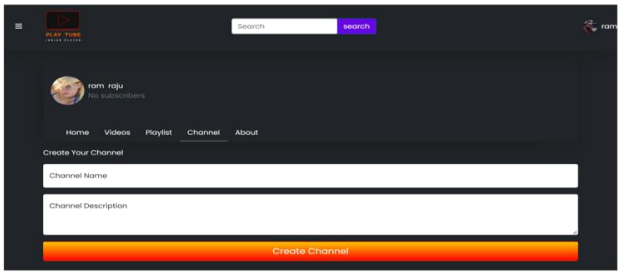

Figure 10. Upload video page

User can upload their videos in their own channel.

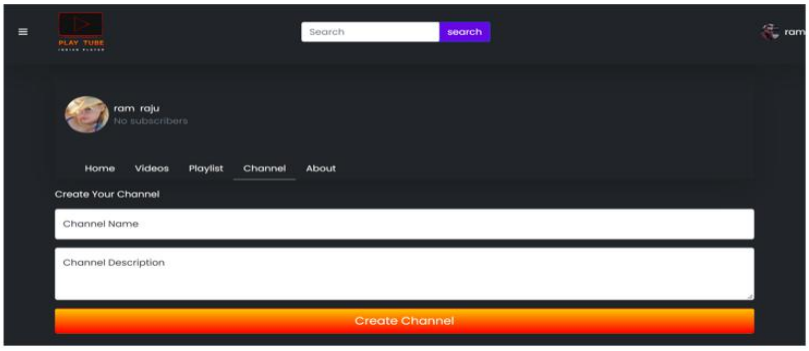

Figure 11. Create Channel page

6. CONCLUSION

The video sharing website is popular in the present world. The people exploring and browsing the videos. They create their video and upload it on the website, where other users watch those videos and like, dislike and comment on it. The people can also subscribe to the channels to watch more upcoming videos. The platform provides the learning, motivational, entertainment and variety of videos. This platform is more interactive with the user. The main aim of this website is to provide a platform for videos with good quality.

REFERENCES

[1] X. Cheng, J. Liu and C. Dale, "Understanding the Characteristics of Internet Short Video Sharing: A YouTube-Based Measurement Study", *IEEE Transactions on Multimedia*, vol. 15, no. 5, pp. 1184-1194, 2013. Available: 10.1109/tmm.2013.2265531.

[2] A. Lo, M. Esser and K. Gordon, "YouTube: A gauge of public perception and awareness surrounding epilepsy", *Epilepsy & Behavior*, vol. 17, no. 4, pp. 541-545, 2010. Available: 10.1016/j.yebeh.2010.02.004.

[3] Q. Zea and J. Heekyoung, "Learning and Sharing Creative Skills with Short Videos: A Case Study of User Behavior in TikTok and Bilibili", *international Association of Societies of Design Research Conference 2019*, p. 15.

[4] P. Lange, "Publicly Private and Privately Public: Social Networking on YouTube", *Journal of Computer-Mediated Communication*, vol. 13, no. 1, pp. 361-380, 2007. Available: 10.1111/j.1083-6101.2007.00400.x [Accessed 27 September 2022].

[5] H. Li, F. Wang, J. Liu and K. Xu, "SNACS: Social Network-Aware Cloud Assistance for Online Propagated Video Sharing", *2015 IEEE 8th International Conference on Cloud Computing*, 2015. Available: 10.1109/cloud.2015.120.

[6] M. Saxena, U. Sharan and S. Fahmy, "Analyzing Video Services in Web 2.0: A Global Perspective", *NOSSDAV '08 Braunschweig, Germany*, p. 6. Available: ACM 978-1-60588-157-6/05/2008.

[7] M. Ferhatoglu, A. Kartal, U. Ekici and A. Gurkan, "Evaluation of the Reliability, Utility, and Quality of the Information in Sleeve Gastrectomy Videos Shared on Open Access Video Sharing Platform YouTube", *Obesity Surgery*, vol. 29, no. 5, pp. 1477-1484, 2019. Available: 10.1007/s11695-019-03738-2.

[8] M. Tatsuya, K. Ryoichi, H. Haruhisa and S. Shinsuke, "Characterizing Traffic Flows Originating from Large-Scale Video Sharing Services", 2010. Available: 10.1007/978-3-642-12365-8_2

[9] M. Li, M. Claypool, R. Kinicki and J. Nichols, "Characteristics of streaming media stored on the Web", *ACM Transactions on Internet Technology*, vol. 5, no. 4, pp. 601-626, 2005. Available: 10.1145/1111627.1111629.

[10] R. L. T. and B. P. S, "Characterizing the YouTube video-sharing community", p. 8, 2022. Available: MG 31270-901.

Framework of a Health Care Information Retrieval System

Pandaram Sathish Kumar, Shashi Mehrotra*

Department of Computer Science and Engineering, Koneru Lakshmaiah Education Foundation, Vaddeswaram, AP, India

**sethshashi11@gmail.com*

Abstract

In these years, digital medical data has increased exponentially, and web search is becoming very common. Information Retrieval (IR) provides users with the needed information. However, it is tedious retrieving relevant information for several reasons. One important reason is more than one meaning of the word. The medical domain is sensitive, and appropriate and timely information retrieval is necessary. To enhance medical information retrieval, we present an information retrieval framework for retrieving articles and medical information according to the query given by the user. We used a vector space model. The health care information retrieval system would be helpful for doctors, patients, and researchers to get information related to their queries. The retrieved related medical records could help in diagnosing and treatment of associated diseases. We used data set TREC-15, for experimental evaluation of the model and obtained promising experimental results.

Keywords- Machine Learning, Information retrieval, Document Term Matrix

1. INTRODUCTION

Medical information searching is becoming very common in present days of digital era and the availability of huge digital data. Health care retrieval systems are very help full for various types of users, such as patients, doctors, and researchers, to access medical information [19]. An information system is understood as a method of searching of information from the web. Users expect relevant retrieval of contents for the query given by them. The query given is matched with the metadata that is about the details in the contents collection. The user needs some sort of information, and the need is formed as a query. Matched documents with the query are returned as a search result. The information is now available on many types of platforms like websites, social media platforms like Twitter, Github, and records of hospital. Searching for health content is very popular these days, and it is the foremost important domain in information retrieval [22]. Physicians want evidence related to the best curing methods for their patients' diseases.

These evidences are available in articles, historical books, and reports which are earlier faced by some expert physicians, researchers. The analysis presented in [22] shows that most commonly search is done for the following information, specific disease related information, treatment, doctors, hospitals, medical insurance, food, drug safety, health or environmental threat [22].

Information retrieval for medical is challenging as medical sciences is very vast and diverse [18, 22]. Publications and organizations are some examples of information resources [22]. The major challenge of IR is the heterogeneity of the information resources. Search engines display retrieved information in the list form. It is very tedious searching for information relevant to the user from the long list [3,4]. Information retrieved and stored in the meaningful cluster would be helpful for efficient searching, where clustering could be used [5,6,7,8]. In [9], the author explored the evolutionary approach of clustering for searching [9].

The remainder of the paper is organised as follows: Section 2 is literature survey discusses related research, and section 3, presents the methodology of our study. Section 4 presents experimental results and analysis, and section 5 is the conclusion and future work.

3. DESIGN AND METHODOLOGY

Medical information retrieval is a sensitive and challenging task. This section discusses some related research. Abadeh MS [1] discussed approaches to dilute fuzzy systems with learning methods made in soft computing. Neural and fuzzy systems will dilute the approximate reasoning method of fuzzy systems with the capabilities of learning neural networks and algorithms. He also said that genetics-based learning algorithm and discussed its usage to detect intrusion in a computer network. Aravind et al.[2], He presented that they will describe a magnificent approach to fetch related medical articles from PubMed collection, based on a required given query. So his Information Retrieval system consists of 3 parts: inverted indexing using Lucene, lexical query expansion to increase recall with Meta Map, and reranking aimed at optimizing the system. He evaluated his system using 30 medical queries. Yang [10], disc ered in his study that the present search engines in web often cannot handle the medical search efficiently because of not considering the special requirements of search. An uncertain procedure for a medical information searcher about questions and is unfamiliar with medical terminology. So, the author sometimes prefers to pose long queries, saying symptoms and the situation in English to receive information relevant from the search results. Eysenbach Gunther [11] identified that e-Health is an essential field in bisecting the medical informatics, business, referring to health services and information enhanced by searching on the Internet or related technologies. More broadly, it characterizes both technical development and state of mind and attributes like attitude, commitment, global thinking, to improve health care logically, and communication technology. Estrela [12] discussed the importance of Medical Image Processing in e-health and telemedicine. This will enable rapid diagnosis with visual, quantitative, and analytical assessment. Remote care could reveal some important changes that indicate a therapy progression. For example, Covid disease evaluation uses behavioural tests, PET scans and MRI of the whole brain. The collection of diverse images offers some chances to improve diagnosis the evidence-based. So there is some need for proper methods to search some of these collections for images with similar images. Wang et al. [13], stated that medical information retrieval set a goal to discover the scientific evidence to support decision making with some knowledge in the medical domain. Knowledge developed by domain experts is able to enhance the understanding of the free text with some knowledge in the domain. Structured knowledge bases represent the information as a group of knowledge graphs consisting of nodes and edges. This representation has a long history in logic and artificial intelligence. Strictly, UMLS is used chiefly knowledge base in the medical domain. UMLS

is a classroom of biomedical terms and concepts. Kasban et al. [14], presented a method to retrieve the medical images for searching the required image for the query image in the database. Nishant et al. [16], experimented with Random Forest. Bayesian Classification, Decision Tree, and SVM for medical Data. The SVM algorithm demonstrate highest precision and F-measure. Nishant et al. [17] presented an experiment with sampling methods to improve classifiers' performance. Most of the data in the medical is a class imbalance. Therefore, it is required to apply some sampling methods before any classification to improve the performance. Di Girolamo, Nicola [20], used and evaluated the Bayesian algorithm for information retrieval and clinical decision support.

4. DESIGN AND METHODOLOGY

This section present methodology we used in our study, and the data details used for the experiments.

3.1 Vector Space Model:

It is a very popular framework for applying term weighted. Term frequency inverse (TF-IDF) is used to weight the term, which shows the term's importance [25].

Following formulas for representing the documents as a vector space model. In this model, each document is considered as a vector in the term-space.

Inverse document Frequency = 1/(log(DF)+1) (1)

TF-IDF = TF*(1/(log(DF)+1)) (2)

TF – (count of a required word in query)/ (Total no of words in the document)

DF – (No of documents that contain the required word)/(Total number of documents present in the corpus)

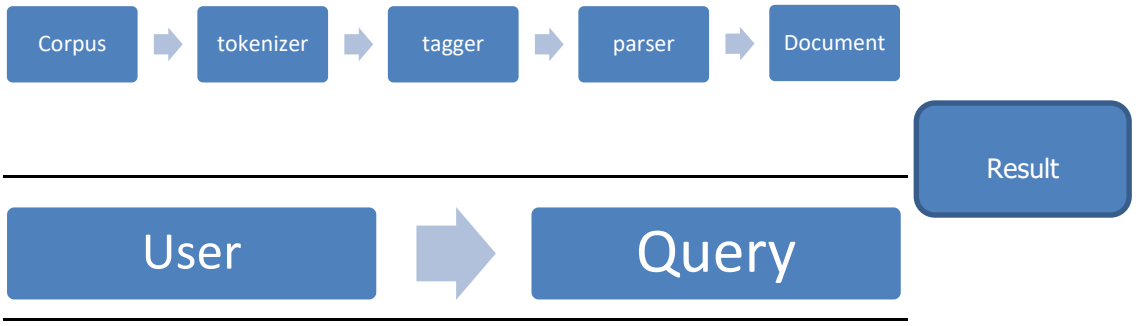

Figure 1. Workflow of our process

3.2 Data Description

We used the TREC-15 dataset for this project. TREC-15 consists of 128491 rows and four columns.

Dataset consists of columns like topic-id, query, question, and narrative.

Topic id refers to the id of the topics. Query refers to the type of query that the user is giving. The second dataset consists of country, latest, long, and dates columns. The country says the country in which the given covid cases are registered. The latest gives the number of cases up to then those are registered. Long gives the largest number of cases registered in a period. Dates represent the covid cases recorded on the specific date.

3.3 Relevance based Evaluation:

The main goal of the IR system is to retrieve relevant information/documents. We considered the relevance and diversity of the search for the evaluation. To measure how the models performed in this regard, we use precision, recall, and f-measure matrices. Information retrieved could be true positive (TP), false positive (FP), true negative (TN), or false negative (FN). TP + FP are the total numbers of documents retrieved, while TP+FN are the relevant documents [23].

Precision is a fraction of the relevant documents retrieved.

Precision = (TP) / (TP + FP) (3)

Recall is fraction of the relevant documents retrieved from the data.

Recall = (TP) / (TP + FN) (4)

F-measure is harmonic mean of precision and recall.

F-measure = 2*(precision*recal)/(precision + recall) (5)

5. EXPERIMENT AND RESULT ANALYSIS

The Figure 2, presents pie chart with various categories of queries in the data.

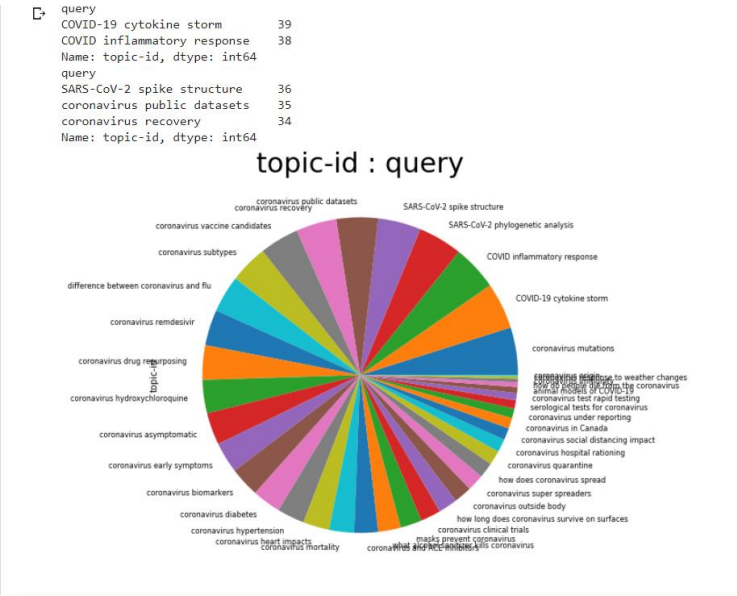

Figure 2. Number of occurrences queries

We can observe in the Figure 2 queries and their count, and pie chart with classification of queries.

	topic-id	cord-id
0	1	010vptx3
1	1	02f0opkr
2	1	04ftw7k9
3	1	05qglt1f
4	1	0604jed8
...	...	...
20723	35	zp4oddrt
20724	35	zppc6p20
20725	35	zrobzakn
20726	35	zwjvvio0
20727	35	zzmfhr2s

20728 rows × 2 columns

Figure 3. Documents retrieved

6. CONCLUSION AND FUTURE WORK

The paper presents a health care information retrieval framework. Searching for various information is becoming very common in our day-to-day life due to the massive usage of internet and the availability of digital data. Various health related people such as doctors, patients, health insurance seekers, researchers etc. could be benefited from a lot of available information on web.

REFERENCES

[1] Abadeh, M. S., Habibi, J., & Lucas, C. (2007). Intrusion detection using a fuzzy genetics-based learning algorithm. *Journal of Network and Computer Applications*, *30*(1), 414-428.

[2] Aravind, M., Viswanath, S., Mohan, N., Adarsh, R., & Bhaskar, J. (2019, December). A modified medical information retrieval system. In *2019 IEEE 9th International Conference on Advanced Computing (IACC)* (pp. 218-222). IEEE.

[3] Mehrotra, S., & Sharan, A. (2020). Comparative Analysis of K-Means Algorithm and Particle Swarm Optimization for Search Result Clustering. In *Smart Trends in Computing and Communications* (pp. 109-114). Springer, Singapore.

[4] Nishant, P. S., Mehrotra, S., Sree, P. R., & Srikanth, P. (2020, August). Hierarchical clustering based intelligent information retrieval approach. In *2020 Third International Conference on Smart Systems and Inventive Technology (ICSSIT)* (pp. 862-866). IEEE.

[5] Mehrotra, S., & Kohli, S. (2016). Application of clustering for improving search result of a website. In *Information Systems Design and Intelligent Applications* (pp. 349-356). Springer, New Delhi.

[6] Mehrotra, S., & Kohli, S. (2015, October). Comparative analysis of K-Means with other clustering algorithms to improve search result. In *2015 International Conference on Green Computing and Internet of Things (ICGCIoT)* (pp. 309-313). IEEE.

[7] Mehrotra, S., Kohli, S., & Sharan, A. (2018). To identify the usage of clustering techniques for improving search result of a website. *International Journal of Data Mining, Modelling and Management*, *10*(3), 229-249.

[8] Mehrotra, S., Kohli, S., & Sharan, A. (2019). An intelligent clustering approach for improving search result of a website. *International Journal of Advanced Intelligence Paradigms*, *12*(3-4), 295-304.

[9] Mehrotra, S., & Kohli, S. (2016, March). Identifying evolutionary approach for search result clustering. In *2016 3rd International Conference on Computing for Sustainable Global Development (INDIACom)* (pp. 3778-3782). IEEE.

[10] Change to [2.2]Yang, L., Mei, Q., Zheng, K., & Hanauer, D. A. (2011). Query log analysis of an electronic health record search engine. In *AMIA annual symposium proceedings* (Vol. 2011, p. 915). American Medical Informatics Association.

[11] Eysenbach, G. (2001). What is e-health?. *Journal of medical Internet research*, *3*(2), e20.

[12] Estrela, V. V., & Herrmann, A. E. (2016). Content-based image retrieval (CBIR) in remote clinical diagnosis and healthcare. In *Encyclopedia of E-Health and Telemedicine* (pp. 495-520). IGI Global.

[13] Wang, H., Zhang, Q., & Yuan, J. (2017). Semantically enhanced medical information retrieval system: a tensor factorization based approach. *Ieee Access*, *5*, 7584-7593.

[14] Kasban, H., & Salama, D. H. (2019). A robust medical image retrieval system based on wavelet optimization and adaptive block truncation coding. *Multimedia Tools and Applications*, *78*(24), 35211-35236.

[15] Mourão, A., Martins, F., & Magalhaes, J. (2015). Multimodal medical information retrieval with unsupervised rank fusion. *Computerized Medical Imaging and Graphics*, *39*, 35-45.

[16] Nishant, P. S., Mehrotra, S., Mohan, B. G. K., & Devaraju, G. (2020). Identifying Classification Technique for Medical Diagnosis. In *ICT Analysis and Applications* (pp. 95-104). Springer, Singapore.

[17] Nishant, P. S., Rohit, B., Chandra, B. S., & Mehrotra, S. (2021). HOUSEN: Hybrid Over–Undersampling and Ensemble Approach for Imbalance Classification. In *Inventive Systems and Control* (pp. 93-108). Springer, Singapore.

[18] Sheikhshoaei, Fatemeh, Gholamreza Roshandel, Marzieh Zarinbal, MolukoSadat Hosseini Beheshti, Mohammadhiwa Abdekhoda, Auwal Abdullahi Abubakar, and Masoud Mohammadi. "Mapping Global Knowledge Domain, Research in Information Retrieval in Medical Sciences: A Scientometric and Evaluative Study." (2021).

[19] Di Girolamo, Nicola. "Advances in Retrieval and Dissemination of Medical Information." *Veterinary Clinics: Exotic Animal Practice* 22, no. 3 (2019): 539-548.

[20] Balaneshinkordan, Saeid, and Alexander Kotov. "Bayesian approach to incorporating different types of biomedical knowledge bases into information retrieval systems for clinical decision support in precision medicine." *Journal of Biomedical Informatics* 98 (2019): 103238.

[21] Gudivada, Akhil, and Nasseh Tabrizi. "A literature review on machine learning based medical information retrieval systems." In *2018 IEEE symposium series on computational intelligence (SSCI)*, pp. 250-257. IEEE, 2018.

[22] Hersh, William, Hersh, and Weston. *Information retrieval: A biomedical and health perspective*. New York: Springer, 2020.

[23] Hersh, William. "Evaluation of biomedical text-mining systems: lessons learned from information retrieval." *Briefings in bioinformatics* 6, no. 4 (2005): 344-356.

[24] Xu, Bo, Hongfei Lin, Yuan Lin, Yunlong Ma, Liang Yang, Jian Wang, and Zhihao Yang. "Improve biomedical information retrieval using modified learning to rank methods." *IEEE/ACM Transactions on Computational Biology and Bioinformatics* 15, no. 6 (2016): 1797-1809.

[25] Baeza-Yates, Ricardo, and Berthier Ribeiro-Neto. *Modern information retrieval*. Vol. 463. New York: ACM press, 1999.

Biographies

Pandaram Sathish Kumar received the bachelor's degree in computer science and engineering from K L University in 2020, pursing the master's degree in computer science and engineering from KL University, respectively. He contributed research papers in international conferences. He participated workshops/seminars related to machine learning. His area of interest is Natural Language Processing, Artificial Intelligence, Machine Learning, and Deep Learning.

Shashi Mehrotra completed her Ph. D from Birla Institute of Technology, Mesra, Ranchi, in the area of Information retrieval. M.Tech in Computer Engineering from ITM Gurgaon, MCA, and M.Phil from Madurai Kamaraj University. She is actively engaged in teaching and research in areas of Computer Science. Currently working as an Associate Professor in the Department of Computer Science and Engineering at KL University, Vaddeswaram, India, since 1/12/2017. She contributed research papers in national/international journals/conferences/symposiums of repute, participated in keynote speech delivery, and invited talk. She has organized many professional activities like special sessions in conferences/FDPs, workshops, and expert lectures as an editorial board member or as a reviewer for several international journals and conferences. Her research interest includes Text mining, Machine learning, and Deep learning.

Design of an Optical Filter using Side Coupled Series of Optical Ring-Resonators

Yash R Bawankar and Anamika Singh

Department of Electronics and Communications Engineering, Visvesvaraya National Institute of Technology, Nagpur, India

yash.bawankar7@gmail.com, anamikasingh@ece.vnit.ac.in

Abstract

Silicon Photonics is one of the emerging technologies which offer variety of applications and several advantages over the current technology once unified with Photonic Integrated Circuits (PIC's). This integration of both the fields is possible due to over the decade research and the compatibility of PIC's which can be fabricated using the CMOS fabrication technique once they are designed and used along with Silicon Photonics technology. In this paper, a design of optical micro-ring resonator which includes multiple rings between two waveguides adjacently placed to obtain an optical filter to drop certain band of wavelengths has been proposed. These micro-ring resonators find various applications in different fields due to their high-speed readout, compact size and very low to almost zero electromagnetic interference.

Keywords: Silicon photonics, optical filters, micro-ring resonators.

1. INTRODUCTION

Optical micro-ring resonators can be considered as one of the best example amongst the passive photonic devices. An optical micro-ring resonator is basically an integrated optic travelling wave resonator which is constructed by bending and forming a closed loop of an optical waveguide, generally racetrack and circular shape [1]. When this round-trip length is exactly equivalent to an integral multiple of wavelength of light within the waveguide, large intensity buildup and sharp resonances occurs due to constructive interference of light inside microring cavity [2]. This is possible due to bus or access waveguides through which light couples in and out of the waveguide and the microring waveguide placed adjacent to it. Depending on the number of bus waveguides placed adjacent to the microring, they are classified into different configurations. Most common configuration are "All pass ring-resonator" and "Add Drop ring-resonator". Different configuration possesses different spectral characteristics and spectral response which is shown in Fig. 1.

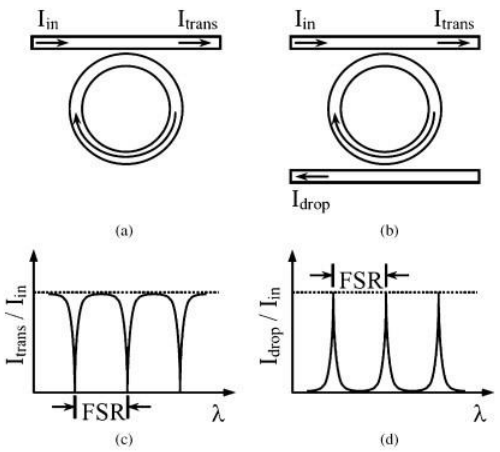

Figure 1 Two basic configuration of micro-ring resonators: (a) All Pass configuration. (b) Add-Drop configuration. (c) Spectral response at transmission ports in both configurations. (d) Spectral response at drop port in Add-Drop configuration [3]

On the basis of different configuration of microring resonators, transmission spectrum with single ring cavity placed adjacent to the bus waveguides shows dips after regular time intervals when the ring is in resonance i.e., they support multiple resonances [3]. Supporting multiple resonances is considered as one of the major property of microring resonators and spacing between respective resonances is called as *free spectral range* (FSR) which is directly proportional to the resonator length. In this way, due to its spectral response, a microring resonator can be utilized as a spectral filter in optical communication field. However, this spectral response changes due to several factors such as ring radius, distance between the waveguides, number of rings and also distance between waveguides and rings. Depending on multiple rings placed between the waveguides, two configurations named as coupled optical resonator and side coupled sequence of ring resonators were introduced.

In this paper, we have explored the side coupled sequence of ring resonators configuration of microring resonators to obtain an optical filter to drop certain band of wavelengths.

2. THEORETICAL BACKGROUND ON OPTICAL FILTERS

A filter is a device or structure which alters characteristics such as phase, amplitude or group delay in a desired fashion of an input signal. Synthesis of optical filters is one of the most important applications of optical microring resonators. Due to their compact size and strong dispersive characteristics around a resonant frequency, ring resonators are widely used for construction of higher order integrated optical filters. In optical networks, important characteristic which makes optical microring resonators to be used as optical filters is their tunability. Micro-ring resonators also enables synthesis of large scale photonic integrated circuits due to their small dimensions and non requirement of grating and facets for optical feedback [4].

As shown in Fig. 2, all pass and add-drop ring resonators gives a sharp dip and highs in filter responses, they are mainly used to add and drop particular wavelengths. Hence are mostly used as optical notch filter. But to add and drop certain range of wavelengths i.e. to have control over certain band of frequencies, it was found that on adding multiple rings between waveguides similar ring resonators which acts as notch filter can be used as band stop filter [5]. This new design lead to new configuration with multiple rings namely coupled optical resonator and side coupled sequence of ring resonators configuration. The parallel cascaded array of add-drop and all pass microring resonators are called single-channel and dual-channel side coupled sequence of ring resonators, whereas serially coupled arrays are called as coupled optical resonator [6]. The double-channel side coupled sequence of ring resonators and coupled optical resonator configuration both demonstrate similar feature that distributed resonances with feedback results in photonic band structures which consists alternate transmission and stop bands in their spectrum [7].

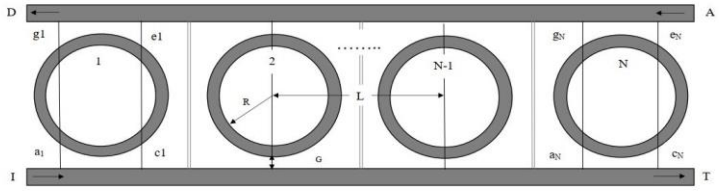

Figure 2 Sketch of a side coupled sequence of ring resonators configuration device consisting of N ring-resonators. L is distance between centres of two adjacently placed ring-resonators [7]

3. DESIGN OF SIDE COUPLED SEQUENCE OF RING RESPONSES CONFIGURATION

A single channel side coupled sequence of ring resonators where multiple rings are coupled to a single waveguide is not of much interest to investigate, since it's transfer function can be obtained by multiplying transfer function of single APF with the number of rings in the configuration. In Fig. 2, a side coupled sequence of ring resonators composed by N ring-resonators coupled indirectly between two waveguides is shown.

For calculating transfer function of N ring-resonators, we construct a new matrix P_L^N to determine the fields propagating between *(N-1)-th* and *N-th* ring resonators [7].

$$\begin{pmatrix} a_N \\ g_N \end{pmatrix} = \begin{pmatrix} e^{-i\pi L\beta_S} & 0 \\ 0 & e^{i\pi L\beta_S} \end{pmatrix} \begin{pmatrix} c_{N-1} \\ e_{N-1} \end{pmatrix} \equiv P_L^N \begin{pmatrix} c_{N-1} \\ e_{N-1} \end{pmatrix} \quad (1)$$

where β_S is the propagation constant of the bus waveguide, L is distance between two ring-resonators. The suffix N indicates that all the resonators in the configuration can possess different parameters. Let us define matrix M^N which describes input and output fields of *N-th* ring-resonator. Hence overall matrix can be written as [7]:

$$\begin{pmatrix} a_N \\ g_N \end{pmatrix} = M^N P_L^N M^{N-1} \cdots P_L^1 M^1 \begin{pmatrix} c_{N-1} \\ e_{N-1} \end{pmatrix} \equiv s \begin{pmatrix} c_{N-1} \\ e_{N-1} \end{pmatrix} \quad (2)$$

As shown in Fig. 2, we will consider the configuration as ideal side coupled sequence of ring resonators, where the rings are identical and are separated by similar distances from each other. This side coupled sequence of ring resonators configuration also has two photonic bands i.e. bragg band (BB) and resonators band (RB) [8].

The condition of resonance for RB is that optical path in a ring resonator must be an integral multiple of wavelength ($m_R\lambda_R = 2\pi R n^b_{eff}$), where m_R is the order of the band, λ_R is the resonance wavelength, n^b_{eff} is the effective index of bend mode and R is the radius of the ring resonator. Whereas, the condition of resonance for BB is that optical path between centres of two adjacent ring resonators is half integral multiple of wavelength, i.e. $\frac{m_R}{2}\frac{\lambda_B}{} = L n^s_{eff}$ [9]. Here, m_B is the order of the band, λ_B is Bragg Band wavelength, n^s_{eff} is the effective index of the straight mode and L is the distance between the ring resonators.

Our proposed side coupled sequence of ring resonators configuration is shown in Fig. 2. In Fig. 2, R is the radius of micro-ring resonator, G is the gap between micro-ring and adjacent bus waveguide whereas L represents distance between two respective microring resonators. Also, I represent input port from where input signal will be applied, D represents drop port where the wavelengths in resonance with ring cavity are obtained, T represents the transmission port where the remaining wavelengths not in resonance with ring cavity is measured and A represents add port from which additional wavelengths required or to be detected can be separately added provided they are in resonance with the ring cavity. Here we have used 8 rings for our side coupled sequence of ring resonators configuration i.e. N=8, where N is the number of rings in the design. We have used COMSOL Multiphysics 5.6 which is finite element analysis and multiphysics simulation software.

4. RESULTS AND DISCUSSION

In this section, we have demonstrated our proposed model in COMSOL Multiphysics 5.6 software for side coupled sequence of ring resonators configuration of 8 rings. Fig. 3. shows the simulation of side coupled sequence of ring resonators configuration in COMSOL. For our design we have considered refractive indices of 3.48 and 1.45 for core and cladding respectively.

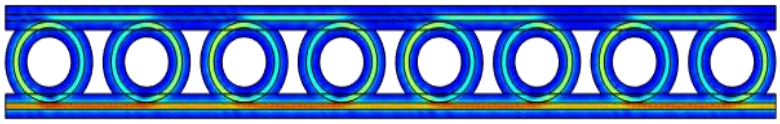

Figure 3 Simulation of proposed side coupled sequence of ring resonators configuration in COMSOL Multiphysics 5.6 software

The design parameters are: R = 1.6 μm, G = 0.931 μm and L = 4.5 μm. We have chosen width of core as 0.26 μm and width of cladding as 1μm. These parameters were chosen on the basis of the simulation performed on radius of the rings R and distance between them L as shown in Fig. 4 and Fig. 5 respectively. In Fig. 3 we can see that for R = 1.6 μm, power outflow at D port is around 0.95, which means power at input port I is coupled to D port, due to resonance within the ring. Whereas, for R = 1.6 μm if we vary distance between the rings, it was observed that for L = 4.5 μm maximum power couples to the drop port D from input port I. However, the range of the analysis was selected on the basis of calculations performed from equations

(1) and (2) respectively. On simulating the design over the range of wavelengths, we obtained reflectance, transmission and absorptance graph as shown in Fig. 6. As we can observe from the response graph, wavelengths from 1.54 μm to 1.55 μm shows the transmittance of value 0.1, means these band of frequencies are in resonance and hence their transmission coefficient is taking a dip.

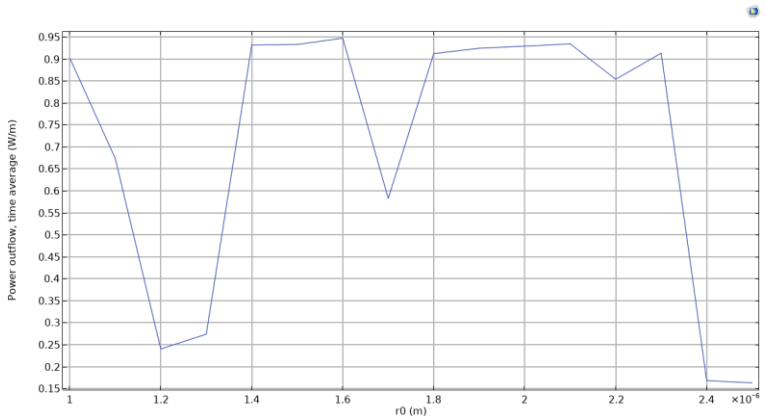

Figure 4 Power outflow (W/m) at port D with variation of ring radius R from 1 μm to 2.5 μm with step size of 0.1 μm.

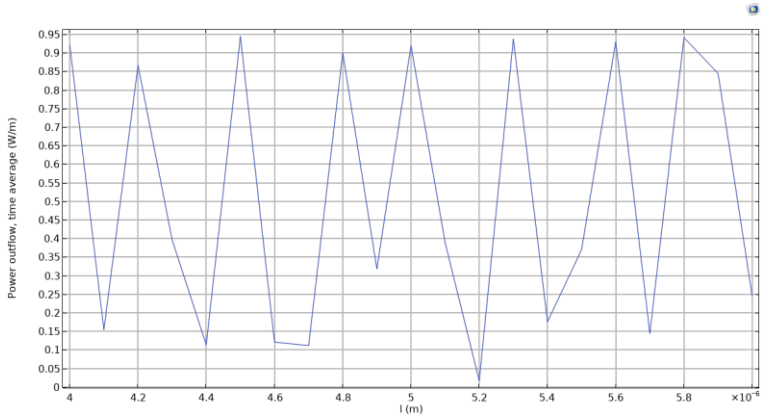

Figure 5 Power outflow (W/m) at port D with variation of distance between the rings L from 1 μm to 2.5 μm with step size of 0.1 μm.

When we compare this result with all pass notch filter which take a dip at the wavelength of the order 10^{-3}, this side coupled sequence of ring resonators configuration shows dip in transmission coefficient for the order of 10^{-1}. For optical frequencies where for large amount of bandwidths, frequencies are in nanometers, this dip for 0.1 μm range is huge or we can say 100 nm range of dip in optical frequencies. For optical frequencies range this configuration can easily be used to drop a range of frequencies. This transmission coefficient of 0.1 can be neglected for certain applications. However, further study is required with the coupling coefficient and certain parameters to rectify this error.

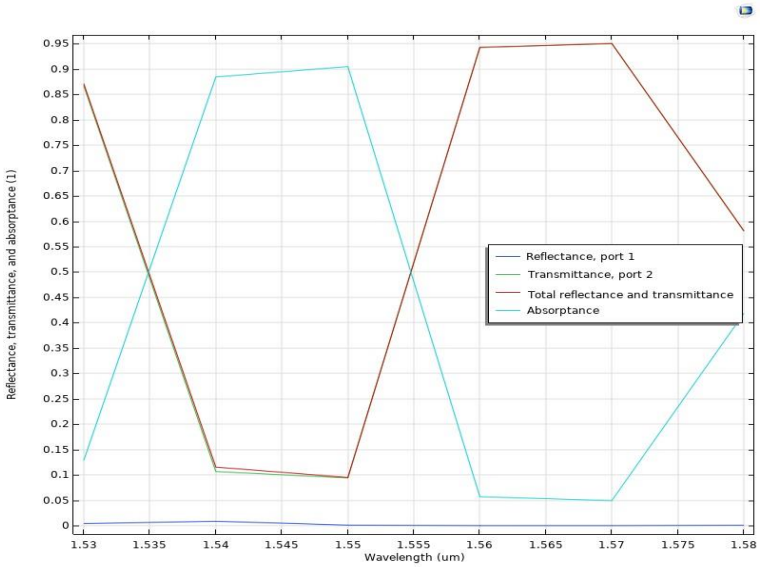

Figure 6 1.53 μm to 1.58 μm spectral response of designed side coupled sequence of ring resonators configuration for R = 1.6 μm, G = 0.931 μm and L = 4.5 μm

5. CONCLUSION AND FUTURE PERSPECTIVES

In this paper, a design to obtain an optical filter using side coupled sequence of ring resonators configuration of micro-ring resonators has been proposed. In this study we found that the optical micro-ring resonators with various different configuration along with suitable parameters can be used to obtain optical filters as per our need. The optical filter design also shows different behaviour for different number of rings, their radius and distance between them. These parameters must be primarily considered while designing the optical filter required for certain application. However, integration of Silicon Photonics and CMOS fabrication have led path and open various opportunities for fabrication of various Photonic Integrated Circuits (PIC's) at affordable prices which was never possible before. In our design study it was also observed that with increase in number of rings between the waveguides, the width of stop band can be increased. However, this was only observed for ring radius taken into account under study. This design can be further extended by studying the variations of ring radius between the two waveguides and also by choosing different materials having large refractive index difference between them.

REFERENCES

[1] S. Kumari and S. Gupta, "Cladding stress induced performance variation of silicon mmi coupler," *Photonics and Nanostructures-Fundamentals and Applications*, vol. 33, pp. 55– 65, 2019.

[2] Y. R. Bawankar and A. Singh, "Microring resonators based applications in silicon photonics-a review," in *2021 5th Conference on Information and Communication Technology (CICT)*, pp. 1–6, IEEE, 2021.

[3] C.-Y. Chao, W. Fung, and L. J. Guo, "Polymer microring resonators for biochemical sensing applications," *IEEE journal of selected topics in quantum electronics*, vol. 12, no. 1, pp. 134–142, 2006.

[4] V. Zamora, P. Lutzow, M. Weiland, and D. Pergande, “Investigation of cascaded sin¨ microring resonators at 1.3 μm and 1.5 μm,” *Optics express*, vol. 21, no. 23, pp. 27550– 27557, 2013.

[5] H. Hairi, T. Saktioto, D. Irawan, and J. Ali, “A design of twisted double channel scissors for optical filter,” *Komunikasi Fisika Indonesia*, vol. 10, no. 6, pp. 452–459, 2013.

[6] V. Van, *Optical microring resonators: theory, techniques, and applications*. CRC Press, 2016.

[7] M. M. Mancinelli, *Linear and non linear coupling effects in sequence of microresonators*. PhD thesis, University of Trento, 2013.

[8] A. Liu, L. Liao, D. Rubin, H. Nguyen, B. Ciftcioglu, Y. Chetrit, N. Izhaky, and M. Paniccia, “High-speed optical modulation based on carrier depletion in a silicon waveguide,” *Optics express*, vol. 15, no. 2, pp. 660–668, 2007.

[9] X. Fan, I. M. White, S. I. Shopova, H. Zhu, J. D. Suter, and Y. Sun, “Sensitive optical biosensors for unlabeled targets: A review,” *analytica chimica acta*, vol. 620, no. 1-2, pp. 8–26, 2008.

Biographies

Yash R Bawankar, currently in the final year of M.Tech in Communication System Engineering at Visvesvaraya National Institute of Technology. Academic interests consist of Optical Communication Systems.

Dr. Anamika Singh, works as an Assistant Professor at Electronics and Communications Engineering, Visvesvaraya National Institute of Technology. General interests include Optical Communication and Silicon Photonics.

Analysis of VHO Parameters based on Polynomial Regression

[1]Siddharth Goutam, [2]Srija Unnikrishnan, [3]Pradeep Singh, [4]Aradhana Goutam

[1]Dr. B. R. Ambedkar University of Social Sciences, Dr. Ambedkar Nagar (Mhow), Indore (M.P)

[2,3]Father Conceicao Rodrigues College of Engineering, Mumbai, Maharashtra, India

[4]Research & Business Analytics, Prin. L. N. Welingkar Institute of Management Development and Research, Matunga, Mumbai 400019

[1]sgoutam07@gmail.com, [2]srija@frcrce.ac.in, [3]pradeep@frcrce.ac.in, [4]aradhana.goutam@welingkar.org

Abstract

The continuous & ever growing demand of high data rate various mobile applications can be dealt by Next Generation Networks (NGNs). This demand of high data rate is also coupled with least cost for the mobile user. This combination is feasible by considering Vertical Handover (VHO) in NGNs. This research paper aims in capturing the design and simulation of an algorithm for Vertical Handover. The input parameters considered are Received Signal Strength (RSS), bandwidth, cost and user velocity. The statistical analysis based polynomial regression model is also presented in the research paper

Keywords. Vertical Handover (VHO), Vertical Handover Decision Algorithm (VHDA), Received Signal Strength (RSS), Fuzzy Inference System (FIS), Next Generation Networks (NGNs).

1. INTRODUCTION

The nature of Next Generation Networks is heterogeneous, and they will be constituting of IP-based networks. NGNs will be diverse because of the presence of numerous Radio Access Technologies (RATs) [1] [2]. The presence of NGNs is depicted in Figure 1.

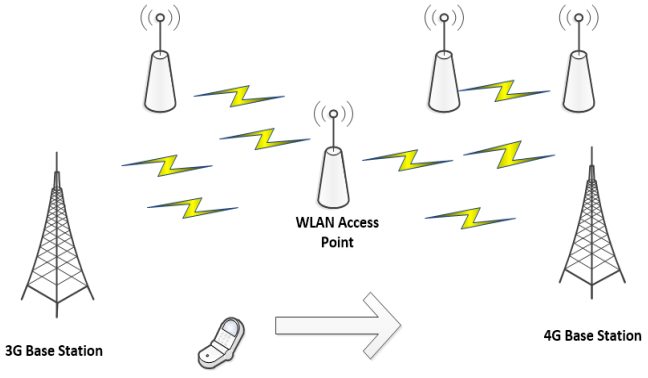

Figure 1 Presence of NGNs

Mobile customers' increasing demand for high bandwidth can be satisfied to some extent by NGNs.

Vertical Handover allows for seamless mobility across the various RATs [2] [3].

The paper has been organized as follows: Section II provides the theoretical background. Section III captures the system model. Section IV gives implementation results and analysis. Section V presents the conclusion & future work.

2. THEORETICAL BACKGROUND

2.1. VHO

VHO can be categorized in 3 steps. Fig 2 represents the steps of VHO [4].

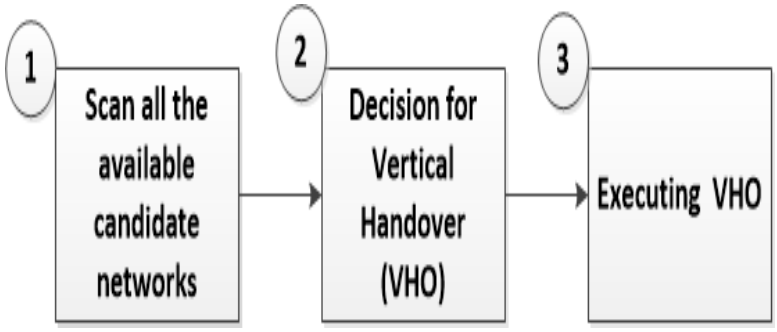

Figure 2. Phases of VHO

Figure 3 captures the i/p attributes for VHO. The handover value of the n/w is described as under by eq (1)

$$HV = f(RSS, Bandwidth, Cost, Velocity) \quad (1)$$

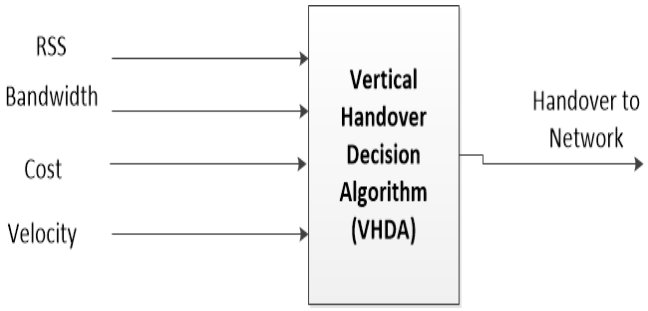

Figure 3. Parameters of VHDA

2.2. Fuzzy Inference System (FIS)

FIS is represented in fig 4.

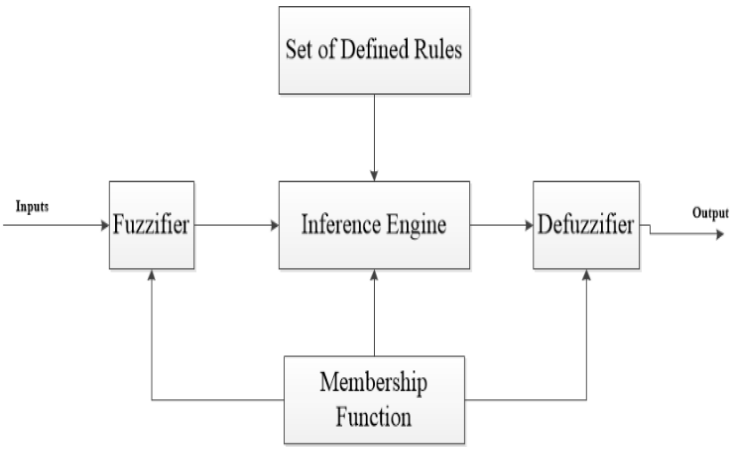

Figure 4. FIS

The membership function is represented in equation 2. [2]

$$\mu(x{:}\,r,s,t) = \begin{cases} 0, & x \le r \\ \frac{(x-r)}{(s-t)}, & r \le x \le s \\ \frac{(t-x)}{(t-s)}, & s \le x \le t \\ 0, & x \ge t \end{cases} \quad (2)$$

2.3. Polynomial Regression Analysis

The polynomial regression analysis is performed for representation of the relationship between two variables which is modeled as an nth degree polynomial in x.

x; independent variable

y; dependent variable

The equation is shown as under:

$$y = a + bx + cx^2 \quad (3)$$

The normal equations are described as under:

$$\sum y = na + b\sum x + c\sum x^2 \quad (4)$$

$$\sum xy = a\sum x + b\sum x^2 + c\sum x^3 \quad (5)$$

$$\sum x^2 y = a\sum x^2 + b\sum x^3 + c\sum x^4 \quad (6)$$

The values of a,b and c is found using above equations [5].

3. SYSTEM MODEL

Figure 5 represents block diagram of FIS [6].

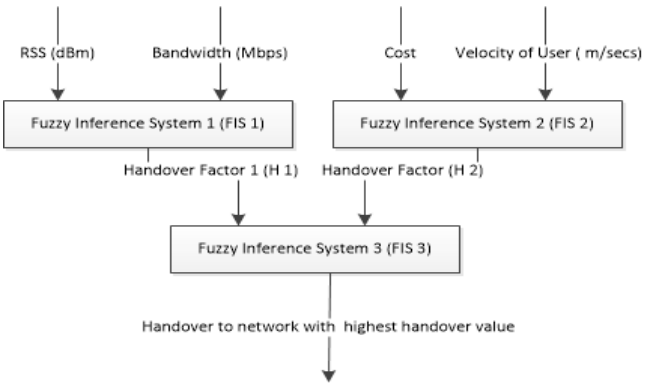

Figure 5. Block diagram for FIS

Figures 6 & 7 represent VHO flowchart & VHDA respectively.

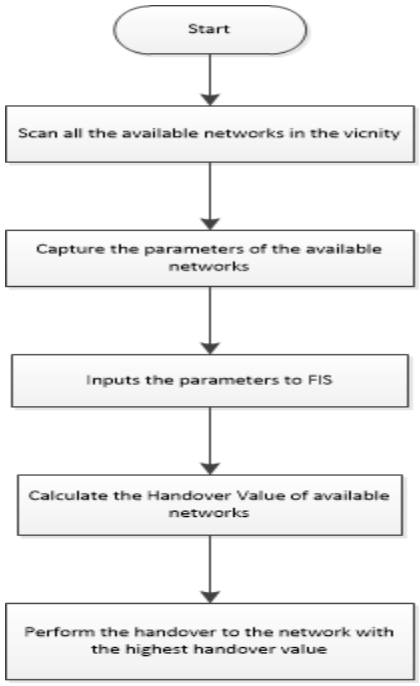

Figure 6. Flowchart of VHO

Algorithm ; VHO based on Fuzzy Logic

Input(s) :
- RSS
- Bandwidth
- Cost
- Velocity

Output :
- Handover to the network

Steps to be followed :

1. Scan all the available candidate networks in vicinity
2. Capture the parameters of the available networks
3. Input the parameters to Fuzzy Inference System (FIS)
4. Calculate the handover value of each candidate network
5. Handover to the network with highest score

Figure 7. Algorithm for VHO

4. IMPLEMENTATION RESULTS & ANALYSIS

The implementation of algorithm has been performed in Python. . The parameters are captured in Table 1.

Table 1 Parameters used in Implementation

S. No	Parameter	4G	WLAN
1	RSS (in dBm)	-104 to-110	-105 to -110
2	Cost (INR)	10-20	0-4
3	Bandwidth (in Mbps)	1-6	8-10
4	Velocity (in m/sec)	15-30	0-5

The dataset of parameters has been generated by using the values measured. The polynomial regression analysis has been done for bandwidth & handover value (while keeping RSS, velocity cost as constant) for 4G & WLAN. Also, we have performed the polynomial regression analysis of velocity & handover value (while keeping RSS, bandwidth, cost as constant) for 4G & WLAN.

4.1. Polynomial Regression Analysis for Bandwidth & Handover Value for 4G

The values of other parameters have been kept fixed/constant at following values :

RSS (in dBm) = -110

Cost (INR) = 15-20

Velocity (in m/sec) = 25-50
x : Bandwidth
y : Handover value

$\sum x$ = 8580

$\sum y = 2972.26$

$\sum xy = 16411.12$

$\sum x^2y = 115022.5$

$\sum x^2 = 60060$

$\sum x^3 = 471900$

$\sum x^4 = 3951948$

$n = 1560$

Solving normal eq. 3 to eq.6 we will get the following

a=1.8487, b = 0.0196, c = -0.0013

$y = 1.8487 + 0.0196x - 0.0013x^2$

4.2. Polynomial Regression Analysis for Bandwidth & Handover Value for WLAN

The values of other parameters have been kep fixed/constant at following values :

RSS (in dBm) = -110

Cost (INR) = 0 - 3

Velocity (in m/sec) = 0-4
x : Bandwidth
y : Handover value

$\sum x$ = 1090

$\sum y = 417.4108$

$\sum xy = 826.7362$

$\sum x^2y = 2468.115$

$\sum x^2 = 7600$

$\sum x^3 = 59500$

$\sum x^4 = 496660$

$n = 200$

Solving normal eq.3 to eq. 6 we will get the following

a=11.5263 , b= -3.2596 , c= 0.2191

$$y = 11.5263 - 3.2596x + 0.2191x^2$$

4.3. Polynomial Regression Analysis for Velocity & Handover Value for 4G

The values of other parameters have been kept fixed/constant at following values:

RSS (in dBm) = -110

Cost (INR) = 15-20

Bandwidth (in Mbps) = 1-5

x : Velocity
y : Handover value

$\sum x$ = 30600

$\sum y = 2325.5$

$\sum xy = 57887.3$

$\sum x^2y = 1943234$

$\sum x^2 = 1030200$

$\sum x^3 = 39015000$

$\sum x^4 = 1575999960$

$n = 815$

Solving normal eq. 3 to eq. 6 we will get the following

a=-1.0711 , b=0.236816 , c=-0.003929

$$y = -1.0711 + 0.236816x - 0.003929x^2$$

4.4. ***Polynomial Regression Analysis for Velocity & Handover Value for WLAN***

The values of other parameters have been keep fixed/constant at following values :

RSS (in dBm) = -110

Cost (INR) = 0-3

Bandwidth (in Mbps) = 7-10

x : Velocity
y : Handover value

$\sum x$ = 20400

$\sum y = 1664.09868$

$\sum xy = 41148.5962$

$\sum x^2y = 1378086.22$

$\sum x^2 = 686800$

$\sum x^3 = 26010000$

$\sum x^4 = 1050666640$

$n = 815$

Solving normal eq.3 to eq. 6 we will get the following

a=2.1274 , b= -0.00455 , c= 0.000034

$$y = 2.1274 - 0.00455x + 0.000034x^2$$

5. CONCLUSION & FUTURE SCOPE

This research paper aims at the analysis of the parameters of Vertical Handover (VHO) based on polynomial regression analysis. The analysis has been presented for bandwidth and handover value, velocity and handover value for 4G & WLAN. The practical values have been considered for analysis. In our future work, we intend to consider more number of parameters for VHO and also intend to consider more number of networks.

REFERENCES

[1] Y. N. Gyekye and J. I. Agbinya, "A Vertical Handoff Decision Algorithm for Next Generation Wireless Networks," in *Third International Conference on Broadband Communications, Information technology and Biomedical Applications, IEEE Computer Society*, 2008, pp. 358-364.

[2] S. Goutam and S. Unnikrishnan, "QoS based Vertical Handover Decision Algorithm using Fuzzy Logic," in *IEEExplore*, Mumbai, 2019.

[3] Siddharth Goutam, Srija Unnikrishnan, Sundary Prabavathy, and Neel Kudu, "Prediction of Vertical Handover Using Multivariate Regression Model," *International Journal of Innovative Technology and Exploring Engineering (IJITEE) (ISSN: 2278-3075)*, vol. 8, no. 10, pp. 2626-2633, August 2019.

[4] Siddharth Goutam and Srija Unnikrishnan, "Algorithm for handover decision in IEEE 802.11 WLAN Environment based on Fuzzy Logic," in *International WIE Conference on Electrical and Computer Engineering (WIECON - ECE 2019), IEEE*, Bangalore, 2019.

[5] M. K. Jain, S. R.K. Iyengar, and R. K. Jain, *Numerical Methods for Scientific and Engineering Computation*.

[6] S. Goutam ,S. Unnikrishnan P. Singh and A.Karandikar, "Algorithm for handover decision using Fuzzy Logic," in IEEExplore, Mumbai, 2021

Biographies

Siddharth Goutam completed his bachelor degree in Electronics & Telecommunication Engineering and Masters in Engineering in Electronics & Telecommunication Engineering with specialization in Communication Systems Engineering. He has completed Ph.D. in Electronics Engineering with specialization in Communication engineering.

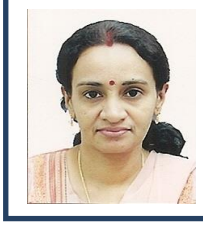

Dr. Srija Unnikrishnan is Principal at Fr. Conceicao Rodrigues College of Engineering affiliated with the University of Mumbai, India. She has over 35 years of teaching experience at the UG and PG level. She received her Bachelor's Degree in Engineering from the University of Kerala, a Master's Degree from Osmania University, and Ph.D. from the University of Mumbai. Her broad areas of interest are Mobile Communication and Signal Processing.

Pradeep Singh is working as an Assistant Professor in Department of Humanities & Science at Father Conceicao Rodrigues College OF Engineering, Band-stand, Bandra (West),Mumbai from June 2006. He has completed Master of Science (M.Sc.) in Mathematics from Indian Institute of Technology (IIT) – Bombay in the year 2004. He has qualified NET – CSIR with Rank -21. His main area of interest are Linear Algebra, Statistics, Partial Differential Equations, Theory of Complex Analysis

Dr. Aradhana Goutam holds a Ph.D. in the area of Computer Science Engineering & Information Technology, from Faculty of Engineering Sciences, Devi Ahilya Vishwavidyalaya, Indore (M.P.), coupled with a Master of Technology (M.Tech) in Information Technology Degree from the Devi Ahilya Vishwavidyalaya, Indore (M.P.). She has experience in developing software solutions on multiple platforms. Her academics experience spans across M.Tech. Information Technology, Mobile Computing, M.Sc. - Electronics & Communication, Electronics, B.E. Computer Science and B.E. Information Technology . She has been associated with premier and reputed institutions like DAVV Indore, FRCRCE Mumbai and IES MCRC Mumbai.Her 17 years of experience spans across Teaching, Industry and Research domains. She has taught many subjects Like Project Management, Software Engineering, Mobile Computing, DBMS, JAVA, ERP, and many others. She has published 16 research papers in various International and national Journals. Her tryst with academics as a knowledge facilitator has been for the past 8 years. Dr. Aradhana Goutam is currently associated with IES Institute of Management College.

PGForYou: A Framework for Facilitating Paying Guest Search Method

[1]Lavish Saini, [2]Harshit Lomas, [3]Pushpa Singh

[1,2,3]Computer Science and Information Technology, KIET Group of Institutions, Delhi-NCR, Ghaziabad, India

[1]lavish.1822csi1018@kiet.edu, [2]harshit.1822csi1014@kiet.edu, [3]pushpa.gla@gmail.com

Abstract

Every individual who wants to relocate from their city or house just wants to get a place where he feels at home. If a student is relocating for studies or an employee is relocating for his job, then they need a living place near their school/college or office. Paying guests (PG) is a perfect and affordable option for such an individual as they do not need to care about security, food, or cleaning, and also it feels like home when it gets compared with a Hostel room or rented flat. Available solution is primarily focused on buying and selling property and renting commercial and residential property. PG is a secondary option. This paper suggests a dedicated web application for PG searching facilities in their nearby location. PGs are ranked with the help of a keyword extraction mechanism. Application is developed with Android framework, Angular JS, Express JS, Msg91, Mapbox and Cloudinary. The proposed application will solve the accommodation problem of the user in an efficient and optimized way.

Keywords. Paying Guest, Web applications, Android, rating

1. INTRODUCTION

Metro cities of India are the foremost centre of education, businesses and jobs. People are migrating from rural areas to urban areas or metro cities for better education and employment. These people are mainly facing issues related to accommodation. Each and everyone expects a neat, clean, stable and low-cost accommodation. There may be various options of accommodation such as hostel, rented house, rented flat and Paying Guest (PG). PG is one of the best choices among all other available options due to its benefit, as shown in figure 1. [1]. A PG is a better option than a flat or hotel room as you don't have to worry about food, security, etc. Consider a scenario where a first-year student belongs to a different state or locality. Being a stranger in the city will be hectic and take lots of time and energy as a student, and their parents visit PG by themselves and ask for pricing, security, etc. He needs accommodation around his nearby Institute which can save transport costs, provide good food facility, low-cost maintenance, and a homely environment. If all these problems are solved by browsing a particular application, a user's life will turn out to be very easy and accessible. This problem is the same for the employee relocating from their city to work. So, in this paper, we are trying to overcome all such problems with our android based framework. The user can search the PG in their nearby location.

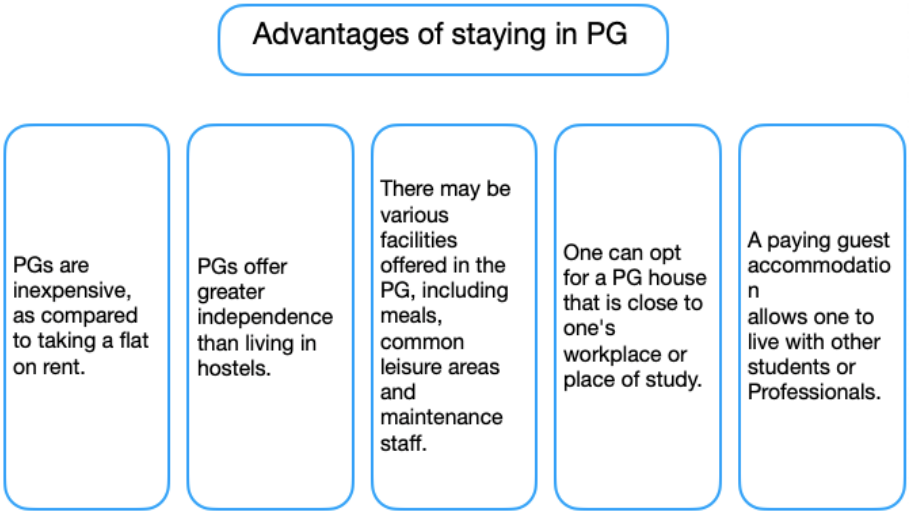

Figure 1. Advantages of PG

PGs are rated on the basis of user feedback utilizing the concept of natural language processing (NLP). This application will be useful to anyone searching for an efficient place to stay.

This paper is organized into subsequent sections. Section 2 represents a brief related work. Section 3 represents the proposed methodology. Section 4 represents the result and discussion. Finally, section 5 concludes the work.

2. RELATED WORK

India has the world's largest population of 5-24 years, which provides a great opportunity for the education sector [2] and observes a rapid growth in the number of educational institutions [3]. Many Android-based apps are proposed and used to connect students and college[4-6]. PGs and Hostels are also an integrated part of education and seeking attention. PG is a place where users/students can stay for three or four years in a very convenient manner that too very low cost. We have researched multiple sites related to PG search and came across they were primarily focused on buying and selling property, Residential and Commercial places for rent, etc. PG is a secondary option. Reference [7] proposed online accommodation, but we would like to focus only on PG. The user wants to search PG for accommodation; he only needs information like pricing, distance from college/office, food, security, the experience of other users, photos, and price comparison. Existing available solutions have their broad view, while students are only looking for their own perspective. However, students can also select a hostel and a flat, but PG is a combination of both and hence becomes a key solution for accommodation [8]. There is always a need for specific solutions that can only be dedicated to students or trainees. During Covid-19, small houses in the metro city are one of the main reasons to spread of this infectious disease among their

family member. PG can also play a pivotal role in mitigating the spread of infection [9]. Keyphrase extraction is extensively used in many fields, particularly website ranking [10], and provides recommendations of any product or brand based on customer feedback [11]. Further, the rank of PG will also assist the user in searching the PG in less time. AI and Machine Learning techniques with Natural language processing (NLP) extract the most important keywords from text [12] for PG recommendation.

This motivates us to propose a key solution that can primarily focus on students' requirements. Apart from the user side, we can also give PG owner a separate window where he provides description, pricing, availability of PG, etc., on the website. PG on site will rate/rank according to NLP based on positive or negative comments of the user. So overall, our objective behind this paper is to provide a single platform for paying guest solutions to users that is very easy to understand by him, saves time and energy, and also on which he can trust.

3. PROPOSED METHODOLOGY

Our objective is to propose an online application to book a paying guest that is available nearer to colleges/offices. In this application, there is a separate module for the user and a PG owner. There are various websites and applications working in the current framework, but they are discrete and arbitrary. Now we are trying to convert it into one particular website. Our application helps users take a virtual tour of PGs via photos and videos; by this, they don't need to visit the different PGs physically.

3.1. Technology Used:

This application mostly utilized free and open-source software (FOSS) to build the front end and backend. FOSS is offered active tools that can be quickly employed in corporate, research and academia [13]. The following tools are used to build the proposed work:

- **Bootstrap:** An open-source framework, i.e., Bootstrap, is used to build a proposed web application where HTML is used for front-end design, CSS beautify the web page, and Java Script offers the facility of validations. Bootstrap contains different design templates for forms, buttons, navigation, and other components. Bootstrap support all browser and offers lightweighted and customizable.
- **Node.js** provides a runtime javascript environment that implements javascript outside a web browser with the help of the V8 engine.
- **Express.js** is the backend web framework for Node js.
- **MongoDB** is a NoSQL, document-oriented database in which data is in the JSON format.This is used to store all

  kinds of information related to PG. It also provides technical support for the cloud environment.
- **Msg91** provides API's for SMS, Email, Whatsapp, Voice, and Authentication. This is used for mobile phone OTP. Verification of a user in the proposed application.

- **Cloudinary**: It provides cloud-based Image management services.This is used for managing and storing all PG's Images.
- **Mapbox**: It is a custom online map provider. This is used to locate PG on a map. Mapbox can quickly deal with heavy traffic websites with simple coding.

3.2. System Design

After identifying of problem, tools and technologies required for the system, the next step is to design the framework or system. How the system entity interacts with the proposed system and how the data flow from one process to another process or entity during login and registration of a user represented by a login and registration Data Flow Diagram (DFD), as shown in figure 2 and how user and PG owner entity interacts with the system and how the data is flowing from process to another process shown in Figure 3. and Figure 4 respectively. OTP mechanism is used to verify and validate the user.

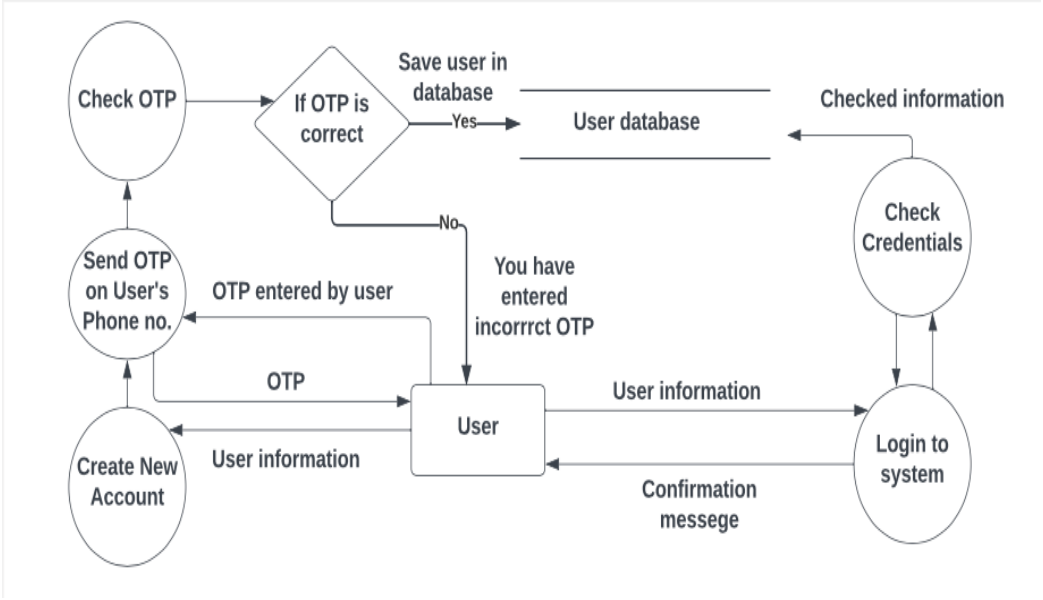

Figure 2. Login and Registration DFD

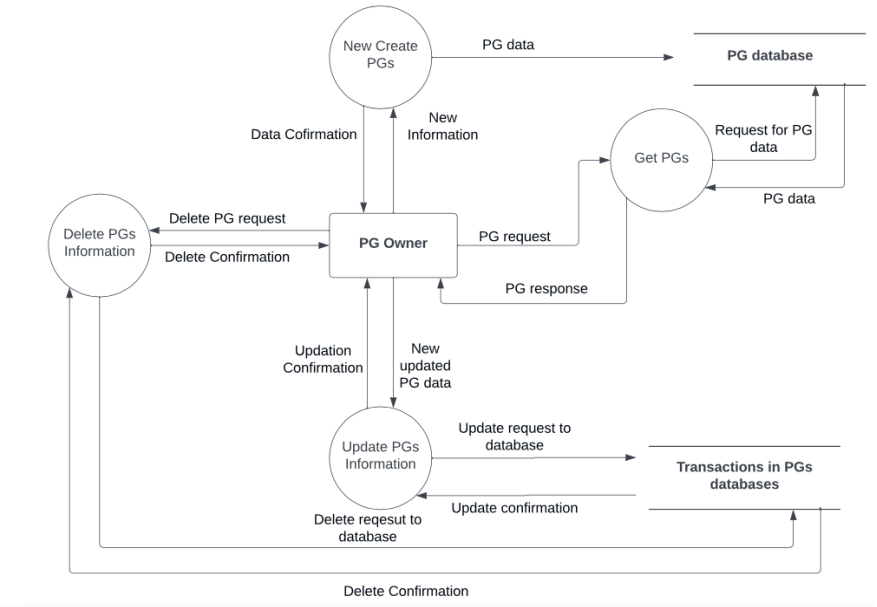

Figure 3. PG owner DFD

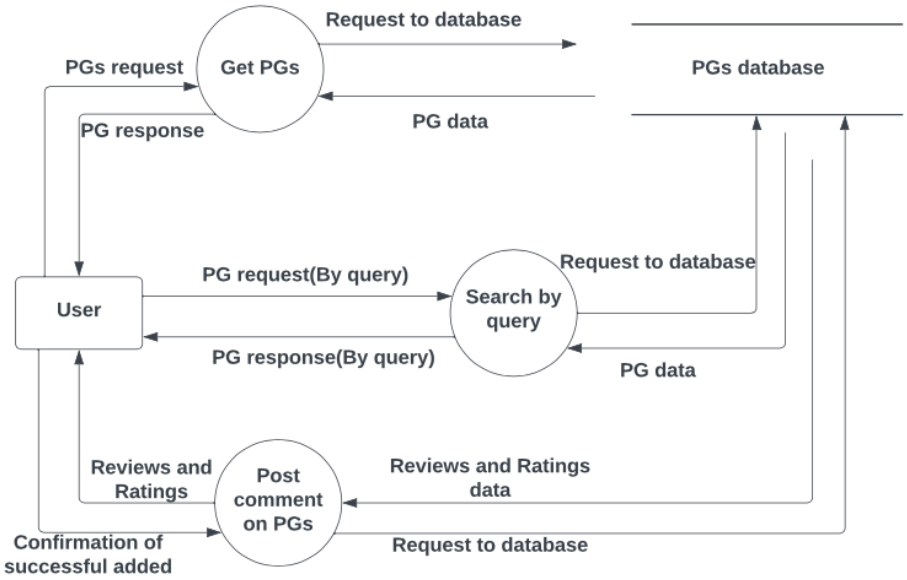

Figure 4. User DFD

An interesting feature of this proposed android based framework is its ability to rate/rank PG. According to figure 3.3, the system collects comments or feedback from the user who has been admitted in PG. User feedback/comments are keywords such as 'good' or 'bad', and their synonyms are extracted from the feedback text and utilized for the rating of PG. The concept of NLP has been taken into consideration to extract keywords from the posted comment of the authenticated users. Here, authenticated user means whoever has taken admission/exit in a specific PG. Not all users' comments who have just visited the site will be counted for rating purposes.

3.3. Module Description:

The proposed android-based framework consists of four main modules.

Admin Module: Manages all the data and corresponding access rights of PG owner and user. This module can View/Edit the details of the PG owner and user.

PG Owner Module: The PG Owner can start the process with login after signup with a phone number. PG owners can quick add/delete/update the PG room details with images and videos. Images can store in the cloud and hence optimize the storage capacity. Figure 3.2 represents work flow of PG owner.

User Module: The user will also register with the signup process and connect with the user ID and password. Users can search for location-wise PG, room details, and price and can take a virtual tour of PG via photos and videos. Mapbox will help the user to find PG on the map. User can view list of top ten PGs, which is rated on the basis of the authenticated user.

Rating of PG: Generally, users wish to search for a top ten PG in their respective location. How to rate the PG is a challenging task. The proposed framework solves this problem. The system automatically rate the PG according to the feedback of users in particular PG. Positive keywords such as ‘good’, ‘best’, ‘ok’ and other synonyms are extracted from the feedback and rate according to maximum number of positive keywords for a particular PGs.

4. RESULT AND DISCUSSION

The proposed framework named as "PGForYou" offers online PG searching services to users. Application is developed by using HTML, CSS and ReactJS. Screenshots of developed applications are represented in figures 5, 6,7, and 8. On the website, the location of PG is also viewed on the map by which a user gets satisfaction with the exact location of PG. If a user selects a PG for booking, then he is required to SignUp with his phone number via OTP verification. Then a user is allowed to talk with the PG owner directly if he wants.

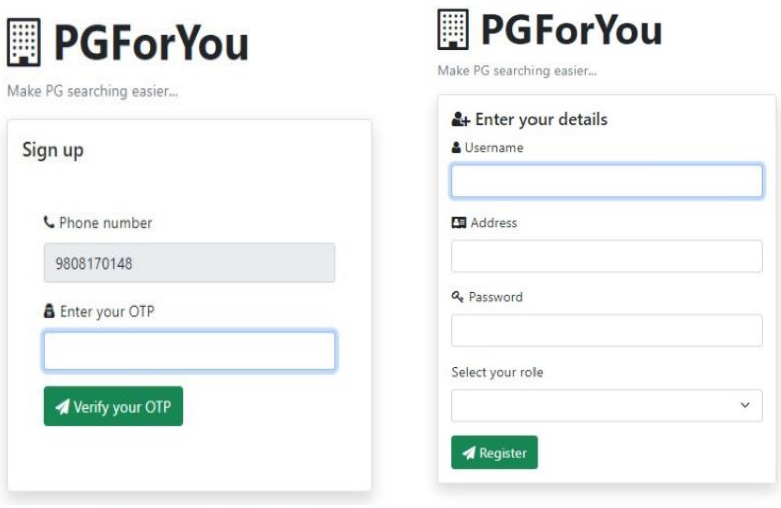

Figure 5. Sign up and login page

In case, If requested PG and rooms are not available currently, then the user can add his request in his wishlist.

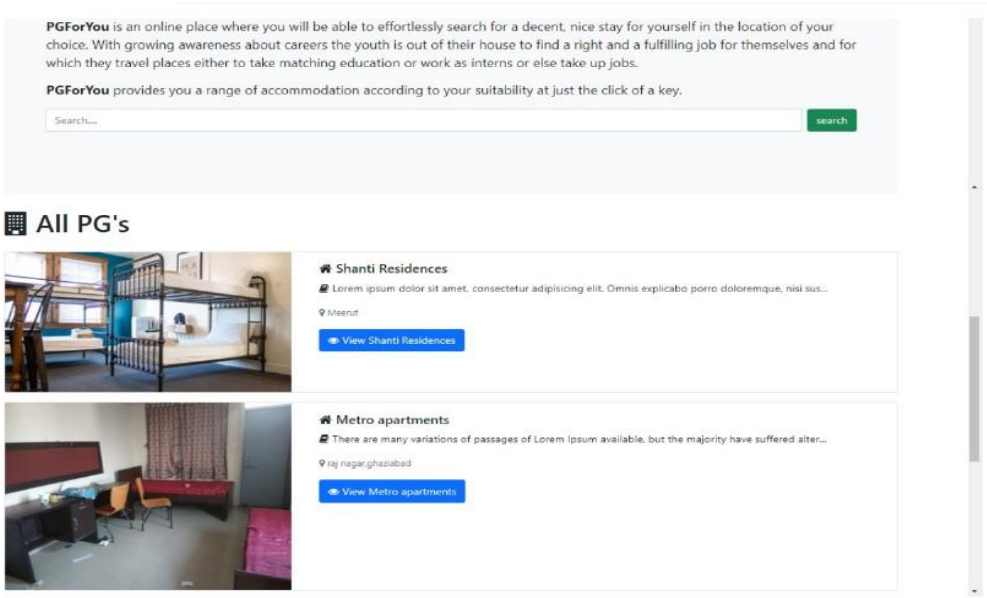

Figure 6. Home Page of PGForYou Application

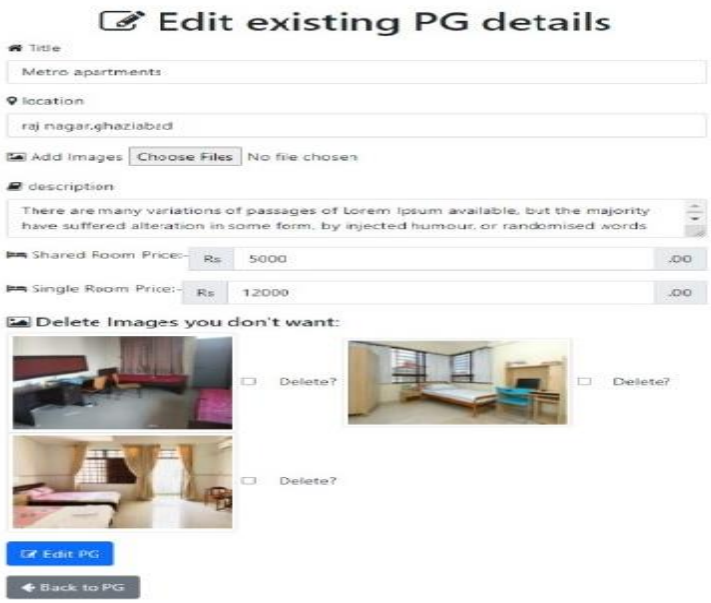

Figure 7. Edit of Existing PG Details

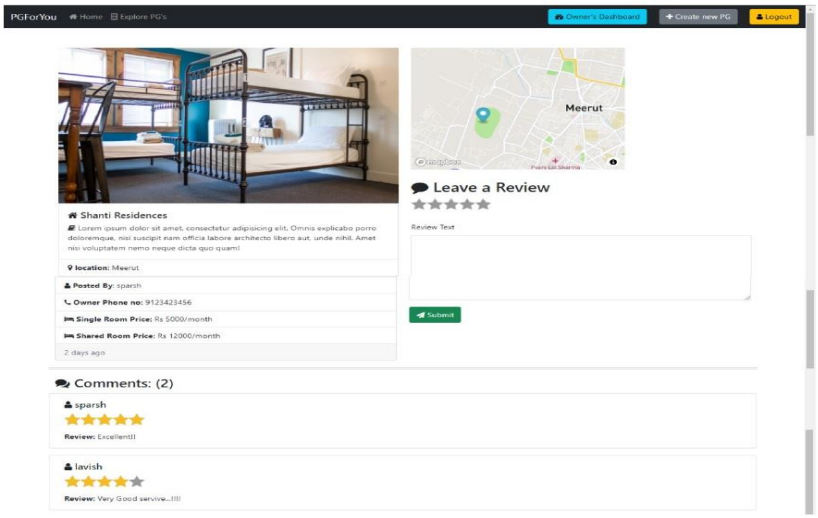

Figure 8. Glimpse of PGForYou

We want to extend this work with the advanced technology of flask and flutter [14]. Rating of PG may be implemented by the page rank algorithm [15]. AI and Cloud-based technology

may make PG finding activity smart and intelligent [16]. With the help of ratings provided by different authenticated PG users, a new user will be able to choose the best PG from the available options. With the help of a page ranking algorithm, a user will automatically suggest the best PG according to their requirements and budget.

5. CONCLUSION

'PGForYou' is a user-friendly android based framework that enables the user to search PG with respect to location. The application utilized node.js, express.js, Msg91, Mapbox and Cloudinary. Mapbox provides PG on map, and Cloudinary offers cloud storage to image data. The application helps the user to search best PG in their nearby location. The rating of PG is based on feedback to make the search easy. NLP is used to extract keywords from feedback and rate them according to the maximum number of positive keywords.

REFERENCES

[1] PG Accommodation" accessed on 8 Jan 2022 from https://www.magicbricks.com/blog/benefits-of-pg-accommodation-paying-guest/126427.html.

[2] IBEF, 'EDUCATION SECTOR IN INDIA INDUSTRY REPORT*'* accessed on 28 March 2022 from https://www.ibef.org/industry/education-sector-india, Mar 2021.

[3] B. Dhanalaxmi et al., 'An User-Friendly Android based Application for Online Rental System', In *2021 Fifth International Conference on I-SMAC (IoT in Social, Mobile, Analytics and Cloud)(I-SMAC)*, pp. 1030-1038, IEEE, Nov. 2021.

[4] R. Malhotra, D. Kumar, D.P. Gupta, 'An android application for campus information system', *Procedia Computer Science*, *172*, pp. 863-868, 2020.

[5] S. Kumar, S. kumar Sharma, D. Dagwar, 'Android Based College Campus App', In *2018 Second International Conference on Computing Methodologies and Communication (ICCMC)*, pp. 328-333, IEEE, Feb. 2018.

[6] S. Harnale, T. Ganeshsingh, S. A. Hussain, 'Android College Campus', *International Journal of Ethics in Engineering & Management Education*, pp. 2348-4748, 2014.

[7] G. Kamath, '*A Project Report On Online Accomodation Finder*' (Doctoral dissertation, CMR Institute of Technology. Bangalore), 2020.

[8] Meghali , 'Hostel vs PG vs Rented Flat', Online accessed on 28 March 2022 from https://www.reviewadda.com/institute/article/226/hostel-vs-pg-vs-rented-flat, Jul 07, 2020.

[9] S. R Marella, K. Priya, & P.V. D'Souza, 'COVID-19 and precarious housing: paying guest accommodation in a metropolitan Indian city', *Global Discourse: An interdisciplinary journal of current affairs*, 2022.

[10] T. Haarman, B. Zijlema, & M. Wiering, 'Unsupervised keyphrase extraction for web pages', *Multimodal Technologies and Interaction*, *3*(3), pp. 58, 2019.

[11] K. A. Tarnowska, Z. Ras, 'NLP-based customer loyalty improvement recommender system', *Big Data and Cognitive Computing*, *5*(1), pp. 4, 2021.

[12] F. Liu et al., 'Performance evaluation of keyword extraction methods and visualization for student online comments', *Symmetry*, 12(11), pp. 1923, 2020.

[13] P. Singh, N. Singh, 'Analysis of Free and Open Source Software (FOSS) Product in Web Based Client-Server Architecture', *International Journal of Open Source Software and Processes (IJOSSP)*, *9*(3), pp. 36-47, 2018.

[14] A. Hardiyanto, D. Fitrianah, 'Android application for extractive text summarization', *Library Hi Tech News*, 2021.

[15] M. Coppola et. al., 'The PageRank algorithm as a method to optimize swarm behavior through local analysis', *Swarm Intelligence*, 13(3), pp. 277-319, 2019.

[16] P. Singh et al., 'Artificial Intelligence for Smart Data Storage in Cloud-Based IoT', In *Transforming Management with AI, Big-Data, and IoT*, pp. 1-15, Springer, Cham, 2022.

Biographies

Lavish received the bachelor's degree in computer engineering from KIET group of institutions, Delhi-NCR in 2022.He is currently working as a Data engineer in Gemini solutions pvt ltd. His area of expertise includes SQL and NoSql databases, ETL frameworks and Cloud services.

Harshit received the bachelor's degree in computer engineering from KIET group of institutions, Delhi-NCR in 2022. He is currently working as an Associate software engineer trainee in Naggaro technologies pvt ltd. His area of expertise includes backend and frontend development using javascript frameworks and libraries.

Dr. Pushpa Singh is an Associate Professor of CSIT Department at the KIET Group of Institutions, Delhi-NCR, Ghaziabad, India. She has more than 18+ years of experience teaching B.Tech and MCA students. Dr. Singh has acquired MCA, M.Tech (CSE), and Ph.D. (CSE) in Wireless Networks from AKTU Lucknow. Her current areas of research include performance evaluation of heterogeneous wireless networks, machine learning, blockchain and cryptography. She has published 50 research publications in reputed international journals, conference and edited book. She has published four books and contributed six book chapters in international publication. She is one of active reviewers of IGI, Springer, and other conference proceedings and journals. She has been invited to serve on various technical program committees